

TOOLS TOWARDS THE EXPLORATION AND LEVERAGE OF NOVEL PHOTOCATALYTIC METHODOLOGIES

Durbis Javier Castillo Pazos



Department of Chemistry, McGill University

Montreal, QC, Canada

October 2024

A thesis submitted to McGill University in partial fulfillment of the requirements of the degree of Doctor of Philosophy

©Durbis Javier Castillo Pazos 2024

“El proceso creativo es tan importante como el resultado final, es en él donde descubrimos quiénes somos.”

- Remedios Varo

Dedicated to my mother, Milagros.

Thank you for your love, your strength, and your wisdom.

You are always missed, but never missing.

Abstract

Photocatalytic methodologies have become a cornerstone of synthetic chemistry, offering new ways to access high-value intermediates under mild reaction conditions. Due to the widespread demand for more efficient photocatalytic approaches, constant innovation is required to reach the desired reactivity, selectivity, and stability, while making these methods sustainable and accessible. For this reason, during the last decade, the Li lab has reported numerous tools that provide solutions to existing challenges on diverse fronts, including but not limited to: the development of new reagents to access facile and streamlined functionalization reactions, the in-depth study of new catalytic pathways for the exploration of diversified reactivities, and the design of new and accessible devices that allow for accelerated optimization of reaction conditions. Herein, we report 3 tools in the same order. Chapter 1 introduces the necessary background regarding modern methodologies in homogeneous photocatalysis, identifying areas of opportunity, and current efforts to address these challenges while providing standardized solutions. Chapter 2 (“New Reagents”) provides insight into developing a series of bench-stable photocleavable reagents for the perfluoroalkylation of electron-rich aromatics under metal-free and redox- and pH-neutral conditions. Chapter 3 (“New Catalytic Pathways”) describes the application of simple triarylamine as catalytic electron donors in Electron Donor-Acceptor (EDA) complexes. In this project, we discuss the photophysical characterization of the complex formed between these amines and the photocleavable reagents described in Chapter 2. Chapter 4 (“New Devices”) provides insight into the design of a 3D-printed photoreactor for High-Throughput Experimentation (HTE). Such a low-cost prototype is modular and accelerates the discovery and optimization of novel reactions promoted by visible light in a parallel fashion. Lastly, Chapter 5 discusses contributions to fundamental knowledge and future work related to these three projects.

Résumé

Les méthodologies photocatalytiques sont devenues un pilier de la chimie de synthèse, offrant de nouvelles voies d'accès à des intermédiaires de grande valeur sous des conditions de réactions douces. En raison de la demande croissante pour des approches photocatalytiques plus efficaces, une innovation constante est nécessaire pour atteindre la réactivité, la sélectivité et la stabilité souhaitées, tout en rendant ces méthodes durables et accessibles. C'est pourquoi, au cours de la dernière décennie, le groupe de recherche du professeur Li mis au point de nombreux outils apportant des solutions aux défis existants sur divers fronts, notamment, mais sans s'y limiter : le développement de nouveaux réactifs permettant des réactions de fonctionnalisation simples et efficaces, l'étude approfondie de nouvelles voies catalytiques pour l'exploration de réactivités diversifiées, ainsi que la conception de nouveaux dispositifs accessibles permettant une optimisation accélérée des conditions de réaction. Dans ce document, nous présentons trois outils dans le même ordre. Le chapitre 1 introduit les bases nécessaires concernant les méthodologies modernes en photocatalyse homogène, en identifiant les opportunités et les efforts actuels pour relever ces défis et en proposant des solutions standardisées. Le chapitre 2 (« Nouveaux réactifs ») présente le développement d'une série de réactifs photoclivables stables à l'air, permettant la perfluoroalkylation d'aromatiques riches en électrons dans des conditions sans métal, neutres en termes de redox et de pH. Le chapitre 3 (« Nouvelles voies catalytiques ») décrit l'application d'amines triaryliques simples en tant que donneurs d'électrons catalytiques dans des complexes donneur-accepteur d'électrons (EDA). Ce projet discute de la caractérisation photophysique du complexe formé entre ces amines et les réactifs photoclivables décrits dans le chapitre 2. Le chapitre 4 (« Nouveaux dispositifs ») décrit la conception d'un photoréacteur imprimé en 3D pour l'expérimentation à haut débit (HTE). Ce prototype peu coûteux est modulaire et accélère la découverte et l'optimisation de nouvelles réactions promues par la lumière visible de manière parallèle. Enfin, le chapitre 5 expose les contributions à la connaissance fondamentale et les perspectives liées à ces trois projets.

Acknowledgements

First and foremost, I would like to express my deepest gratitude to my supervisor, Dr. Chao-Jun Li, for his unwavering guidance, support, and patience throughout the course of my PhD journey. I am incredibly thankful to you for providing me with an opportunity and space to grow professionally and become an independent scientist. Your expertise and kindness have been nothing but invaluable for my career. At the same time, I am incredibly fortunate to have had the opportunity to work under the mentorship and guidance of the members of my committee, Dr. Gonzalo Cosa, Dr. Audrey Moores, and Dr. Dmytro Perepichka. Without your constructive criticism, thoughtful suggestions, and continuous support, this thesis would not have been possible.

I am deeply indebted to my collaborators, Ehsan Hamzehpoor, Jan Michael Salgado, Cory Ruchlin, Jorge Ramos Sánchez, Alexander Logozzo, Evan Chen, Guillermo Lozano, and Jean-Philippe Guay. Your contributions and stimulating discussions have significantly improved the outcome of my research. Thank you for your lessons, your hard work, and the fun moments amidst the daily grind. I also thank my mentees Malcolm Sim, Loric Lefebvre, and Alexei Kieran for all their hard work. I hope you learned as much from me as I did from you. Lastly, I extend my special gratitude to Juan Lasso. Thank you for sharing the path with me during 6 years through hardships and celebrations. We have grown a lot together.

I would also like to extend my heartfelt thanks to present and past members of my research group. Especially to Sosthène Ung, Alain Li, Alejandra Domínguez, Zihang Qiu, Zoë Hearne, Jingtian Han, Hui Su, and Daliah Farajat, thank you for your camaraderie, technical assistance, and for making the lab my second home. However, my biggest thanks go to Inna Perepichka, for being our daily support from start to finish. Without your motherly kindness and sense of humour it would not have been the same.

My deepest appreciation goes to Chantal Marotte for being the G.O.A.T and the absolute pillar of the Department of Chemistry. You have positively impacted so many of our lives as students, thank you for always standing on our side and building a safe space for us. My appreciation extends to all the administrative staff of the department, including

Linda del Paggio, Chelsea Briand-Pitts, and Edith Salifou. Your daily work has made many of my achievements possible. Additionally, I am thankful to all the technical staff: Robin Stein, Hatem Titi, Nadim Saadé, Petr Fiurasek and Violeta Toader for sharing your expertise patiently in the most stressful times of my degree. You have all been instrumental at shaping the direction of this work. Beyond the department, I thank to all the members of the McGill community that helped me so much along the way: Chris Corkery, David Nguyen, April Colosimo, Yvonne Hung, and Iris Papaemmanouil.

To my friends in Montreal, Juan, JM, Anne, Chris, Benedetta, Arthur, Jessie, Hariz, Evan, Tom, Cory, Ehsan, Yeganeh, Mohammad, Konstantin, Juanjo, Alicia, and Laurence. Thank you for being my family away from home, for the dinners and the board game nights. For the serious advice, and for the silly jokes, for your constant encouragement and for always being there to share in both the triumphs and challenges of this journey. Your friendship means the world to me.

Alida, I am incredibly fortunate to be your partner. You bring color and music to my life, and I am nothing but grateful for all the good moments by your side. Thank you for showing me what being a team means. Through better and worse, thank you for your patience, love, and unfaltering belief in me. I look forward to celebrating life every day with you.

I want to thank Jade for being my lighthouse in the middle of the storm. I am deeply thankful for your insight, understanding, and all your loving support. You helped me create a space to grow into who I am today. I also want to thank Perla for being a second mother to me. Thanks to your support, I have found my inner voice.

I owe an immeasurable debt of gratitude to my Anvargasa (Rodrigo). Your constant presence, wisdom, and unwavering support have been a source of strength throughout my degree. You have been my champion, my cheerleader, and my confidant in times of doubt and uncertainty. You have helped me navigate both the academic and personal challenges of this degree, and your encouragement has pushed me forward when I needed it most. I could not have come this far without you.

I am incredibly fortunate to have had the opportunity to work with all the people at Merck: Jack, Shane, Guy, Mycah, Jennifer, Nancy, Helen, Kevin, Ron, Qi, Tim, the Michaels, Spencer, and everyone that made my doctoral internship an amazing experience. I cannot wait to join you soon.

To all my friends outside Montreal and the families that have adopted me like one of your own: The Sánchez-Mejorada García, the López Jaimez, the Libien, Abraham, Luis, David and Lillian, Diana, Luis Ángel, El Abuelo, Eduardo, Paco Valencia, Jorge, Marah, Joaquín, and Karina. You have been my support and home all these years, and for that I am forever in debt.

Lastly, I want to acknowledge the incredible financial support I have received throughout my degree: the Vanier Canada Graduate Scholarship, the Dr. Richard H. Tomlinson Fellowship, the CONACYT scholarship, and the Lawrence Light Graduate Fellowship. The generous support granted by these funding agencies not only have made my degree possible but have also provided me with a platform to reach my dreams and life goals.

To everyone else who has contributed to this work and my degree, in ways big or small, thank you. This achievement is also yours to celebrate.

List of Publications and Work Output

Throughout my degree, I have contributed to a total of 12 publications and 2 reports of invention. Items 2, 4, and 8 are included in full length as Chapters 2, 3, and 4 of this thesis, respectively. Items 1, 3 and 7 are directly related to the topics discussed, but will not be included herein. Sections of items 5 and 6 have been discussed in Chapter 1; however, the reader may consult them separately for a more comprehensive background.

Publications as first author or co-first author:

(‡Equal contribution, #mentored undergraduate collaborators)

1. Juan D. Lasso,‡ Durbis J. Castillo-Pazos,‡ Jan Michael Salgado,‡ Cory Ruchlin, Loric Lefebvre,# Daliah Farajat, Dmytro F. Perepichka, Chao-Jun Li (2024). A general platform for visible light sulfonylation reactions enabled by catalytic triarylamine EDA complexes. *Journal of the American Chemical Society*. 146, 4, 2583-2592.
2. Durbis J. Castillo-Pazos,‡ Juan D. Lasso,‡ Ehsan Hamzhepoor,‡ Jorge Ramos-Sánchez, Jan Michael Salgado, Gonzalo Cosa, Dmytro F. Perepichka, Chao-Jun Li (2023). Triarylmines as catalytic donors in light-mediated electron donor–acceptor complexes. *Chemical Science*. 14, 3470-3481
3. Juan D. Lasso,‡ Durbis J. Castillo-Pazos,‡ Malcolm Sim,# Joaquín Barroso-Flores, Chao-Jun Li (2022). EDA mediated S–N bond coupling of nitroarenes and sodium sulfinate salts. *Chemical Science*. 14, 525-532
4. Durbis J. Castillo-Pazos,‡ Juan D. Lasso,‡ Chao-Jun Li (2022). Synthesis of α -(perfluoroalkylsulfonyl)propiophenones: a new set of reagents for the light-mediated perfluoroalkylation of aromatics. *Beilstein Journal of Organic Chemistry*. 18, 788–795.
5. Durbis J. Castillo-Pazos,‡ Juan D. Lasso,‡ Chao-Jun Li (2021). Modern methods for the synthesis of perfluoroalkylated aromatics. *Organic & Biomolecular Chemistry*. 19(33): 7116-7128.

-
6. Juan D. Lasso,[‡] Durbis J. Castillo-Pazos,[‡] Chao-Jun Li (2021). Green chemistry meets medicinal chemistry: a perspective on modern metal-free late-stage functionalization reactions. *Chemical Society Reviews*. 50: 10955-10982.
7. Cory Ruchlin,[‡] Durbis J. Castillo-Pazos,[‡] Juan D. Lasso, Ehsan Hamzehpoor, Aleksandr Mikov, Chao-Jun Li, Dmytro F. Perepichka. (2024) Carbonyl-Bridged Triphenylamines: Divergent Synthesis and Photophysical Characterization of Organic Room-Temperature Phosphorescent Solids. (Under review)
8. Durbis J. Castillo-Pazos, Jean-Philippe Guay, Alexander Logozzo, Juan D. Lasso, Loric Lefebvre, Alexei Kieran, Thomas C. Preston, Chao-Jun Li. Design of a 3D Printed Photoreactor for Accessible High Throughput Experimentation. (Under review)

Publications as collaborator:

9. Jan Michael Salgado, Durbis J. Castillo-Pazos, Juan D. Lasso, Konstantin Stock, Chao-Jun Li (2024). Manganese-catalyzed nucleophilic addition of aldehydes to carbonyl compounds via hydrazone umpolung on water. *Green Chemistry*. 26: 7357-7362.
10. Alexander Logozzo, Benjamin Vennes, Ravleen Kaur Kohli, James F. Davies, Durbis J. Castillo-Pazos, Chao-Jun Li, Catherine D. Neish, Thomas C. Preston. (2024) Photochemically driven peptide formation in supersaturated aerosol droplets. *Angewandte Chemie International Edition*. 63, e202409788
11. Zihang Qiu, Hanh D. M. Pham, Jianbin Li, Chen-Chen Li, Durbis J. Castillo-Pazos, Rustam Z. Khaliullin, Chao-Jun Li (2019). Light-enabled metal-free pinacol coupling by hydrazine. *Chemical Science*. 10:10937-10943

12. Daliah Farajat D, Lea Philippe, Anastasiia Afanassenko, Durbis J. Castillo-Pazos, Juan D. Lasso, Yiram Kim, Joaquín Barroso-Flores, Chao-Jun Li (2023) Nickel-catalyzed cross-coupling methylation of aryl and heteroaryl electrophiles via hydrazone umpolung. (In progress, ChemRxiv: 10.26434/chemrxiv-2023-4bc19)

Reports of invention:

1. Design of a 3D-printed modular photoreactor for small-scale High-Throughput Experimentation (2024) (Under review)
2. Expedient synthesis and derivatization of 2-sulfonyl-1-phenylethanones as photochemical functionalization agents (2019). Commercialization of the reagent as Sigma-Aldrich product 911941

Additionally, during my degree I secured a 3-month internship at the Discovery Chemistry department of the pharmaceutical company Merck & Co., Inc., in its headquarters in New Jersey, USA. I worked at the interface of the DNA Encoded Libraries (DEL) and High-Throughput Experimentation (HTE) groups, in which I applied some of the methodologies developed in the Li Research Group. These projects are still under progress.

Copyright Statement

Some of the material included in this thesis is adapted from published papers, which are protected by copyright by the corresponding editorials.

Chapter 2:

© 2022 Castillo-Pazos et al.; licensee Beilstein-Institut.

This is an open access article licensed under the terms of the Beilstein-Institut Open Access License Agreement (<https://www.beilstein-journals.org/bjoc/terms>), which is identical to the Creative Commons Attribution 4.0 International License (<https://creativecommons.org/licenses/by/4.0>). The reuse of material under this license requires that the author(s), source and license are credited. Third-party material in this article could be subject to other licenses (typically indicated in the credit line), and in this case, users are required to obtain permission from the license holder to reuse the material.

You are free to:

Share — copy and redistribute the material in any medium or format for any purpose, even commercially.

Adapt — remix, transform, and build upon the material for any purpose, even commercially.

The licensor cannot revoke these freedoms as long as you follow the license terms.

Under the following terms:

 **Attribution** — You must give appropriate credit, provide a link to the license, and indicate if changes were made. You may do so in any reasonable manner, but not in any way that suggests the licensor endorses you or your use.

No additional restrictions — You may not apply legal terms or technological measures that legally restrict others from doing anything the license permits.

Notices:

You do not have to comply with the license for elements of the material in the public domain or where your use is permitted by an applicable exception or limitation.

No warranties are given. The license may not give you all of the permissions necessary for your intended use. For example, other rights such as publicity, privacy, or moral rights may limit how you use the material.

Chapter 3:

Triarylamines as catalytic donors in light-mediated electron donor-acceptor complexes

D. J. Castillo-Pazos, J. D. Lasso, E. Hamzehpoor, J. Ramos-Sánchez, J. M. Salgado, G. Cosa, D. F. Perepichka and C. Li, *Chem. Sci.*, 2023, **14**, 3470 DOI: 10.1039/D2SC07078B

This article is licensed under a [Creative Commons Attribution-NonCommercial 3.0 Unported Licence](#). **You can use material from this article in other publications, without requesting further permission** from the RSC, provided that the correct acknowledgement is given and it is not used for commercial purposes.

To request permission **to reproduce material from this article in a commercial publication**, please go to the [Copyright Clearance Center request page](#).

If you are **an author contributing to an RSC publication, you do not need to request permission** provided correct acknowledgement is given.

If you are **the author of this article, you do not need to request permission to reproduce figures and diagrams** provided correct acknowledgement is given. If you want to reproduce the whole article in a third-party commercial publication (excluding your thesis/dissertation for which permission is not required) please go to the [Copyright Clearance Center request page](#).

Read more about [how to correctly acknowledge RSC content](#).

Co-first authors Consent Statements

I, Juan David Lasso, as collaborator of Durbis Javier Castillo Pazos, agree to share the data from two co-authored papers (Beilstein J. Org. Chem., 2022, 18, 788-795 and Chem. Sci., 2023, 14, 3470-3481), including the totality of the published manuscripts and supporting information.

I acknowledge that he is permitted to incorporate this work into his thesis for submission to McGill University as part of the requirements for his Ph.D. degree. Durbis will include these two papers as published, along with a manuscript under preparation in which I also collaborated. I also confirm that we contributed equally to both publications, and the author contribution sections in each chapter are accurate and complete.



Juan David Lasso

I, Ehsan Hamzehpoor, as collaborator of Durbis Javier Castillo Pazos, agree to share the data from one co-authored paper (Chem. Sci., 2023, 14, 3470-3481), including the totality of the published manuscript and supporting information.

I acknowledge that he is permitted to incorporate this work into his thesis for submission to McGill University as part of the requirements for his Ph.D. degree. Durbis will include this paper as published. I also confirm that we contributed equally to this publication and the author contribution sections in each chapter are accurate and complete.



Ehsan Hamzehpoor

TABLE OF CONTENTS

ABSTRACT	V
RÉSUMÉ	VI
ACKNOWLEDGEMENTS	VII
LIST OF PUBLICATIONS AND WORK OUTPUT	X
COPYRIGHT STATEMENT	XIII
TABLE OF CONTENTS	XVI
LIST OF FIGURES	XVIII
LIST OF SCHEMES	XIX
LIST OF TABLES	XX
LIST OF ABBREVIATIONS	XXI
CHAPTER 1: INTRODUCTION	24
CONTEXT AND THESIS SCOPE	24
BASICS OF PHOTOCHEMISTRY AND PHOTOCATALYSIS	26
SYNTHETIC APPLICATIONS OF RADICALS	32
THE CASE FOR METAL-FREE CATALYSIS	40
REFERENCES	42
CHAPTER 2: NEW REAGENTS	51
PREFACE	52
AUTHOR CONTRIBUTIONS	52
ABSTRACT	53
INTRODUCTION	53
RESULTS AND DISCUSSION	55
CONCLUSION	62
EXPERIMENTAL	63
ACKNOWLEDGEMENTS	63
FUNDING.....	63
REFERENCES	64
SUPPORTING INFORMATION	67
CHAPTER 3: NEW CATALYTIC PATHWAYS	81
PREFACE	82
AUTHOR CONTRIBUTIONS	83
ABSTRACT	84
INTRODUCTION	84

RESULTS AND DISCUSSION	87
CONCLUSION	104
ACKNOWLEDGEMENTS	104
REFERENCES	105
SUPPORTING INFORMATION	112
CHAPTER 4: NEW DEVICES.....	129
PREFACE	130
AUTHOR CONTRIBUTIONS	131
ABSTRACT	132
INTRODUCTION	132
RESULTS AND DISCUSSION	134
CONCLUSION	141
ACKNOWLEDGEMENTS	142
REFERENCES	143
SUPPORTING INFORMATION	147
CHAPTER 5: DISCUSSION AND FUTURE REMARKS	171
CONTRIBUTIONS TO ORIGINAL KNOWLEDGE.....	171
OUTLOOK FOR FUTURE RESEARCH	174
CONCLUSION	177
REFERENCES	178
APPENDIX.....	179
CHARACTERIZATION DATA FOR CHAPTER 2	179
CHARACTERIZATION DATA FOR CHAPTER 3	227
CHARACTERIZATION DATA FOR CHAPTER 4	319

List of Figures

Figure 1.1: Simplified Jablonski diagram. Wave arrows indicate radiative processes, while boxes illustrate the corresponding multiplicities.	27
Figure 1.2: A) Identification of EDA complexes by empirical (top) and spectroscopic (bottom) means, B) Melchiorre's metal-free cross coupling	31
Figure 3.1. Overview of catalytic EDA complexes in synthetic chemistry.....	87
Figure 3.2. Catalytic EDA system design and application	88
Figure 3.3. Mechanistic studies on triphenylamine as an EDA.....	91
Figure 3.4. Radical trapping and control experiments	94
Figure 3.5. Proposed mechanism for the catalytic EDA complex formation between TPA and the perfluoroalkylating reagent.	95
Figure 3.6. Demonstrative scope for the catalytic EDA-mediated perfluoroalkylation of electron-rich aromatics. Note: PF9 is done under modified conditions (25% benzene v/v as solvent).....	100
Figure 3.7. Demonstrative scope for the catalytic EDA-mediated trifluoromethylation of electron-rich aromatics	103
Figure 4.1: Current state of the art for photochemical setup design for homogeneous photocatalysis, where HTE compatible 3D printed setups still represent a major gap.	133
Figure 4.2: Main structural components of the HERMES photoreactor	136
Figure 4.3: Model reaction yields before completion (A), and after completion (B). Duplicate plates are shown in Section 5 of the SI.	140

List of Schemes

Scheme 1.1: Main photocatalytic pathways for the initiation of organic reactions. PC stands for photocatalyst, A for acceptor, and D for Donor.....	28
Scheme 1.2: Stoichiometric Electron Donor Acceptor (EDA) complexes	30
Scheme 1.3: Minisci-type reactions	35
Scheme 1.4: Examples of perfluoroalkylating methodologies	38
Scheme 1.5: Melchiorre’s perfluoroalkylation of phenols.....	39
Scheme 2.1: Envisioned Minisci perfluoroalkylation facilitated by “dummy group” reagents	55
Scheme 2.2: Control experiments for the nucleophilic substitution of perfluoroalkyl sulfonates and halogenated electrophilic partners	57
Scheme 2.3: Left: isolated yields of synthesized perfluoroalkylating reagents: perfluorobutyl (1a), perfluorohexyl (1b), and perfluorooctyl (1c) analogues (after conversion of byproduct); middle: gram amounts of perfluorooctyl product 1c ; right: UV–vis absorption of reagents 1b and 1c	59
Scheme 2.4: Radical trapping experiment with 1,1-diphenylethylene (7) and 1b confirming the initially proposed mechanism.....	59
Scheme 2.5: Demonstrative scope for the perfluoroalkylation of aromatics. Isolated yields are shown in parentheses.	62
Scheme 4.1: Redox-neutral sulfonylation of olefins promoted by blue light and catalyzed by TMPA (4-(trismethoxy) triphenylamine).	138
Scheme 5.1: Proposed radical acylation of olefines	174
Scheme 5.2: Examples of triaryl amines that will be explored as electron donors.....	175

List of Tables

Table 2.1: Optimization for the nucleophilic substitution between α -iodopropiophenone and sodium perfluoroalkylsulfonates.	57
Table 2.2: Optimization for the perfluoroalkylation of aromatics under UV light.....	61
Table 3.1. Optimization of reaction conditions—perfluoroalkylation of electron-rich aromatics.....	97
Table 3.2. Optimization of reaction conditions—trifluoromethylation of electron-rich aromatics.....	102

List of abbreviations

APCI	atmospheric pressure chemical ionization
BET	back electron transfer
CDC	cross-dehydrogenative coupling
CFL	compact fluorescent lamp
DBU	1,8-diazabicyclo[5.4.0]undec-7-ene
DCM	dichloromethane
DFT	density functional theory
DHC0	dihydrocarbazole in the ground state
DIPEA	<i>N,N</i> -diisopropylethylamine
DMA	dimethylacetamide
DMSO	dimethylsulfoxide
EDA	electron donor-acceptor
EPR	electron paramagnetic resonance
ESI	electro-spraying ionization
ET	energy transfer
EtOAc	ethyl acetate
FDM	fused deposition modelling
FRET	Förster resonance energy transfer
GC	gas chromatography
HAT	hydrogen atom transfer
HOMO	highest occupied molecular orbital
HPLC	high performance liquid chromatography
HRMS	high resolution mass spectrometry
HTE	high-throughput experimentation
IC	internal conversion
IPA	isopropanol
ISC	intersystem crossing
LCD	liquid crystal display
LED	light emitting diode

LFP	laser flash photolysis
LSF	late-stage functionalization
LUMO	lowest unoccupied molecular orbital
MeCN	acetonitrile
MeDPA	methyldiphenylamine
MeOH	methanol
MesAcr	mesityl acridinium
MHz	megahertz
NMR	nuclear magnetic resonance
N-PhCbz	<i>N</i> -phenyl carbazole
OD	optical density
PC	photocatalyst
PCB	printed circuit board
PET	polyethylene terephthalate
PET-CF	polyethylene terephthalate with carbon fiber
PETG	polyethylene terephthalate glycol
PFAS	polyfluoroalkyl substances
PLA	polylactic acid
PP	polypropylene
PRE	persistent radical effect
PTH	phenylphenothiazine
PVC	polyvinyl chloride
PWM	pulse width modulation
RPM	revolutions per minute
SAR	structure-activity relationships
SCXRD	single-crystal X-ray diffraction
SET	single-electron transfer
SN2	bimolecular nucleophilic substitution
SOMO	singly occupied molecular orbitals
SuFEx	sulfur (VI) fluoride exchange

TCSPC	time-correlated single-photon counting
TLC	thin layer chromatography
TMB	1,3,5-trimethoxybenzene
TMEDA	tetramethylethylenediamine
TMPA	tris(4-methoxy)triphenylamine
TMS	tetramethylsilane
TPA	triphenylamine
TPB	tetraphenyl benzidine
UV	ultraviolet

1 Introduction

1.1 Context and Thesis Scope

This introduction aims to provide the necessary context to evaluate the importance of the projects discussed in subsequent chapters. We will also provide a brief overview of the fundamental topics needed to understand the results presented, including the basics of photochemistry and photocatalysis, the importance of radical-mediated reactions, and the need for metal-free methodologies. However, specific background will be more thoroughly explained in each one of the chapter's introductions.

In 2018, Blakemore and colleagues published a perspective in the journal *Nature Chemistry*, stating the importance of organic chemistry within the industrial context, and highlighting significant synthetic challenges and areas of opportunity.¹ This perspective has served both as inspiration and a directive for young and established researchers alike, presenting a clear outline of the areas that could accelerate the development of the synthetic domain. Our group has been no exception, dedicating resources to the design of novel methodologies compatible with more complex scaffolds, as well as the creation of new technologies.

Within the research areas covered by the Li group, photocatalysis represents a major opportunity to deal with some of the aforementioned challenges in a sustainable way. However, the photocatalysis field itself can present a unique set of issues including the following:²⁻⁴

1. Development and characterization of new photocatalytic strategies: The drive for new synthetic disconnections and the accessibility of a wider chemical space has prompted the development of new photocatalytic strategies capable of

enabling new reactivities. At the same time, the underlying mechanisms of many novel photocatalytic methodologies are not fully understood, highlighting the need for thorough characterization from a perspective of rational design.¹

2. Sustainable photocatalysis: As a tool, photocatalysis must thrive to be accessible and cost-effective. Among the many ways to achieve this, two points stand out. The first refers to a drive for the development of metal-free photocatalytic methodologies. The second points at designing approaches that work efficiently under mild conditions (ambient temperature and pressure, neutral pH).⁵

3. Setup standardization: Homogeneous photocatalytic reactions rely heavily on the conditions of light irradiation. While industrial setups have well developed devices that allow for the control of light sources, thermal regulation and proper mixing, there is a major gap in the development of affordable and easily accessible photocatalytic reactors or setups for academic purposes.⁶

The main objective of this thesis is to discuss some of the advances and contributions made by our lab to tackle said challenges in photocatalysis. The research described herein is organized within the context of 3 research projects, corresponding to three different types of improvement or tools: the development of new reagents, the study of new catalytic pathways, and the design of novel devices for photocatalysis.

1.2 Basics of Photochemistry and Photocatalysis

It has been more than a century since the Italian chemist Giacomo Ciamician highlighted the importance of harnessing light as a powerful tool for the transformation of organic matter, and as an agent of change facing scientific, industrial, and economic challenges.⁷ Following his rudimentary but seminal experiments with sunlight, the 20th century witnessed the birth of photochemistry as a formal discipline, carried on by chemists and physicists alike. Photochemistry can be defined as the study of interactions between matter and light, most seen as the excited states produced upon light absorption by a molecule.⁸ Light is a type of electromagnetic radiation composed by photons, usually classified into ultraviolet (UV), visible light, and infrared light. UV light is commonly divided into short-wave (UVC from 200 to 280 nm), middle-wave (UVB from 280-320 nm), and long-wave (from 320 to 400 nm), while the visible region of light is loosely delimited between 400 nm to 700 nm. These different wavelengths are associated with the amount of energy available to interact with a molecule, governed by the first law of photochemistry: only absorbed photons can cause a chemical change. This means that photons must be absorbed by the reacting species, and their energy must be sufficient to ensure the molecule traverses the path from reactants to products (through the transition state) within the excited state lifetime.^{8,9}

When a molecule absorbs light, it can access an excited state from which numerous chemical or physical changes can occur. To understand how molecules are photoexcited, we can look at the Jablonski diagram (**Figure 1.1**), a simplistic visualization of the energy and multiplicity of a molecule's electronic states. When an absorbed photon provides enough energy, an electron can be promoted from the highest occupied molecular orbital (HOMO) to the lowest unoccupied molecular orbital (LUMO), bringing the molecule from its ground state (S_0), to higher energy levels in the form of singlets ($S_1, S_2 \dots S_N$). To reach a minimum energy state the molecule can follow two main pathways. On the one hand, it can release energy through internal conversion (IC), dropping to other lower energy singlet states like S_1 or S_0 (Kasha's rule), or it can emit radiation in the form of fluorescence.⁸

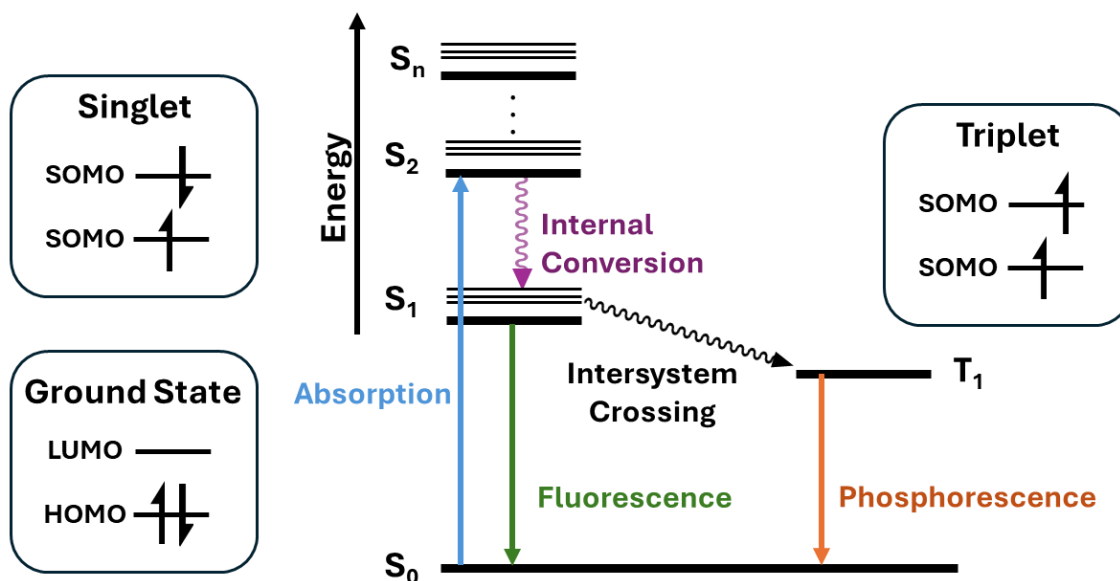
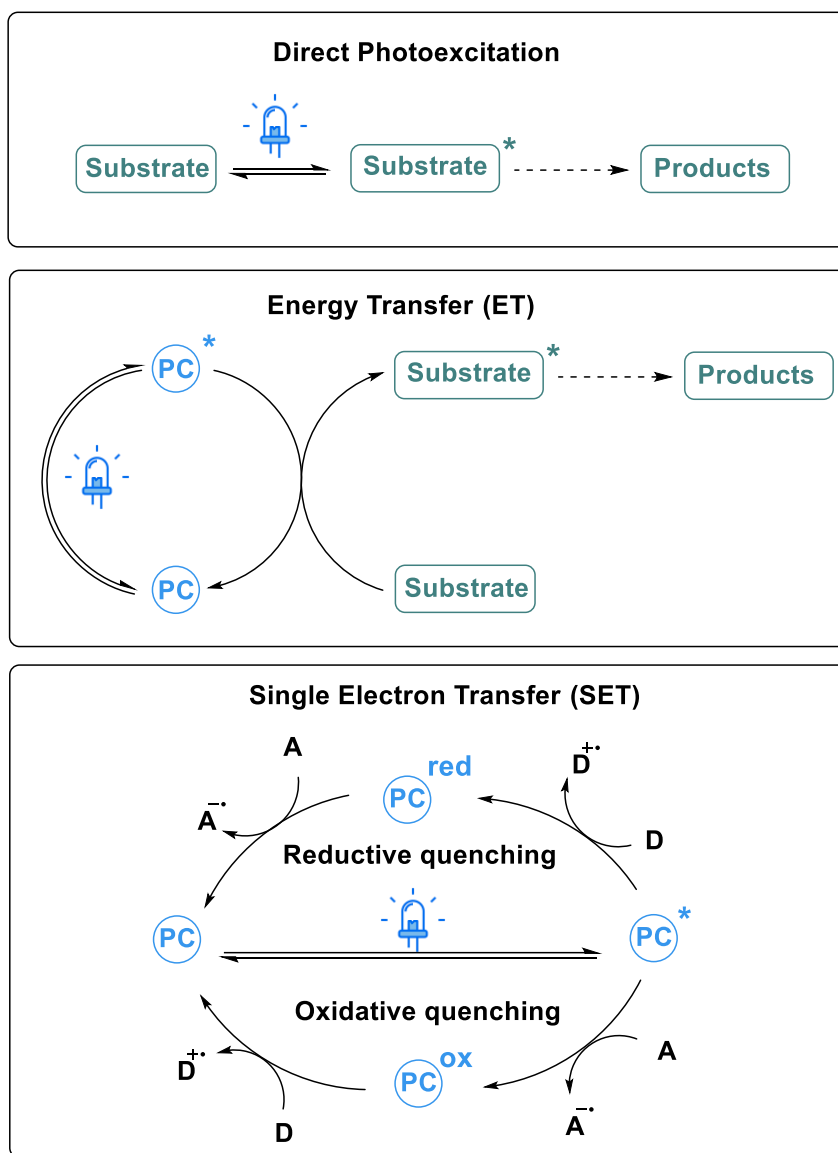


Figure 1.1: Simplified Jablonski diagram. Wave arrows indicate radiative processes, while boxes illustrate the corresponding multiplicities.

On the other hand, the singlet state can undergo intersystem crossing (ISC) to form a more stable triplet excited state (T), where the unpaired electrons have parallel spins. Triplet states have lower energies than their singlet counterparts, as explained by Hund's rule, which dictates that orbital occupancy with maximum multiplicity has the lowest energy. However, transitions between singlet and triplet states are said to be forbidden, consequently slowing down the transition from singlet to triplet. For this reason, triplet states possess longer lifetimes than singlet states but can still return to the ground state (S_0) via phosphorescence—an emission with multiplicity change. While states of higher multiplicity exist, they are rarely observed in the context of organic photochemistry.⁹

Based on the aforementioned processes occurring upon a molecule's excitation, we can exploit the energy provided by a light source to initiate organic reactions. This is the paradigm of organic photochemistry, which states that the irradiation of ground state reactants will eventually lead to ground state products (**Scheme 1.1**).⁹ Nonetheless, this will always be achieved through the formation of excited state reactants and the subsequent formation of the corresponding reaction intermediates (e.g. free radicals in

solution). The additional energy available for these excited states, as well as their multiplicity will set their reactivity apart from ground state molecules. For this reason, photochemistry offers the possibility to access different product profiles than those obtained through thermal means.



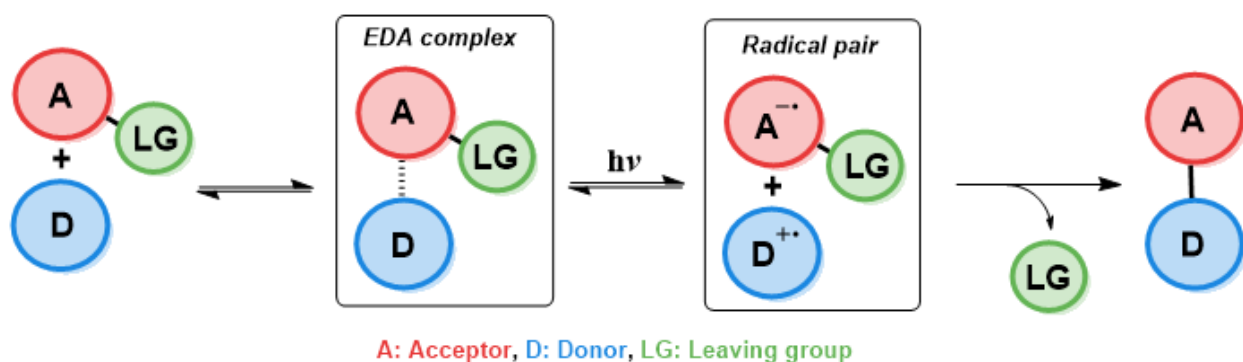
Scheme 1.1: Main photocatalytic pathways for the initiation of organic reactions. PC stands for photocatalyst, A for acceptor, and D for Donor.

In addition to direct photoexcitation, useful chemistry can also be originated from the transfer of energy between an excited molecule (i.e. a photosensitizer) and another species in the ground state (i.e. our substrate). This is commonly referred to as sensitization or Energy Transfer (ET), a favorable tool to generate reactive species when our substrate of interest cannot directly absorb on the irradiated wavelength (**Scheme 1.1**). This process usually occurs through two mechanisms. The first one is called Dexter energy transfer, a fast exchange of electrons between the orbitals of the donor and the acceptor. This process requires proximity of the acting species and can be observed in the context of both singlet and triplet states. The second mechanism is called Förster Resonance Energy Transfer (FRET) and occurs at larger distances (nanometers) when the energy transfer involves two singlets.

Nonetheless, there is a last important photochemical pathway by which we can initiate organic transformations: Single Electron Transfer (SET) (**Scheme 1.1**).¹⁰ SET processes originate when, upon excitation, diamagnetic molecules become both better electron donors and better electron acceptors. In other words, by promoting electrons from the Highest Occupied Molecular Orbital (HOMO) to the Lowest Unoccupied Molecular Orbital (LUMO), we generate a pair of Singly Occupied Molecular Orbitals (SOMO) where redox potentials become larger. As with Dexter's ET, SET processes rely on the proximity between a donor and an acceptor and can occur from both singlet or triplet excited states. If the electron transfer happens between two neutral molecules, this will create a pair of radical ions (namely, radical anion and radical cation) capable of reacting with other molecules in solution upon escape from the solvent cage. However, back electron transfer (BET) represents a major competing pathway that can yield back the initial donor and acceptor in their ground state, resulting in no chemical reactions.⁸

These rules set the base for photoredox catalysis, a subdiscipline of photochemistry that employs small concentration of highly photosensitive molecules capable of starting or accelerating a chemical reaction via SET processes. This type of catalysis has become a cornerstone of modern synthetic chemistry since 2008, thanks to the pioneering work of the groups of MacMillan, Yoon, and Stephenson.¹¹⁻¹³ Photoredox

chemistry can proceed through a diverse range of photocatalysts through reductive or oxidative pathways (**Scheme 1.1**), and in combination with sacrificial reagents—reducing or oxidizing the photocatalyst back to its original state. While such processes can proceed in the presence of organic dyes and heterogeneous catalysts, transition-metal photocatalysts have dominated the field thanks to their well-studied photophysical properties.^{5, 12, 14-17} Moreover, the advent of photoredox catalysis has allowed organic chemists to shift the operational range of wavelengths well into the visible spectrum, opening the door for more selective transformations under milder and safer conditions.

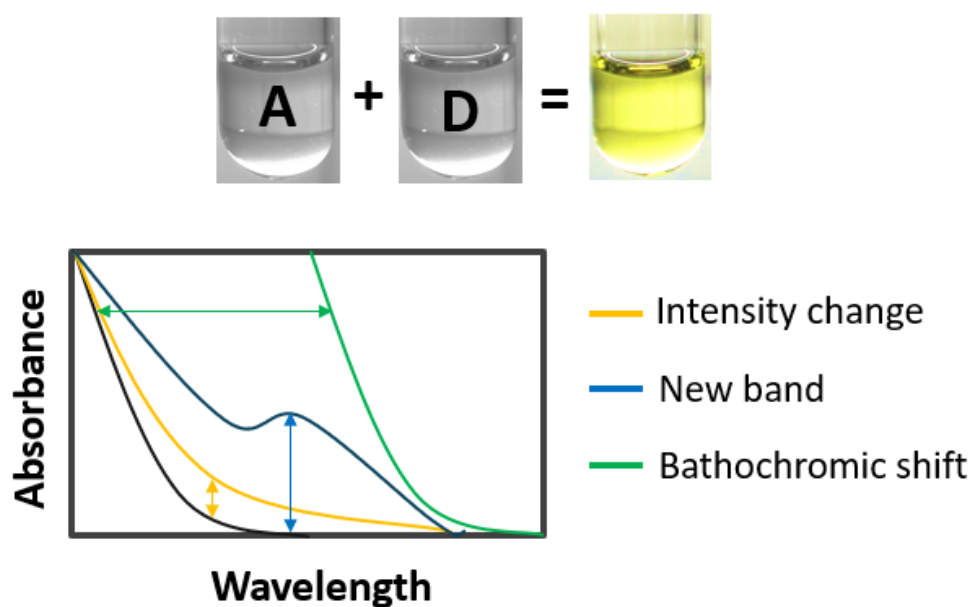


Scheme 1.2: Stoichiometric Electron Donor Acceptor (EDA) complexes

However, the dependence of the field on scarce metal-containing photocatalysts has prompted multiple research groups to explore alternative photocatalytic approaches. A major avenue that has been explored in the last few years has been the use of charge-transfer complexes, better known by organic chemists as Electron Donor Acceptor (EDA) complexes (**Scheme 1.2**).^{18, 19} EDA complexes follow the same basic photophysical principles exposed in previous paragraphs, starting with an electron-rich substrate (donor) associating in solution with an electron-poor molecule (acceptor).²⁰ The newly formed complex will construct a new set of orbitals, populated by the electrons of both species, where the gap between the new ground and excited states is smaller. This directly translates into an easier excitation of the complex by less energetic wavelengths, usually in the visible light range.²¹ In other words, the formation of such new charge transfer band allows us to generate radicals from reactants that do not absorb the irradiated light on

their own. On a more practical note, the formation of the EDA complex can be initially evidenced by the formation of colored solutions (e.g. yellow or orange) due to the absorbance in the visible light range. Additionally, EDA complexes are observed spectroscopically by changes in band absorbption, the appearance of new absorption bands, or even by bathochromic shifts altogether (**Figure 1.2A**). Nonetheless, it is also important to note that some of these effects can also be affected by the solvent of choice. EDA systems are overall sensitive to the nature of the solvent, where polar solvents facilitate and stabilize the electron transfer process.^{22, 23}

A) Initial evidence of an EDA complex formation



B) Example from Melchiorre, et al. (2020)



Figure 1.2: A) Identification of EDA complexes by empirical (top) and spectroscopic (bottom) means, B) Melchiorre's metal-free cross coupling

Lastly, to render this strategy synthetically useful, organic chemists have avoided BET by attaching a leaving group onto one of the reactants. This means that upon light irradiation and subsequent formation of the radical ions, the cleavage of the leaving group yields the process irreversible, leading to the recombination of the radicals formed in solution. This gives a Donor-Acceptor product, such as the one exemplified by the group of Melchiorre through the metal-free cross coupling of anilines and aryl bromides (**Figure 1.2B**).¹⁸ Due to the 1:1 equivalence between Donor and Acceptor present in the final structure of the product, these EDA systems are also known as stoichiometric EDA complexes. In Chapter 3 of this thesis, we present our contributions regarding the development of catalytic EDA complexes, which show improved atom economy and scope diversity.

1.3 Synthetic Applications of Radicals

After discussing the different ways in which we can harness the energy of light to generate reactive species such as radicals, it is important to delve into their synthetic utility within modern organic chemistry. The name radical refers to those atoms or molecules that contain at least one unpaired electron (i.e. open-shell electronic configuration) making them highly reactive species.²⁴ However, within the right time framework, such free radical species can be trapped by other molecules in solution, serving as useful intermediates for the construction of complex molecular architectures.

Historically, the formal study of radical chemistry dates back to the year 1900, more specifically to the pioneering work of Moses Gomberg, who isolated triphenylmethyl as the first persistent organic radical.²⁵ Since then, our understanding of radicals has evolved significantly, leading to their application in diverse fields, including polymer chemistry, medicinal chemistry, and materials science. Regarding organic chemistry, stability and lifetime of radicals are crucial factors influencing their reactivity and utility. Radical stability is often determined by the ability of the unpaired electron to delocalize over adjacent atoms or through resonance structures. Carbon-centered radicals can exhibit varying degrees of stability based on their structure, and such stability is a thermodynamic categorization (destabilized, stabilized) often evidenced by their bond dissociation

energy. For example, tertiary and benzylic radicals are generally more stable than secondary or primary radicals due to hyperconjugation and inductive effects. Additionally, structural and steric factors can also determine the lifetime of radicals, ranging from nanoseconds to several hours. This way, we can kinetically categorize radicals into transient (short lived) and persistent (long lived). While all stable radicals are persistent, different degrees of stabilization can be found in both transient and persistent species.²⁶ This is known as the persistent radical effect (PRE), and it sets the foundation for selective radical transformations in synthesis.²⁴

In synthetic organic chemistry, radicals are useful tools for the initiation of polymerization reactions, cross-coupling reactions, and the diversification of functional groups as chemical handles. More specifically, the projects presented in this thesis deal with the radical C–H functionalization of aromatic molecules. Being a powerful approach, C–H activation methodologies have been mostly geared towards Late-Stage Functionalization (LSF) reactions. For this reason, modern research in this area strives towards substituting previously achieved organometallic C–H activation reactions using novel and highly potent organo-photocatalysts, hypervalent iodine reagents, or by repurposing old radical chemistries.

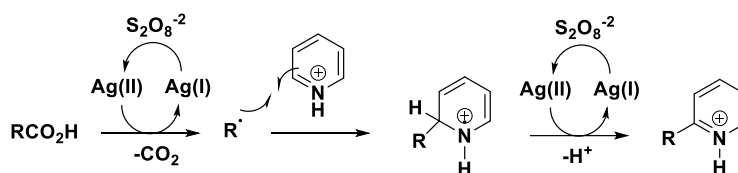
Nowadays, synthetic chemists recognize two main classes of C–H functionalization called “guided” and “innate”.²⁷ The first one makes use of external agents such as metal complexation, directing groups or steric bias. Guided modifications have been extensively studied in the case of traditional organometallic C–H activation reactions, both harnessing the structure of the substrates involved,²⁸ and through design of tailored catalysts.²⁹ Alternatively, “innate” functionalization refer to the addition of radicals onto unsaturated compounds (e.g. aromatics, olefines, alkynes) without previous modification of the substrate, or without the presence of a directing group. They are called innate because their selectivity is controlled by the inherent reactivity of the species involved, dictated by their steric and electronic attributes. Furthermore, radical-based innate functionalization reactions are governed by the nature of the reacting

radical and the energetic compatibility with the molecular orbitals of the substrate, as well as the effect of solvent or pH.

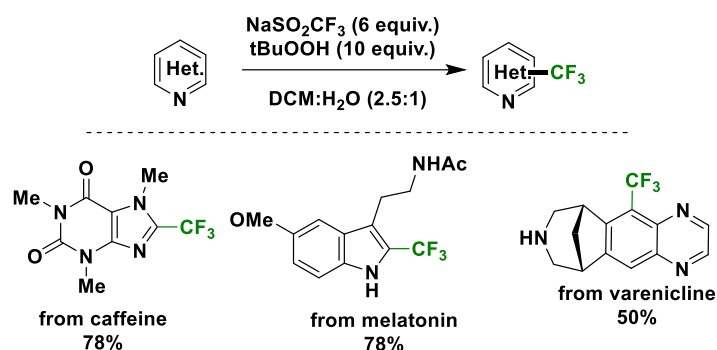
Regarding C(sp²)-H functionalization, Minisci-type reactions represent an important synthetic strategy—employed in Chapters 2 and 3 of this thesis. Described in 1971 by Francesco Minisci, the classical Minisci reaction involved a silver-catalyzed decarboxylation generating alkyl and acyl radicals which subsequently add onto electron-poor aromatic substrates such as pyridine (**Scheme 1.3A**).³⁰ These initial reactions required both stoichiometric quantities of oxidant as well as the aid of a silver catalyst and were limited to the addition of nucleophilic radicals onto electrophilic heteroaromatic compounds. With the renewed interest in radical chemistry, this name reaction resurfaced as an entire family of transformations sharing a common mechanism, acting as a potent tool in medicinal chemistry and synthesis. An exhaustive review of such reactions has been published by Phillips and co-workers.³¹

When studying modern functionalization reactions, the work of Baran and colleagues has become the seminal example of Minisci-type reactions in LSF with the use of sulfinate salts as alkylating reagents.³² In their 2011 report, Langlois reagent (NaSO₂CF₃) was used as an air-stable -CF₃ radical source under traditional oxidative Minisci conditions, leading to facile trifluoromethylation of caffeine and melatonin, among others, in moderate to good yields (**Scheme 1.3B**). Intense interest in this field led to the development of commercially available sulfinate salt LSF kits, which potentially allow drug discovery programs the ability to quickly determine structure-activity relationships (SAR) through the easy synthesis of a molecular library.³³

A) Original Minisci reaction



B) Modern Minisci-type reactions: Baran's trifluoromethylation

**Scheme 1.3:** Minisci-type reactions

After this renewed interest in innate functionalizations, a plethora of functionalities have come to be employed as radical precursors in Minisci-type reactivities such as in the works of Lee,³⁴ and Gopalakrishnan³⁵ research groups. Other notable examples include the use xanthenes,³⁶ 1,4-dihydropyridines³⁷ and aldehydes,³⁸ all of them without the requirement of metal reagents. Additionally, the group of Baran has provided further insights into the regioselectivity rules that control the addition of radicals to aromatic substrates,³⁹ expanding on the existing discussion over regioselectivity rules.^{31, 40, 41}

In recent years, extensive work has led to further design of milder conditions that eliminate the use of metal catalysis or harsh oxidants to generate radicals. For example, metal-free reactions have primarily pivoted on the use of novel and highly potent organo-photoredox catalysts such as mesitylacridinium trifluoroborates ($\text{MesAcr}^+ \text{BF}_4^-$)⁴² capable of reaching similar or greater oxidative potentials to their much more expensive metal counter parts. Thanks to the mild nature of photoredox reactions, many groups have utilized this route to access radicals solely obtained by organometallic methodologies in the past. A representative example of this can

be seen in Molander's group recent use of alkyl trifluoroborates under organo-photocatalytic conditions.⁴³

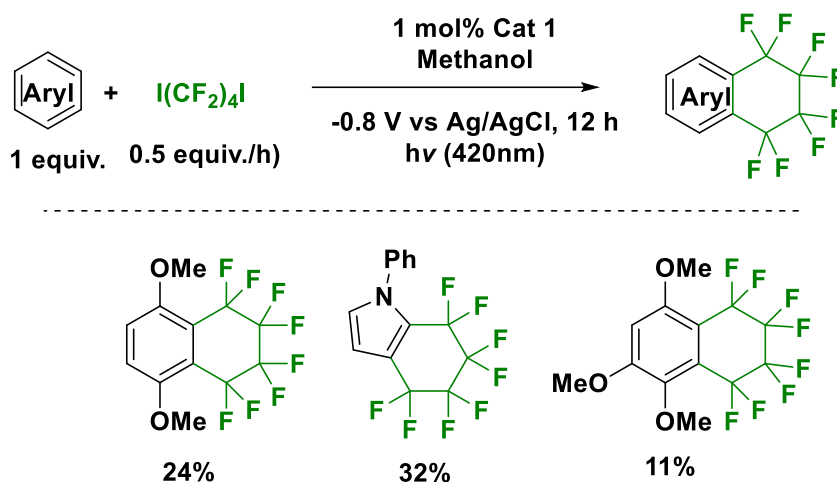
Notably, our group has also contributed to the development of more sustainable Minisci-type reactions. For example, our group has pioneered the formation of C–C bonds through cross-dehydrogenative couplings (CDC), a strategy capable of activating traditionally inert hydrogen bonds and selectively install them onto aromatic substrates.⁴⁴⁻⁴⁷ Regarding photochemical methods, we recently reported a methodology in which benign diacetyl and acetone are utilized as photosensitizer and oxidant respectively, allowing for the direct generation of trifluoromethyl radicals under near-ultraviolet irradiation.⁴⁸ Similarly, our group has also reported the addition of methyl groups to nitrogen-containing heterocycles using methanol.⁴⁹ Finally, our group also developed pH- and redox-neutral conditions for the trifluoromethylation and alkylation of heterocycles in excellent yields.⁵⁰ Chapter 2 builds directly upon the observations discussed in such seminal work.

Since two chapters of this thesis deal with the formation of perfluoroalkyl radicals, it remains significant to discuss their importance in chemistry, as well as their synthesis methods. Traditionally, the fluorination of molecules has been an important but elusive goal for organic chemists due to the lack of mild and chemoselective fluorinating reagents. The past decades have seen the extensive introduction of the trifluoromethyl group into drug discovery programs thanks to their ability to confer improved potency, metabolic stability and improved physicochemical properties onto lead structures. Consequently, the synthetic methods utilized to introduce said functional groups have been extensively reviewed by many research groups.⁵¹⁻⁵⁷ Yet, while trifluoromethyl groups are omnipresent in the organic chemist's lexicon, perfluoroalkyl groups—a class of aliphatic chains in which each hydrogen atom has been replaced by a fluorine atom—are less studied in organic chemistry.

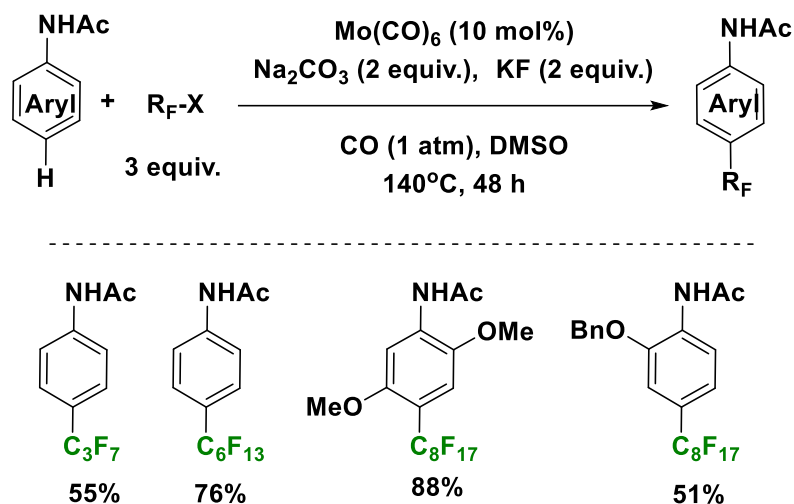
Similar to how the trifluoromethyl group dramatically alters chemical properties in drug molecules, perfluoroalkyl groups are renowned for their ability to bestow chemical resistance and beneficial mechanical properties to materials and fine chemicals, such as flame retardants in fire fighter foams or specialized aviation lubricants.⁵⁸ Thanks to these valuable properties, this class of compounds have become ubiquitous in the modern world. Perfluoroalkylated radicals also hold an important place in organic chemistry as model systems that allow synthetic chemists to study the insertion of new C–C bonds.⁵⁹ Additionally, perfluoroalkyl-containing compounds have found applications in DNA polymer delivery systems for gene transfection⁶⁰ as well as anhydrous proton conducting organic frameworks⁶¹, among many other specialized applications. For this reason, there has been an interest for greener methods for the synthesis of these specialized compounds in applications where no reasonable alternatives exist.

Historically, perfluoroalkyl molecules were synthesized by electrochemical fluorination, which typically requires superstoichiometric fluorine equivalents, resulting in low yields and numerous undesired side-products. In 1960, George Triers reported the first perfluoroalkylation of aromatics, in which perfluoroheptyl iodide was observed to add directly to arenes without the aid of catalyst or other reagents at 250 °C.⁹ Then, in 1969, McLoughlin and Thrower succeeded at lowering the temperature requirement of said reaction through the addition of stoichiometric amounts of copper.^{62, 63} Since then, the literature of perfluoroalkylation methods of aromatics has focused intensely on activation of perfluoroalkyl iodides, either by radical initiators and tandem catalysis,⁶⁴⁻⁶⁸ or assisted by metal catalysts in a homogeneous or heterogeneous fashion (**Scheme 1.4**).⁶⁹⁻⁷⁷ Several groups have extensively covered these classical reactions developed for synthesis of perfluorinated aromatics and polymers, reviewing the accumulated literature from the past 70 years.⁷⁸⁻⁸⁰

A) Hisaeda's electrochemical cycloperfluoroalkylation



B) Zhao's molybdenum-mediated perfluoroalkylation

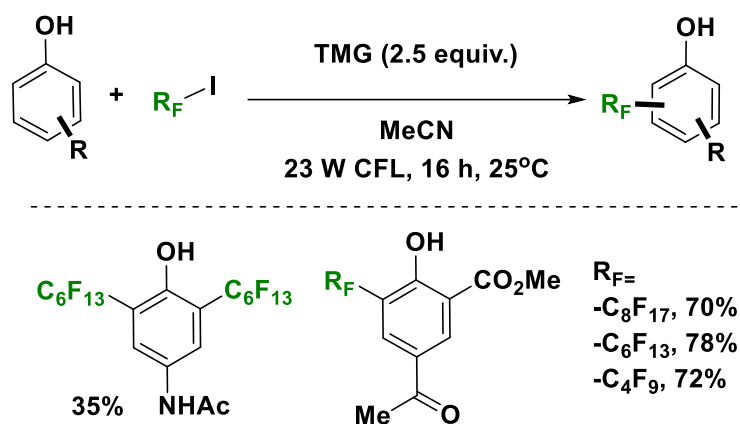


Scheme 1.4: Examples of perfluoroalkylating methodologies

Even though most research on perfluoroalkylation focuses on organometallic reactions, metal-free and photocatalyzed synthetic methods have also been extensively promoted. The first report of a UV light-driven reaction for the perfluoroalkylation of aromatics dates back to 1967, found in a patent from the Minnesota Mining and Manufacturing Company,⁸¹ establishing an alternative method to copper-mediated syntheses of perfluoroalkylated aryl products. Due to the lability of the R_F-I bond, and the ubiquity of these iodides as starting materials, photochemical perfluoroalkylation methods

commonly implement the use of EDA complexes,⁸²⁻⁸⁵ for which a thorough review has been written by Postigo and co-workers.⁸⁶ In 2014 Melchiorre and co-workers rediscovered the potential of these reactions, reporting on the perfluoroalkylation of α -cyano arylacetates through the use of electron donor-acceptor (EDA) complexes under mild conditions,^{87, 88} opening the door for the exploration of new techniques with photoredox chemistry (**Scheme 1.5**). After these initial reports, this group also described a photochemical strategy for the modification of phenols from the perfluoroalkyl iodide at ambient temperature under the irradiation of a Compact Fluorescent Lamp (CFL).⁸⁹ Currently, photochemical methods for the installation of perfluoroalkyl moieties remains an area of interest; something we have summarized in a review published in the *Journal of Organic & Biomolecular Chemistry*.⁸⁰ However, challenges still remain, including the need for selective photocleavable perfluoroalkyl sources in benign solvents, an aspect that we have focused on throughout Chapter 2.

Melchiorre's SET-mediated perfluoroalkylation of phenols



Scheme 1.5: Melchiorre's perfluoroalkylation of phenols

1.4 The Case for Metal-Free Catalysis

The synthetic methodologies exposed in this thesis have the ultimate goal of being useful in the context of LSF reactions. For this reason, it is important to explain in deeper detail their relationship with sustainability and our vision as a green chemistry group, particularly from the need of metal-free reactions.

In 2020, Börgel and Ritter defined LSF reactions as the modification of pharmaceutically or biologically relevant complex molecules through chemoselective methodologies which utilize native moieties as chemical handles and avoids the precursory introduction of functional groups for said modification.⁹⁰ Requirements for LSF reactions and some of the directives established in green chemistry overlap significantly.^{91, 92} The first of these shared objectives pertains to the reduction of derivatives and prevention of waste. LSF reactions exclude the installation of precursory handles and directing groups, a step that inherently prevents the unnecessary elongation of synthetic routes. Also, their chemoselective character and the needed tolerance towards other functional groups minimizes the introduction of protecting groups, thus improving the atom economy of a given transformation. The second branch of shared objectives deals with the design of reactions for energy efficiency. Development of LSF reactions calls for a precautionary approach based on the use of milder methods for the introduction of new functionalities, namely transition-metal catalysis with high turnover numbers or stoichiometric reagents with yields high enough to be pharmaceutically relevant.

While modern LSF reactions have recently evolved in parallel to the practice of sustainability, they still display important caveats that need to be tackled. The most important of these is the widespread use of metal-containing compounds for the activation of C–H bonds. While metal catalysis provides endless opportunities for the manipulation of challenging substrates, and has expanded accessible chemical space through fine-tuning of their electronic properties, they also present key disadvantages for the field.⁹³ A notable example is metal contamination in

pharmaceuticals. Even in minimal quantities, metal contamination has the potential to interfere with subsequent development and screening stages. This includes false signals during *in vitro* screenings, side effects during *in vivo* tests, and toxicity risks when administered to the end user.^{94, 95} Furthermore, metal-catalysts can be expensive and less available, limiting the scalability in process chemistry.⁹⁶ Finally, the need for further purification of functionalized products in order to lower the metal residue content to ppm level, defeats the purpose of reducing hazardous waste.

The work discussed in this thesis provides examples of LSF reactions that can be performed without the use of metals and with relative selectivity. For a more thorough discussion on metal free LSF reactions, I have co-authored a comprehensive review in the journal *Chemical Society Reviews*.⁹⁷ This review thoroughly covers examples on C–H functionalization and the use of native heteroatom-containing functionalities as chemical handles, as well as their overlap with green chemistry principles.

References

- (1) Blakemore, D. C.; Castro, L.; Churcher, I.; Rees, D. C.; Thomas, A. W.; Wilson, D. M.; Wood, A. Organic synthesis provides opportunities to transform drug discovery. *Nat. Chem.* **2018**, *10* (4), 383-394.
- (2) Noël, T.; Zysman-Colman, E. The promise and pitfalls of photocatalysis for organic synthesis. *Chem Catalysis* **2022**, *2* (3), 468-476.
- (3) Beil, S. B.; Bonnet, S.; Casadevall, C.; Detz, R. J.; Eisenreich, F.; Glover, S. D.; Kerzig, C.; Næsberg, L.; Pullen, S.; Storch, G.; et al. Challenges and Future Perspectives in Photocatalysis: Conclusions from an Interdisciplinary Workshop. *JACS Au* **2024**, *4* (8), 2746-2766.
- (4) Buglioni, L.; Raymenants, F.; Slattery, A.; Zondag, S. D. A.; Noël, T. Technological Innovations in Photochemistry for Organic Synthesis: Flow Chemistry, High-Throughput Experimentation, Scale-up, and Photoelectrochemistry. *Chem. Rev.* **2022**, *122* (2), 2752-2906.
- (5) Romero, N. A.; Nicewicz, D. A. Organic Photoredox Catalysis. *Chem. Rev.* **2016**, *116* (17), 10075-10166.
- (6) Schrader, M. L.; Schäfer, F. R.; Schäfers, F.; Glorius, F. Bridging the information gap in organic chemical reactions. *Nat. Chem.* **2024**, *16* (4), 491-498.
- (7) Ciamician, G. The Photochemistry of the Future. *Science* **1912**, *36* (926), 385-394.
- (8) Turro, N. J.; Ramamurthy, V.; Scaiano, J. C. *Modern molecular photochemistry of organic molecules*; University Science Books Sausalito, CA, 2010.
- (9) Scaiano, J. C. *Photochemistry Essentials*; American Chemical Society, 2022. DOI: doi:10.1021/acsinfocus.7e5031.
- (10) Plesniak, M. P.; Huang, H.-M.; Procter, D. J. Radical cascade reactions triggered by single electron transfer. *Nature Reviews Chemistry* **2017**, *1* (10), 0077.
- (11) Schultz, D. M.; Yoon, T. P. Solar Synthesis: Prospects in Visible Light Photocatalysis. *Science* **2014**, *343* (6174), 1239176.
- (12) Stephenson, C. R. J.; Yoon, T. P.; MacMillan, D. W. C. *Visible Light Photocatalysis in Organic Chemistry*; Wiley, 2018.
- (13) Shaw, M. H.; Twilton, J.; MacMillan, D. W. C. Photoredox Catalysis in Organic Chemistry. *J. Org. Chem.* **2016**, *81* (16), 6898-6926.

- (14) Chan, A. Y.; Ghosh, A.; Yarranton, J. T.; Twilton, J.; Jin, J.; Arias-Rotondo, D. M.; Sakai, H. A.; McCusker, J. K.; MacMillan, D. W. C. Exploiting the Marcus inverted region for first-row transition metal–based photoredox catalysis. *Science* **2023**, 382 (6667), 191-197.
- (15) Prier, C. K.; Rankic, D. A.; MacMillan, D. W. C. Visible Light Photoredox Catalysis with Transition Metal Complexes: Applications in Organic Synthesis. *Chem. Rev.* **2013**, 113 (7), 5322-5363.
- (16) Bell, J. D.; Murphy, J. A. Recent advances in visible light-activated radical coupling reactions triggered by (i) ruthenium, (ii) iridium and (iii) organic photoredox agents. *Chem. Soc. Rev.* **2021**, 50 (17), 9540-9685.
- (17) Singh, P. P.; Singh, J.; Srivastava, V. Visible-light acridinium-based organophotoredox catalysis in late-stage synthetic applications. *RSC Advances* **2023**, 13 (16), 10958-10986.
- (18) Crisenza, G. E. M.; Mazzarella, D.; Melchiorre, P. Synthetic Methods Driven by the Photoactivity of Electron Donor–Acceptor Complexes. *J. Am. Chem. Soc.* **2020**, 142 (12), 5461-5476.
- (19) Wortman, A. K.; Stephenson, C. R. J. EDA photochemistry: Mechanistic investigations and future opportunities. *Chem* **2023**, 9 (9), 2390-2415.
- (20) Mori, T.; Inoue, Y. Charge-transfer excitation: unconventional yet practical means for controlling stereoselectivity in asymmetric photoreactions. *Chem. Soc. Rev.* **2013**, 42 (20), 8122-8133.
- (21) Lima, C. G. S.; de M. Lima, T.; Duarte, M.; Jurberg, I. D.; Paixão, M. W. Organic Synthesis Enabled by Light-Irradiation of EDA Complexes: Theoretical Background and Synthetic Applications. *ACS Catal.* **2016**, 6 (3), 1389-1407.
- (22) Wang, C.; Li, H.; Bürgin, T. H.; Wenger, O. S. Cage escape governs photoredox reaction rates and quantum yields. *Nat. Chem.* **2024**, 16 (7), 1151-1159.
- (23) Bryden, M. A.; Millward, F.; Lee, O. S.; Cork, L.; Gather, M. C.; Steffen, A.; Zysman-Colman, E. Lessons learnt in photocatalysis – the influence of solvent polarity and the photostability of the photocatalyst. *Chem. Sci.* **2024**, 15 (10), 3741-3757.
- (24) Leifert, D.; Studer, A. The Persistent Radical Effect in Organic Synthesis. *Angew. Chem. Int. Ed.* **2020**, 59 (1), 74-108.

- (25) Gomberg, M. An instance of trivalent carbon: Triphenylmethyl *J. Am. Chem. Soc.* **1900**, *22* (11), 757-771.
- (26) Griller, D.; Ingold, K. U. Persistent carbon-centered radicals. *Acc. Chem. Res.* **1976**, *9* (1), 13-19.
- (27) Brückl, T.; Baxter, R. D.; Ishihara, Y.; Baran, P. S. Innate and Guided C–H Functionalization Logic. *Acc. Chem. Res.* **2012**, *45* (6), 826-839.
- (28) Meng, G.; Lam, N. Y. S.; Lucas, E. L.; Saint-Denis, T. G.; Verma, P.; Chekshin, N.; Yu, J.-Q. Achieving Site-Selectivity for C–H Activation Processes Based on Distance and Geometry: A Carpenter’s Approach. *J. Am. Chem. Soc.* **2020**, *142* (24), 10571-10591.
- (29) Hartwig, J. F. Catalyst-Controlled Site-Selective Bond Activation. *Acc. Chem. Res.* **2017**, *50* (3), 549-555.
- (30) Minisci, F.; Bernardi, R.; Bertini, F.; Galli, R.; Perchinummo, M. Nucleophilic character of alkyl radicals—VI: A new convenient selective alkylation of heteroaromatic bases. *Tetrahedron* **1971**, *27* (15), 3575-3579.
- (31) Proctor, R. S. J.; Phipps, R. J. Recent Advances in Minisci-Type Reactions. *Angew. Chem. Int. Ed.* **2019**, *58* (39), 13666-13699.
- (32) Ji, Y.; Brueckl, T.; Baxter, R. D.; Fujiwara, Y.; Seiple, I. B.; Su, S.; Blackmond, D. G.; Baran, P. S. Innate C-H trifluoromethylation of heterocycles. *PNAS* **2011**, *108* (35), 14411.
- (33) Fujiwara, Y.; Dixon, J. A.; O’Hara, F.; Funder, E. D.; Dixon, D. D.; Rodriguez, R. A.; Baxter, R. D.; Herlé, B.; Sach, N.; Collins, M. R.; et al. Practical and innate carbon–hydrogen functionalization of heterocycles. *Nature* **2012**, *492* (7427), 95-99.
- (34) Westwood, M. T.; Lamb, C. J. C.; Sutherland, D. R.; Lee, A.-L. Metal-, Photocatalyst-, and Light-Free Direct C–H Acylation and Carbamoylation of Heterocycles. *Org. Lett.* **2019**, *21* (17), 7119-7123.
- (35) Noisier, A. F. M.; Johansson, M. J.; Knerr, L.; Hayes, M. A.; Drury Iii, W. J.; Valeur, E.; Malins, L. R.; Gopalakrishnan, R. Late-Stage Functionalization of Histidine in Unprotected Peptides. *Angew. Chem. Int. Ed.* **2019**, *58* (52), 19096-19102.
- (36) Braun, M.-G.; Castanedo, G.; Qin, L.; Salvo, P.; Zard, S. Z. Introduction of Trifluoroethylamine as Amide Isostere by C–H Functionalization of Heteroarenes. *Org. Lett.* **2017**, *19* (15), 4090-4093.

- (37) Gutiérrez-Bonet, Á.; Remeur, C.; Matsui, J. K.; Molander, G. A. Late-Stage C–H Alkylation of Heterocycles and 1,4-Quinones via Oxidative Homolysis of 1,4-Dihydropyridines. *J. Am. Chem. Soc.* **2017**, *139* (35), 12251-12258.
- (38) Siddaraju, Y.; Lamani, M.; Prabhu, K. R. A Transition Metal-Free Minisci Reaction: Acylation of Isoquinolines, Quinolines, and Quinoxaline. *J. Org. Chem.* **2014**, *79* (9), 3856-3865.
- (39) O'Hara, F.; Blackmond, D. G.; Baran, P. S. Radical-Based Regioselective C–H Functionalization of Electron-Deficient Heteroarenes: Scope, Tunability, and Predictability. *J. Am. Chem. Soc.* **2013**, *135* (32), 12122-12134.
- (40) Cernak, T.; Dykstra, K. D.; Tyagarajan, S.; Vachal, P.; Krska, S. W. The medicinal chemist's toolbox for late stage functionalization of drug-like molecules. *Chem. Soc. Rev.* **2016**, *45* (3), 546-576.
- (41) White, M. C.; Zhao, J. Aliphatic C-H Oxidations for Late-Stage Functionalization. *J. Am. Chem. Soc.* **2018**, *140* (43), 13988-14009.
- (42) Jouffroy, M.; Kong, J. Direct C-H Carbamoylation of Nitrogen-Containing Heterocycles. *Chemistry* **2019**, *25* (9), 2217-2221.
- (43) Matsui, J. K.; Primer, D. N.; Molander, G. A. Metal-free C–H alkylation of heteroarenes with alkyltrifluoroborates: a general protocol for 1°, 2° and 3° alkylation. *Chem. Sci.* **2017**, *8* (5), 3512-3522.
- (44) Li, J.; Huang, C.-Y.; Li, C.-J. Cross-dehydrogenative coupling of unactivated alkanes. *Trends in Chemistry* **2022**, *4* (6), 479-494.
- (45) Huang, C.-Y.; Kang, H.; Li, J.; Li, C.-J. En Route to Intermolecular Cross-Dehydrogenative Coupling Reactions. *J. Org. Chem.* **2019**, *84* (20), 12705-12721.
- (46) Li, C.-J. Cross-Dehydrogenative Coupling (CDC): Exploring C–C Bond Formations beyond Functional Group Transformations. *Acc. Chem. Res.* **2009**, *42* (2), 335-344.
- (47) Deng, G.; Ueda, K.; Yanagisawa, S.; Itami, K.; Li, C.-J. Coupling of Nitrogen Heteroaromatics and Alkanes without Transition Metals: A New Oxidative Cross-Coupling at C–H/C–H Bonds. *Chem. Eur. J.* **2009**, *15* (2), 333-337.
- (48) Li, L.; Mu, X.; Liu, W.; Wang, Y.; Mi, Z.; Li, C.-J. Simple and Clean Photoinduced Aromatic Trifluoromethylation Reaction. *J. Am. Chem. Soc.* **2016**, *138* (18), 5809-5812.

- (49) Liu, W.; Yang, X.; Zhou, Z.-Z.; Li, C.-J. Simple and Clean Photo-induced Methylation of Heteroarenes with MeOH. *Chem* **2017**, *2* (5), 688-702.
- (50) Liu, P.; Liu, W.; Li, C.-J. Catalyst-Free and Redox-Neutral Innate Trifluoromethylation and Alkylation of Aromatics Enabled by Light. *J. Am. Chem. Soc.* **2017**, *139* (40), 14315-14321.
- (51) Tomashenko, O. A.; Grushin, V. V. Aromatic Trifluoromethylation with Metal Complexes. *Chem. Rev.* **2011**, *111* (8), 4475-4521.
- (52) Landelle, G.; Panossian, A.; Pazenok, S.; Vors, J.-P.; Leroux, F. R. Recent advances in transition metal-catalyzed Csp²-monofluoro-, difluoro-, perfluoromethylation and trifluoromethylthiolation. *Beilstein J. Org. Chem.* **2013**, *9*, 2476-2536.
- (53) Barata-Vallejo, S.; Lantaño, B.; Postigo, A. Recent Advances in Trifluoromethylation Reactions with Electrophilic Trifluoromethylating Reagents. *Chem. Eur. J* **2014**, *20* (51), 16806-16829.
- (54) Cho, E. J. Radical-Mediated Fluoroalkylations. *Chem. Rec.* **2016**, *16* (1), 47-63.
- (55) Liu, X.; Xu, C.; Wang, M.; Liu, Q. Trifluoromethyltrimethylsilane: Nucleophilic Trifluoromethylation and Beyond. *Chem. Rev.* **2015**, *115* (2), 683-730.
- (56) Charpentier, J.; Früh, N.; Togni, A. Electrophilic Trifluoromethylation by Use of Hypervalent Iodine Reagents. *Chem. Rev.* **2015**, *115* (2), 650-682.
- (57) Xiao, H.; Zhang, Z.; Fang, Y.; Zhu, L.; Li, C. Radical trifluoromethylation. *Chem. Soc. Rev.* **2021**, *50* (11), 6308-6319.
- (58) Brooke, G. M. The preparation and properties of polyfluoro aromatic and heteroaromatic compounds. *J. Fluorine Chem.* **1997**, *86* (1), 1-76.
- (59) Avila, D. V.; Ingold, K. U.; Luszytk, J.; Dolbier, W. R.; Pan, H. Q.; Muir, M. Absolute rate constants for some reactions of perfluoro-n-alkyl radicals in solution. *J. Am. Chem. Soc.* **1994**, *116* (1), 99-104.
- (60) Lv, J.; Cheng, Y. Fluoropolymers in biomedical applications: state-of-the-art and future perspectives. *Chem. Soc. Rev.* **2021**, *50* (9), 5435-5467.
- (61) Wu, X.; Hong, Y.-L.; Xu, B.; Nishiyama, Y.; Jiang, W.; Zhu, J.; Zhang, G.; Kitagawa, S.; Horike, S. Perfluoroalkyl-Functionalized Covalent Organic Frameworks with Superhydrophobicity for Anhydrous Proton Conduction. *J. Am. Chem. Soc.* **2020**, *142* (33), 14357-14364.

- (62) McLoughlin, V. C. R.; Thrower, J. A route to fluoroalkyl-substituted aromatic compounds involving fluoroalkylcopper intermediates. *Tetrahedron* **1969**, *25* (24), 5921-5940.
- (63) Tiers, G. V. D. Perfluoroalkylation of aromatic compounds. *J. Am. Chem. Soc.* **1960**, *82* (20), 5513-5513.
- (64) Leifert, D.; Artiukhin, D. G.; Neugebauer, J.; Galstyan, A.; Strassert, C. A.; Studer, A. Radical perfluoroalkylation – easy access to 2-perfluoroalkylindol-3-imines via electron catalysis. *Chem. Commun.* **2016**, *52* (35), 5997-6000.
- (65) Xu, Z.; Sun, T.; Cai, Q.; Ni, F.; Han, J.; Chen, J.; Deng, H.; Shao, M.; Zhang, H.; Cao, W. Stereoselective synthesis of trans-perfluoroalkylated [1,3]oxazino[2,3-a]isoquinolines from aromatic aldehydes, methyl perfluoroalk-2-ynoates and isoquinolines. *J. Fluorine Chem.* **2016**, *181*, 45-50.
- (66) He, D.; Xu, Y.; Han, J.; Deng, H.; Shao, M.; Chen, J.; Zhang, H.; Cao, W. Facile one-pot tandem synthesis of perfluoroalkylated indolizines under metal-free mild conditions. *Tetrahedron* **2017**, *73* (7), 938-944.
- (67) El Kharrat, S.; Laurent, P.; Boiteau, L.; Blancou, H. Novel Synthesis of Substituted 2-Trifluoromethyl and 2-Perfluoroalkyl N-Arylpyridinium Compounds—Mechanistic Insights. *Molecules* **2019**, *24* (12), 2328.
- (68) Pan, Y.; Li, J.; Li, Z.; Huang, F.; Ma, X.; Jiao, W.; Shao, H. An efficient and facile strategy for trifluoromethylation and perfluoroalkylation of isoquinolines and heteroarenes. *Chem. Commun.* **2020**, *56* (56), 7813-7816.
- (69) Kalkman, E. D.; Mormino, M. G.; Hartwig, J. F. Unusual Electronic Effects of Ancillary Ligands on the Perfluoroalkylation of Aryl Iodides and Bromides Mediated by Copper(I) Pentafluoroethyl Complexes of Substituted Bipyridines. *J. Am. Chem. Soc.* **2019**, *141* (49), 19458-19465.
- (70) Aikawa, K.; Nakamura, Y.; Yokota, Y.; Toya, W.; Mikami, K. Stable but Reactive Perfluoroalkylzinc Reagents: Application in Ligand-Free Copper-Catalyzed Perfluoroalkylation of Aryl Iodides. *Chem. Eur. J* **2015**, *21* (1), 96-100.
- (71) Wang, X.; Hirano, K.; Kurauchi, D.; Kato, H.; Toriumi, N.; Takita, R.; Uchiyama, M. Perfluoroalkyl and -aryl Zinc Ate Complexes: Generation, Reactivity, and Synthetic Application. *Chem. Eur. J* **2015**, *21* (31), 10993-10996.

- (72) Huang, Y.; Ajitha, M. J.; Huang, K.-W.; Zhang, Z.; Weng, Z. A class of effective decarboxylative perfluoroalkylating reagents: [(phen)₂Cu](O₂CRF). *Dalton Trans.* **2016**, 45 (20), 8468-8474.
- (73) Harada, K.; Tezuka, N.; Hirano, K.; Miyamoto, K.; Saito, T.; Uchiyama, M. Rhodium-Catalyzed (Perfluoroalkyl)olefination of Acetanilides Leading to Perfluoroalkylated Aromatics. *Chem. Pharm. Bull.* **2016**, 64 (10), 1442-1444.
- (74) Kirij, N. V.; Filatov, A. A.; Khrapach, G. Y.; Yagupolskii, Y. L. The first nucleophilic C–H perfluoroalkylation of aromatic compounds via (arene)tricarbonylchromium complexes. *Chem. Commun.* **2017**, 53 (13), 2146-2149.
- (75) Yuan, C.; Dai, P.; Bao, X.; Zhao, Y. Highly Site-Selective Formation of Perfluoroalkylated Anilids via a Protecting Strategy by Molybdenum Hexacarbonyl Catalyst. *Org. Lett.* **2019**, 21 (16), 6481-6484.
- (76) He, L.; Natte, K.; Rabeah, J.; Taeschler, C.; Neumann, H.; Brückner, A.; Beller, M. Heterogeneous Platinum-Catalyzed C–H Perfluoroalkylation of Arenes and Heteroarenes. *Angew. Chem. Int. Ed.* **2015**, 54 (14), 4320-4324.
- (77) Zhang, S.; Weniger, F.; Kreyenschulte, C. R.; Lund, H.; Bartling, S.; Neumann, H.; Ellinger, S.; Taeschler, C.; Beller, M. Towards a practical perfluoroalkylation of (hetero)arenes with perfluoroalkyl bromides using cobalt nanocatalysts. *Catal. Sci. Technol.* **2020**, 10 (6), 1731-1738.
- (78) Barata-Vallejo, S.; Bonesi, S. M.; Postigo, A. Perfluoroalkylation reactions of (hetero)arenes. *RSC Adv.* **2015**, 5 (77), 62498-62518.
- (79) Postigo, A. Aromatic radical perfluoroalkylation reactions. *Can. J. Chem.* **2012**, 90 (6), 493-497.
- (80) Castillo-Pazos, D. J.; Lasso, J. D.; Li, C.-J. Modern methods for the synthesis of perfluoroalkylated aromatics. *Org. Biomol. Chem.* **2021**, 19 (33), 7116-7128.
- (81) Process for preparing fluorinated compounds. United States US3326928A, 1967.
- (82) Beatty, J.; Douglas, J.; R. Miller; McAtee, R.; Cole, K.; Stephenson, C. Photochemical Perfluoroalkylation with Pyridine N -Oxides: Mechanistic Insights and Performance on a Kilogram Scale. *Chem* **2016**, 1 (3), 456-472.

- (83) Sun, X.; Wang, W.; Li, Y.; Ma, J.; Yu, S. Halogen-Bond-Promoted Double Radical Isocyanide Insertion under Visible-Light Irradiation: Synthesis of 2-Fluoroalkylated Quinoxalines. *Org. Lett.* **2016**, *18* (18), 4638-4641.
- (84) Wang, Y.; Wang, J.; Li, G.-X.; He, G.; Chen, G. Halogen-Bond-Promoted Photoactivation of Perfluoroalkyl Iodides: A Photochemical Protocol for Perfluoroalkylation Reactions. *Org. Lett.* **2017**, *19* (6), 1442-1445.
- (85) Wang, R.; Guan, W.; Han, Z.-B.; Liang, F.; Suga, T.; Bi, X.; Nishide, H. Ambient-Light-Promoted Three-Component Annulation: Synthesis of Perfluoroalkylated Pyrimidines. *Org. Lett.* **2017**, *19* (9), 2358-2361.
- (86) Postigo, A. Electron Donor-Acceptor Complexes in Perfluoroalkylation Reactions. *Eur. J. Org. Chem.* **2018**, *2018* (46), 6391-6404.
- (87) Fernández-Alvarez, V. M.; Nappi, M.; Melchiorre, P.; Maseras, F. Computational Study with DFT and Kinetic Models on the Mechanism of Photoinitiated Aromatic Perfluoroalkylations. *Org. Lett.* **2015**, *17* (11), 2676-2679.
- (88) Nappi, M.; Bergonzini, G.; Melchiorre, P. Metal-Free Photochemical Aromatic Perfluoroalkylation of α -Cyano Arylacetates. *Angew. Chem. Int. Ed.* **2014**, *53* (19), 4921-4925.
- (89) Filippini, G.; Nappi, M.; Melchiorre, P. Photochemical direct perfluoroalkylation of phenols. *Tetrahedron* **2015**, *71* (26), 4535-4542.
- (90) Börgel, J.; Ritter, T. Late-Stage Functionalization. *Chem* **2020**, *6* (8), 1877-1887.
- (91) Anastas, P.; Eghbali, N. Green Chemistry: Principles and Practice. *Chem. Soc. Rev.* **2010**, *39* (1), 301-312.
- (92) Anastas, P. T.; Warner, J. C. *Green Chemistry: Theory and Practice*; Oxford University Press, 1998.
- (93) Dalton, T.; Faber, T.; Glorius, F. C–H Activation: Toward Sustainability and Applications. *ACS Cent. Sci.* **2021**, *7* (2), 245-261.
- (94) Egorova, K. S.; Ananikov, V. P. Toxicity of Metal Compounds: Knowledge and Myths. *Organometallics* **2017**, *36* (21), 4071-4090.
- (95) Hermann, J. C.; Chen, Y.; Wartchow, C.; Menke, J.; Gao, L.; Gleason, S. K.; Haynes, N.-E.; Scott, N.; Petersen, A.; Gabriel, S.; et al. Metal Impurities Cause False Positives in High-Throughput Screening Campaigns. *ACS Med. Chem. Lett.* **2013**, *4* (2), 197-200.

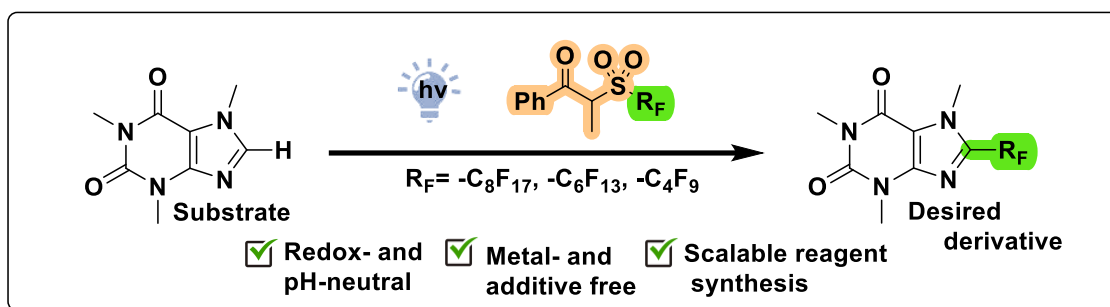
(96) Ludwig, J. R.; Schindler, C. S. Catalyst: Sustainable Catalysis. *Chem* **2017**, 2 (3), 313-316.

(97) Lasso, J. D.; Castillo-Pazos, D. J.; Li, C.-J. Green chemistry meets medicinal chemistry: a perspective on modern metal-free late-stage functionalization reactions. *Chem. Soc. Rev.* **2021**, 50 (19), 10955-10982.

2 New Reagents

Synthesis of α -(perfluoroalkylsulfonyl) propiophenones:

A new set of reagents for the light-mediated perfluoroalkylation of aromatics



Reproduced with permission from “Synthesis of α -(perfluoroalkylsulfonyl)propiophenones: a new set of reagents for the light-mediated perfluoroalkylation of aromatics”, Castillo-Pazos, D.; Lasso, J.; Li, C.-J., *Beilstein J. Org. Chem.*, **2022**, 18, 788-795. Copyright 2022 Beilstein Institut.

Preface

In chapter 1, we highlighted some of the areas of opportunity capable of pushing modern photocatalysis forward. These include, but are not limited to, the exploration of new reagents based on current needs. For example, since the advent of photoredox catalysis, one can notice the strong dependence on methods that require both external catalysts and sacrificial reagents, namely oxidants, reductants, acids or bases that can promote the reaction in question. For this reason, recent literature in photocatalysis has highlighted the need for minimalistic synthetic methodologies; namely, those that can be initiated without such external catalysts or sacrificial reagents, thereby proceeding under redox- or pH-neutral conditions.

Having this need in mind, our group developed in 2017 a propiophenone-based scaffold capable of cleaving upon UV light irradiation to produce free trifluoromethyl and alkyl radicals to subsequently functionalize a wide array of substrates.¹ As my first project within the Li group, we proceeded to expand this proof of concept towards the installation of perfluoroalkyl chains onto aromatic substrates, providing them with valuable properties (e.g. hydrophobicity and stereoelectronics). Until 2018, most perfluoroalkylating methodologies relied on the use of unstable reagents coupled with the use of sacrificial reductants. Therefore, we decided to develop a series of α -(perfluoroalkylsulfonyl) propiophenones as a new family of bench-stable reagents for the redox- and pH-neutral innate functionalization of aromatic molecules.

In this chapter, we describe the design and synthesis of such reagents, describing their reactivity under the irradiation of UV light. Such perfluoroalkylating tools became part of a report of invention and are now commercialized by Millipore-Sigma.

Author contributions:

Durbis Castillo and Prof. Chao-Jun Li contributed to the project conception and design. Durbis Castillo and Juan Lasso performed all optimization and scope experiments as well as their corresponding analysis. Durbis Castillo and Juan Lasso wrote the manuscript under the supervision and editing of Prof. Chao-Jun Li. Durbis Castillo and Juan Lasso contributed equally to this work.

Abstract

In response to the demand for late-stage perfluoroalkylation in synthetic chemistry, we report the synthesis of a series of bench-stable α -(perfluorosulfonyl)propiophenones. Their application as photocleavable reagents was tested with electron-rich aromatics under the metal-free, redox- and pH-neutral conditions to enable late-stage perfluorooctylation, perfluorohexylation and perfluorobutylation.

Introduction

Perfluorinated compounds are a family of molecules containing a backbone where all C–H bonds have been substituted with fluorine atoms. Within this family of molecules, perfluoroalkyl groups represent an industrially relevant moiety, capable of modifying the physicochemical properties of the scaffold that they are attached to. Such properties and a distinctive reactivity—or inert character—have been harnessed in a plethora of applications in modern life: Teflon in non-stick pans, fire-fighting foams, stain-resistant and weatherproof fabrics, etching of circuit boards, and even imaging agents.² Given their importance, multiple synthetic methodologies for the introduction of long perfluorinated chains into aromatic rings have been developed since the first reports of such transformation by George Tiers in 1960, and McLoughlin and Thrower in 1969.^{3, 4} Most approaches have made extensive use of organometallic chemistry, radical initiators, photocatalysis, electrochemistry, and more sophisticated platforms such as metal nanoparticles, all of which have been reviewed thoroughly in the literature.⁵⁻⁹

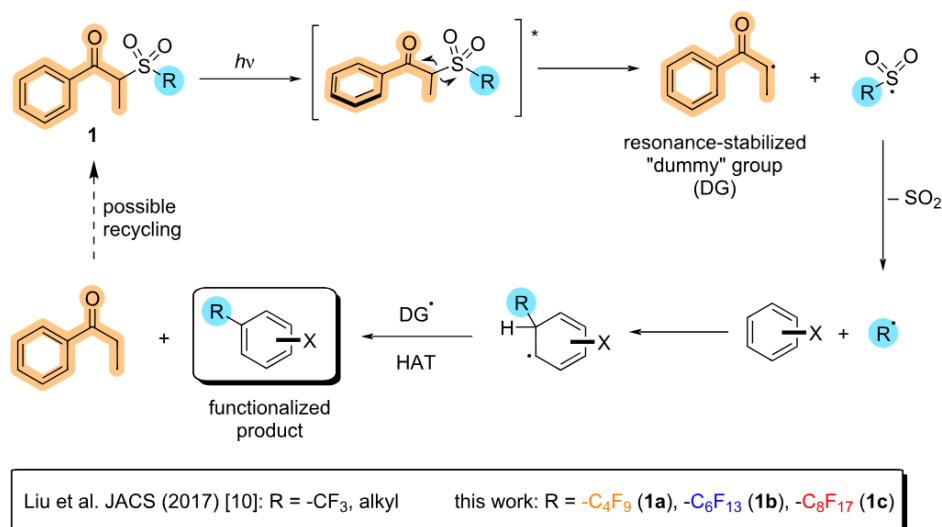
However, the methods referenced so far display one or more of the following setbacks: involvement of harsh oxidants and reductants, use of expensive metal catalysts, need for superstoichiometric amounts of starting materials, generation of undesired perfluoroalkylated byproducts, and poor chemoselectivity. Perfluorinating methodologies are typically predicated on the use of commercially abundant perfluoroalkyl iodides, molecules which are highly sensitive and frequently unstable to laboratory conditions. Modern perfluoroalkylation methodologies exceedingly rely on the use of perfluoroalkyl iodides as their principal source of perfluoroalkyl synthons. Indeed, while these molecules are cheap and abundant starting materials their use is fraught with technical complications. This family of molecules is extremely sensitive to bench

conditions and requires a carefully controlled refrigeration in addition to low light levels to avoid decomposition. Furthermore, true to the unique solubility of this class of molecules, perfluoroalkyl iodides have a tendency to be weakly soluble in common organic solvents (i.e. ethyl acetate, methanol) rendering their application troublesome.¹⁰ Moreover, the homolysis of the perfluoroalkyl iodide produces iodine radicals that can result in stray halogenation reactions or oxidation. For these reasons, it would be ideal to develop an efficient methodology that allows for the generation of perfluoroalkyl radicals in a mild, redox- and pH-neutral manner, without the assistance of external photocatalysts, heavy metal catalysts, or further additives. Thus, the expansion of our previously reported propiophenone family of reagents was envisioned as suitable alternative to produce a bench stable, organic soluble, and iodine free perfluoroalkylation source.

In 2017, our group developed a metal-free and redox-neutral protocol for the photoinduced alkylation of aromatics, for which trifluoromethylation was also possible in good to high yields for electron-rich aromatic rings.¹ In this protocol, inspired by Norrish type I reactions and the elimination of β -substituents after ketone photoexcitation,^{11-13a} a series of reagents containing an α -sulfonylpropiophenone moiety readily undergoes homolysis into 3 parts upon irradiation of light: a propiophenone radical—forming a stabilized and bulky “dummy group”—, a molecule of SO₂, and our radical of interest. Once this radical is formed in solution, radical addition of the aromatic substrate undergoes readily, and is subsequently followed by a hydrogen atom transfer (HAT) process aided by the “dummy group” radical. These reagents thus fit the paradigm of a green methodology as their implicit design and photoactivity allows them to react without the use of external metal catalysts. The intrinsic reactivity of these molecules allows this set of reagents to be both redox- and pH-neutral, while also being highly diversifiable. Additionally, all byproducts generated either during its synthesis or use in following reactions have the potential to be recycled, if so desired.

Based on the fact that both, trifluoromethyl radicals and its longer-chain analogues, share a common electrophilic character and a stabilizing stereoelectronic effect,¹⁴ we envisioned that the “dummy group” methodology could be translated into the formation of sought after perfluoroalkyl radicals (**Scheme 2.1**). In this work, we report the synthesis

and application of three new members of the “dummy group” reagent family, based on the α -(perfluorosulfonyl)propiophenone scaffold for the perfluorooctylation, perfluorohexylation, and perfluorobutylation of electron-rich aromatics. With the insights discussed in this paper, the authors hope to provide a new and amenable synthetic tool for the future academic and industrial demand of perfluorinated molecules and materials.



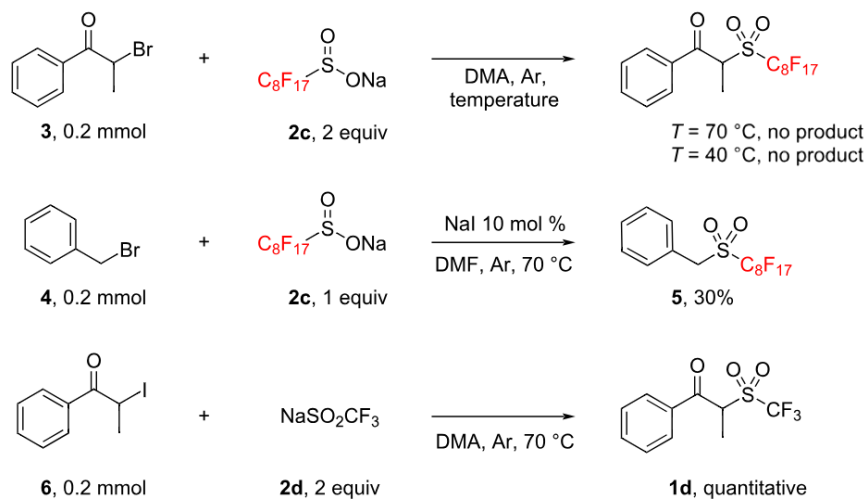
Scheme 2.1: Envisioned Minisci perfluoroalkylation facilitated by “dummy group” reagents

Results and Discussion

To design an efficient and reproducible methodology for the synthesis of α -(perfluorosulfonyl)propiophenones, we envisioned the bimolecular nucleophilic substitution between an α -halopropiophenone as the “dummy group” scaffold and the corresponding perfluorinated sodium sulfinate salt—also visualized as the installation of the photocleavable moiety onto the perfluoroalkyl chain.¹⁵⁻¹⁹ Synthesis of the precursory sulfinate salts **2a-c** were synthesized through the sulfinatodehalogenation, reaction, discovered by Huang and coworkers,^{20, 21} and later on adapted by other research groups.^{22, 23} Pleasingly, the desired -C₄F₉ (**2a**), -C₆F₁₃ (**2b**), and -C₈F₁₇ (**2c**) sulfinate salts were obtained from the perfluoroalkyl iodide precursors in good to quantitative yields as previously described. Additionally, we conceived that this methodology should be

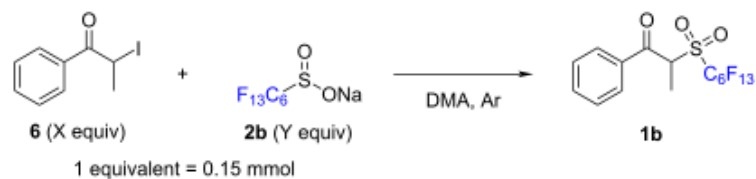
amenable to the synthesis of one of the limited commercially available secondary perfluoroalkyl groups such as perfluoroisopropyl iodide. However, despite being able to obtain the corresponding sulfinate in limited yield, the decomposition of this compound after several days at 4 °C, and within a few minutes under heating deemed its applicability impractical.

After this first step, we proceeded to test the nucleophilic substitution between our perfluoroalkyl sulfinate salts and an α -halopropiophenone. Unfortunately, initial attempts of a nucleophilic attack on α -bromopropiophenone were unsuccessful due to the insufficient nucleophilicity of the sulfinate to substitute a bromide on a secondary carbon atom at 40 °C (**Scheme 2.2**). Furthermore, increasing the temperature to 70 °C was not found to generate product and instead resulted in slight decomposition of the starting materials. Attempting to trap the sulfinate nucleophiles with primary benzyl bromide with catalytic sodium iodide under thermal conditions underscored the sluggish reactivity of these sulfinate derivatives towards undergoing nucleophilic substitution. To solve this problem, we turned to the use of α -iodopropiophenone, generated from its bromide counterpart through a simple Finkelstein reaction.²⁴ After performing a control experiment between α -iodopropiophenone and sodium triflate (quantitative yield), we proceeded to optimize the conditions for the nucleophilic substitution on this substrate by sodium perfluorohexyl sulfinate (**Table 2.1**). Temperature displayed a pivotal role in this synthesis: while room temperature proved insufficient to promote the substitution, the use of heat beyond 70 °C was detrimental for the reaction due to decomposition of the product. Once established that 40 °C was enough to promote the reaction, while limiting decomposition, we proceeded to screen the possible molar ratios between both components in the reaction. Given the higher economic value of the perfluorinated salts, we decided to vary the amounts of α -iodopropiophenone to increase. Ranging from a 2.5:1 until a 10:1 molar ratio, yields increased significantly from 20% to 68%; however, a 5:1 ratio offered us a similar yield with a much shorter workup time when the reaction concentration was doubled.



Scheme 2.2: Control experiments for the nucleophilic substitution of perfluoroalkyl sulfonates and halogenated electrophilic partners

Table 2.1: Optimization for the nucleophilic substitution between α -iodopropiophenone and sodium perfluoroalkylsulfonates.

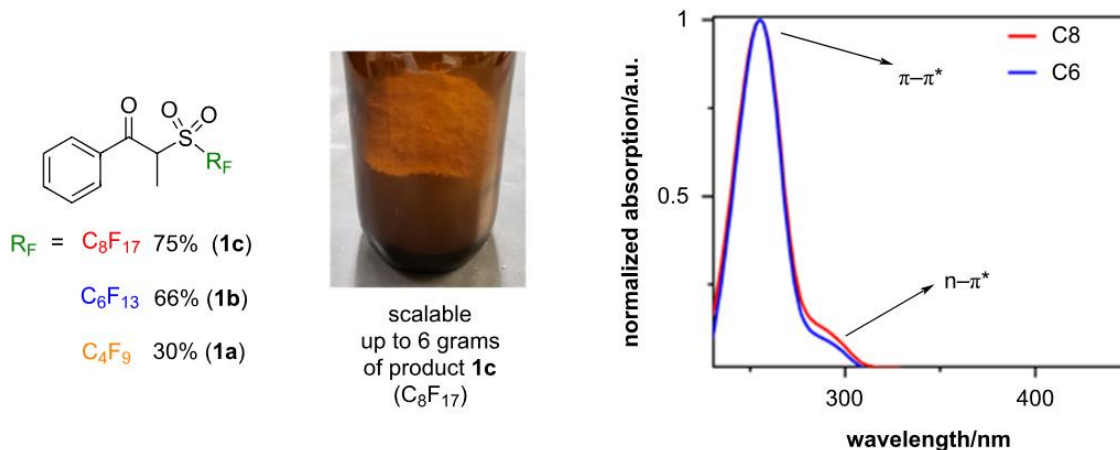


Entry	Molar ratio X:Y	Vol. MeCN (mL)	Temperature ($^\circ\text{C}$)	Time (h)	NMR yield (%) ^a
1	1:1.5	1	70	16	n.d.
2	1:1.5	1	40	16	18
3	1:1.5	1	20	16	traces
4	2.5:1	0.5	40	18	20
5	4:1	0.5	40	18	33
6	10:1	0.5	40	18	68
7	40:1	0.5	40	18	48
8	3:1	0.5	50	18	12
9	4:1	0.5	50	18	19
10	5:1	1	40	18	24
11	5:1	0.5	40	18	38
12	5:1	0.25	40	18	51
13	5:1	0.125	40	18	53

^aUsing dimethylsulfone as a standard

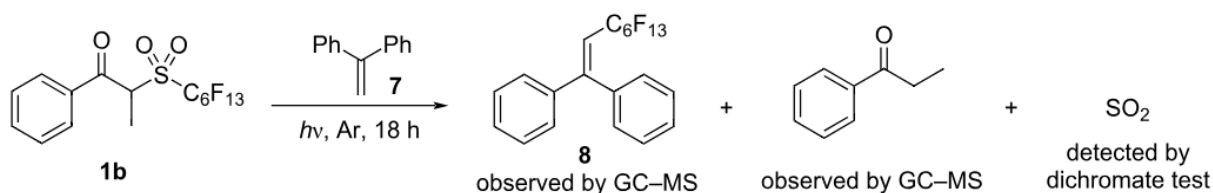
Knowing that nucleophilicity is a key factor in this reaction, we also employed crown ethers 15-crown-5 and 18-crown-6 to test whether a “naked” sulfinate ion would help us achieve a better yield. Unfortunately, the addition of such ethers shut down all reactivity, most likely due to side reactions with the sulfinate salt. Moreover, it is worth mentioning that, while other synthetic approaches were explored to obtain these reagents, the S_N2 strategy described in this work was the most efficient. Such synthetic alternatives included: first, a sulphur(VI) fluoride exchange (SuFEx) between perfluoroalkylsulfonyl fluorides and the corresponding silyl enol ether generated *in situ* from propiophenone, and second, the deprotection of propiophenone α -thioesters in the presence of perfluoroalkyliodides and subsequent oxidation of the formed perfluorothioether into the sulfone. However, none of these proposed pathways gave yields high enough for the reaction to be scalable (i.e. a maximum of 15% by ¹H NMR).

Finally, due to the concentration of α -iodopropiophenone employed, we detected the formation of a byproduct in the last stages of the optimization, namely the condensation of the desired product with α -propiophenone in the form of an enol ether. Once this byproduct was fully characterized by NMR, and the structure was confirmed by SCXRD, we conceived a hydrolysis protocol to break apart the formed enol ether—fully described in section 2.4 of the SI. After brief optimization, we succeeded at recovering the portion of perfluoroalkylating reagent that participated in such condensation (around 30%), giving us the final yields displayed in **Scheme 2.3**. Afterward, to show the practicality of application of these reagents in industry, we proceeded to scale up the reaction in gram-scale. Satisfactorily, the developed synthesis and workup allowed us to produce them in batches of up to six grams, with no decomposition observed over the course of 6 months.



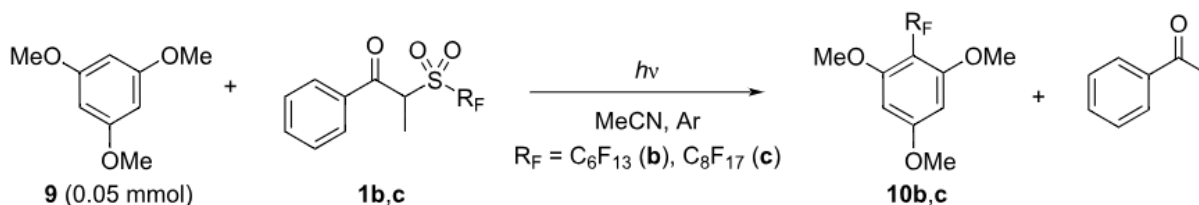
Scheme 2.3: Left: isolated yields of synthesized perfluoroalkylating reagents: perfluorobutyl (**1a**), perfluorohexyl (**1b**), and perfluorooctyl (**1c**) analogues (after conversion of byproduct); middle: gram amounts of perfluorooctyl product **1c**; right: UV-vis absorption of reagents **1b** and **1c**.

For the last section of this work, we proceeded to test the capacity of our reagents to generate the desired perfluoroalkyl radicals under light irradiation for the diversification of arenes. To verify the generation of perfluoroalkyl radicals, we conducted an experiment with 1,1-diphenylethylene as a radical trapping agent. Gratifyingly, we observed the formation of 2-(perfluorohexyl)-1,1-diphenylethylene, and propiophenone through GC/MS. Additionally, the presence of free SO₂ gas was confirmed by the reaction of acidic potassium dichromate solution on paper (green coloration of the exposed surface).



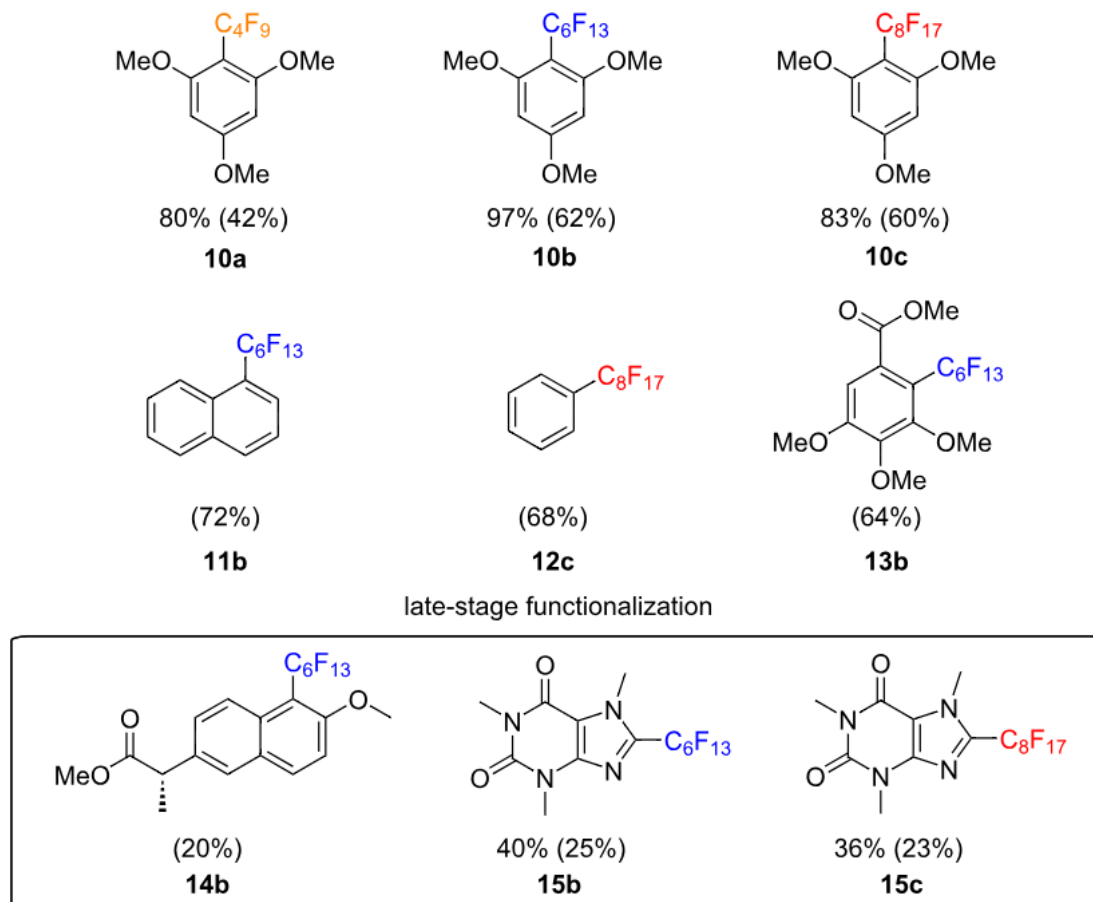
Scheme 2.4: Radical trapping experiment with 1,1-diphenylethylene (**7**) and **1b** confirming the initially proposed mechanism.

Using 1,3,5-trimethoxybenzene (TMB) as a model substrate, we optimized the perfluoroalkylation reaction under irradiation of a 300 W Xenon arc lamp (**Table 2.2**). Based on the UV-Vis absorption of our reagents **1**, we used long-pass filters at either 280 nm or 295 nm, to avoid side reactions caused by shorter wavelengths. During this optimization, 2 to 3 equivalents of the reagent **1** resulted in better yields, along with more concentrated reaction mixtures, reaching almost quantitative yields for the perfluorohexylation of TMB (**10b**) (**Scheme 2.5**) and 83% yield for its perfluorooxylation (**10c**), both in less than 6 hours. Unsubstituted arenes such as naphthalene were well tolerated in this methodology and produced 72% isolated yield of the perfluorohexylated product **11b**. The radical addition to unsubstituted benzene was also found to be possible affording perfluorooxylation product **12c** in 68% isolated yield, but as tends to be the case for inactivated substrates, excess quantities of benzene (50% v/v) were required. Compounds containing esters such as methyl 3,4,5-trimethoxybenzoate and naproxen methyl ester were also tolerated and the desired products **13b** and **14b** were isolated in yields of 64% and 20%, respectively. Arenes containing halogens were attempted, however in accordance to previous reported literature, the compounds were found to decompose under the ultraviolet radiation necessary for the homolysis of the reagent.²⁵ Lastly, some heteroaromatic substrates such as *N*-phenyl pyrrole and 2-phenyl indole were found to produce large quantities of the desired perfluorohexyl and perfluorooxy analogues as observed by both ¹H NMR and GC/MS however these molecules generated large concentrations of fluorinated byproducts which rendered separation of the products impossible. Furthermore, we tested this methodology on caffeine (**Scheme 2.5**), obtaining a lower yield of products **15b** and **c**, due to its less electron-rich nature²⁶. However, this yield is concordant with other radical innate functionalizations reported in the literature, showing the potential of these reagents as late-stage functionalization agents.^{26, 27} For a trend in reactivity, a more comprehensive scope of arenes and heteroarenes has been explored with the innate trifluoromethylation methodology previously reported by our group.¹

Table 2.2: Optimization for the perfluoroalkylation of aromatics under UV light.

Entry ^a	Equiv. reagent	Vol. MeCN (mL)	Time (h)	Filter (nm)	NMR yield (%) ^c
1	1	0.75	6	>295	20
2	2	0.75	6	>280	25
3	3	0.75	6	>295	35
4	1	0.75	12	>295	20
5	1	0.75	6	No filter	20
6	1	0.75	24	CFL ^b	Traces
7	1	0.75	18	>295	20
8	1	0.50	6	>295	47
9	1	0.25	6	>280	47
10	2	0.25	6	>280	97
11	3	0.25	6	>295	97
12	2	0.25	4	>295	90
13	1	0.75	6	>295	36
14	2	0.5	6	>295	83

^aEntries 1-12 carried out with the perfluorohexyl analogue **1b**, entries 13 and 14, with the perfluorooctyl analogue **1c**; ^bCompact Fluorescent Lamp, 23W; ^cUsing dimethylsulfone as a standard



Scheme 2.5: Demonstrative scope for the perfluoroalkylation of aromatics. Isolated yields are shown in parentheses.

Conclusion

In summary, we have successfully developed a robust synthetic methodology for α -(perfluoroalkylsulfonyl)propiophenones, envisioned as a new members of photocleavable perfluoroalkylating reagents. In this work, we have demonstrated their scalability and applicability in the metal-, catalyst- and additive-free, redox- and pH-neutral perfluoroalkylation of electron-rich aromatics, as well as in the late-stage functionalization of small molecules such as caffeine, which is of great interest in the current literature.²⁸ In future work, we will explore the reach and applicability of these reagents for the functionalization of compounds of interest in academia and industry, namely, for the synthesis of molecules with novel properties in the fields of material and bioorganic chemistry.

Experimental

All detailed experimental procedures and compound characterization data can be found in the supporting information.

CCDC 2163755 contains the supplementary crystallographic data byproduct B (perfluorooctyl analogue). These data can be obtained free of charge through the Cambridge Crystallographic Data Center (www.ccdc.cam.ac.uk/data_request/cif).

Acknowledgements

We gratefully acknowledge the McGill Chemistry Characterization Facility (MC²) for their contribution to this work, especially Robin Stein and Tara Sprules on the NMR data, Hatem Titi on SCXRD interpretation, Nadim Saadé and Alexander Wahba on HRMS, and Petr Fiurasek and Ehsan Hamzehpoor on UV-Vis spectroscopy.

Funding

The authors acknowledge the Canada Research Chair (Tier I) foundation, the E.B. Eddy endowment fund, the CFI, NSERC, and FQRNT for support of our research. DJCP acknowledges the financial support granted by the Vanier Canada Graduate Scholarships, CONACYT Mexico, and the Richard H. Tomlinson Fellowship.

References

- (1) Liu, P.; Liu, W.; Li, C.-J. Catalyst-Free and Redox-Neutral Innate Trifluoromethylation and Alkylation of Aromatics Enabled by Light. *J. Am. Chem. Soc.* **2017**, *139* (40), 14315-14321.
- (2) Glüge, J.; Scheringer, M.; Cousins, I. T.; DeWitt, J. C.; Goldenman, G.; Herzke, D.; Lohmann, R.; Ng, C. A.; Trier, X.; Wang, Z. An overview of the uses of per- and polyfluoroalkyl substances (PFAS). *Environ. Sci. Process Impacts* **2020**, *22* (12), 2345-2373.
- (3) Tiers, G. V. D. Perfluoroalkylation of aromatic compounds. *J. Am. Chem. Soc.* **1960**, *82* (20), 5513-5513.
- (4) McLoughlin, V. C. R.; Thrower, J. A route to fluoroalkyl-substituted aromatic compounds involving fluoroalkylcopper intermediates. *Tetrahedron* **1969**, *25* (24), 5921-5940.
- (5) Castillo-Pazos, D. J.; Lasso, J. D.; Li, C.-J. Modern methods for the synthesis of perfluoroalkylated aromatics. *Org. Biomol. Chem.* **2021**, *19* (33), 7116-7128.
- (6) Barata-Vallejo, S.; Bonesi, S. M.; Postigo, A. Perfluoroalkylation reactions of (hetero)arenes. *RSC Adv.* **2015**, *5* (77), 62498-62518.
- (7) Postigo, A. Electron Donor-Acceptor Complexes in Perfluoroalkylation Reactions. *Eur. J. Org. Chem.* **2018**, *2018* (46), 6391-6404.
- (8) Barata-Vallejo, S.; Cooke, M. V.; Postigo, A. Radical Fluoroalkylation Reactions. *ACS Catal.* **2018**, *8* (8), 7287-7307.
- (9) Yerien, D. E.; Lantano, B.; Barata-Vallejo, S.; Postigo, A. Catalytic Fluoroalkylation Reactions of Alkoxy-substituted (Hetero)Arenes. *ChemCatChem* **2021**, *13* (21), 4497-4506.
- (10) These properties are usually reflected in the material safety data sheet of any of these building blocks. For example: Perfluorooctyl iodide, MSDS No. P286505; Toronto Research Chemicals: Toronto, ON, 2020. <https://www.trc-canada.com/product/img/MSDS/P286505MSDS.pdf> (accessed 05/24/2022)
- (11) Zimmerman, H. E. H., K.G; Licke, G.C. . Mechanistic organic photochemistry. XXXII. Stereochemistry and mechanism of photochemical interconversion of cis-and trans-5,6-diphenylbicyclo[3.1.0] hexan-2-ones. *J. Am. Chem. Soc.* **1968**, *90*.

- (12) Sheehan, J. C.; Wilson, R. M.; Oxford, A. W. Photolysis of methoxy-substituted benzoin esters. Photosensitive protecting group for carboxylic acids. *J. Am. Chem. Soc.* **1971**, *93* (26), 7222-7228.
- (13) Sheehan, J. C.; Wilson, R. M. Photolysis of Desyl Compounds. A New Photolytic Cyclization. *J. Am. Chem. Soc.* **1964**, *86* (23), 5277-5281.
- (14) Song, H. Research progress on trifluoromethyl-based radical reaction process. *IOP Conference Series: Earth and Environmental Science* **2017**, *100*, 012061.
- (15) Fujiwara, Y.; Dixon, J. A.; O'Hara, F.; Funder, E. D.; Dixon, D. D.; Rodriguez, R. A.; Baxter, R. D.; Herlé, B.; Sach, N.; Collins, M. R.; et al. Practical and innate carbon-hydrogen functionalization of heterocycles. *Nature* **2012**, *492* (7427), 95-99.
- (16) O'Hara, F.; Blackmond, D. G.; Baran, P. S. Radical-Based Regioselective C-H Functionalization of Electron-Deficient Heteroarenes: Scope, Tunability, and Predictability. *J. Am. Chem. Soc.* **2013**, *135* (32), 12122-12134.
- (17) Fujiwara, Y.; Baran, P. S. Radical-Based Late Stage C-H Functionalization of Heteroaromatics in Drug Discovery. In *New Horizons of Process Chemistry: Scalable Reactions and Technologies*, Tomioka, K., Shioiri, T., Sajiki, H. Eds.; Springer Singapore, 2017; pp 103-120.
- (18) Aziz, J.; Hamze, A. An update on the use of sulfinato derivatives as versatile coupling partners in organic chemistry. *Org. Biomol. Chem.* **2020**, *18* (45), 9136-9159.
- (19) Liang, S.; Hofman, K.; Friedrich, M.; Manolikakes, G. Recent Advances in the Synthesis and Direct Application of Sulfinato Salts. *Eur. J. Org. Chem.* **2020**, *2020* (30), 4664-4676.
- (20) Huang, X.-T.; Long, Z.-Y.; Chen, Q.-Y. Fluoroalkylation of aromatic compounds with per(poly)fluoroalkyl chlorides initiated by sodium dithionite in DMSO. *J. Fluorine Chem.* **2001**, *111* (2), 107-113.
- (21) Weiyuan, H.; Bingnan, H.; Wei, W. Studies on sulfinato-dehalogenation iii. the sulfinato-dehalogenation of primary perfluoroalkyl iodides and α,ω -perfluoroalkylene diiodides by sodium dithionite. *Acta Chim. Sinica* **1985**, *43* (7), 663-668.
- (22) Cao, H.-P.; Chen, Q.-Y. Practical and efficient synthesis of perfluoroalkyl iodides from perfluoroalkyl chlorides via modified sulfinatodehalogenation. *J. Fluorine Chem.* **2007**, *128* (10), 1187-1190.

- (23) Dmowski, W.; Piasecka-Maciejewska, K. An easy preparation of per- and poly-fluoroalkyl propenyl sulfones. *J. Fluorine Chem.* **2005**, *126* (6), 877-882.
- (24) Finkelstein, H. Darstellung organischer Jodide aus den entsprechenden Bromiden und Chloriden. *Ber. Dtsch. Chem. Ges.* **1910**, *43* (2), 1528-1532.
- (25) Li, L.; Liu, W.; Zeng, H.; Mu, X.; Cosa, G.; Mi, Z.; Li, C.-J. Photo-induced Metal-Catalyst-Free Aromatic Finkelstein Reaction. *J. Am. Chem. Soc.* **2015**, *137* (26), 8328-8331.
- (26) Beatty, J. W.; Douglas, J. J.; Cole, K. P.; Stephenson, C. R. J. A scalable and operationally simple radical trifluoromethylation. *Nat. Comm.* **2015**, *6* (1), 7919.
- (27) Yin, D.; Su, D.; Jin, J. Photoredox Catalytic Trifluoromethylation and Perfluoroalkylation of Arenes Using Trifluoroacetic and Related Carboxylic Acids. *Cell Rep. Phys. Sci.* **2020**, *1* (8), 100141.
- (28) Lasso, J. D.; Castillo-Pazos, D. J.; Li, C.-J. Green chemistry meets medicinal chemistry: a perspective on modern metal-free late-stage functionalization reactions. *Chem. Soc. Rev.* **2021**, *50* (19), 10955-10982.

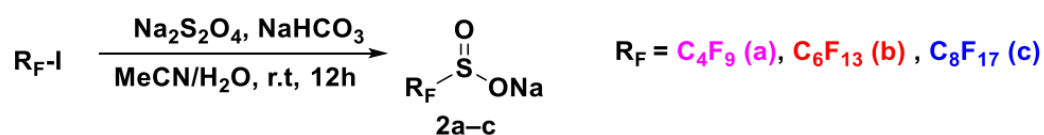
Supporting Information

1. General experimental procedures:

All reactions were carried out under argon atmosphere using standard Schlenk technique. ^1H NMR (500 MHz), ^{13}C NMR (126 MHz) and ^{19}F NMR (471 MHz) were recorded on an NMR spectrometer with CDCl_3 or d^6 -acetone as the solvent. Chemical shifts of ^1H , ^{13}C and ^{19}F NMR spectra are reported in parts per million (ppm). The residual solvent signals were used as references and the chemical shifts were converted to the TMS scale (CDCl_3 : $\delta \text{H} = 7.26$ ppm, $\delta \text{C} = 77.16$ ppm). All coupling constants (J values) are reported in Hertz (Hz). High-resolution mass spectrometry was conducted through using atmospheric pressure chemical ionization (APCI) or electro-spraying ionization (ESI), and was performed at McGill University on a Thermo-Scientific Exactive Orbitrap. Protonated molecular ions $[\text{M}+\text{H}]^+$ or sodium adducts $[\text{M}+\text{Na}]^+$ were used for empirical formula confirmation. Column chromatography was performed either on silica gel 200–300 mesh, or on C8-reversed phase perfluorinated silica gel.

2. General procedure for the synthesis of the perfluoroalkylating reagents 1a-c (alkyl chains: $-\text{C}_8\text{F}_{17}$, $-\text{C}_6\text{F}_{13}$, $-\text{C}_4\text{F}_9$)

2.1 Step 1: Synthesis of sodium perfluoroalkyl sulfinates 2a-c



The reaction was performed in an open 100 mL flask with a magnetic stir bar. Sodium dithionite (5.22 g, 30 mmol) and sodium bicarbonate (2.0 g, 24 mmol) were suspended in a water-acetonitrile solution (2:1, 45 mL) cooled with a bath of ice and salt. Then, 25 mmol of the corresponding perfluoroalkyl iodide (perfluorooctyl-, perfluorohexyl-, perfluorobutyl-) were added. The reaction was left overnight to reach ambient temperature.¹ During this time, the generation of gas (carbon and sulfur dioxides) is

observed, and the solution turns from colorless to pale transparent yellow with no presence of suspended salts.

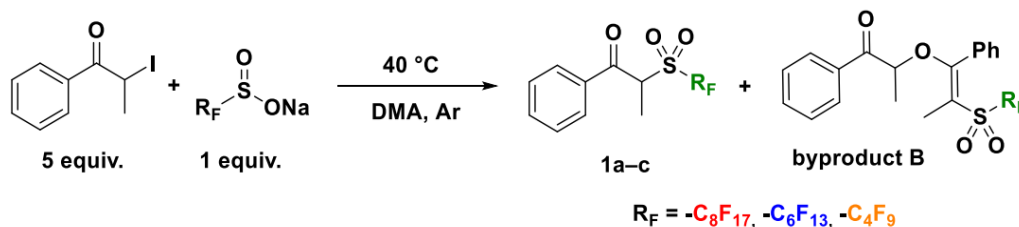
Once the reaction finished, the crude was evaporated to dryness while stirring at 82–100 °C. The solids at the bottom of the flask were washed with acetone until the fractions collected were colorless and passed through a fritted glass filter. For perfluorohexyl (**2b**) and perfluorooctyl sulfinate (**2c**) salts, the collected acetone fractions were evaporated with a rotary evaporator and under high vacuum to yield a pale-yellow solid that was later recrystallized from acetonitrile to give the final sodium sulfinate salt as a white crystalline salt. The crude sodium perfluorobutyl sulfinate (**2a**), was too soluble in acetonitrile and was instead washed with DCM until colorless on a fritted glass filter and allowed to dry. Isolated yields might range from quantitative to 50%, depending on the correct performance of the recrystallization step.

2.2 Step 2: Synthesis of 2-iodopropiophenone (**6**)



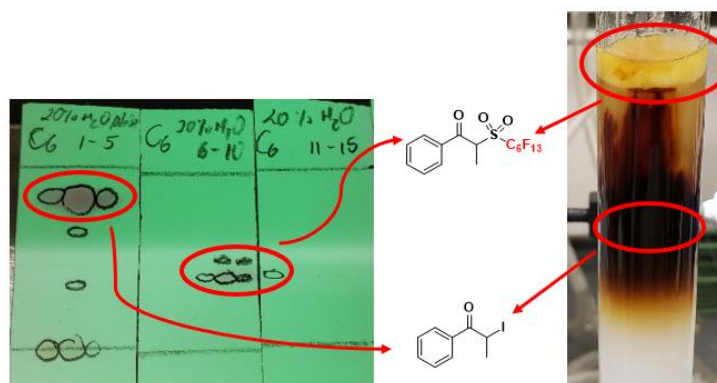
A solution of 20 mmol of sodium iodide (3.0 g) in 50 mL of acetone was stirred in a 100 mL open flask at room temperature for one or two minutes until saturation of the salt was evidenced by the appearance of a pale-yellow color. 2-bromopropiophenone (2.13 g, 10 mmol) was added dropwise while stirring vigorously, leading to the formation of a cloudy yellow suspension due to the precipitation of sodium bromide (Finkelstein reaction).² After 15 minutes, acetone was evaporated on a rotary evaporator and the product was extracted 3 times with ethyl acetate, washed with brine, and dried over anhydrous sodium sulfate. If the solution turned to a darker tone of brown, washing with saturated sodium thiosulfate would suffice to eliminate the forming iodine. The dried organic phases were evaporated to give a yellow oil in quantitative yield. The resulting product is sensitive to light and was typically synthesized for use on same day.

2.3 Step 3: Synthesis of the perfluoroalkyl-2-sulfonyl-1-1-phenylethanones 1a-c

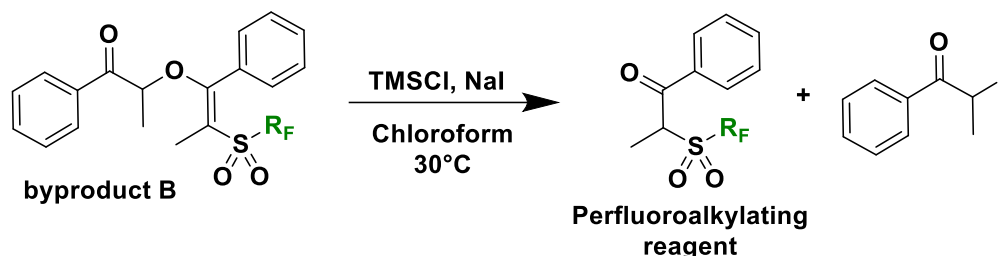


In a 25 mL flask equipped with a stirring bar, 3 mmol of the corresponding sodium sulfinate and 5 equivalents of 2-iodopropiophenone (13 g) were dissolved into 5 mL of dried DMA. The reaction was stirred vigorously for 16 h at 40°C under inert atmosphere. Over time, the reaction turned black due to the generation of iodine in solution. Once it was finished, the reaction was quenched with 30 mL of water, and the product was extracted with ethyl acetate (3x10 mL). The organic fractions were collected, washed with saturated sodium thiosulfate and brine, and evaporated. The excess of 2-iodopropiophenone was separated from the desired product through a C8 perfluorinated silica plug (40 g) using the following gradient: methanol/water (2:1) → methanol → acetone. The methanol and acetone fractions were collected and evaporated to give a clean mixture products **1a-c** and byproduct B (2:1, respectively) as a white powder. Isolated yield of the product at this stage can be up to 50%. The reaction demonstrated a scalability of up to 6 grams of product. Recycling of excess 2-iodopropiophenone utilized can be achieved by silica column with a gradient of 0% to 10% ethyl acetate in hexanes.

Note: When running the crude through the perfluorinated silica plug, constant pressure must be maintained for optimal separation. A successful separation is shown below:

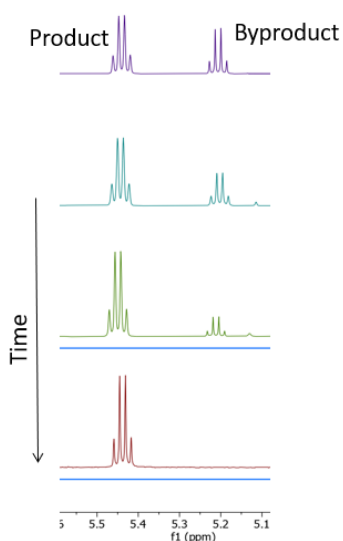


2.4 Step 4: Conversion of byproduct B



In a 50 mL flask, dissolve the mixture obtained in step 3 in the minimum amount possible of chloroform (to form a solution around 0.4 M). While stirring vigorously, add 5 equivalents of chlorotrimethylsilane and 5 equivalents of sodium iodide (calculated against the amount of byproduct B detected by NMR). Monitor the reaction at 30°C until completion (approximately 1-3 hours) and wash with one portion of each: saturated bicarbonate solution, saturated sodium thiosulfate solution, and brine. After evaporating the chloroform on a rotary evaporator, the crude is purified through a C8 perfluorinated silica plug (40 g) using the following gradient: methanol/water (2:1) → methanol → acetone. The methanol and acetone fractions are collected and evaporated to give the final perfluoroalkylating reagent as a white powder. Isolated yield of the product at this final stage can be up to 70%.

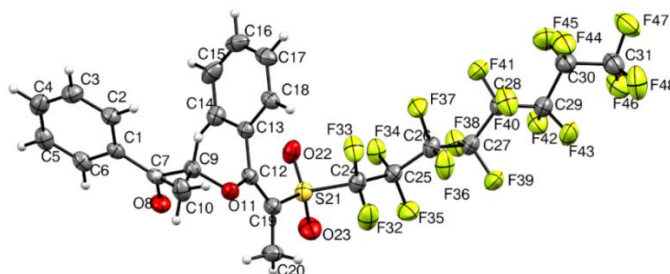
The most efficient way of monitoring the amount of byproduct present in the crude (if any) is to trace the proton in the alpha position through NMR as shown in the right:



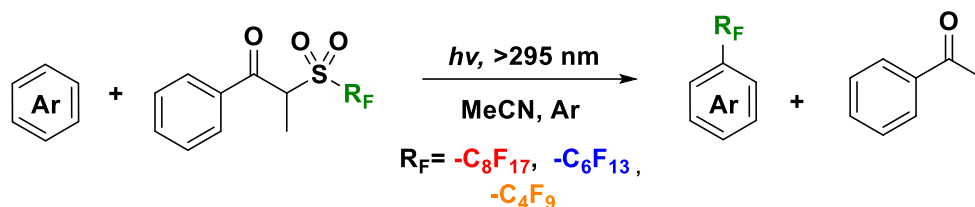
2.5 Single-crystal X-Ray Diffraction of byproduct B (perfluorooctyl analogue)

The byproduct was separated via column chromatography (100% toluene) and recrystallized from methanol over the course of 3 days at 4 °C to yield colorless needles. A Bruker D8 Advance powder X-ray diffractometer was used for the structure refinement and collection of the following crystal data:

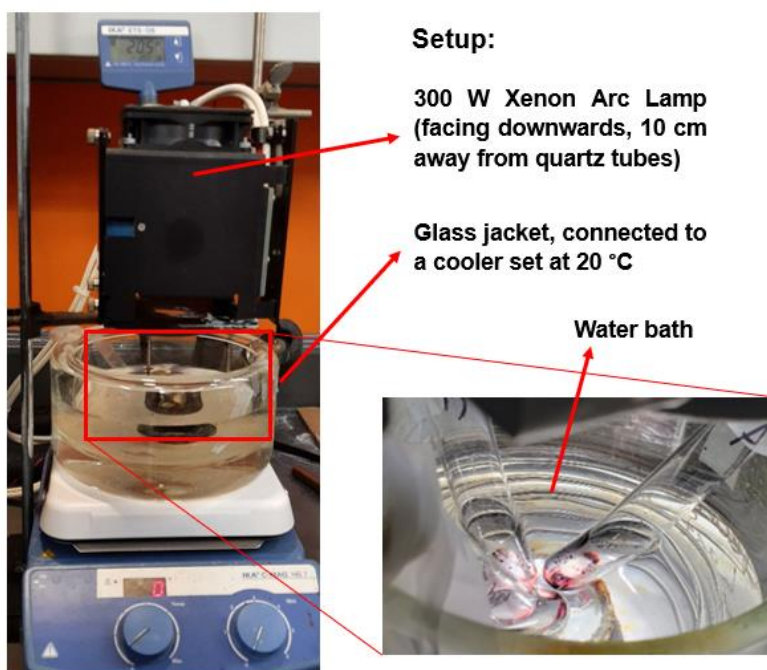
Empirical formula: C ₂₆ H ₁₇ F ₁₇ O ₄ S	Crystal size/mm ³ 0.540 × 0.320 × 0.310
Formula weight: 748.46	Radiation CuKα (λ = 1.54178)
Temperature/K: 180(2)	2θ range for data collection/° 7.416 to 144.608
Crystal system: monoclinic	Index ranges -58 ≤ h ≤ 58, -10 ≤ k ≤ 10, -12 ≤ l ≤ 17
Space group: C2/c	Reflections collected: 53403
a/Å: 47.7488(17)	Independent reflections: 5678 [Rint = 0.0485, Rsigma = 0.0260]
b/Å: 8.7035(3)	Data/restraints/parameters: 5678/0/435
c/Å: 14.0715(5)	Goodness-of-fit on F ² : 1.042
α/°: 90, β/°: 93.0800(10), γ/°: 90	Final R indexes [I ≥ 2σ (I)] R1 = 0.0406, wR2 = 0.1067
Volume/Å ³ : 5839.4(4)	Final R indexes [all data] R1 = 0.0427, wR2 = 0.1090
Z: 8	Largest diff. peak/hole / e Å ⁻³ 0.28/-0.37
ρ _{calc} /cm ³ : 1.703	
μ/mm ⁻¹ : 2.329	
F(000): 2992.0	



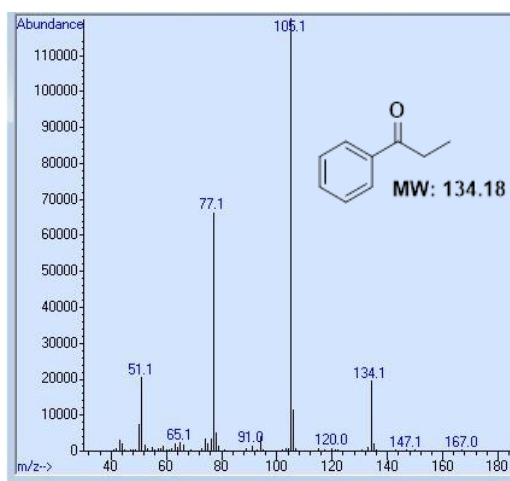
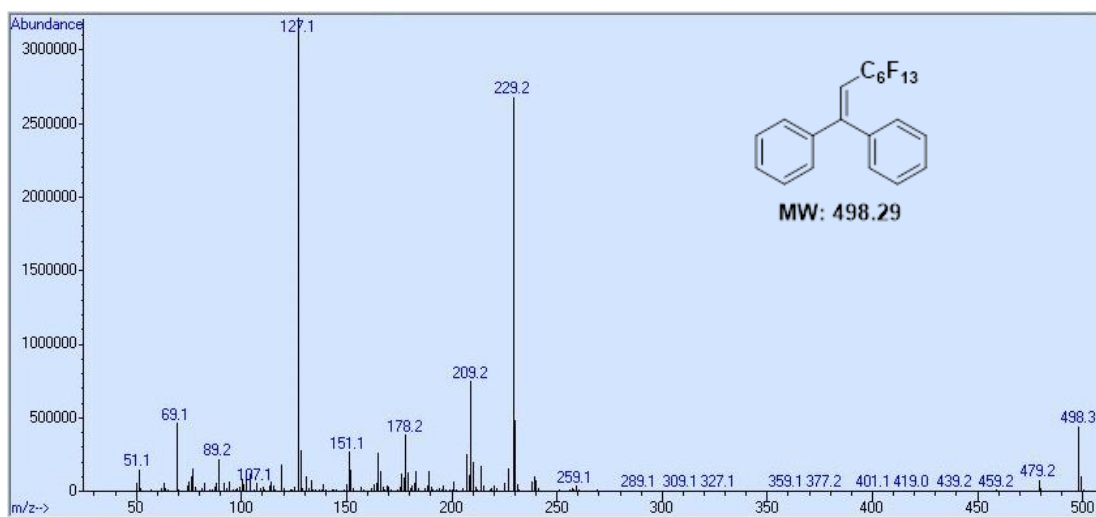
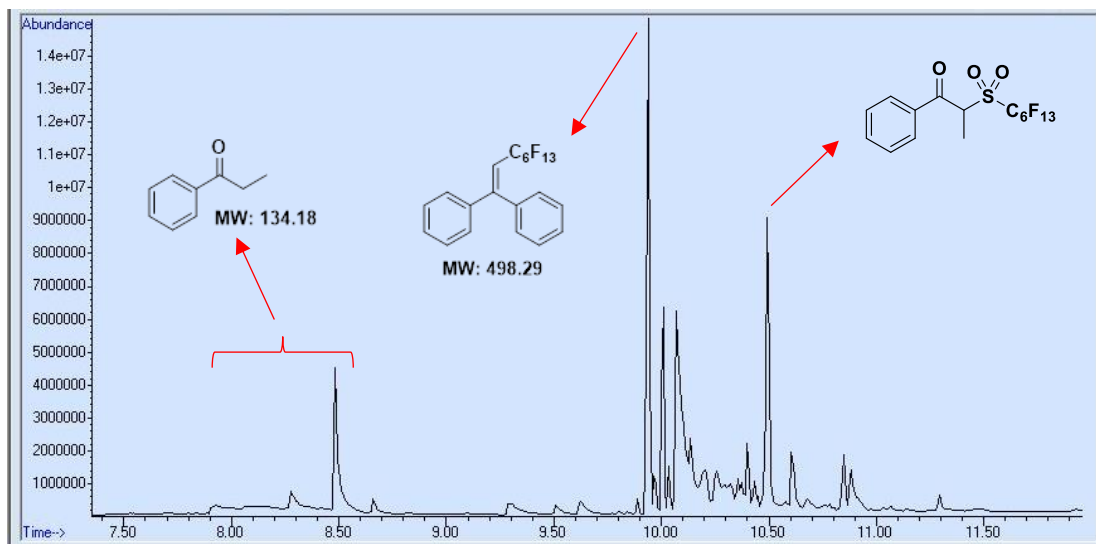
3. General procedure for the perfluoroalkylation of aromatics



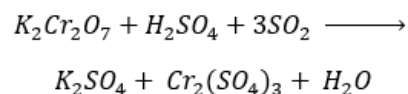
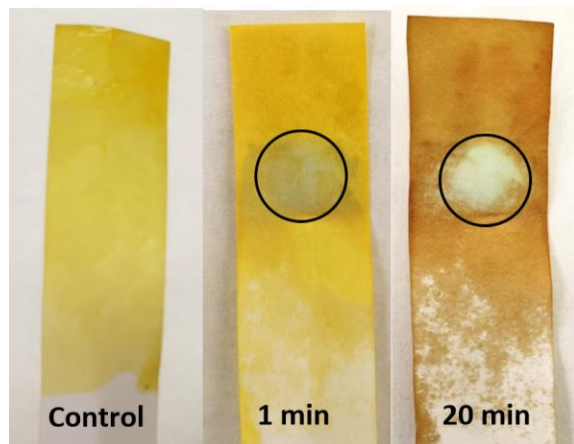
The aromatic substrate (0.1 mmol) and corresponding perfluoroalkylating reagent **1** (0.15-0.2 mmol) were added into 0.5 mL acetonitrile inside an air-tight quartz. Three freeze-pump-thaw cycles were carefully performed before setting the reaction under light irradiation at 20°C using a 300 W xenon lamp. Temperature was controlled by a cold-water bath in a jacketed glass container connected to a cooler. After the reaction was finished (4-12 h), the product diluted with dichloromethane or acetone, evaporated under reduced pressure, and purified through a C8 perfluorinated silica plug (10-20 g) using the following gradient: methanol/water (2:1) → methanol → acetone. Methanol and acetone fractions were collected and evaporated to give the final product. An alternative purification method consists of preparative thin-layer chromatography, using ethyl acetate/hexanes or dichloromethane/hexanes as the eluent.



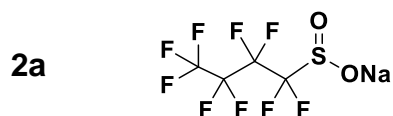
3.1 Mechanistic evidence



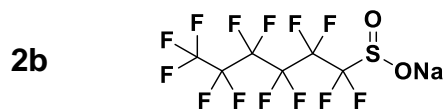
Detection of sulfur dioxide: A paper strip was coated in an acidic solution of potassium dichromate and was used to cap a needle that punctured the sealed reaction vessel. Over the course of 20 min, a blue-green coloration developed in the exposed area, indicating the presence of SO₂



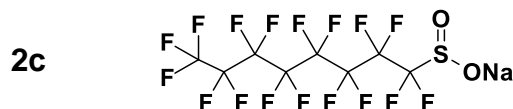
4. Characterization data of reported compounds:



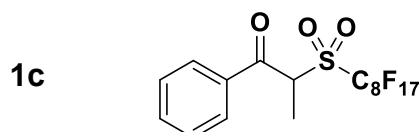
Sodium perfluorobutylsulfinate (2a)³: White crystals. Yield: 54%. ¹⁹F NMR (471 MHz, Acetone) δ -81.90 – -82.00 (m), -124.32 (dd, *J* = 14.6, 7.3 Hz), -127.01 – -127.12 (m), -132.58 (td, *J* = 10.5, 9.1, 6.5 Hz). HRMS: *m/z* = 282.94816, theoretical = 282.94808.



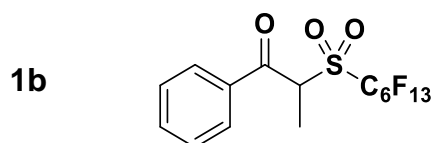
Sodium perfluorohexylsulfinate (2b)³: White crystals. Quantitative yield (highly dependent on workup conditions). ¹⁹F NMR (471 MHz, Acetone) δ -81.58 – -81.85 (m), -115.16 – -115.45 (m), -121.11, -122.36, -123.36, -126.78 (ddd, *J* = 18.8, 11.1, 5.5 Hz). HRMS: *m/z* = 382.94052, theoretical = 382.94169.



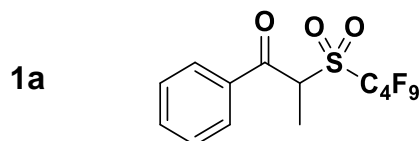
Sodium perfluorooctylsulfinate (2c)⁴: White crystals. Quantitative yield (highly dependent on workup conditions). ¹⁹F NMR (471 MHz, Acetone) δ -81.67 (t, J = 10.1 Hz), -122.55 (d, J = 12.7 Hz), -123.26 (d, J = 19.5 Hz), -126.74, -132.39. HRMS: m/z = 482.93492, theoretical = 382.93530.



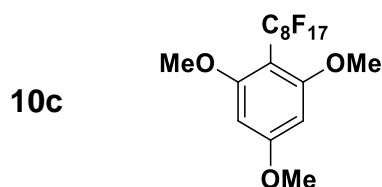
2-((perfluorooctyl)sulfonyl)-1-phenylpropan-1-one (1c): White powder. 75% yield. ¹H NMR (500 MHz, CDCl₃) δ 8.00 – 7.94 (m, 2H), 7.72 – 7.65 (m, 1H), 7.58 – 7.51 (m, 2H), 5.42 (q, J = 7.0 Hz, 1H), 1.84 (dd, J = 7.0, 1.0 Hz, 3H). ¹³C NMR (126 MHz, Acetone) δ 155.2, 150.9, 146.9, 136.5, 134.0, 128.7, 110.3, 33.4, 27.2. ¹⁹F NMR (471 MHz, CDCl₃) δ -80.76, -109.18, -119.94, -121.36, -121.69, -121.90, -122.72, -126.11.



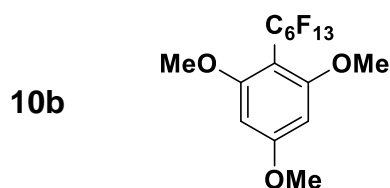
2-((perfluorohexyl)sulfonyl)-1-phenylpropan-1-one (1b): White powder. 66% yield. ¹H NMR (500 MHz, CDCl₃) δ 8.02 – 7.96 (m, 2H), 7.75 – 7.68 (m, 1H), 7.61 – 7.54 (m, 2H), 5.44 (q, J = 7.0 Hz, 1H), 1.87 (d, J = 7.0 Hz, 3H). ¹³C NMR (126 MHz, CDCl₃) δ 188.8, 135.0, 134.9, 129.2, 128.9, 61.8, 13.1. ¹⁹F NMR (471 MHz, CDCl₃) δ -80.72 (t, J = 10.0 Hz), -109.19 (t, J = 14.9 Hz), -119.97 (ddt, J = 30.5, 18.6, 7.6 Hz), -121.59 (d, J = 22.6 Hz), -122.50 – -122.72 (m), -126.05 (ddq, J = 14.3, 10.9, 4.0 Hz).



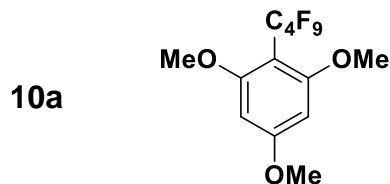
2-((perfluorobutyl)sulfonyl)-1-phenylpropan-1-one (1a): Yellow solid (melts at room temperature). 30% yield. ^1H NMR (500 MHz, Acetone) δ 8.20 – 8.14 (m, 4H), 7.82 – 7.74 (m, 2H), 7.68 – 7.61 (m, 4H), 6.19 – 6.11 (m, 1H), 1.90 – 1.84 (m, 3H), 1.86 (s, 3H), 1.31 (s, 2H), 0.90 (t, J = 6.3 Hz, 1H). ^{19}F NMR (471 MHz, Acetone) δ -81.56 – -81.68 (m), -110.44 – -110.62 (m), -121.70 – -121.91 (m), -126.52 (td, J = 14.6, 14.1, 7.0 Hz).



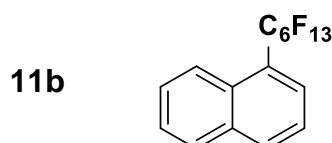
2-(perfluorooctyl)-1,3,5-trimethoxybenzene (10c)⁵: White solid. 60% yield. ^1H NMR (500 MHz, CDCl_3) δ 6.17 (s, 2H), 3.86 (s, 3H), 3.83 (s, 6H). ^{13}C NMR (126 MHz, CDCl_3) δ 163.8, 161.7, 161.7, 91.7, 56.2, 55.2. ^{19}F NMR (471 MHz, CDCl_3) δ -80.88 (t, J = 10.0 Hz), -102.51 – -102.80 (m), -121.61 – -121.91 (m), -121.91 – -122.21 (m), -122.75 (dq, J = 26.7, 13.2, 11.2 Hz), -126.18 (dq, J = 14.5, 6.6 Hz).



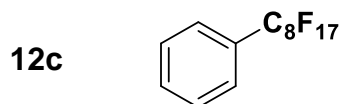
2-(perfluorohexyl)-1,3,5-trimethoxybenzene (10b)⁵: White solid. 62% yield. ^1H NMR (500 MHz, CDCl_3) δ 6.17 (s, 2H), 3.86 (s, 3H), 3.83 (s, 6H). ^{13}C NMR (126 MHz, CDCl_3) δ 163.8, 161.7, 91.7, 56.3, 55.3. ^{19}F NMR (471 MHz, CDCl_3) δ -80.78 – -80.98 (m), -102.56 – -102.72 (m), -122.03 – -122.33 (m), -122.69 (qd, J = 16.8, 13.2, 5.7 Hz), -126.17 (td, J = 14.3, 6.4 Hz).



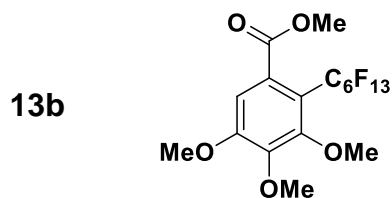
2-(perfluorobutyl)-1,3,5-trimethoxybenzene (10a)⁵: White solid. 42% yield. ¹H NMR (500 MHz, CDCl₃) δ 6.17 (d, *J* = 1.0 Hz, 2H), 3.86 (s, 3H), 3.83 (s, 6H). ¹³C NMR (126 MHz, CDCl₃) δ 163.8, 161.7, 91.7, 56.3, 55.3. ¹⁹F NMR (471 MHz, CDCl₃) δ -80.89 – -81.05 (m), -102.83 (td, *J* = 13.6, 3.0 Hz), -122.97 (pq, *J* = 10.2, 4.6 Hz), -126.33 – -126.48 (m).



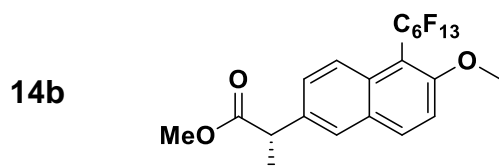
1-perfluorohexylnaphthalene (11b): White solid. 72% yield. ¹H NMR (500 MHz, CDCl₃) δ 8.26 (d, *J* = 8.7 Hz, 1H), 8.09 (d, *J* = 8.2 Hz, 1H), 7.95 (dt, *J* = 9.1, 2.7 Hz, 1H), 7.86 (dd, *J* = 7.4, 1.2 Hz, 1H), 7.67 – 7.56 (m, 3H). ¹³C NMR (201 MHz, CDCl₃) δ 134.1, 133.43, 130.2, 129.0, 128.0, 127.6, 127.1, 126.3, 124.8, 124.2. ¹⁹F NMR (471 MHz, CDCl₃) δ -80.77, -104.42, -120.26, -121.46, -122.73, -126.07.



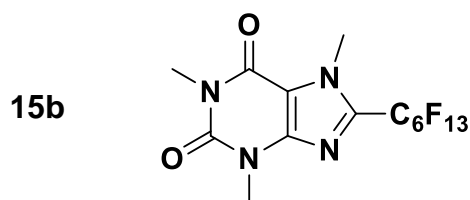
Perfluorooctylbenzene (12c): Yellow oil. 68% yield. ¹H NMR (500 MHz, CDCl₃) δ 7.64 – 7.57 (m, 3H), 7.53 (t, *J* = 7.6 Hz, 2H). ¹³C NMR (201 MHz, CDCl₃) δ 131.9, 128.6, 126.7. ¹⁹F NMR (471 MHz, CDCl₃) δ -80.81, -110.73, -121.27, -121.90, -122.73, -126.19.



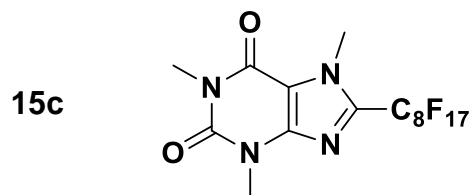
Methyl 3,4,5-trimethoxy-2-(perfluorohexyl)benzoate (13b)⁶: White solid. 64% yield. ¹H NMR (500 MHz, CDCl₃) δ 6.78 (s, 1H), 3.94 (d, *J* = 1.5 Hz, 6H), 3.91 (s, 3H), 3.89 (s, 3H). ¹³C NMR (201 MHz, CDCl₃) δ 168.6, 156.1, 153.9, 144.0, 136.8, 136.1, 133.3, 132.9, 130.1, 128.7, 128.6, 128.5, 128.4, 107.3, 61.9, 60.8, 56.2, 52.8. ¹⁹F NMR (471 MHz, CDCl₃) δ -80.74, -100.99.



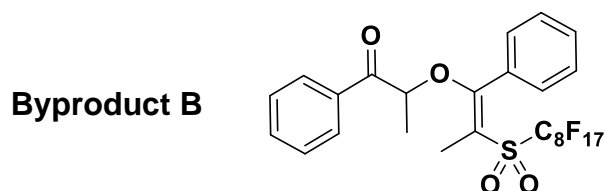
Naproxen methyl ester-C₆F₁₃ (14b): White solid. 20% yield. ¹H NMR (800 MHz, CDCl₃) δ 8.15 (d, *J* = 9.2 Hz, 1H), 7.98 (d, *J* = 9.1 Hz, 1H), 7.70 (d, *J* = 2.1 Hz, 1H), 7.49 (dd, *J* = 9.2, 2.1 Hz, 2H), 7.34 (d, *J* = 9.1 Hz, 1H), 3.97 (s, 3H), 3.87 (q, *J* = 7.3 Hz, 1H), 3.68 (s, 3H), 1.58 (d, *J* = 7.1 Hz, 5H). ¹³C NMR (201 MHz, CDCl₃) δ 174.7, 159.0, 136.1, 134.9, 131.3, 129.4, 126.8, 125.1, 114.6, 57.4, 52.1, 44.9, 18.3. ¹⁹F NMR (471 MHz, CDCl₃) δ -80.72, -100.17, -120.67, -121.94, -122.61, -126.06.



Caffeine-C₆F₁₃ (15b)⁷: White solid. 25% yield. ¹H NMR (500 MHz, Acetone) δ 4.26 (t, *J* = 2.0 Hz, 6H), 3.51 (s, 6H), 3.33 (s, 6H), 2.10 (d, *J* = 1.2 Hz, 1H), 1.31 (s, 1H). ¹³C NMR (126 MHz, Acetone) δ 155.2, 150.9, 146.9, 129.5, 128.4, 110.3, 33.4, 27.2. ¹⁹F NMR (471 MHz, Acetone) δ -81.51 – -81.84 (m), -81.71, -109.18 (t, *J* = 14.4 Hz), -121.34 – -121.70 (m), -121.84, -122.32, -123.28, -126.69 (ddq, *J* = 19.5, 11.7, 4.0 Hz).



Caffeine-C₈F₁₇ (15c)⁷: White solid. 23% yield. ¹H NMR (500 MHz, Acetone) δ 4.26 (t, *J* = 2.0 Hz, 3H), 3.52 (s, 3H), 3.33 (s, 3H). ¹⁹F NMR (471 MHz, Acetone) δ -81.64 (t, *J* = 10.3 Hz), -109.16 (t, *J* = 14.3 Hz), -121.27 – -121.80 (m), -122.22, -122.33, -123.21, -126.51 – -126.89 (m).



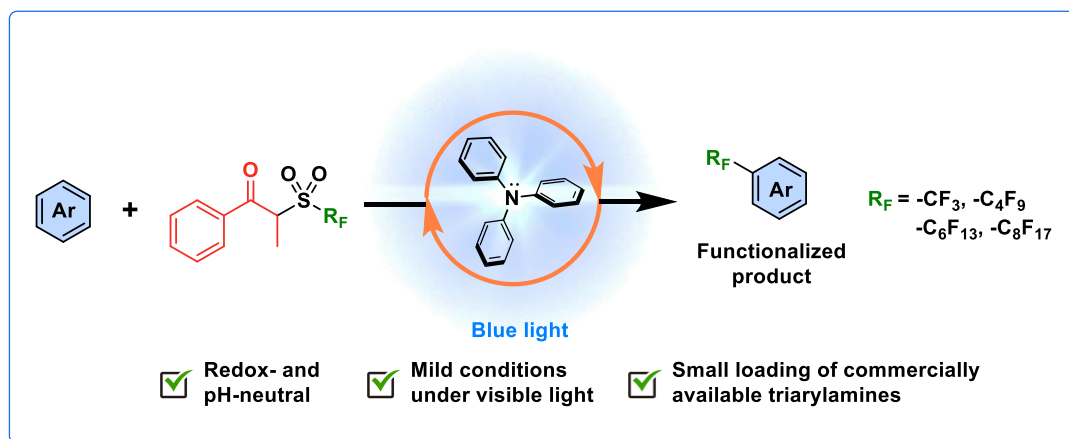
(E)-2-((2-((perfluorooctyl)sulfonyl)-1-phenylprop-1-en-1-yl)oxy)-1-phenylpropan-1-one (byproduct B): White solid. ¹H NMR (500 MHz, acetone) δ 7.58 – 7.54 (m, 2H), 7.45 – 7.41 (m, 2H), 7.37 (tt, *J* = 7.5, 1.3 Hz, 1H), 5.50 (q, *J* = 6.9 Hz, 1H), 2.33 (d, *J* = 0.8 Hz, 3H), 1.55 (d, *J* = 6.9 Hz, 3H). ¹³C NMR (126 MHz, acetone) δ 205.1, 197.0, 189.5, 173.10, 142.5 – 120.6 (m), 133.7, 130.2, 129.1, 129.0, 128.7, 127.8, 109.7, 77.1, 62.3, 17.9, 12.7, 12.7. ¹⁹F NMR (471 MHz, Acetone) δ -81.58 – -81.69 (m), -111.91 (dd, *J* = 17.3, 13.0 Hz), -120.88 (tt, *J* = 14.0, 5.5 Hz), -121.47 – -122.86 (m), -123.22, -126.02 – -128.00 (m).

References

- (1) Dmowski, W.; Piasecka-Maciejewska, K. An easy preparation of per- and poly-fluoroalkyl propenyl sulfones. *J. Fluorine Chem.* **2005**, *126* (6), 877-882.
- (2) Finkelstein, H. Darstellung organischer Jodide aus den entsprechenden Bromiden und Chloriden. *Ber. Dtsch. Chem. Ges.* **1910**, *43* (2), 1528-1532.
- (3) Hu, C.; Qing, F.; Huang, W. Reaction of perfluoroalkanesulfinates with allyl and propargyl halides. A convenient synthesis of 3-(perfluoroalkyl)prop-1-enes and 3-(perfluoroalkyl)allenes. *J. Org. Chem.* **1991**, *56* (8), 2801-2804.
- (4) Clavel, J.-L.; Langlois, B.; Nantermet, R.; Tordeux, M.; Wakselman, C. Reactions of bromotrifluoromethane and related halides. Part 12. Transformation of disulfides into perfluoroalkyl sulfides in the presence of sulfoxylate anion radical precursors. *J. Chem. Soc., Perkin Trans. 1* **1992**, (24), 3371-3375.
- (5) Tasnim, T.; Ryan, C.; Christensen, M. L.; Fennell, C. J.; Pitre, S. P. Radical Perfluoroalkylation Enabled by a Catalytically Generated Halogen Bonding Complex and Visible Light Irradiation. *Org. Lett.* **2022**, *24* (1), 446-450.
- (6) JP Patent: JPS5775932A
- (7) Wei, Z.; Qi, S.; Xu, Y.; Liu, H.; Wu, J.; Li, H.; Xia, C.; Duan, G. Visible Light-Induced Photocatalytic C–H Perfluoroalkylation of Quinoxalinones under Aerobic Oxidation Condition. *Adv. Synth. Catal.* **2019**, *361* (23), 5490-5498.

3 New Catalytic Pathways

Triarylamines as Catalytic Donors in Light-Mediated Electron Donor-Acceptor Complexes



Reproduced with permission from “Triarylamines as catalytic donors in light-mediated electron donor–acceptor complexes”, Castillo-Pazos, D.; Lasso, J.D.; Hamzehpoor, E.; Ramos-Sánchez, J.; Salgado, J.M.; Cosa, G.; Perepichka, D.F.; and Li, C.-J. *Chem. Sci.*, **2023**, 14, 3470-3481. Copyright 2023 Royal Society of Chemistry.

Preface

In Chapter 2, we provided an example of how desired reactivities and methodology modalities can be achieved through the design and development of new reagents. However, developing new synthetic paradigms through the study of new reaction mechanisms and novel catalytic pathways also constitutes a powerful instrument to address current needs in the field. Since 2008, the paradigm of photocatalysis has been represented by the use of iridium and ruthenium photocatalysts. These noble-metal complexes are well characterized regarding their photophysical behavior, making them ideal tools for the exploration of new light-promoted reactions. However, their use comes at the expense of caveats such as scarcity and high prices, poor accessibility, the need for subsequent removal.

In recent years, Electron Donor-Acceptor (EDA) complexes have witnessed a dramatic surge of interest as an alternative strategy to rival well-established photoredox methods in photocatalysis. EDA complexes have shifted the synthetic paradigm allowing organic chemists to perform photochemistry with substrates that do not absorb light independently. Despite this success, EDA systems are frequently limited by stoichiometric amounts of prudently chosen donor and acceptor components in which both components end in the product structure. Thus, it would be ideal to develop EDA complexes employing catalytic amounts of donors or acceptors to decouple photoactivation steps from substrate functionalization. In this strategy, the substrates are no longer restricted to structures containing specific moieties required to engage in complex formation, significantly increasing the versatility of EDA complex photochemistry.

However, such catalytic donors or acceptors are very scarce, requiring high amounts of additives, or immoderate reaction conditions to close their catalytic cycle. For this reason, in 2020 our group took on the task of exploring new efficient catalytic donors, that could be characterized by their accessibility, tunability, and low cost. Throughout this project, we established the capability of triarylamine, a well-known electron-donating scaffold used in organic optoelectronics, as a highly efficient and inexhaustibly tunable photocatalyst. During preliminary studies, we discovered an EDA complex between

commercially available triarylamine and the α -perfluorosulfonyl propiophenone reagents discussed in Chapter 2, catalyzing C–H perfluoroalkylation of arenes and heteroarenes under visible light irradiation in pH- and redox-neutral conditions. In this chapter, we describe the formation of such an EDA complex under the irradiation of blue light (427 nm) and the mechanism behind its successful turnover. Furthermore, we showcase the tunability of this scaffold to fine-tune the photocatalyst toward efficient trifluoromethylation of aromatic substrates. Lastly, we provide thorough photophysical characterization and mechanistic insight, a feature that filled an important gap in the literature of catalytic EDA systems at the time of publication.

Author contributions:

Durbis Castillo, Juan Lasso, and Prof. Chao-Jun Li conceived the catalytic system. Durbis Castillo and Juan Lasso conducted the experiments for optimization and scope. Ehsan Hamzehpour and Jorge Ramos performed all spectroscopic studies (UV Vis, EPR, fluorescence quenching, time-correlated single-photon counting spectra, and transient absorption measurements). Jan Michael Salgado helped validate the reproducibility of the experiments and purify the final products. Durbis Castillo wrote the manuscript, and all authors and coauthors contributed to data analysis and the revision of the manuscript. Prof. Chao-Jun Li, Prof. Gonzalo Cosa, and Prof. Dmytro Perepichka supervised the work, providing mentorship regarding mechanistic studies. Durbis Castillo, Juan Lasso, and Ehsan Hamzehpour contributed equally.

Abstract

Recently, photochemistry of Electron Donor-Acceptor (EDA) complexes employing catalytic amounts of electron donors have become of interest as a new methodology in the catalysis field, allowing for decoupling of the electron transfer (ET) from the bond-forming event. However, examples of practical EDA systems in the catalytic regime remain scarce, and their mechanism is not yet well-understood. Herein, we report the discovery of an EDA complex between triarylaminines and α -perfluorosulfonyl propiophenone reagents catalyzing C–H perfluoroalkylation of arenes and heteroarenes under visible light irradiation in pH- and redox- neutral conditions. We elucidate the mechanism of this reaction using a detailed photophysical characterization of the EDA complex, the resulting triarylamine radical cation, and its turnover event.

Introduction

Modern photocatalysis explores myriad ways of accelerating chemical reactions by channeling energy from a light source. Currently, the paradigm for light-powered reactions in industry and academia is mostly represented by the use of transition metal complexes—for example, iridium and ruthenium photocatalysts—which pose challenges of elevated cost and contamination of the final product with often toxic metals.¹ Therefore, it is highly desirable to find alternative photocatalytic approaches based on commercially available organic (metal-free) molecules. Complementary to the many advances in the field of organic photoredox catalysis in the last decade,^{2, 3} the synthetic potential of EDA complexes has become of great recent interest through the pioneering studies by Kochi and later by the groups of Melchiorre and Chatani.⁴⁻⁶

EDA complexes are formed by association of an electron donor molecule and an acceptor molecule in the ground state. They are characterized by a reduction of the HOMO-LUMO gap compared to individual components, and a new charge-transfer absorption band often appears in the UV-Vis spectra. Irradiation of EDA complexes with visible light can lead to a single-electron transfer (SET), which upon the irreversible cleavage of a leaving group in either the donor or the acceptor, can be exploited to trigger further radical reactivity.⁷ This SET enables new chemical transformations under mild conditions with substrates that do not absorb visible light without the need for an

exogenous photocatalyst. However, a caveat of traditional EDA-mediated synthetic platforms comprises the need for stoichiometric amounts of donor and acceptor, where both components end in the product structure.⁸⁻¹⁰ This drawback can be overcome by a catalytic approach to EDA complex formation, in which either the donor or acceptor is added in a catalytic amount, decoupling the complexation/photoactivation steps from the substrate functionalization.¹¹

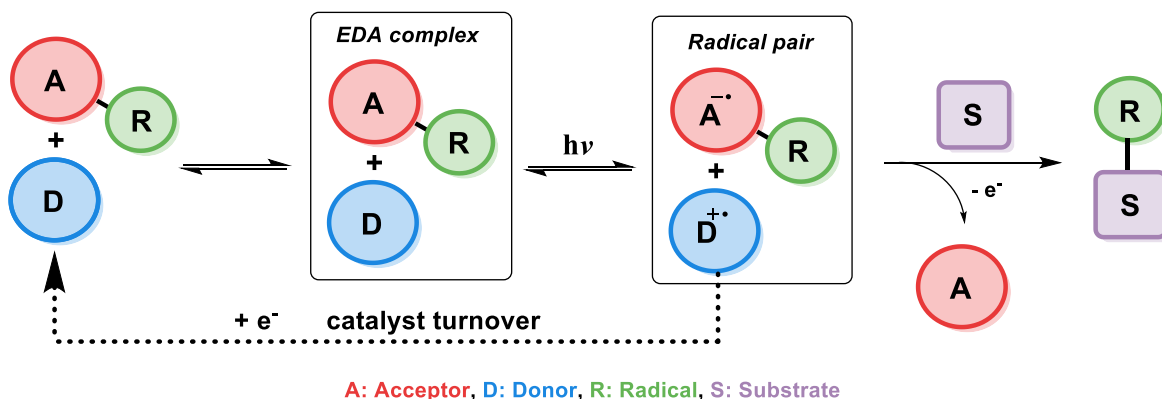
In 2019, Fu *et al.* reported a modified EDA-mediated system consisting of an electron-deficient acceptor (*N*-(acyloxy)phthalimides) in association with a catalytic donor (triphenylphosphine) and sodium iodide as an additive, where a substrate of interest traps the resulting radical species, and the donor is later regenerated by a one-electron reduction in a turnover event (**Figure 3.1a**).¹² Using this catalytic EDA-system they promoted the photodecarboxylative alkylation of silyl enol ethers and heteroaromatics. Since this seminal work, a limited number of catalytic donors for EDA-mediated transformations have been reported (**Figure 3.1b**), categorized into ionic and neutral EDA systems. Milestone examples of the former category include Melchiorre's decarboxylative Giese additions employing dithiocarboxylate anions,¹³ the use of tetramethylethylenediamine (TMEDA) and phosphonium iodide salts for the monofluoromethylation of alkenes,¹⁴ Stephenson's 2-methoxynaphthalene-mediated trifluoromethylation and alkylation of aromatics,¹⁵ and the synthesis of benzo[b]phosphine oxides by the photoredox catalyst Eosin Y.¹⁶ On the other hand, more scarce reports on neutral catalytic EDA systems include the quinuclidine-catalyzed aminodecarboxylation of tetrachlorophthalamide esters¹⁷ and hydroquinones/organophosphines in the halogen bonding-mediated modification of arenes and heterocycles.^{18, 19}

While all these reports showcase the expansion of the catalytic donor toolbox in the last three years, there still exist challenges that hamper their efficacy when compared to transition metal photocatalysts; for example, the instability of most donors in the catalytic cycle, the need for superstoichiometric amounts of additives (i.e. acids, bases, or inorganic salts), heating of the photoreaction solution, long reaction times (> 24 h), or catalyst loadings above 10 mol%. Therefore, it is important to explore new functionalities capable of addressing such limitations.

Triarylamines are among the most studied electron donors for their versatility, stability, and the easy tunability of the electronic levels by permutations of the aryl groups synthesized in one step by well-established methodologies. The parent molecule of this family, triphenylamine (TPA), is widely used in materials chemistry as a redox-active scaffold, spanning numerous applications such as dyes, semiconductors, or electrochemical redox mediators.²⁰⁻²⁴ In its ground state, TPA is also one of the least basic organic amines, making it compatible with a wide range of functional groups, useable in pH-neutral reactions, and orthogonal to acid-base processes within the same system.²⁵ However, until a recent report by Procter and co-workers²⁶—published after the preparation of this manuscript—, triarylamines remained unexplored as catalytic donors in a general synthetic platform for radical generation and functionalization of arenes. In their work, a naphthyldiphenylamine donor proved successful in the alkylation and cyanation of arenes from their corresponding thianthrenium salts. Nevertheless, in addition to their elegant C–H activation for the formation of aryl radicals—challenging to form without the use of highly reducing photoredox catalysts such as 10-phenylphenothiazine²⁷—, it would also be advantageous for the field to explore the capability of EDA catalytic triarylamine donors in the context of Minisci-type reactions onto aromatic substrates.²⁸

For the reasons exposed above, we were compelled to study triphenylamine—the simplest of triarylamines, until now synthetically relegated to cyclization and dimerization reactions—as a suitable catalytic donor that is not only readily available, economically accessible, and synthetically tunable; but also safe, efficient and obtainable from renewable feedstocks. In this work, we describe the design of an EDA system utilizing TPA as a catalytic donor and study the mechanism behind its association with a propiophenone redox tag as a suitable acceptor for the first time. Additionally, we explore the catalytic turnover ability of triarylamines towards the innate perfluoroalkylation and trifluoromethylation of electron-rich arenes and biologically relevant scaffolds as a benchmark reaction. Finally, we provide comprehensive photophysical studies that describe the catalytic cycle in detail, establishing a general reference framework for the design of future EDA-mediated catalytic donors and acceptors.

a) Catalytic Electron Donor-Acceptor Systems



b) Previous literature

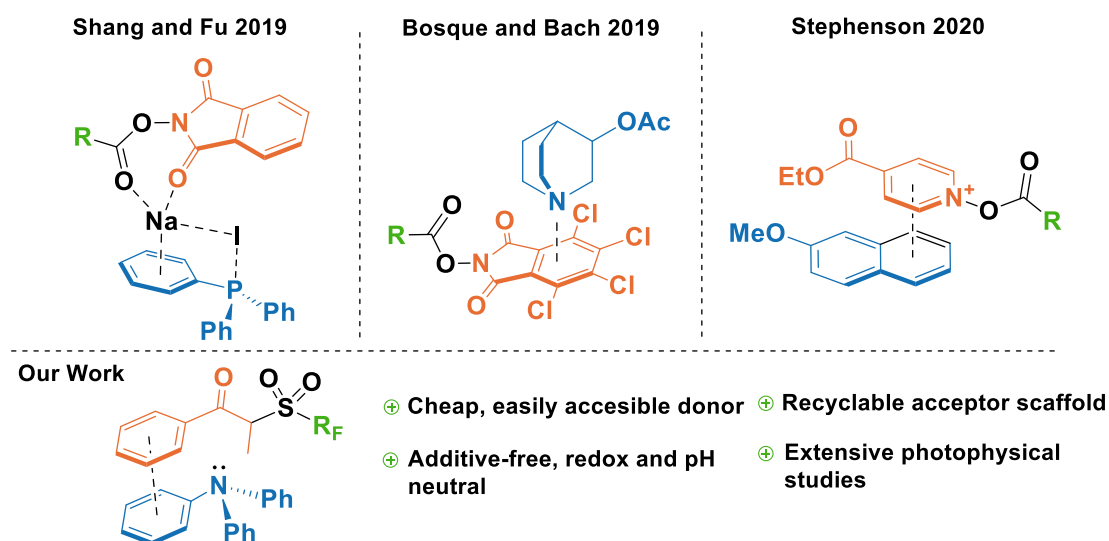


Figure 3.1: Overview of catalytic EDA complexes in synthetic chemistry.

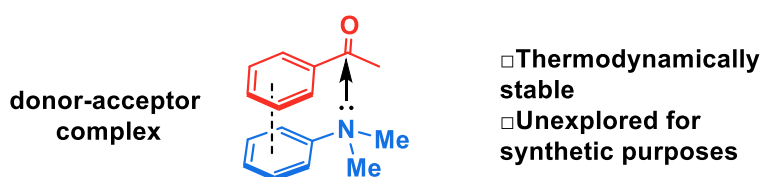
Results and discussion

I. Design of a catalytic system: Triphenylamine in the context of β -cleavage reactions

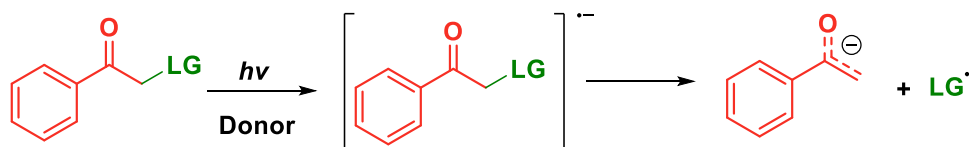
The first step in the design of an acceptor complementary to TPA in EDA catalysis was to find a suitable “recognition element” pertaining to an electron-deficient moiety capable of interacting with the lone pair of the amine. Kannappan and coworkers studied the charge transfer complexes between arylamines and aryl ketones and showed that the

thermodynamic stability of such complexes is aided by secondary interactions such as dipole-dipole or π -stacking (**Figure 3.2a**).²⁹ Reactions involving ketone β -cleavage have been studied previously under high intensities of ultraviolet light (450 W Xenon lamp) with the presence of a suitable leaving group such as a halogen, acetoxy group, or sulfones.³⁰⁻³³ Thus, we hypothesized that the addition of an electron (photoreduction) into such scaffolds would lead to the generation of a stabilized anion and a radical species (**Figure 3.2b**), providing an opportunity to study the capability of triphenylamine as a catalytic electron donor in a general synthetic platform.

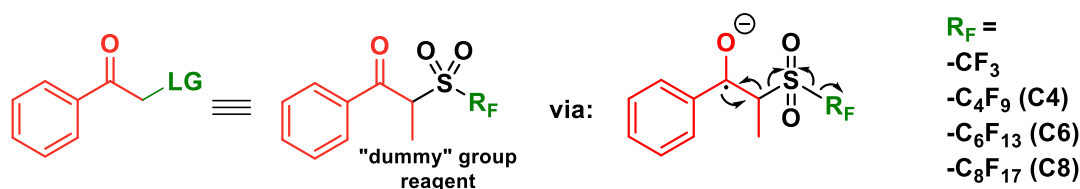
a) *Charge-transfer complexes between arylamines and arylketones*



b) *Beta-cleavage pathway of aryl ketones*



c) *Arylketones as photocleavable agents: "dummy" group reagent as model acceptor*



d) *Triphenylamine as a catalytic donor in EDA photocatalysis*

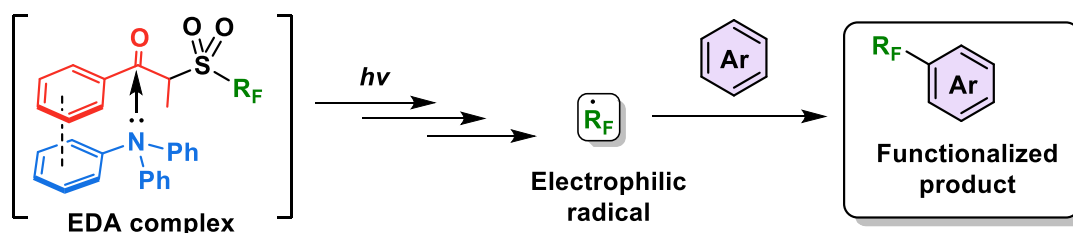


Figure 3.2: Catalytic EDA system design and application

Recently, the β -cleavage of ketones was included in the design of a series of alkylating reagents reported by our laboratory, exploiting propiophenone as a photocleavable fragment (**Figure 3.2c**).³⁴ In this work, inspired by García-Garibay's engineering of Norrish I reactions^{35, 36} and the captodative effect,^{37, 38} these reagents were capable of homolytic cleavage into three elements upon irradiation of light with a xenon arc lamp (> 295 nm): a propiophenone radical—nicknamed “dummy” due to its stability—, a molecule of SO₂ gas, and the radical of interest, which is then trapped by the aromatic substrate to be functionalized innately.³⁴ Such propiophenone-based reagents have several advantages versus the well-established perfluoroalkyl iodides: they are thermally and photostable and can be used under redox- and pH-neutral condition in late-stage functionalization. These “dummy group” reagents allow for easy installation of perfluoroalkyl (perfluorooctyl, perfluorohexyl, perfluorobutyl and trifluoromethyl) group and also alkyl radicals (such as isopropyl and n-hexyl) on electron-rich aromatics and various biologically relevant substrates.³⁹ However, while a diverse set of perfluoroalkyl and alkyl radicals were successfully utilized in this approach, the scope of the substrate is limited to molecules with minimal absorptions overlap to that of the “dummy” group (< 290 nm) to achieve high photoconversion yields. It is noteworthy that while the literature pertaining to perfluoroalkylation reactions is vast,⁴⁰⁻⁴⁴ methods for the metal-free C–H perfluoroalkylation of aromatic molecules through the use of EDA complexes in the catalytic regime remain limited.^{18, 19, 45}

We thus hypothesized that these *dummy* group reagents constituted the ideal candidates as the benchmark reaction to test TPA's capability as a catalytic donor (**Figure 3.2d**): firstly, they contain a benzoyl moiety that can be used as a recognition element, second, their structure is designed for a facile cleavage leading to the generation of the desired radicals, and thirdly, the formation of an EDA complex with TPA would allow for the photoactivation to be initiated under milder conditions with the use of blue LEDs rather than a high energy ultraviolet light source.

II. Mechanistic studies: Exploring the EDA catalytic cycle

EDA complexes are evidenced by the appearance of a new absorption band typically within the visible range of light, beyond the absorption of pure donor or acceptor. Upon

mixing solutions of TPA in MeCN with ketone C8 (or C6) —1:5 ratio, 0.02 M and 0.1M, respectively— an immediate shift in the absorption with a new broad feature (attributed to charge transfer) was observed compared to the absorption profile of the separate components (**Figure 3.3a,c**). Furthermore, the sequential dilution of a mixture of TPA (0.005 M) and C6 (0.02 M) showed a quadratic concentration dependency for the charge transfer band consistent with its bimolecular complexation origin ($\lambda_{\text{mon}} = 427$ nm; **Figure S3.2a,c**), whereas that of the π - π^* band ($\lambda_{\text{mon}} = 295$ nm; **Figure S3.2b,d**), linearly decreased upon dilution as is to be expected based on Beer-Lambert law, further confirming the bimolecular nature of the new charge transfer band. Overlapping the emission profile of our 427 nm LED lamp suggests that this freshly mixed solution absorbs light from the photoreactor as a result of the EDA complex formation, having *ca.* 20% light absorption (absorbance of 0.097) at 427 nm (maximum of our photoreactor incident light) for the given concentrations. Furthermore, after irradiating the sample under blue light for ten minutes, the sample's absorption surged considerably by reaching 64%, and a new absorption band was formed at ~ 660 nm. We attributed this new species to triphenylamine radical cation (TPA^{•+}), previously observed upon SET events.^{46, 47}

Consistent with TPA^{•+} formation upon irradiation of the TPA and acceptor mixture in acetonitrile at room temperature (5 minutes of irradiation under blue light, 427nm), a strong and long-lived electron paramagnetic resonance (EPR) signal was recorded confirming the presence of a radical species, **Figure 3.3d**. Fitting of the observed EPR spectra suggests a hyperfine coupling (hfc) attributed to a single electron coupled with an N nucleus ($S = 1$, hfc ~ 8.5 G) and nine H nuclei ($3H_{\text{para}}$ with $hf_{\text{CH}(\text{para})} \sim 1.9$ G and $6H_{\text{ortho}}$, hfc ~ 1.4 G), which is in line with the previous reports⁴⁸⁻⁵² and the density functional theory calculations (**Figure 3.3e, Table S3.1**). Such observation not only confirmed the *in situ* formation of the TPA radical cation but also substantiated the formation of an EDA complex, as discussed in the work of Stamires and Turkevich.⁵³ Importantly, no EPR signal was observed in a freshly mixed solution of TPA and the acceptor before irradiation, wherefrom a relatively weak charge transfer between the donor (TPA) and acceptor (perfluoroalkyl) may be inferred.⁵³

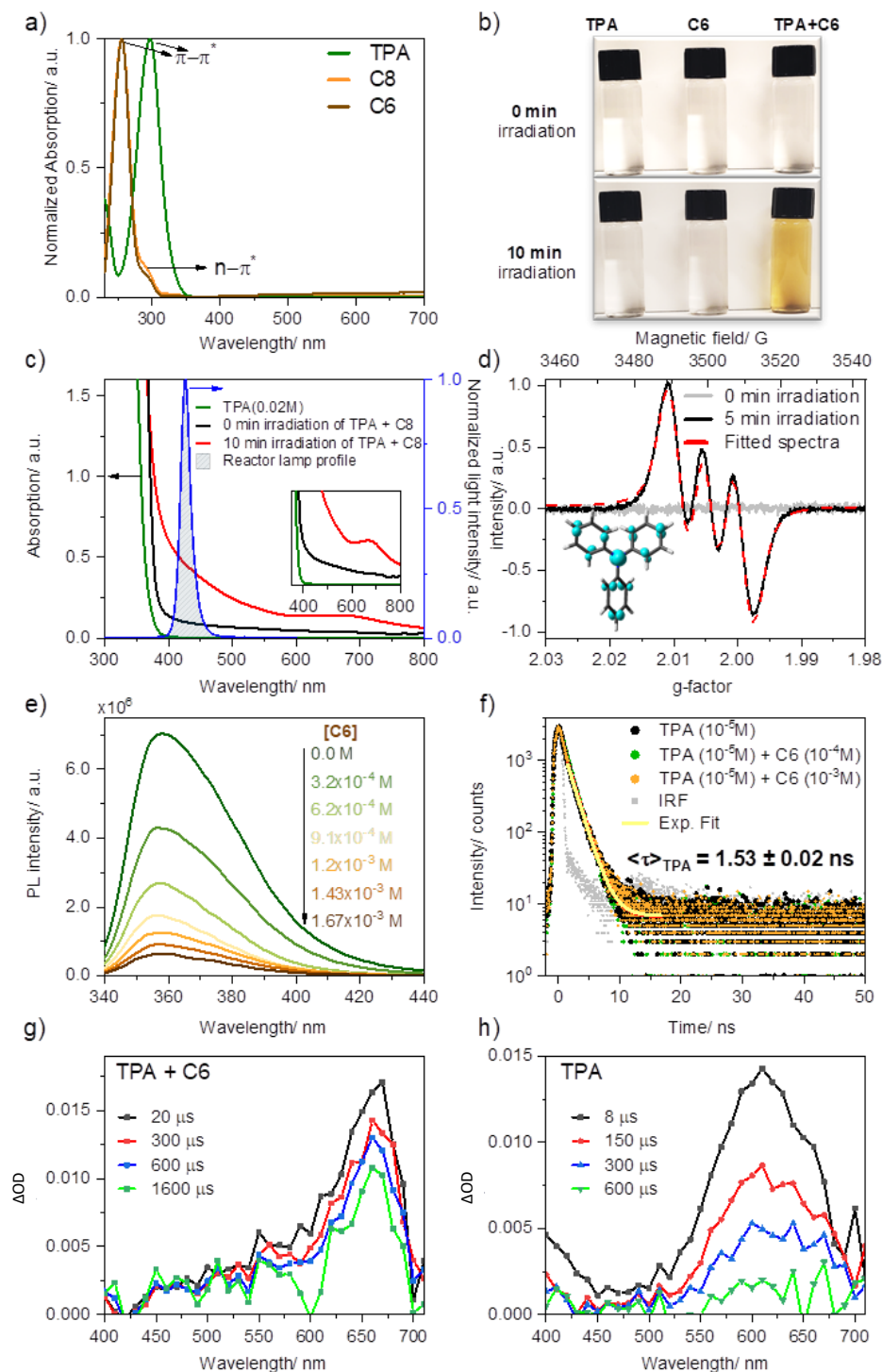


Figure 3.3: Mechanistic studies on triphenylamine as an EDA

(a) UV-Visible spectra of TPA (1×10^{-5} M) and the perfluoroalkylating reagents C8 and C6 (1×10^{-5} M) **(b)** Formation of color by the mixture of TPA (0.02 M) and C8 (0.1 M, 5

equiv.) solutions, freshly made (0 min irradiation) and after 10 min irradiation using blue light (10 min, 40W Kessil lamp 427 nm). **(c)** Absorption evolution of the EDA complex formed between TPA (0.02 M) and C8 (0.1 M, 5 equiv.) and its absorption overlap with the employed light source. **(d)** EPR spectrum of a mixture of C8 with TPA at room temperature before and after shining light (5 min, 40W Kessil lamp 427 nm). Below the spectra: spin distribution for TPA radical cation calculated by density functional theory (DFT; B3LYP 6-31g(d)) as a visual reference of spin delocalization. **(e)** Quenching of TPA (1×10^{-5} M) by forming an EDA complex with various concentrations of C6. **(f)** Time-correlated single-photon counting spectra of TPA in the absence of perfluoroalkylating agent (black), 10 equiv. C6 (green) and 100 equiv. C6 (orange) (1×10^{-4} M and 1×10^{-3} M, respectively); the decreasing emission intensity and the constant lifetime upon the addition of the quencher indicate a static quenching. **(g)** Transient absorption spectrum of TPA (0.005 M) and C6 (0.02 M) upon excitation with a 355 nm laser yielding the TPA radical cation. **(h)** Transient absorption of TPA (0.005 M) showing the formation of 4a,4b-dihydrocarbazole in the ground state upon excitation with a 355 nm laser.

Quenching of TPA emission in the presence of increasing amounts of acceptor (C6) provided further insights into the nature of their interaction, studied through steady-state and time-resolved fluorescence quenching experiments (**Figure 3.3e,f**). Here we sought to reveal whether the TPA interaction with the dummy group existed *a priori* of their excitation (static quenching, no diffusion required) or rather, following photoexcitation of TPA, the electronically excited donor and the acceptor (C6) encounter in solution (dynamic quenching). The drop in intensity of TPA with increasing C6 (**Figure 3.3e**) was analyzed using Stern-Volmer formula. A linear relationship was obtained with a Stern-Volmer quenching constant of $K_{SV} \sim 3.1 \times 10^3 \text{ M}^{-1}$. Combining this value and the fluorescence decay lifetime of TPA in acetonitrile (1.53 ns, **Figure 3.3e**), a bimolecular quenching rate constant $k_q = 2.1 \times 10^{12} \text{ M}^{-1} \cdot \text{s}^{-1}$ (**Figure S3.4a**) was estimated. The resulting k_q far exceeds the diffusion-controlled rate constant value in acetonitrile, i.e. $2.0 \times 10^{10} \text{ M}^{-1} \cdot \text{s}^{-1}$,⁵⁴ indicating that “dynamic quenching” is not a major pathway involved in TPA-C6 interaction. Consistent with a preformed complex, static emission quenching was

confirmed in time-resolved emission studies by the lack of changes in the TPA emission decay lifetime, recorded from time-correlated single-photon counting (TCSPC) upon the addition of C6 up to 10^{-3} M concentrations. In the case of a dynamic process, both intensity and emission decay lifetime would vary proportionally to the increasing C6 concentration. Analysis of the quenching plot using static equilibrium conditions and assuming no emission from the EDA complex (see SI **Figure S3.4, Equation S3.2**) suggests the formation of a 1:1 ratio complex with a binding constant of $K = 1.04 \pm 0.40 \times 10^4 \text{ M}^{-1}$, which is significantly higher than the previously studied charge transfer complexes between a similar system of *N,N*-dimethylaniline and acetophenone derivatives.^{29, 55}

To gain further mechanistic insight, we also conducted transient absorption studies via laser flash photolysis upon 355 nm excitation of TPA in argon-purged acetonitrile solutions, alone or in the presence of C6. Following excitation in the presence of C6 we observed the formation of a transient band with a peak at 660 nm consistent with that previously reported for $\text{TPA}^{+\cdot}$ (**Figure 3.3g**).^{46, 56} Formation of $\text{TPA}^{+\cdot}$ was observed immediately within excitation; however, we note that the high sample absorption at the excitation wavelength generated a thermal wave that prevented accurate spectral assignments within the first $\sim 1 \mu\text{s}$ upon excitation. Notably, excitation of TPA in the absence of C6 but under otherwise identical conditions, rendered the spectra of 4a,4b-dihydrocarbazole in the ground state (DHC_0) with a characteristic absorption at 610 nm (**Figure 3.3h**). This transient species is consistent with the previously reported photo-processes of TPA.⁵⁷⁻⁵⁹ In short, for the latter, upon excitation, rapid intersystem crossing (ISC) from the singlet excited state ($^1\text{TPA}^*$) generates TPA in the triplet excited state ($^3\text{TPA}^*$) with a quantum yield of 0.9. The $^3\text{TPA}^*$ in turn, cyclizes to quantitatively generate $^3\text{DHC}^*$, which decays into its ground state upon intersystem crossing (DHC_0). In the absence of oxygen, DHC_0 converts back to TPA. Importantly, while we were unable to excite at a wavelength where only the EDA complex absorbs, our LFP results position SET as an active mechanism operating when TPA is in the presence of C6. Here $\text{TPA}^{+\cdot}$ is unequivocally observed within the first few microseconds following excitation. Combined with the absorption and fluorescence studies that indicate the formation of an EDA complex and the radical formation at lower excitation energies (427 nm) measured

by EPR, transient absorption studies altogether confirm that electron transfer originates from the complex and not from the excitation of TPA alone.

The observed high stability of the TPA radical cation in the solution (~3h in air, as confirmed by EPR analysis) is likely due to its low concentration, which suppresses the coupling of radical cations, as studied by Creason, Wheeler, and Nelson.⁶⁰ Moreover, we see no evidence for the formation of *N,N,N',N'*-tetraphenyl benzidine (TPB)—the product of dimerization between two TPA units—neither by GCMS of reaction mixtures nor by fluorescence spectroscopy (**Figure S3.3a**),^{46, 61, 62} ruling out the possibility of TPB being a secondary catalyst formed *in situ* by photooxidation of TPA.

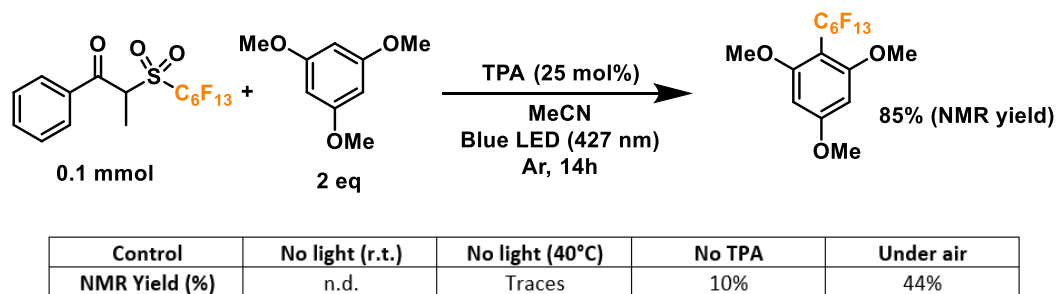


Figure 3.4: Radical trapping and control experiments

Finally, we proceeded to confirm the formation of the desired perfluoroalkyl radicals with a trapping experiment (**Figure 3.4**). These radicals are electrophilic in nature, making them more prone to addition to electron-rich aromatics. The first trial using 1,3,5-trimethoxybenzene as the trapping substrate provided an NMR yield of 85% when irradiated overnight (14 h) in the presence of a 25 mol% load of TPA with respect to the C6 perfluoroalkylating reagent. The formation of propiophenone was confirmed by GCMS and NMR, corroborating the proposed cleavage pathway for the C6 reagent. Regarding controls for this system, light irradiation is essential for the formation of product given the yields obtained when running a dark reaction, both at room temperature and 40°C—none and traces, respectively. Most importantly, when a TPA-free reaction was run under light irradiation, less than 10% of the product was formed, indicating that the functionalization of the aromatic substrate is clearly driven by the addition of the donor. Lastly, we

investigated the tolerance of the EDA catalytic cycle to oxygen. The reaction still proceeds in air, albeit with a 50% decrease in the yield, which we attribute to possible interference of oxygen in the radical cascade derived from the cleavage of the perfluoroalkylating reagent. Furthermore, since commercially available triphenylamines are usually synthesized through metal-mediated cross-coupling reactions (e.g. the traditional Ullman coupling), we wanted to rule out the possibility of trace metals such as Cu and Pd promoting the reaction. For this, an extra control was run with sublimated TPA, giving the same yield as the commercial-grade reagent (98% purity).

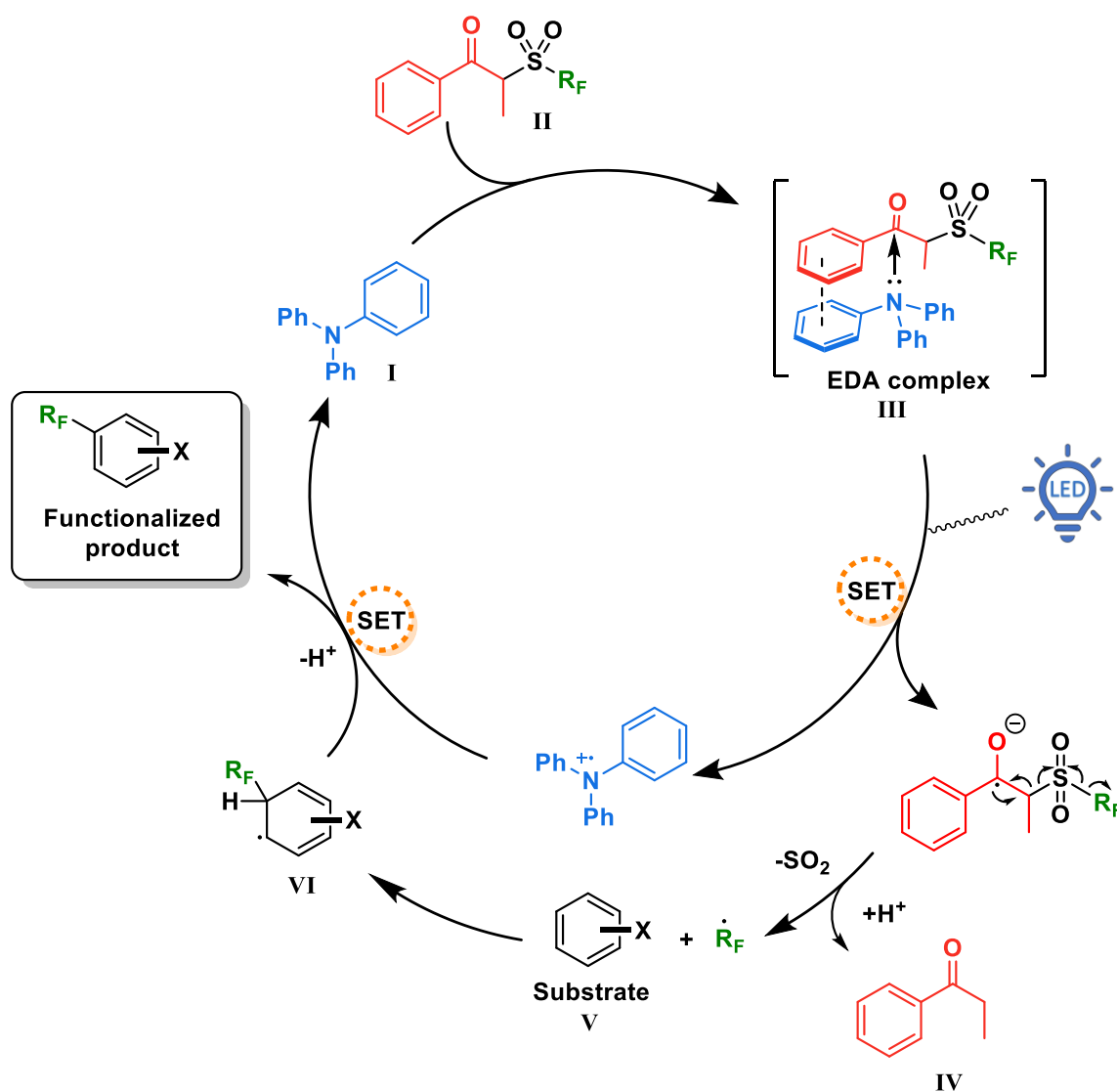
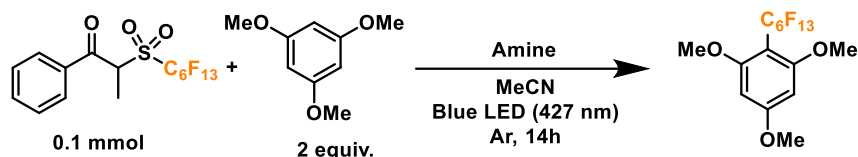


Figure 3.5: Proposed mechanism for the catalytic EDA complex formation between TPA and the perfluoroalkylating reagent.

With this information in mind, a proposed mechanism is depicted in **Figure 3.5**. When present in solution, our TPA catalyst **I** and the propiophenone-containing perfluoroalkylating reagent **II** form a charge transfer complex **III** (absorbing in the visible spectra). Upon excitation with blue light at 427nm, SET creates a radical pair of the triphenylaminium radical cation and the radical anion of the perfluoroalkylating reagent. Due to a weakened C–S bond and driven by entropy, this radical anion breaks into three components: a resonance-stabilized enolate, an SO₂ molecule, and the free perfluoroalkyl radical. The latter thereupon adds to the aromatic substrate **V**, forming the intermediate **VI** which is then oxidized by the triphenylaminium radical cation releasing the functionalized product and regenerating the TPA catalyst.

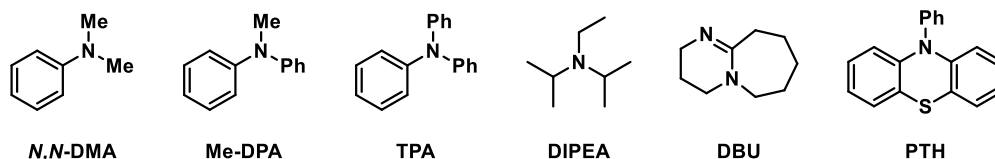
III. Optimization of conditions and expansion of scope: Visible-light promoted perfluoroalkylation and trifluoromethylation of aromatics

Having placed the pieces together in our mechanistic puzzle, we proceeded to optimize the proposed conditions and study the scope, while using our previously reported UV-light promoted perfluoroalkylating methodology as a reference.³⁹ In the original report, 2 equivalents of the propiophenone-based perfluoroalkylating reagent were used to functionalize electron-rich aromatics under irradiation of a 300-watt xenon arc lamp with a long-pass filter of >295 nm, reaching almost quantitative NMR yields for the perfluorohexylation of 1,3,5-trimethoxybenzene.³⁹ Here we aimed to attain the same yields albeit with an electron donor—preferably in catalytic amounts—and using commercial blue LEDs.

Table 3.1. Optimization of reaction conditions—perfluoroalkylation of electron-rich aromatics

Entry	Amine	Mol % amine	Solvent	Product yield (%) ^a
1	TPA	25	MeCN	85
2	<i>N,N</i> -DMA	25	MeCN	37
3	MeDPA	25	MeCN	52
4	DIPEA	25	MeCN	25
5	DBU	25	MeCN	traces
6	PTH	25	MeCN	21, 39 ^b
7	TPA	25	MeCN	80 ^c
8	TPA	25	MeCN	65 ^d
9	TPA	25	IPA	18
10	TPA	25	EtOAc	77
11	TPA	25	MeOH	48
12	TPA	25	DMSO	47
13	TPA	50	MeCN	59
14	TPA	75	MeCN	54
15	TPA	100	MeCN	47
16	TPA	5	MeCN	82
17	TPA	5	MeCN	87 ^e
18	TPA	5	MeCN	88 ^{e,f}

Amines



^a NMR yields using dimethylsulfone as a standard, ^b yields of mono- and di-functionalized products, respectively, ^c 24h reaction, ^d double concentration (0.4 M), ^e inverted equivalents of substrate and reagent, ^f perfluorooctylation. TPA: triphenylamine, *N,N*-DMA: *N,N*-dimethylaniline, MeDPA: *N*-methyldiphenylamine, DIPEA: *N,N*-diisopropylethylamine/Hünig's base, DBU: 1,8-diazabicyclo[5.4.0]undec-7-ene, PTH: 10-phenylphenothiazine.

Firstly, taking the conditions shown in **Figure 3.4** as our starting point (**Table 3.1, entry 1**), we explored the use of other amines to study their efficiency and behavior compared to TPA (**entries 2-6**). Starting with *N,N*-dimethylaniline (*N,N*-DMA) as a reference, the yield of functionalization decreased to 37%, possibly due to both a lower affinity towards the C6 reagent and a lower turnover number. Also, despite its structural similarity with TPA, *N*-methyldiphenylamine (MeDPA) presented a lower yield at 52%. Such observation could be explained by the known reactivity of tertiary amines in photocatalysis, where upon abstraction of one electron α -aminoalkylradicals are readily formed.⁶³ Trials with amines bearing no aromatic substituents (e.g., Hünig's base) resulted in even lower yield of 25%, suggesting that, while the amine could reduce the reagent, it acts as a stoichiometric (sacrificial) donor. Additionally, when switching to another strong organic base such as 1,8-diazabicyclo[5.4.0]undec-7-ene (DBU)—traditionally known as a suitable electron donor in thermochemistry—the reaction was shut down, suggesting that the donating power of the amine may not depend on its basicity in the ground state. Finally, the highly reducing 10-phenylphenothiazine (PTH) photocatalyst showed lower selectivity towards the mono-perfluorohexylated product with 21%, in addition to a 39% yield for the di-perfluorohexylated product. These results confirm that the reactivity between TPA and propiophenone-based redox tags is significantly different from previous literature reports employing other types of amines, including the closely related phenothiazines.

Further extension of the reaction time to 24 h resulted in no change in the yield (**entry 7**), prompting us to keep the initially proposed 14 hours as the optimum timeframe. Moreover, by doubling the crude concentration to around 0.4 M, a slight decrease in yield was noticed (**entry 8**), possibly due to decreased light penetration in the reaction mixture. Next, we moved on to analyze the influence of solvent in the reaction (**entries 9-12**). Trials to optimize the conditions selecting more polar solvents (higher chance of EDA complexation)⁸ such as isopropanol (IPA), ethyl acetate (EtOAc), methanol (MeOH) and dimethylsulfoxide (DMSO), showed lower yields compared to acetonitrile. Next, we proceeded to find the optimal amount of TPA in our system. Interestingly, increasing the amine's load proved counter-productive to the reaction, with yield dropping to ~50% when using 50-100 mol% of TPA (**entries 13-15**). On the other hand, the use of 5 mol% of TPA

allowed us to replicate a >80% yield observed in our initial radical trapping experiment, with just one fifth of the original catalyst loading (**entry 16**). Motivated by this result, we moved on to test whether an inversion of the equivalents between the aromatic substrate and the perfluoroalkylating reagent would have an effect on the yield, allowing us to apply these conditions when the substrate is available in very limited amounts for applications such as late-stage functionalization. By keeping a 5 mol% load of TPA with respect to the limiting reagent —2.5 mol% with respect to the perfluoroalkylating reagent (a very low loading of catalyst compared to the literature on EDA catalytic donors), we successfully obtained a yield of ~87% (**entries 17, 18**).

With these encouraging results we moved on to show the wide scope of our optimized conditions (**Figure 3.6**). As already discussed above, perfluorooxylation and perfluorohexylation of 1,2,3-trimethoxybenzene resulted in good yields after purification, reaching 80% yield for product **PF1** and 79% yield for product **PF2**. An additional test for perfluorobutylation of the same substrate yielded similar amounts by NMR, albeit a lower isolated yield for the perfluorobutylated **PF3**. When looking at less electron-rich aromatics such as 1,4- and 1,2-dimethoxybenzene we observed moderate yields of 49% (**PF4**) and 46% (**PF5**), respectively, with high regioselectivity towards the 4-position in the latter case. On the other hand, an inseparable mixture of monoperfluoroalkylated isomers with approximately equimolar distribution, as determined by GCMS, was obtained for 1,2,3-trimethoxybenzene (**PF6**) with a total yield of 20%.

We then decided to test substrates that have proved challenging to perfluoroalkylate in the literature, such as those that absorb at wavelengths similar to the perfluoroalkylating reagent. For example, 2,6-dimethoxynaphthalene is strongly absorbing at 295 nm, preventing the cleavage of the dummy group reagent and the subsequent generation of radicals in solution. However, when subject to the conditions of this work, perfluorooxylation was successful in the 1- position, giving the product **PF7** with a yield of 43%. Unsubstituted aromatic rings constitute another challenging family of molecules in perfluoroalkylation reactions due to their less electron-rich character. Nevertheless, the proposed EDA catalysis proved useful for the perfluorohexylation of naphthalene and the perfluorooxylation of benzene in good yields giving products **PF8**

and **PF9**, respectively. Monofunctionalized products were observed for both substrates, with the latter having modified reaction conditions—25% v/v in solution. Lastly, UV light also prevented the application of these perfluoroalkylating reagents for the addition to olefins due to the generation of inseparable mixtures. When submitting *N*-methacryloyl-*N*-methylbenzamide to our conditions, the addition of the perfluorooctyl radical and the subsequent cascade cyclization with the benzene ring were observed, yielding product **PF10** in 45% yield.

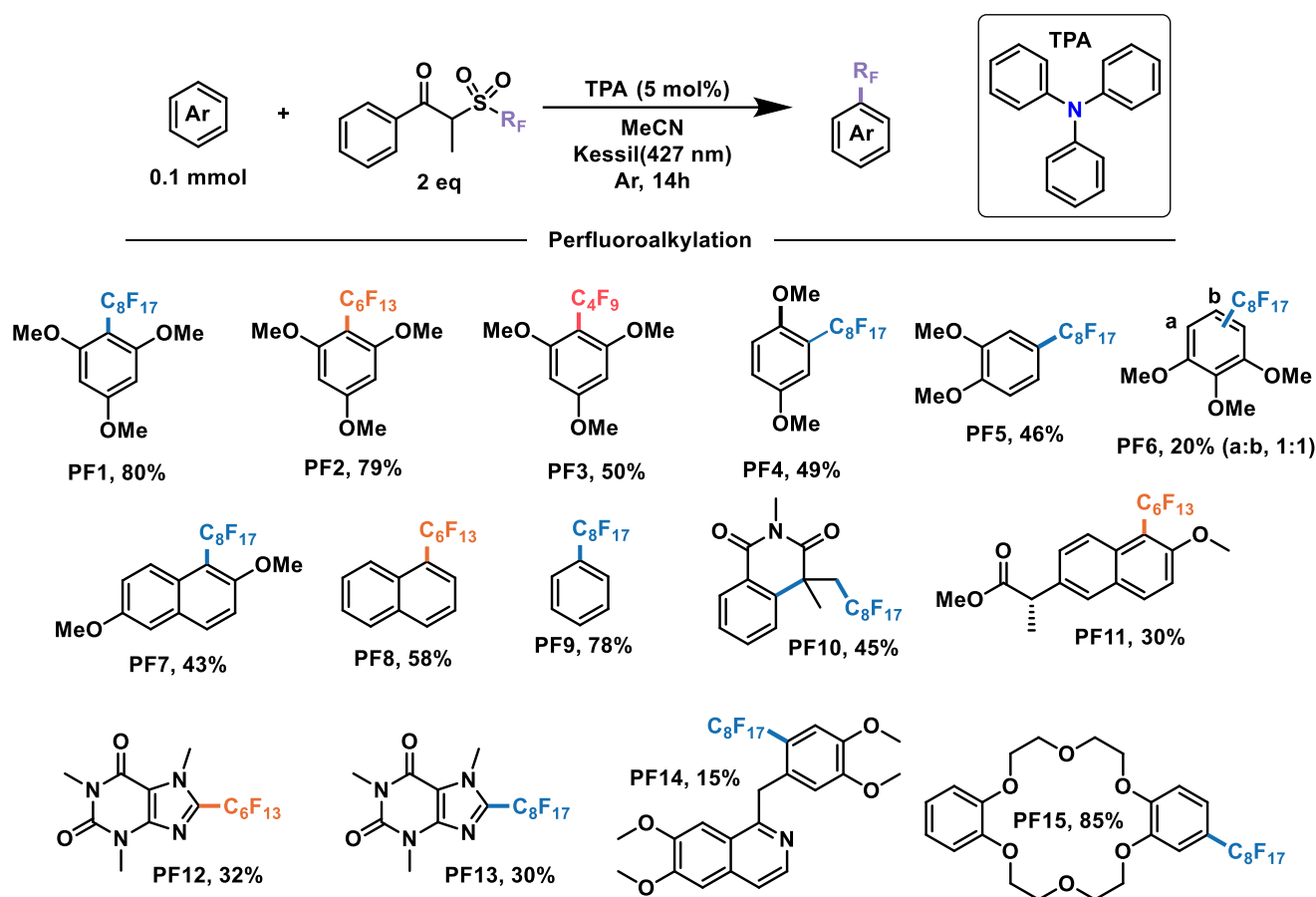
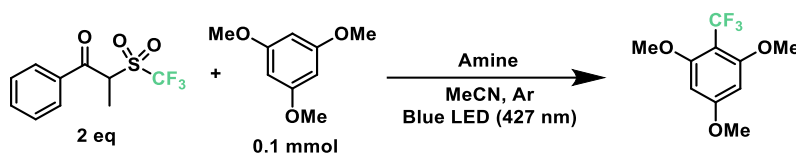


Figure 3.6: Demonstrative scope for the catalytic EDA-mediated perfluoroalkylation of electron-rich aromatics. Note: PF9 is done under modified conditions (25% benzene v/v as solvent).

In addition to the electron-rich substrates presented here, our strategy proved applicable for the late-stage functionalization of some molecules of biological importance. For example, a methylated derivative of naproxen proved responsive towards

perfluorohexylation in 30% yield to give product **PF11**. In addition, similar yields were observed for free caffeine to give the perfluorohexylated product **PF12** and its perfluorooctylated analogue **PF13** under our conditions. Monosubstituted **PF14** was also obtained with high selectivity albeit in low yield (15%) by perfluorooctylation of papaverine—an antispasmodic alkaloid—in its free base form. Finally, we tested our conditions on dibenzo-18-crown-6, a popular phase-transfer agent, obtaining the 4-perfluorooctylated product **PF15** in excellent yield. We envision that the late-stage perfluoroalkylation of aromatic substrates shown in this work will find applications beyond this scope, such as the study of their physical-chemical properties for the modification of materials, the study of their interactomes in biological systems⁶⁴ their use as probes and the development of new analytical techniques for their binding and detection,^{65, 66} among others.

The previously described results motivated us to turn next to a highly-sought reaction in medicinal chemistry: the radical late-stage trifluoromethylation of aromatic scaffolds.^{67, 68} The introduction of the trifluoromethyl moiety allows for the control of fundamental properties in the drug development process such as potency, conformation, metabolism and membrane permeability, making it a valuable transformation for the pharmaceutical industry.^{69, 70} Following the same principle as the previous section, we began to optimize the trifluoromethylation of 1,3,5-trimethoxybenzene in the presence of the CF₃ reagent and TPA at 427 nm. Starting with similar conditions to the optimized perfluoroalkylation of aromatics, TPA reached a yield of only 15% towards the desired product (**Table 3.2, entries 1 and 2**). Such a decrease in the yield against a different reagent can be explained by the difference in bond dissociation energies between the carbon atom alpha to the ketone and the sulfone moiety, showing 174.9 kJ/mol and 185.0 kJ/mol for C6 and CF₃, respectively (calculated using density functional theory, DFT-B3LYP 6-31g(d)). Nonetheless, this represented an opportunity to modify the triphenylamine scaffold without compromising the simplicity of the catalytic design. In our search for more electron-donating amines, tris(4-methoxyphenyl)amine (TMPA) appeared to be a viable commercially-available alternative to TPA. A reaction with a 5 mol% loading of TMPA showed a significant increase in yield at 64% under the same conditions (**entries 3 and 4**).

Table 3.2 Optimization of reaction conditions—trifluoromethylation of electron-rich aromatics

Entry	Amine	Mol % amine	Volume (mL)	Product yield (%) ^a
1	TPA	0	0.5	Traces
2	TPA	5	0.5	15
3	TMPA	0	0.5	Traces
4	TMPA	5	0.5	64
5	TMPA	10	0.5	63
6	TMPA	2.5	0.5	77
7	TMPA	1	0.5	13
8	TMPA	5	0.25	74
9	TMPA	5	0.5	89^b
10	TMPA	2.5	0.5	75 ^c
11	TMPA	2.5	0.25	91
12	TMPA	2.5	0.25	45 ^{b,d}
13	TMPA	2.5	0.25	45 ^{d,e}
14	TMPA	2.5	0.25	50 ^{c,d}

^aNMR yields using dimethylsulfone as a standard, ^b18 hours of irradiation ^cUsing 2.5 equivalents of CF₃ reagent, ^d440 nm light, ^e24 hours of irradiation.

Similar to our previous optimization, lower loadings of catalyst provided higher yields of up to 77% with 2.5 mol% of catalyst (**entries 4,5,6**); however, loadings of ≤1 mol% led to poor results (**entry 7**). On the other hand, using half the amount of acetonitrile brought the yield of the reaction up to 74% (**entry 8**), similar to the use of 2.5 equivalents of trifluoromethylating reagent (**entry 10**). A longer reaction time of up to 18h further increased the yield to 89% (**entry 9**). Combining these factors together, a yield of 91% was achieved when running the reaction for 18 hours in 0.25 mL of acetonitrile with a 2.5 mol% loading of TMPA (**entry 11**). Additionally, we tested the efficiency of this system

under a 440 nm light source (**entries 12–14**); however, a maximum yield of 50% was obtained even after 24 hours of irradiation.

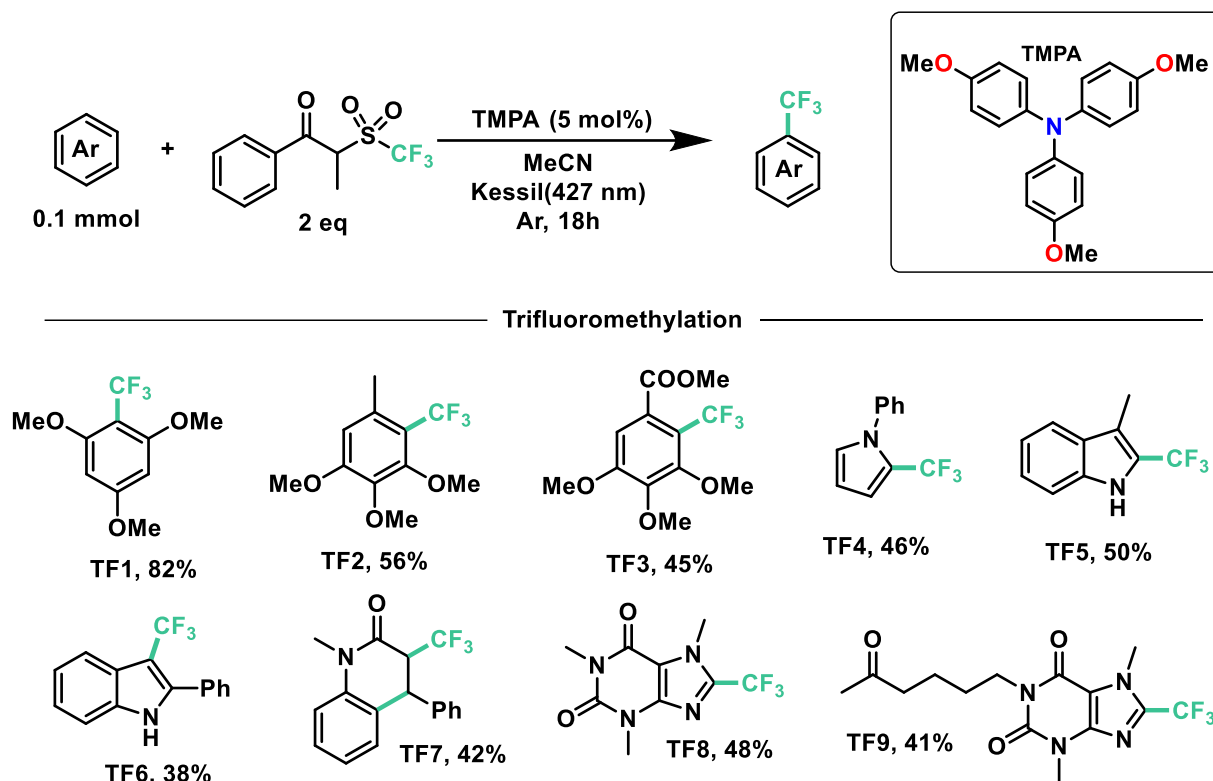


Figure 3.7: Demonstrative scope for the catalytic EDA-mediated trifluoromethylation of electron-rich aromatics

Next, we proceeded to explore the substrate scope for trifluoromethylation. As with our perfluoroalkylation scope, the addition of trifluoromethyl radicals proceeds readily with electron-rich arenes such as trimethoxyarenes. After isolating our first trifluoromethylated product **TF1** at 82%, we tested our conditions against 3,4,5-trimethoxytoluene (**TF2**) and methyl 3,4,5-trimethoxybenzoate (**TF3**) resulting in yields of 56% and 45%, respectively. Moreover, nitrogen-containing heterocycles proved successful with moderate yields: *N*-phenylpyrrole (**TF4**) at 46% and indoles such as 3-methylindole (**TF5**) and 2-phenylindole (**TF6**) with yields of 50% and 38%, respectively. Similarly, as with our perfluoroalkylation of PF10, the trifluoromethylation of olefins was proven feasible with the cyclization of *N*-methyl-*N*-phenylcinnamide (**TF7**) in 42% yield. Lastly, in the context of late-stage

functionalization, trifluoromethylation of caffeine proved more efficient than its perfluorohexyl and perfluorooctyl analogues with a yield of 48%. Given this result, we proceeded to test our conditions on pentoxifylline (**TF9**)—a hemorheological agent used in the treatment of muscle pain—resulting in a 41% yield.

Conclusions

We have performed a comprehensive mechanistic study of perfluoroalkylation reactions using Electron Donor-Acceptor (EDA) complexes of triarylamines as photocatalytic donors and α -(perfluoroalkylsulfonyl)propiophenones as the model acceptor for the generation of perfluorooctyl, perfluorohexyl, perfluorobutyl, and trifluoromethyl radicals. We have confirmed the formation of an EDA complex via UV-Vis absorption and fluorescence quenching experiments and studied the mechanism behind its successful turnover under blue light irradiation. We showed a great synthetic utility of this catalytic system at low catalytic loading (2.5 mol%) in the Minisci-type perfluoroalkylation and trifluoromethylation reactions for the diversification of aromatics, including the late-stage functionalization of biologically relevant scaffolds in moderate to good yields. This work opens the new applications of triarylamines in synthetic chemistry as photocatalysts. We also envisage that our results will open new avenues for general applications EDA-mediated systems in photocatalysis.

Acknowledgements

We would like to acknowledge the McGill Chemistry Characterization (MC²) Facility for their contribution to the compound characterization in this work, specifically, Robin Stein on the NMR and Nadim Saadé and Alexander Wahba on HRMS. We also thank Chia-Yu Huang for providing the starting materials for products PF10 and TF7.

The authors acknowledge the Canada Research Chair (Tier I) foundation, the E.B. Eddy endowment fund, the CFI, NSERC, and FRQNT for support of our research. DJCP acknowledges the financial support granted by the Vanier Canada Graduate Scholarship, CONACYT Mexico, and the Richard H. Tomlinson Fellowship. JRS acknowledges the financial support granted by CONACYT Mexico.

References

- (1) Prier, C. K.; Rankic, D. A.; MacMillan, D. W. C. Visible Light Photoredox Catalysis with Transition Metal Complexes: Applications in Organic Synthesis. *Chem. Rev.* **2013**, *113* (7), 5322-5363.
- (2) Romero, N. A.; Nicewicz, D. A. Organic Photoredox Catalysis. *Chem. Rev.* **2016**, *116* (17), 10075-10166.
- (3) Lee, Y.; Kwon, M. S. Emerging Organic Photoredox Catalysts for Organic Transformations. *Eur. J. Org. Chem.* **2020**, *2020* (38), 6028-6043.
- (4) Arceo, E.; Jurberg, I. D.; Álvarez-Fernández, A.; Melchiorre, P. Photochemical activity of a key donor–acceptor complex can drive stereoselective catalytic α -alkylation of aldehydes. *Nat. Chem.* **2013**, *5* (9), 750-756.
- (5) Tobisu, M.; Furukawa, T.; Chatani, N. Visible Light-mediated Direct Arylation of Arenes and Heteroarenes Using Diaryliodonium Salts in the Presence and Absence of a Photocatalyst. *Chem. Lett.* **2013**, *42* (10), 1203-1205.
- (6) Kim, E. K.; Bockman, T. M.; Kochi, J. K. Electron-transfer mechanism for aromatic nitration via the photoactivation of EDA (electron donor-acceptor) complexes. Direct relationship to electrophilic aromatic substitution. *J. Am. Chem. Soc.* **1993**, *115* (8), 3091-3104.
- (7) Crisenza, G. E. M.; Mazzarella, D.; Melchiorre, P. Synthetic Methods Driven by the Photoactivity of Electron Donor–Acceptor Complexes. *J. Am. Chem. Soc.* **2020**, *142* (12), 5461-5476.
- (8) Lima, C. G. S.; de M. Lima, T.; Duarte, M.; Jurberg, I. D.; Paixão, M. W. Organic Synthesis Enabled by Light-Irradiation of EDA Complexes: Theoretical Background and Synthetic Applications. *ACS Catal.* **2016**, *6* (3), 1389-1407.
- (9) Rosokha, S. V.; Kochi, J. K. Fresh Look at Electron-Transfer Mechanisms via the Donor/Acceptor Bindings in the Critical Encounter Complex. *Acc. Chem. Res.* **2008**, *41* (5), 641-653.
- (10) Yuan, Y.-q.; Majumder, S.; Yang, M.-h.; Guo, S.-r. Recent advances in catalyst-free photochemical reactions via electron-donor-acceptor (EDA) complex process. *Tetrahedron Lett.* **2020**, *61* (8), 151506.

- (11) Tasnim, T.; Ayodele, M. J.; Pitre, S. P. Recent Advances in Employing Catalytic Donors and Acceptors in Electron Donor–Acceptor Complex Photochemistry. *J. Org. Chem.* **2022**, *87* (16), 10555-10563.
- (12) Fu, M.-C.; Shang, R.; Zhao, B.; Wang, B.; Fu, Y. Photocatalytic decarboxylative alkylations mediated by triphenylphosphine and sodium iodide. *Science* **2019**, *363* (6434), 1429-1434.
- (13) de Pedro Beato, E.; Spinnato, D.; Zhou, W.; Melchiorre, P. A General Organocatalytic System for Electron Donor–Acceptor Complex Photoactivation and Its Use in Radical Processes. *J. Am. Chem. Soc.* **2021**, *143* (31), 12304-12314.
- (14) Liu, Q.; Lu, Y.; Sheng, H.; Zhang, C.-S.; Su, X.-D.; Wang, Z.-X.; Chen, X.-Y. Visible-Light-Induced Selective Photolysis of Phosphonium Iodide Salts for Monofluoromethylations. *Angew. Chem. Int. Ed.* **2021**, *60* (48), 25477-25484.
- (15) McClain, E. J.; Monos, T. M.; Mori, M.; Beatty, J. W.; Stephenson, C. R. J. Design and Implementation of a Catalytic Electron Donor–Acceptor Complex Platform for Radical Trifluoromethylation and Alkylation. *ACS Catal.* **2020**, *10* (21), 12636-12641.
- (16) Quint, V.; Morlet-Savary, F.; Lohier, J.-F.; Lalevée, J.; Gaumont, A.-C.; Lakhdar, S. Metal-Free, Visible Light-Photocatalyzed Synthesis of Benzo[b]phosphole Oxides: Synthetic and Mechanistic Investigations. *J. Am. Chem. Soc.* **2016**, *138* (23), 7436-7441.
- (17) Bosque, I.; Bach, T. 3-Acetoxyquinuclidine as Catalyst in Electron Donor–Acceptor Complex-Mediated Reactions Triggered by Visible Light. *ACS Catal.* **2019**, *9* (10), 9103-9109.
- (18) Tasnim, T.; Ryan, C.; Christensen, M. L.; Fennell, C. J.; Pitre, S. P. Radical Perfluoroalkylation Enabled by a Catalytically Generated Halogen Bonding Complex and Visible Light Irradiation. *Org. Lett.* **2022**, *24* (1), 446-450.
- (19) Lu, H.; Wang, D.-y.; Zhang, A. Visible Light-Promoted Phosphine-Catalyzed Difluoroalkylation of Arenes and Heterocycles. *J. Org. Chem.* **2020**, *85* (2), 942-951.
- (20) Blanchard, P.; Malacrida, C.; Cabanetos, C.; Roncali, J.; Ludwigs, S. Triphenylamine and some of its derivatives as versatile building blocks for organic electronic applications. *Polym. Int.* **2019**, *68* (4), 589-606.
- (21) Liang, M.; Chen, J. Arylamine organic dyes for dye-sensitized solar cells. *Chem. Soc. Rev.* **2013**, *42* (8), 3453-3488.

- (22) Ho, P.-Y.; Wang, Y.; Yiu, S.-C.; Yu, W.-H.; Ho, C.-L.; Huang, S. Starburst Triarylamine Donor-Based Metal-Free Photosensitizers for Photocatalytic Hydrogen Production from Water. *Org. Lett.* **2017**, *19* (5), 1048-1051.
- (23) Dai, C.; Zhong, L.; Gong, X.; Zeng, L.; Xue, C.; Li, S.; Liu, B. Triphenylamine based conjugated microporous polymers for selective photoreduction of CO₂ to CO under visible light. *Green Chem.* **2019**, *21* (24), 6606-6610.
- (24) Yuan Chiu, K.; Xiang Su, T.; Hong Li, J.; Lin, T.-H.; Liou, G.-S.; Cheng, S.-H. Novel trends of electrochemical oxidation of amino-substituted triphenylamine derivatives. *J. Electroanal. Chem.* **2005**, *575* (1), 95-101.
- (25) Tshepelevitsh, S.; Kütt, A.; Lõkov, M.; Kaljurand, I.; Saame, J.; Heering, A.; Plieger, P. G.; Vianello, R.; Leito, I. On the Basicity of Organic Bases in Different Media. *Eur. J. Org. Chem.* **2019**, *2019* (40), 6735-6748.
- (26) Dewanji, A.; van Dalsen, L.; Rossi-Ashton, J. A.; Gasson, E.; Crisenza, G. E. M.; Procter, D. J. A general arene C–H functionalization strategy via electron donor–acceptor complex photoactivation. *Nat. Chem.* **2022**.
- (27) Discekici, E. H.; Treat, N. J.; Poelma, S. O.; Mattson, K. M.; Hudson, Z. M.; Luo, Y.; Hawker, C. J.; de Alaniz, J. R. A highly reducing metal-free photoredox catalyst: design and application in radical dehalogenations. *Chem. Commun.* **2015**, *51* (58), 11705-11708.
- (28) Proctor, R. S. J.; Phipps, R. J. Recent Advances in Minisci-Type Reactions. *Angew. Chem. Int. Ed.* **2019**, *58* (39), 13666-13699.
- (29) Kumar, R.; Jayakumar, S.; Kannappan, V. Thermodynamic properties of donor–acceptor complexes of tertiary amine with aryl ketones in hexane medium. *Thermochim. Acta* **2012**, *536*, 15-23.
- (30) Sheehan, J. C.; Wilson, R. M.; Oxford, A. W. Photolysis of methoxy-substituted benzoin esters. Photosensitive protecting group for carboxylic acids. *J. Am. Chem. Soc.* **1971**, *93* (26), 7222-7228.
- (31) Zimmerman, H. E.; Flechtner, T. W. Excited-state three-ring bond opening in cyclopropyl ketones. Mechanistic organic photochemistry. LX. *J. Am. Chem. Soc.* **1970**, *92* (23), 6931-6935.
- (32) Zimmerman, H. E.; Hancock, K. G.; Licke, G. C. Mechanistic organic photochemistry. XXXII. Stereochemistry and mechanism of photochemical interconversion of cis-and

trans-5,6-diphenylbicyclo[3.1.0] hexan-2-ones. *J. Am. Chem. Soc.* **1968**, *90* (18), 4892-4911.

(33) Sheehan, J. C.; Wilson, R. M. Photolysis of Desyl Compounds. A New Photolytic Cyclization. *J. Am. Chem. Soc.* **1964**, *86* (23), 5277-5281.

(34) Liu, P.; Liu, W.; Li, C.-J. Catalyst-Free and Redox-Neutral Innate Trifluoromethylation and Alkylation of Aromatics Enabled by Light. *J. Am. Chem. Soc.* **2017**, *139* (40), 14315-14321.

(35) Campos, L. M.; Dang, H.; Ng, D.; Yang, Z.; Martinez, H. L.; Garcia-Garibay, M. A. Engineering Reactions in Crystalline Solids: Predicting Photochemical Decarbonylation from Calculated Thermochemical Parameters. *J. Org. Chem.* **2002**, *67* (11), 3749-3754.

(36) Yang, Z.; Garcia-Garibay, M. A. Engineering Reactions in Crystalline Solids: Radical Pairs in Crystals of Dialkyl 1,3-Acetonedicarboxylates. *Org. Lett.* **2000**, *2* (13), 1963-1965.

(37) Viehe, H. G.; Merényi, R.; Stella, L.; Janousek, Z. Captodative Substituent Effects in Syntheses with Radicals and Radicophiles [New synthetic methods (32)]. *Angew. Chem. Int. Ed. Engl.* **1979**, *18* (12), 917-932.

(38) Viehe, H. G.; Janousek, Z.; Merenyi, R.; Stella, L. The captodative effect. *Acc. Chem. Res.* **1985**, *18* (5), 148-154.

(39) Castillo-Pazos, D. J.; Lasso, J. D.; Li, C.-J. Synthesis of α -(perfluoroalkylsulfonyl)propiophenones: a new set of reagents for the light-mediated perfluoroalkylation of aromatics. *Beilstein J. Org. Chem.* **2022**, *18*, 788-795.

(40) Guan, Z.; Wang, H.; Huang, Y.; Wang, Y.; Wang, S.; Lei, A. Electrochemical Oxidative Aryl(alkyl)trifluoromethylation of Allyl Alcohols via 1,2-Migration. *Org. Lett.* **2019**, *21* (12), 4619-4622.

(41) Zhang, L.; Zhang, G.; Wang, P.; Li, Y.; Lei, A. Electrochemical Oxidation with Lewis-Acid Catalysis Leads to Trifluoromethylative Difunctionalization of Alkenes Using CF₃SO₂Na. *Org. Lett.* **2018**, *20* (23), 7396-7399.

(42) Muralirajan, K.; Kancherla, R.; Bau, J. A.; Taksande, M. R.; Qureshi, M.; Takanabe, K.; Rueping, M. Exploring the Structure and Performance of Cd-Chalcogenide Photocatalysts in Selective Trifluoromethylation. *ACS Catal.* **2021**, *11* (24), 14772-14780.

(43) Nagib, D. A.; MacMillan, D. W. C. Trifluoromethylation of arenes and heteroarenes by means of photoredox catalysis. *Nature* **2011**, *480* (7376), 224-228.

- (44) Choi, W. J.; Choi, S.; Ohkubo, K.; Fukuzumi, S.; Cho, E. J.; You, Y. Mechanisms and applications of cyclometalated Pt(II) complexes in photoredox catalytic trifluoromethylation. *Chem. Sci.* **2015**, *6* (2), 1454-1464.
- (45) Castillo-Pazos, D. J.; Lasso, J. D.; Li, C.-J. Modern methods for the synthesis of perfluoroalkylated aromatics. *Org. Biomol. Chem.* **2021**, *19* (33), 7116-7128.
- (46) Nelson, R. F.; Philp, R. H. Electrochemical and spectroscopic studies of cation radicals. 4. Stopped-flow determination of triarylammonium radical coupling rate constants. *J. Phys. Chem.* **1979**, *83* (6), 713-716.
- (47) Sreenath, K.; Suneesh, C. V.; Gopidas, K. R.; Flowers, R. A. Generation of Triarylamine Radical Cations through Reaction of Triarylamines with Cu(II) in Acetonitrile. A Kinetic Investigation of the Electron-Transfer Reaction. *J. Phys. Chem. A* **2009**, *113* (23), 6477-6483.
- (48) Mao, L.; Zhou, M.; Shi, X.; Yang, H.-B. Triphenylamine (TPA) radical cations and related macrocycles. *Chin. Chem. Lett.* **2021**, *32* (11), 3331-3341.
- (49) Talipov, M. R.; Hossain, M. M.; Boddada, A.; Thakur, K.; Rathore, R. A search for blues brothers: X-ray crystallographic/spectroscopic characterization of the tetraarylbenzidine cation radical as a product of aging of solid magic blue. *Org. Biomol. Chem.* **2016**, *14* (10), 2961-2968.
- (50) Schaub, T. A.; Mekelburg, T.; Dral, P. O.; Miehlich, M.; Hampel, F.; Meyer, K.; Kivala, M. A Spherically Shielded Triphenylamine and Its Persistent Radical Cation. *Chem. Eur. J.* **2020**, *26* (15), 3264-3269.
- (51) Munshi, M. U.; Berden, G.; Martens, J.; Oomens, J. Gas-phase vibrational spectroscopy of triphenylamine: the effect of charge on structure and spectra. *Phys. Chem. Chem. Phys.* **2017**, *19* (30), 19881-19889.
- (52) Cias, P.; Slugovc, C.; Gescheidt, G. Hole Transport in Triphenylamine Based OLED Devices: From Theoretical Modeling to Properties Prediction. *J. Phys. Chem. A* **2011**, *115* (50), 14519-14525.
- (53) Stamiros, D. N.; Turkevich, J. Electron Paramagnetic Resonance in Some Molecular Charge Transfer Complexes. *J. Am. Chem. Soc.* **1963**, *85* (17), 2557-2561.
- (54) Ware, W. R. Oxygen Quenching of Fluorescence in Solution: An Experimental Study of the Diffusion Process. *J. Phys. Chem.* **1962**, *66* (3), 455-458.

- (55) Kannappan, V.; Gandhi, N. I. Ultrasonic method of determination of stability constants of charge transfer complexes of certain carbonyl compounds and diethylamine in n-hexane. *Phys. Chem. Liq.* **2008**, *46* (5), 510-521.
- (56) Oyama, M.; Higuchi, T.; Okazaki, S. An Intermediate State of the Triphenylamine Cation Radical Revealed Using an Electron-Transfer Stopped-Flow Method. *Electrochem. Solid-State Lett.* **2002**, *5* (2), E1.
- (57) Forster, E. W.; Grellman, K. H. The light-induced conversion of triphenylamine to the excited triplet state of 11,12-dihydrocarbazole. *Chem. Phys. Lett.* **1972**, *14* (4), 536-538.
- (58) Görner, H. Photoinduced Oxygen Uptake of Diphenylamines in Solution and Their Ring Closure Revisited. *J. Phys. Chem. A* **2008**, *112* (6), 1245-1250.
- (59) Sanmartín, R. A.; Salum, M. L.; Protti, S.; Mella, M.; Bonesi, S. M. The Photoinduced Electrocyclization Reaction of Triphenylamine (TPA) in Sustainable and Confined Micellar Solutions: A Steady-State and Laser Flash Photolysis Approach. *ChemPhotoChem* **2022**, *6* (4), e202100247.
- (60) Creason, S. C.; Wheeler, J.; Nelson, R. F. Electrochemical and spectroscopic studies of cation radicals. I. Coupling rates of 4-substituted triphenylaminium ion. *J. Org. Chem.* **1972**, *37* (26), 4440-4446.
- (61) Yurchenko, O.; Freytag, D.; zur Borg, L.; Zentel, R.; Heinze, J.; Ludwigs, S. Electrochemically Induced Reversible and Irreversible Coupling of Triarylaminines. *J. Phys. Chem. B* **2012**, *116* (1), 30-39.
- (62) Vallat, A.; Laviron, E. Étude de l'oxydation de triphénylaminines par voltammétrie à variation linéaire de tension en couche mince. *J. Electroanal. Chem. Interf. Electrochem.* **1976**, *74* (3), 309-314.
- (63) Nakajima, K.; Miyake, Y.; Nishibayashi, Y. Synthetic Utilization of α -Aminoalkyl Radicals and Related Species in Visible Light Photoredox Catalysis. *Acc. Chem. Res.* **2016**, *49* (9), 1946-1956.
- (64) Zhang, Q.; Dong, X.; Lu, J.; Song, J.; Wang, Y. Chemoproteomic Approach toward Probing the Interactomes of Perfluoroalkyl Substances. *Anal. Chem.* **2021**, *93* (27), 9634-9639.

- (65)** Khan, R.; Andreescu, D.; Hassan, M. H.; Ye, J.; Andreescu, S. Nanoelectrochemistry Reveals Selective Interactions of Perfluoroalkyl Substances (PFASs) with Silver Nanoparticles. *Angew. Chem. Int. Ed.* **2022**, *61* (42), e202209164.
- (66)** Kralj, M.; Tušek-Božić, L.; Frkanec, L. Biomedical Potentials of Crown Ethers: Prospective Antitumor Agents. *ChemMedChem* **2008**, *3* (10), 1478-1492.
- (67)** Lasso, J. D.; Castillo-Pazos, D. J.; Li, C.-J. Green chemistry meets medicinal chemistry: a perspective on modern metal-free late-stage functionalization reactions. *Chem. Soc. Rev.* **2021**, *50* (19), 10955-10982.
- (68)** Xiao, H.; Zhang, Z.; Fang, Y.; Zhu, L.; Li, C. Radical trifluoromethylation. *Chem. Soc. Rev.* **2021**, *50* (11), 6308-6319.
- (69)** Purser, S.; Moore, P. R.; Swallow, S.; Gouverneur, V. Fluorine in medicinal chemistry. *Chem. Soc. Rev.* **2008**, *37* (2), 320-330.
- (70)** Meanwell, N. A. Fluorine and Fluorinated Motifs in the Design and Application of Bioisosteres for Drug Design. *J. Med. Chem.* **2018**, *61* (14), 5822-5880.

Supporting Information

1. General experimental procedures:

All reactions were carried out under an argon atmosphere using standard Schlenk technique. ^1H NMR (500 MHz), ^{13}C NMR (126 MHz), and ^{19}F NMR (471 MHz) were recorded on an NMR spectrometer with CDCl_3 or d^6 -acetone as the solvent. Chemical shifts of ^1H , ^{13}C and ^{19}F NMR spectra are reported in parts per million (ppm). The residual solvent signals were used as references and the chemical shifts were converted to the TMS scale (CDCl_3 : $\delta \text{H} = 7.26$ ppm, $\delta \text{C} = 77.16$ ppm). All coupling constants (J values) are reported in Hertz (Hz). High-resolution mass spectrometry was conducted through using atmospheric pressure chemical ionization (APCI) or electro-spraying ionization (ESI), on a Thermo-Scientific Exactive Orbitrap. Protonated molecular ions $[\text{M}+\text{H}]^+$ or sodium adducts $[\text{M}+\text{Na}]^+$ were used for empirical formula confirmation. Column chromatography was performed either on silica gel 200–300 mesh, or on C8-reversed phase perfluorinated silica gel. Analytical thin layer chromatography (TLC) was performed using Merck silica gel 60 F254 pre-coated plates (0.25 mm). All reactions were conducted in 10x75 mm Fisher culture-tubes and were irradiated utilizing Kessil PR160L 427nm (45W) LED lamps. All perfluoroalkylating reagents were synthesized, purified and characterized as reported previously in the literature.¹

2. General procedure for the perfluoroalkylation of aromatics



Scheme S3.1. The aromatic substrate (0.1 mmol), the corresponding perfluoroalkylating reagent (0.15 – 0.2 mmol, and 0.005 mmol of triphenylamine were added into 0.5 mL acetonitrile inside a glass test tube capped with a rubber septum. Three freeze-pump-thaw cycles under argon were carefully performed before setting the reaction under light irradiation at 20°C using a Kessil PR160L 427nm (45W) LED lamp. Two desk fans were

used to keep the temperature below 25°C. After the reaction was finished (14-18 h), the reaction crude was evaporated under reduced pressure, and purified through preparative thin-layer chromatography, using ethyl acetate/hexanes or dichloromethane/hexanes systems as the eluent.

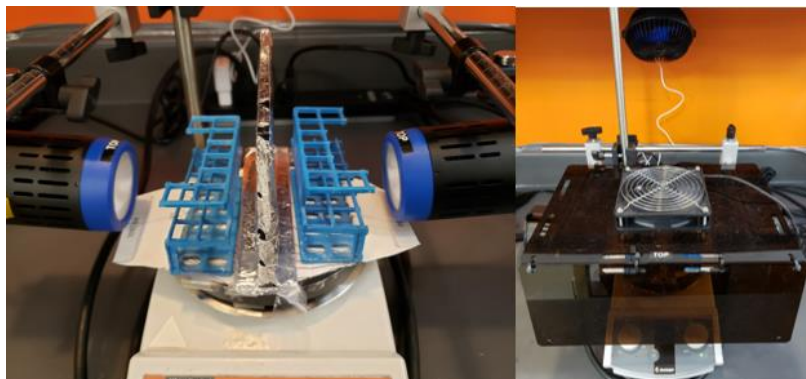
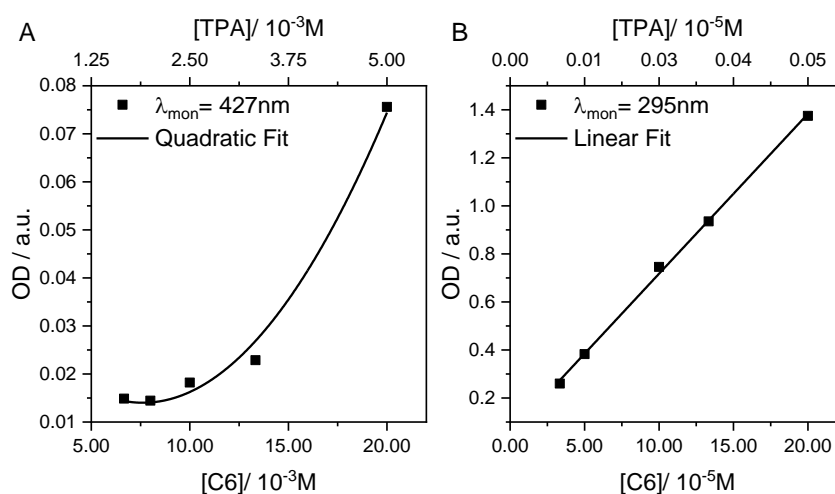


Figure S3.1. Left: close-up of the Kessil lamp setup, allowing for multiple reactions at the same time, all-absorbing around 200000 mW/cm². Right: Covered setup and the two auxiliary fans to keep the temperature below 25°C.

3. Mechanistic Studies

3.1 Fluorescence quenching experiments

Solution UV-vis absorption spectra were collected on a JASCO V-670 spectrophotometer in quartz cuvettes from Starna Cells, Inc.



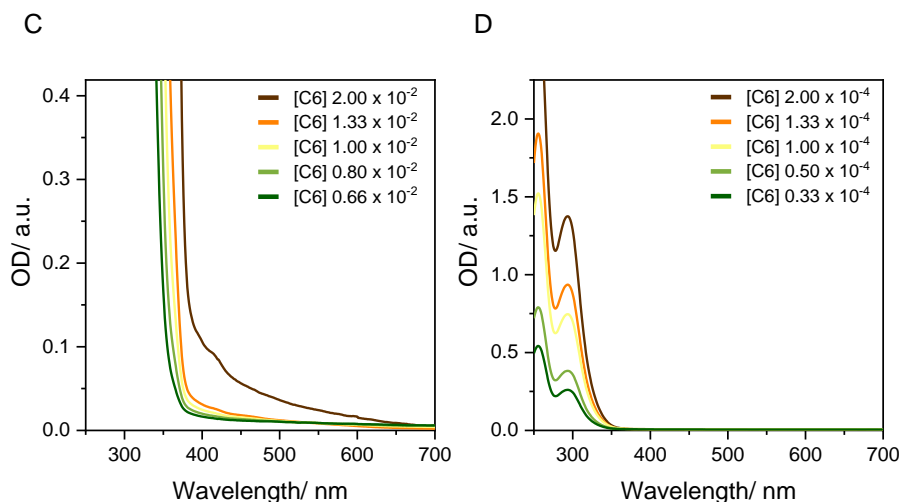


Figure S3.2. The dependency of absorbance on the concentration of a 1:4 mixture of TPA and C6(0.02 for A,C and 0.0002 for B,D, respectively), following a sequential dilution; which shows quadratic relationship for $\lambda_{CT}=427$ nm and a linear relationship for the $\lambda_{p^*}=427$ nm.

Steady-state photoluminescence spectra were collected using a Fluorolog 3 fluorometer from Horiba Jobin-Yvon. **The emission lifetimes** of the samples were determined by the Time-Correlated Single Photon Counting (TCSPC) technique using a DeltaDiode 373 nm pulsed laser diode controlled by a DeltaHub controller, both from Horiba Scientific.

A quenching plot for TPA in the presence of C6 was obtained by preparing the solutions of TPA (10^{-5} M) mixed with the corresponding amount of C6 solution (10^{-5} M) in acetonitrile. It is noteworthy that each sample was scanned once (quick scan 0.01s/nm) due to the rapid cyclization of TPA into *N*-phenylcarbazole in the presence of oxygen, as reported previously in the literature.²

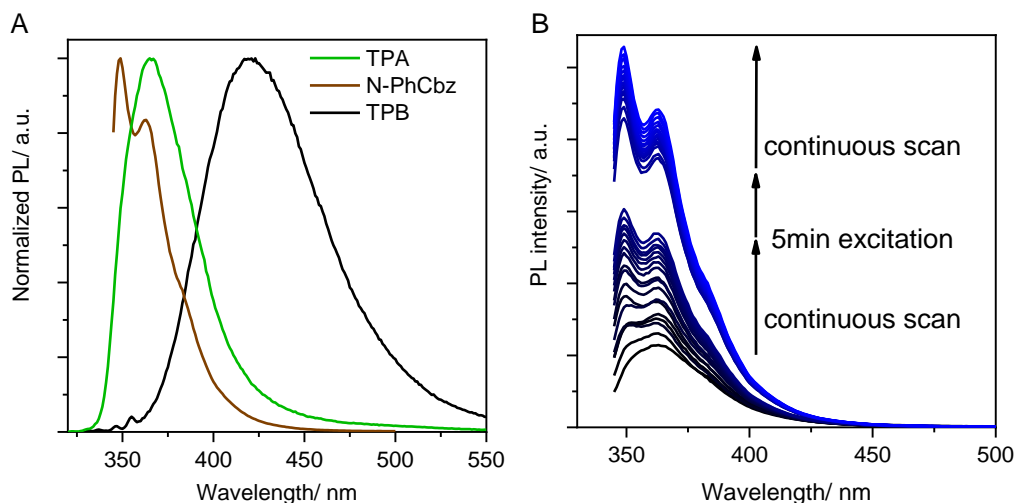


Figure S3.3. (A) Normalized photoluminescent spectra of TPA, TPB and *N*-phenyl carbazole (*N*-PhCbz) in MeCN. (B) The emergence of a new species (*N*-phenylcarbazole) when a TPA (10^{-5}M)-C6 (10^{-4}M) solution is scanned and excited multiple times (scan rate of 0.1s/nm ; $\lambda_{\text{ex}}=340\text{nm}$).

The Stern-Volmer plot was obtained from single point emission intensity measurement at 360nm to minimize the amount of photobleaching of TPA. Fluorescence quenching data were analyzed with the Stern–Volmer equation 1:

Equation S3.1
$$\frac{I}{I_0} = 1 + K_{SV}[Q] = 1 + k_q\tau_0[Q]$$

Where I_0 and I are the relative fluorescence intensities in the absence and presence of a quencher, respectively, $[Q]$ is the concentration of the quencher, K_{SV} is the Stern–Volmer quenching constant, k_q is the bimolecular quenching rate constant and τ_0 the average lifetime of the fluorophore in the excited state (1.5 ns for TPA).

When small molecules bind independently to a set of equivalent sites on a fluorophore, the equilibrium between free and bound molecules is given by the Hill equation:³

Equation S3.2
$$\log\left(\frac{I_0 - I}{I}\right) = \log K_b + n \log [Q]$$

where I_0 , I , and $[Q]$ are the same as those in Equation S3.1. K is the binding constant, and n is the number of binding sites per fluorophore.

Plotting $\log((I_0-I)/I)$ versus $\log [Q]$ (Figure S3.3B) gives a straight line whose slope equals n (1.2), and the intercept on the Y-axis equals $\log K$ (4.02). The complex of TPA with C6 is determined to be a 1:1 ratio with a binding constant of $\sim 1.04 \times 10^4$.

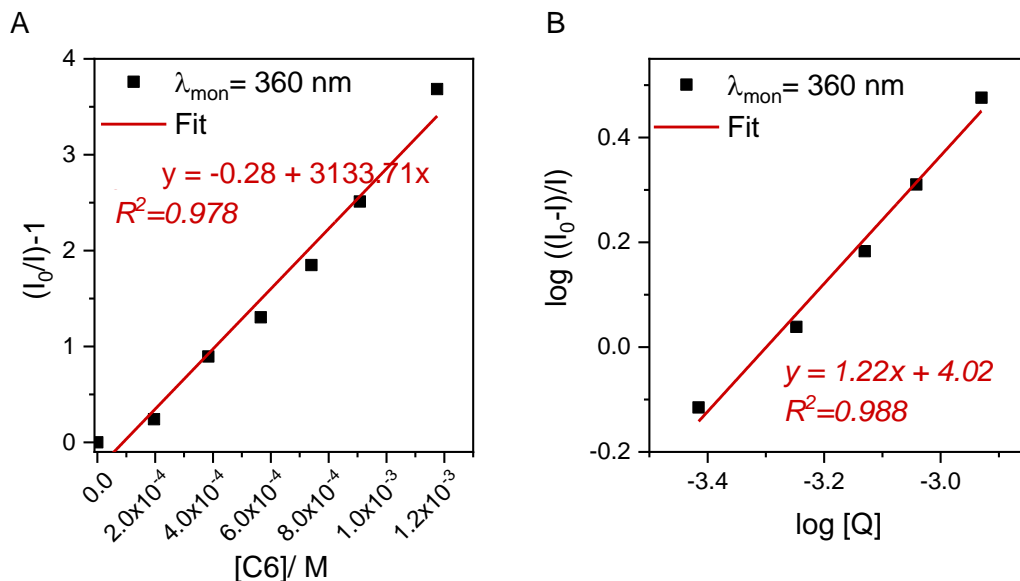


Figure S3.4. (A) The Stern-Volmer quenching plot for TPA($10^{-5}M$) and various concentrations of C6. (B) Quenching plot, according to the equation S2 and the fitted linear function (red), the calculated error for the y-intercept (i.e., $\log(K_b)$) is 0.24, which corresponds to the binding constant of $K_b = 1.04 \pm 0.44 \times 10^4$

3.2 Density Functional Theory calculations

Density functional theory (DFT) calculations were performed using B3LYP functional and 6-31G(d) basis set, using geometry optimization and frequency options implemented in Gaussian 16. Rev. B.01.⁴ The homolytic bond dissociation energies were calculated by the difference in energy of separated molecular segments (as neutral radicals) with the optimized structure energies.

Table S3.1

Atom	counts	Theoretical* hfc(G)	Fitted hfc (G)
¹⁵ N	1	8.8	8.5
¹ H ortho	6	2.4	1.4
¹ H para	3	3.6	1.9
¹ H meta	6	1.5	N.A.

*Obtained from the isotropic fermi contact coupling, in the DFT (B3LYP, 6-31g(d)) optimized TPA^{•+}.

3.3 EPR Measurements

Continuous-wave EPR measurements were carried out using a Bruker (Billerica, Elexsys E580) X-band spectrometer fitted with a standard EPR flat cell, from Wilmad-lab glass. The data were obtained at room temperature in air, using MeCN solutions of TPA and C8 (10⁻³ M). An equimolar mix was done in situ and irradiated with a Kessil PR160L 427nm (45W) LED lamp for 5 minutes before introducing the resulting yellow-coloured solution in the flat cell for measurement. The baseline of the obtained EPR signal was corrected using polynomial baseline functions (in the Xepr software from Bruker) and the data were fitted with a single radical with hyperfine interactions through N:Ho:HP 1:6:3 matching with the TPA radical cation using a built in software from Bruker.

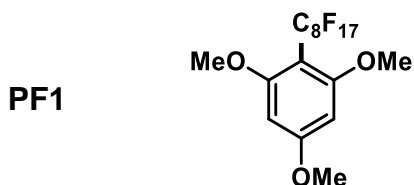
3.4 Transient absorption setup and sample preparation

Experiments were conducted using a laser flash photolysis setup (Luzchem). A Nd:YAG (Continuum Surelite CLII-10, 10 Hz, 450 mJ at 1064 nm) laser was used for excitation using its third harmonic with a wavelength centered at 355 nm. 10 mJ laser pulses were used with a pulse width of 6 ns. A 150 W Xe lamp was used as the monitoring light source. The detector consisted of a photomultiplier tube (PMT) connected to a digital oscilloscope (Tektronix TDS2012). All data was collected via the commercially available LFP 7.0 software (Luzchem).

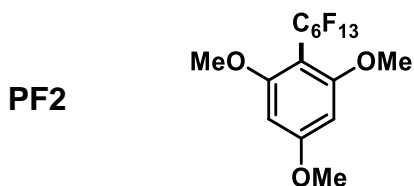
Samples containing TPA alone (~5mM) or in the presence of C6 (~20mM) in acetonitrile were freshly prepared in a 10 x 10 mm quartz cell. O₂ was removed by bubbling argon

through the solution and sealed with a septum. Samples were irradiated with at least 10 laser shots to acquire ΔOD temporal evolution traces. The time per division recorded by the detector was varied from 10 μs to 250 μs on a sample-to-sample basis to optimize the time window to fully capture the temporal events. Spectra were acquired at 10 nm intervals in the 400-710 nm range.

4. Characterization data of reported compounds:

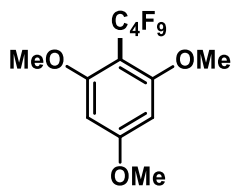


2-(perfluorooctyl)-1,3,5-trimethoxybenzene (1)⁵: White solid. 80% yield. ¹H NMR (500 MHz, CDCl₃) δ 6.15 (s, 2H), 3.82 (d, $J = 18.0$ Hz, 9H). ¹³C NMR (126 MHz, CDCl₃) δ 163.7, 161.7, 161.6, 91.6, 56.1, 55.2. ¹⁹F NMR (471 MHz, CDCl₃) δ -80.86, -102.66, -121.70, -122.07, -122.81, -126.00.



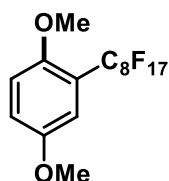
2-(perfluorohexyl)-1,3,5-trimethoxybenzene (2)⁵: White solid. 79% yield. ¹H NMR (500 MHz, CDCl₃) δ 6.15 (s, 2H), 3.82 (d, $J = 18.3$ Hz, 9H). ¹³C NMR (126 MHz, CDCl₃) δ 164.2, 162.1, 92.1, 56.7, 55.7. ¹⁹F NMR (471 MHz, CDCl₃) δ -80.69, -102.71, -122.04, -122.16, -122.62, -126.10.

PF3



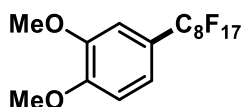
2-(perfluorobutyl)-1,3,5-trimethoxybenzene (3)⁵: White solid. 50% yield. ¹H NMR (500 MHz, CDCl₃) δ 6.14 (d, *J* = 1.0 Hz, 2H), 3.82 (d, *J* = 19.0 Hz, 9H). ¹³C NMR (126 MHz, CDCl₃) δ 164.2, 162.1, 92.1, 56.7, 55.7. ¹⁹F NMR (471 MHz, CDCl₃) δ -80.64, -102.90, -122.97, -126.44.

PF4



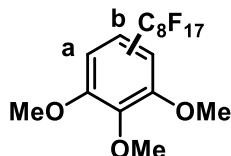
2-(perfluorooctyl)-1,4-dimethoxybenzene (4)⁶: White solid. 49% yield. ¹H NMR (500 MHz, CDCl₃) δ 7.11 – 6.91 (m, 3H), 3.81 (d, *J* = 10.7 Hz, 6H). ¹³C NMR (126 MHz, CDCl₃) δ 153.5, 119.1, 114.6, 57.1, 56.3. ¹⁹F NMR (471 MHz, CDCl₃) δ -80.77, -107.66, -121.09, -121.65, -121.91, -122.69, -126.12.

PF5



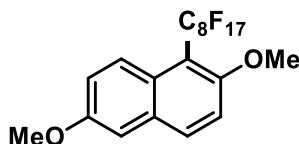
4-(perfluorooctyl)-1,2-dimethoxybenzene (5)⁶: White solid. 46% yield. ¹H NMR (500 MHz, CDCl₃) δ 7.18 (dd, *J* = 8.5, 2.1 Hz, 1H), 7.02 (d, *J* = 2.1 Hz, 1H), 6.95 (d, *J* = 8.4 Hz, 1H), 3.93 (d, *J* = 7.5 Hz, 6H). ¹³C NMR (126 MHz, CDCl₃) δ 151.7, 148.8, 120.0, 110.7, 109.3, 55.9. ¹⁹F NMR (471 MHz, CDCl₃) δ -80.60, -109.60, -121.26, -121.81, -122.71, -126.08.

PF6



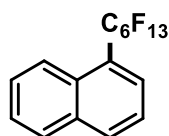
4- and 5-(perfluorooctyl)-1,2,3-trimethoxybenzene (6): White solid. 20% yield (inseparable mixture of isomers 1:1). ^1H NMR (500 MHz, CDCl_3) δ 7.20 (d, $J = 9.0$ Hz, 1H), 6.78 (s, 2H), 6.73 (d, $J = 9.0$ Hz, 1H), 3.96 – 3.85 (m, 16H). ^{13}C NMR (126 MHz, CDCl_3) δ 157.3, 153.7, 143.3, 124.0, 107.0, 104.6, 62.1, 61.3, 61.1, 56.7, 56.4. ^{19}F NMR (471 MHz, CDCl_3) δ -80.78, -103.27, -104.64, -106.63, -109.98, -120.94, -121.27, -121.61, -121.92, -122.69, -126.05.

PF7



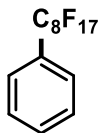
1-(perfluorooctyl)-2,6-dimethoxynaphthalene (8): White solid. 43% yield. ^1H NMR (500 MHz, CDCl_3) δ 8.09 (d, $J = 9.7$ Hz, 1H), 7.90 (d, $J = 9.1$ Hz, 1H), 7.31 (d, $J = 9.1$ Hz, 1H), 7.21 (dd, $J = 9.6, 2.8$ Hz, 1H), 7.10 (d, $J = 2.8$ Hz, 1H), 3.93 (d, $J = 20.4$ Hz, 6H). ^{13}C NMR (126 MHz, CDCl_3) δ 155.8, 149.8, 136.2, 128.6, 126.1, 115.1, 57.5, 55.1. ^{19}F NMR (471 MHz, CDCl_3) δ -80.76, -99.99, -120.64, -121.66, -122.09, -122.66, -126.07.

PF8



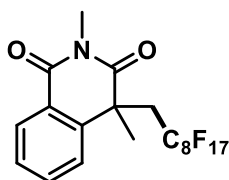
1-perfluorohexylnaphthalene (9)¹: White solid. 58% yield. ^1H NMR (500 MHz, CDCl_3) δ 8.23 (d, $J = 8.6$ Hz, 1H), 8.06 (d, $J = 8.2$ Hz, 1H), 7.95 – 7.90 (m, 1H), 7.83 (d, $J = 7.3$ Hz, 1H), 7.65 – 7.53 (m, 3H). ^{13}C NMR (126 MHz, CDCl_3) δ 134.1, 133.4, 129.0, 126.3, 124.2. ^{19}F NMR (471 MHz, CDCl_3) δ -80.78, -104.40, -120.21, -121.48, -122.68, -126.12.

PF9



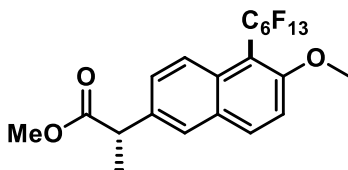
Perfluorooctylbenzene (10)¹: Yellow oil. 78% yield. ¹H NMR (500 MHz, CDCl₃) δ 7.66 – 7.54 (m, 3H), 7.51 (dd, *J* = 8.3, 6.8 Hz, 2H). ¹³C NMR (126 MHz, CDCl₃) δ 132.3, 129.3, 129.2, 129.0, 127.2, 127.2, 127.1. ¹⁹F NMR (471 MHz, CDCl₃) δ -80.82, -110.88, -121.30, -121.90, -122.73, -126.12.

PF10



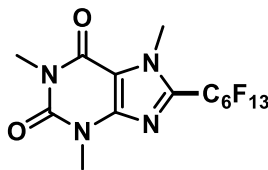
4-(perfluorooctyl)-2,4-dimethylisoquinoline-1,3(2H,4H)-dione (11): Off-white solid. 15% yield. ¹H NMR (500 MHz, CDCl₃) δ 8.30 (dd, *J* = 7.9, 1.5 Hz, 1H), 7.66 (td, *J* = 7.6, 1.5 Hz, 1H), 7.56 – 7.39 (m, 2H), 3.42 (s, 4H), 2.84 – 2.65 (m, 1H), 1.68 (s, 3H). ¹³C NMR (126 MHz, CDCl₃) δ 175.0, 164.1, 141.0, 134.1, 129.7, 128.4, 126.1, 124.4, 43.7, 41.2, 32.3, 30.1, 27.8. ¹⁹F NMR (471 MHz, CDCl₃) δ -80.82, -107.59, -108.18, -112.52, -113.10, -121.53, -121.94, -122.75, -123.77, -126.09.

PF11



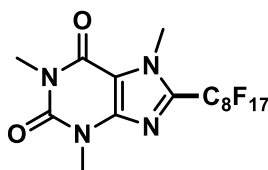
Naproxen methyl ester-C₆F₁₃ (13)¹: White solid. 30% yield. ¹H NMR (500 MHz, CDCl₃) δ 8.15 (d, *J* = 9.2 Hz, 1H), 7.98 (d, *J* = 9.1 Hz, 1H), 7.70 (d, *J* = 2.1 Hz, 1H), 7.49 (dd, *J* = 9.2, 2.1 Hz, 1H), 7.34 (d, *J* = 9.1 Hz, 1H), 3.97 (s, 3H), 3.87 (q, *J* = 7.1 Hz, 1H), 3.68 (s, 3H), 1.58 (d, *J* = 7.2 Hz, 3H). ¹³C NMR (126 MHz, CDCl₃) δ 175.1, 159.4, 136.5, 135.3, 131.7, 129.8, 128.4, 127.2, 125.4, 115.0, 57.8, 52.5, 45.3, 18.7. ¹⁹F NMR (471 MHz, CDCl₃) δ -80.77, -100.14, -120.66, -121.95, -122.60, -126.03.

PF12



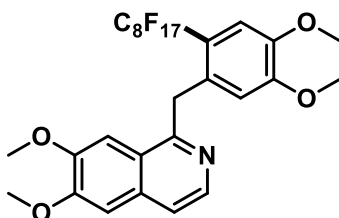
Caffeine-C₆F₁₃ (14)¹: White solid. 32% yield. ¹H NMR (500 MHz, CDCl₃) δ 4.19 (s, 3H), 3.59 (s, 3H), 3.42 (s, 3H). ¹³C NMR (126 MHz, CDCl₃) δ 155.4, 147.4, 147.0, 33.8, 29.9, 28.2. ¹⁹F NMR (471 MHz, CDCl₃) δ -80.69, -108.96, -120.96, -121.36, -122.67, -126.03.

PF13

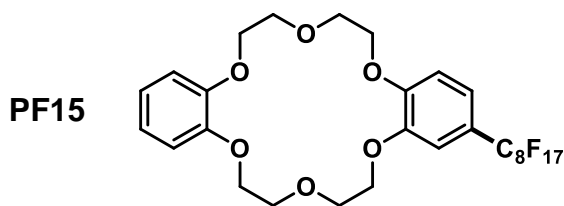


Caffeine-C₈F₁₇ (15)¹: White solid. 30% yield. ¹H NMR (500 MHz, CDCl₃) δ 4.19 (d, *J* = 1.9 Hz, 3H), 3.60 (s, 3H), 3.42 (s, 3H). ¹³C NMR (126 MHz, CDCl₃) δ 155.4, 151.2, 33.8, 29.9, 28.2. ¹⁹F NMR (471 MHz, CDCl₃) δ -80.68, -108.89, -120.91, -121.13, -121.67, -122.65, -126.05.

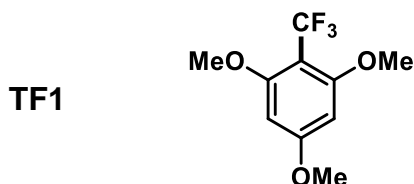
PF14



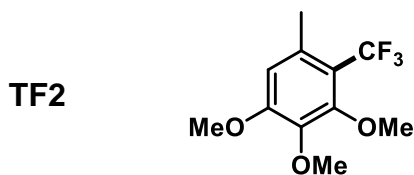
Papaverine-C₈F₁₇ (16)¹: White solid. 15% yield. ¹H NMR (500 MHz, CDCl₃) δ 8.40 (d, *J* = 5.8 Hz, 1H), 7.53 (d, *J* = 5.8 Hz, 1H), 7.22 (s, 1H), 7.10 (s, 1H), 7.03 (s, 1H), 6.44 (s, 1H), 4.76 (s, 2H), 4.03 (s, 3H), 3.89 (s, 3H), 3.83 (s, 3H), 3.55 (s, 3H). ¹³C NMR (201 MHz, CDCl₃) δ 151.8, 147.6, 123.3, 119.8, 117.9, 113.8, 111.4, 105.6, 104.1, 56.4, 56.4, 56.15, 56.0, 30.0. ¹⁹F NMR (471 MHz, CDCl₃) δ -80.73, -104.30, -120.37, -121.47, -122.65, -126.04.



2-(perfluorooctyl)dibenzo[b,k][1,4,7,10,13,16]hexaoxacyclooctadecane(17): White solid. 85% yield. ^1H NMR (500 MHz, CDCl_3) δ 7.14 (dt, $J = 8.5, 2.2$ Hz, 1H), 7.00 (d, $J = 2.3$ Hz, 1H), 6.88 (dddd, $J = 17.2, 9.6, 7.1, 3.0$ Hz, 5H), 4.31 – 3.89 (m, 16H). ^{13}C NMR (126 MHz, CDCl_3) δ 151.7, 148.7, 129.0, 121.6, 120.8, 113.3, 112.2, 111.3, 70.1, 69.8, 69.0, 68.7, 68.6. ^{19}F NMR (471 MHz, CDCl_3) δ -80.99, -109.76, -121.48, -121.95, -122.83, -126.18.

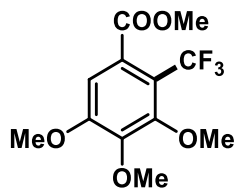


2-(trifluoromethyl)-1,3,5-trimethoxybenzene (TF1)⁷: White solid. 82% yield. ^1H NMR (500 MHz, CDCl_3) δ 6.13 (s, 2H), 3.83 (d, $J = 1.3$ Hz, 10H). ^{13}C NMR (126 MHz, CDCl_3) δ 163.5, 160.4, 125.4, 123.2, 100.7, 91.2, 56.2, 55.3. ^{19}F NMR (471 MHz, CDCl_3) δ -53.96.



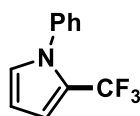
1,2,3-trimethoxy-5-methyl-4-(trifluoromethyl)benzene (TF2)⁷: Colorless oil. 56% yield. ^1H NMR (500 MHz, CDCl_3) δ 6.49 (s, 1H), 3.95 – 3.80 (m, 9H), 2.42 (q, $J = 3.4$ Hz, 3H). ^{13}C NMR (126 MHz, CDCl_3) δ 155.0, 153.2, 140.8, 132.9, 128.6, 125.8, 123.6, 115.2, 110.5, 61.6, 60.7, 55.8, 21.4. ^{19}F NMR (471 MHz, CDCl_3) δ -54.30.

TF3



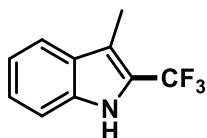
methyl 3,4,5-trimethoxy-2-(trifluoromethyl)benzoate (TF3)⁷: Colorless oil. 45% yield. ¹H NMR (500 MHz, CDCl₃) δ 6.75 (s, 1H), 3.95 (s, 3H), 3.90 (d, *J* = 8.2 Hz, 9H). ¹³C NMR (126 MHz, CDCl₃) δ 168.8, 156.2, 144.5, 128.8, 124.5, 122.3, 115.1, 107.2, 62.2, 61.3, 56.6, 53.4. ¹⁹F NMR (471 MHz, CDCl₃) δ -56.86.

TF4



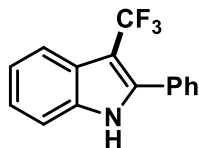
1-phenyl-2-(trifluoromethyl)-1H-pyrrole (TF4)⁷: Yellow oil. 46% yield. ¹H NMR (500 MHz, CDCl₃) δ 7.51 – 7.35 (m, 5H), 6.88 (dd, *J* = 2.8, 1.7 Hz, 1H), 6.73 (dd, *J* = 4.0, 1.8 Hz, 1H), 6.32 – 6.22 (m, 1H). ¹³C NMR (126 MHz, CDCl₃) δ 139.5, 129.3, 128.8, 127.6, 126.9, 122.6, 120.5, 113.1, 108.6. ¹⁹F NMR (471 MHz, CDCl₃) δ -55.95.

TF5



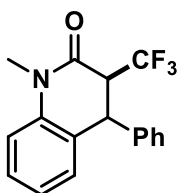
3-methyl-2-(trifluoromethyl)-1H-indole (TF5)⁷: White solid. 50% yield. ¹H NMR (500 MHz, CDCl₃) δ 8.19 (s, 1H), 7.65 (d, *J* = 8.0 Hz, 1H), 7.42 – 7.29 (m, 2H), 7.20 (ddd, *J* = 8.0, 6.8, 1.1 Hz, 1H), 2.45 (d, *J* = 1.2 Hz, 3H). ¹³C NMR (126 MHz, CDCl₃) δ 135.5, 128.4, 125.1, 123.5, 120.7, 120.4, 114.4, 111.9, 8.7. ¹⁹F NMR (471 MHz, CDCl₃) δ -58.64.

TF6



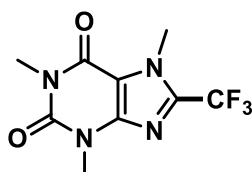
2-phenyl-3-(trifluoromethyl)-1H-indole (TF6)⁷: Yellow solid. 38% yield. ¹H NMR (500 MHz, CDCl₃) δ 8.35 (s, 1H), 7.89 – 7.80 (m, 1H), 7.63 – 7.56 (m, 2H), 7.54 – 7.37 (m, 4H), 7.35 – 7.21 (m, 3H). ¹³C NMR (126 MHz, CDCl₃) δ 138.9, 135.2, 131.4, 129.7, 129.4, 129.0, 123.8, 122.1, 120.4, 111.4, 103.8. ¹⁹F NMR (471 MHz, CDCl₃) δ -52.91.

TF7

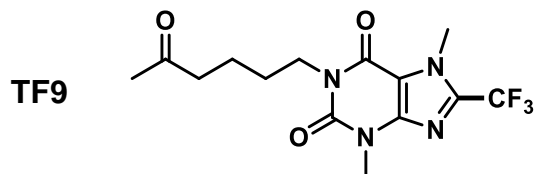


3-(trifluoromethyl)-1-methyl-4-phenyl-3,4-dihydroquinolin-2(1H)-one (TF7)⁸: Colorless oil. 42% yield. ¹H NMR (500 MHz, CDCl₃) δ 7.37 (ddd, *J* = 8.6, 7.3, 1.6 Hz, 1H), 7.29 – 7.26 (m, 2H), 7.24 – 7.19 (m, 2H), 7.14 – 7.09 (m, 2H), 7.01 (dd, *J* = 7.4, 1.7 Hz, 2H), 4.51 (s, 1H), 3.66 (qd, *J* = 9.4, 1.4 Hz, 1H), 3.46 (s, 3H). ¹³C NMR (126 MHz, CDCl₃) δ 161.6, 140.2, 139.3, 129.3, 128.8, 127.7, 127.0, 124.6, 124.3, 115.3, 53.2, 42.1, 30.3. ¹⁹F NMR (471 MHz, CDCl₃) δ -67.29.

TF8



Caffeine-CF₃ (TF8)⁷: White solid. 48% yield. ¹H NMR (500 MHz, CDCl₃) δ 4.16 (s, 3H), 3.59 (s, 3H), 3.42 (s, 3H). ¹³C NMR (126 MHz, CDCl₃) δ 155.4, 151.3, 146.5, 119.2, 117.1, 109.6, 33.2, 29.9, 28.2. ¹⁹F NMR (471 MHz, CDCl₃) δ -62.39.



Pentoxifylline- CF_3 (TF9):⁹ Off-white solid. 41% yield. ^1H NMR (500 MHz, CDCl_3) δ 4.14 (d, $J = 1.4$ Hz, 3H), 4.01 (t, $J = 6.9$ Hz, 2H), 3.57 (s, 3H), 2.49 (t, $J = 6.9$ Hz, 2H), 2.13 (s, 3H), 1.70 – 1.59 (m, 4H). ^{13}C NMR (126 MHz, CDCl_3) δ 208.9, 155.7, 151.4, 146.9, 139.4, 139.1, 128.8, 119.6, 117.5, 110.0, 43.4, 41.5, 33.5, 33.5, 30.3, 30.2, 29.6, 27.6, 21.2. ^{19}F NMR (471 MHz, CDCl_3) δ -62.41.

5. References

- (1) Castillo-Pazos, D. J.; Lasso, J. D.; Li, C.-J. Synthesis of α -(perfluoroalkylsulfonyl)propiophenones: a new set of reagents for the light-mediated perfluoroalkylation of aromatics. *Beilstein J. Org. Chem.* **2022**, *18*, 788-795.
- (2) Protti, S.; Mella, M.; Bonesi, S. M. Photochemistry of triphenylamine (TPA) in homogeneous solution and the role of transient N-phenyl-4a,4b-dihydrocarbazole. A steady-state and time-resolved investigation. *New J. Chem.* **2021**, *45* (36), 16581-16593.
- (3) Feng, X.-Z.; Lin, Z.; Yang, L.-J.; Wang, C.; Bai, C.-I. Investigation of the interaction between acridine orange and bovine serum albumin. *Talanta* **1998**, *47* (5), 1223-1229.
- (4) Gaussian 16, Revision B.01, M. J. Frisch, G. W. Trucks, H. B. Schlegel, G. E. Scuseria, M. A. Robb, J. R. Cheeseman, G. Scalmani, V. Barone, G. A. Petersson, H. Nakatsuji, X. Li, M. Caricato, A. V. Marenich, J. Bloino, B. G. Janesko, R. Gomperts, B. Mennucci, H. P. Hratchian, J. V. Ortiz, A. F. Izmaylov, J. L. Sonnenberg, D. Williams-Young, F. Ding, F. Lipparini, F. Egidi, J. Goings, B. Peng, A. Petrone, T. Henderson, D. Ranasinghe, V. G. Zakrzewski, J. Gao, N. Rega, G. Zheng, W. Liang, M. Hada, M. Ehara, K. Toyota, R. Fukuda, J. Hasegawa, M. Ishida, T. Nakajima, Y. Honda, O. Kitao, H. Nakai, T. Vreven, K. Throssell, J. A. Montgomery, Jr., J. E. Peralta, F. Ogliaro, M. J. Bearpark, J. J. Heyd, E. N. Brothers, K. N. Kudin, V. N. Staroverov, T. A. Keith, R. Kobayashi, J. Normand, K. Raghavachari, A. P. Rendell, J. C. Burant, S. S. Iyengar, J. Tomasi, M. Cossi, J. M. Millam, M. Klene, C. Adamo, R. Cammi, J. W. Ochterski, R. L. Martin, K. Morokuma, O. Farkas, J. B. Foresman, and D. J. Fox, Gaussian, Inc., Wallingford CT, 2016.
- (5) Tasnim, T.; Ryan, C.; Christensen, M. L.; Fennell, C. J.; Pitre, S. P. Radical Perfluoroalkylation Enabled by a Catalytically Generated Halogen Bonding Complex and Visible Light Irradiation. *Org. Lett.* **2022**, *24* (1), 446-450.
- (6) Hossain, M. J.; Ono, T.; Wakiya, K.; Hisaeda, Y. A vitamin B12 derivative catalyzed electrochemical trifluoromethylation and perfluoroalkylation of arenes and heteroarenes in organic media. *Chem. Commun.* **2017**, *53* (79), 10878-10881.

(7) Liu, P.; Liu, W.; Li, C.-J. Catalyst-Free and Redox-Neutral Innate Trifluoromethylation and Alkylation of Aromatics Enabled by Light. *J. Am. Chem. Soc.* **2017**, *139* (40), 14315-14321.

(8) Chen, L.; Ma, P.; Yang, B.; Zhao, X.; Huang, X.; Zhang, J. Photocatalyst and additive-free visible light induced trifluoromethylation–arylation of N-arylacrylamides with Umemoto's reagent. *Chem. Commun.* **2021**, *57* (8), 1030-1033.

(9) McClain, E. J.; Monos, T. M.; Mori, M.; Beatty, J. W.; Stephenson, C. R. J. Design and Implementation of a Catalytic Electron Donor–Acceptor Complex Platform for Radical Trifluoromethylation and Alkylation. *ACS Catal.* **2020**, *10* (21), 12636-12641.

4 New Devices

Design of a 3D Printed Photoreactor for Accessible High Throughput Experimentation



High-Throughput Experimentation Reactor and
Modular Environment for Synthesis



This manuscript is under revision. Currently it is also under evaluation as a report of invention titled “A 3D printed photoreactor for High-Throughput Experimentation” with track code D2025-0002

Preface

In Chapters 2 and 3, we provided an overview of two projects that aimed to advance the understanding and applicability of new reactivities in homogeneous photocatalysis. More specifically, these works represent a proof of concept regarding the development of new reagents and new catalytic pathways, respectively. As it is custom in most synthetic fields, the advantages, impact, and future opportunities of these methodologies were discussed focusing on the novelty of the proposal, along with metrics such as yields, atom-economy, or scope diversity. However, standardization of photocatalytic methods requires us to also pay attention to technical specifications such as the nature and reproducibility of the setup, the type of irradiation source, or the vessel employed.

After a short internship at the Capabilities group of the pharmaceutical company Merck & Co., Inc., I realized the importance of investing time and resources towards the development of new tools to solve pressing chemistry problems. Within the High-Throughput Experimentation (HTE) laboratory, many of these tools took the shape of new methodologies and reagents, but also new software and devices that could speed the efficiency of day-to-day work. While many of these advancements remain currently out of reach for the academic photocatalysis research community, they still provide inspiration to develop similar tools for educational settings at a fraction of the cost.

For this reason, upon my return to McGill, we decided to develop an accessible apparatus that would help closing the existing gap between “homemade” non-standardized photocatalytic setups, and the highly engineered HTE devices employed by the chemical industry. After one year of collaborative design efforts, we were able to develop an affordable open source photoreactor through 3D printing. This device can run 24 reactions in parallel with the help of a single LED lamp and can be easily sourced from commercially available parts. In Chapter 4, we describe its operational components and modules and discuss its efficiency through radiometric and chemical testing (i.e. using a model reaction).

Author contributions:

Durbis Castillo and Juan Lasso contributed to the project conception under the supervision of Prof. Chao-Jun Li. Durbis Castillo and Jean-Philippe Guay designed and built the photoreactor, along with all its prototypes. Durbis Castillo tested all functioning modules. Durbis Castillo and Juan Lasso set up and analyzed the corresponding reaction plates. Alexander Logozzo designed and tested the absorptive filter employed to homogenize incident light under the supervision of Prof. Thomas Preston. Loric Lefebvre and Alexei Kieran prepared duplicate reaction plates to test for reproducibility. Durbis Castillo and Alexander Logozzo wrote the manuscript with the help and editing of Prof. Chao-Jun Li and Juan Lasso.

Abstract

We report the design and validation of a first-in-kind 3D-printed photoreactor capable of running 24 reactions simultaneously, employing a standard reaction block and a single Kessil lamp. The reactor features stirring and temperature control modules, making it an efficient tool for photochemical research. It provides an accessible and reproducible platform for accelerating reaction discovery and optimization, while also serving as a valuable training tool for students in high-throughput experimentation (HTE).

Introduction

Within the realm of synthetic chemistry, photocatalysis has become a vital instrument enabling innovative and selective transformations under mild conditions, often using visible light at room temperature.¹ Advances in LED technology have provided energy-efficient, high-intensity, and controllable light sources which allow for streamlining of operations and lowering costs while expanding accessibility. Despite these advances, inconsistencies in published methods due to the wide variety of light sources and experimental setups remains a key challenge, highlighting the need for standardization in photochemical equipment.^{2, 3} While multiple commercially available photoreactors (e.g. Hepatochem, Lumidox, SynLED, LuzChem, among others) have successfully solved reproducibility issues and their performance has been extensively compared in the literature,^{2, 4} they remain mostly out of reach for academic research due to their cost.

In the last five years, 3D printed photoreactors have recently emerged as a more accessible solution to this problem, leveraging additive manufacturing (3D printing) as a valuable resource for homogeneous and heterogeneous photocatalysis alike.⁵⁻⁸ Main examples include the works published by the teams of Rossi,⁹ Gellman,¹⁰ Brown and Sherwood,¹¹ Ananikov,¹² López,¹³ Martins,¹⁴ and Aubineau.¹⁵ Most of these designs support versatile applications in photoredox catalysis, and have adapted commercially available LED sources to work with common microscale batch vessels such as vials and test tubes (**Figure 4.1**). This ability underscores the potential for 3D printing to democratize access to advanced photochemical techniques, allowing researchers to replicate and innovate upon existing methodologies. Moreover, recent designs have been geared towards the inclusion of other valuable capabilities such as flow chemistry and

multi-purpose reactor platforms. This is well exemplified in the reports showcased by the teams of Schiel,¹⁶ Liauw,¹⁷ Penny and Hilton,¹⁸ and Noël,¹⁹ emphasizing the possibility to tailor photoreactors to specific reaction conditions. However, despite these accomplishments, the absence of an open-source 3D printed photoreactor compatible with High-Throughput Experimentation (HTE) techniques remains a major gap in the field.

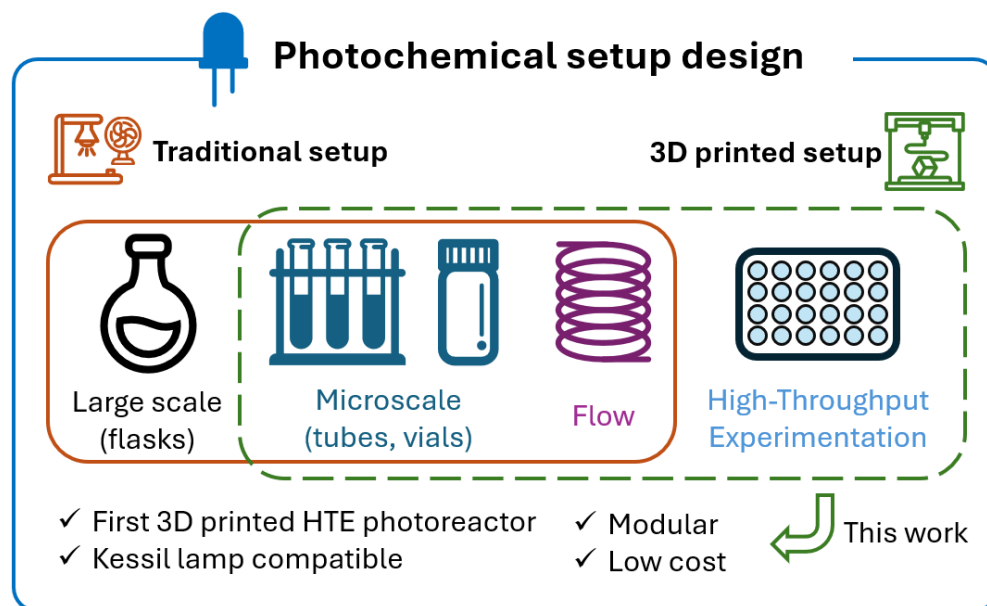


Figure 4.1: Current state of the art for photochemical setup design for homogeneous photocatalysis, where HTE compatible 3D printed setups still represent a major gap.

HTE capabilities in chemistry comprise setting up and analyzing large arrays of miniaturized chemical reactions in parallel, usually inside a matrix plate with several vials ranging from 24 to 1536.²⁰⁻²² Implementing HTE in a laboratory provides powerful improvements and benefits such as accelerated exploration of chemical space for synthesis and reaction optimization and reduced set up time. Additionally, it employs smaller amounts of starting materials, and provides the capacity to observe second-degree correlations between reaction parameters that are usually ignored during traditional monoparametric reaction optimizations.^{20, 23, 24} For this reason, numerous sectors of industry—notably drug development campaigns or material discovery programs—have invested significant effort and resources to improve and develop new and sophisticated HTE tools.^{25, 26}

More than 25 years after the first attempts to implement HTE techniques within the field of chemistry,²⁷ many of these tools remain inaccessible to most academic research and teaching laboratories, mainly due to three factors: the prohibitive cost of equipment needed to reproduce reported methodologies, limited access to adequate analytical capabilities,²⁸ and the subsequent lack of familiarity and skepticism regarding its benefits.²⁹ On that account, multiple academic groups have since demonstrated the feasibility of adapting HTE techniques within their projects and developing new tools for their democratization.^{23, 30-33} However, these projects heavily depend on industrial collaboration and have been mostly focused on metal- and organocatalyzed methodologies that require no light input. For these reasons, a cheap, modular, and accessible reactor capable of facilitating photocatalyzed HTE using standardized light sources under a controlled environment has become a major area of opportunity. Such development would bring together both the wide accessibility of 3D printing and the accelerated discovery capabilities of HTE.

Herein, we disclose the design and testing of the first 3D printed photoreactor aimed at running photocatalytic reactions in parallel under a controlled-temperature environment. This apparatus can be sourced from inexpensive and commercially available parts, including a 24-well reaction block and a Kessil LED lamp, and represents a valuable resource for academic training regarding the use of HTE.

Results and Discussion

Design of the photoreactor

According to Schiel and co-workers,¹⁶ new 3D printed setups must attempt to meet a series of requirements in order to contribute standardization and increase the chances of widespread adoption. These requirements include fixed vial and lamp positions for reproducibility, variable light intensity across defined light sources, temperature control, and the possibility to perform several reactions at the same time, preferably using different vessels—according to the type of reaction of interest. Additionally, setups must strive for affordability and practicality (i.e. adequate size, safe to use).

To conceive our photoreactor, we had to build our design around its two most important elements: the light source, and the HTE plate. As a light source, we chose to work with the PR160L LED series sold by Kessil due to their ubiquitous presence throughout academic laboratories and the wide selection of available lamps with distinct wavelengths. Regarding the HTE plate, we decided to test our concept using a 24-well Para-dox block from Analytical Sales for its compatibility with smaller analytical settings. With respect to the method of manufacture, we set to use Fused Deposition Modelling (FDM) as it is the simplest, most widely available, and least expensive 3D printing technique. This technique is based on the use of a thermoplastic filament (e.g. PLA, PP, or PET), which is melted and extruded through a heated nozzle to form 3D structures. In this process, 2D layers are built one on top of another to create a three-dimensional object.⁶

Having pinned down these 3 features, our objective was to develop a 3D printed framework capable of directing light irradiation into the bottom holes of the HTE plate. Hence, our design had two additional specifications: an alternative stirring method was required to ensure proper mixing at the height of the plate, and cooling was required to keep both the lamp and the plate at a regulated temperature. To meet all requirements, we came up with the layout shown in **Figure 4.2**.

This layout consists of the following main components (A detailed list can be found in **Section 1 of the SI**, along with building instructions):

1. A cylindrical body with an upper chamber containing a support for a 24-well reaction block which is directly irradiated by the lamp from below. To address overheating, we opted for a tandem approach: The chamber's temperature is regulated through liquid-assisted cooling in the form of Tygon tubing connected to an external recirculating chiller, while overheating of the lamp is prevented thanks to two fans venting the interior of the body.
2. A drawer supporting the lamp in a vertical fashion, capable of sliding inside the body of the reactor and surrounded by channels that allow for the flow of air created by the fans located on the back of the main body.

3. Lastly, a lid containing electronic components comprising the stirring module, including a temperature sensor and display, a motor and its speed control. Such motor extends inside the upper chamber of the main body in the form of a rotor containing two magnets that assist the stirring of the reactions.

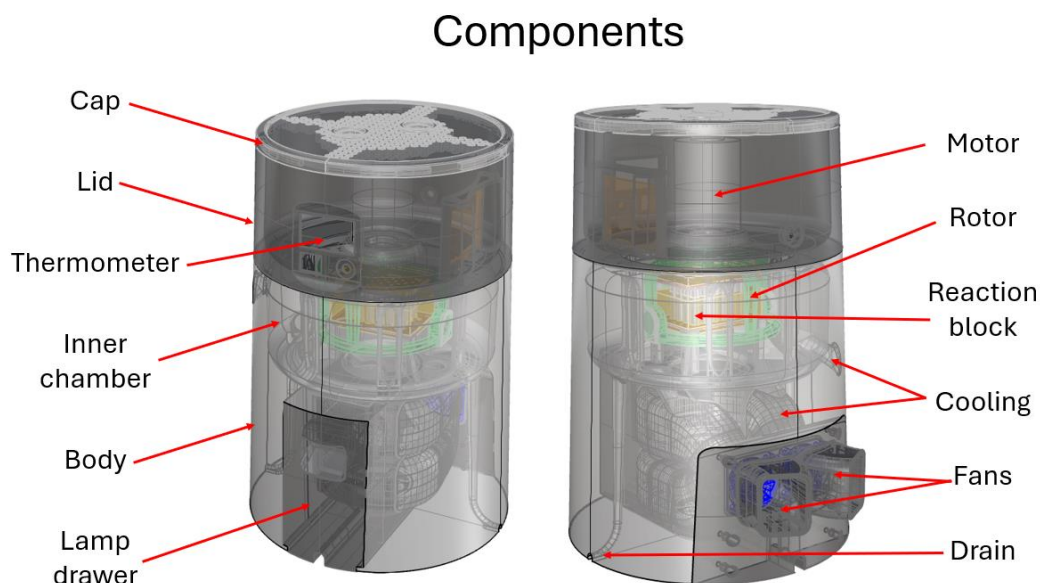


Figure 4.2: Main structural components of the HERMES photoreactor

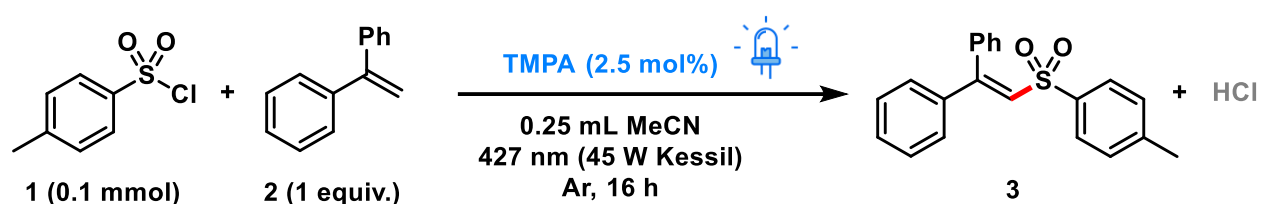
For easier identification, we have named our photoreactor HERMES, which stands for High-throughput Experimentation Reactor and Modular Environment for Synthesis. This name includes a reference to the 3 modules needed for this reactor to operate (a light source, an overhead stirrer, and a cooling system), while hinting at the increased speed of discovery and exploration that comes with the use of HTE. Lastly, but very importantly, the total cost of manufacturing for this photoreactor amounts to a range of 164 to 224 USD, which presents a stark difference when compared to the prices of commercially available photoreactors, in the range of thousands of dollars.¹⁶ A brief breakdown of the cost calculation is provided in **Section 1 of the SI**.

Reactor characterization and testing

After printing the first functional prototype of the photoreactor, we set to determine the correct operation of its different modules. Initially, we confirmed the efficacy of stirring via visual inspection of the stir bars placed across the 24 vials of the block, all of which moved uniformly—even when solids are added in solution. Next, we decided to test the photoreactor's temperature control capacity (Results summarized in **Section 2 of the SI**). Firstly, a thermal imaging camera allowed us to inspect the temperature reached by different elements of the photoreactor. This helped us confirm that the recirculation effectively kept the inner chamber of the photoreactor at controlled lower temperatures (e.g. 25 °C) with or without an operating lamp. Additionally, we also verified that the internal electronic components—including the lamp and fans—do not reach temperatures above 37 °C, ensuring their continuous operability. Secondly, we monitored the temperature stability inside the chamber for a period of 24 hours with a Kessil lamp operating at 100% intensity. Gratifyingly, the temperature values measured both by the thermal camera and the digital thermometer appeared stable after an induction period of one hour. Lastly, to rule out temperature anisotropy throughout the reaction block, we registered the temperature of each well after two hours of irradiation, showing negligible temperature changes across all positions.

Next, we turned our attention to the light irradiation module of the photoreactor. To guarantee the homogeneity of the light incident on the reaction wells, a laser-jet printed absorptive filter was designed in house via a radiometric approach.³⁴ Initially, a calibration curve was constructed to determine the transmittance as a function of printed filter opacity (**SI, Section 3**). The measured intensity distribution ~3.5 cm from the front of the Kessil lamp was used to generate the filter opacity by applying the calibration curve and printing an individual filter for each well. The final filter is shown in **Figure S4.15**. The maximum intensity of the output beam is limited by the intensity at vials A1,6 and D1,6. The filter profile was then printed on commercially available transparent PET sheets (Uinkit, Laser Transparency Film). Upon letting the light pass through the filter, a homogenous light distribution was achieved, with the intensity only varying by a few percent.

Once we had established the correct function of all the elements within the photoreactor and corroborated the efficacy of the absorptive filter through radiometry, we selected a validation reaction to test yield consistency across a 24-well plate. We chose to perform a triarylamine-catalyzed radical sulfonylation recently published by our group (**Scheme 4.1**).³⁵ In this reaction, a catalytic Electron Donor Acceptor (EDA) complex between one equivalent of tosyl chloride (**1**) and a catalytic amount of 4-(trismethoxy) triphenylamine (TMPA) triggers the formation of sulfonyl radicals upon blue light irradiation. These radicals subsequently add to a suitable alkene, such as 1,1-diphenylethylene (**2**), to form the corresponding vinyl sulfone (**3**) in high yields (For a detailed mechanism, consult **Section 4 of the SI**). This transformation is easy to set up, proceeds within a reasonable timeframe (12-16 hours), and shows a straightforward product profile—hydrochloric acid is the only byproduct—, making it an ideal synthetic exercise to evaluate our photoreactor.



Scheme 4.1: Redox-neutral sulfonylation of olefins promoted by blue light and catalyzed by TMPA (4-(trismethoxy) triphenylamine).

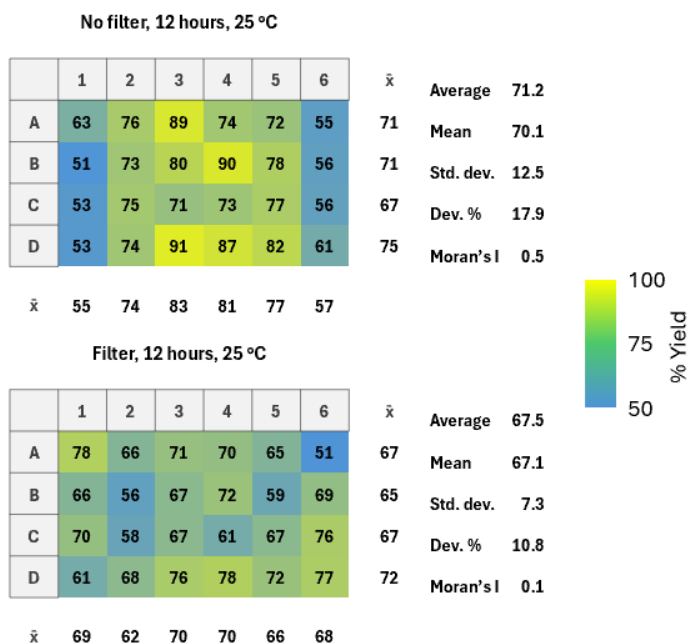
After scaling down the original reaction methodology (**SI, Section 4**), we then proceeded to test yield consistency through a series of plate controls; namely, with and without filter. To better understand yield consistency as the reaction evolved, we analyzed the product area percent (**SI, Section 5**) before reaction completion (after 12 hours at 25°C), and after reaction completion (after 16 hours at 28 °C). Yields for these controls are displayed in **Figure 4.3**, along with the average yields for each row and column, as well as 5 representative statistic measurements for comparison (average, mean, standard deviation, relative deviation, and Moran's I). While reactions before completion showed similar average and mean yields (**Figure 4.3A**), the use of an iterated and final version of the absorptive filter³⁶ led to decreased standard and relative deviations, with a noticeable change in the distribution of high yields across the plate. Visually, the yields on an

unfiltered plate follow a clear pattern with higher values at the center of the plate, correlated to the incident light intensity. For reactions at the point of completion (**Figure 4.3B**), both plates displayed a similar behavior, albeit within a smaller yield range. While an unfiltered reaction plate kept showing lower yields across the edges of the array, its filtered counterpart exhibits a clearly homogeneous layout with a relative deviation of 0.4%.

Nonetheless, to more rigorously determine whether the yield deviations in both the filtered and unfiltered reactions were due to the inhomogeneity of light, a spatial autocorrelation model was implemented. As mentioned above, reaction wells which receive the most intense light are expected to have the highest yields and should be clustered in the center of the reaction plate, while the samples on the perimeter receive significantly less light and are therefore expected to have the lowest yields. Moran's I (I) was calculated to determine whether the reaction yield spatial distribution was randomly or positively spatially autocorrelated. I values between -1 and 0 have a negative spatial autocorrelation (i.e. alternated), which we do not expect here. I values close to zero, are said to be randomly distributed, and I values close to one have a strong positive spatial autocorrelation (i.e. grouped).

On the one hand, Moran's I was evaluated for the model reaction yields without the addition of the absorptive filter. The 12-hour and 16-hour reaction yields without light filtering have I values of 0.46 and 0.37, respectively. This indicates that there is a medium positive autocorrelation between the yields, which can be interpreted as the lamp intensity distribution (**Figure 4.3**) having a significant impact on the yields. The lower I value for the 16-hour samples is also expected, as most of the reactions are allowed to run to completion, and therefore the distinct features of the lamp intensity distribution are less apparent.

A) Model reaction yields (before completion)



B) Model reaction yields (at completion)

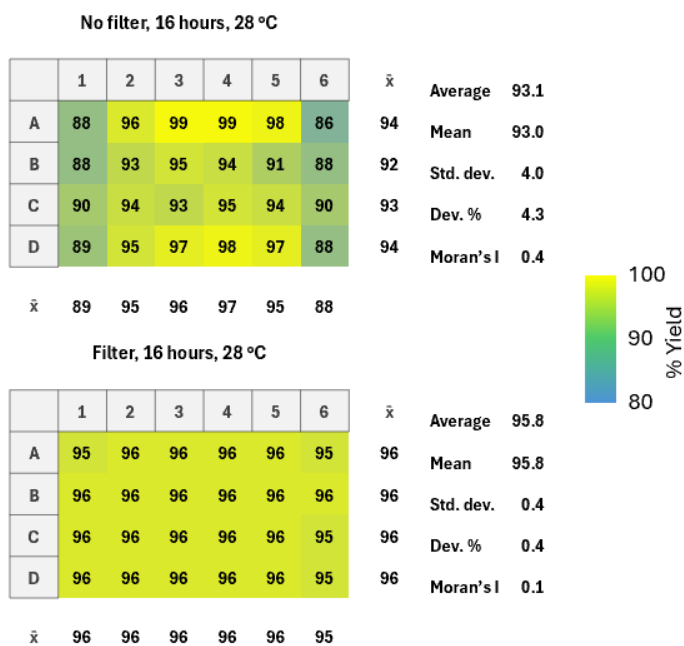


Figure 4.3: Model reaction yields before completion (A), and after completion (B). Duplicate plates are shown in Section 5 of the SI.

On the other hand, when the reactions are conducted with the absorptive filter in place, significantly higher homogeneity between samples is achieved. The *I* value for the model reaction after 12-hours and 16-hours is 0.14 and 0.09, respectively. This indicates that there is a weak positive autocorrelation between the samples, but the yields are mostly randomly distributed. Therefore, the deviation between sample yields is unlikely to be caused by the light intensity distribution, but rather by other random sources of error (i.e. stock solution dispensing, reaction block sealing, analytical sample preparation, etc.). For this reason, it should be noted that rigorous, well-applied HTE campaigns rely on good practices such as reproduction of plates, validation of hits at larger scale, and adequate statistical analysis.²⁰

Having demonstrated the correct operation of all photoreactor modules, as well as the effectiveness of the absorptive filter to even out the light absorption across the 24 reaction wells, we have included a quick user guide (**Section 1, SI**) and a filter template that can be printed on a transparency film with the help of a jet-laser printer (**Section 3, SI**). The authors believe that the accessibility of this photoreactor will allow students and researchers of all levels to become acquainted with the basics of HTE, and successfully apply these skills to their synthetic needs.

Conclusions:

Herein, we have designed, developed, and tested a 3D-printed photoreactor capable of running 24 reactions at the same time with the help of a standard reaction block from Analytical Sales, while employing a single Kessil LED lamp. To achieve this, we have integrated a stirring module and a temperature control module within the same device. Such apparatus, paired with basic analytical techniques such as gas or liquid chromatography (GC, LC), can be used to accelerate the rate of discovery and optimization of photochemical reactions for researchers in academic contexts. Additionally, it will provide an accessible and reproducible platform for students to train in the basics of HTE techniques, a highly valuable skill and standard practice in modern-day chemical industry. We hope this work will help solidify the idea that HTE methods can be integrated into academic settings and teaching labs, without the need for expensive

equipment such as automated robots, specialized software, or cutting-edge analytical capabilities. Future developments of this photoreactor will focus on the introduction of other commercially available light sources, as well as making it compatible with larger standard HTE plates (e.g. 96 wells).

Acknowledgements:

We would like to thank Vahid Shahabadi for his useful advice on the improvement of the absorptive filter. We thank Richard Rossi and Weihua Wang for their technical assistance with the assembly of electronic components, and we also thank Benedetta di Erasmo for her assistance in the development of the GCMS method used to analyze the samples. D.J.C.P. acknowledges the financial support granted by the Vanier Canada Graduate Scholarship, and the Dr. Lawrence Light Graduate Fellowship in Sustainability. J.D.L. thanks the Walter C. Sumner Foundation and NuChem Sciences for their financial support.

References

- (1) Romero, N. A.; Nicewicz, D. A. Organic Photoredox Catalysis. *Chem. Rev.* **2016**, *116* (17), 10075-10166.
- (2) Svejstrup, T. D.; Chatterjee, A.; Schekin, D.; Wagner, T.; Zach, J.; Johansson, M. J.; Bergonzini, G.; König, B. Effects of Light Intensity and Reaction Temperature on Photoreactions in Commercial Photoreactors. *ChemPhotoChem* **2021**, *5* (9), 808-814.
- (3) Bonfield, H. E.; Knauber, T.; Lévesque, F.; Moschetta, E. G.; Susanne, F.; Edwards, L. J. Photons as a 21st century reagent. *Nat. Comm.* **2020**, *11* (1), 804.
- (4) Pijper, B.; Saavedra, L. M.; Lanzi, M.; Alonso, M.; Fontana, A.; Serrano, M.; Gómez, J. E.; Kleij, A. W.; Alcázar, J.; Cañellas, S. Addressing Reproducibility Challenges in High-Throughput Photochemistry. *JACS Au* **2024**, *4* (7), 2585-2595.
- (5) Buglioni, L.; Raymenants, F.; Slattery, A.; Zondag, S. D. A.; Noël, T. Technological Innovations in Photochemistry for Organic Synthesis: Flow Chemistry, High-Throughput Experimentation, Scale-up, and Photoelectrochemistry. *Chem. Rev.* **2022**, *122* (2), 2752-2906.
- (6) Aguirre-Cortés, J. M.; Moral-Rodríguez, A. I.; Bailón-García, E.; Davó-Quiñonero, A.; Pérez-Cadenas, A. F.; Carrasco-Marín, F. 3D printing in photocatalysis: Methods and capabilities for the improved performance. *Appl. Mater. Today* **2023**, *32*, 101831.
- (7) Jones, N. Science in three dimensions: The print revolution. *Nature* **2012**, *487* (7405), 22-23.
- (8) Bogdan, E.; Michorczyk, P. 3D Printing in Heterogeneous Catalysis—The State of the Art. In *Materials*, 2020; Vol. 13.
- (9) Rossi, S.; Dozzi, M. V.; Puglisi, A.; Pagani, M. 3D-printed, home-made, UV-LED photoreactor as a simple and economic tool to perform photochemical reactions in high school laboratories. **2020**, *2* (2).
- (10) Lampkin, P. P.; Thompson, B. J.; Gellman, S. H. Versatile Open-Source Photoreactor Architecture for Photocatalysis Across the Visible Spectrum. *Org. Lett.* **2021**, *23* (13), 5277-5281.
- (11) Brown, G. D.; Batalla, D.; Cavallaro, C. L.; Perez, H. L.; Wroblewski, S. T.; Sherwood, T. C. A compact, practical photoreactor for multi-reaction arrays. *React. Chem. Eng.* **2022**, *7* (9), 1945-1953.

- (12) Gordeev, E. G.; Erokhin, K. S.; Kobelev, A. D.; Burykina, J. V.; Novikov, P. V.; Ananikov, V. P. Exploring metallic and plastic 3D printed photochemical reactors for customizing chemical synthesis. *Sci. Rep.* **2022**, *12* (1), 3780.
- (13) Puente, C.; Pineda Aguilar, N.; Gómez, I.; López, I. Morphology Effect of Photoconverted Silver Nanoparticles on the Performance of Surface-Enhanced Raman Spectroscopy Substrates. *ACS Omega* **2023**, *8* (14), 12630-12635.
- (14) Castro, N.; Queirós, J. M.; Alves, D. C.; Fernandes, M. M. M.; Lanceros-Méndez, S.; Martins, P. M. A 3D-Printed Portable UV and Visible Photoreactor for Water Purification and Disinfection Experiments. In *Nanomaterials*, 2024; Vol. 14.
- (15) Aubineau, T.; Laurent, J.; Olanier, L.; Guérinot, A. Design, Characterization and Evaluation of a Lab-made Photoreactor: A First Step Towards Standardized Procedures in Photocatalysis**. *Chemistry–Methods* **2023**, *3* (11), e202300002.
- (16) Schiel, F.; Peinsipp, C.; Kornigg, S.; Böse, D. A 3D-Printed Open Access Photoreactor Designed for Versatile Applications in Photoredox- and Photoelectrochemical Synthesis. *ChemPhotoChem* **2021**, *5* (5), 431-437.
- (17) Rößler, M.; Liauw, M. A. The PhotoFlexys: A Multi-Purpose Reactor Platform to Simplify Process Intensification and Mechanistic Studies in Photochemistry. *Chemistry–Methods* **2021**, *1* (6), 261-270.
- (18) Penny, M. R.; Hilton, S. T. 3D printed reactors and Kessil lamp holders for flow photochemistry: design and system standardization. *J. Flow Chem*, **2023**, *13* (4), 435-442.
- (19) Masson, T. M.; Zondag, S. D. A.; Schuurmans, J. H. A.; Noël, T. Open-source 3D printed reactors for reproducible batch and continuous-flow photon-induced chemistry: design and characterization. *React. Chem. Eng.* **2024**, *9* (8), 2218-2225.
- (20) Shevlin, M. Practical High-Throughput Experimentation for Chemists. *ACS Med. Chem. Lett.* **2017**, *8* (6), 601-607.
- (21) Cernak, T.; Dykstra, K. D.; Tyagarajan, S.; Vachal, P.; Krska, S. W. The medicinal chemist's toolbox for late stage functionalization of drug-like molecules. *Chem. Soc. Rev.* **2016**, *45* (3), 546-576.

- (22) Krska, S. W.; DiRocco, D. A.; Dreher, S. D.; Shevlin, M. The Evolution of Chemical High-Throughput Experimentation To Address Challenging Problems in Pharmaceutical Synthesis. *Acc. Chem. Res.* **2017**, *50* (12), 2976-2985.
- (23) Caldentey, X.; Romero, E. High-Throughput Experimentation as an Accessible Technology for Academic Organic Chemists in Europe and Beyond. *Chemistry–Methods* **2023**, *3* (5), e202200059.
- (24) Felten, S.; Shevlin, M.; Emmert, M. H. Introduction to High-Throughput Experimentation (HTE) for the Synthetic Chemist. In *Enabling Tools and Techniques for Organic Synthesis*, 2023; pp 197-257.
- (25) Allen, C. L.; VanGelder, K. F.; Maguire, C. K. Implementation of High Throughput Experimentation across Medicinal Chemistry, Process Chemistry and Materials Science. In *The Power of High-Throughput Experimentation: General Topics and Enabling Technologies for Synthesis and Catalysis (Volume 1)*, ACS Symposium Series, Vol. 1419; American Chemical Society, 2022; pp 23-33.
- (26) Kalyani, D.; Uehling, M.; Wleklinski, M. High-Throughput Experimentation for Medicinal Chemistry: State of the Art, Challenges, and Opportunities. In *The Power of High-Throughput Experimentation: Case Studies from Drug Discovery, Drug Development, and Catalyst Discovery (Volume 2)*, ACS Symposium Series, Vol. 1420; American Chemical Society, 2022; pp 37-66.
- (27) Ruck, R. T.; Strotman, N. A.; Krska, S. W. The Catalysis Laboratory at Merck: 20 Years of Catalyzing Innovation. *ACS Catal.* **2023**, *13* (1), 475-503.
- (28) Grainger, R.; Whibley, S. A Perspective on the Analytical Challenges Encountered in High-Throughput Experimentation. *Org. Process Res. Dev.* **2021**, *25* (3), 354-364.
- (29) Gaunt, M. J.; Janey, J. M.; Schultz, D. M.; Cernak, T. Myths of high-throughput experimentation and automation in chemistry. *Chem* **2021**, *7* (9), 2259-2260.
- (30) Cook, A.; Clément, R.; Newman, S. G. Reaction screening in multiwell plates: high-throughput optimization of a Buchwald–Hartwig amination. *Nat. Protoc.* **2021**, *16* (2), 1152-1169.
- (31) Leitch, D. C. High-Throughput Synthetic Chemistry in Academia: Case Studies in Overcoming Barriers through Industrial Collaborations and Accessible Tools. In *The Power of High-Throughput Experimentation: General Topics and Enabling Technologies*

for *Synthesis and Catalysis (Volume 1)*, ACS Symposium Series, Vol. 1419; American Chemical Society, 2022; pp 35-57.

(32) Mahjour, B.; Hoffstadt, J.; Cernak, T. Designing Chemical Reaction Arrays Using Phactor and ChatGPT. *Org. Process Res. Dev.* **2023**, *27* (8), 1510-1516.

(33) Mahjour, B.; Zhang, R.; Shen, Y.; McGrath, A.; Zhao, R.; Mohamed, O. G.; Lin, Y.; Zhang, Z.; Douthwaite, J. L.; Tripathi, A.; et al. Rapid planning and analysis of high-throughput experiment arrays for reaction discovery. *Nat. Comm.* **2023**, *14* (1), 3924.

(34) Zondag, S. D. A.; Schuurmans, J. H. A.; Chaudhuri, A.; Visser, R. P. L.; Soares, C.; Padoin, N.; Kuijpers, K. P. L.; Dorbec, M.; van der Schaaf, J.; Noël, T. Determining photon flux and effective optical path length in intensified flow photoreactors. *Nat. Chem. Eng.* **2024**, *1* (7), 462-471.

(35) Lasso, J. D.; Castillo-Pazos, D. J.; Salgado, J. M.; Ruchlin, C.; Lefebvre, L.; Farajat, D.; Perepichka, D. F.; Li, C.-J. A General Platform for Visible Light Sulfonylation Reactions Enabled by Catalytic Triarylamine EDA Complexes. *J. Am. Chem. Soc.* **2024**, *146* (4), 2583-2592.

(36) A first iteration of the absorptive filter was tested and analyzed through the same process. The resulting yields for this filter are shown in Section 4 of the SI, and display a clear difference between rows A,D and rows B,C of the plate (most likely due to internal lamp reflection patterns). The second and final version of this filter was achieved by adjusting the opacity of the top and bottom rows of the filter by a factor of 10%.

Supporting Information

1. Section 1: Photoreactor building

A. 3D printing Specifications and Parts Inventory:

All printings were made with the help of a Bambu Lab X1-Carbon 3D printer. Rhino 8 was used to design all parts, and Bambu Studio was used for slicing and printing. All assembly parts were printed with a 0.6 mm diameter nozzle using a cubic infill pattern except for the body, where an adaptive cubic pattern is recommended. The authors recommend parts to be printed with either of the following filaments, available from the Bambu Lab website:

- **PET-CF (Carbon fiber reinforced polyethylene terephthalate):** Diameter 1.75 ± 0.03 mm, 1 kg package (324 m), acquired from Bambu Lab (33 USD per spool)
- **PETG (polyethylene terephthalate):** Diameter 1.75 ± 0.03 mm, 1 kg package (324 m), acquired from Bambu Lab (13 USD per spool)

Table S4.1: 3D printed parts inventory

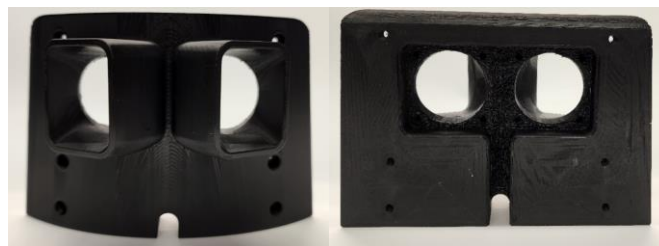
Part name	File name	Comments
Body	Body.stl	Main body of the photoreactor.
Lamp drawer	Lamp Drawer.stl	Drawer to position the Kessil lamp. Includes a space where acetate filters can be stored.
Overhead rotor	Overhead Rotor.stl	To be inserted in the motor with the help of a spring pin. Magnets must be placed in the side pockets.
Magnet caps	Magnet Caps.stl	Cover both magnets. Needs to be glued.
Lid	Lid.stl	Contains all electronic components including the motor, the digital thermometer, and the speed regulators board, switch and plug.
PCB cap	PCB Cap.stl	Holds motor regulator board in place within the lid.
Fan cover	Fan Cover.stl	Holds both fans and their wiring.
Top cap	Top Cap v2.stl	Covers the electronic components in the lid.

Pictures:

Main body (Front, side, back, bottom, interior chamber):



Fan holder (front and back):



Lamp drawer (side, front, back, top, bottom):



Overhead rotor (side, top, bottom):



Lid (front, top with PCB cap, bottom):



Cap (top, bottom):



Table S4.2: Purchased parts inventory

Part name	Amount	Specifications	
Motor	1	Reversible DC electric motor (brush) 30W, 12 V, 35000 RPM. Model XD-3420 (Rod needs to be resized) Purchased from Amazon CA (28 USD)	
Speed controller	1	Adjustable PWM controller for DC brush motor, 5-30 V, 6A, 150W Purchased from Amazon CA (10 USD)	

<u>Thermometer</u>	1	Digital LCD thermometer, range from -50°C to 110°C (5 USD) Purchased from Amazon CA	
<u>Motor power supply</u>	1	Power supply adapter, AC 100-240 V to DC 12V 2A, 24W max + US plug 2.1 mm x 5.5 mm (10 USD) Purchased from Amazon CA	
<u>Fan</u>	2	SUNON MagLev fan HA40101V4-1000U-A99 DC 12V, 0.43W, 5.4 CFM 40mm L x 40mm H x 10 mm W (12 USD) Purchased from Amazon	
Cooling tube	1	Tygon tube E-3603 (ACF0032) 7/16 in, 50 ft package (50 USD) Purchased from Fisher	
Magnets	2	Neodymium magnets (N52) 1/4" thick, 3/4" OD. Pull 23 lbs (5 USD) Purchased from McMaster-Carr	
Threaded inserts	16	Bras heat-set inserts for plastic M3 x 0.5 mm, 4.3 mm installed length (14 USD per pack of 50) Purchased from McMaster-Carr	

Spring pin	1	1050-1095 spring steel slotted spring pin 1/8" diameter, 7/8" long (14 USD per pack of 250) Purchased from McMaster-Carr	
-------------------	---	---	---

*pictures taken from vendor site

Other tools required for the assembly of this photoreactor could include (but is not limited to): Wire, screwdrivers, multimeter, tubing cutter, soldering-iron, 2-part epoxy glue, hot-melt glue gun with glue sticks, 2 screws (3mm x 10mm), 14 screws (3 mm x 15 mm), a 33 ohm resistor, and a 0.125" drill bit (for rotor/spring pin installation)

Other equipment needed to operate the photoreactor:

1. Kessil lamp PR160L with a Y split cable
2. Recirculator chiller with a minimum temperature of at least 0°C (recirculatory employed: Lauda WK300)
3. Analytical sales standard 24-position photoredox reaction block (SKU 24253) and accessories.
4. Laser printer
5. Optional: Timer switch

B. Building instructions:

Step 1: Print all parts mentioned in section B (only the magnet caps need to be printed twice).

Step 2: From the purchased parts, connect the speed controller to the corresponding switch, knob, and power source inlet, as well as the motor, as shown in the diagrams below (left). After fixing the motor to the base of the lid and sliding the controller board on the side, put two inserts and fix the controller with the PCB cap. Lastly, insert the digital

thermometer display in the front of the lid, and place the cylindrical sensor inside the hole placed next to the motor. Final arrangement of electronic shown below (right).

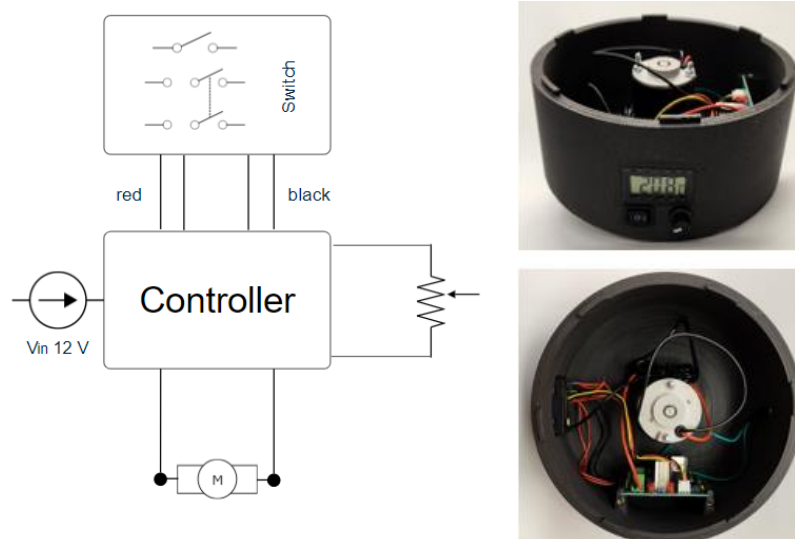


Figure S4.1: Circuit diagram for assembly of electronic parts (left). Distribution of electronics within the photoreactor lid (right top and bottom).

Step 3: Insert both magnets into the rotor piece and glue the caps on each side. Cut the motor shaft to size, and fix the rotor piece by inserting the spring pin. Make sure that the rotor can spin freely in a leveled manner, without hitting the thermometer sensor (see picture).



Figure S4.2: Fixed rotor piece in place. Note the thermometer sensor placement in the bottom.

Step 4: Take the fan cover and assemble the fans and the power inlet as shown below (left), fix the resistor to one of the fans with hot-melt glue. Make sure that no wires stick out of the channel, as shown below (right). **IMPORTANT:** It is worth noting that one fan must push the air inwards, while the other fan should blow in the opposite direction to evacuate the hot air coming from the lamp once the photoreactor is assembled.

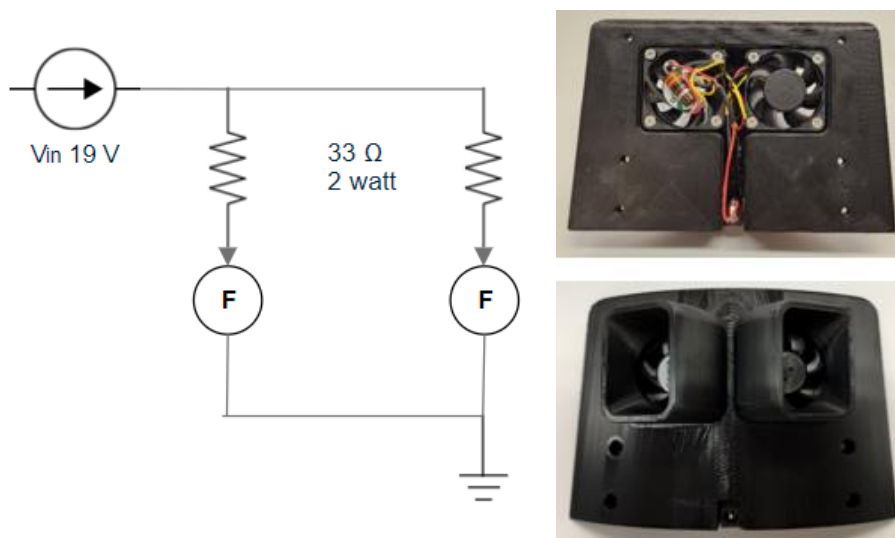


Figure S4.3: Circuit diagram for fan assembly (left). Final placement of fans (right top and bottom).

Step 5: To assemble the body, place the corresponding inserts in its back and screw the fan cover in. Next, insert the Tygon tubing through the lateral holes and around the external part of the chamber until 6 full turns have been completed, as shown below.



Figure S4.4: Interior of the photoreactor body bearing 6 tubing turns. Notice the lamp placement underneath (Always make sure to align and level the lamp before running reactions).

C. User guide:

Step 1: Prepare your 24-well reaction block and place on top of the four central columns above the lamp opening (see picture below). If a filter is used, place right below the reaction block.

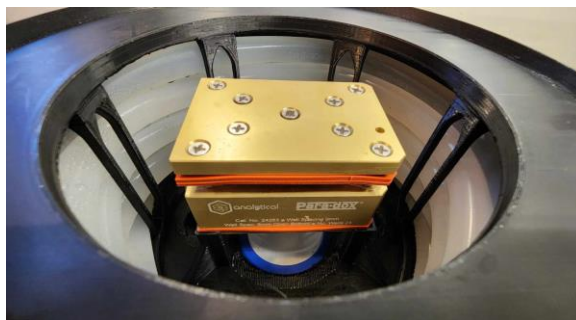


Figure S4.5: Analytical Sales 24-well Para-dox photocatalysis reaction block placed in the inner chamber of the photoreactor.

Step 2: Place the lid on top of the body, making sure that the rotor fits correctly between the reaction block and the chamber supports (See below). Start stirring in either direction by activating the switch and adjust the speed with the knob. The temperature shown in the thermometer must be adjusted manually by setting a lower temperature in the recirculator. To calculate the difference between the displayed temperature and the actual temperature in the reaction, consult Part 3 of the supporting information.

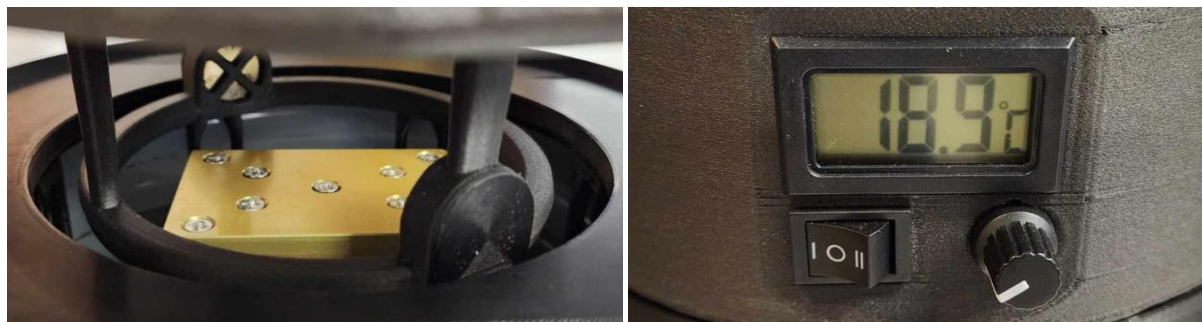


Figure S4.6: Fit of the rotor between the reaction block and the inner chamber (left). Digital thermometer, stirring switch and speed control (right).

Step 3: Adjust the desired intensity of light and insert the Kessil lamp inside the drawer and slide the drawer inside the body of the photoreactor, making sure that the plug sticks out of the channel at the bottom of the drawer. Finally, connect the lamp charger to a Y split, feeding the fans and the lamp at the same time.



Figure S4.7: Placement of the lamp within the drawer (Left, note that it includes a pocket for filter storage). Fully assembled photoreactor (right).

Note 1: Place the photoreactor on a leveled surface to avoid alignment problems with the overhead rotor.

Note 2: While the photoreactor has a built-in channel for the drain of water caused by excessive condensation of air humidity, the user must ensure that no water enters in contact with the electrical parts of the photoreactor.

Note 3: The user must make sure that the fans at the back of the photoreactor are running at all times while the lamp is on. Failure to do so will result in overheating of the lamp, causing it to turn off during the reaction.

Note 4: Avoid the spillage of organic solvents near or on the photoreactor, as these might dissolve the plastic and cause structural damage.

D. Technical drawing

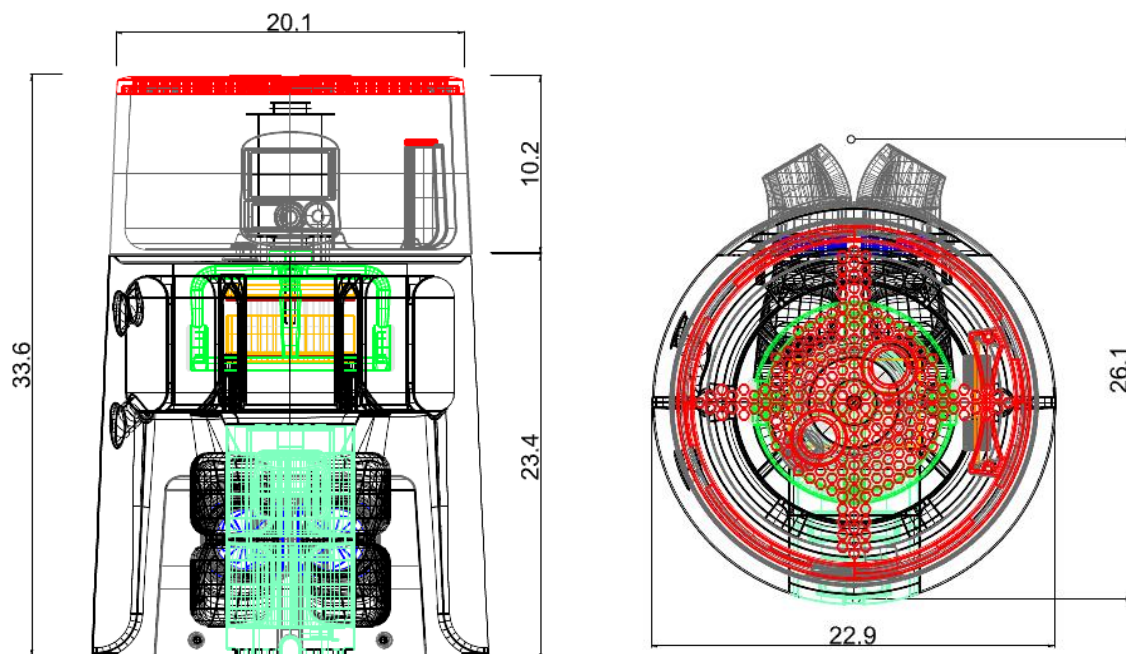


Figure S4.8: Technical drawing, side and top views. All distances shown in centimeters.

E. Estimated price

Based on rounded up prices as of September 2024, the estimated total price for this photoreactor, excluding the lamp and the reaction block, is between **164 USD and 224 USD**.

This estimation based on a printed assembly total weight of is 2070 g when printed with 2 walls and 2890 g when printed using 5 walls. This amounts to an average of 99 USD for 3 spools of PET-CF or 39 USD for 3 spools PETG. In addition to this cost, the components shown in section C average a total of 125 USD.

We do not recommend lowering the cost of the assembly by using cheaper filaments such as PLA due to its melting temperature.

2. Section 2: Temperature control

To standardize and compare the temperature reached by different components of the photoreactor, a HIKMICRO handheld compact thermal imaging camera was used with a reflectance of 0.97 (See below).



Figure S4.9: Thermal imaging measurements of the photoreactor attached to recirculation tubing (far left), the top of the photoreactor, showing electronic components and motor inside (center left), the fan and interior of the lamp holder (center right), and the inner chamber showing the reaction block bottom (far right).

Additionally, the temperature of the inner chamber was monitored over the course of 24 hours, registering a difference of approximately 3 to -5 °C between the digital thermometer, and the actual temperature of the block. For a reaction temperature of 25 °C, the recirculating chiller must be set at around 5 °C, and for a reaction temperature of 28 °C it must be set at around 9 °C.

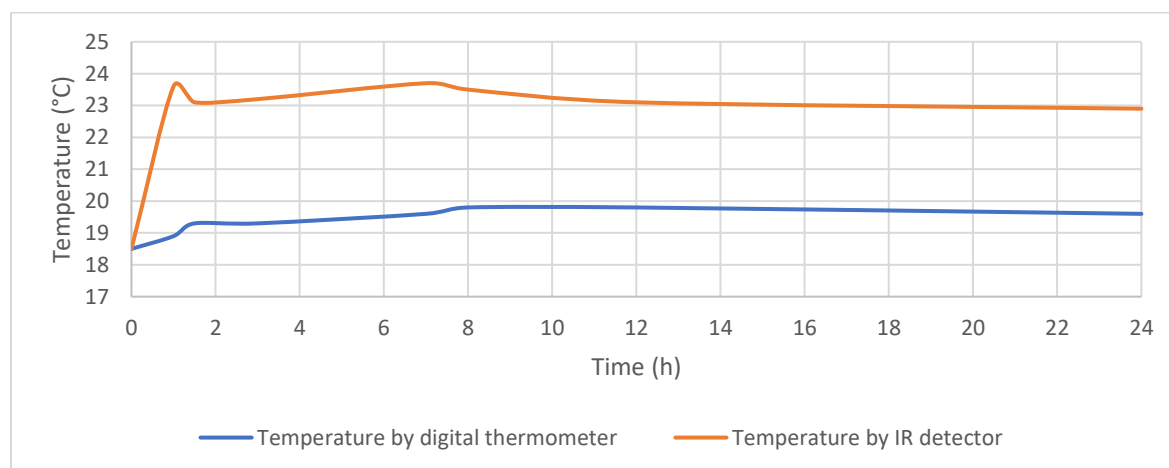


Figure S4.10: Reaction block temperature evolution

Anisotropy effects at a set temperature of 28 °C. During this experiment, the reading of the digital thermometer was 23.3 °C with a room temperature of 22.6 °C and a recirculator temperature of 9.1 °C.



Figure S4.11: Plate temperatures inside the reaction solution

3. Section 3: Filter development

Technical aspects:

Light distribution measurements were conducted by translating a photodiode (Thorlabs, SM1PD1A) along the axis of propagation of the Kessil lamp. Intensity measurements at each position were recorded using a photodiode amplifier (Thorlabs, PDA200C). A neutral density filter (Thorlabs, NE09B-A) was mounted to the photodiode to reduce the intensity of the incident light. The intensities were measured along the x-, y- and z-axis. The intensity distribution of the Kessil lamp without a diffuser is shown in Figure S4.12. The measurements are consistent with the measured intensity maps provided by the manufacturer. To achieve more uniform illumination, a ground glass diffuser and a PVC sheet diffuser were placed at the front of the lamp. However, neither diffuser provided a significant improvement to the homogeneity of light. Therefore, a custom filter was developed which limited the intensity of light at each individual reaction well.

To design the custom absorptive filter, firstly a calibration curve was constructed by measuring the power at the most intense region of the Kessil lamp for different laser-jet printed ink opacities. The power was then normalized to the maximum intensity. Then, the power was measured at each individual reaction well location by translating the

sensor along the x and y-dimensions. The sensor diameter (10 mm) was similar in size to the individual vial diameter (8 mm). Once the power was measured for each well, the power was normalized to the minimum intensity well and the calibration curve was applied to determine the required opacity at each well location. For the reaction yield adjusted filter, the normalized power at the top and bottom well rows was adjusted by 10%.

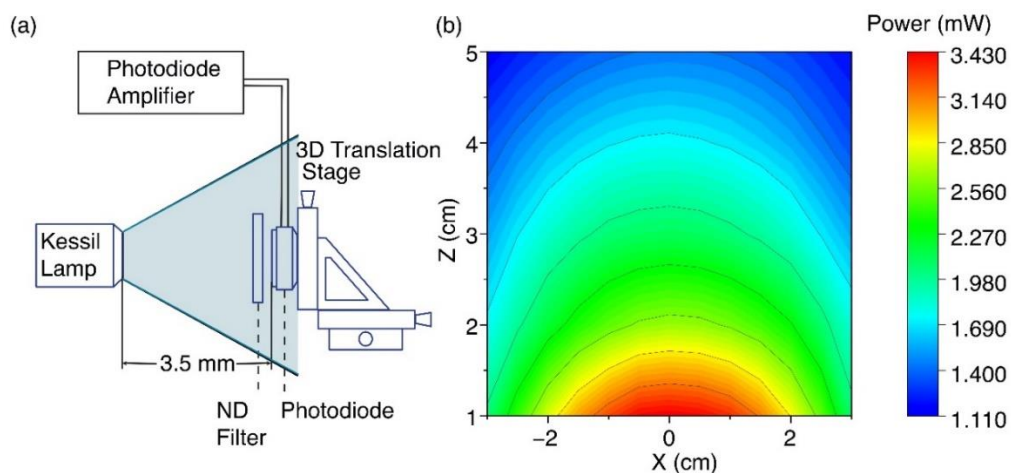


Figure S4.12: (a) Schematic of the experimental setup used to measure the light intensity as a function of individual well position (b) the intensity distribution of the Kessil lamp without light filtration measured along different Z and X positions.

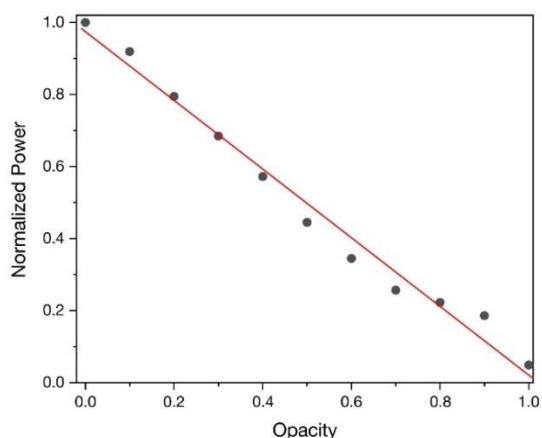


Figure S4.13: Normalized power measured 3.5 mm from the Kessil lamp output at different laser printed filter opacities. Linear fit used to determine the required filter opacity is shown on top of the measurements with a formula of $y = -1.031x + 1.0131$.

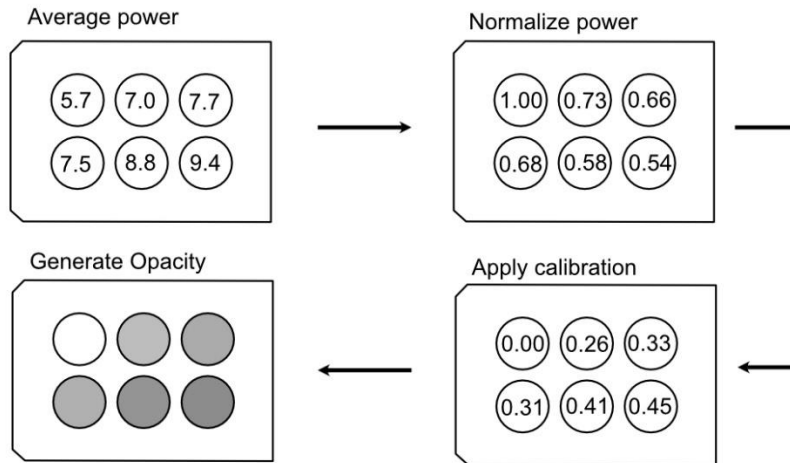


Figure S4.14: Flow chart showing the steps required to generate the absorptive filter.

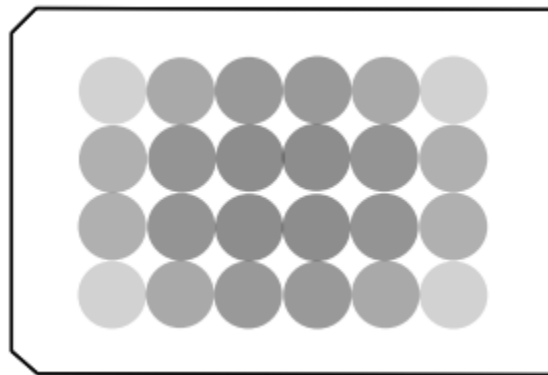


Figure S4.15: Final absorptive filter (real scale).

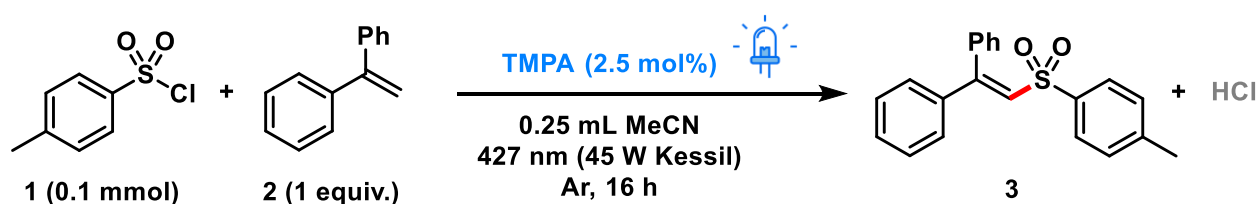
4. Section 4: Chemistry

a. General Experimental Procedures:

Solvents and reagents were purchased from Sigma-Aldrich, Fisher scientific, and Ambeed chemical companies and were used without further purification unless otherwise specified. ^1H and ^{13}C NMR were recorded on Bruker 500 MHz spectrometers, which uses the deuterium lock signal to reference the spectra. The solvent residual peaks, e.g., of chloroform (CDCl_3 : δ 7.26 ppm and δ 77.23 ppm), were used as references. Data are reported as follows: multiplicity (s = singlet, d = doublet, t = triplet, q = quartet, quint = quintet, m = multiplet, dd = doublet of doublets, etc), coupling constant (J/Hz) and integration. All NMR spectra were recorded at room temperature. Mass spectrometry was conducted by using atmospheric pressure chemical ionization (APCI) or electro-spraying ionization (ESI) performed by McGill University on a Thermo-Scientific Exactive Orbitrap. Protonated/deprotonated molecular ions or sodium adducts were used for empirical formula confirmation.

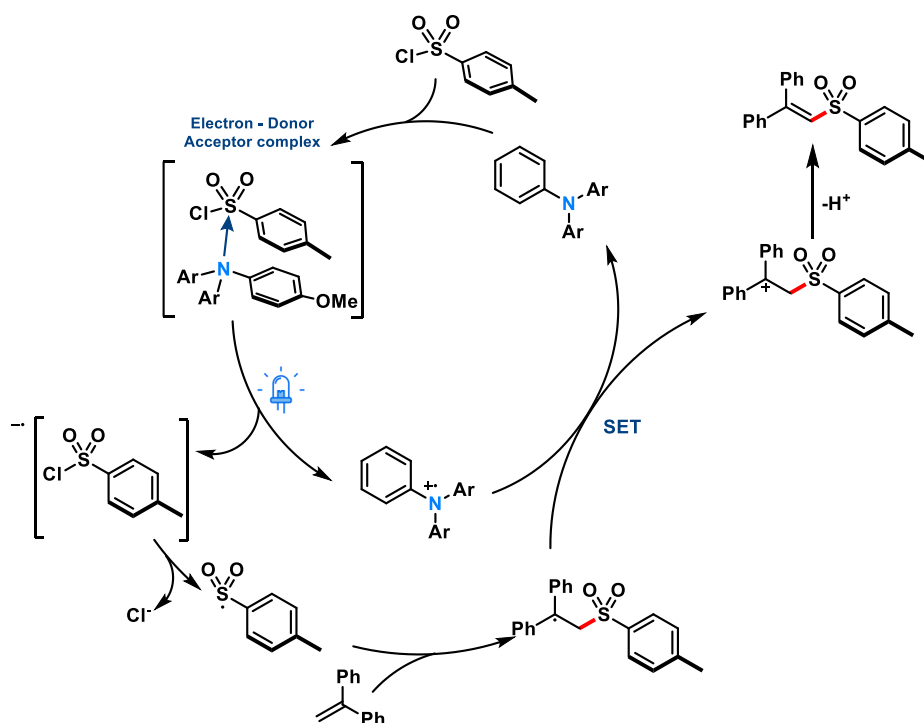
All reactions are stirred magnetically unless otherwise specified. Short-packed column chromatography was performed with Silicycle SiliaFlash silica gel F60 (230–400 mesh) or Biotage Sfär silica HC D 20 μm . Flash column chromatography was performed with IsoleraTM Prime advanced automatic flash purification system.

b. Benchmarking experiments: Triarylamine-catalyzed sulfonylations



Scheme S4.1: Redox-neutral sulfonylation of olefins promoted by blue light and catalyzed by TMPA (4-(trismethoxy) triphenylamine).

Method adapted from a previous publication by our group¹: Using degassed acetonitrile, two solutions were prepared: solution A containing 27 mg of TMPA (4-(trismethoxy)triphenylamine) and 608 mg of tosyl chloride, and solution B, containing 564 μL of 1,1-diphenylethylene. Inside the glovebox, 125 μL of each solution were added to a standard 1 mL 24-well photoredox reaction block (Analytical Sales). Each well was pre-charged with stir bars, while the addition was done with the help of a multichannel pipette. The reaction block was then stirred for one minute, leading to the display of a faint yellow color that quickly develops into a deep blue. The reaction block was sealed and irradiated with a 427 nm Kessil lamp through a transparency filter, inside the photoreactor at 28 $^{\circ}\text{C}$ for 12 hours. Once completed, the reaction block was opened, and the analytical samples were prepared as described in Section 5.



Scheme S4.2: Reaction mechanism for the model reaction¹

5. Section 5: Analytical

a. GCMS calibration curve:

Prior to the sample analysis, a calibration curve was run with 5 prepared samples of known concentration. To an empty 9-dram vial, 27.1 mg of tosyl chloride were weighed out as accurately as possible. Next, the vial was primed with 50.1 mg of 1-[(2',2'-diphenylethenyl)sulfonyl]-4-methylbenzene (2',2'-DPE-1-Ts) previously prepared. Separately, a 10 mL stock of Fisher Scientific HPLC grade acetonitrile was sparged for 15 minutes utilizing ultra-pure argon. Then, 5 mL from the degassed solvent were taken with a 10 mL Thermofisher Finnpiquette F2 micropipette and dispensed to the previously weighed compounds to create a stock solution. Next, to 5 vials GC/MS vials was dispensed the required amount of HPLC grade acetonitrile for the desired dilution, after which the appropriate amount of analyte stock solution was added (**Table S4.3** denotes the quantities utilized to create the appropriate stock solutions at a total volume of 1050 μL). The finished standards were then capped and inverted three times to ensure appropriate mixing. These standards were placed on an Agilent 7890B GC coupled to 5977A MSD equipped with a 50 sample autosampler and were allowed to run using a custom method (Initial temperature of 80 °C for 2 minutes, followed by a ramp of 35 °C/min up to a final temperature of 300 °C for 5 minutes, accounting for a total run time of 13.3 minutes)

Table S4.3. Data sheet for creation of the sulfonylation standard curve

1-[(2',2'-diphenylethenyl)sulfonyl]-4-
methylbenzene

Tosyl chloride

mmol	mg	(mg/mL)	(mmol/mL)	mmol	mg	(mg/mL)	(mmol/mL)	Volume Stock (mL)	Volume MeCN (mL)
0.005	1.67	1.590	0.00476	0.005	0.95	0.904	0.00476	0.175	0.875
0.01	3.34	3.181	0.00952	0.01	1.9	1.809	0.00952	0.35	0.7
0.015	5.01	4.771	0.0143	0.015	2.85	2.714	0.0143	0.525	0.525
0.02	6.68	6.361	0.0190	0.02	3.8	3.619	0.0190	0.7	0.35
0.025	8.35	7.952	0.0238	0.025	4.75	4.523	0.0238	0.875	0.175

After the runs were complete, they were analyzed utilizing the MSD ChemStation software (F.01.03.2357). From here the integration values of the analyte peaks were taken from the chromatograms without further processing. Finally, in Microsoft Excel, the data was plotted versus concentration utilizing the basic linear regression function in this program to produce the desired standard curve.

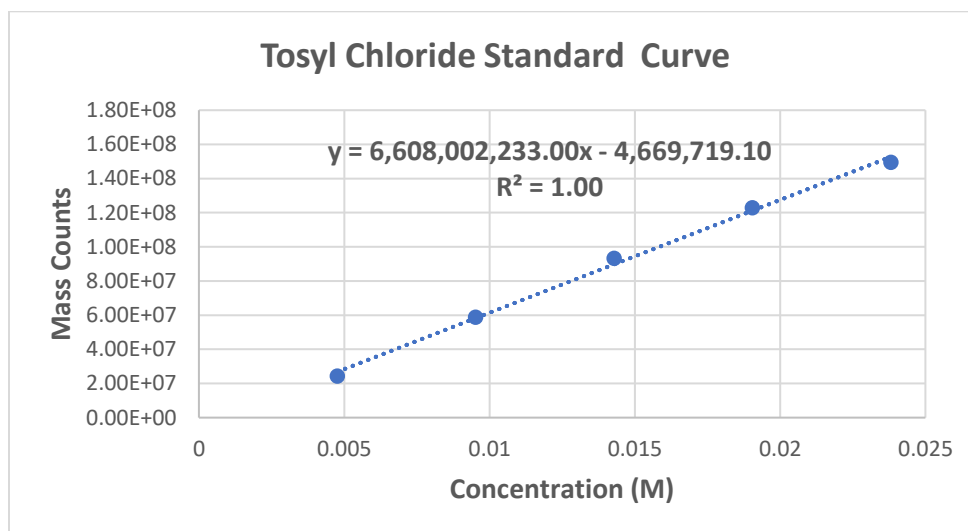


Figure S4.16: Standard curve for the determination of tosyl chloride in HTE 24-well plates.

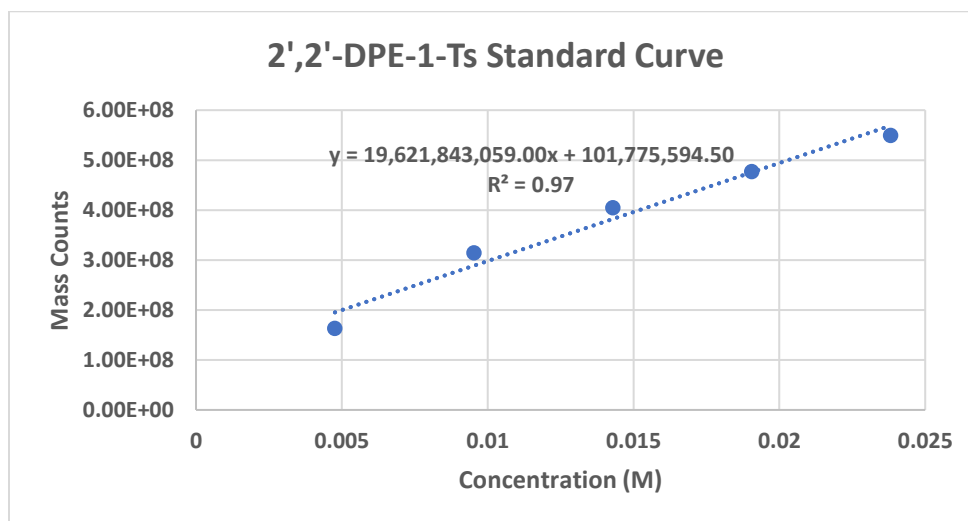


Figure S4.17: Standard curve for the determination of 1-[(2',2'-diphenylethenyl)sulfonyl]-4-methylbenzene in HTE 24-well plates.

Note: Attempts to get a standard curve for 1,1- diphenylethylene were unsuccessful as this molecule displayed a non-linear relationship between concentration and GC/MS area at the concentrations desired.

b. Analysis of 24-well Plates:

After the desired time had elapsed, the reaction plate was taken off the HERMES reactor and opened utilizing a DeWalt 8V MAX Cordless Screwdriver. From the unsealed reactions, utilizing an IKA Pette 8 20-200 μL 100 μL of Fisher Scientific HPLC grade acetonitrile of each individual reaction was utilized to dilute all reaction samples to 350 μL total. (Note: This step is important as the final product tends to crystallize if left standing for prolonged periods of time). From here, 30 μL of the reaction was sampled and placed into individual GC/MS vials. These samples were then finished by the addition of 1 mL of HPLC grade acetonitrile utilizing a Thermofisher Finnpiquette F2 100 μL -1000 μL . The finished samples were securely capped, flipped once to ensure appropriate mixing, and finally placed on the Agilent autosampler utilizing the same method as stated for the standards.

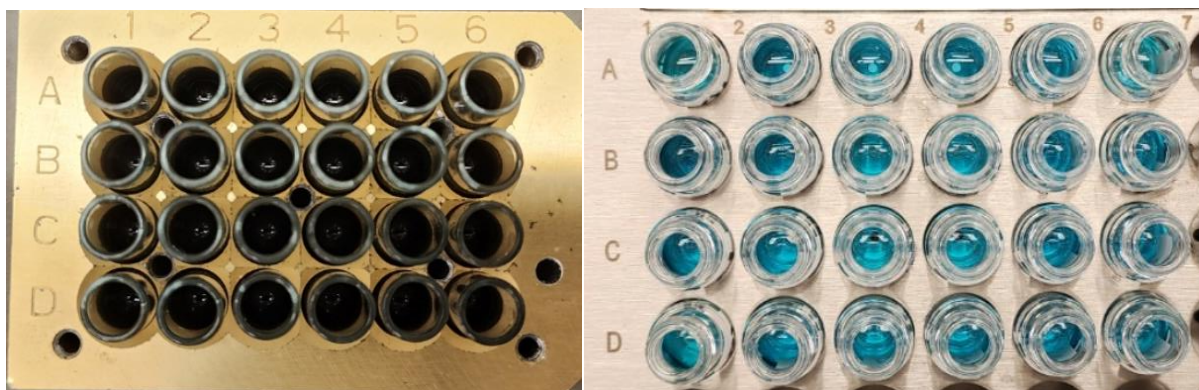


Figure S4.18: Appearance of sulfonylation reactions after 12 hours (left), and the finished GC/MS samples (right).

Once the samples were completed, the chromatograms were integrated utilizing MSD ChemStation software and the analyte areas were transferred to excel from which a pre-prepared excel sheet calculated the analyte concentration in the diluted sample utilizing the standard curve linear regression. The yields were then calculated using simple dilution and yield equations. The data for "Filter, 12 h, 25 °C" is provided below to serve as a demonstration of the data acquisition and the calculations done.

Area Counts of DPE-TS

	1	2	3	4	5	6
A	229595431	208917578	216961470	215795483	207778755	184240805
B	208820956	193283836	211636805	219261319	197915318	215186837
C	216626433	196238804	211895436	201945965	211435595	226505195
D	201803733	212360738	225831182	229500850	218576143	227315025

Concentration Dilute

	1	2	3	4	5	6
A	0.006514161	0.00546	0.00587	0.005811	0.005402	0.004203
B	0.005455418	0.004664	0.005599	0.005987	0.0049	0.00578
C	0.005853214	0.004814	0.005612	0.005105	0.005589	0.006357
D	0.005097795	0.005636	0.006322	0.006509	0.005953	0.006398

Concentration Reaction

	1	2	3	4	5	6
A	0.223652846	0.187472	0.201547	0.199506	0.185479	0.144294
B	0.187302695	0.160117	0.19223	0.205571	0.168221	0.198441
C	0.200960333	0.165287	0.192682	0.175273	0.191878	0.218246
D	0.175024304	0.193496	0.217066	0.223487	0.204372	0.219663

mmol of DPE-TS

	1	2	3	4	5	6
A	0.078278496	0.065615	0.070541	0.069827	0.064918	0.050503
B	0.065555943	0.056041	0.06728	0.07195	0.058877	0.069454
C	0.070336117	0.05785	0.067439	0.061346	0.067157	0.076386
D	0.061258506	0.067724	0.075973	0.078221	0.07153	0.076882

Yield

	1	2	3	4	5	6
A	78.27849627	65.61512	70.5413	69.82723	64.91769	50.50275
B	65.55594311	56.04081	67.2804	71.94975	58.87719	69.45449
C	70.33611667	57.85047	67.43879	61.34561	67.15718	76.386
D	61.25850635	67.72375	75.97322	78.22057	71.53014	76.88195

To determine the concentration of 2',2'-DPE-1-Ts in the diluted GC/MS sample, we can obtain the equation:

$$C_{dilute}(M) = \frac{X - 101775594.5}{19621843059}$$

This equation is derived from rearrangement of the standard curve linear regression, where X represents the area counts obtained from the integration of the GC/MS chromatogram.

Therefore, for the plate “**Filter, 12 h, 25 °C**” at position **A6** it follows:

$$C_{dilute}(M) = \frac{184240805 - 101775594.5}{19621843059} = 0.00420 M$$

From here the concentration of the compound in its original reaction vessel can be calculated from a simple dilution equation, where $V_{sampled}$ represents the 30 μ L utilized to create the dilution:

$$C_{dilute} * V_{dilute} = C_{Rxn} * V_{sampled}$$

Therefore, as the starting and final volumes are known, the concentration of the reaction can be calculated as follows:

$$C_{Rxn}(M) = \frac{C_{dilute} * V_{dilute}}{V_{sampled}} = \frac{0.00420 M * 1.03 mL}{0.03 mL} = 0.144 M$$

Thus, having determined the original concentration, we can simply calculate the millimoles of product present in the total sample using:

$$n_{DPE-Ts}(mmol) = C_{Rxn} * V_{Rxn} = 0.144 M * 0.350 mL = 0.0505 mmol$$

Finally, having the millimoles of product we can divide this quantity by the theoretical yield in millimoles to give the yield of the reaction:

$$Yield \% = \frac{n_{DPE-Ts}}{n_{theoretical}} * 100 = \frac{0.0505 mmol}{0.1 mmol} * 100 = 50\%$$

c. Other plate readings

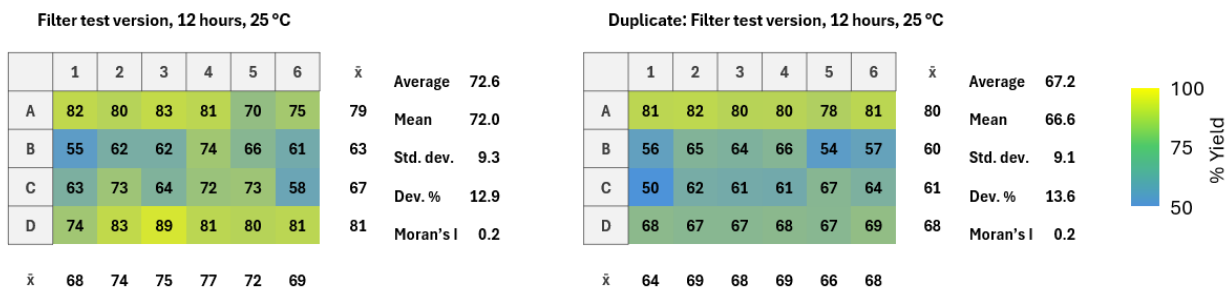


Figure S4.19: Plate readings for the filter's first iteration

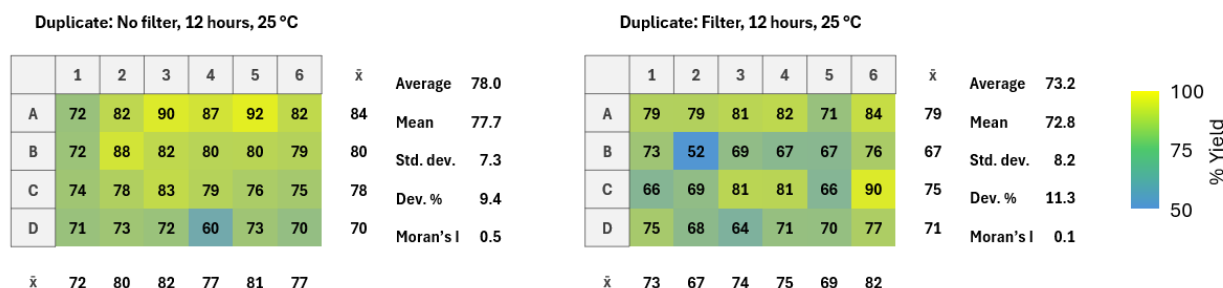
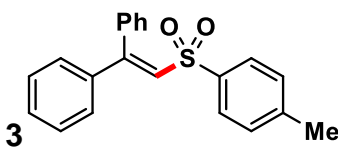


Figure 4.20: Duplicate readings for filter and unfiltered controls shown in the main text

d. Characterization data of compounds:



1-[(2',2'-diphenylethenyl)sulfonyl]-4-methylbenzene (3): White Solid. Purified with a 0-50% EtOAc/Hexanes gradient over silica ($R_f=0.40$ at 20% EtOAc/Hexanes) from the recollection of a plate with 24 reactions. ^1H NMR (500 MHz, CD_3CN) δ 7.52 – 7.49 (m, 2H), 7.42 – 7.38 (m, 2H), 7.36 – 7.31 (m, 4H), 7.28 – 7.25 (m, 2H), 7.24 – 7.20 (m, 2H), 7.09 – 7.05 (m, 3H), 2.39 (s, 3H). ^{13}C NMR (126 MHz, CD_3CN) δ 155.4, 145.2, 140.2, 139.8, 136.9, 131.1, 130.5, 130.4, 129.6, 129.6, 129.5, 129.1, 128.7, 128.3, 21.5. Data is consistent with literature report.¹

6. References

(1) Lasso, J. D.; Castillo-Pazos, D. J.; Salgado, J. M.; Ruchlin, C.; Lefebvre, L.; Farajat, D.; Perepichka, D. F.; Li, C.-J. A General Platform for Visible Light Sulfonylation Reactions Enabled by Catalytic Triarylamine EDA Complexes. *J. Am. Chem. Soc.* **2024**, *146* (4), 2583-2592.

5 Discussion and Future Remarks

5.1 Contributions to Original Knowledge

In **Chapter 2**, we explored the development of photocatalytic synthetic methods that prescind from external catalysts or sacrificial reagents, promoting reactions under redox- and pH-neutral conditions. By developing a series of α -(perfluoroalkylsulfonyl) propiophenones, we created a new family of commercially available and bench-stable reagents that enable perfluoroalkylation of aromatic molecules using UV light. Throughout this project, we also contributed to the expansion of the field of homolytic beta cleavage in ketones, a phenomenon known in photochemistry since 1964, but that has limited synthetic applications to this date.^{1, 2} Lastly, the lack of reproducible methods to obtain perfluoroalkyl sulfinate salts, as well as their commercial unavailability, prompted us to report the first fully characterized methodology for their synthesis.

Chapter 3 focuses on developing new catalytic pathways that contribute to the field of metal-free photocatalysis. Within this project, we made three main contributions. The first contribution relates to the improvement of modern perfluoroalkylating methodologies, a topic that I have discussed in detail as a review in the journal *Organic & Biomolecular Chemistry*.³ In essence, this project was conceived to address some of the shortcomings derived from work reported in Chapter 2: the need for UV light, limited selectivity, and a challenging isolation procedure, all of which were addressed by the addition of a donor under blue light irradiation.

However, the next two contributions have a deeper footprint. The second contribution revolves around the expansion of EDA systems that involve catalytic amounts of donor. In 2022, our laboratory developed the first photochemical and catalyst-free synthesis of *N*-hydroxysulfonamides, which I published as a co-first author in the journal *Chemical Science*.⁴ In this work—our first publication in the field of EDA

catalysis—, we described the stoichiometric charge transfer complex formed between nitroarenes and sulfinate salts under blue light irradiation. During this time, we realized that stoichiometric EDA systems are limited by the functionalities of the carefully chosen donor and acceptors. Additionally, literature reviews at the time suggested a change in paradigm, where donors are added in catalytic amounts to allow the radical addition to happen on any substrate of interest. With the results reported in Chapter 3, we have expanded the toolbox of EDA complexes employing a catalytic donor, a list that remains limited to date.

The third contribution is reporting the first photocatalytic methodology that employed simple triaryl amines as donors. While this family of molecules has been long exploited in the materials field, their synthetic potential was not appreciated until recently. Moreover, our work displays one of the most complete sets of mechanistic studies within the literature of EDA complexes, providing tools for future rational design of catalytic donors. Furthermore, this will assist underfunded institutions and research groups where the use of iridium and ruthenium complexes remains out of reach.

Finally, **Chapter 4** describes the development of an affordable, open-source 3D-printed photoreactor capable of running 24 reactions in parallel using a single Kessil lamp. This device is the first 3D printed photoreactor of its kind designed specifically for HTE purposes, allowing academic research groups to accelerate their photocatalytic methodology development process. At the same time, this photoreactor creates a platform for students to become familiar with a technique that has become the new *modus operandi* for synthetic groups in industry. Lastly, we have described the design of a low-cost absorptive filter for the homogenization of incident light across a reaction block. To the best of our knowledge, this is the first filter of its kind reported for synthetic purposes. We hope that the characterization performed will set a new standard for the diffusion of light, compared to previous attempts in the literature.⁵

5.2 Outlook for Future Research

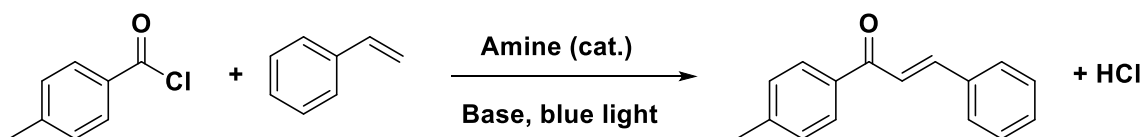
Currently, our research group is working to expand and improve all lines of research presented throughout the chapters of this thesis. For the photocleavable “dummy group” reagents presented in **Chapter 2**, three main future lines of work were devised. The most immediate improvement had to do with tackling the need for UV light irradiation. While UV light is useful to promote transformations that require high activation energies, its use has been phased-out in recent years due to the associated operational hazard.⁶ For this reason, in 2021 we started exploring ways to shift the required wavelength into the visible range. The first strategy to solve this was the employment of external catalytic donors, which eventually led us to explore the EDA complexes described in Chapter 3.⁷ However, an alternative solution focuses on the installation of visible-light absorbing chromophores onto the propiophenone scaffold. With an adequate synthetic route, this modification would allow for the perfluoroalkylation of aromatics bearing UV-sensitive functional groups and improve the radical addition selectivity. Another area for future work revolves around the improvement of atom economy in this reaction.⁸ While the generated propiophenone can be easily recycled into the starting reagent within two synthetic steps (i.e. bromination in the alpha position and subsequent S_N2 by the corresponding sulfinate), a more efficient solution would involve the installation of smaller carbonyl-containing moieties capable of stabilizing the generated radical (e.g. a diacetyl derivative).

Next, the catalytic EDA complexes reported in **Chapter 3** opened several new avenues of research that will be explored in coming years. The first improvement we implemented revolved around the aforementioned atom economy problem. Shortly after finishing this project, and during the years 2022 and 2023, we worked on a new triarylamine-promoted catalytic EDA complex where the acceptor did not require the preinstallation of redox active moieties (e.g. propiophenone). Instead, we focused on employing inherently electron-poor moieties as electron acceptors, preferably in the form of common functional groups in commercially available substrates. Radical sulfonylation reactions allowed us to test this proposal by demonstrating the capability of triarylamines to form catalytic EDA complexes with easily accessible sulfonyl chlorides. Results from

this study were published in January 2024 in the *Journal of the American Chemical Society* as a research article in which I am a co-first author.⁹

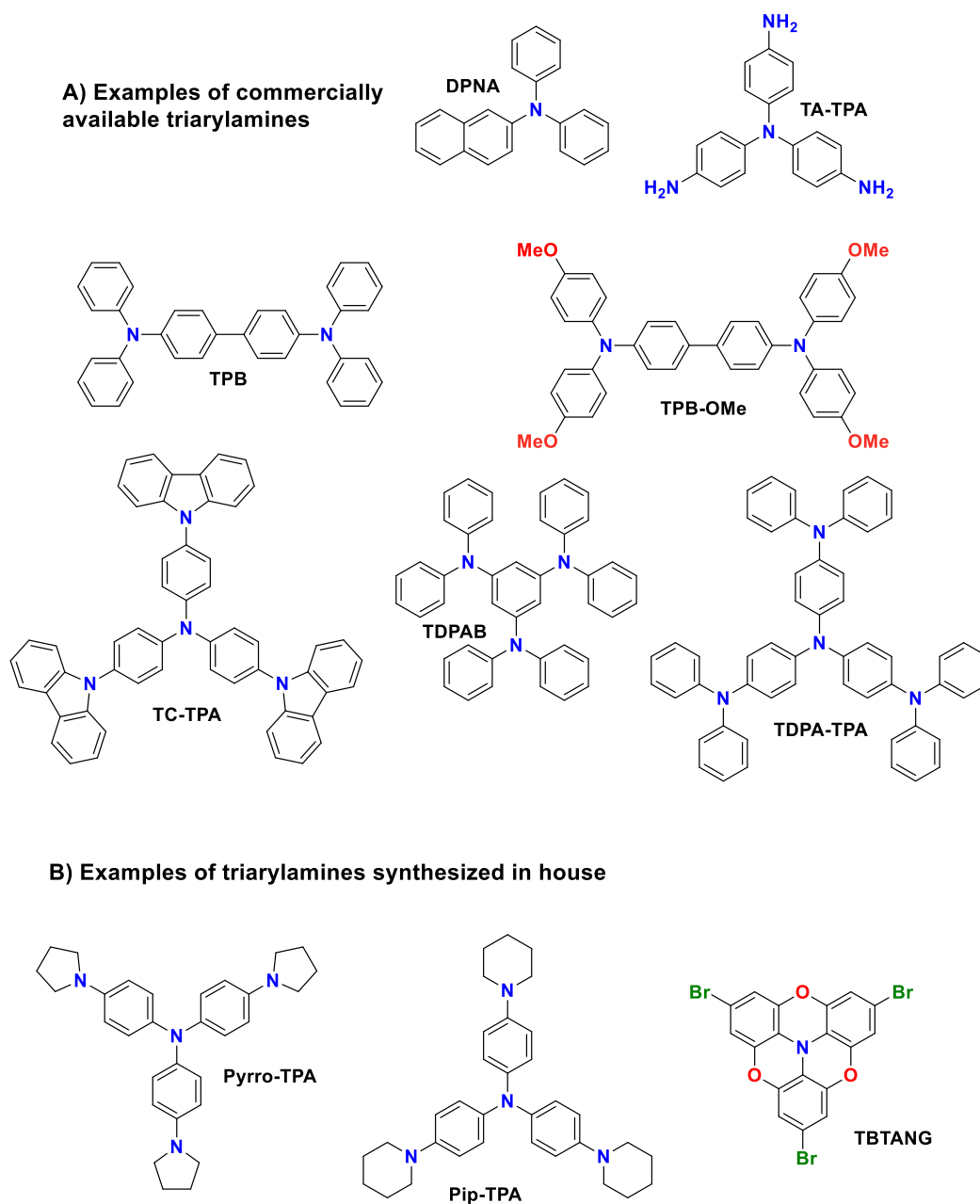
Soon, two main projects will be derived from these findings:

1. An acylation reaction, aimed to functionalize unsaturated molecules such as alkenes, alkynes, and aromatics. This will be explored in the context of a catalytic EDA complex between triarylamines and acyl chlorides, a widely available synthon. If successful, this methodology (Scheme 5.1), will grant rapid access to valuable and biologically relevant synthetic architectures (e.g. chalcones).



Scheme 5.1: Proposed radical acylation of olefins

2. A general metal-free cross-coupling synthetic platform, employing triarylamines as donors against aryl and alkyl halides. This will allow for their subsequent dehalogenation, addition to alkenes (Heck coupling), addition to alkynes (Sonogashira coupling), and functionalization (borylation, phosphorylation, etc.). This study will involve the characterization of a series of triaryamine analogues (both commercially available and synthesized in our laboratory, (Scheme 5.2) by photophysical and electrochemical means. If successful, this study will offer unprecedented insights into the photoredox properties of triarylamines as catalytic donors and provide an alternative route to traditional metal-dependent methodologies.



Scheme 5.2: Examples of triarylamines that will be explored as electron donors.

Finally, the photoreactor presented in **Chapter 4**, while a functional and efficient first prototype, can be expanded and improved in two main directions. Future work for improvement will focus firstly on the reengineering of parts, and secondly in the integration of new capabilities and reactivity platforms.¹⁰

Regarding reengineering of parts, we suggest the following improvements:

1. Developing drawer adaptors that make the photoreactor compatible with other commercially available light sources (e.g. Hepatochem lamps, CFL lamps). This will allow future users to accurately reproduce most methodologies without worrying about changes in the light source specifications.
2. Creating a series of filters, tailored to the most widely used commercial LED lamps.
3. Developing filters with other materials that grant more durability and improved transmittance, especially at wavelengths below 390 nm.
4. Replacing the liquid-assisted cooling module with thermoelectric cooling. By using a series of Peltier plates, electricity will be the only input needed for the operation of the photoreactor. Additionally, this can be coupled with an automatic temperature control, added to the lid's control board.

Regarding the integration and expansion of capabilities, we will explore the following proposals:

1. Integrating the use of larger arrays, such as 96 and 384 well plates. This will require modifying the plate support columns, as well as the width of the stirring module. If successful, these changes will be adapted to other types of plates, such as those that hold HPLC vials for preparative purposes.
2. Designing holders for flow chemistry capabilities. This will include integrating a pump module, as well as new openings for the corresponding tubing. If successful, this will turn the reactor into a multi-purpose platform, opening the door for more opportunities in both educational and professional contexts.
3. Integrating heterogeneous catalysis. By designing the appropriate 3D printed elements, the photoreactor will be capable of performing reactions that remain traditionally out of reach within HTE photocatalysis. For example, this would allow students to perform fast screenings that involve catalytic transformations in the solid-liquid and solid-gas interface.

Lastly, most of these changes will be performed while ensuring that the photoreactor remains affordable, modular, and easily accessible by commercial means.

5.3 Conclusion

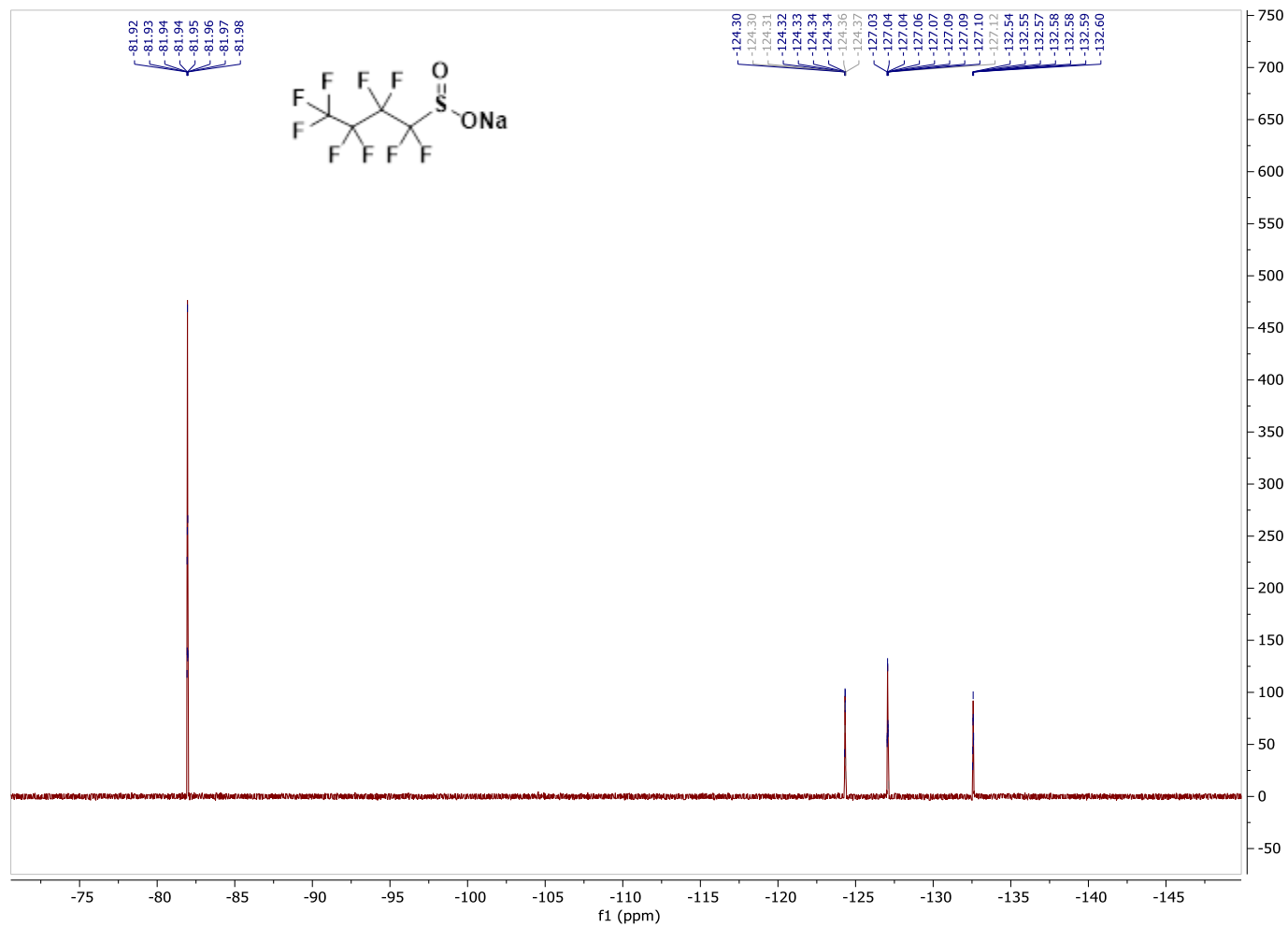
Photocatalysis has evolved to play a crucial role in modern synthetic chemistry, offering environmentally friendly and efficient pathways towards the construction of complex architectures, and the development of new methodologies involving mild and selective conditions. The research presented in this thesis successfully contributed to the advancement of the field of photocatalysis on three critical fronts: the development of new reagents, catalytic pathways, and experimental tools. Such contributions can be summarized as follows: the creation of a new family of bench-stable and photocleavable reagents for the redox- and pH-neutral perfluoroalkylation of aromatics, the discovery and mechanistic study of a new EDA complex using triarylaminines as catalytic donors under blue light, and finally, the development and characterization of an accessible 3D printed HTE photoreactor. In this thesis, not only we present results that expanded on the work of previously established research areas of the Li Group, but we also describe the establishment of new lines of research that will help open new avenues for the accelerated advancement of photocatalysis while considering sustainability and green chemistry implications.

References:

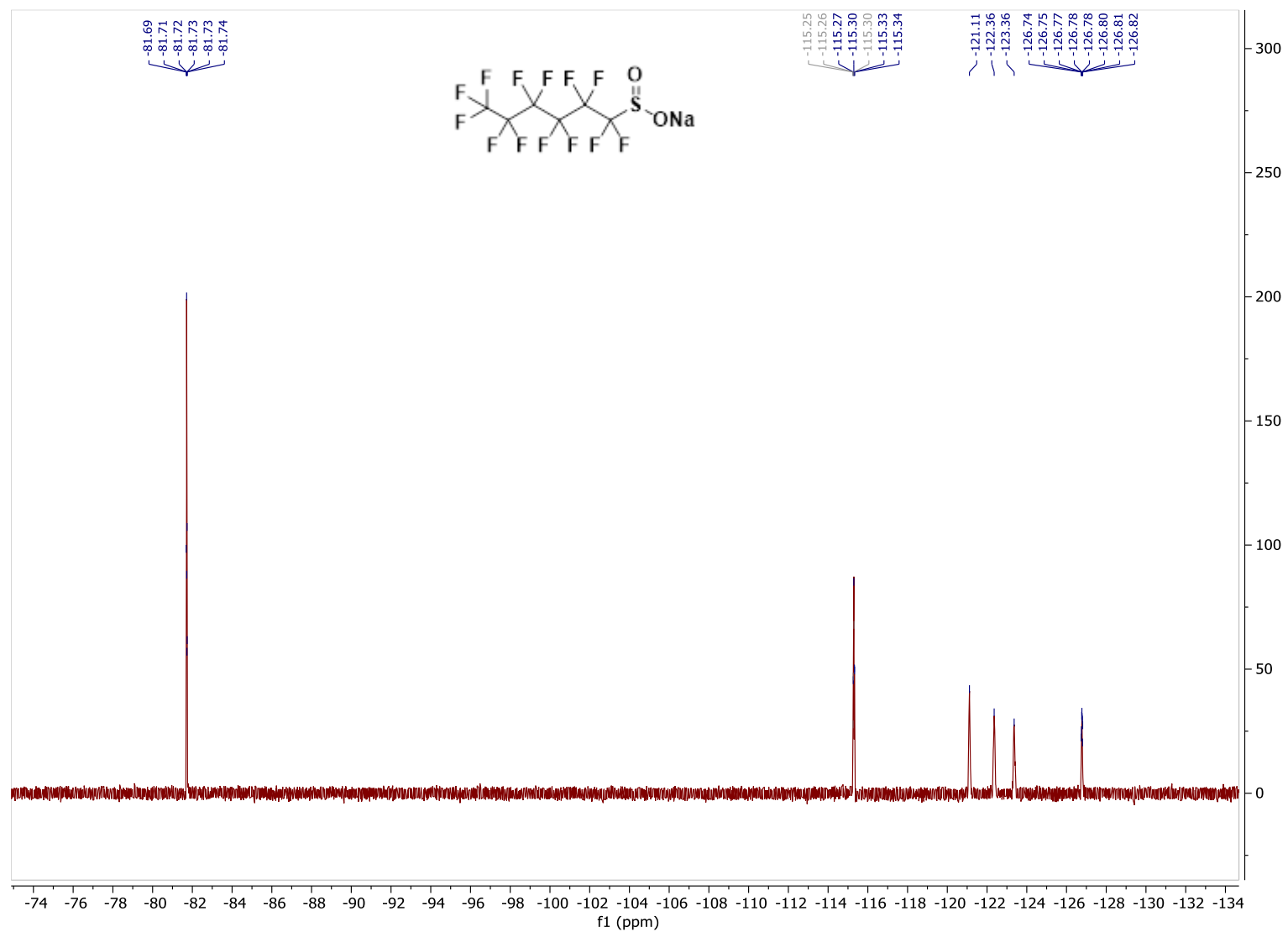
- (1)** Sheehan, J. C.; Wilson, R. M. Photolysis of Desyl Compounds. A New Photolytic Cyclization. *J. Am. Chem. Soc.* **1964**, *86* (23), 5277-5281.
- (2)** Sheehan, J. C.; Wilson, R. M.; Oxford, A. W. Photolysis of methoxy-substituted benzoin esters. Photosensitive protecting group for carboxylic acids. *J. Am. Chem. Soc.* **1971**, *93* (26), 7222-7228.
- (3)** Castillo-Pazos, D. J.; Lasso, J. D.; Li, C.-J. Modern methods for the synthesis of perfluoroalkylated aromatics. *Org. Biomol. Chem.* **2021**, *19* (33), 7116-7128.
- (4)** Lasso, J. D.; Castillo-Pazos, D. J.; Sim, M.; Barroso-Flores, J.; Li, C.-J. EDA mediated S–N bond coupling of nitroarenes and sodium sulfinate salts. *Chem. Sci.* **2023**, *14* (3), 525-532.
- (5)** González-Esguevillas, M.; Fernández, D. F.; Rincón, J. A.; Barberis, M.; de Frutos, O.; Mateos, C.; García-Cerrada, S.; Agejas, J.; MacMillan, D. W. C. Rapid Optimization of Photoredox Reactions for Continuous-Flow Systems Using Microscale Batch Technology. *ACS Central Science* **2021**, *7* (7), 1126-1134.
- (6)** Goti, G.; Manal, K.; Sivaguru, J.; Dell'Amico, L. The impact of UV light on synthetic photochemistry and photocatalysis. *Nat. Chem.* **2024**, *16* (5), 684-692.
- (7)** Castillo-Pazos, D. J.; Lasso, J. D.; Hamzehpoor, E.; Ramos-Sánchez, J.; Salgado, J. M.; Cosa, G.; Perepichka, D. F.; Li, C.-J. Triarylamine as catalytic donors in light-mediated electron donor–acceptor complexes. *Chem. Sci.* **2023**, *14* (13), 3470-3481.
- (8)** Trost, B. M. The Atom Economy—A Search for Synthetic Efficiency. *Science* **1991**, *254* (5037), 1471-1477.
- (9)** Lasso, J. D.; Castillo-Pazos, D. J.; Salgado, J. M.; Ruchlin, C.; Lefebvre, L.; Farajat, D.; Perepichka, D. F.; Li, C.-J. A General Platform for Visible Light Sulfonylation Reactions Enabled by Catalytic Triarylamine EDA Complexes. *J. Am. Chem. Soc.* **2024**, *146* (4), 2583-2592.
- (10)** Buglioni, L.; Raymenants, F.; Slattery, A.; Zondag, S. D. A.; Noël, T. Technological Innovations in Photochemistry for Organic Synthesis: Flow Chemistry, High-Throughput Experimentation, Scale-up, and Photoelectrochemistry. *Chem. Rev.* **2022**, *122* (2), 2752-2906.

APPENDIX

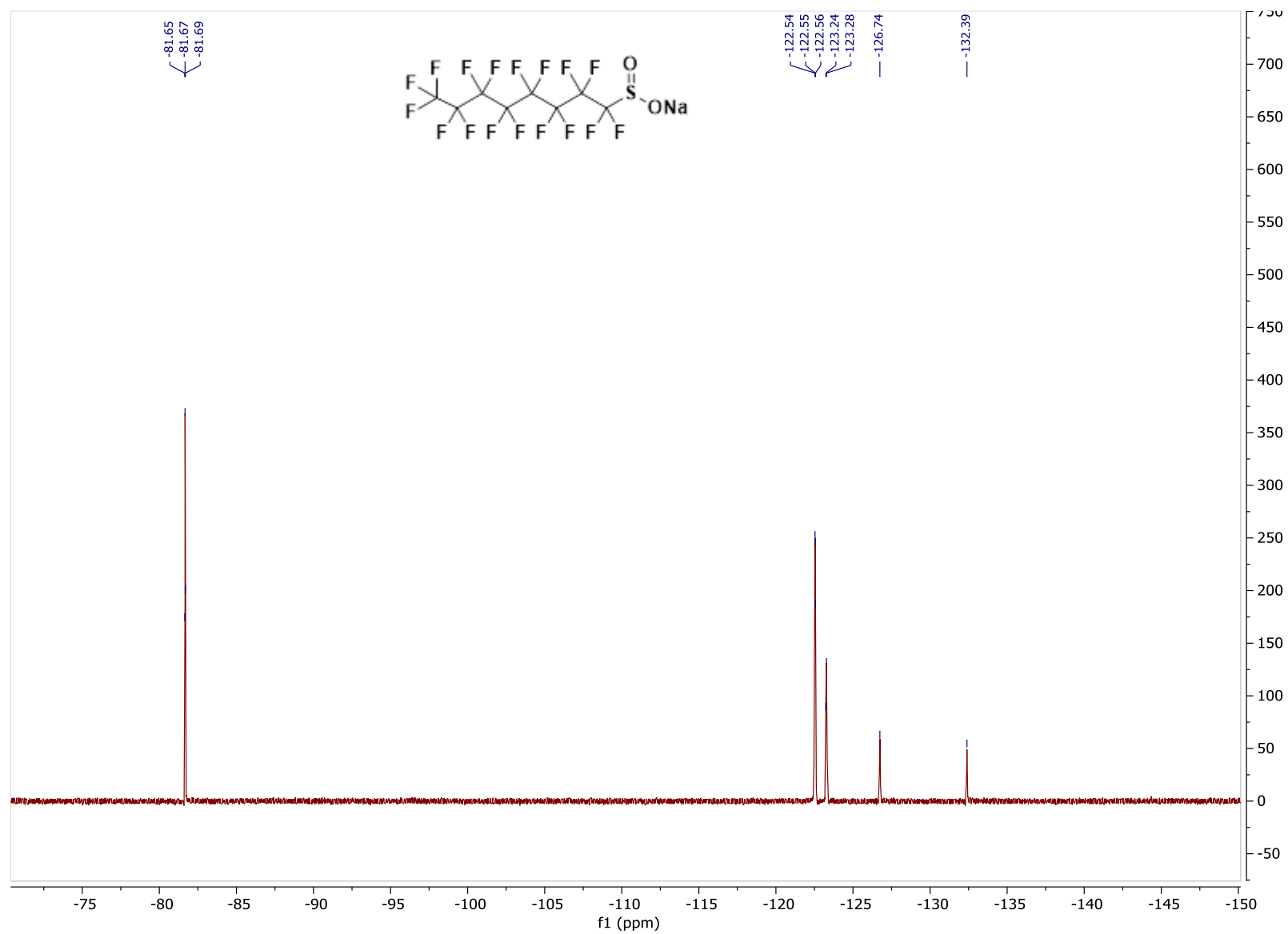
Characterization data for Chapter 2

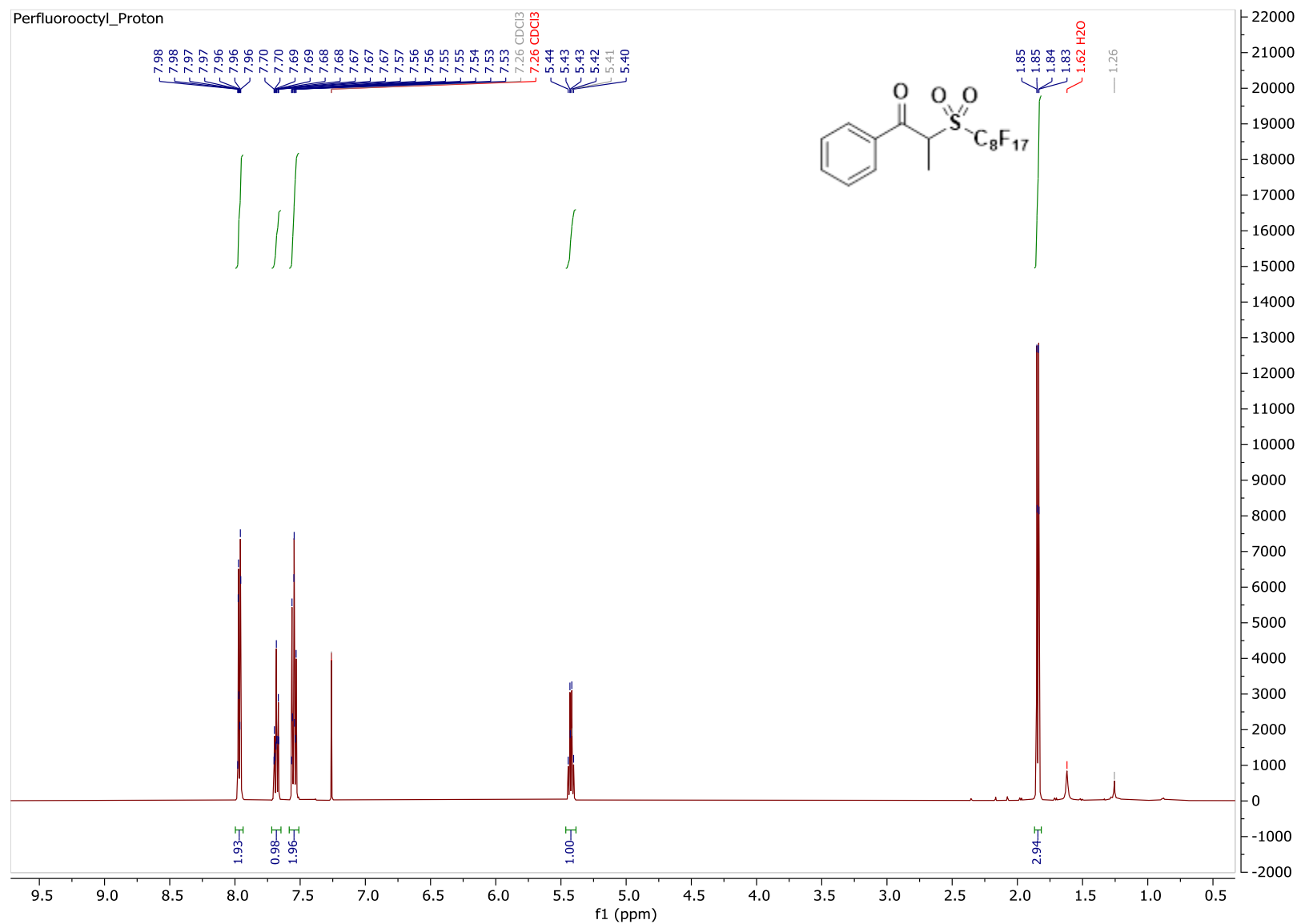
 ^{19}F NMR of **2a**, acetone- d_6 , 471 MHz

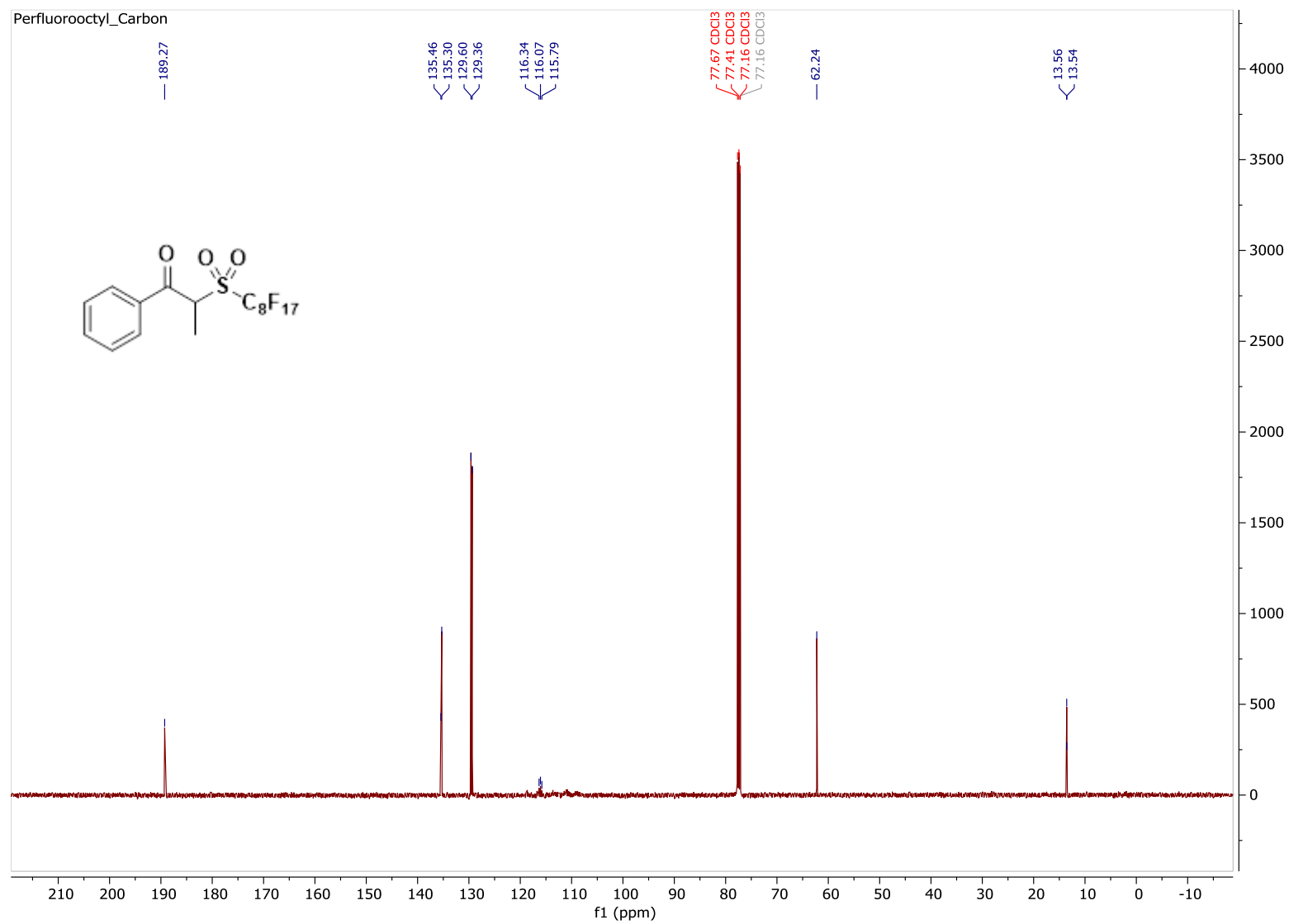
^{19}F NMR of **2b**, acetone- d_6 , 471 MHz



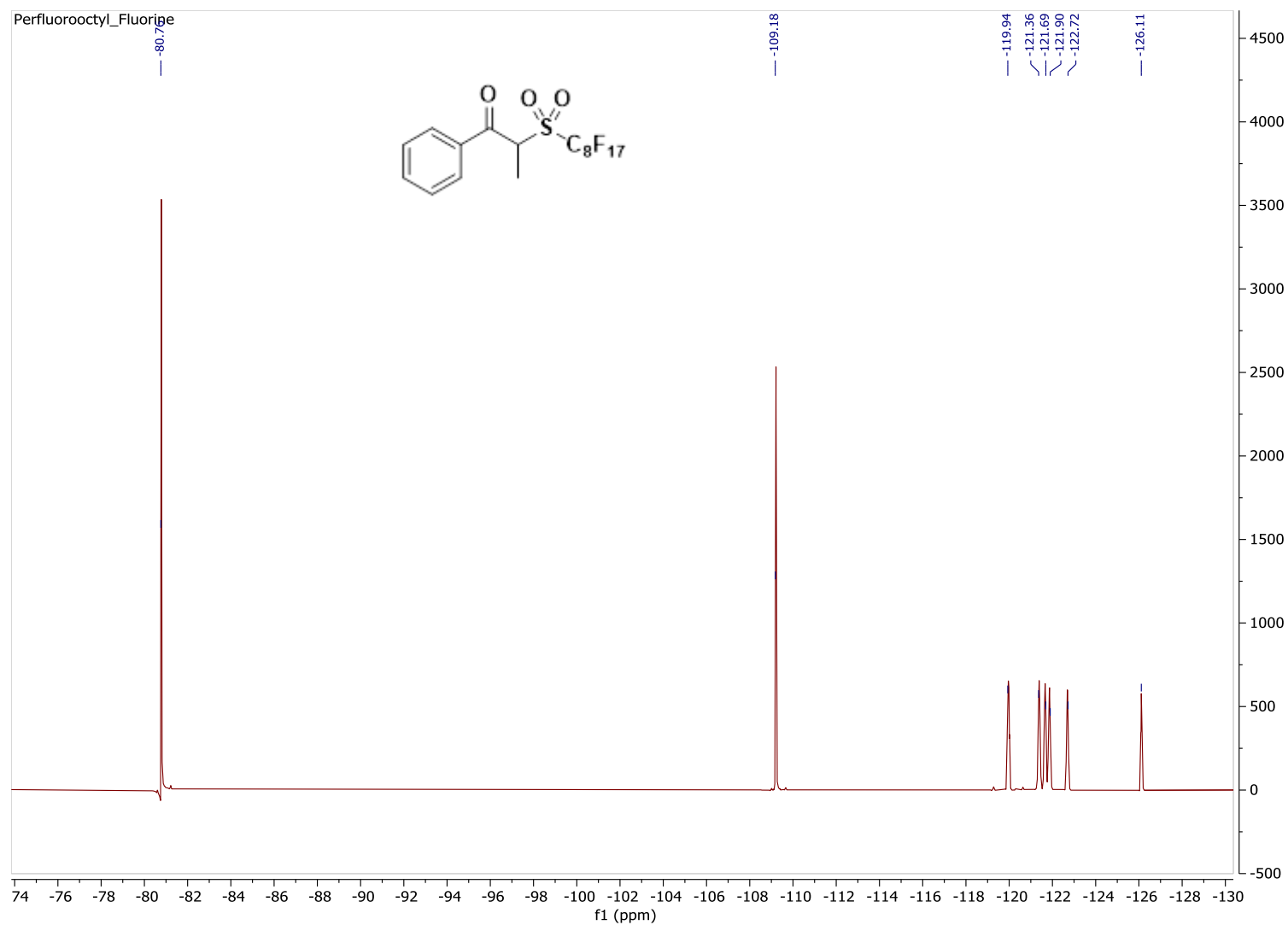
^{19}F NMR of **2c**, acetone- d_6 , 471 MHz

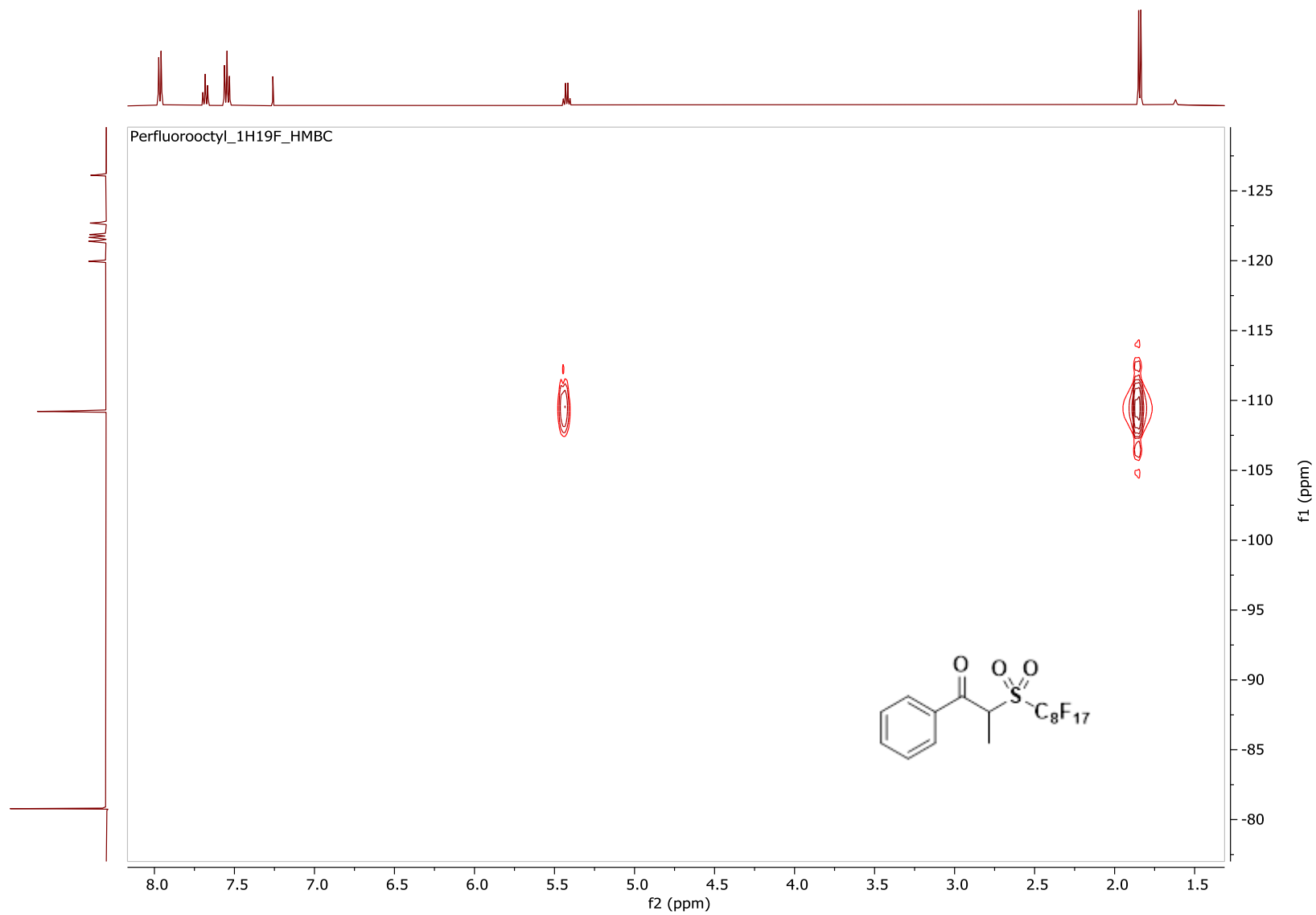


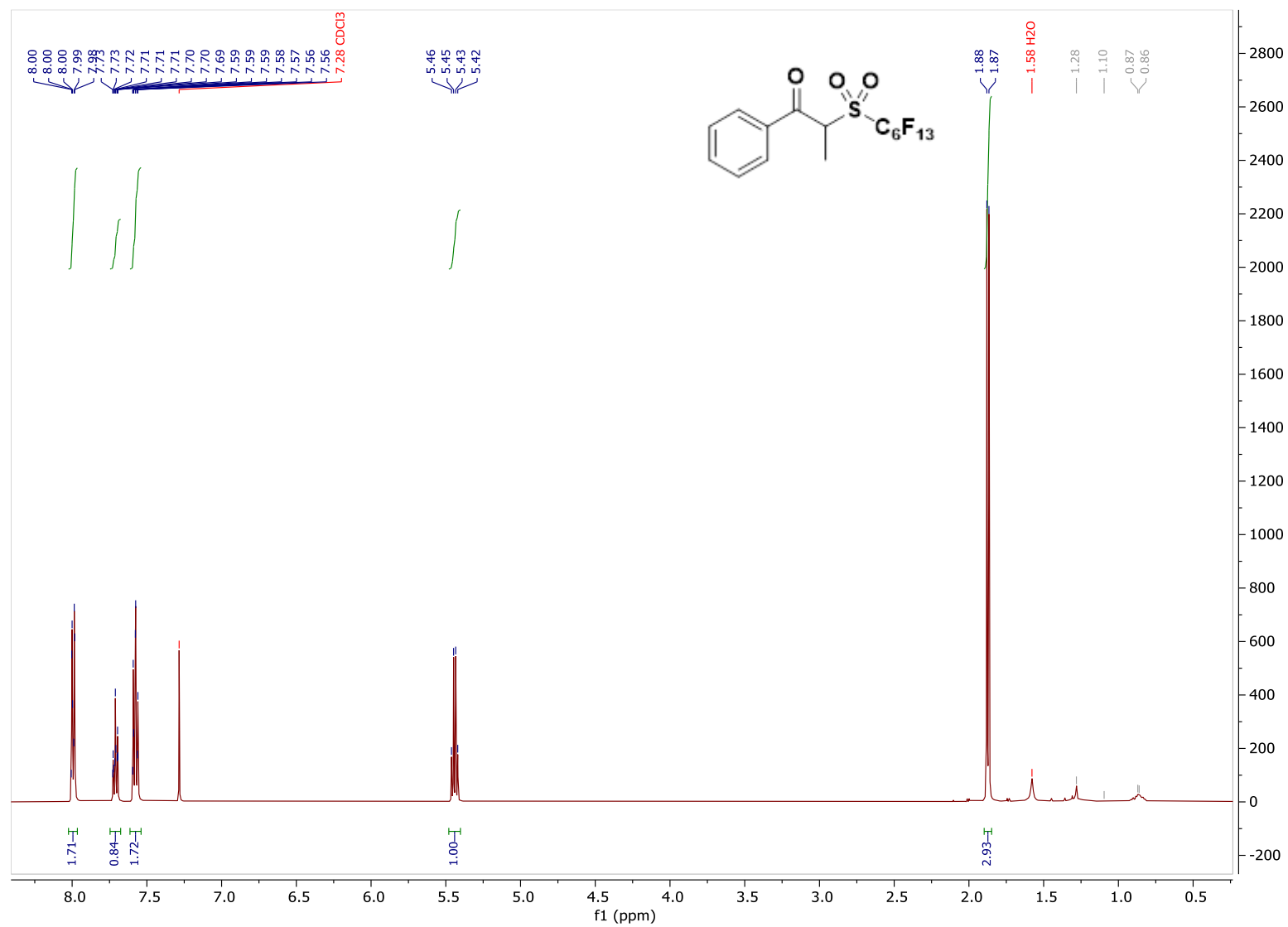
^1H NMR of **1c**, CDCl_3 , 500 MHz

^{13}C NMR of **1c**, CDCl_3 , 126 MHz

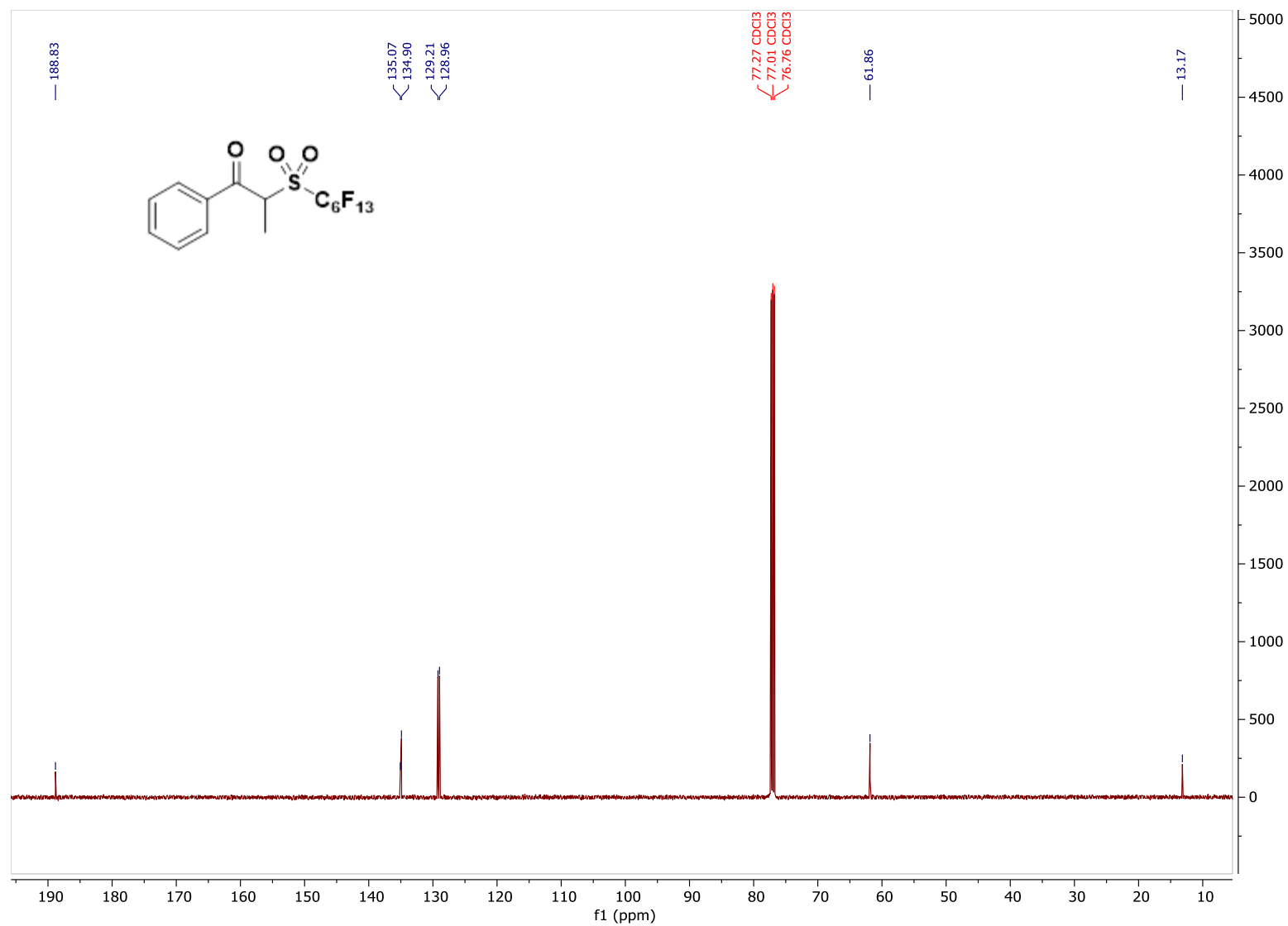
^{19}F NMR of **1c**, CDCl_3 , 471 MHz



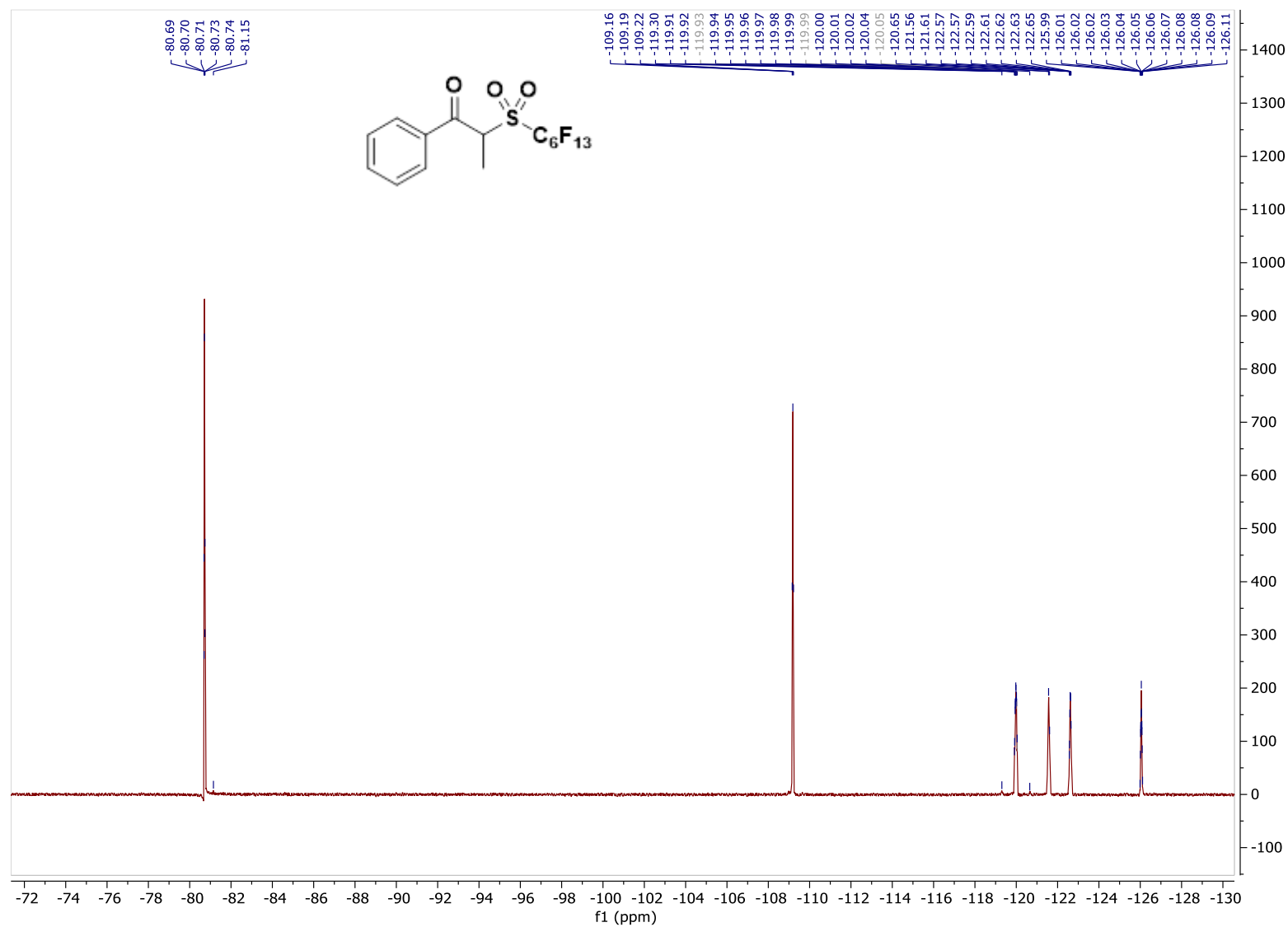
^1H - ^{19}F HMBC of **1c**

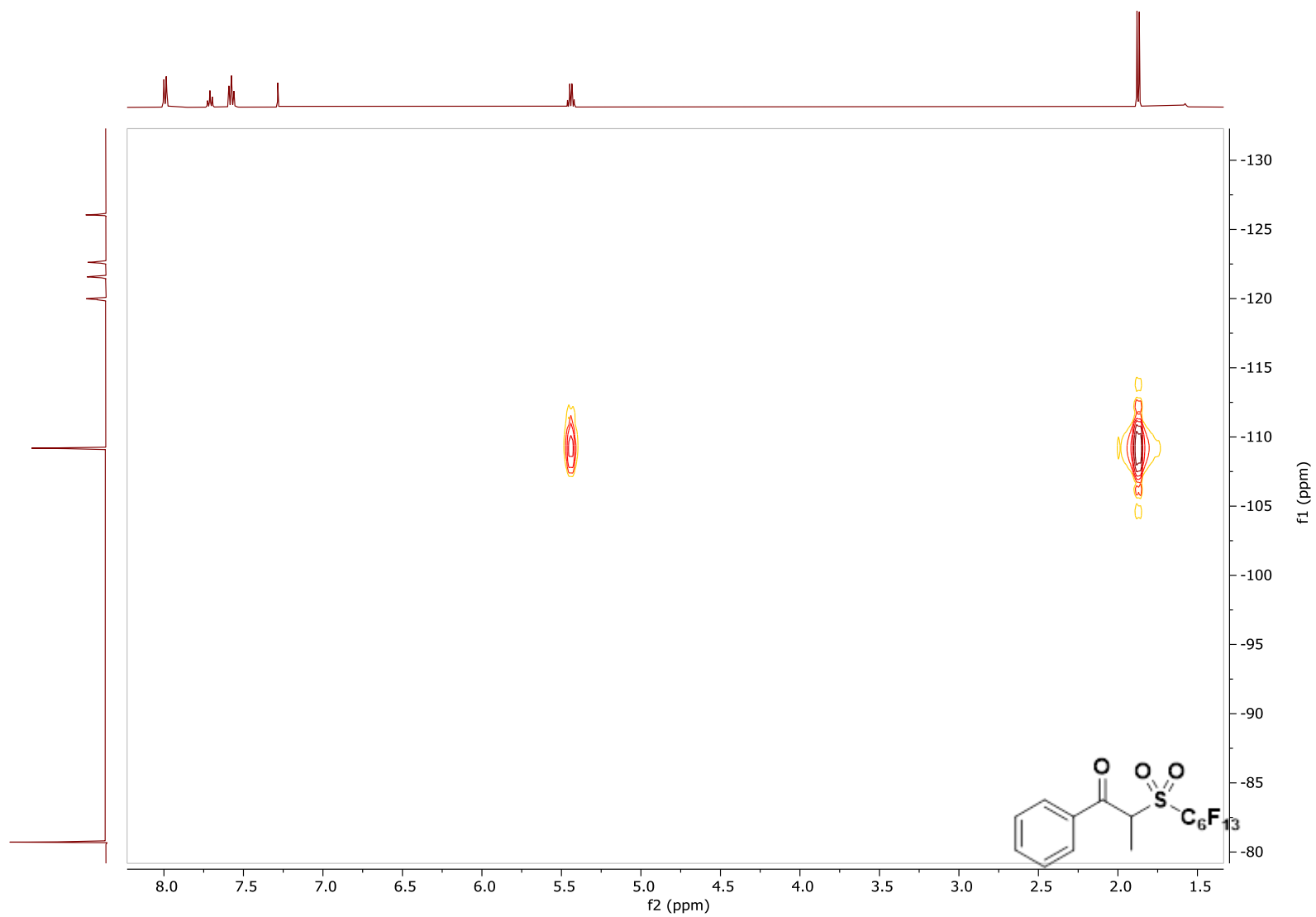
^1H NMR of **1b**, CDCl_3 , 500 MHz

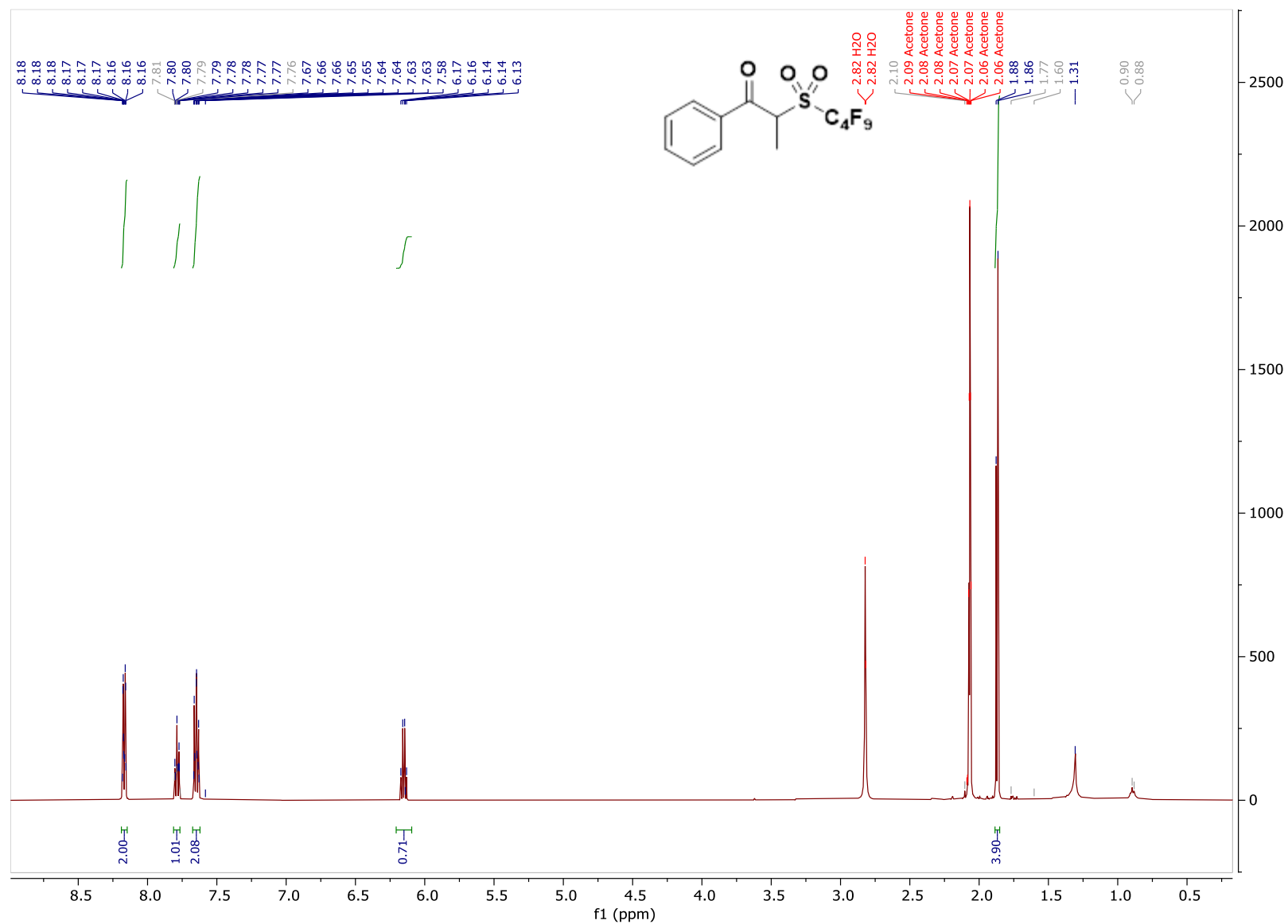
^{13}C NMR of **1b**, CDCl_3 , 126 MHz



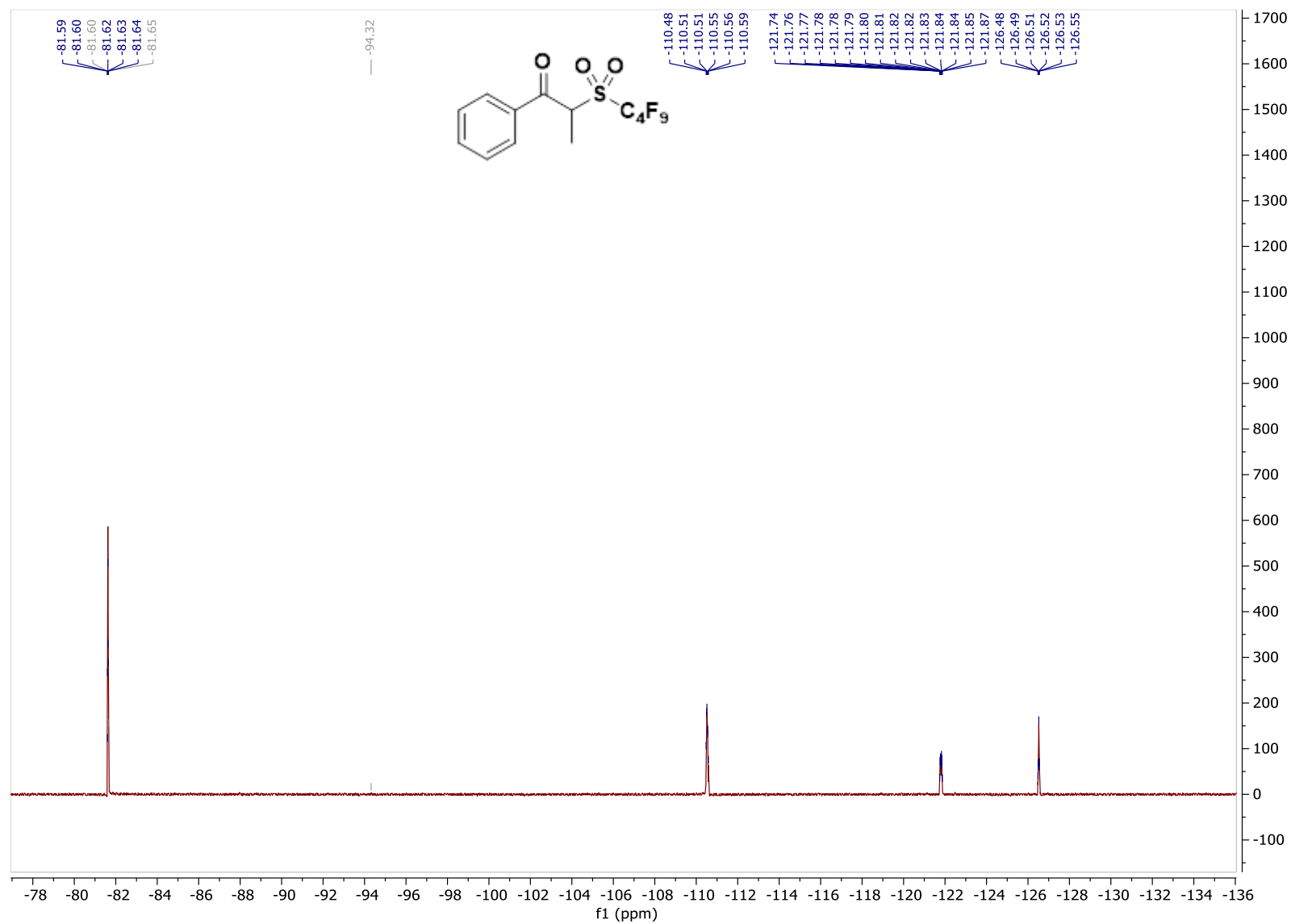
^{19}F NMR of **1b**, CDCl_3 , 471 MHz

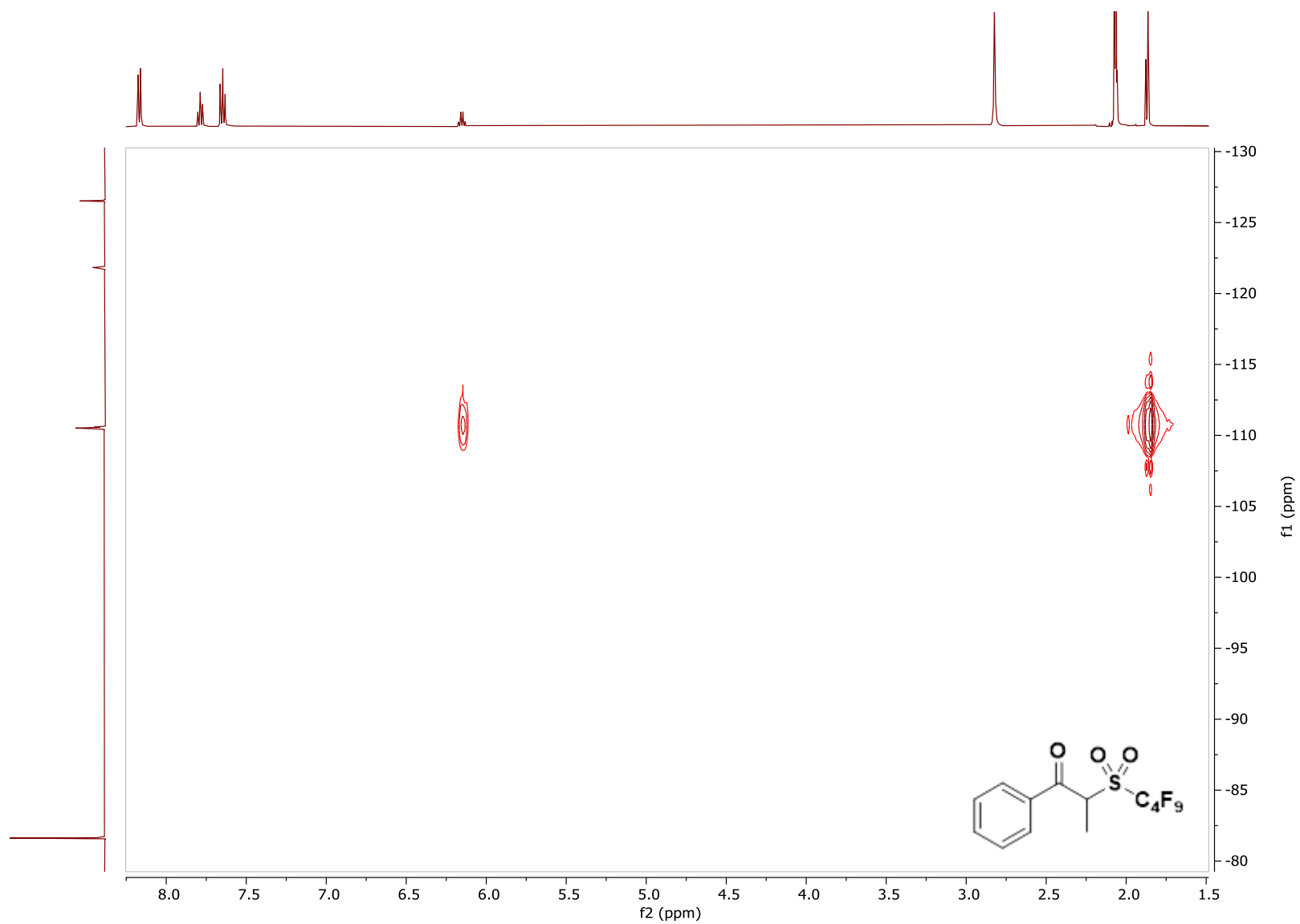


^1H - ^{19}F HMBC of **1b**

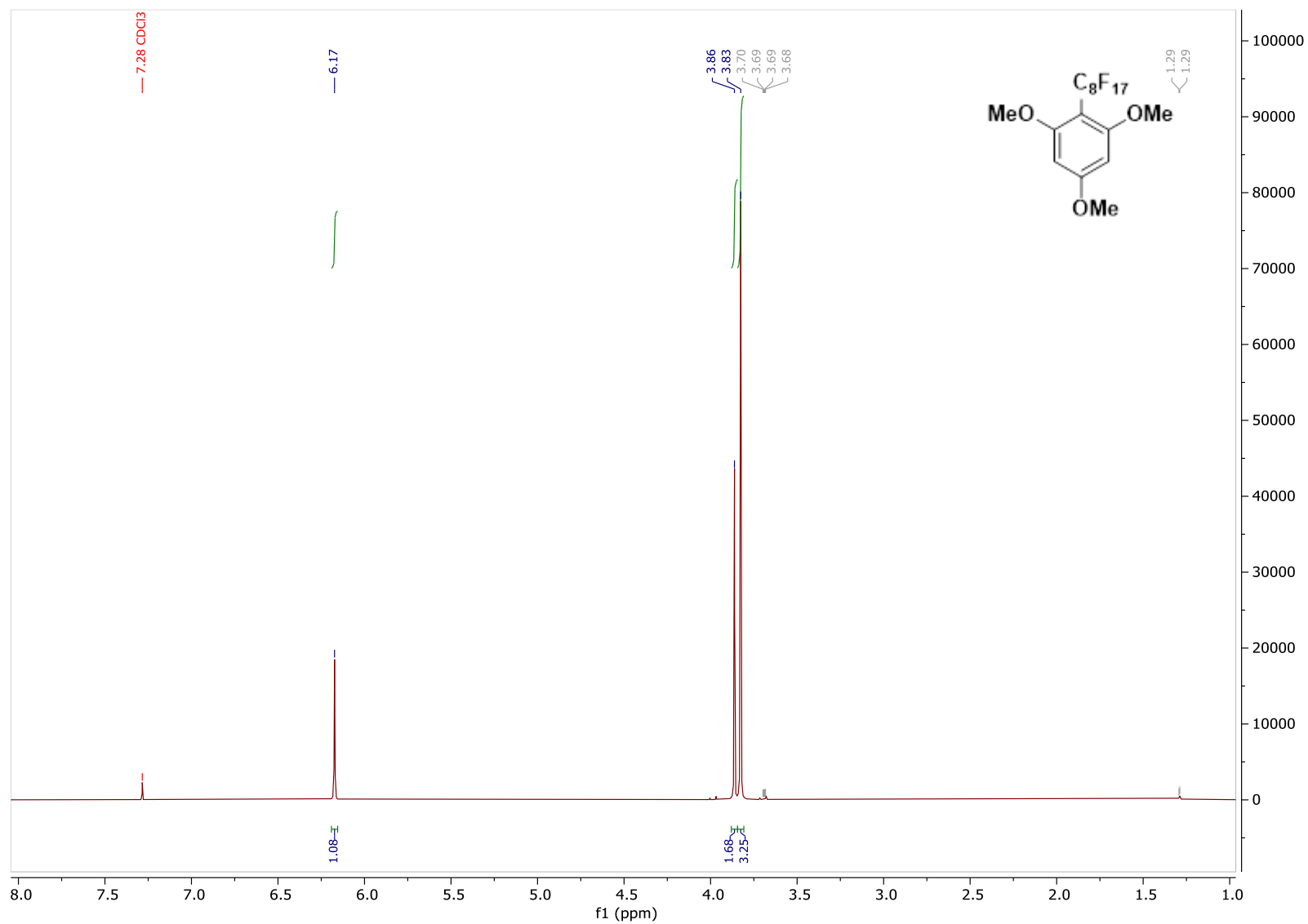
^1H NMR of **1a**, acetone- d_6 , 500 MHz

^{19}F NMR of **1a**, acetone- d_6 , 471 MHz

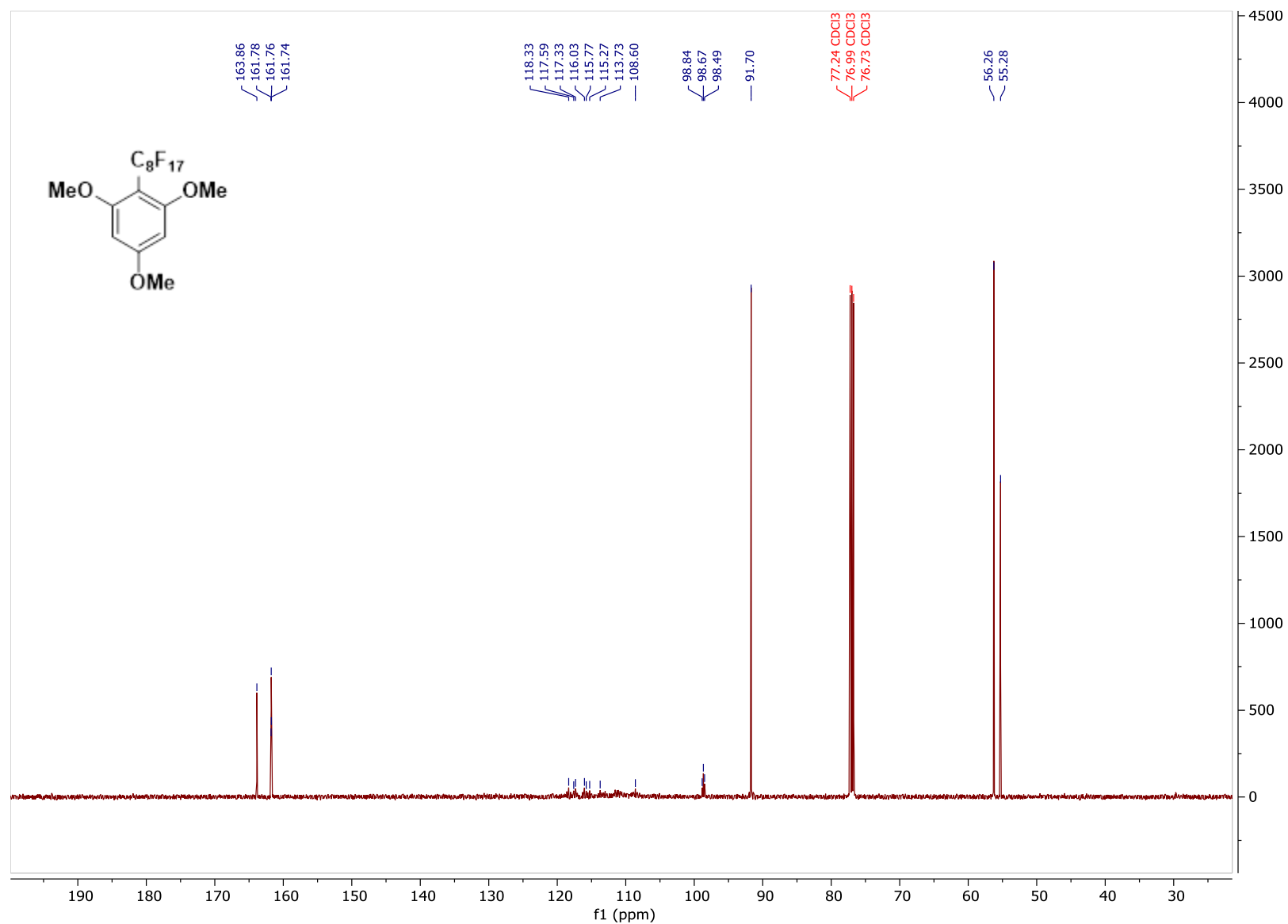


^1H - ^{19}F HMBC of **1a**

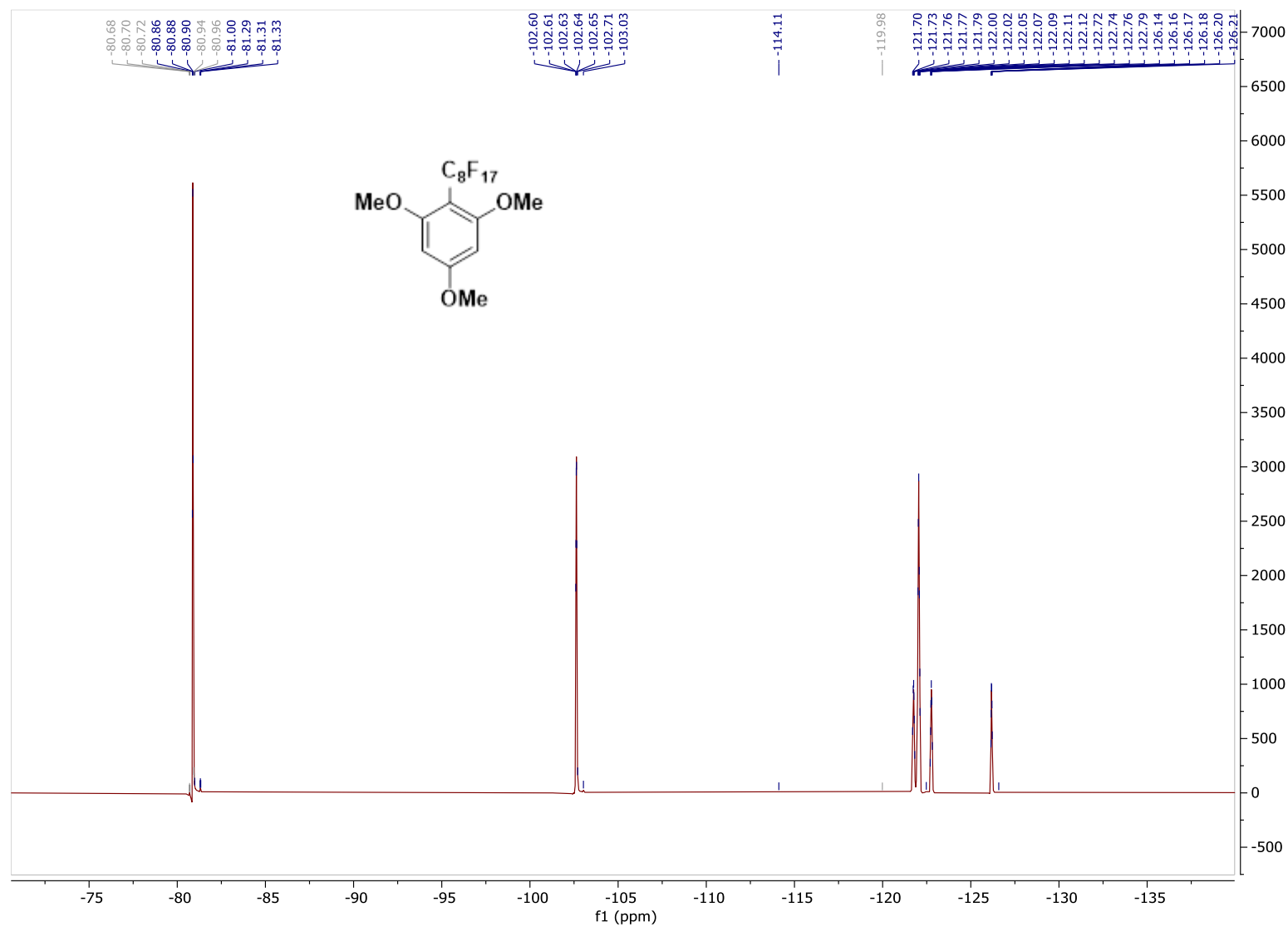
^1H NMR of **10c**, CDCl_3 , 500 MHz



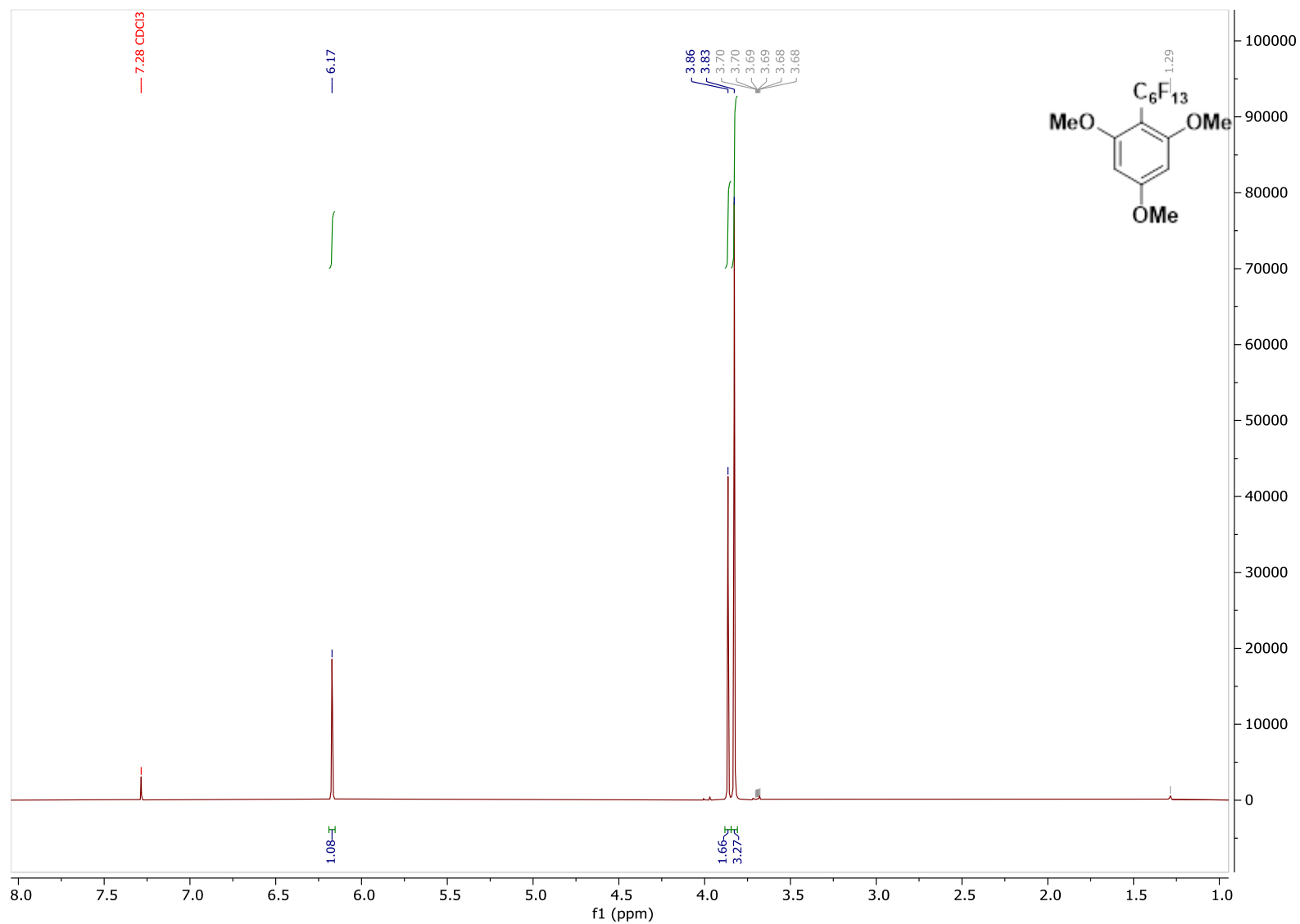
^{13}C NMR of **10c**, CDCl_3 , 126 MHz



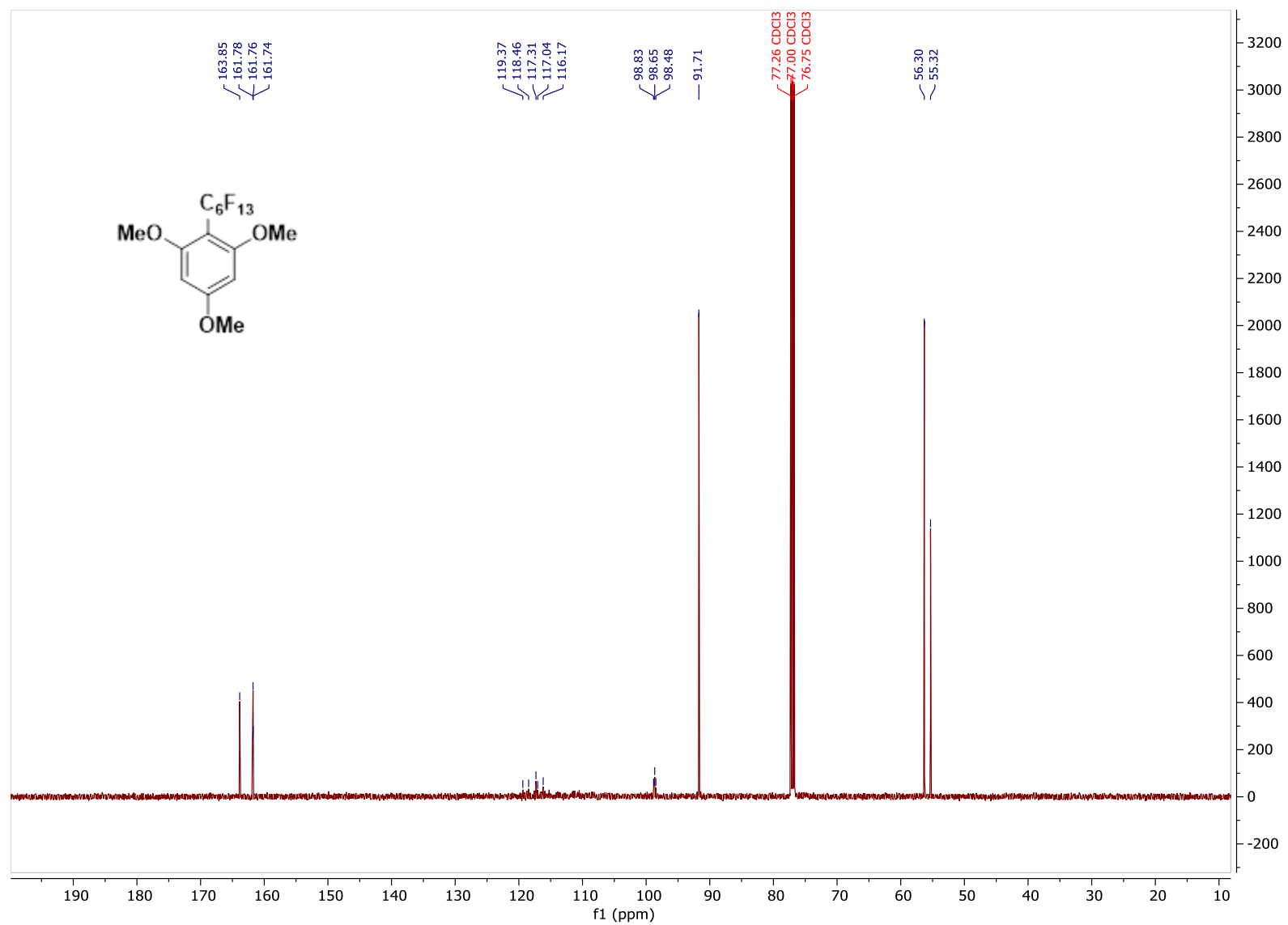
^{19}F NMR of **10c**, CDCl_3 , 471 MHz

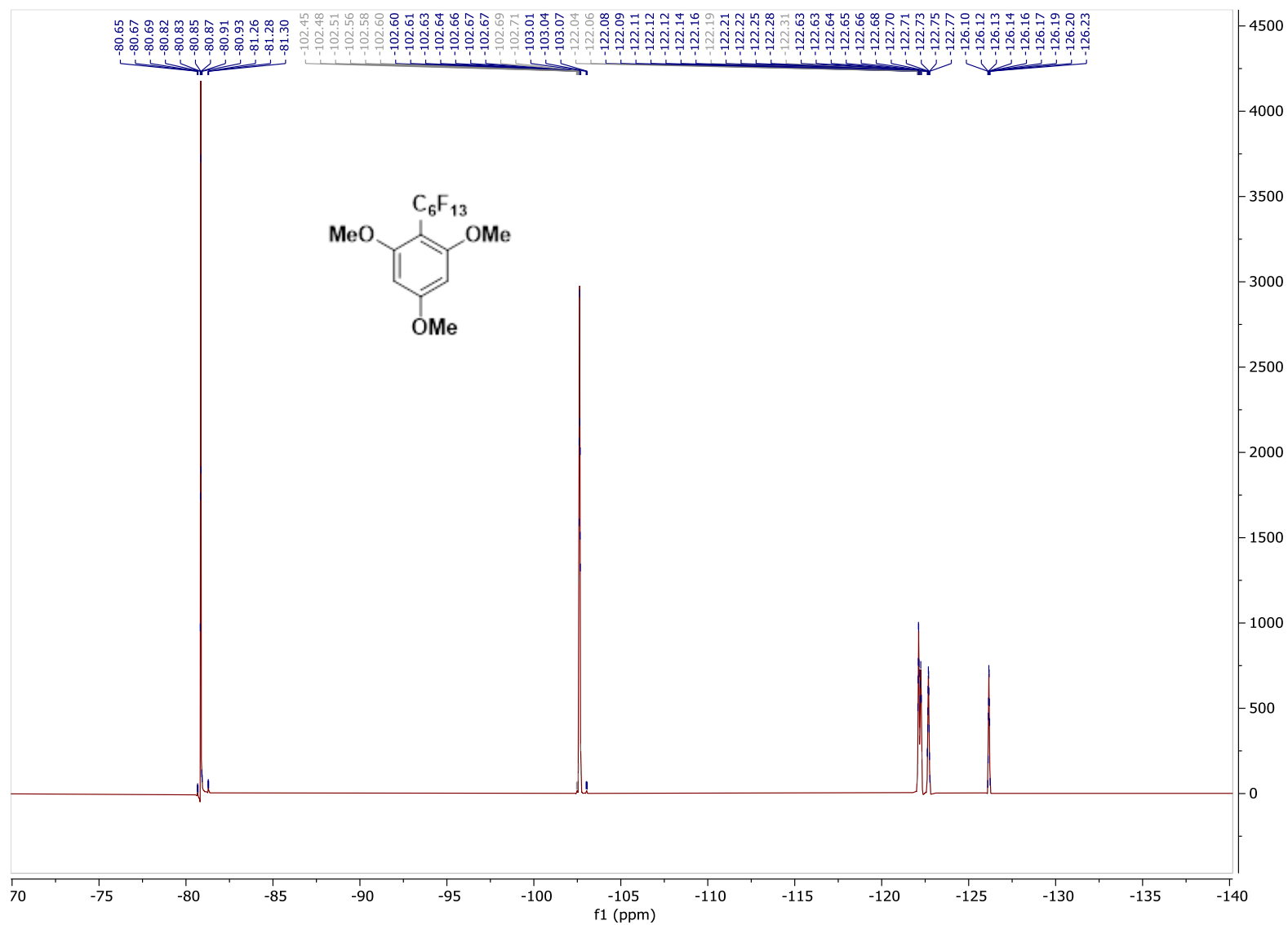


^1H NMR of **10b**, CDCl_3 , 500 MHz

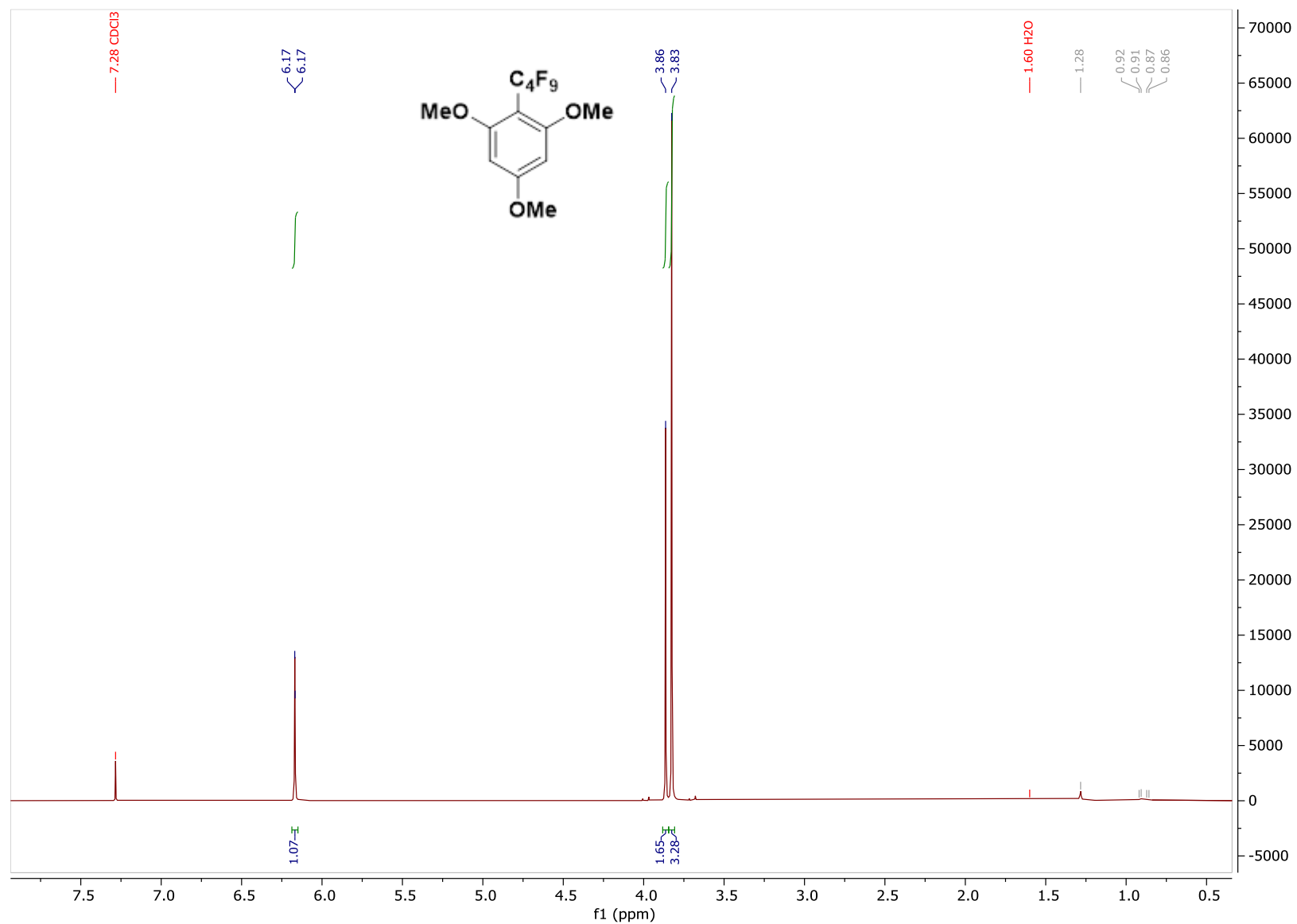


^{13}C NMR of **10b**, CDCl_3 , 126 MHz

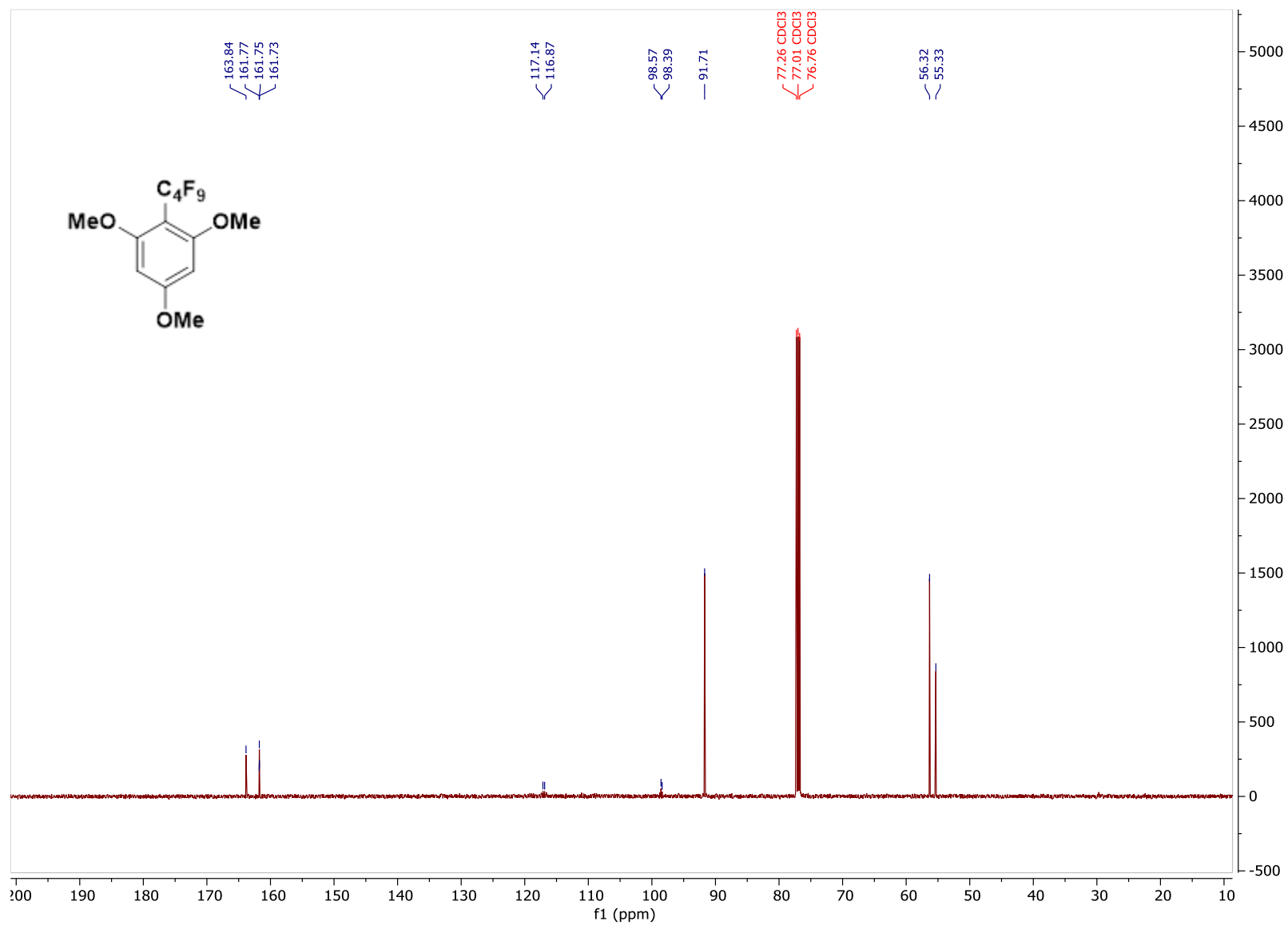


^{19}F NMR of **10b**, CDCl_3 , 471 MHz

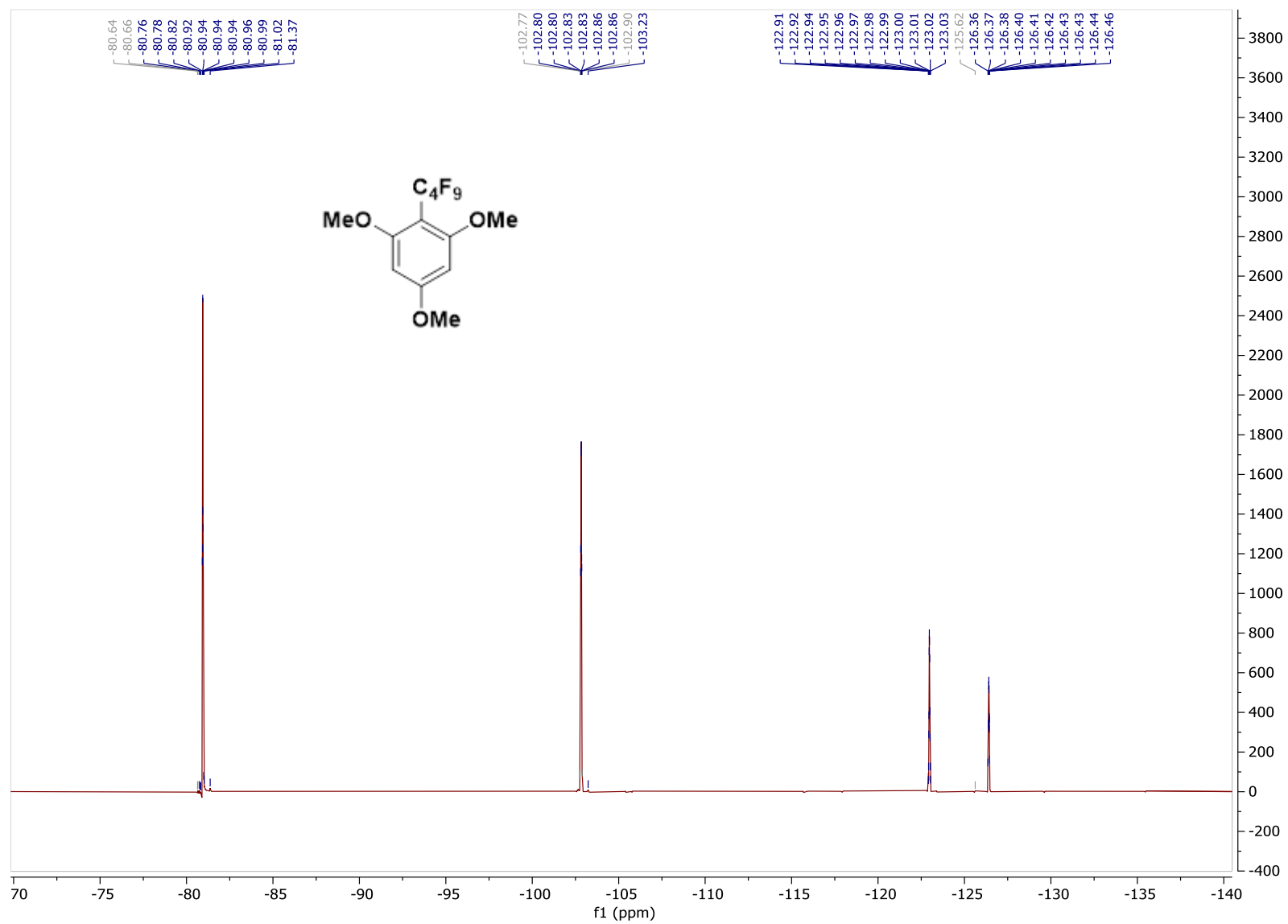
^1H NMR of **10a**, CDCl_3 , 500 MHz



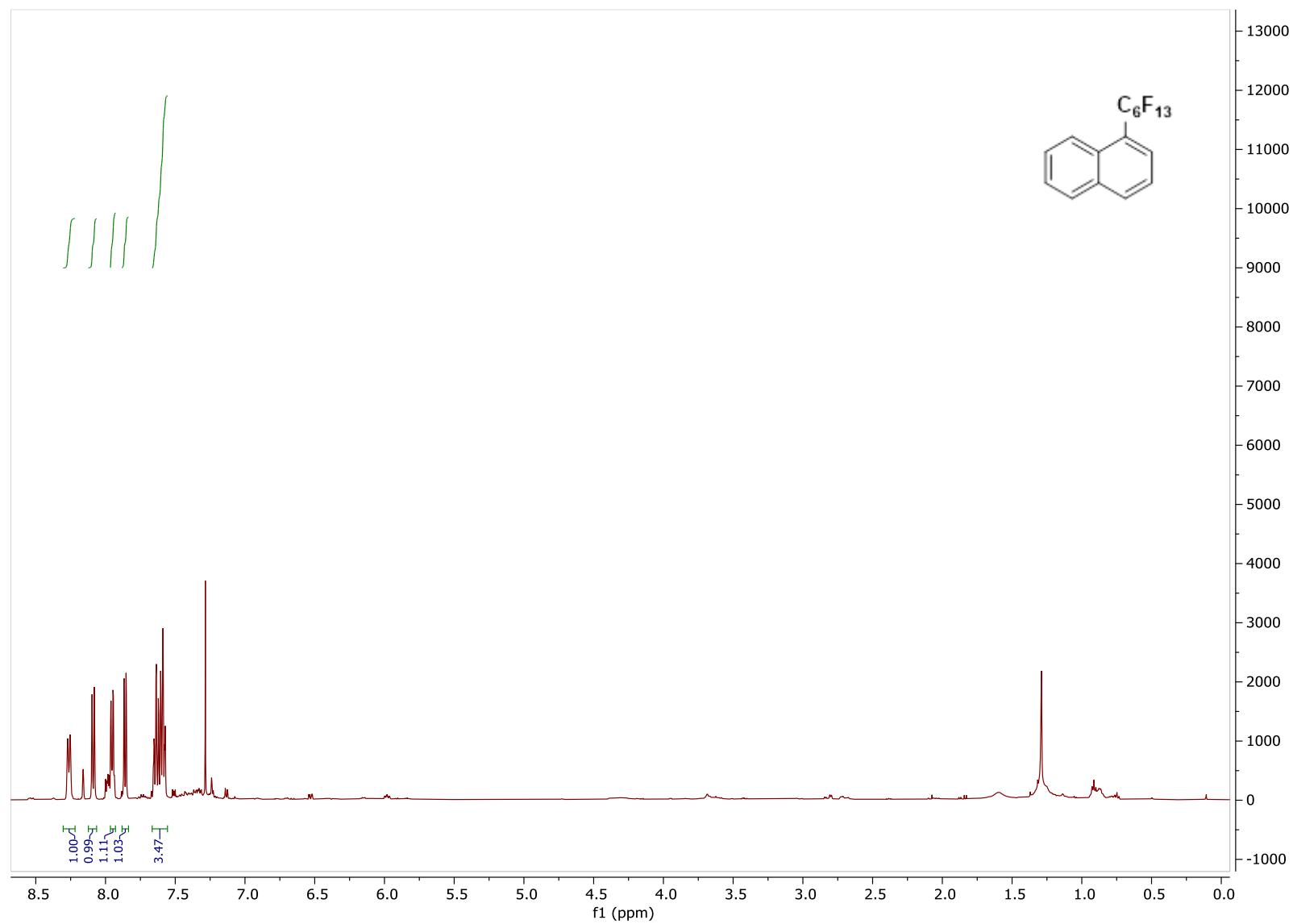
^{13}C NMR of **10a**, CDCl_3 , 126 MHz



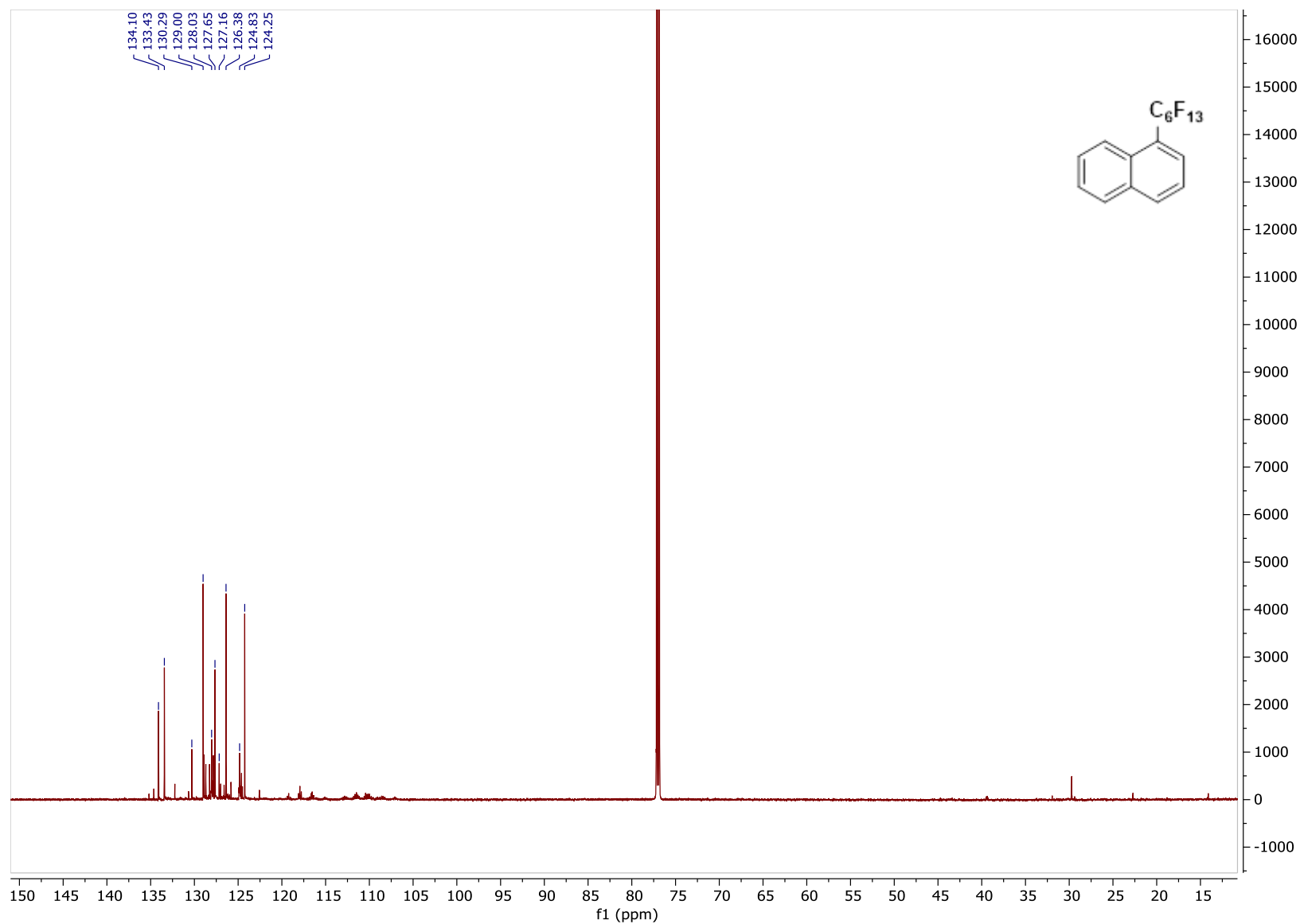
^{19}F NMR of **10a**, CDCl_3 , 471 MHz



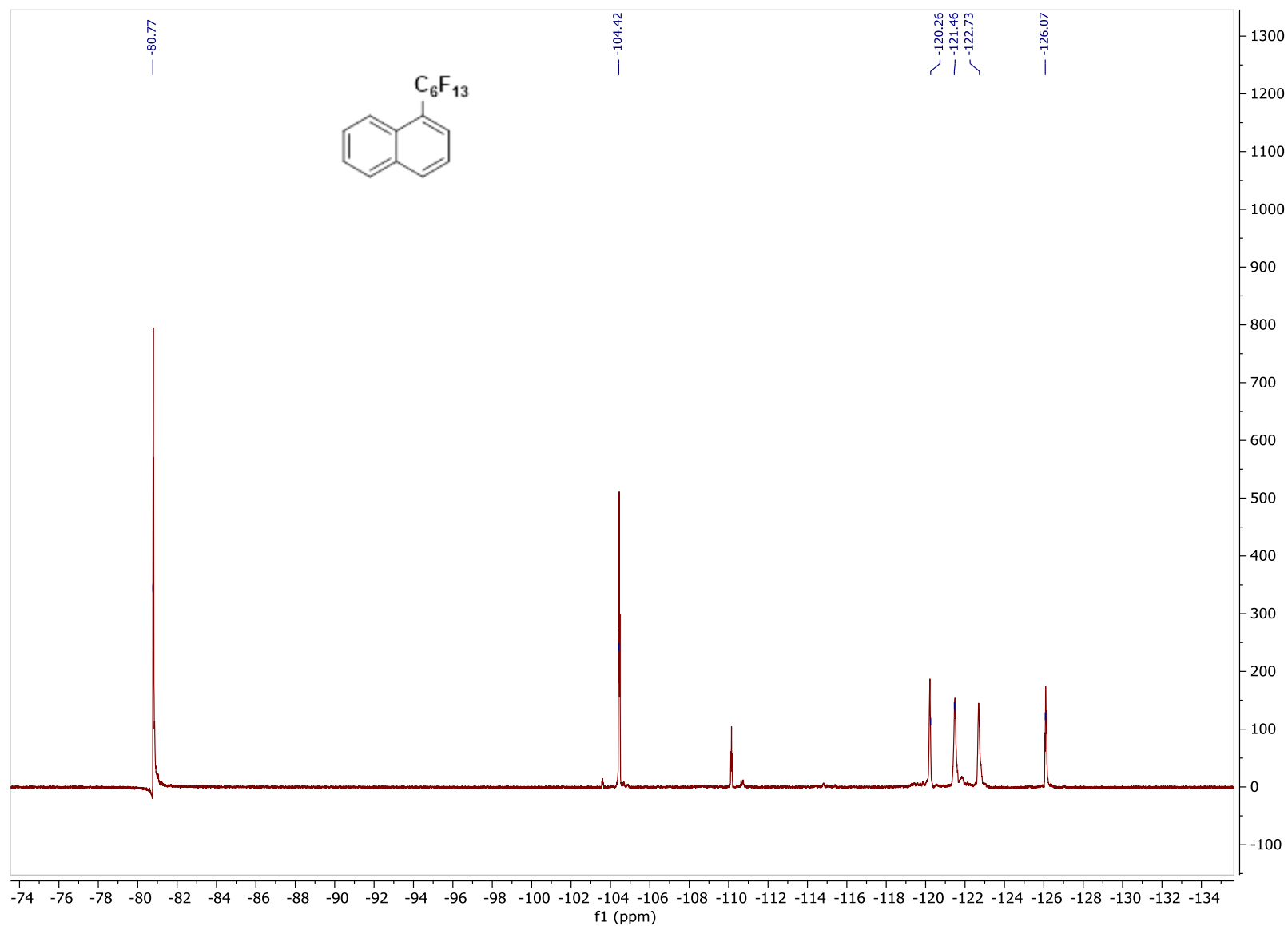
^1H NMR of **11b**, CDCl_3 , 500 MHz

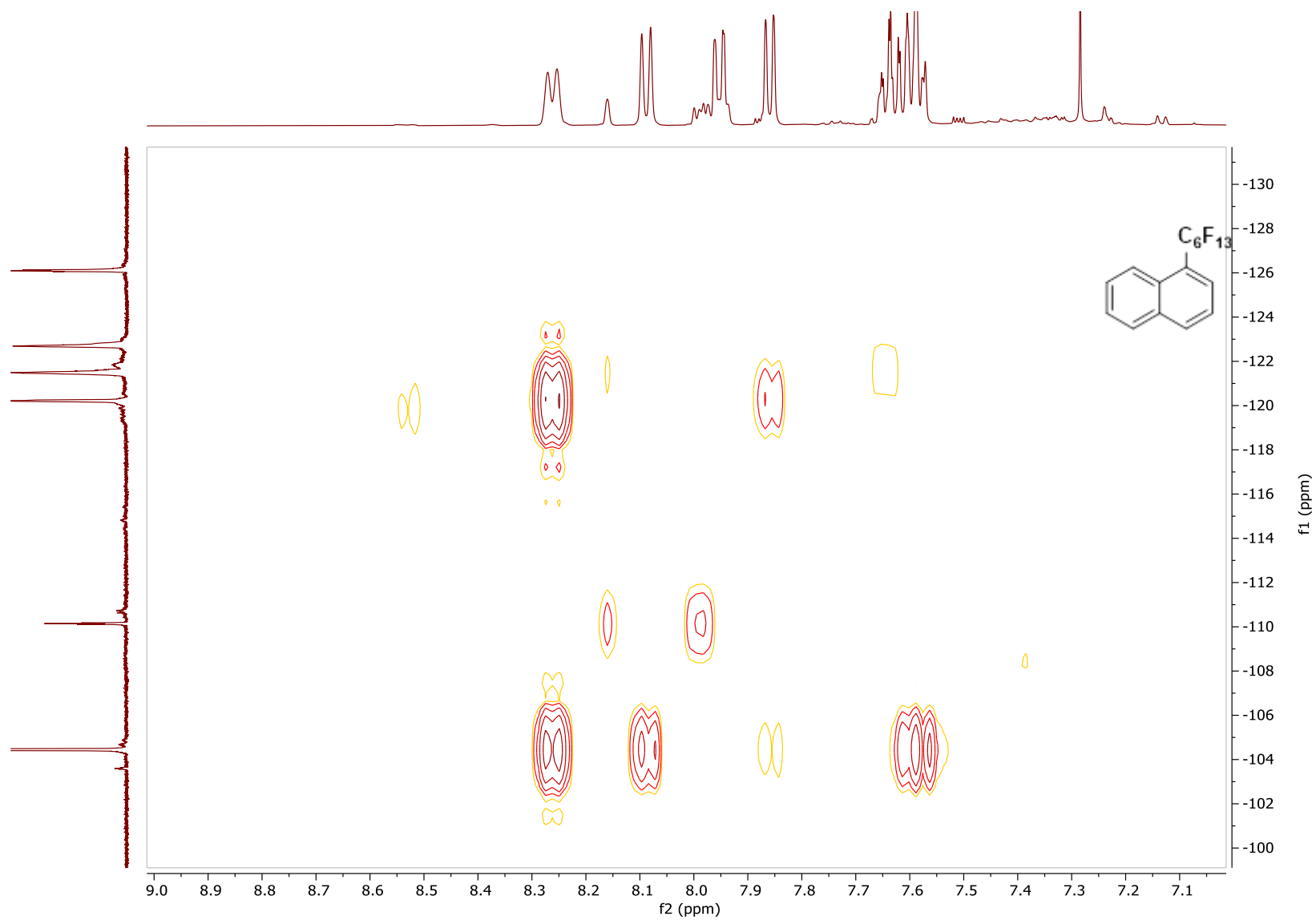


^{13}C NMR of **11b**, CDCl_3 , 126 MHz

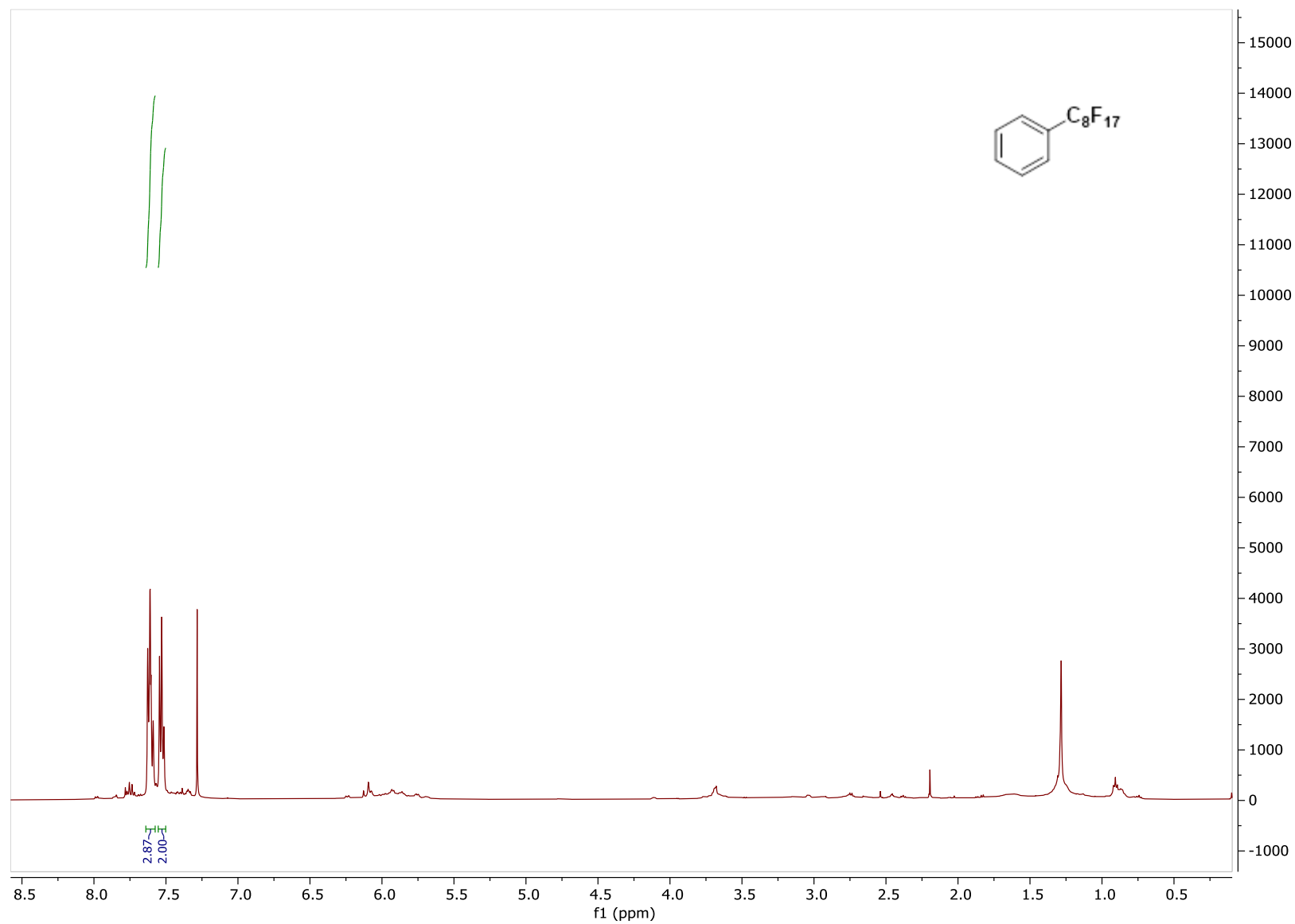


^{19}F NMR of **11b**, CDCl_3 , 471 MHz

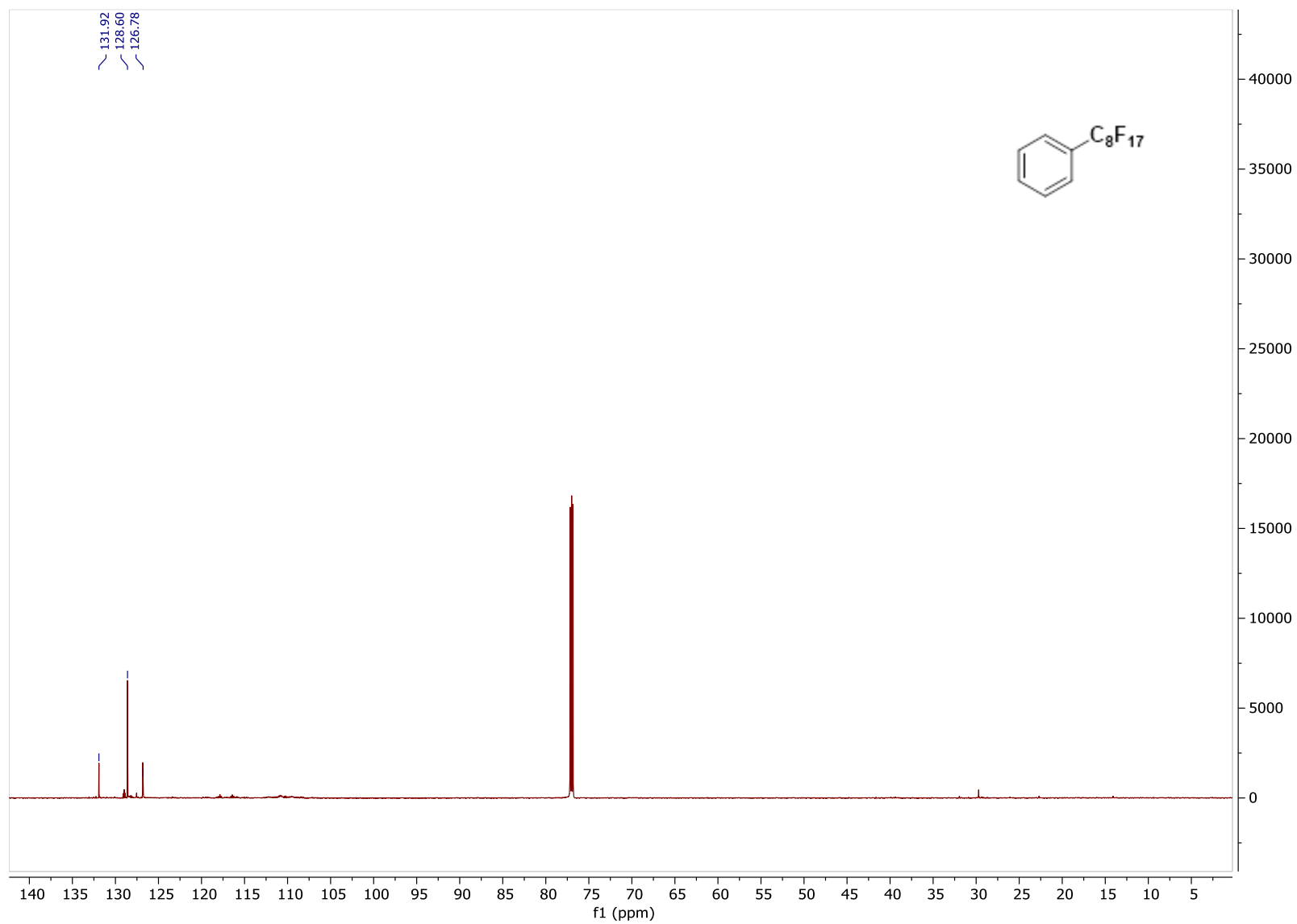


^1H - ^{19}F HMBC of **11b**

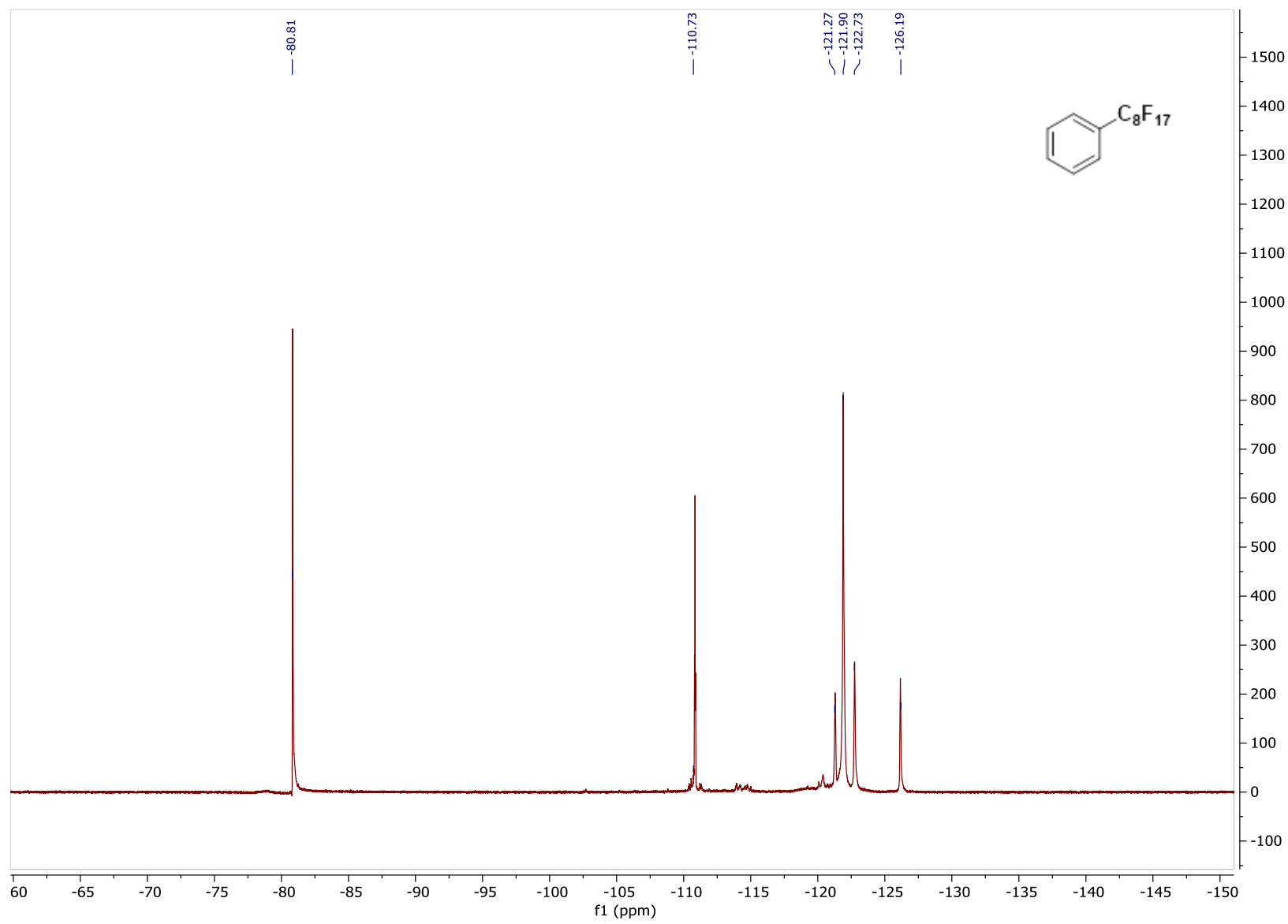
^1H NMR of **12c**, CDCl_3 , 500 MHz

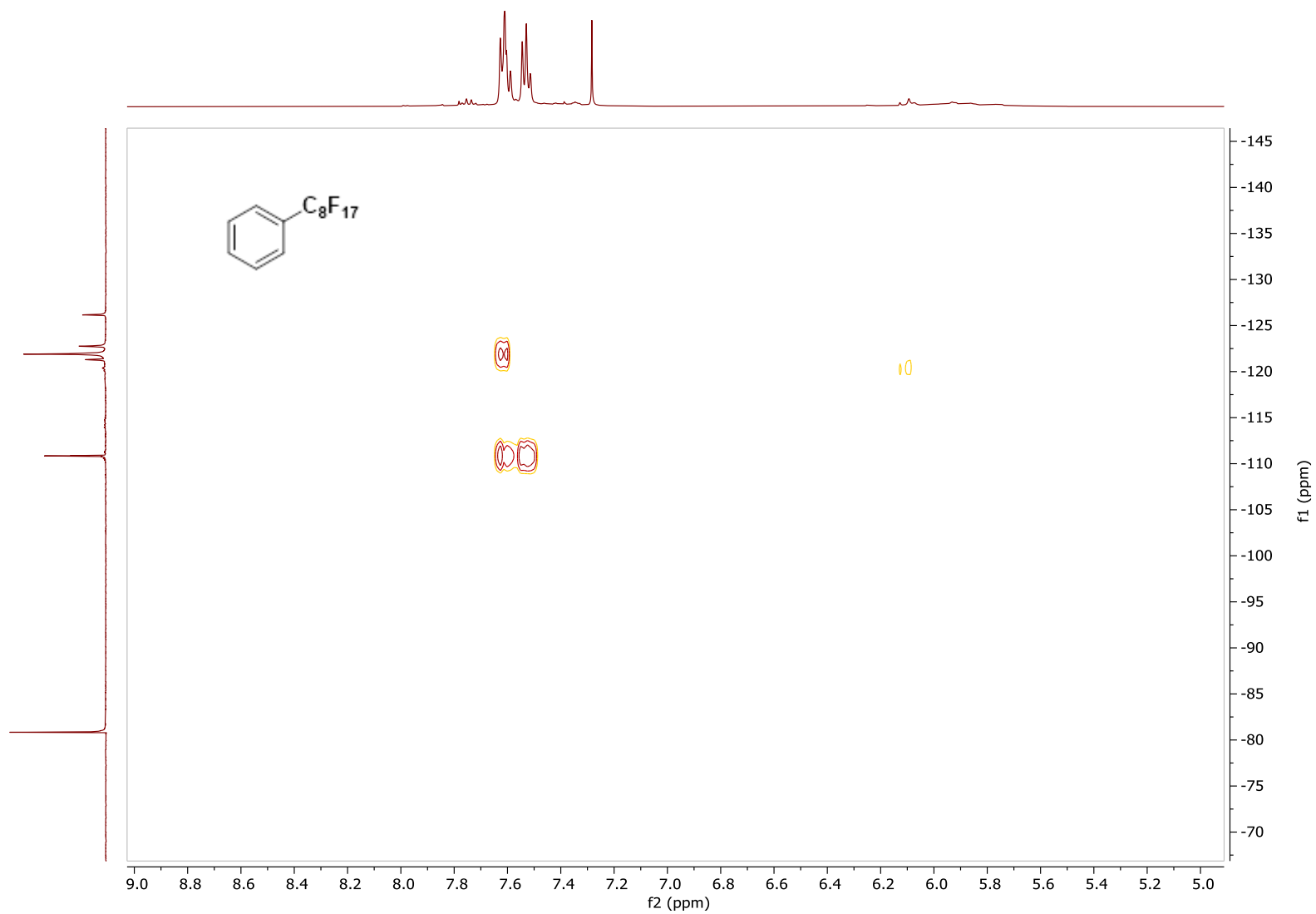


^{13}C NMR of **12c**, CDCl_3 , 126 MHz

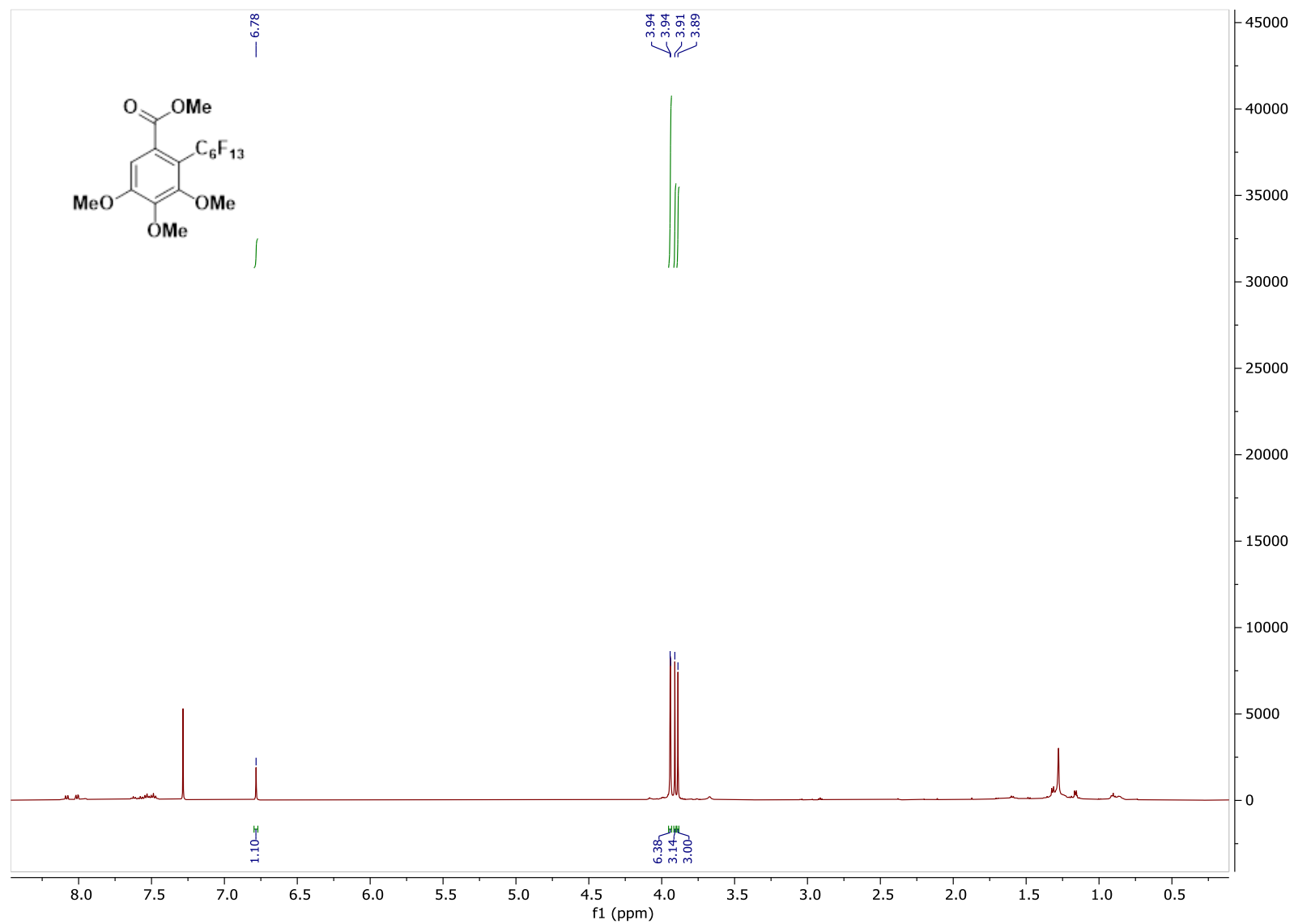


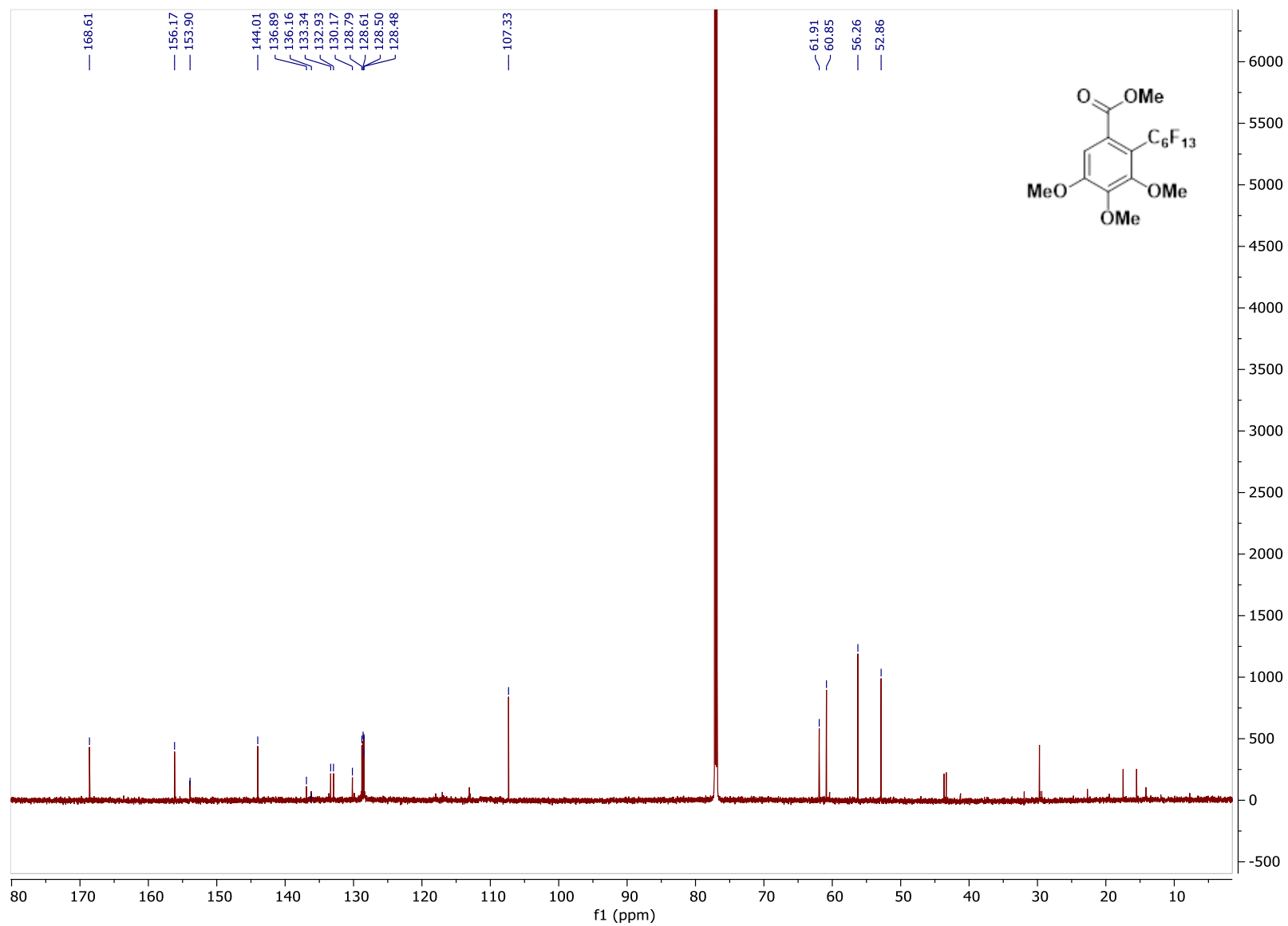
^{19}F NMR of **12c**, CDCl_3 , 471 MHz



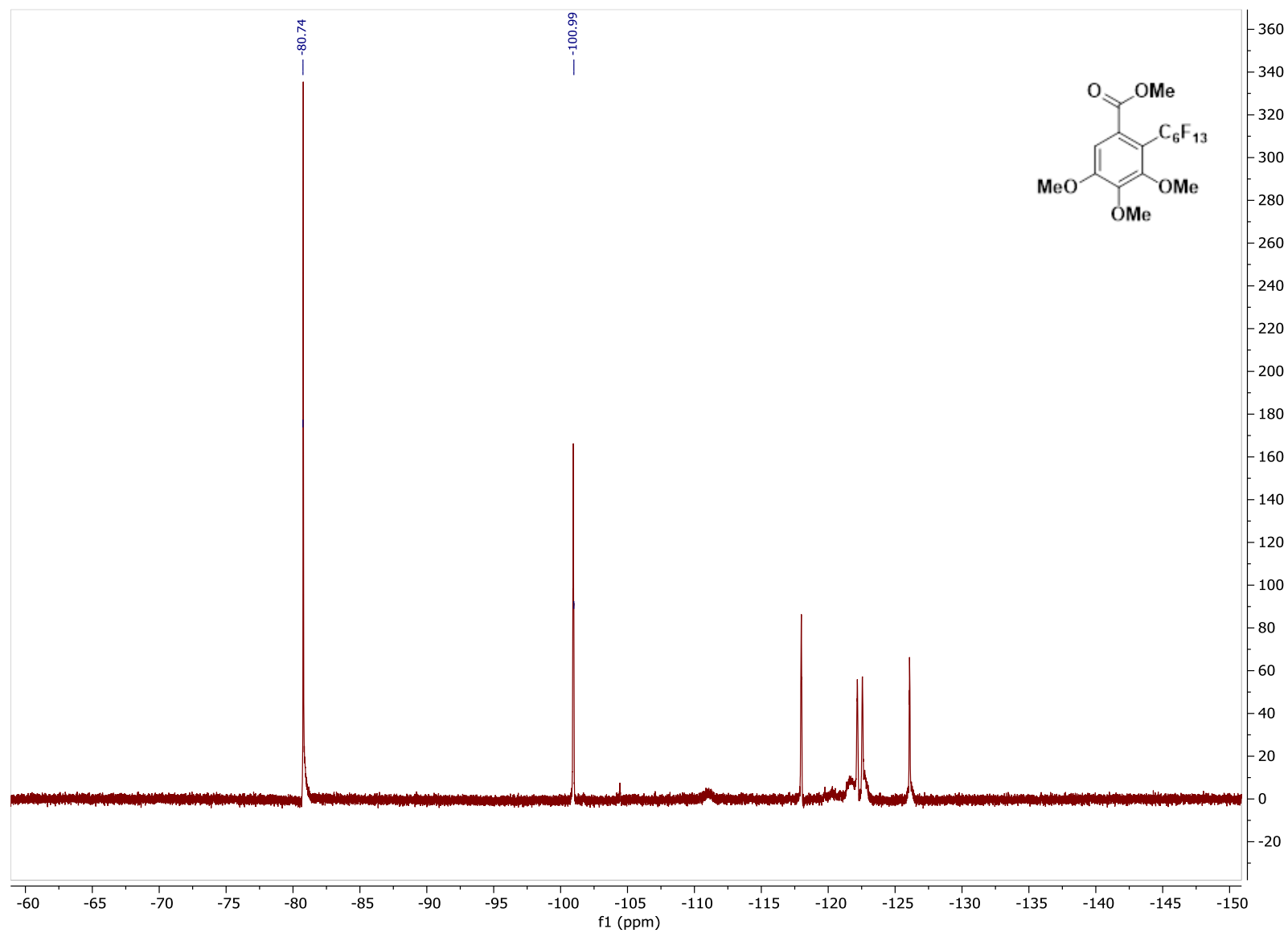
^1H - ^{19}F HMBC of **12c**

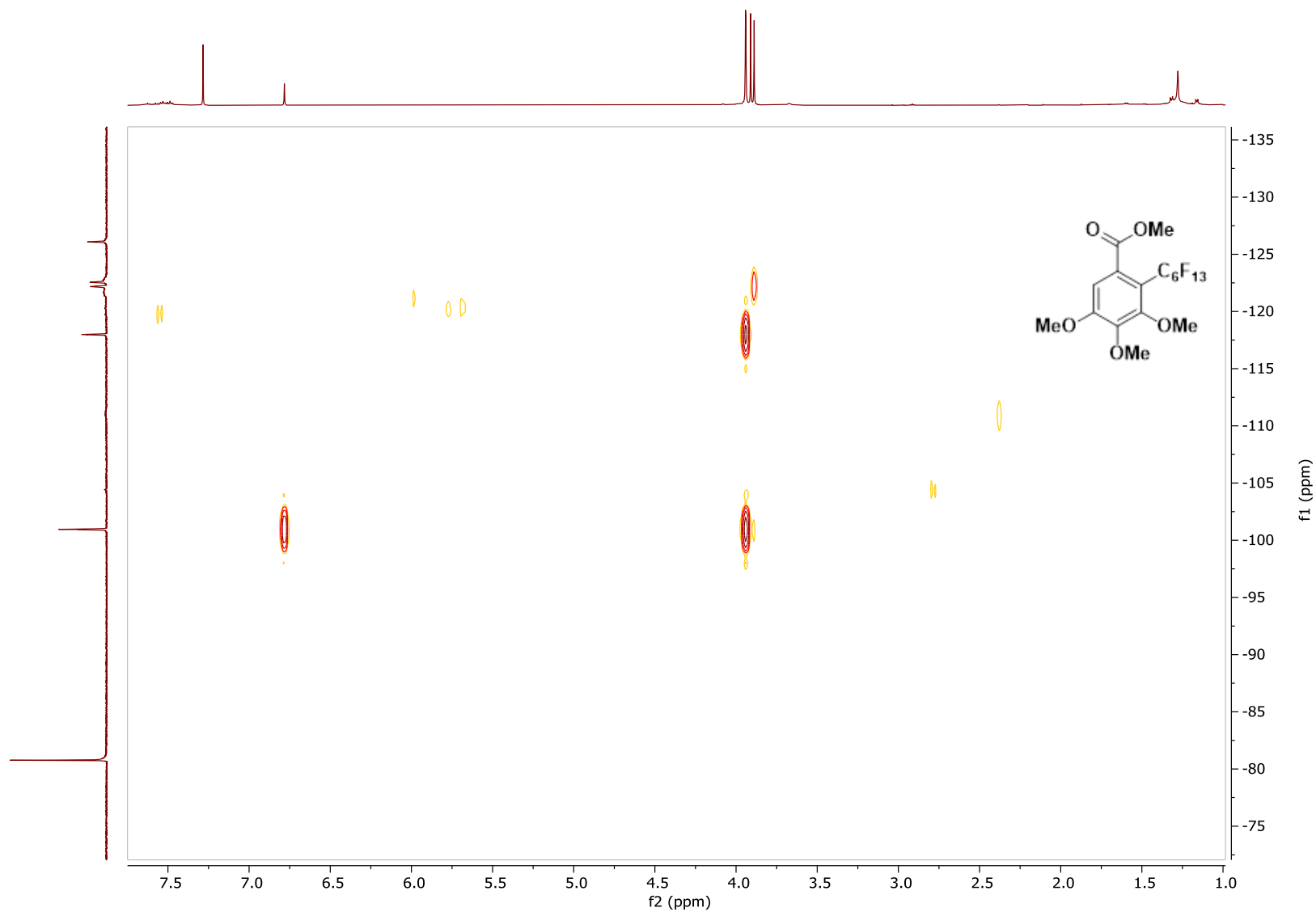
^1H NMR of **13b**, CDCl_3 , 500 MHz



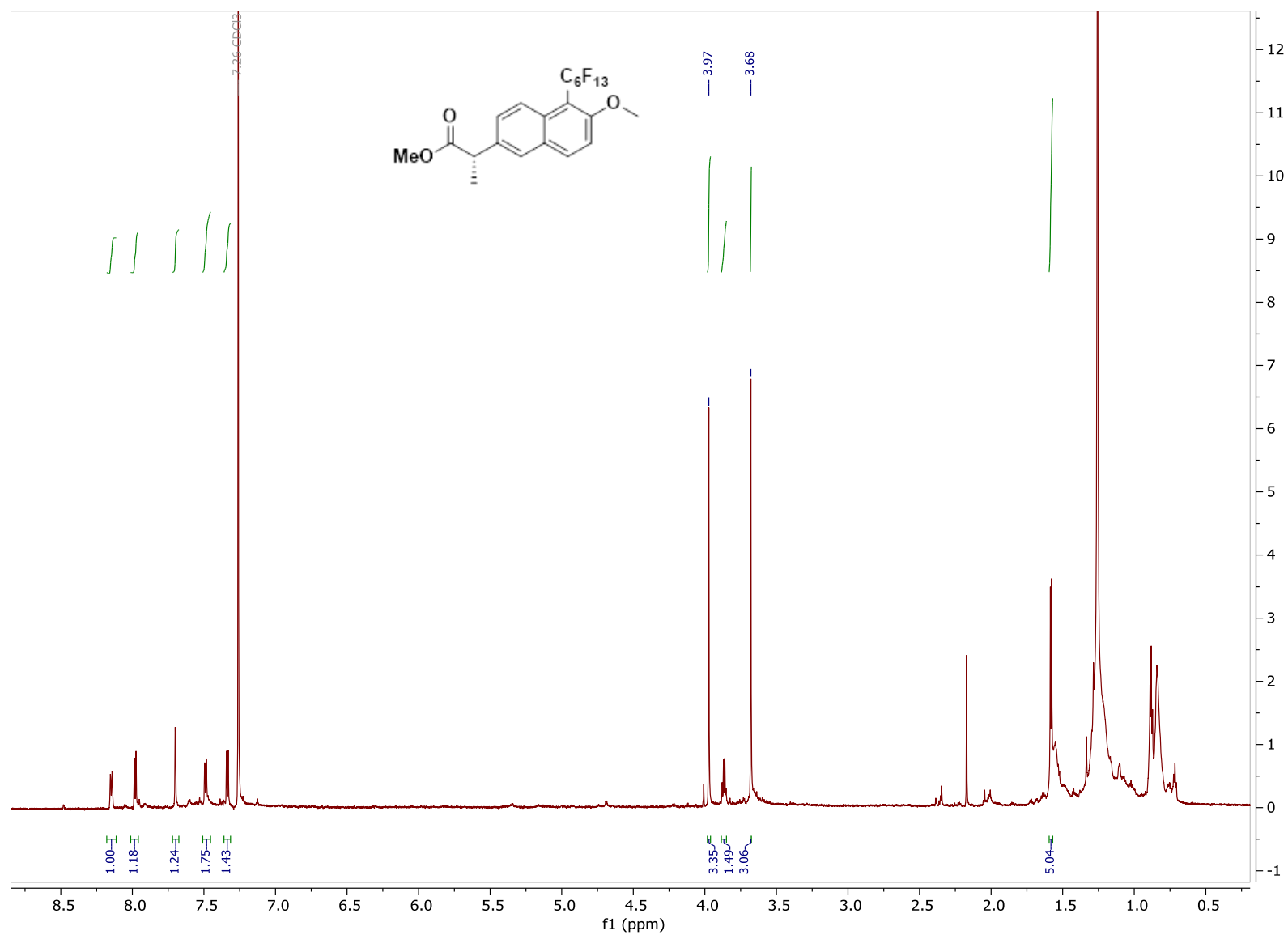
^{13}C NMR of **13b**, CDCl_3 , 126 MHz

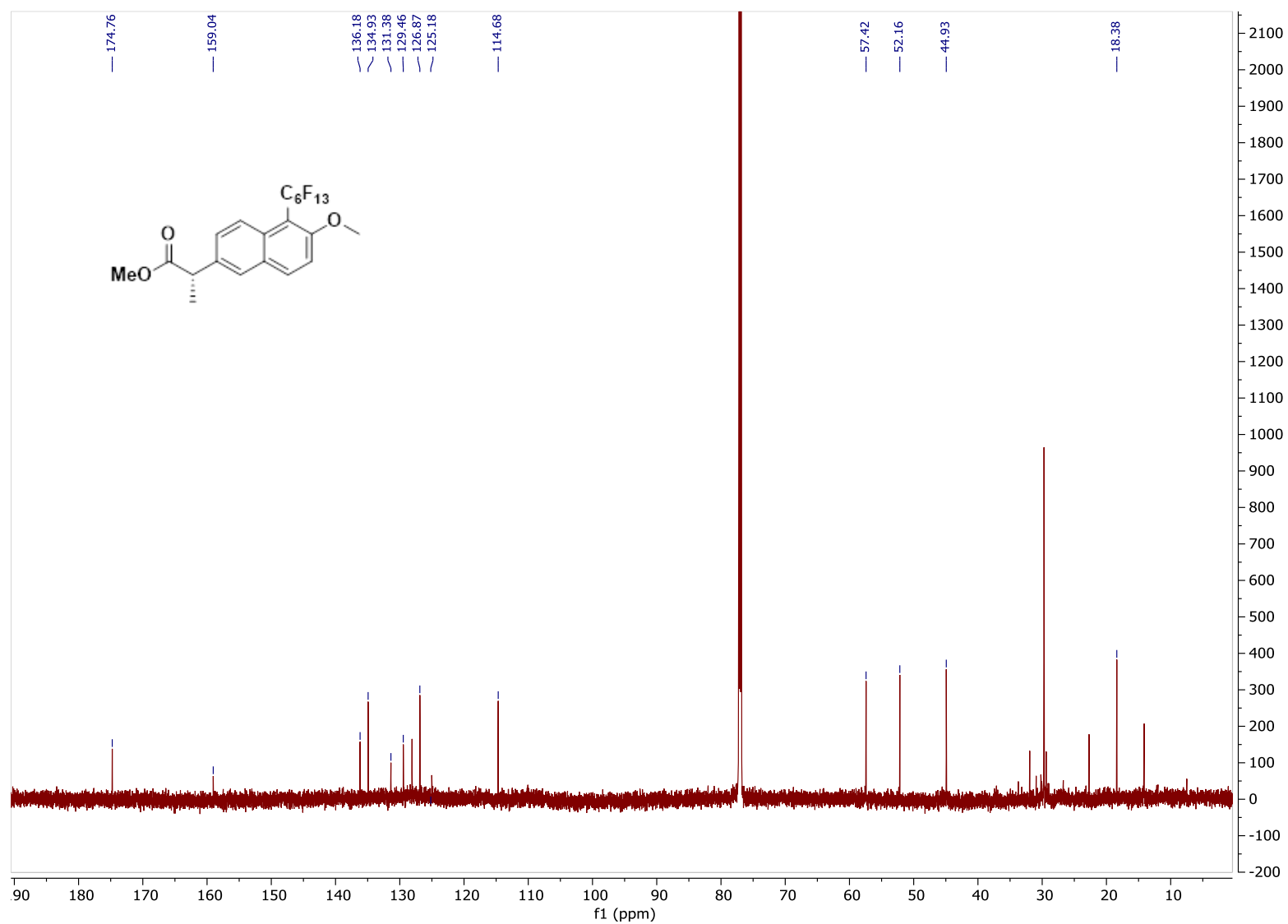
^{19}F NMR of **13b**, CDCl_3 , 471 MHz



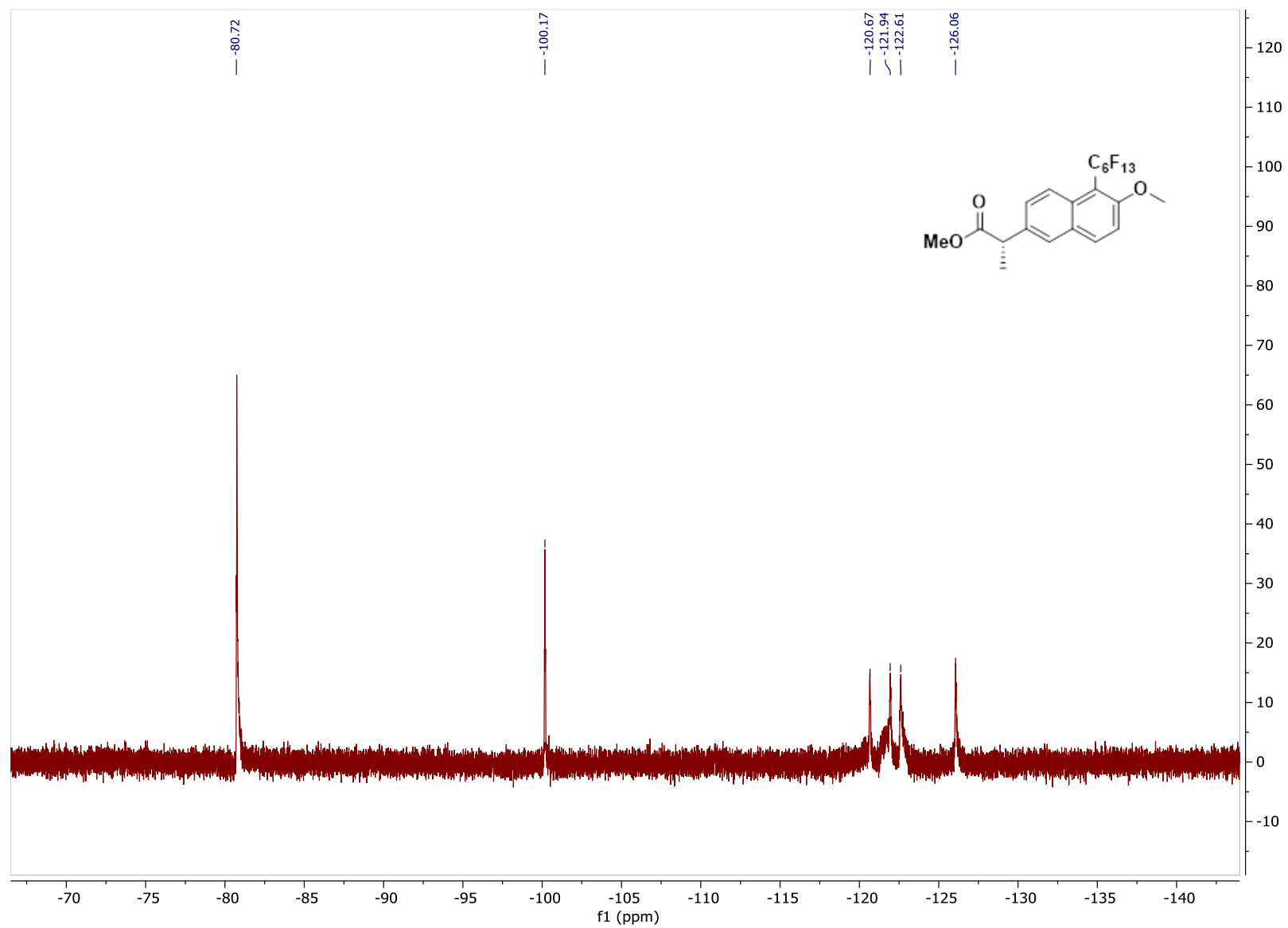
^1H - ^{19}F HMBC of **13b**

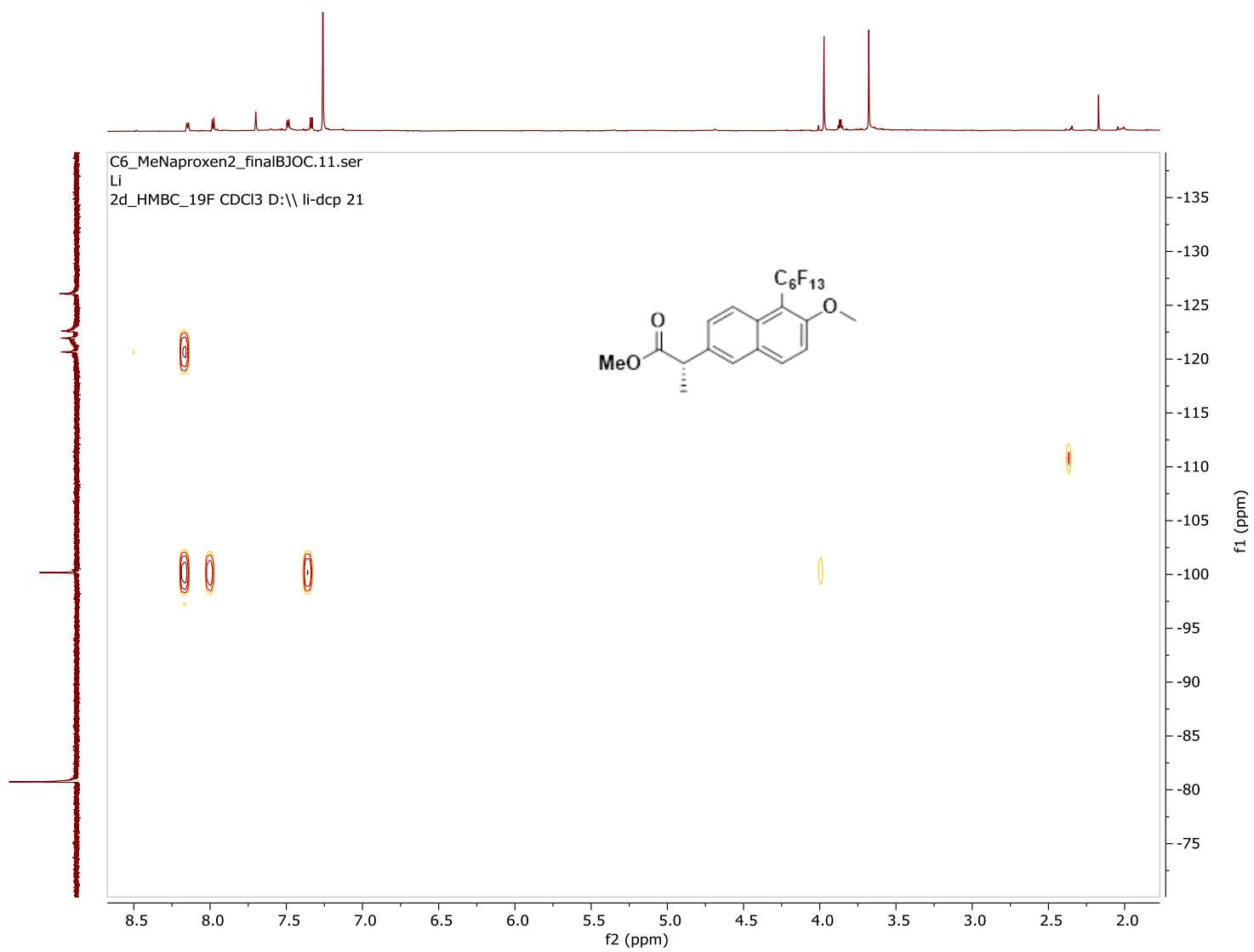
^1H NMR of **14b**, CDCl_3 , 500 MHz



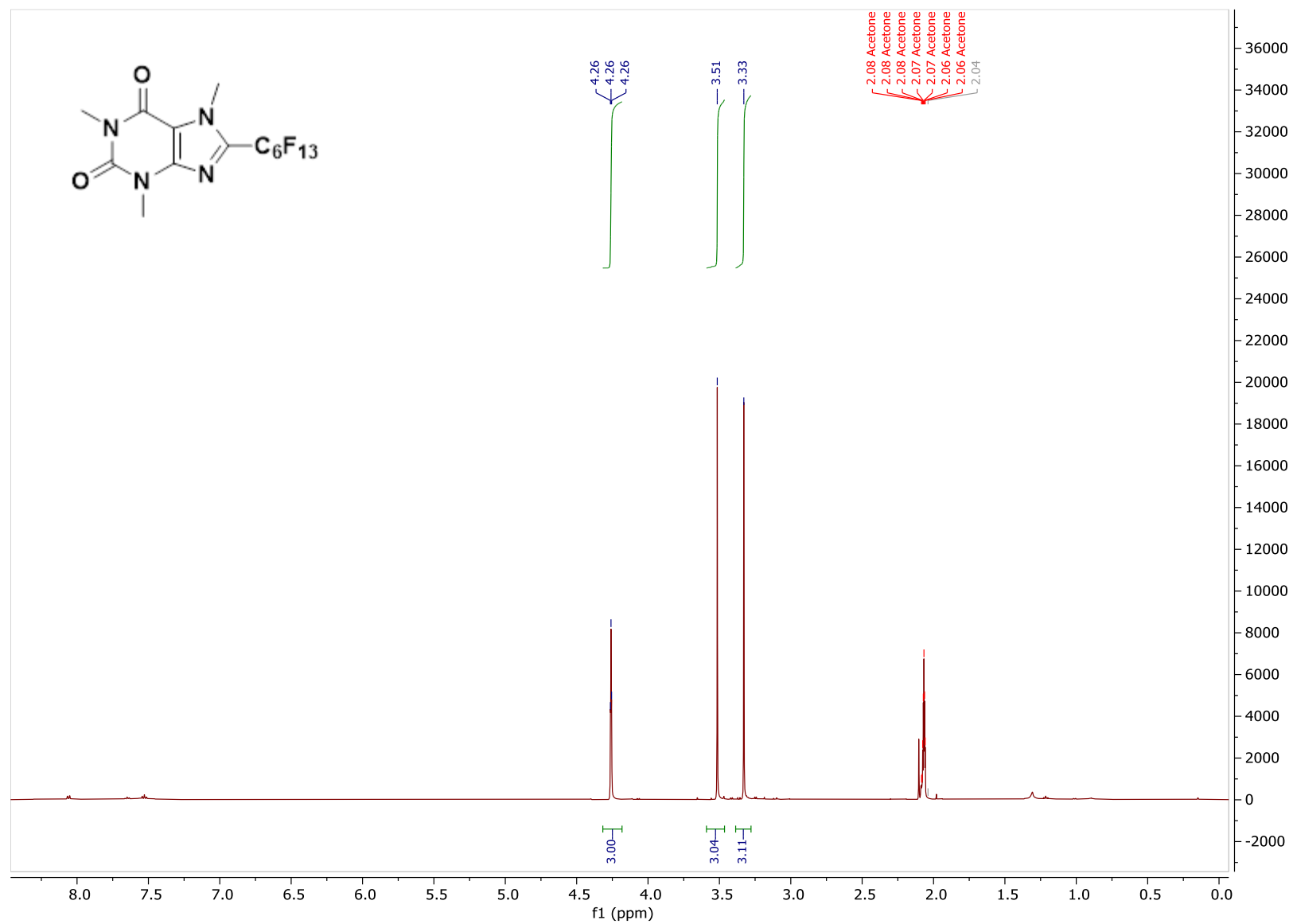
^{13}C NMR of **14b**, CDCl_3 , 126 MHz

^{19}F NMR of **14b**, CDCl_3 , 471 MHz

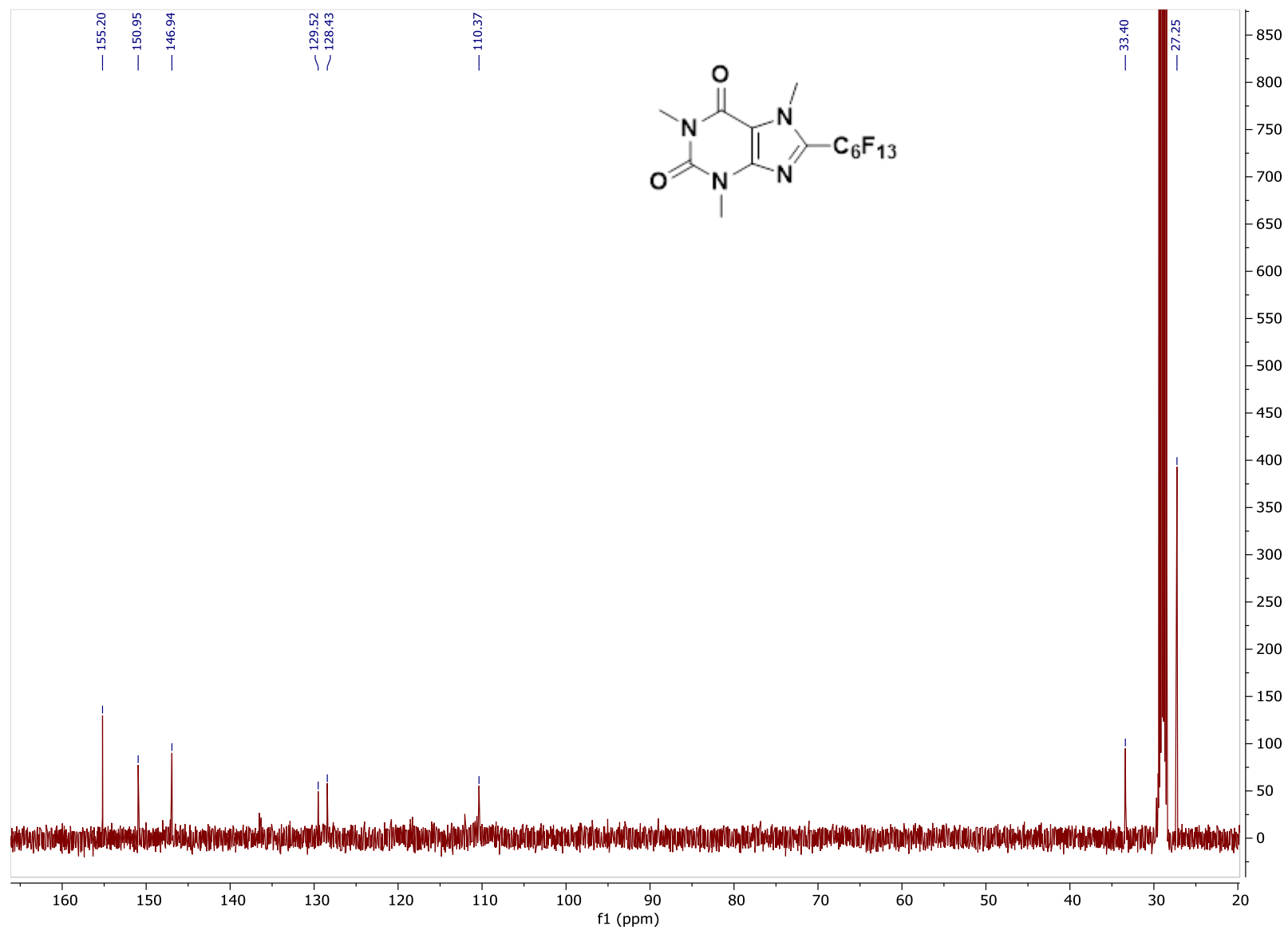


^1H - ^{19}F HMBC of **14b**

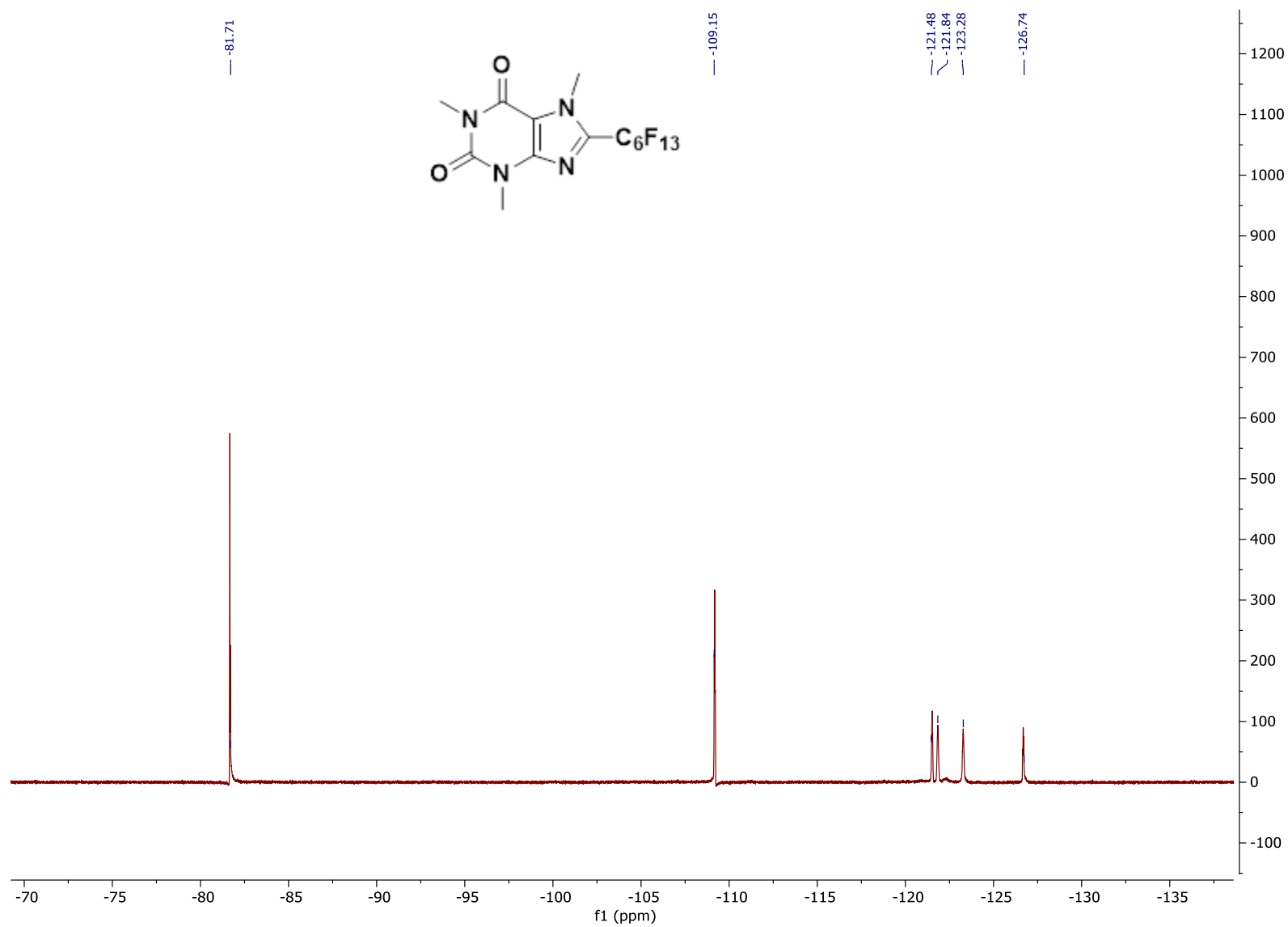
^1H NMR of **15b**, acetone- d_6 , 500 MHz



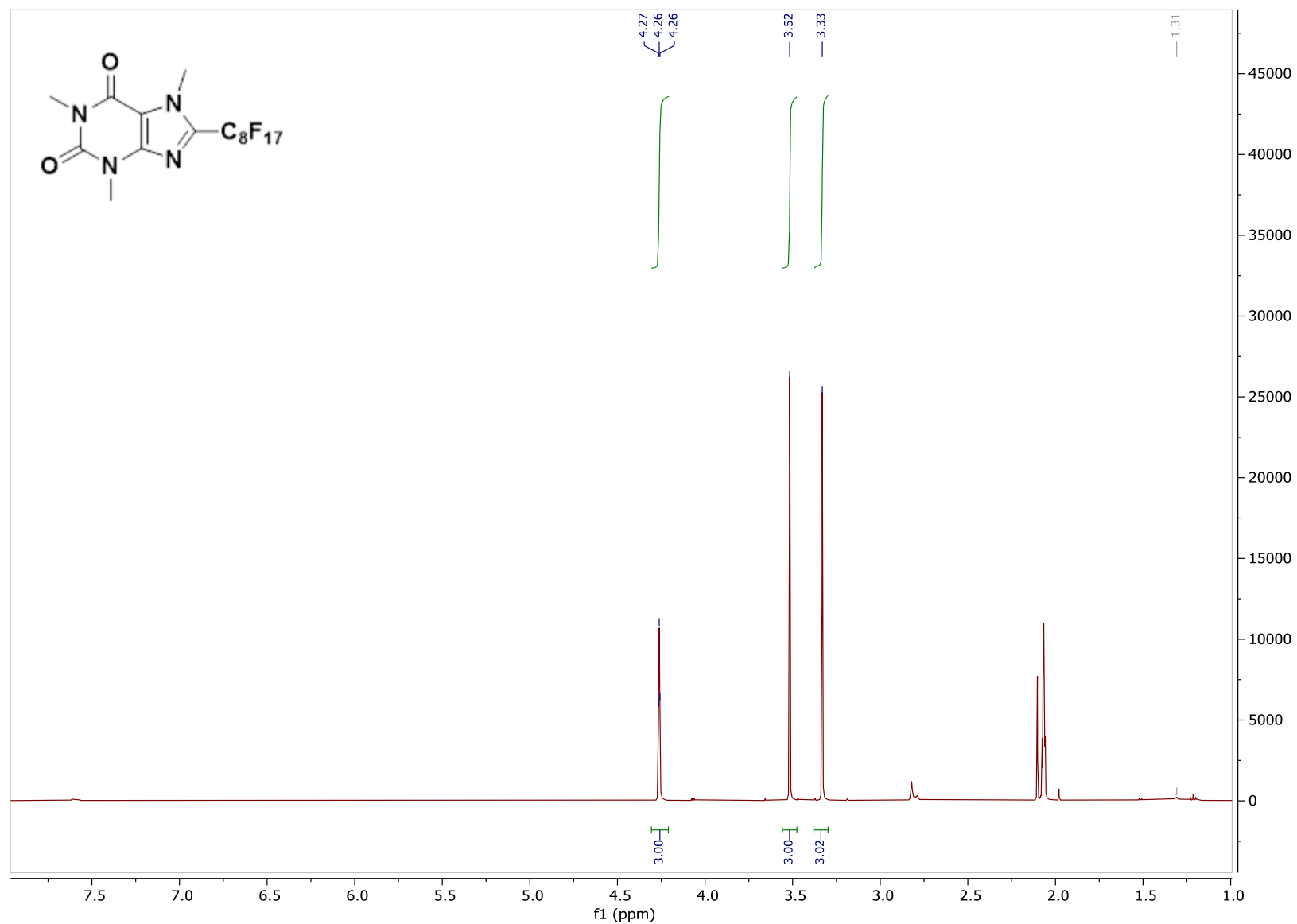
^{13}C NMR of **15b**, acetone- d_6 , 126 MHz



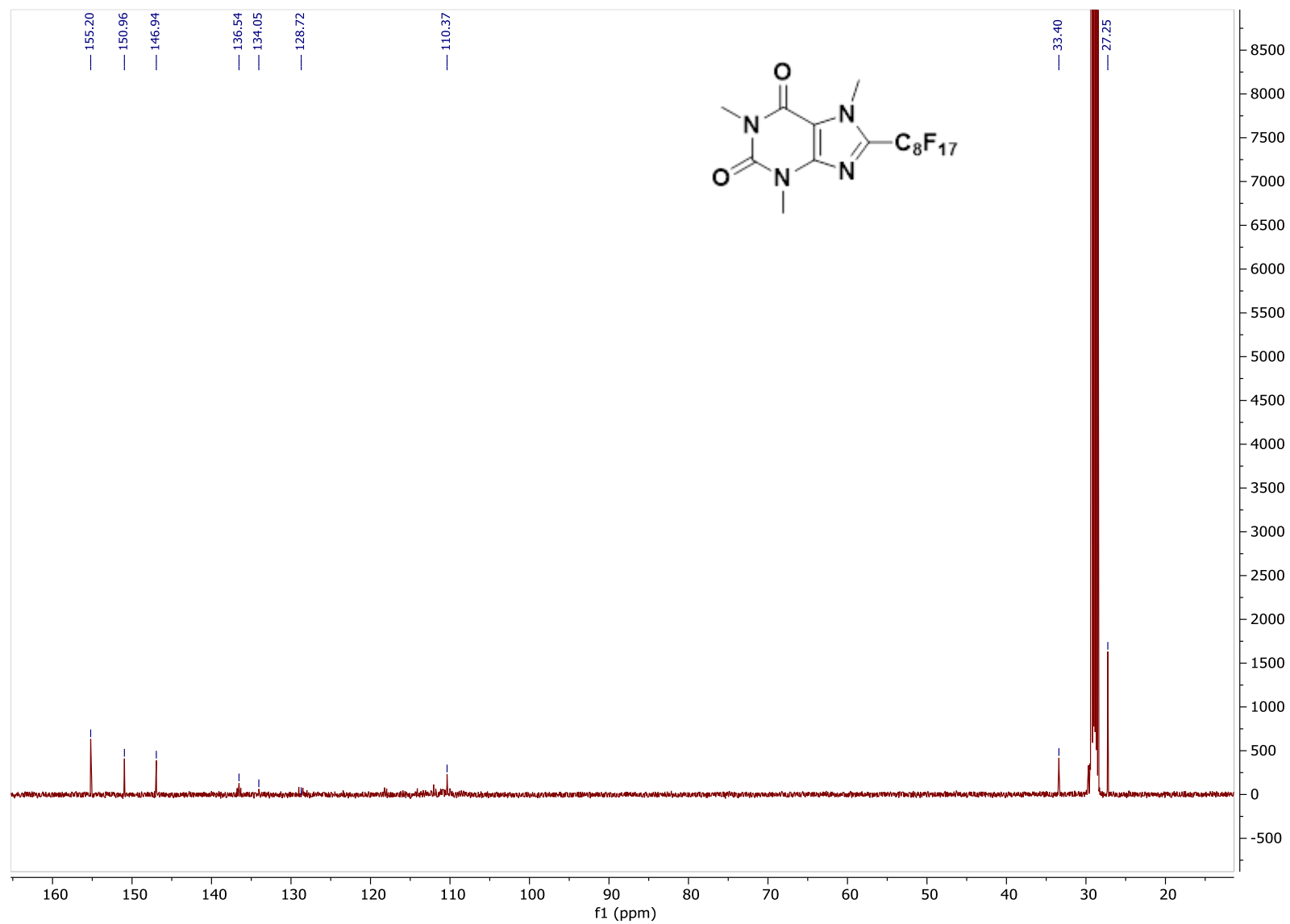
^{19}F NMR of **15b**, acetone- d_6 , 471 MHz



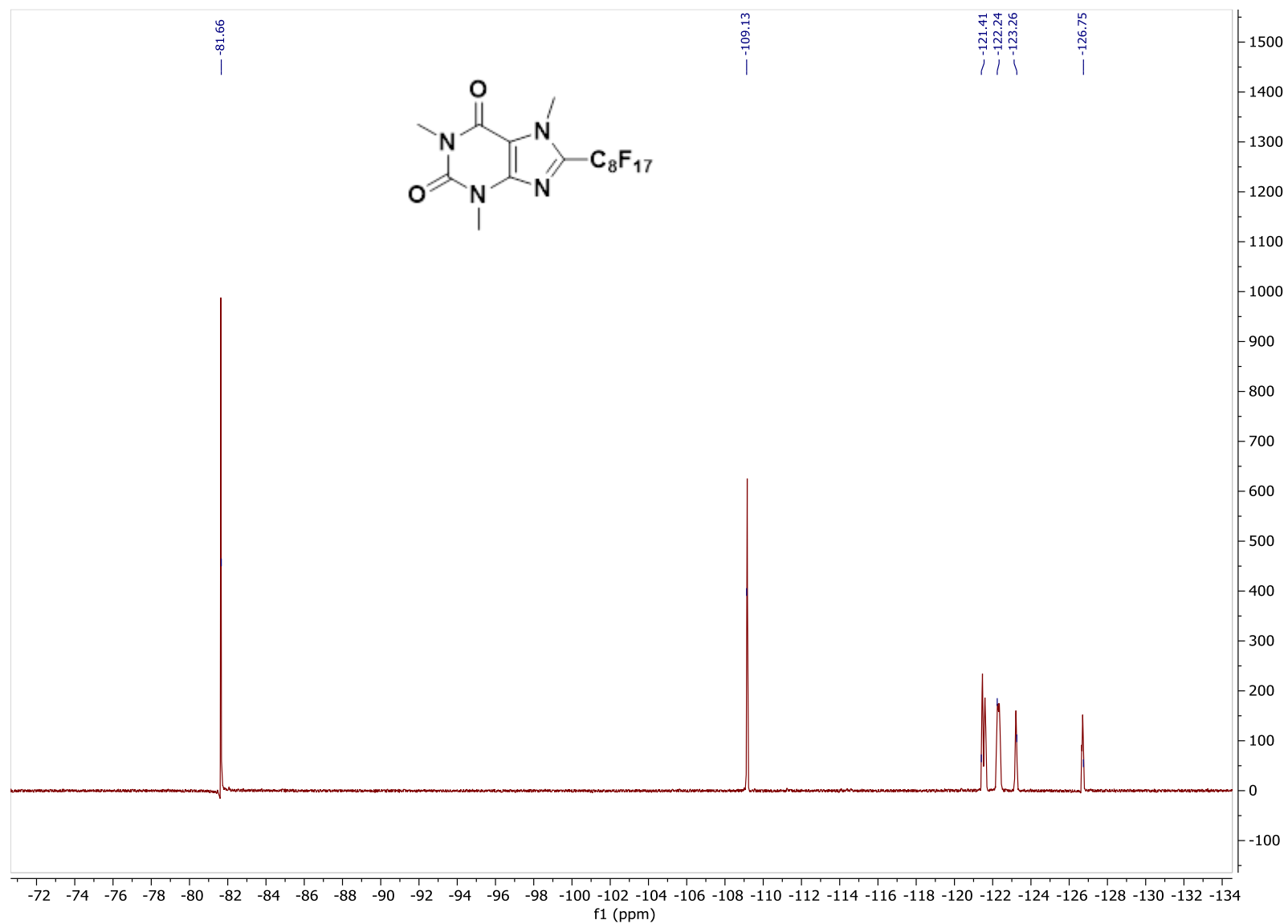
^1H NMR of **15c**, acetone- d_6 , 500 MHz

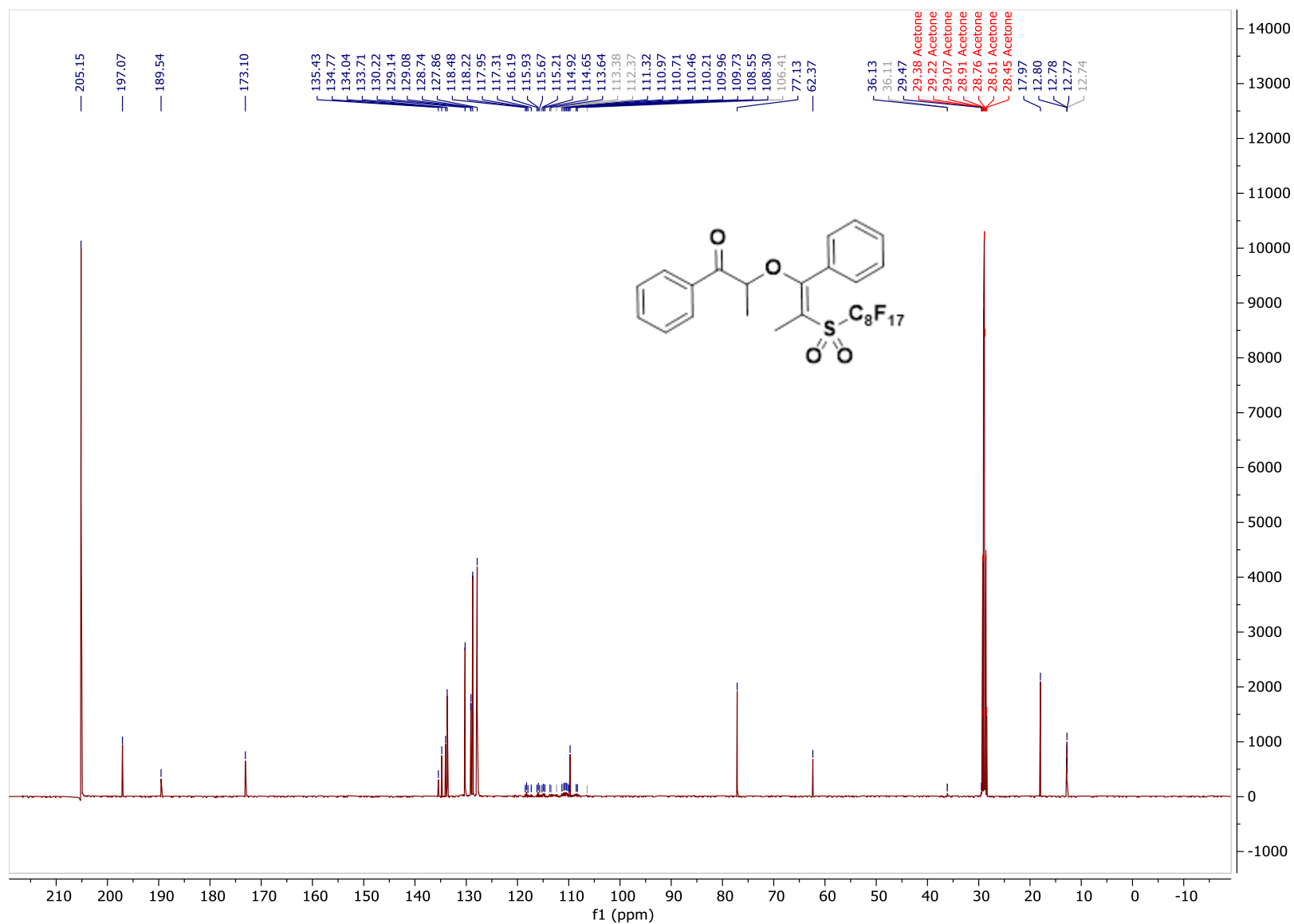


^{13}C NMR of **15c**, acetone- d_6 , 126 MHz

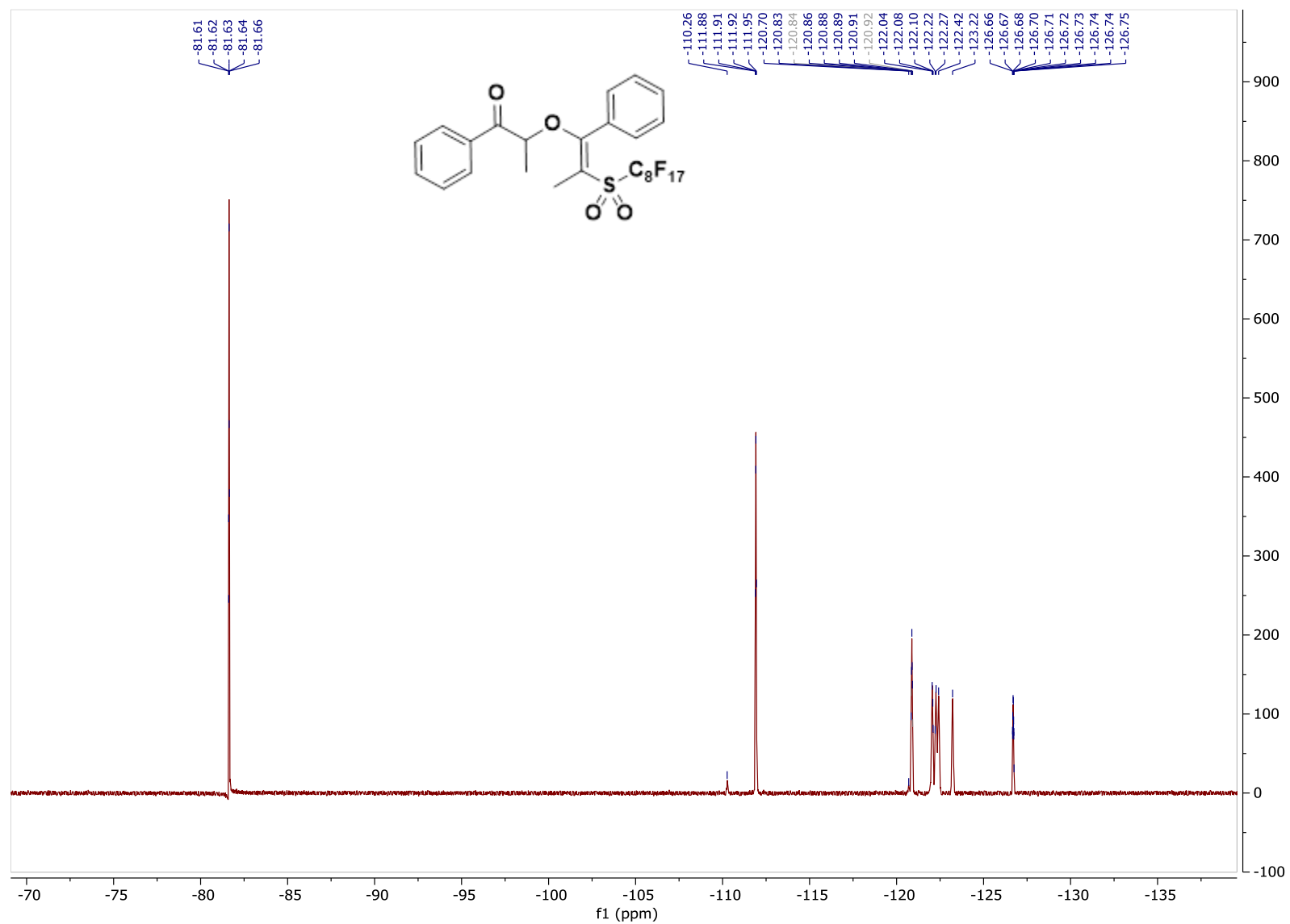


^{19}F NMR of **15c**, acetone- d_6 , 471 MHz

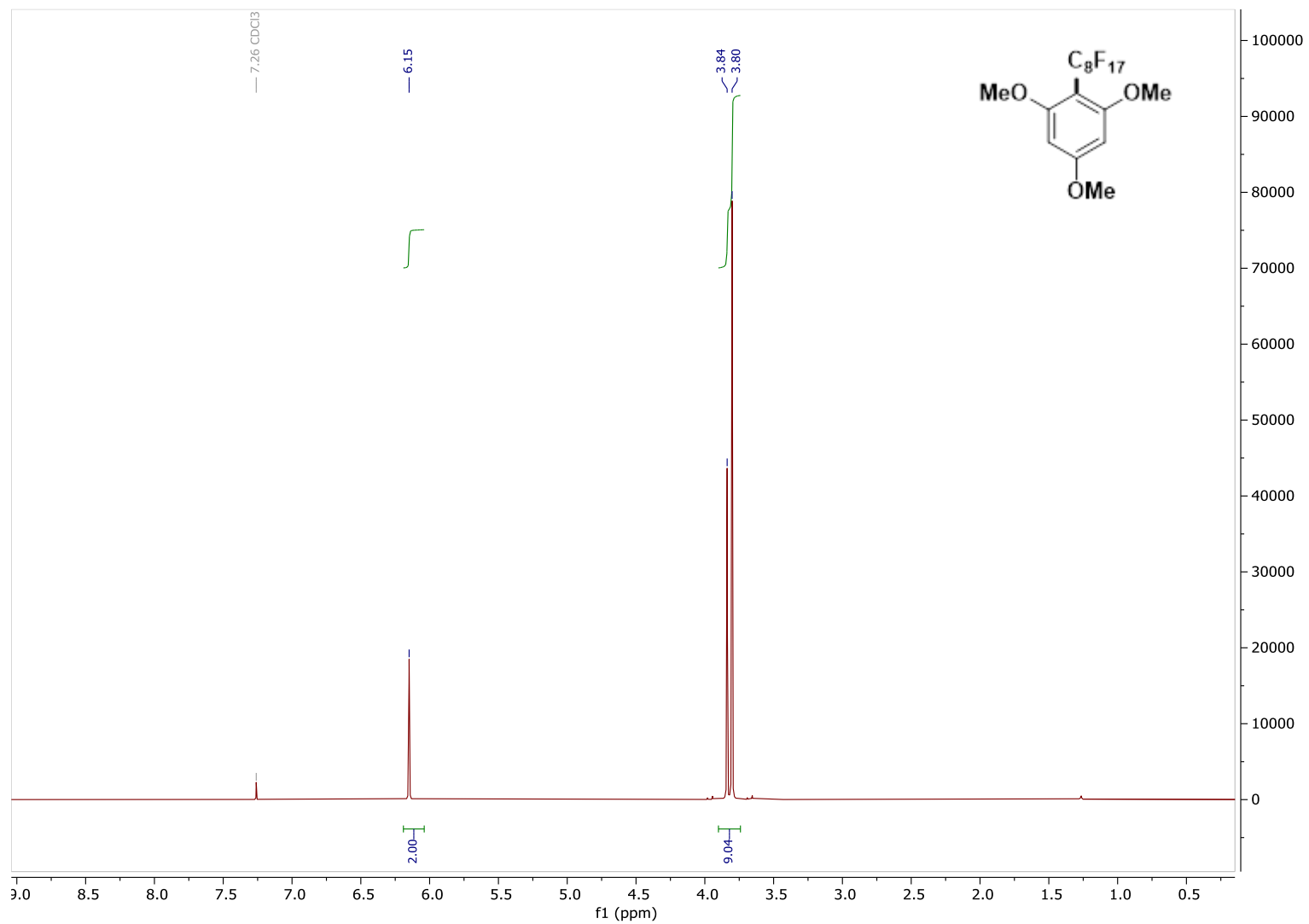


^{13}C NMR of **byproduct B** (perfluorooctyl analogue), acetone- d_6 , 126 MHz

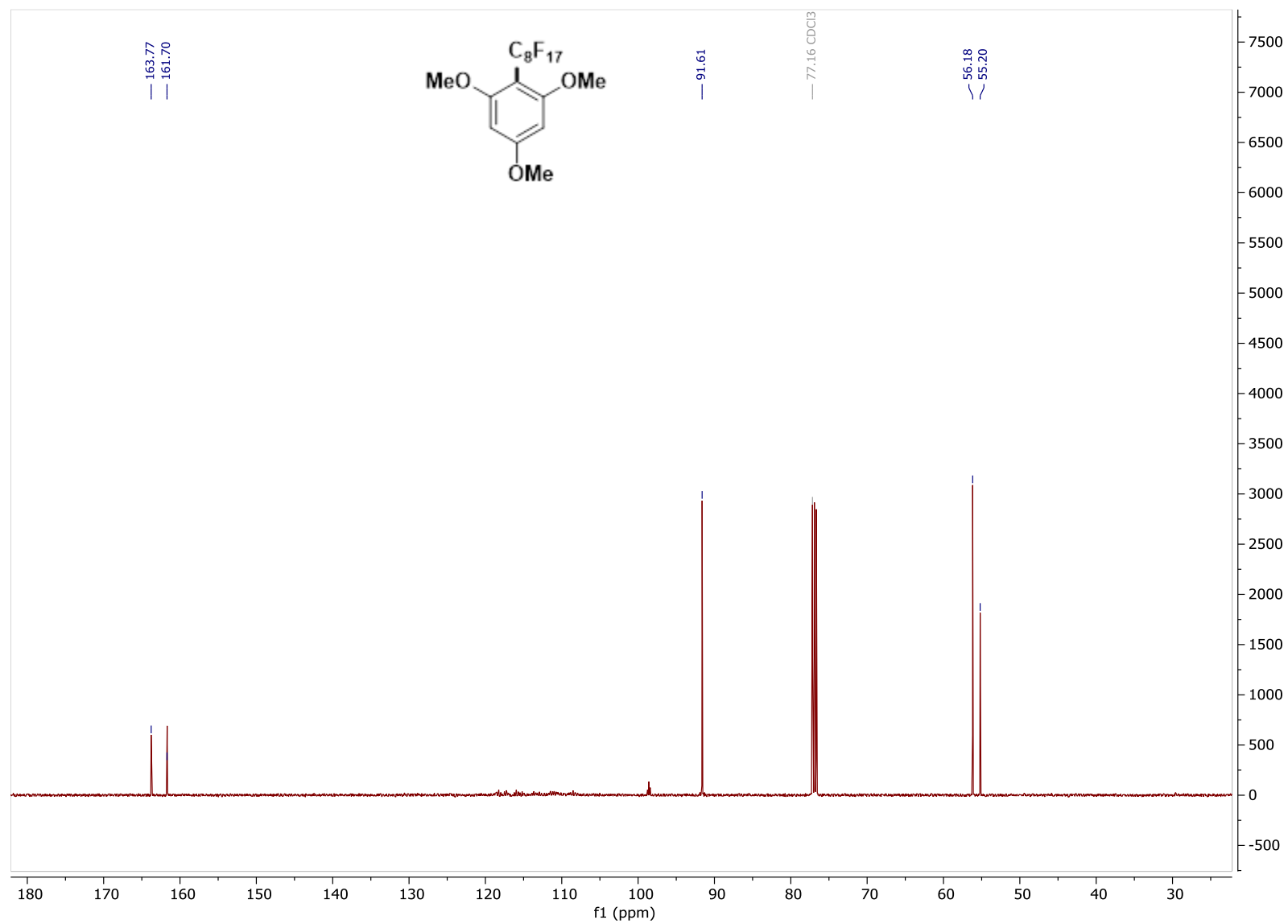
^{19}F NMR of **byproduct B** (perfluorooctyl analogue), acetone- d_6 , 471 MHz



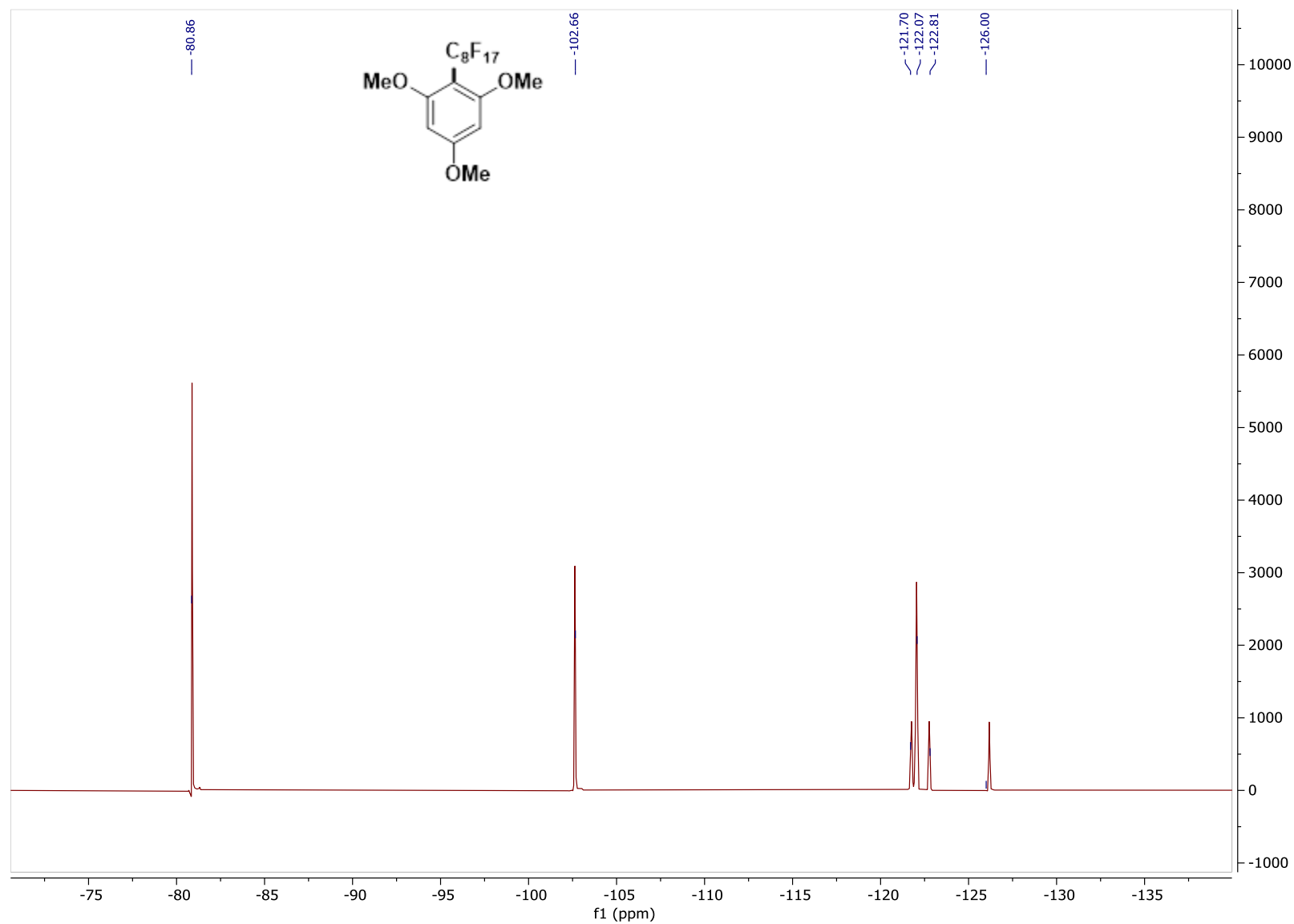
Characterization data for Chapter 3

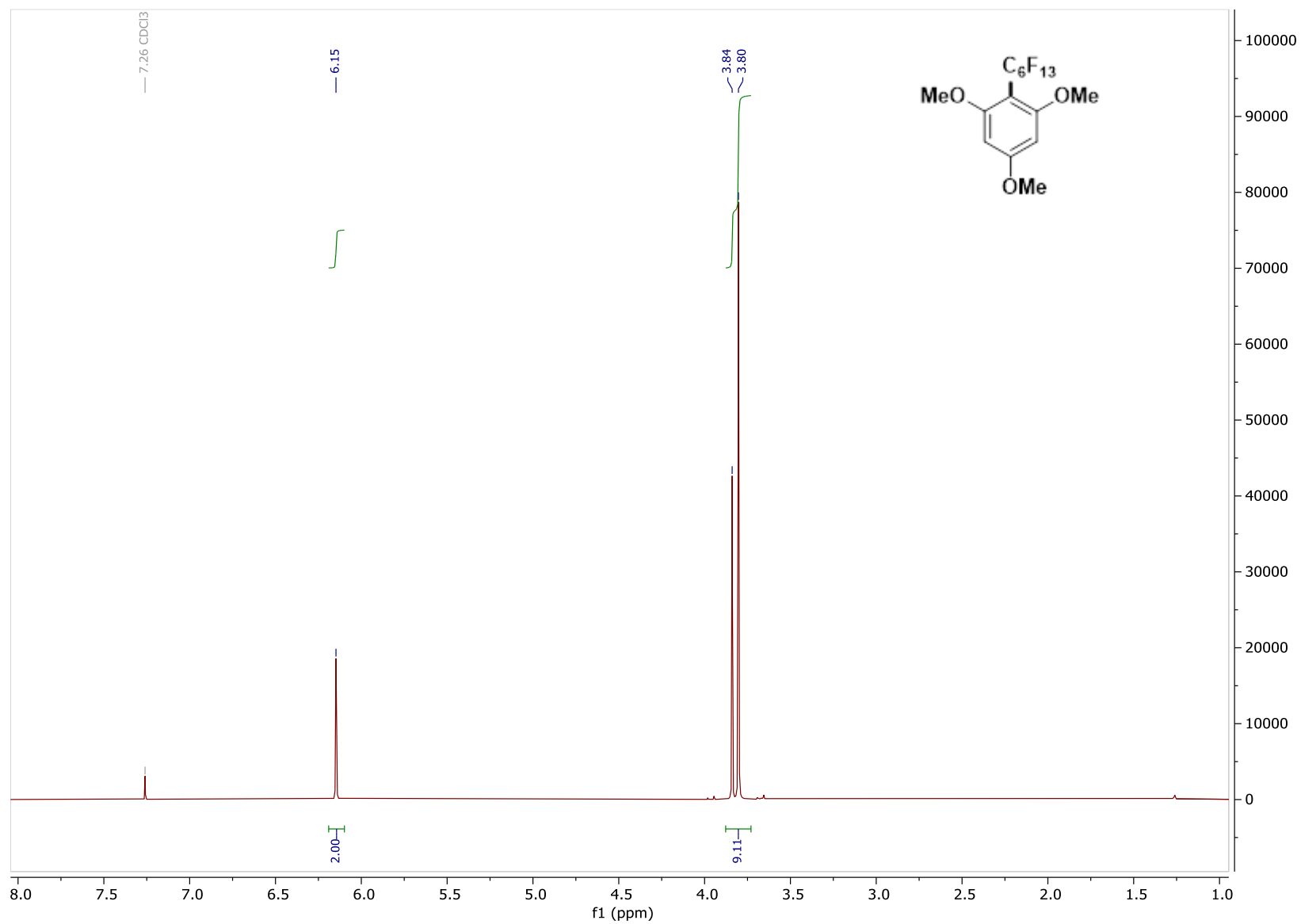
 ^1H NMR of PF1, CDCl_3 , 500 MHz

^{13}C NMR of **PF1**, CDCl_3 , 126 MHz

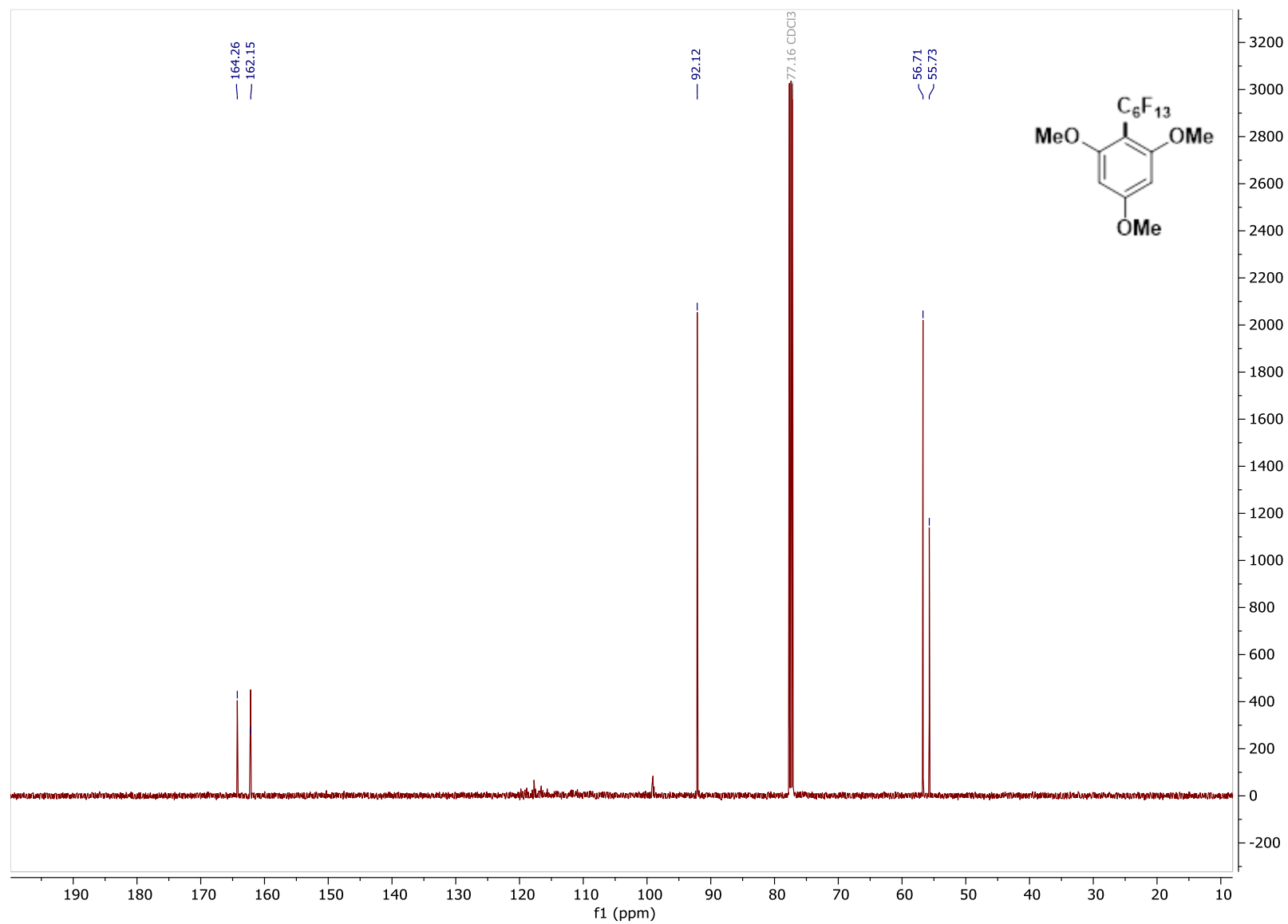


^{19}F NMR of **PF1**, CDCl_3 , 471 MHz

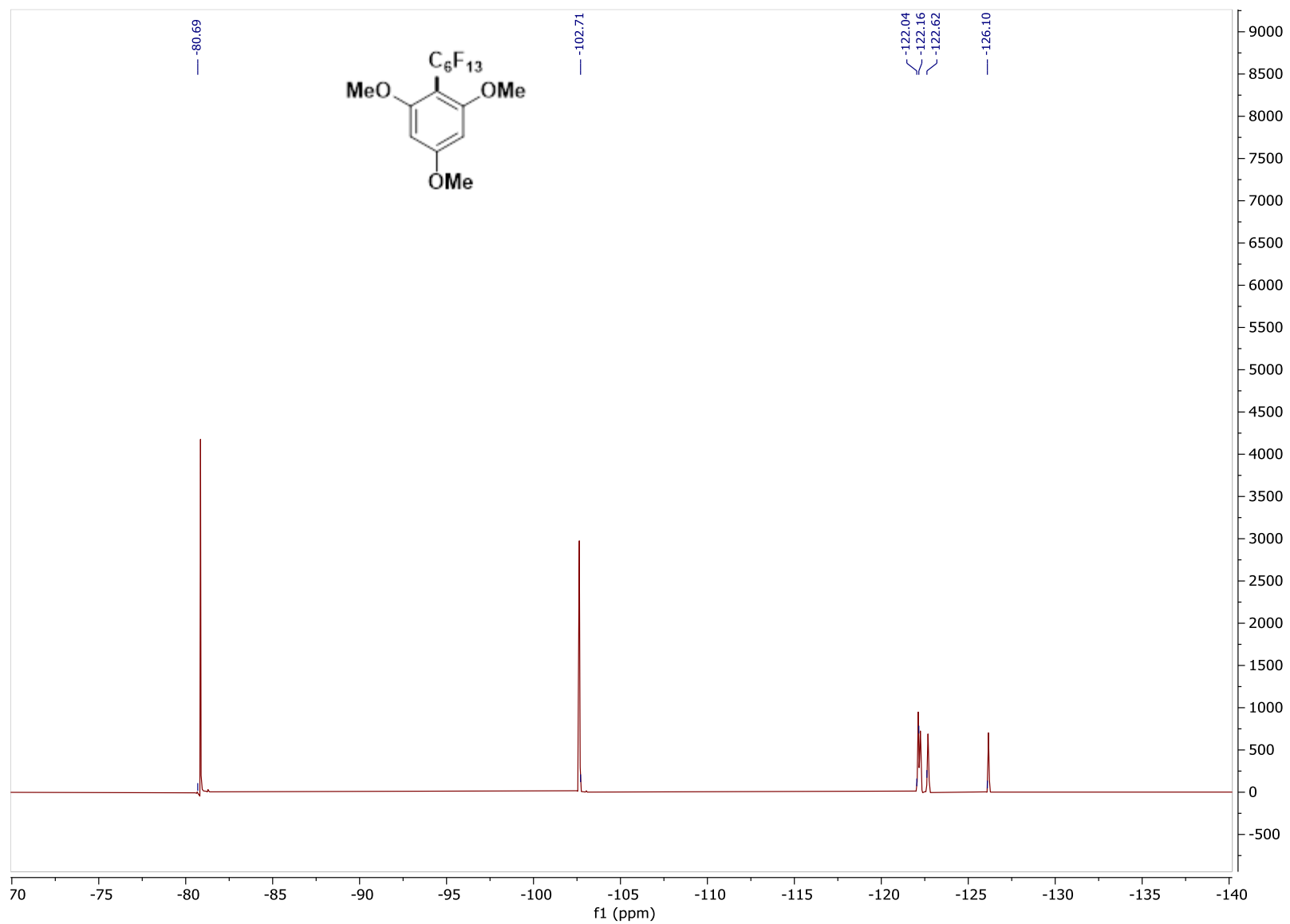


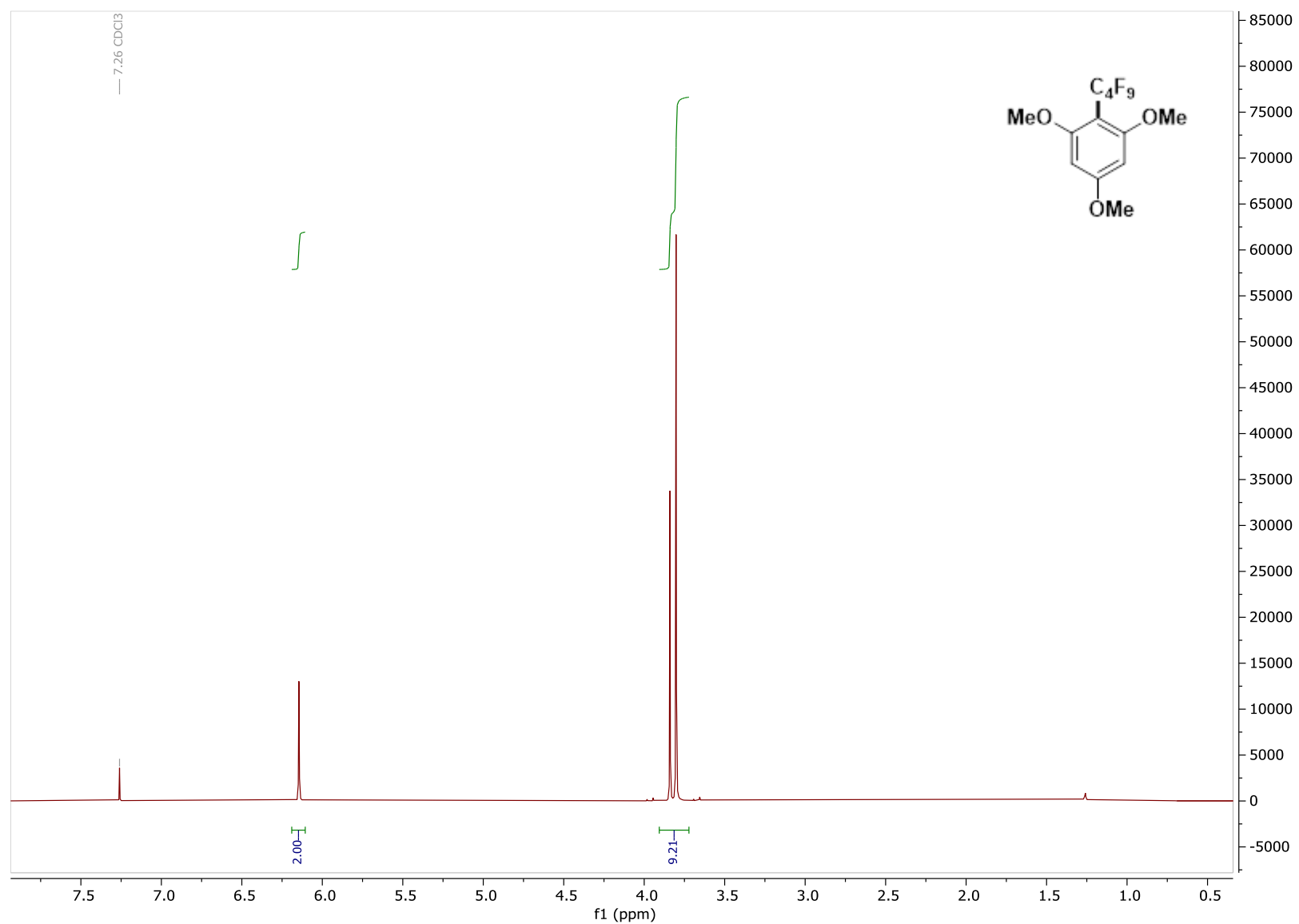
^1H NMR of **PF2**, CDCl_3 , 500 MHz

^{13}C NMR of **PF2**, CDCl_3 , 126 MHz

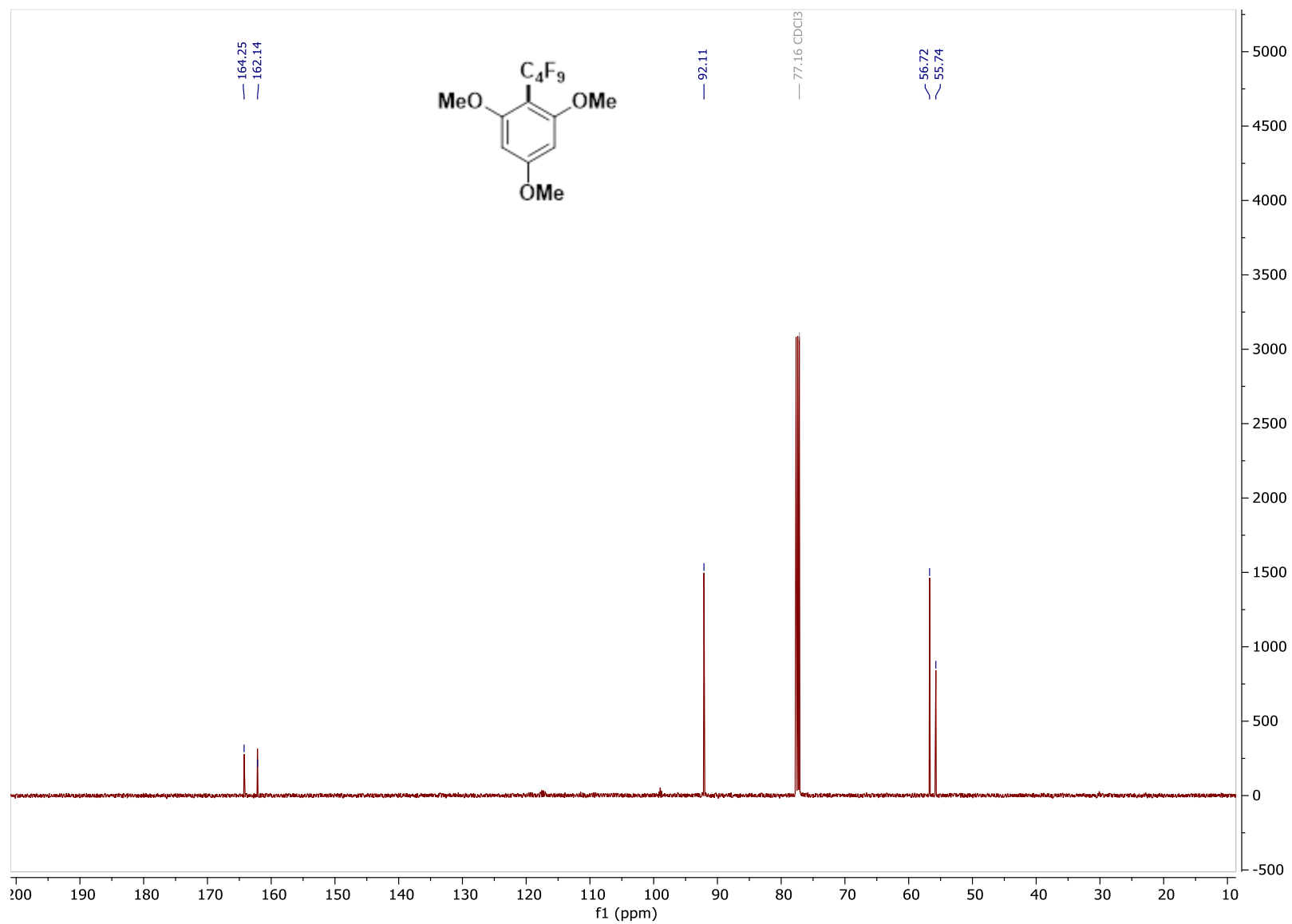


^{19}F NMR of **PF2**, CDCl_3 , 471 MHz

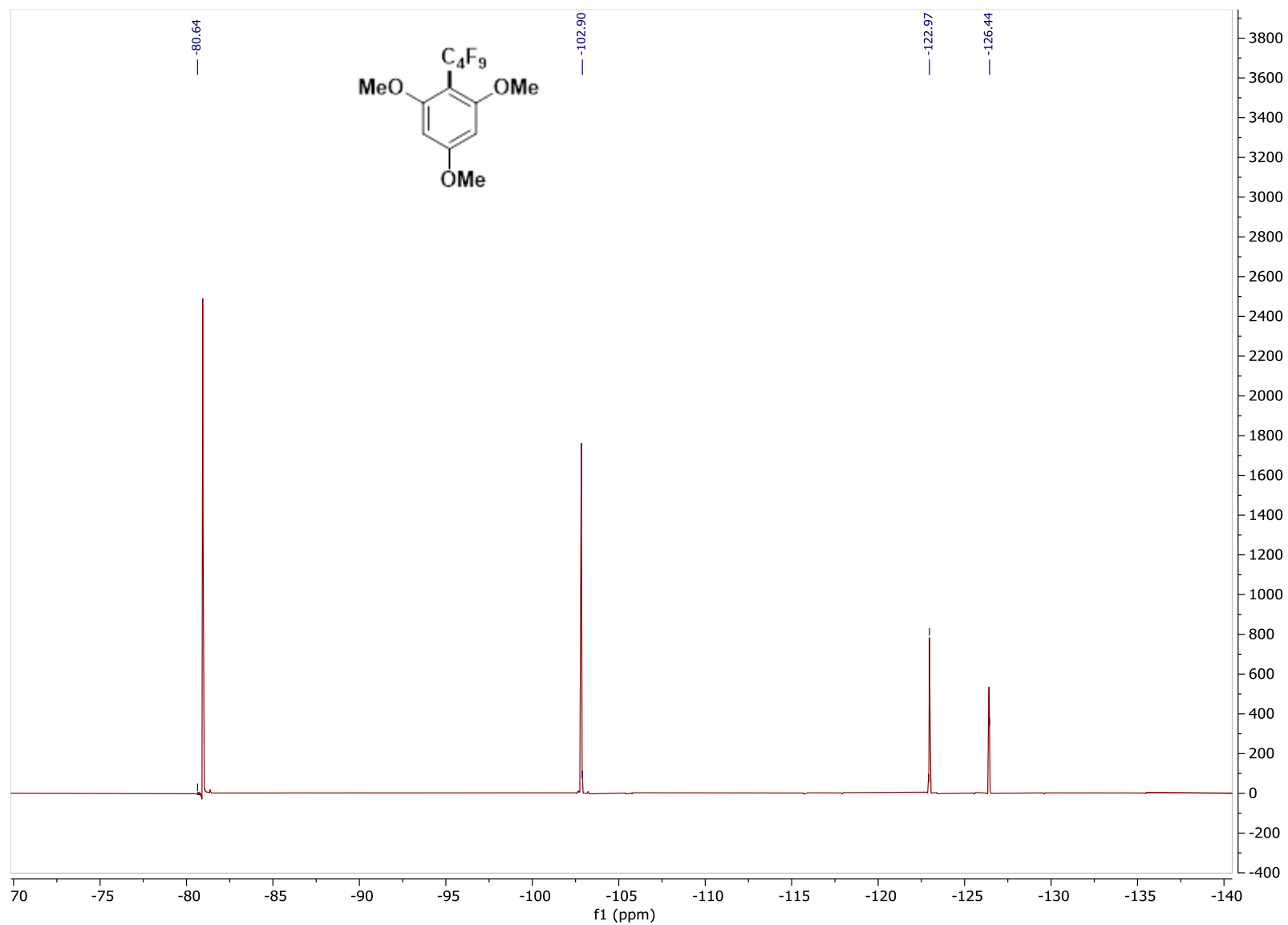


^1H NMR of **PF3**, CDCl_3 , 500 MHz

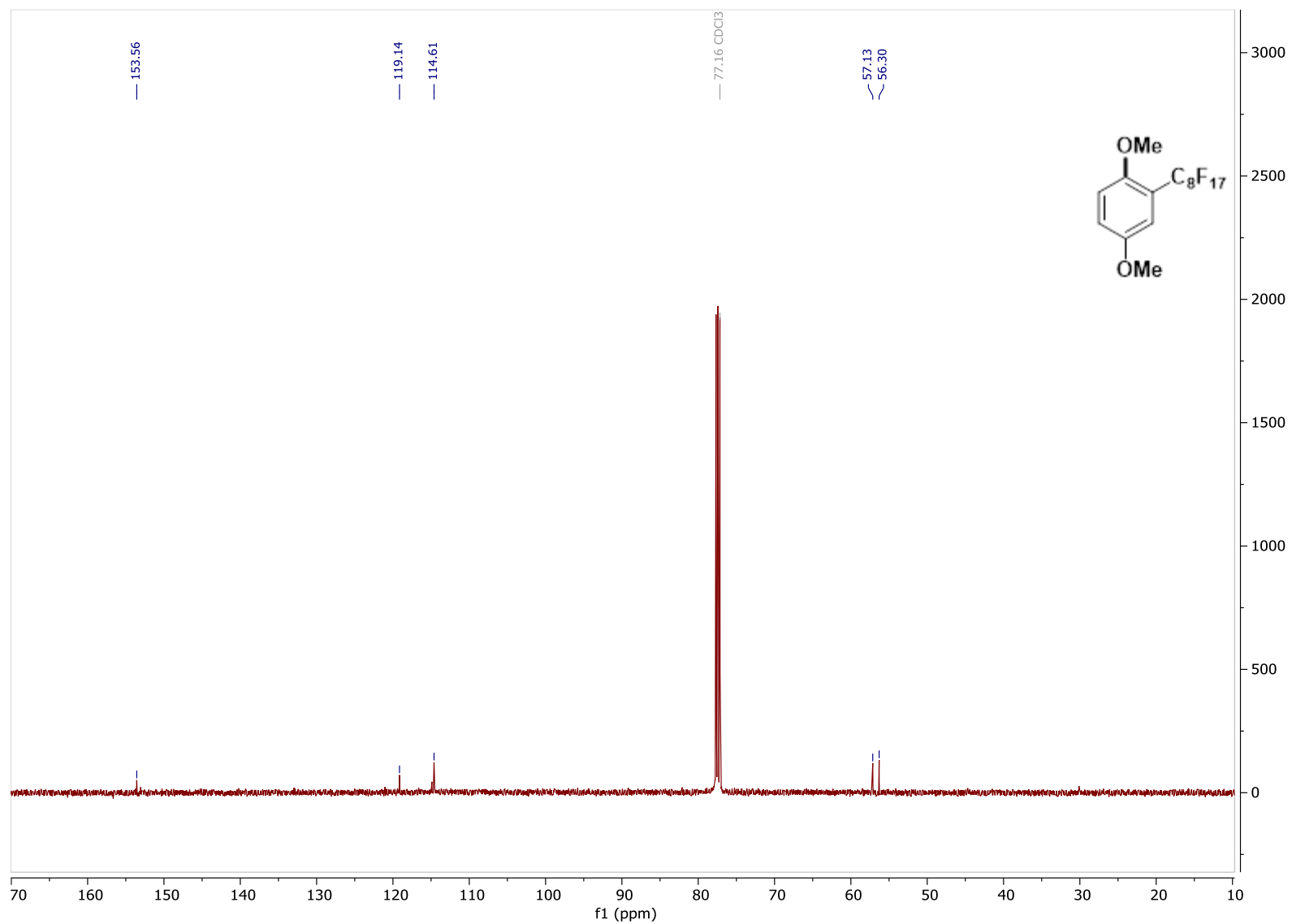
^{13}C NMR of **PF3**, CDCl_3 , 126 MHz



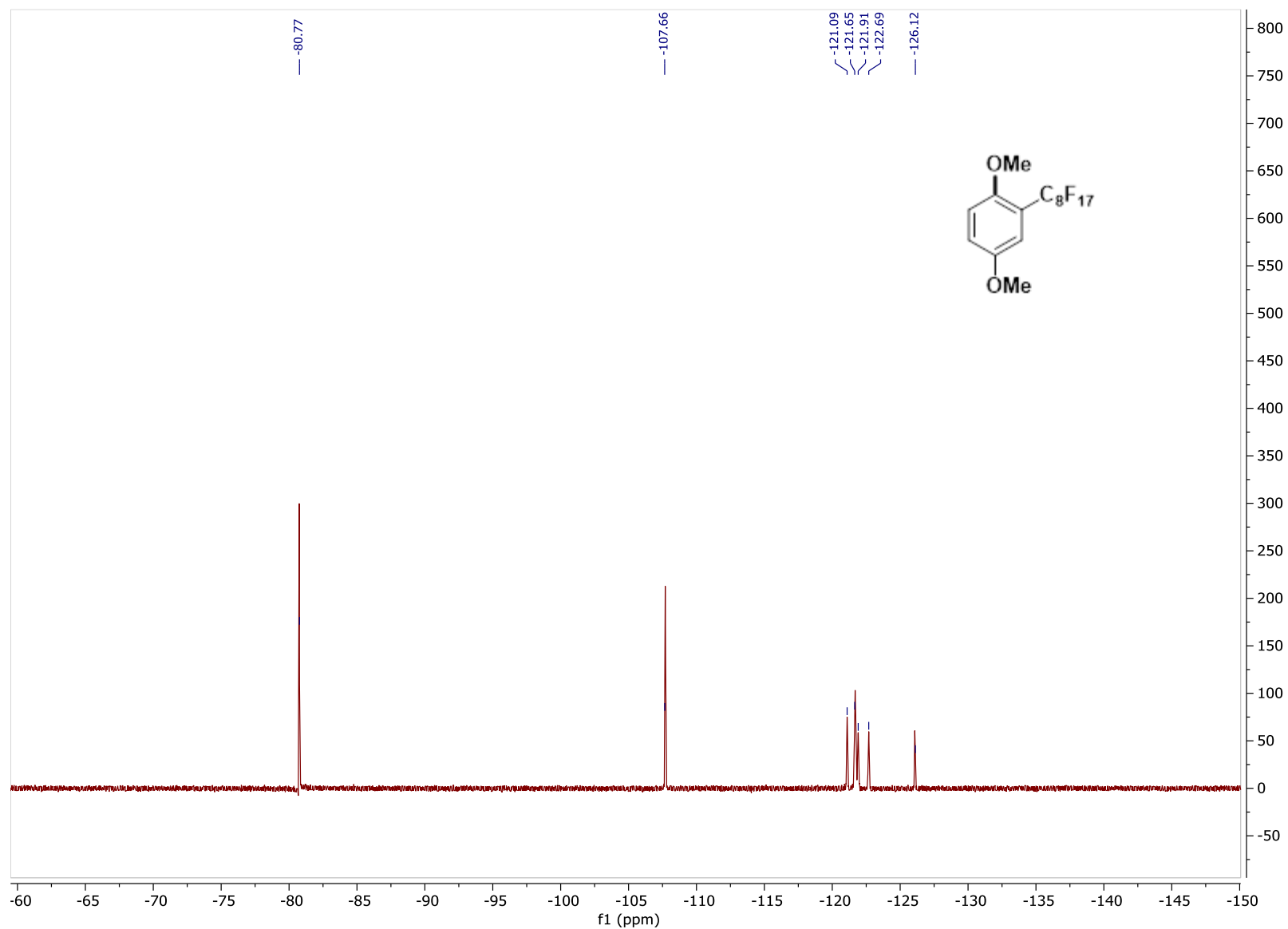
^{19}F NMR of **PF3**, CDCl_3 , 471 MHz

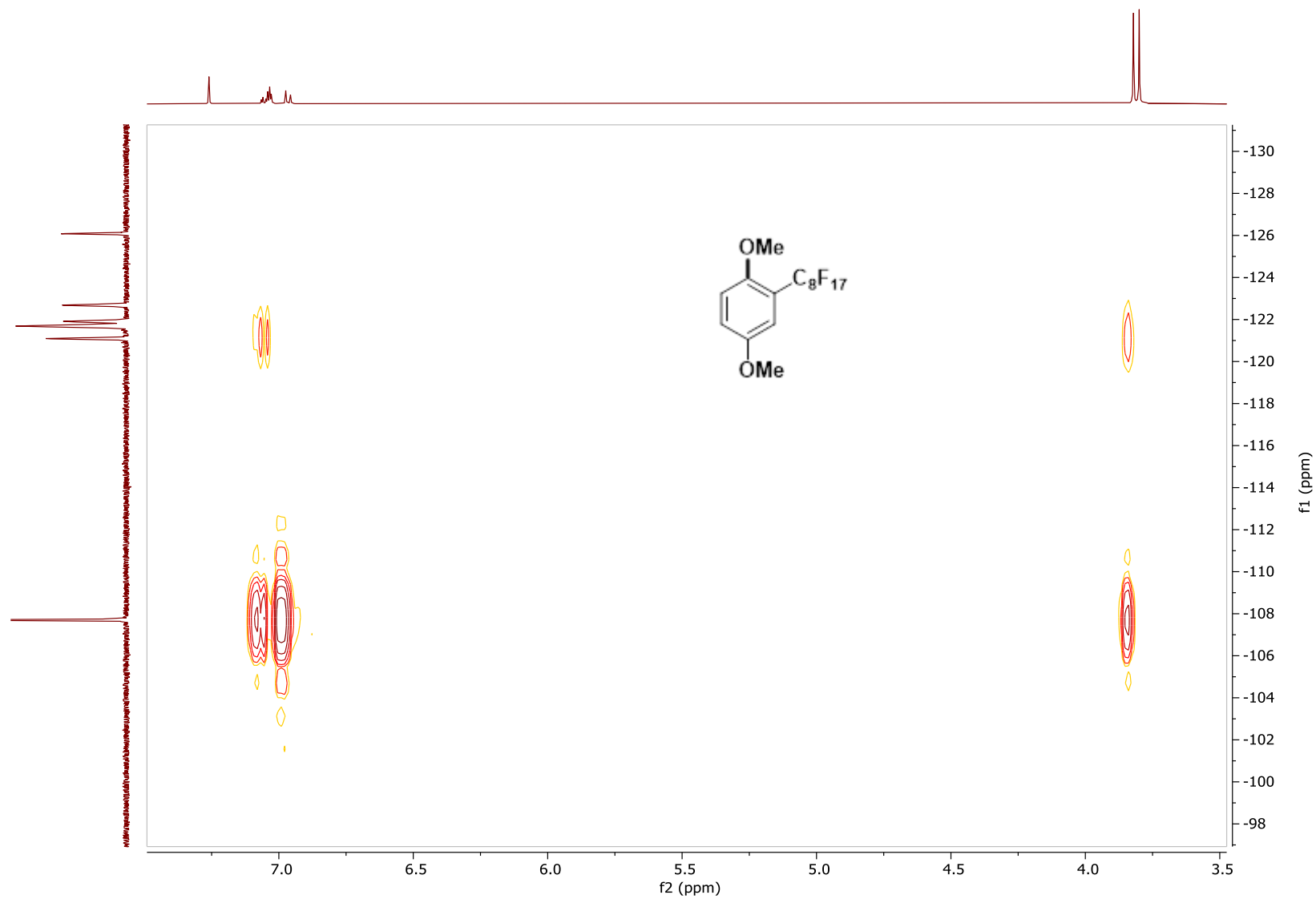


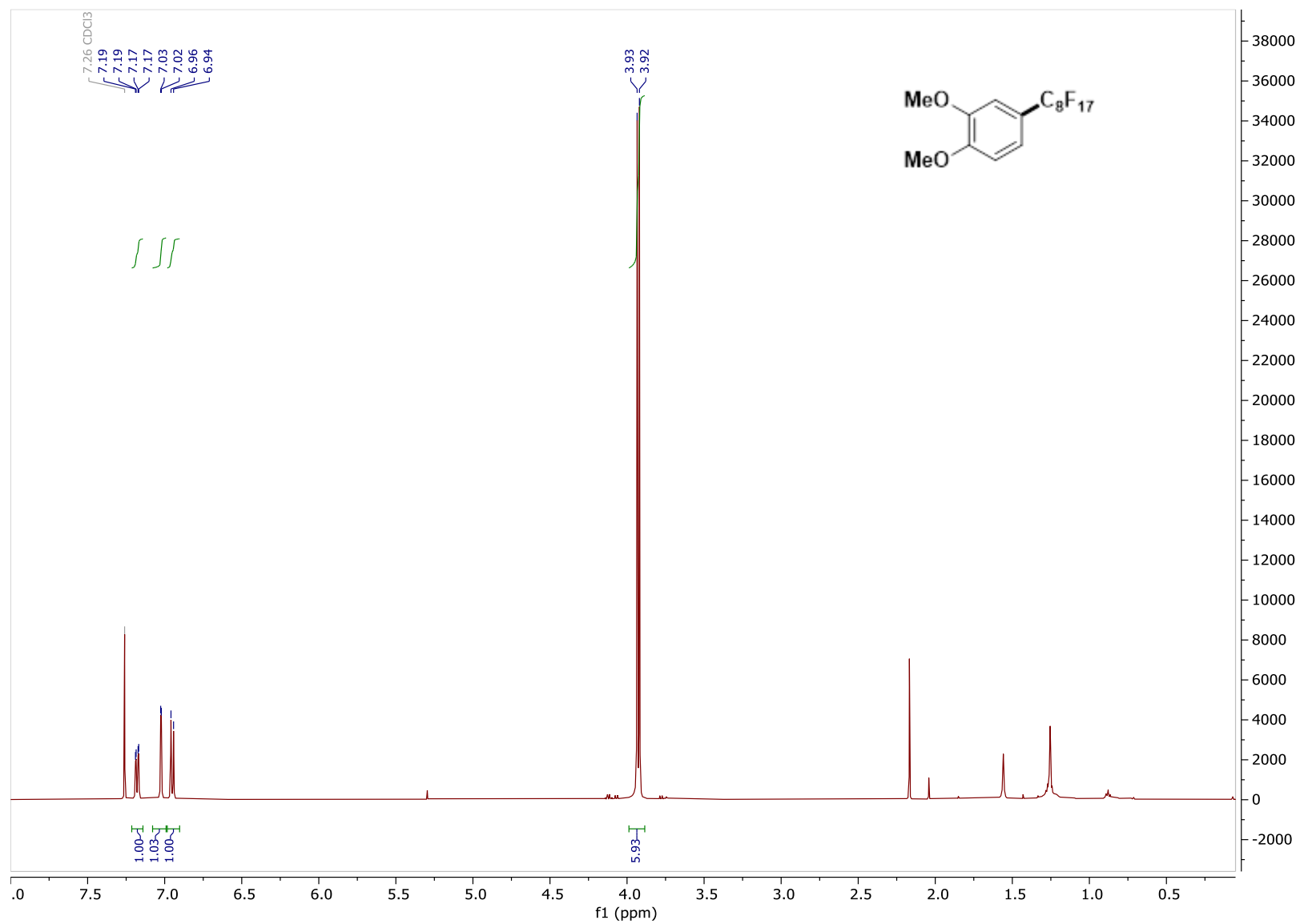
^{13}C NMR of **PF4**, CDCl_3 , 126 MHz



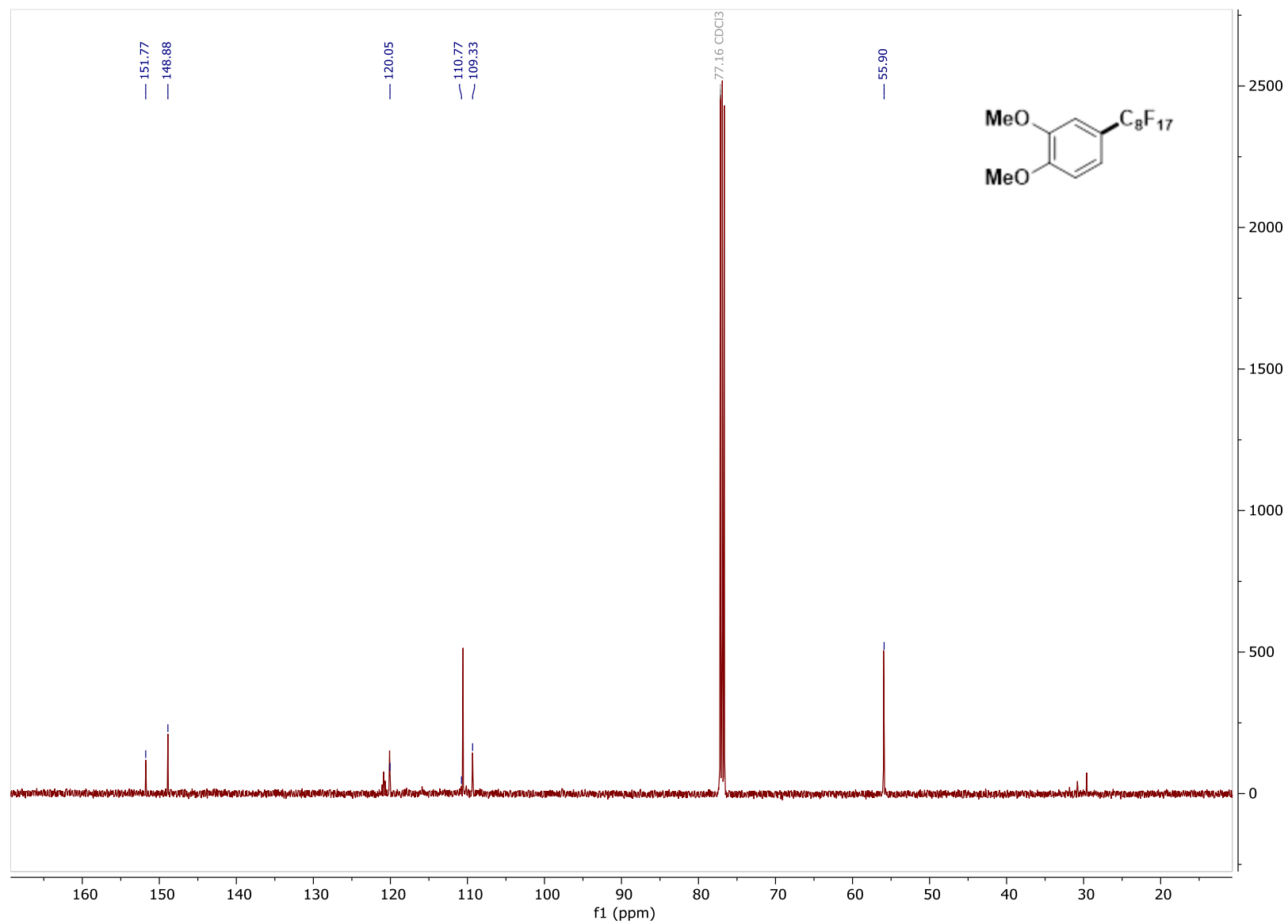
^{19}F NMR of **PF4**, CDCl_3 , 471 MHz



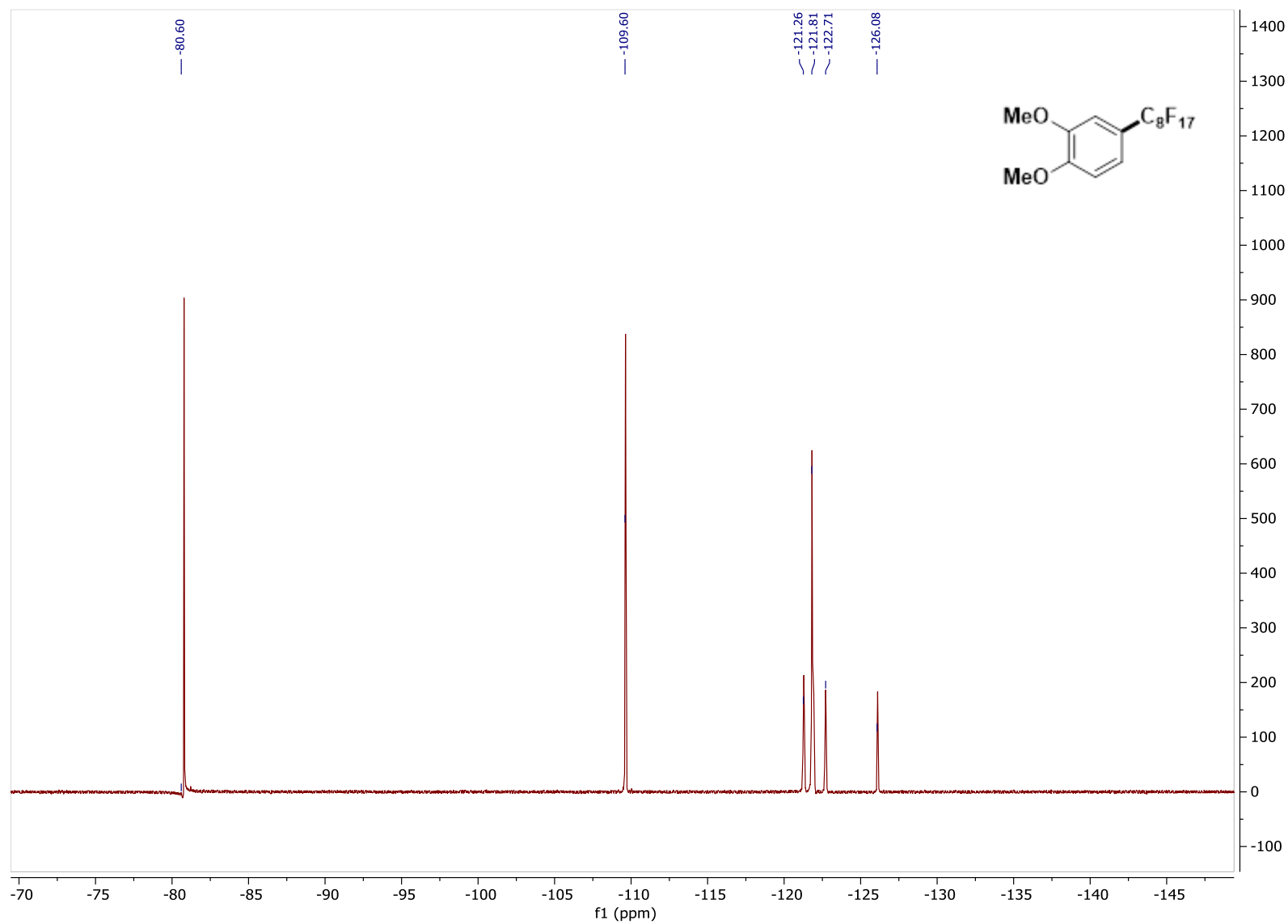
^1H - ^{19}F HMBC of PF4

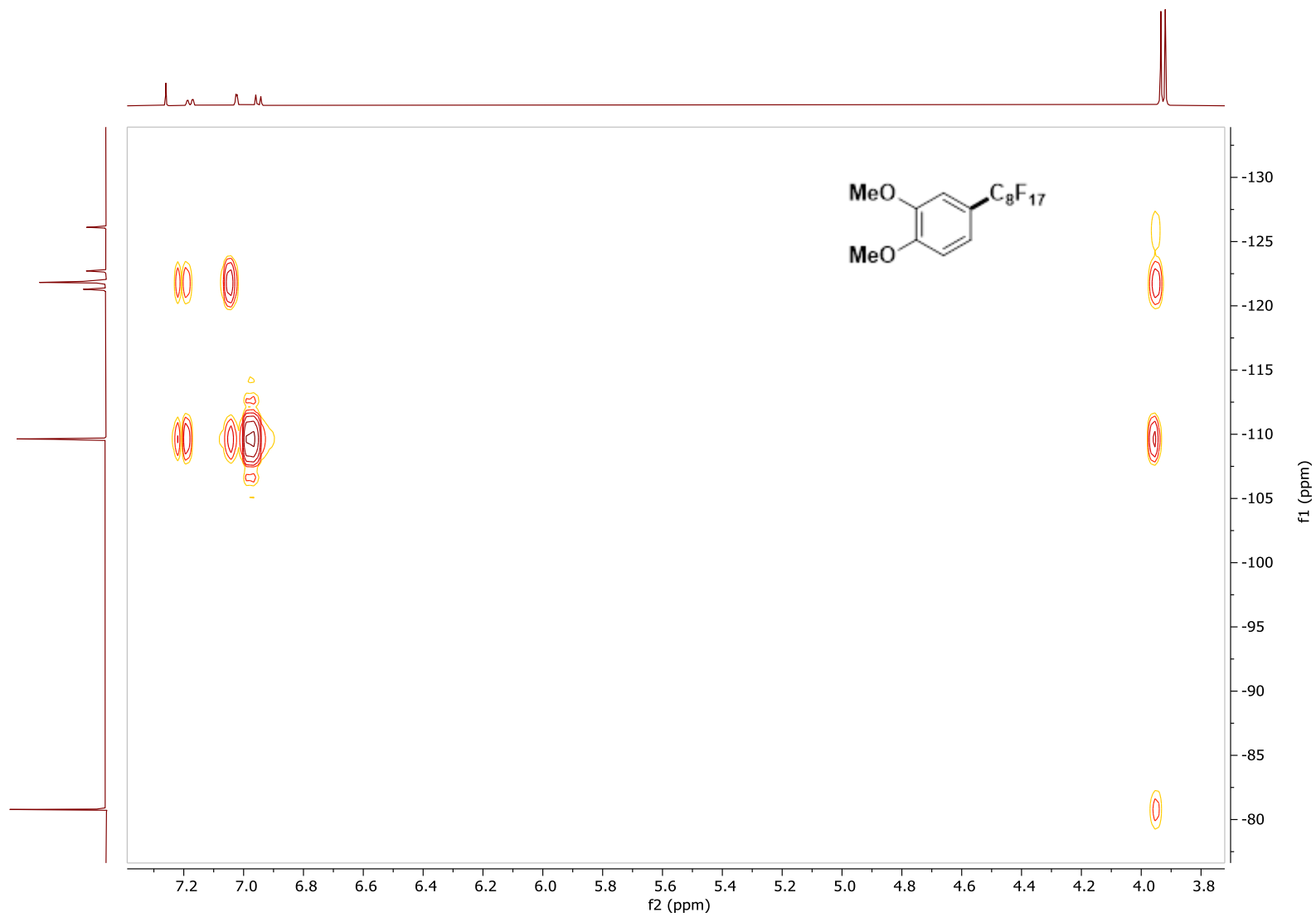
^1H NMR of **5**, CDCl_3 , 500 MHz

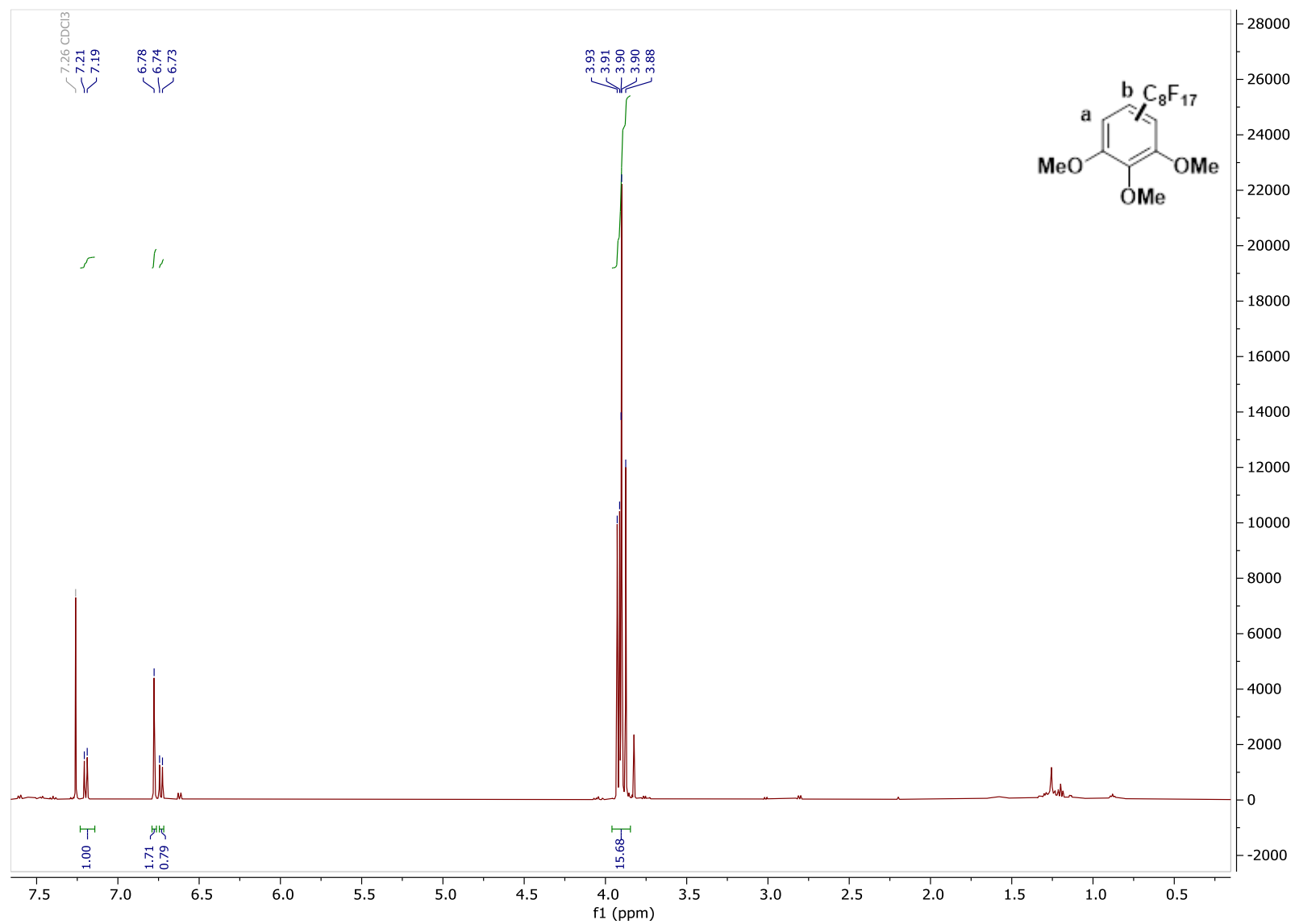
^{13}C NMR of **PF5**, CDCl_3 , 126 MHz



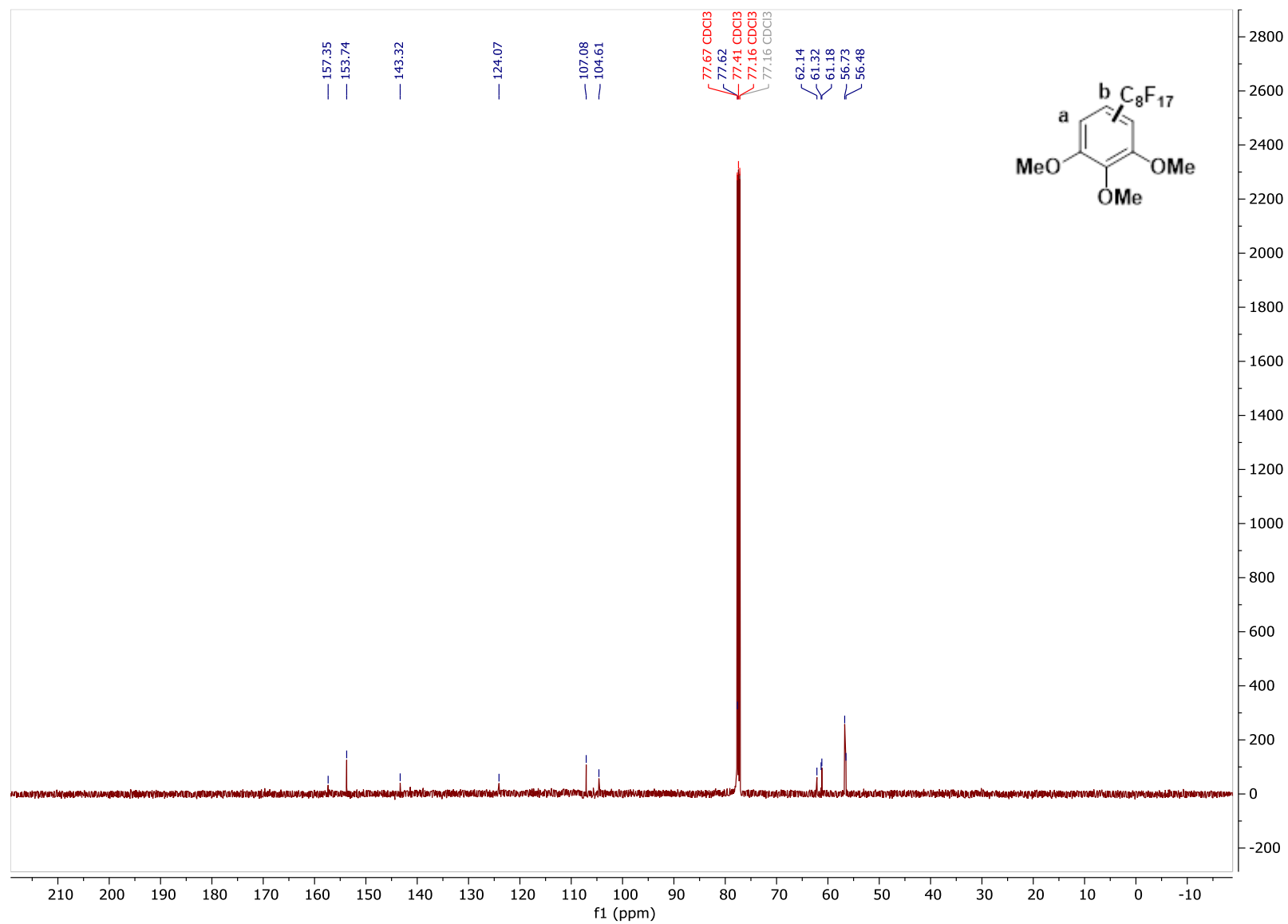
^{19}F NMR of **PF5**, CDCl_3 , 471 MHz



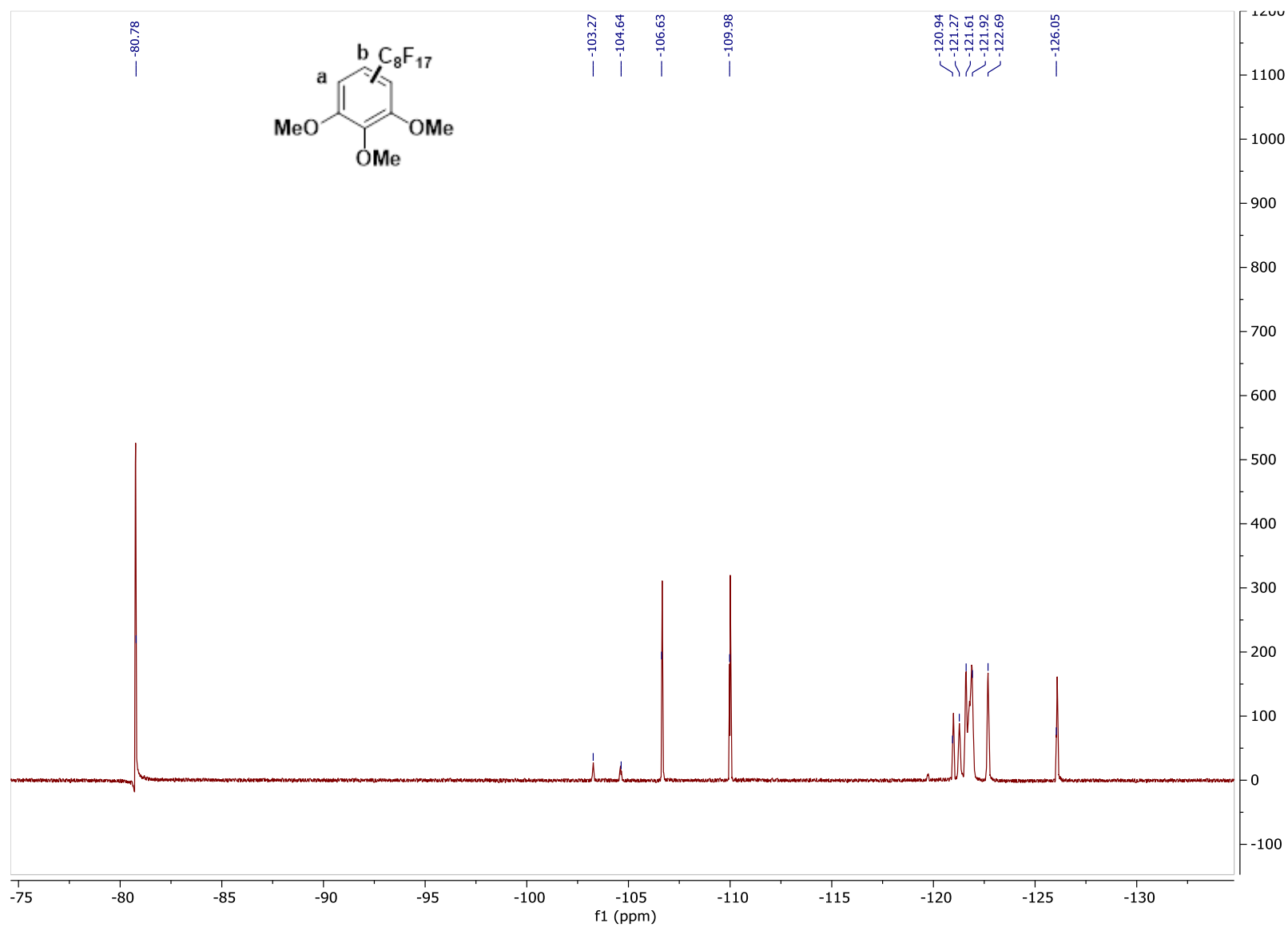
^1H - ^{19}F HMBC of PF5

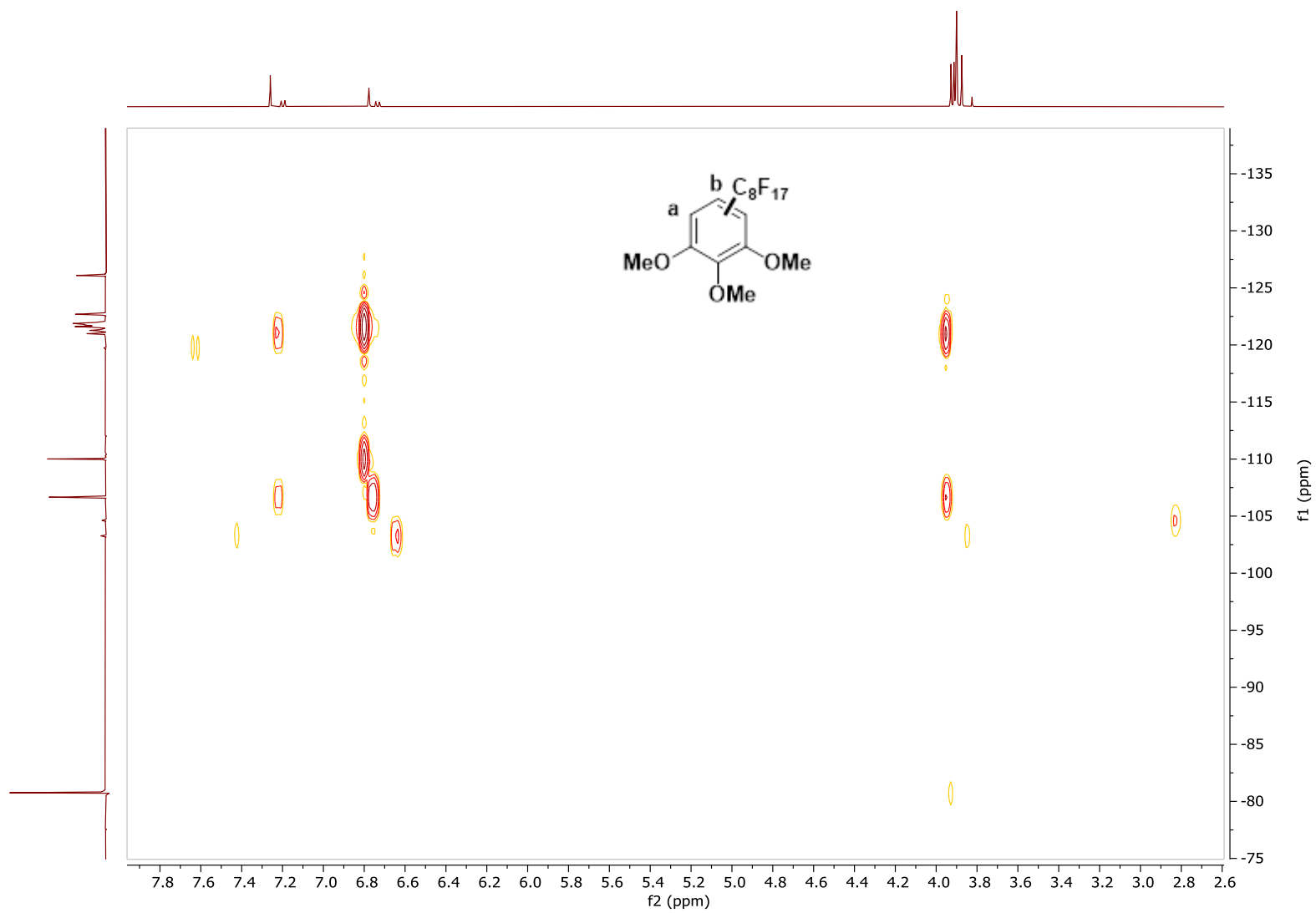
^1H NMR of PF6, CDCl_3 , 500 MHz

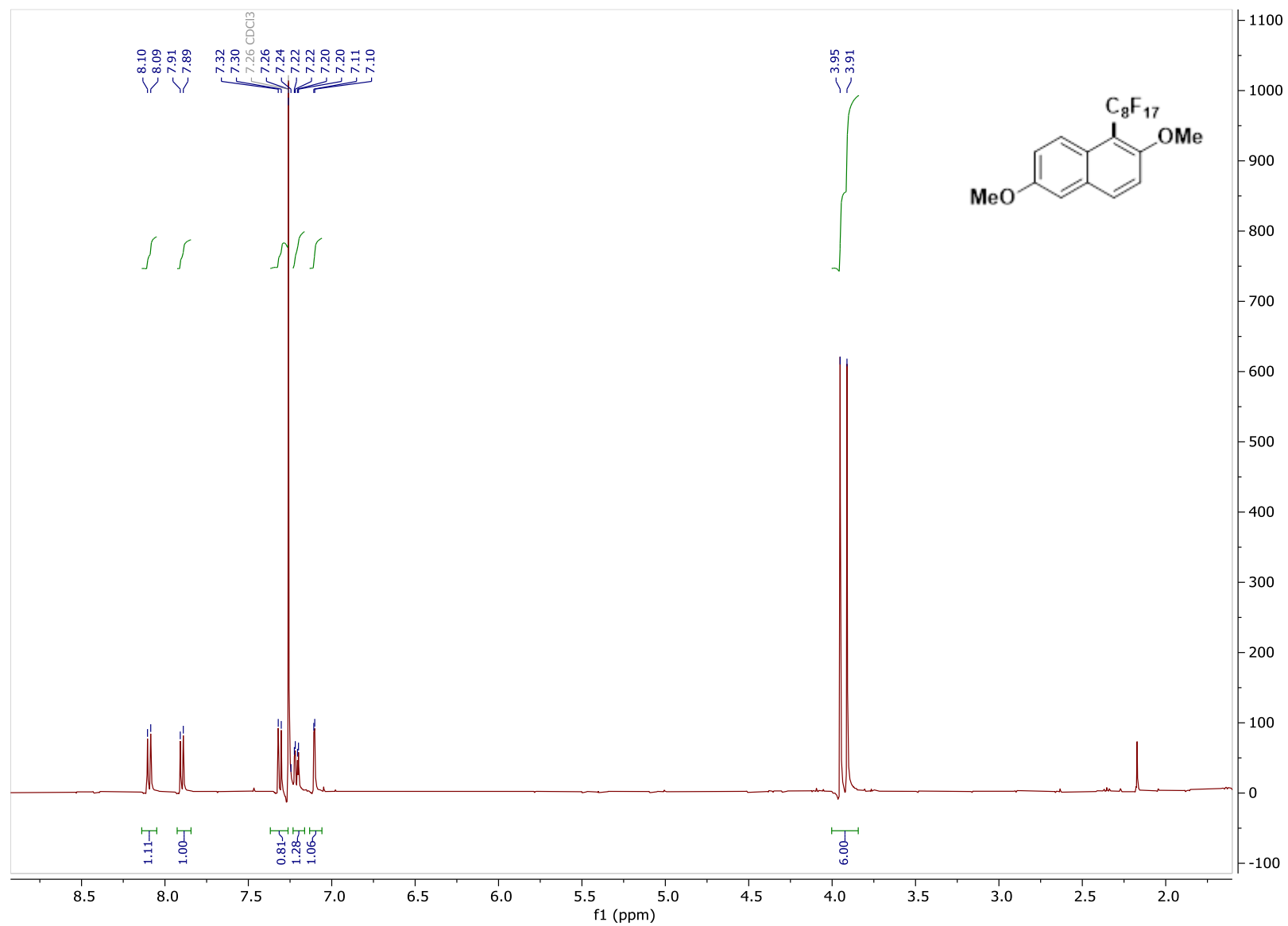
^{13}C NMR of PF6, CDCl_3 , 126 MHz



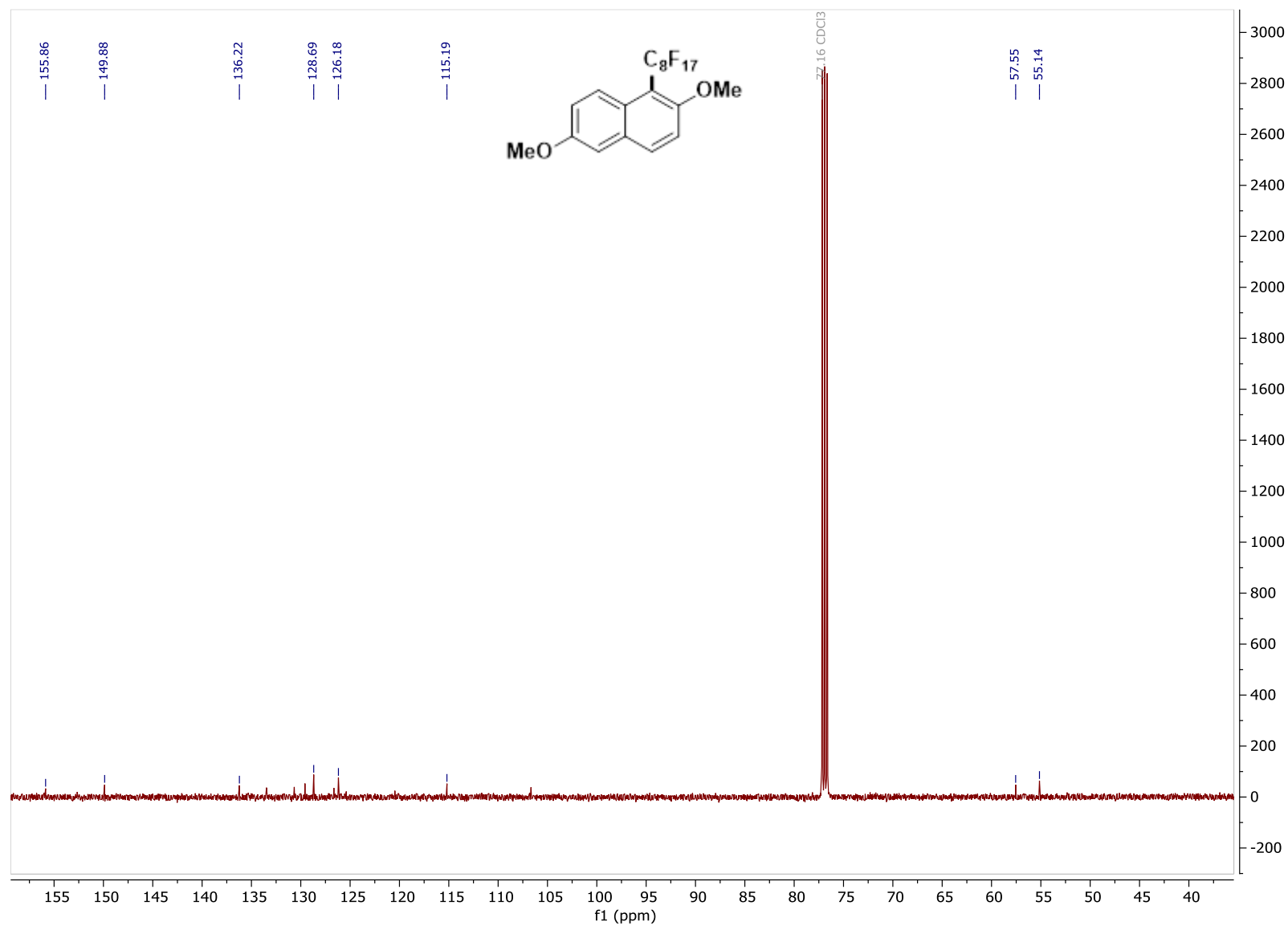
^{19}F NMR of **PF6**, CDCl_3 , 471 MHz



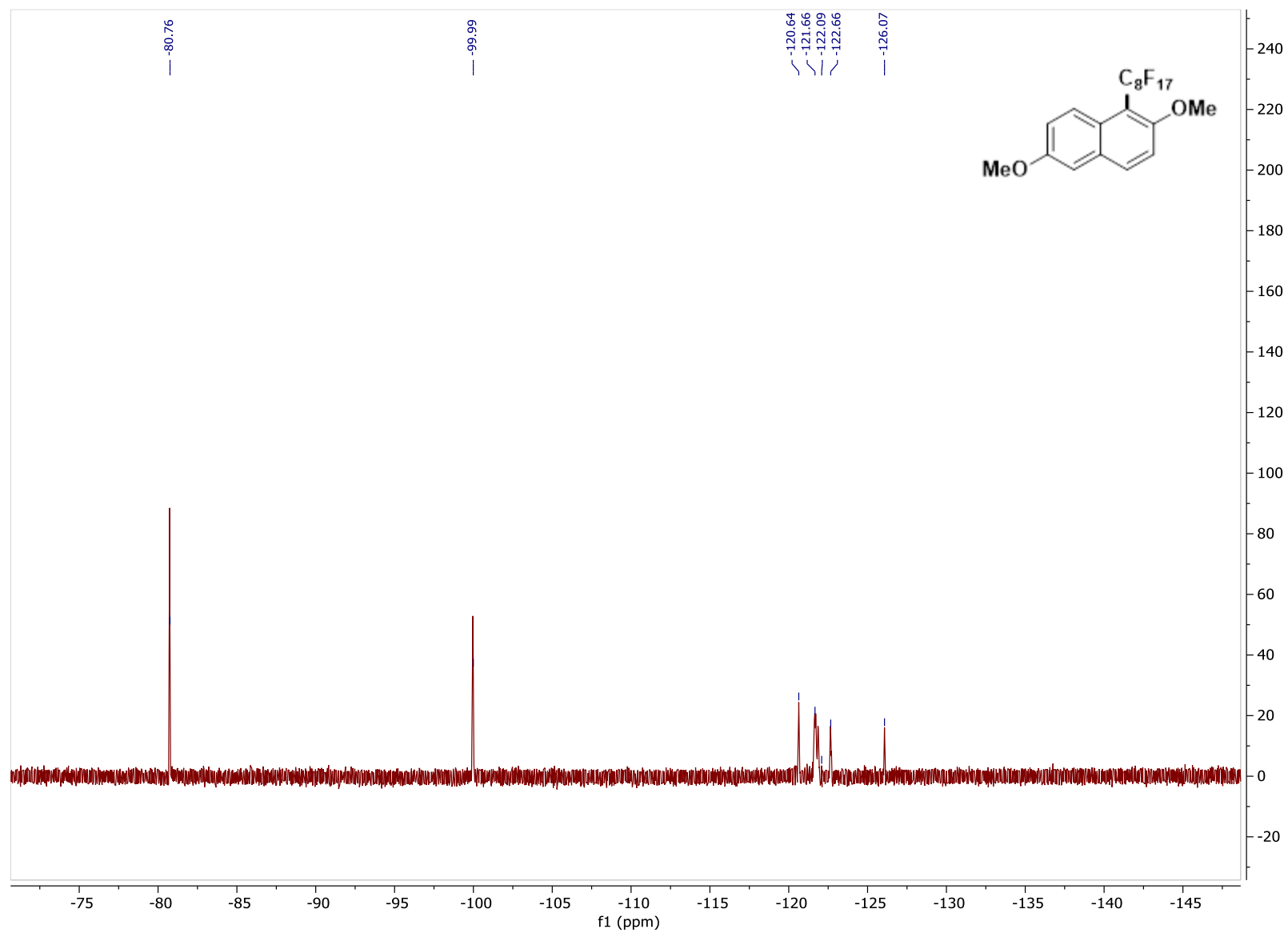
^1H - ^{19}F HMBC of PF6

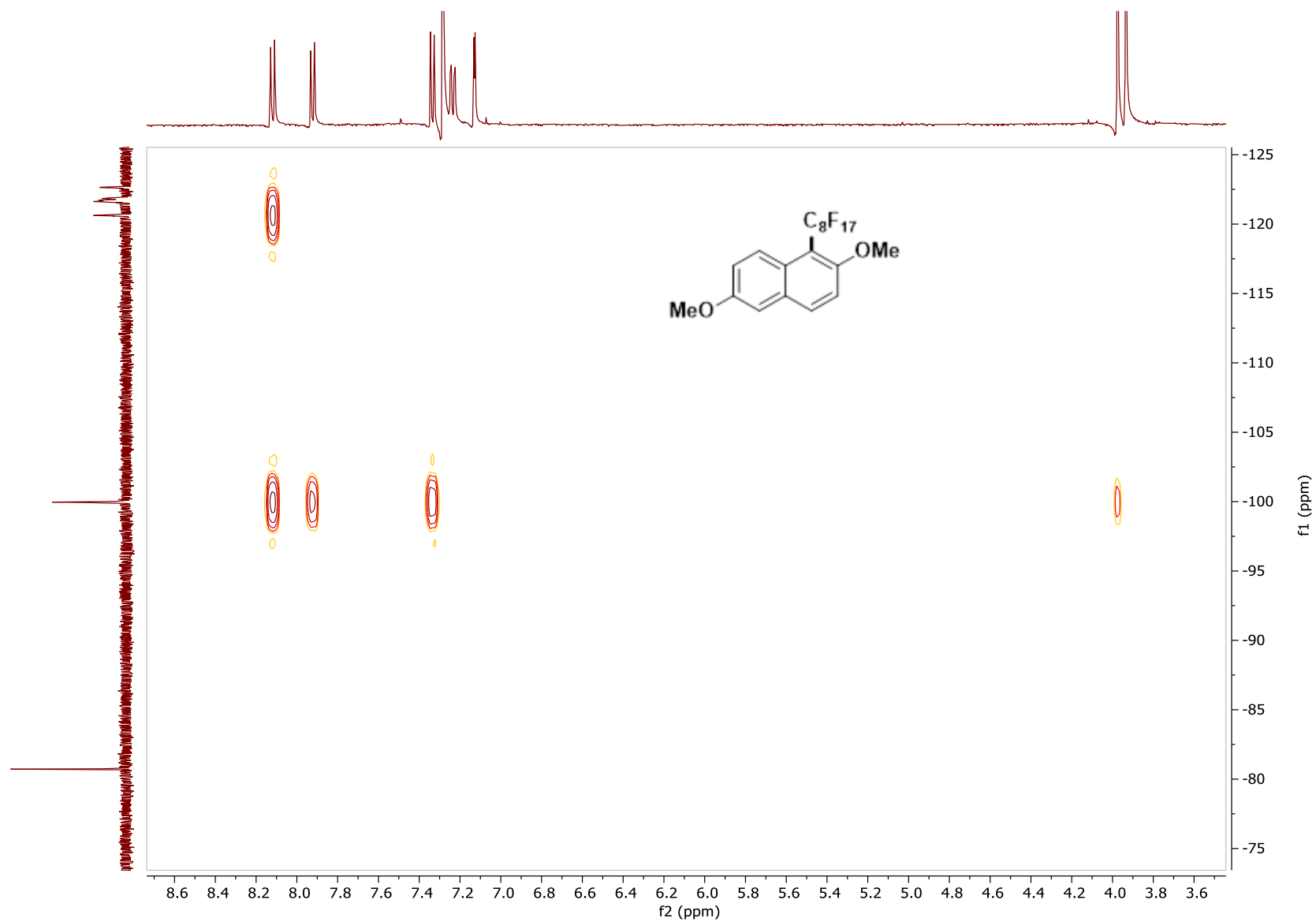
^1H NMR of PF7, CDCl_3 , 500 MHz

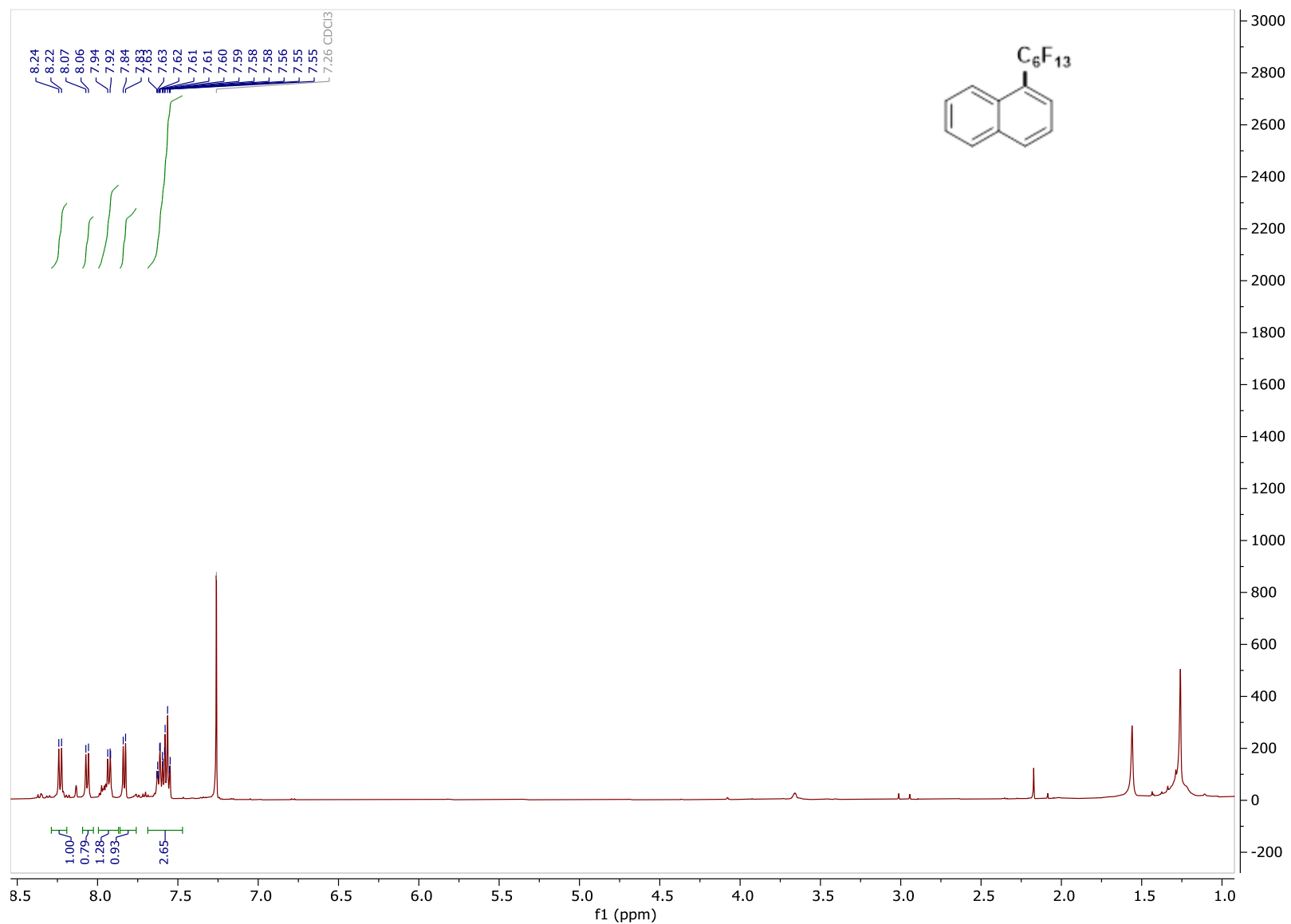
^{13}C NMR of PF7, CDCl_3 , 126 MHz

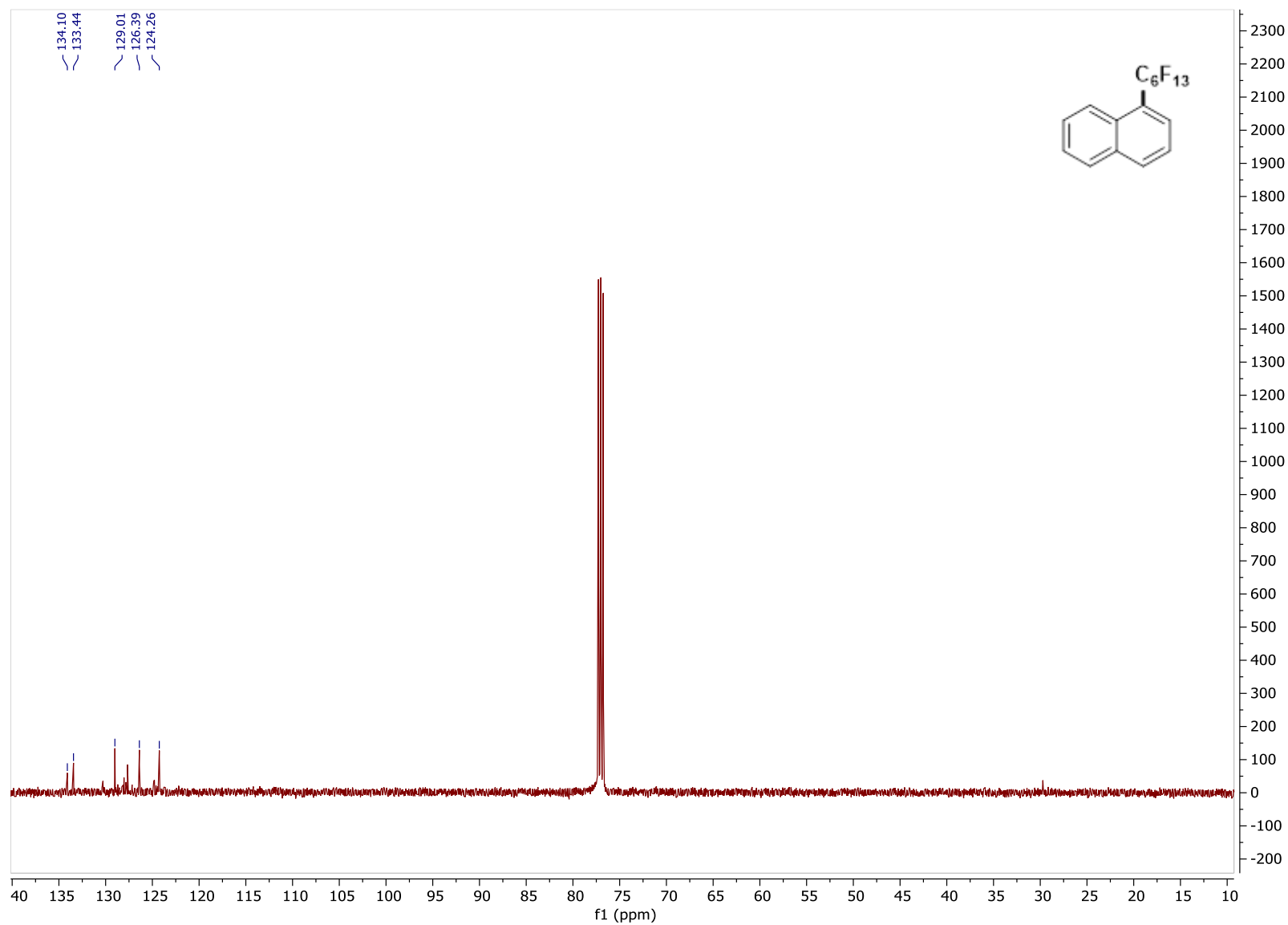


^{19}F NMR of **PF7**, CDCl_3 , 471 MHz

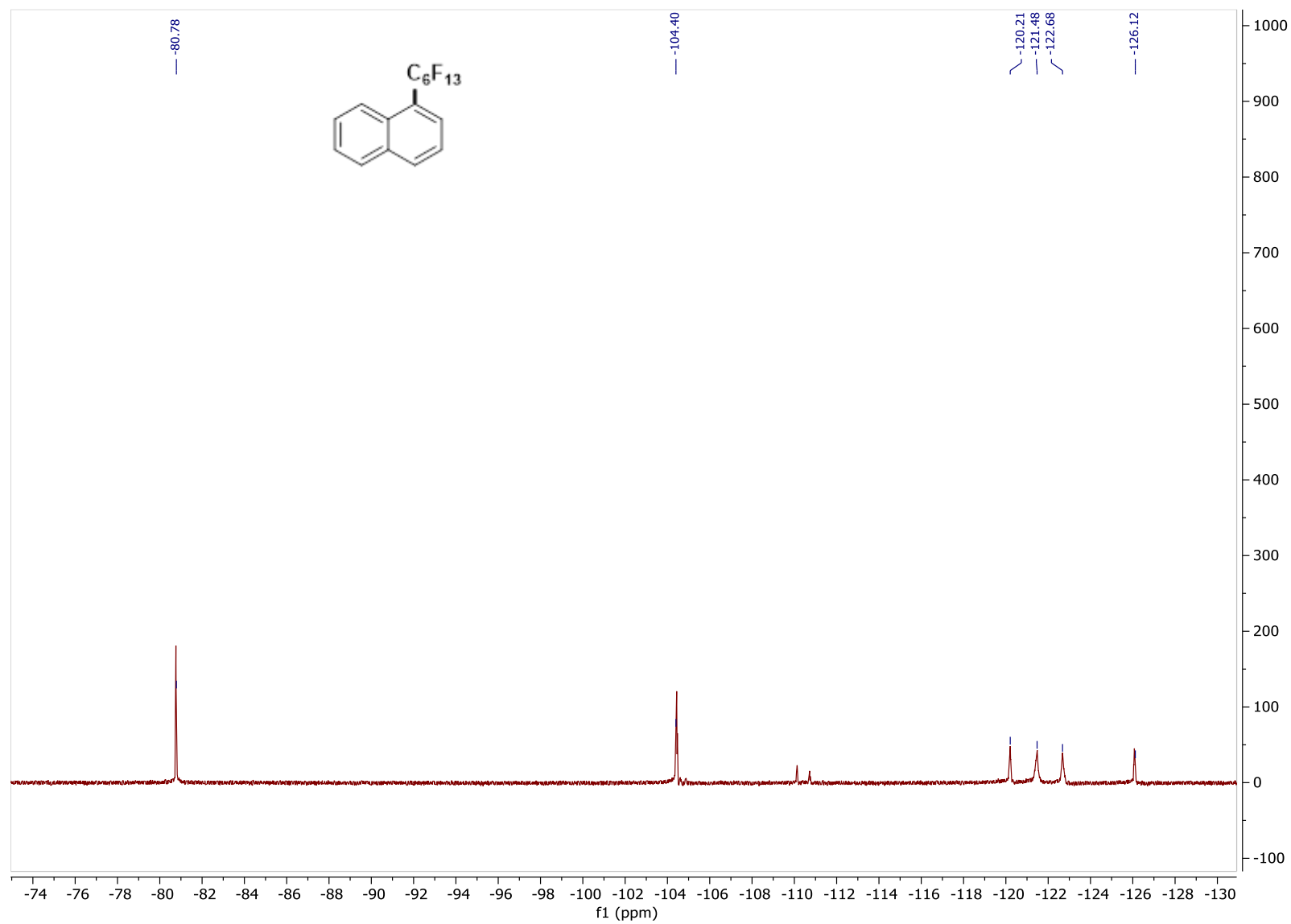


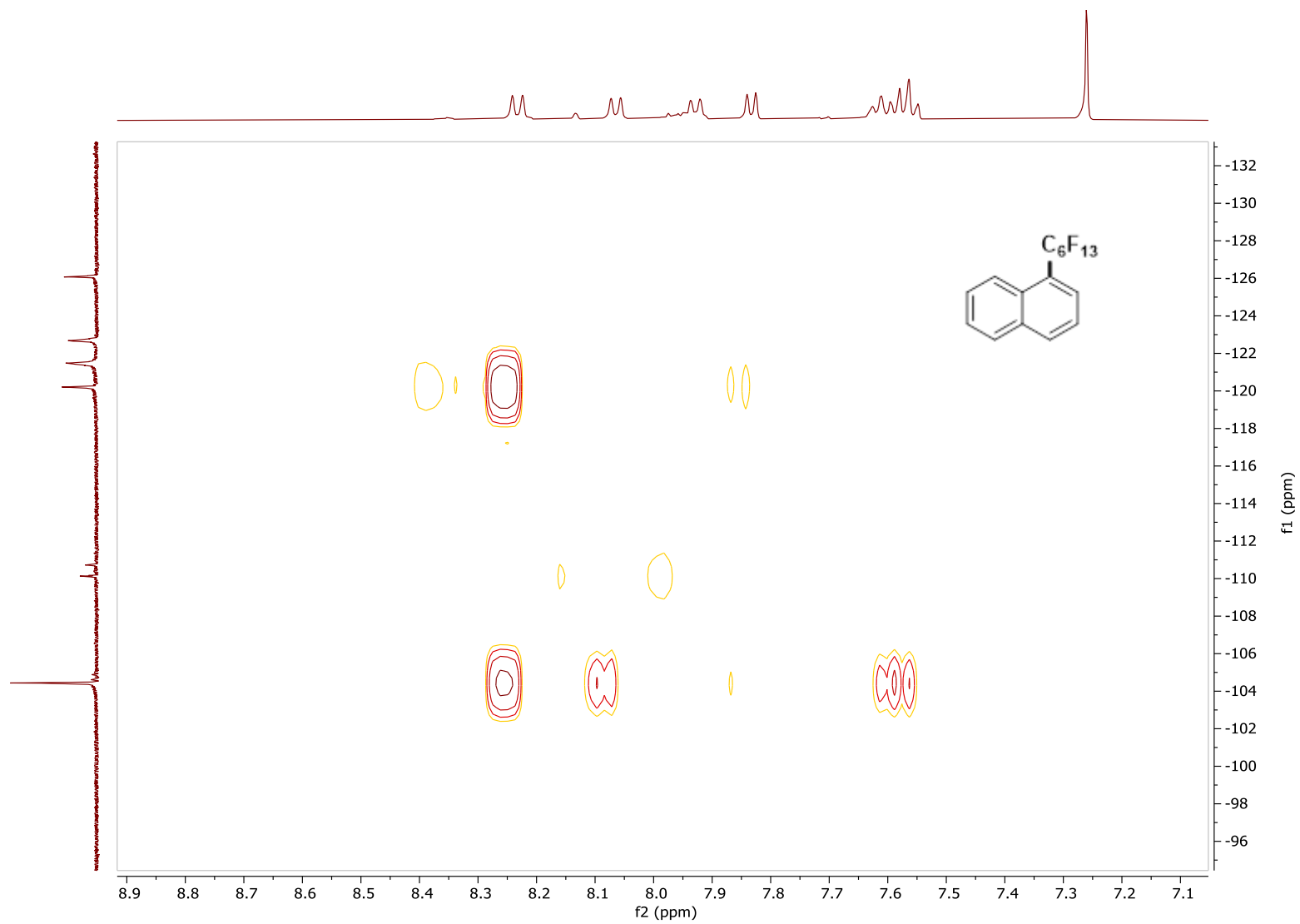
^1H - ^{19}F HMBC of PF7

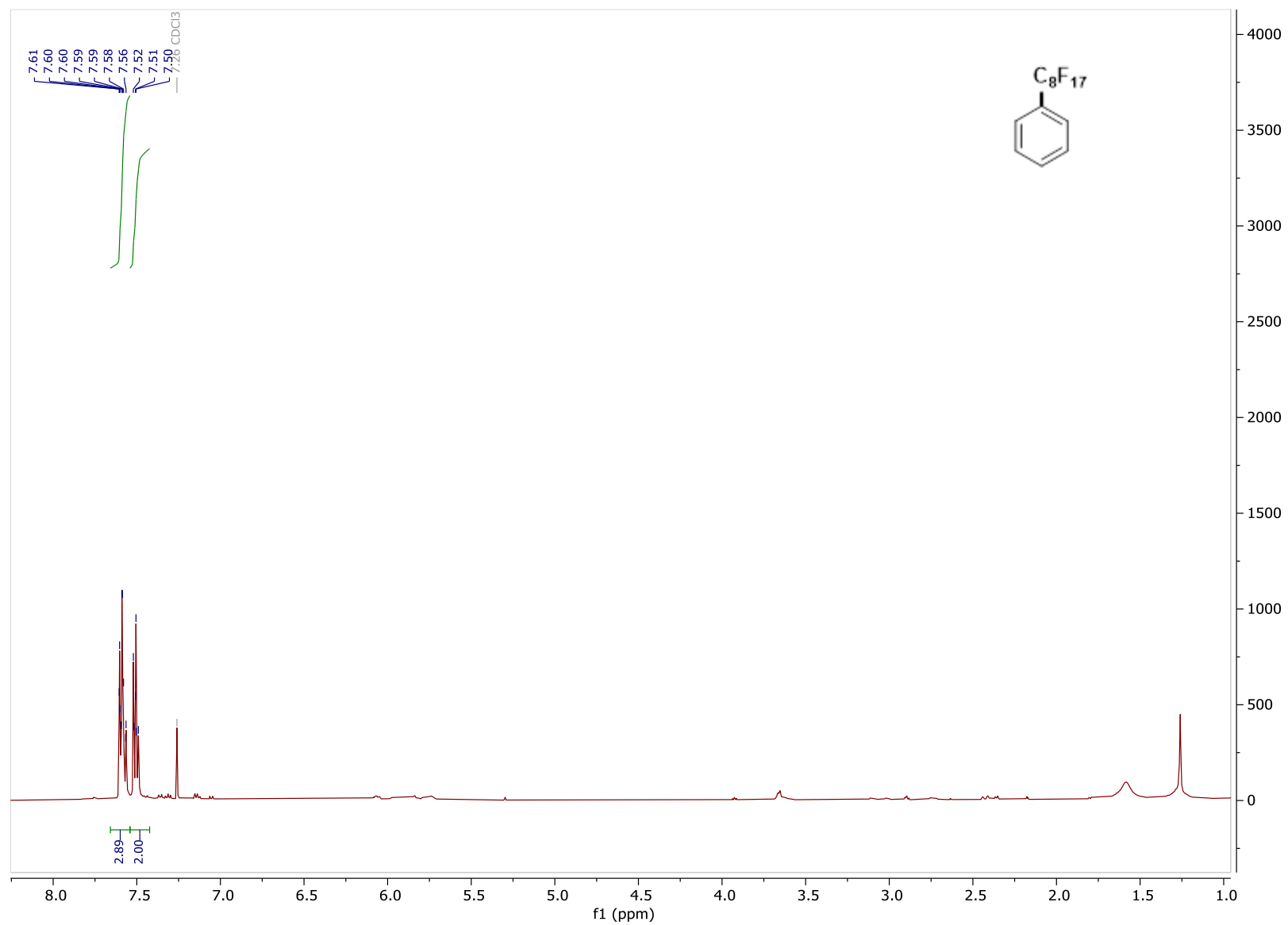
^1H NMR of **PF8**, CDCl_3 , 500 MHz

^{13}C NMR of PF8, CDCl_3 , 126 MHz

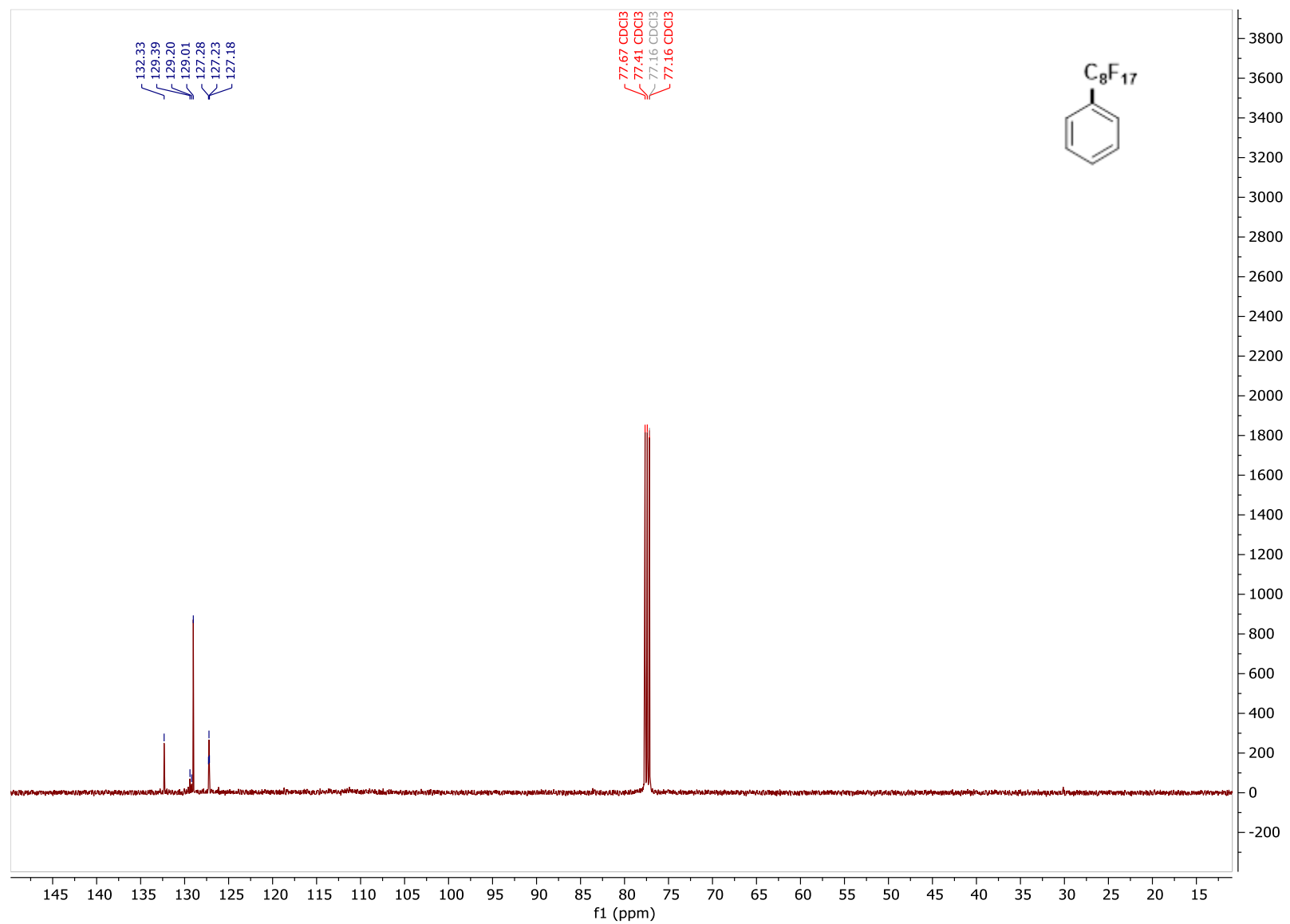
^{19}F NMR of **PF8**, CDCl_3 , 471 MHz



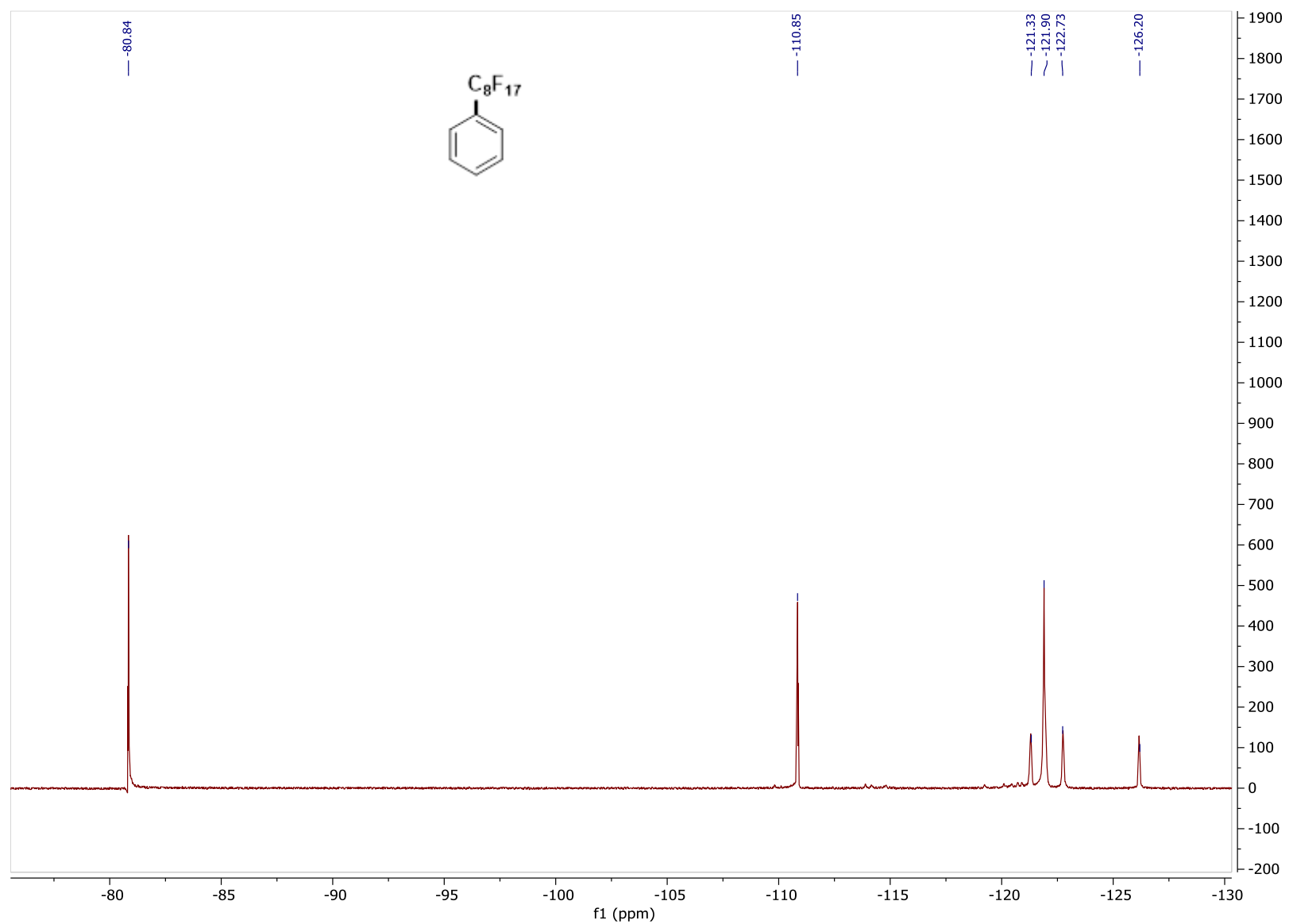
^1H - ^{19}F HMBC of PF8

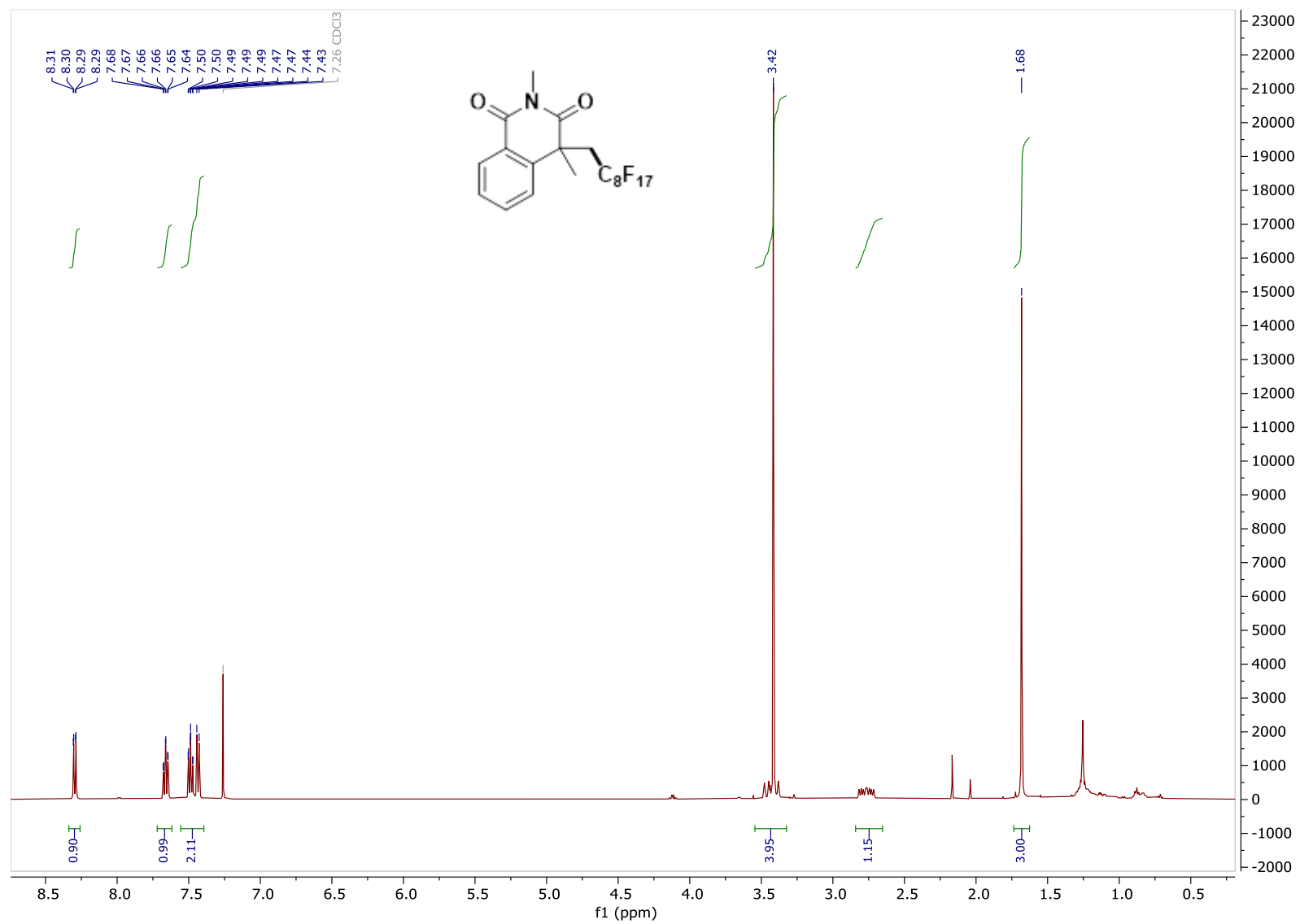
^1H NMR of **PF9**, CDCl_3 , 500 MHz

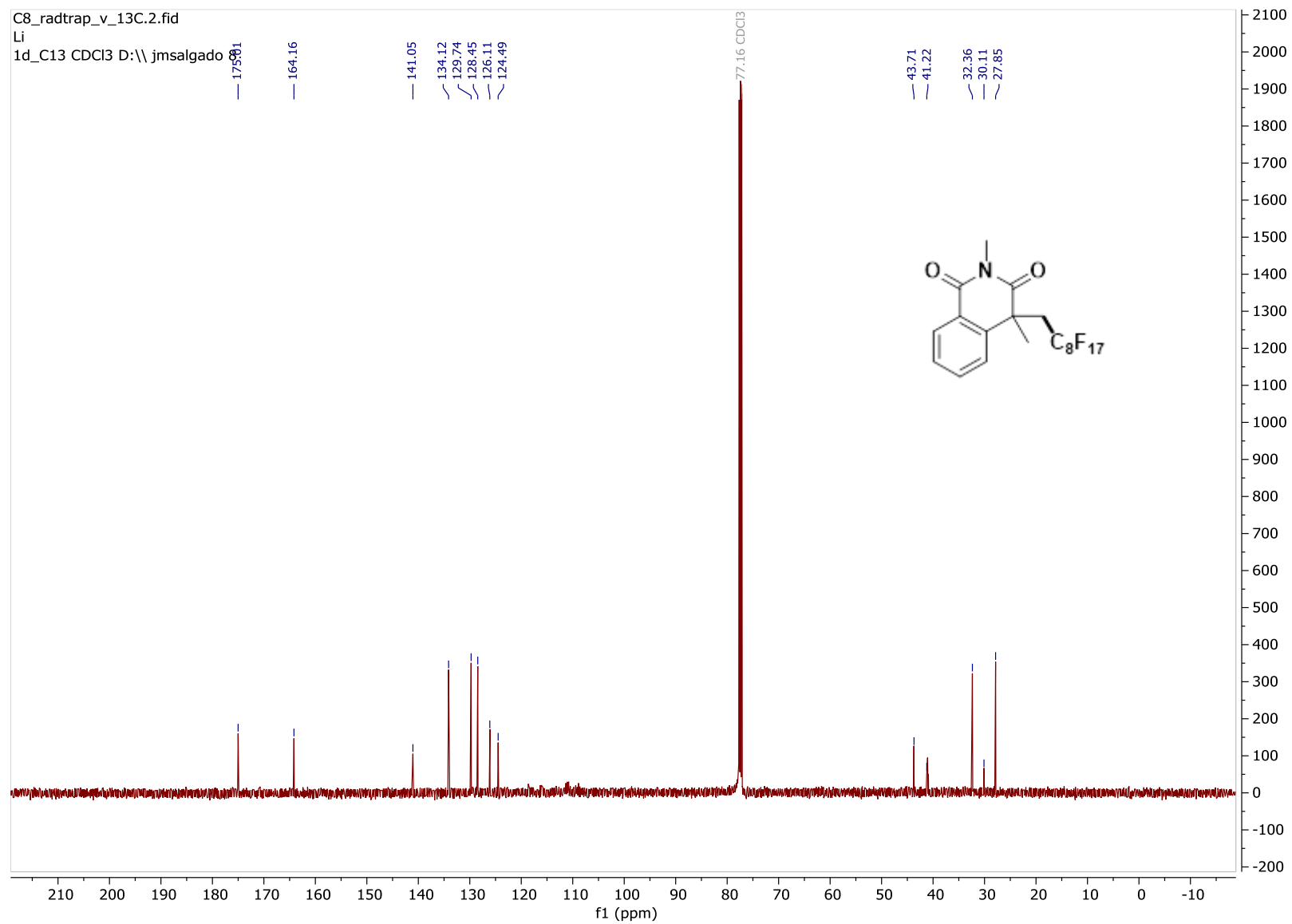
^{13}C NMR of **PF9**, CDCl_3 , 126 MHz



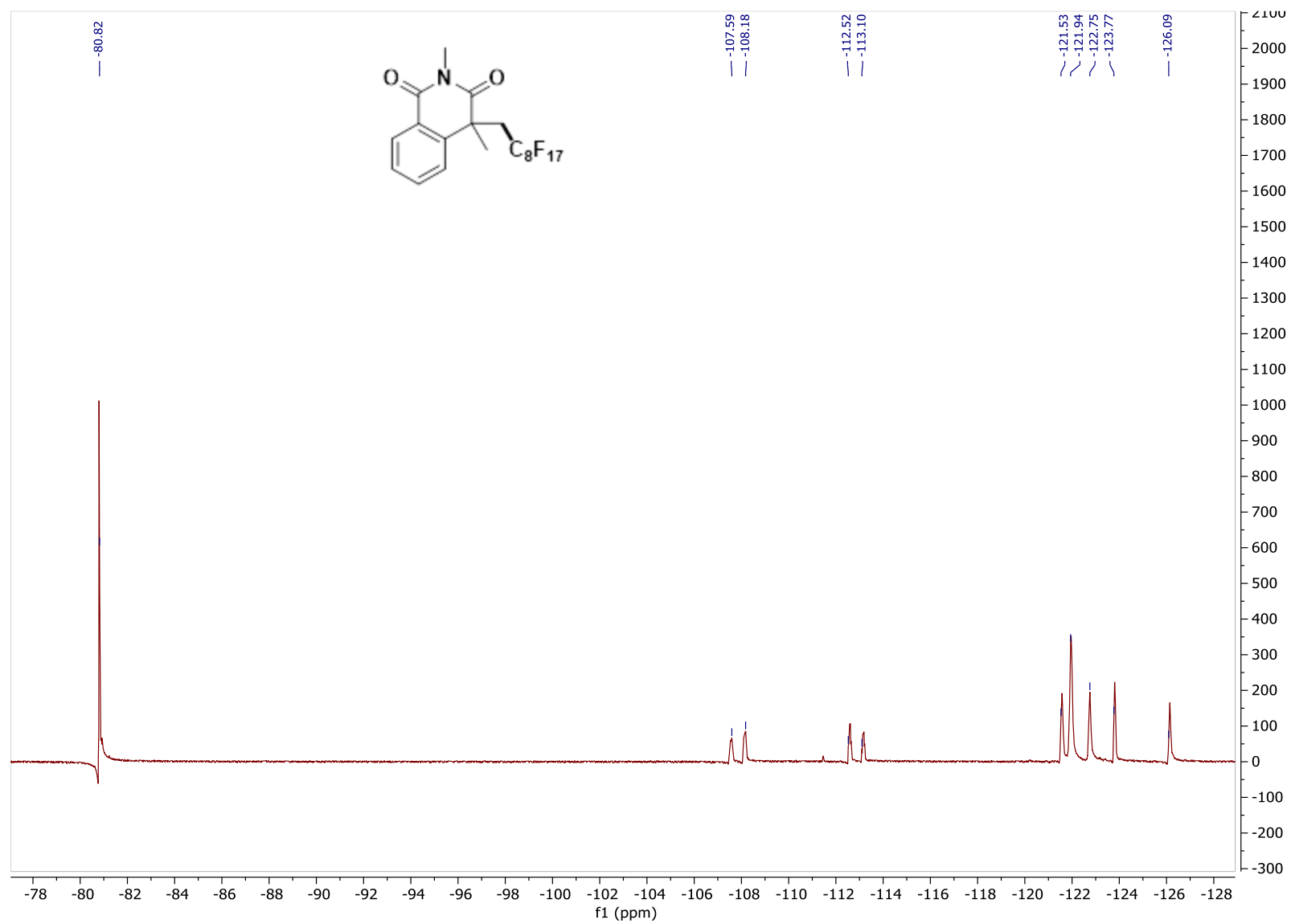
^{19}F NMR of **PF9**, CDCl_3 , 471 MHz

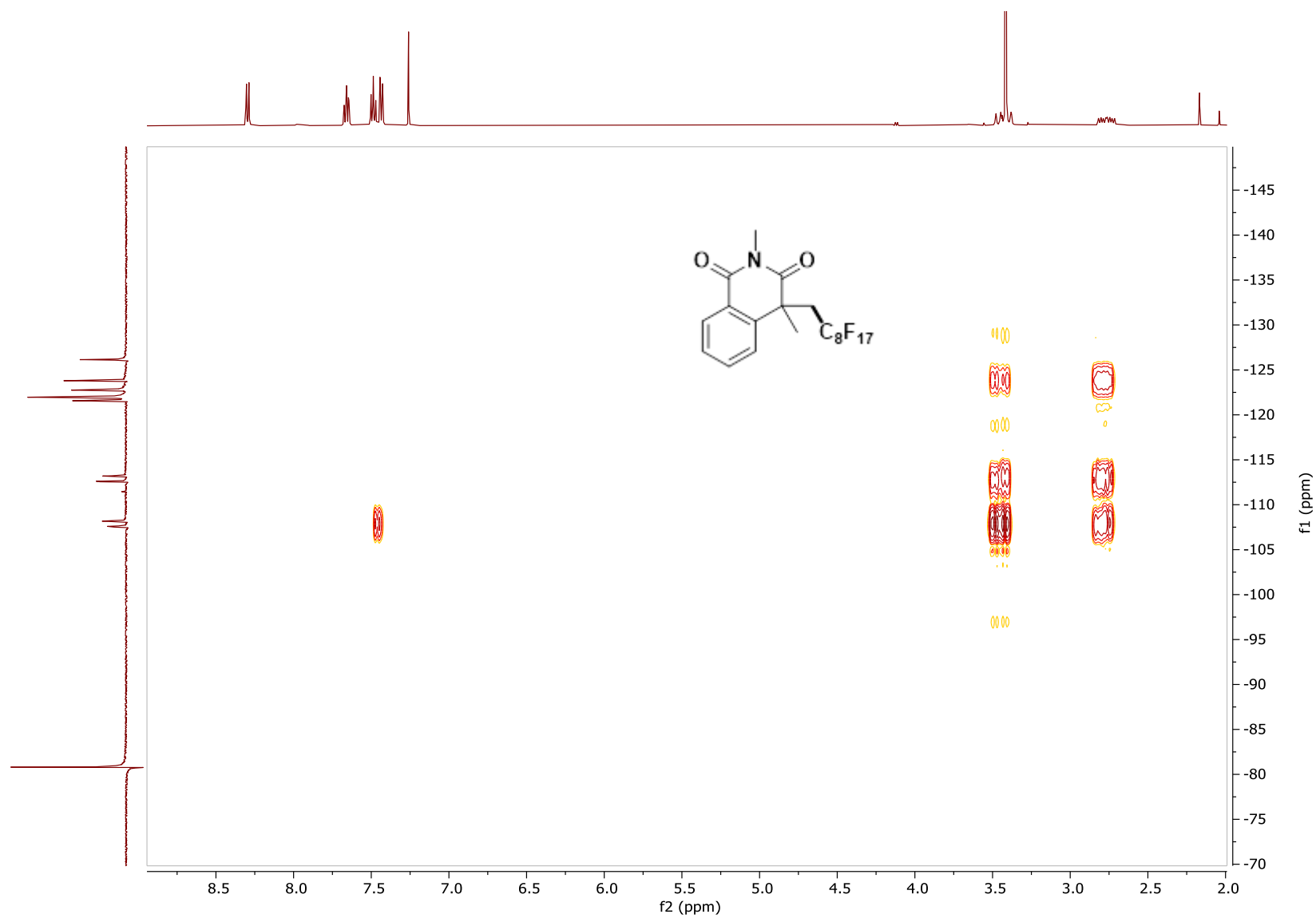


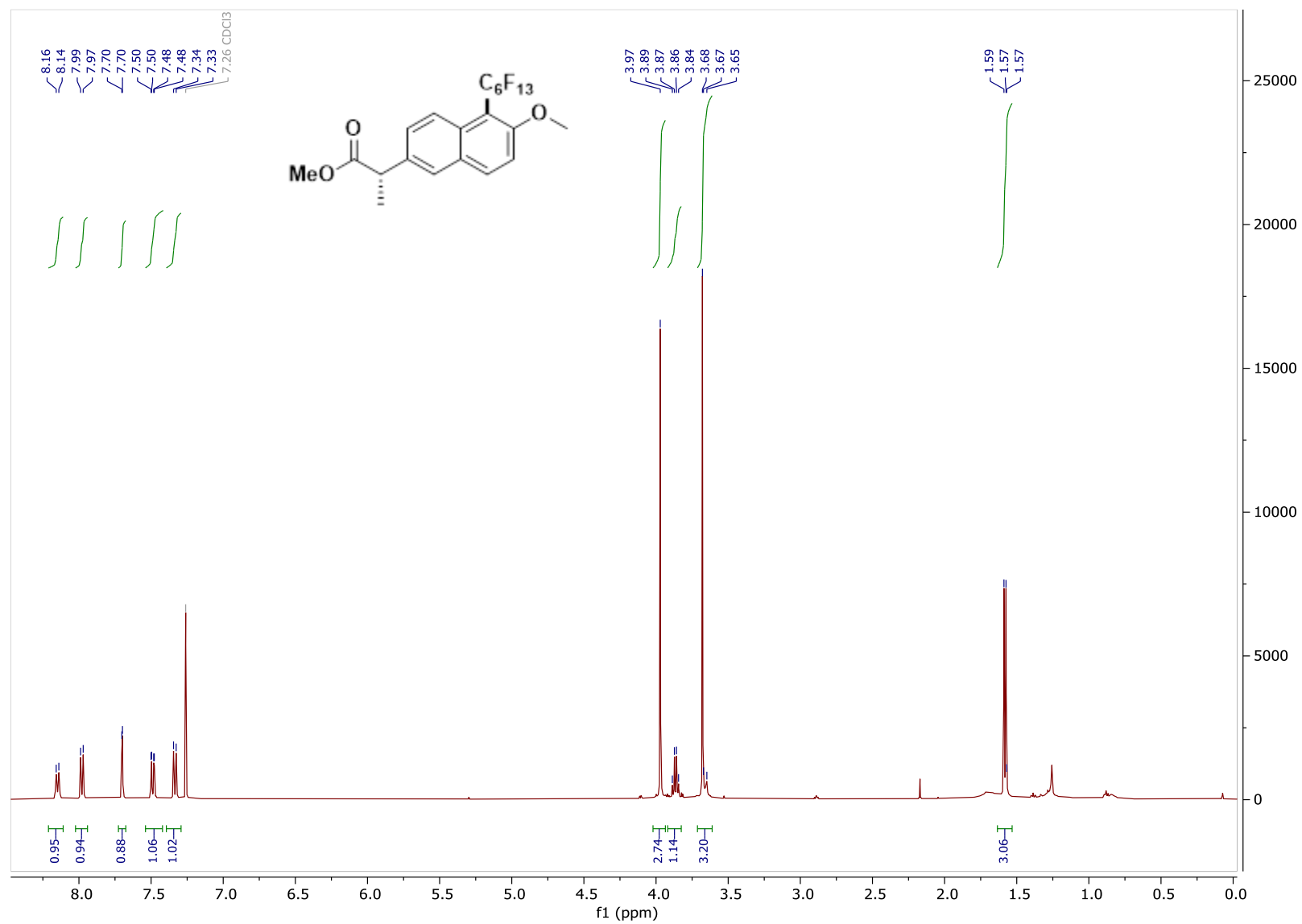
^1H NMR of PF10, CDCl_3 , 500 MHz

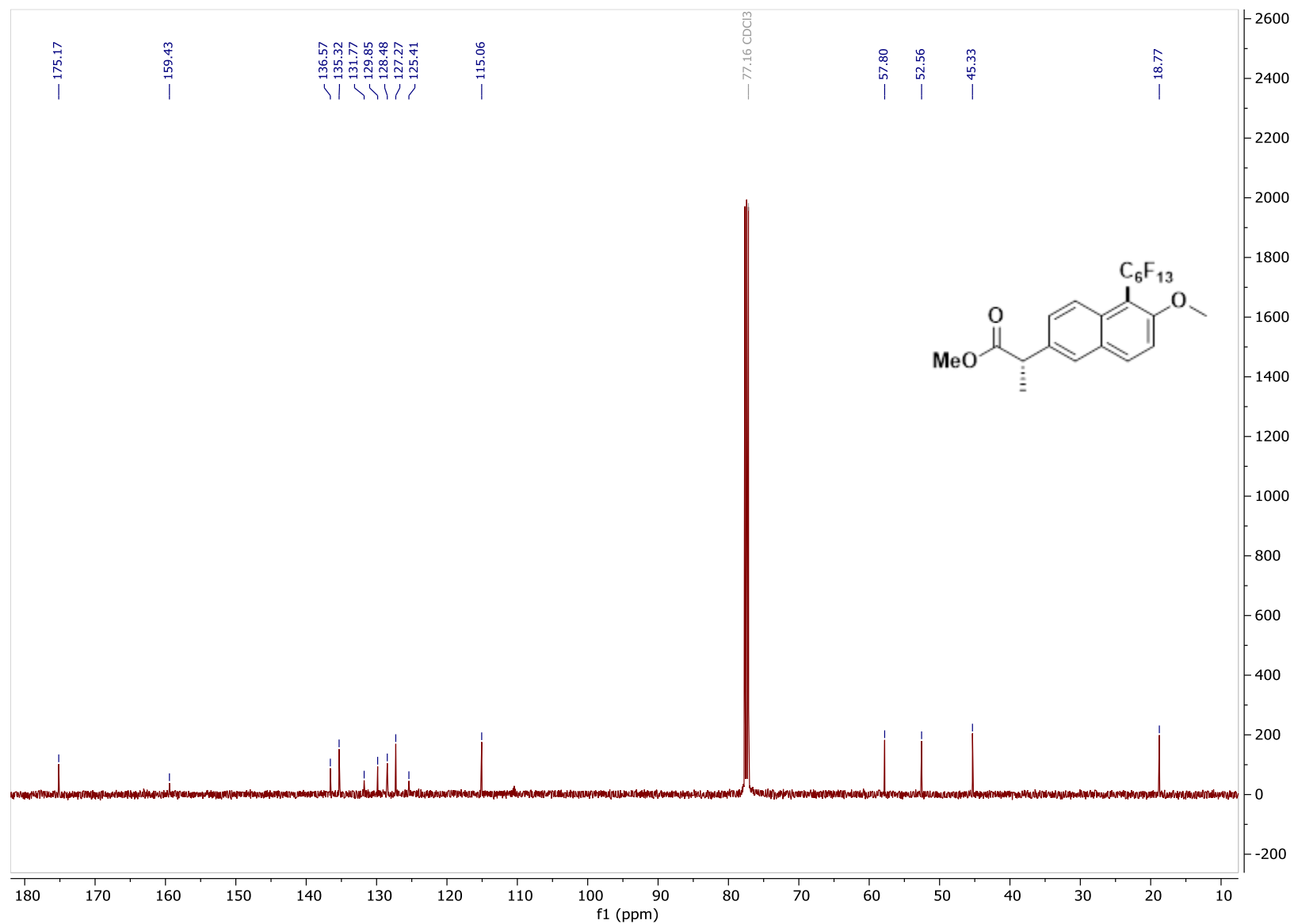
^{13}C NMR of PF10, CDCl_3 , 126 MHz

^{19}F NMR of **PF10**, CDCl_3 , 471 MHz

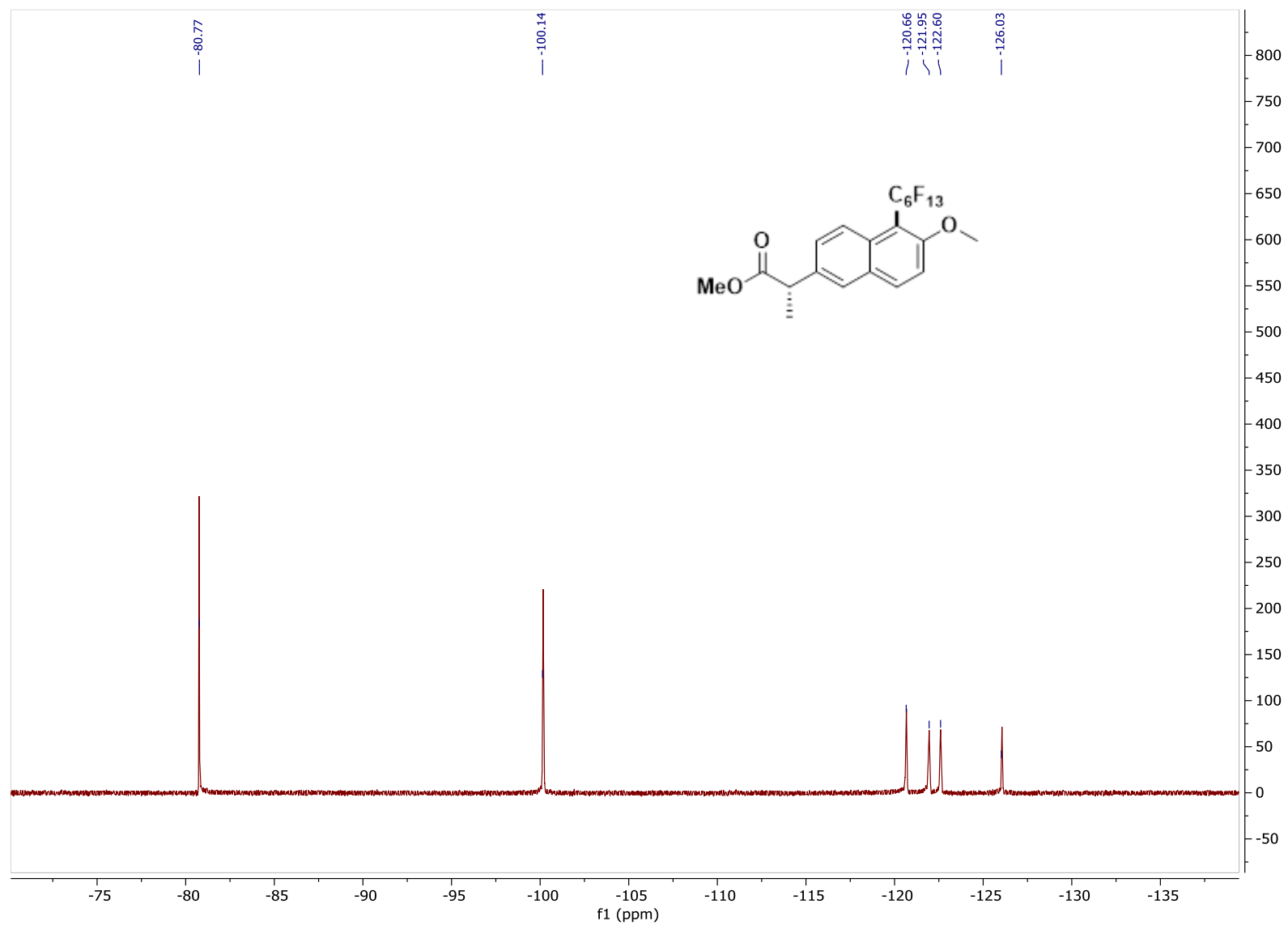


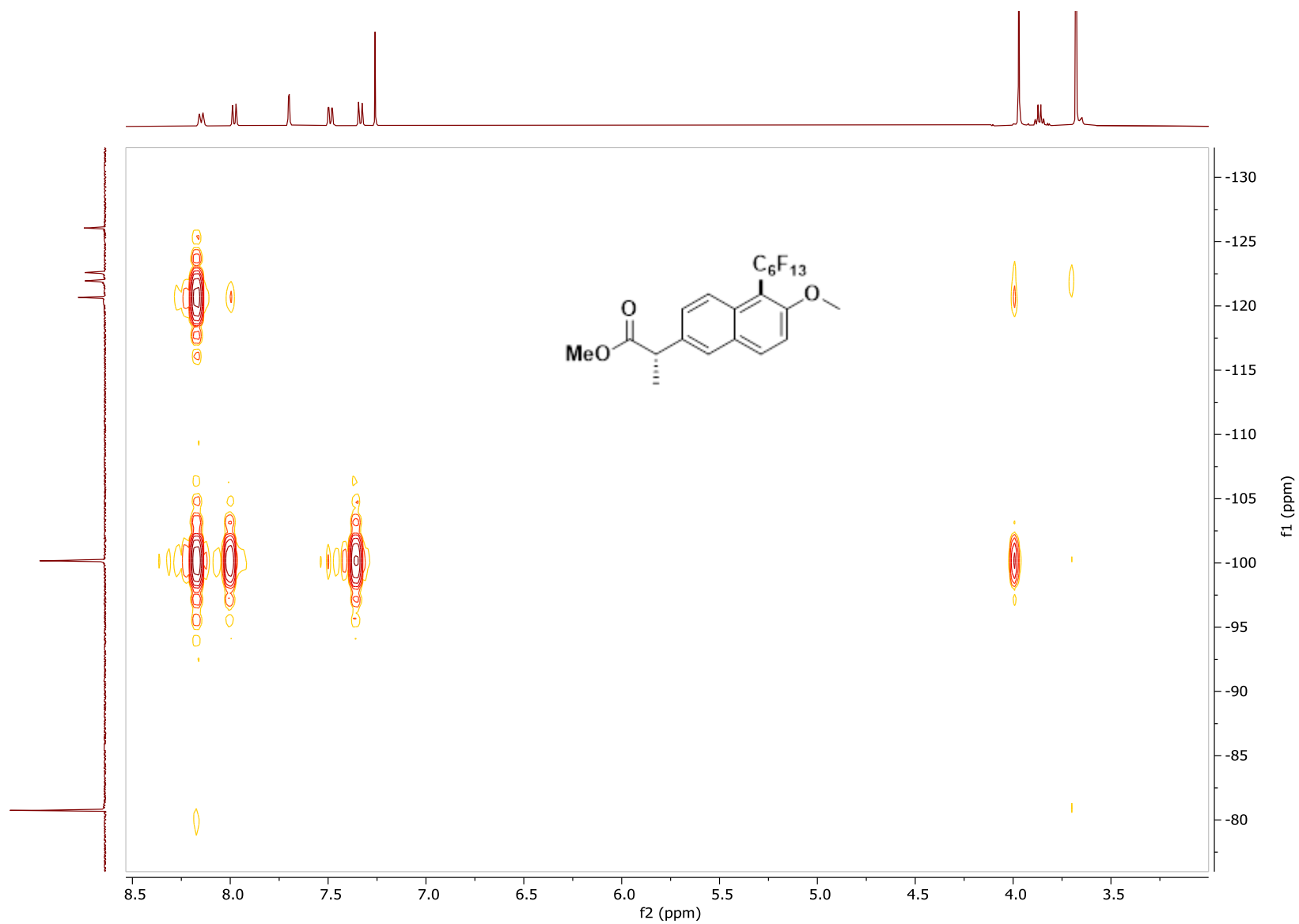
^1H - ^{19}F HMBC of PF10

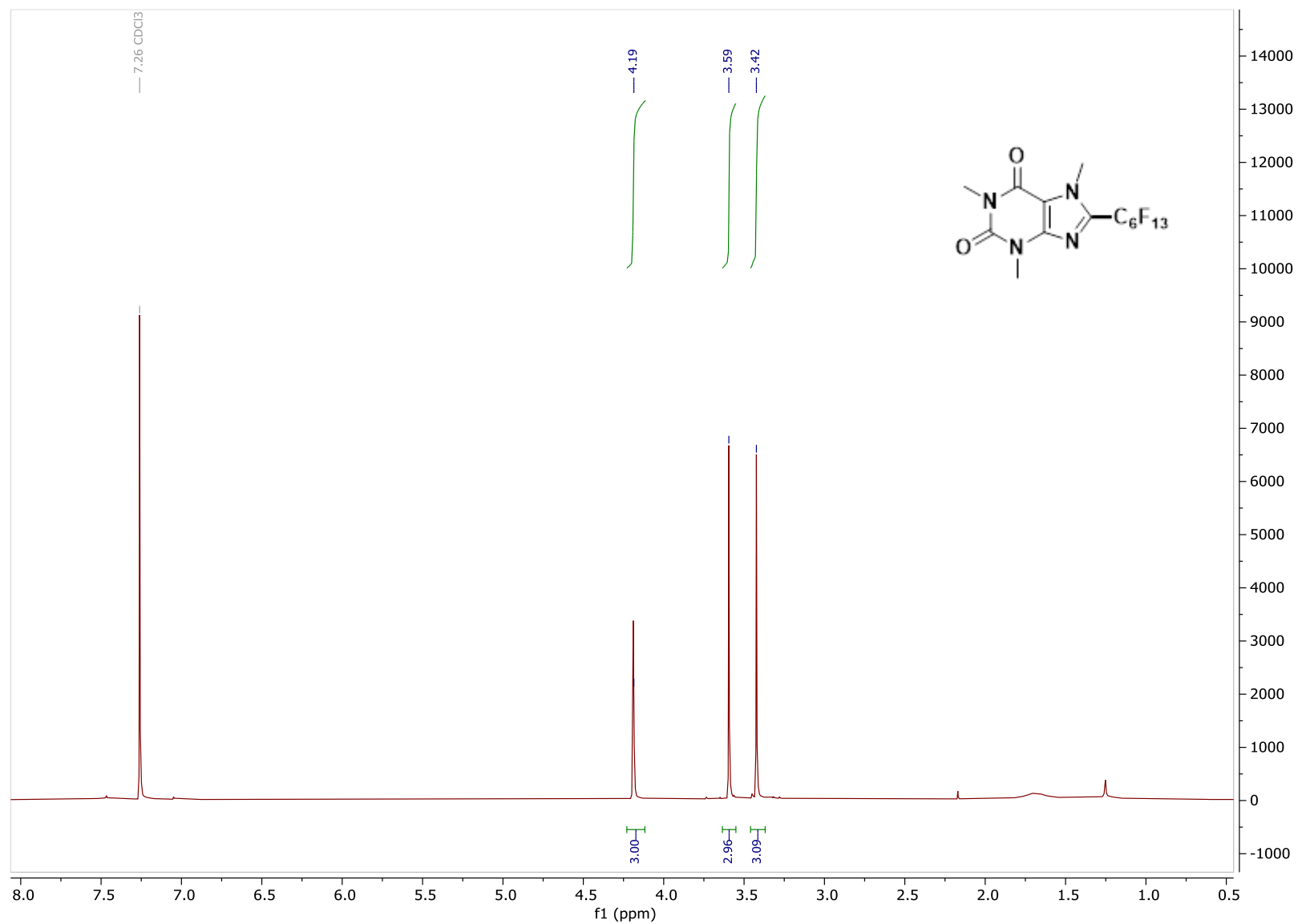
^1H NMR of PF11, CDCl_3 , 500 MHz

^{13}C NMR of PF11, CDCl_3 , 126 MHz

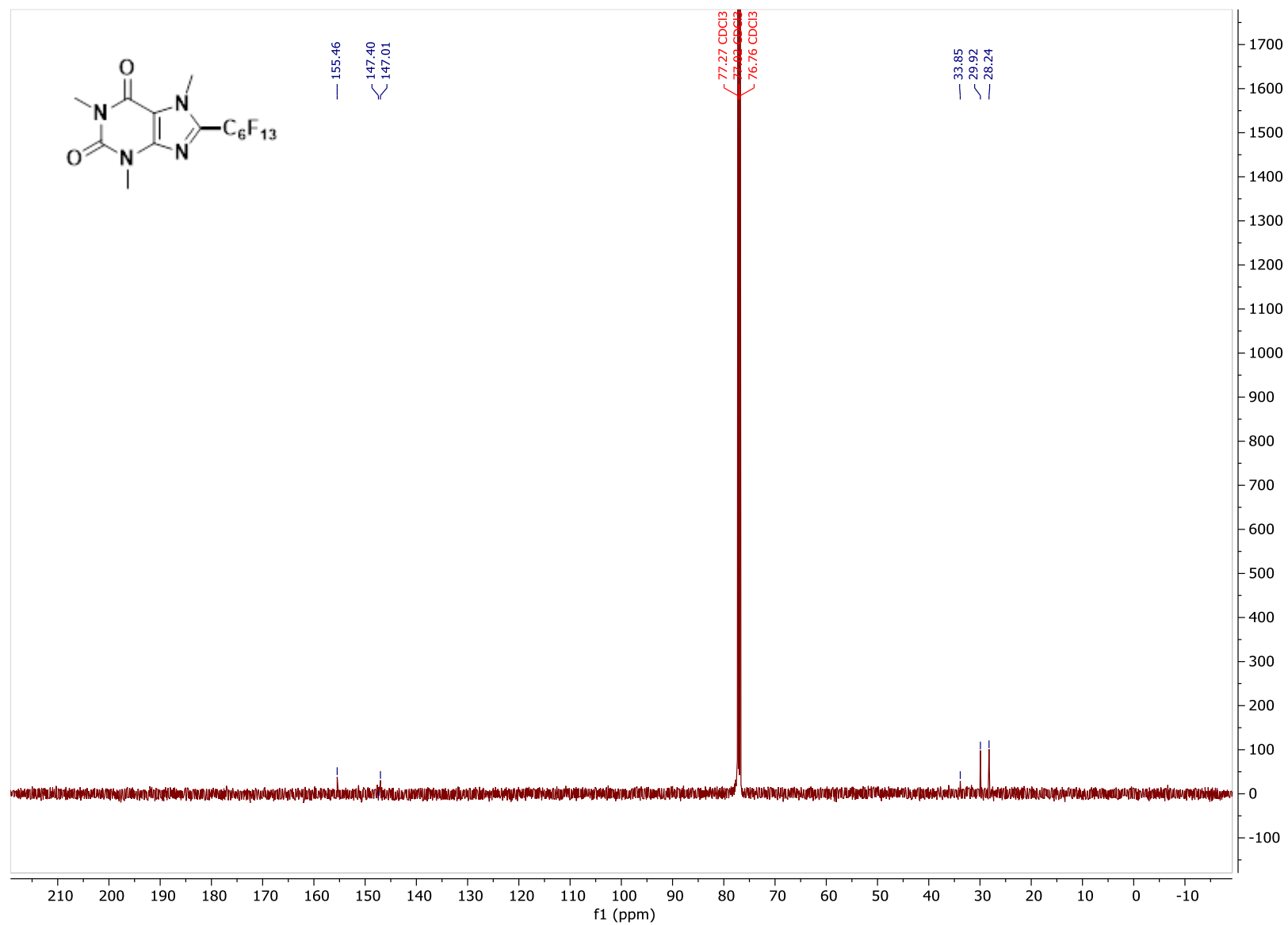
^{19}F NMR of PF11, CDCl_3 , 471 MHz



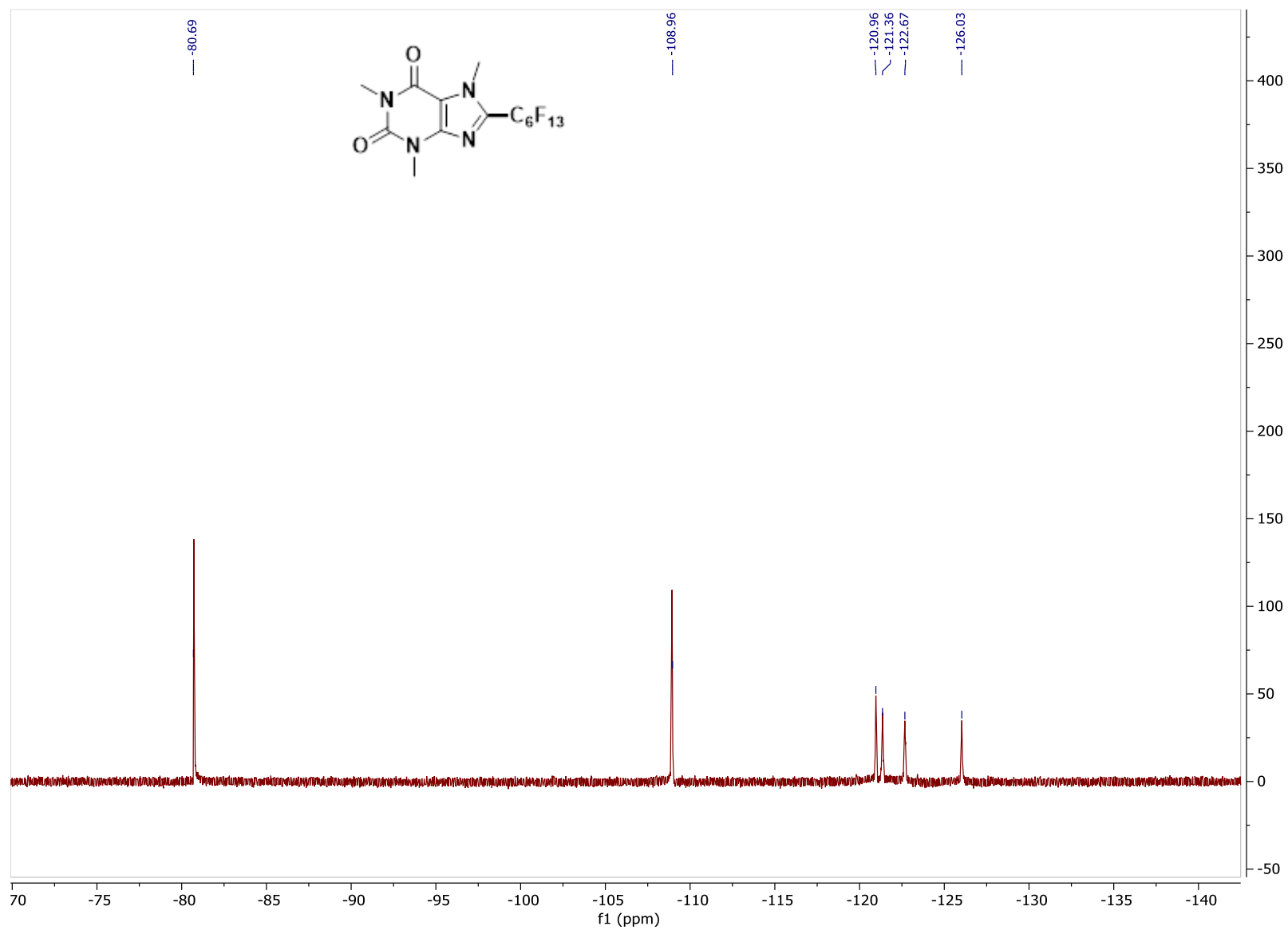
^1H - ^{19}F HMBC of PF11

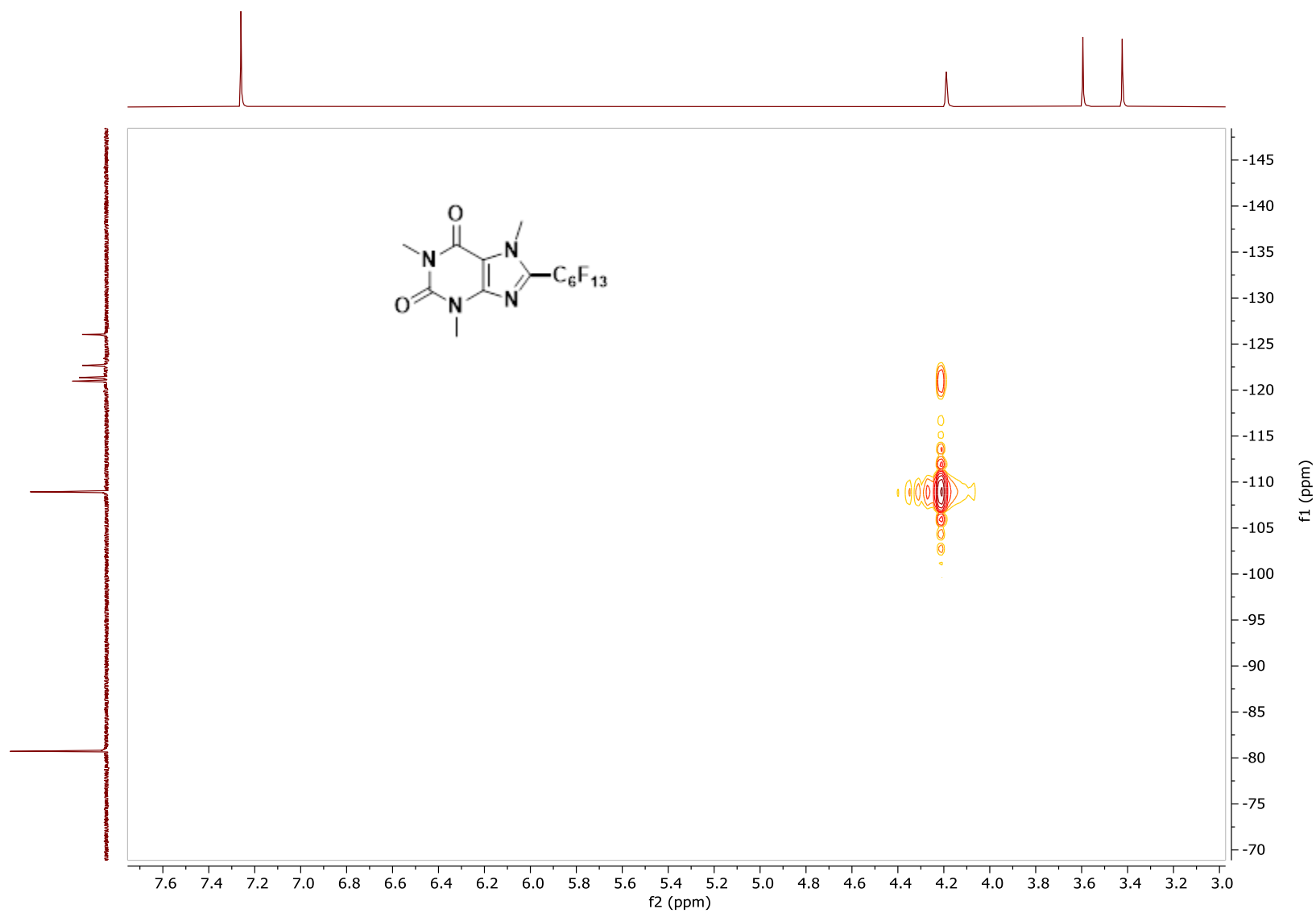
^1H NMR of PF12 CDCl_3 , 500 MHz

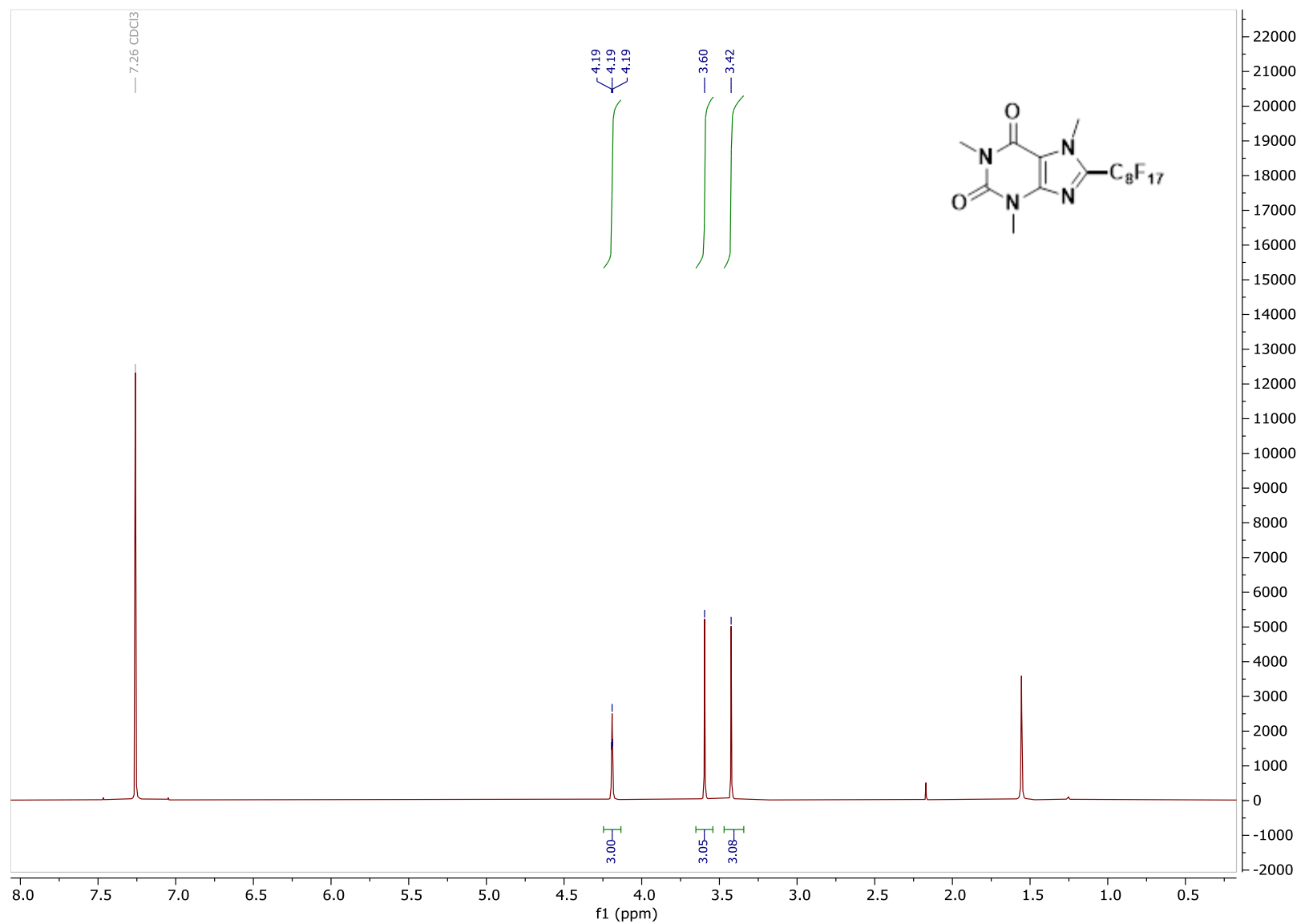
^{13}C NMR of **PF12**, CDCl_3 , 126 MHz



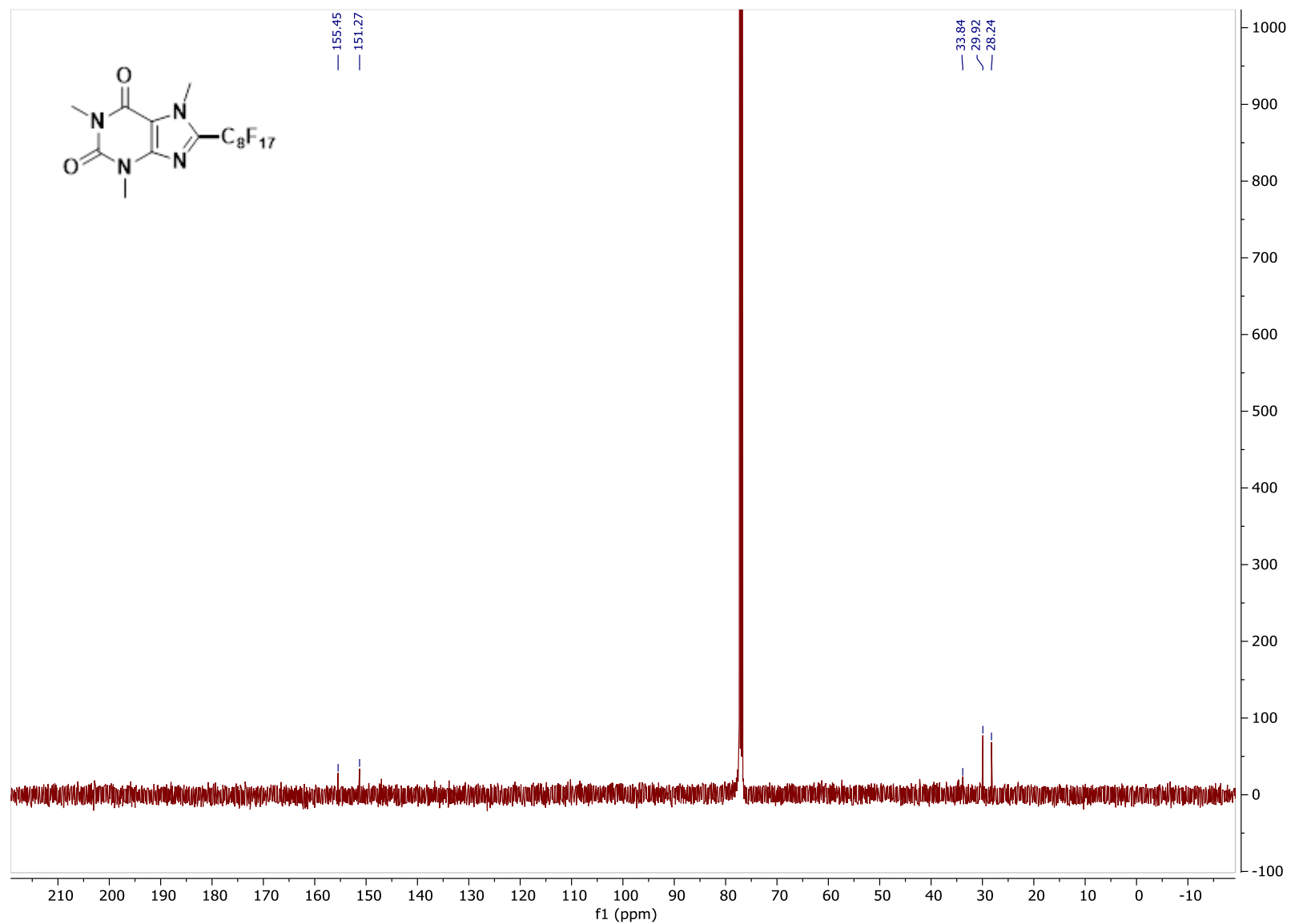
^{19}F NMR of **PF12**, CDCl_3 , 471 MHz



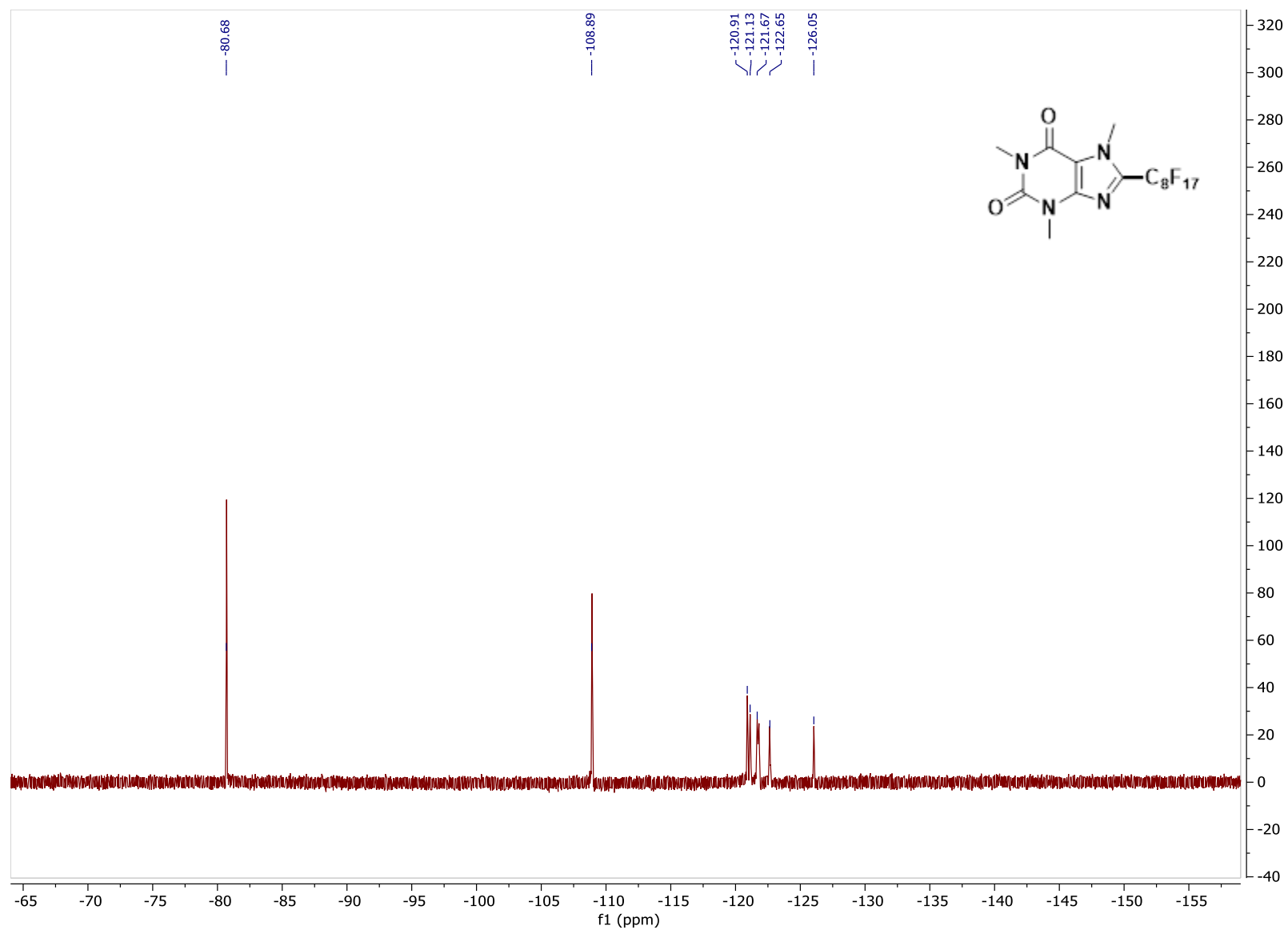
^1H - ^{19}F HMBC of PF12

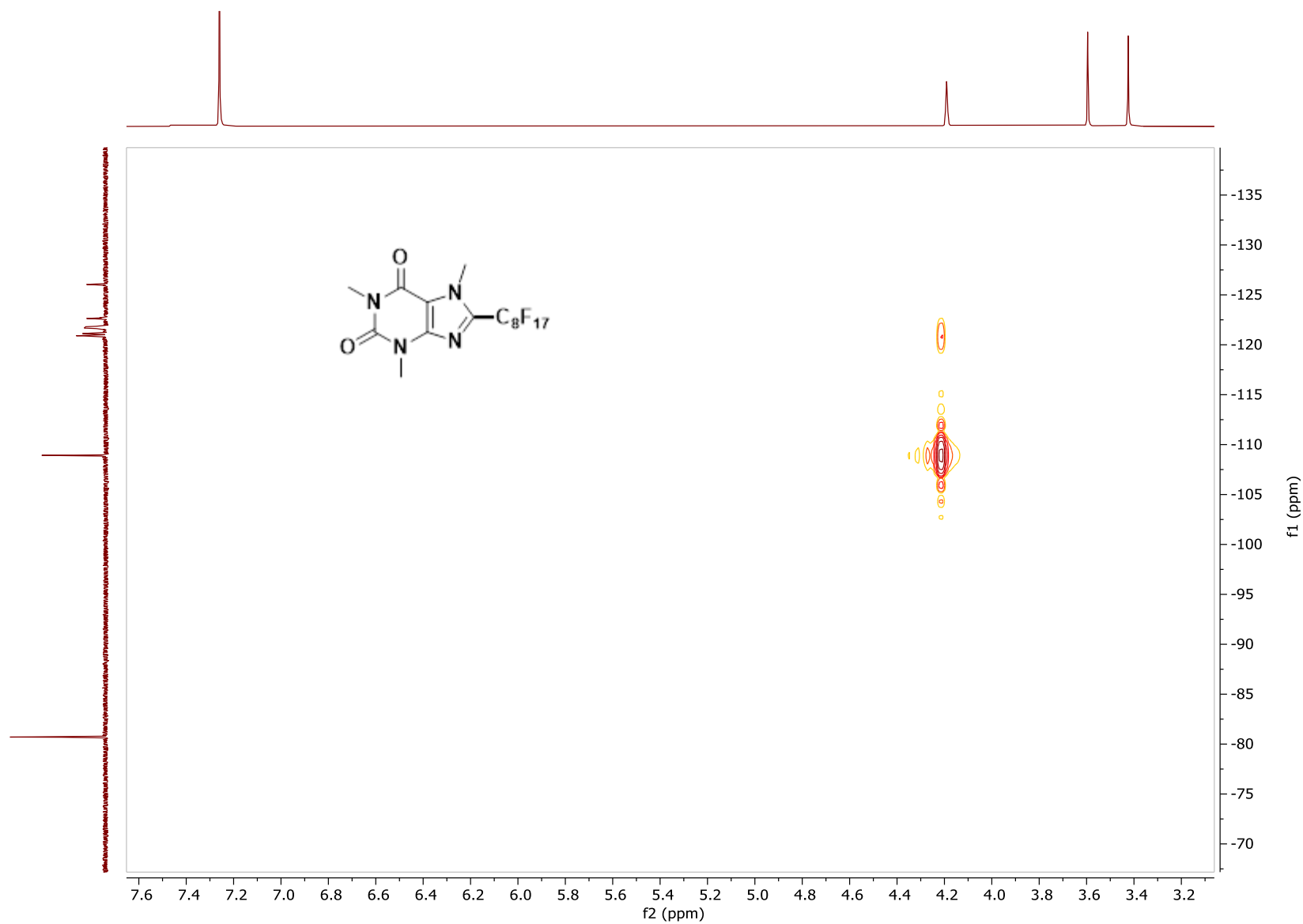
^1H NMR of PF13, CDCl_3 , 500 MHz

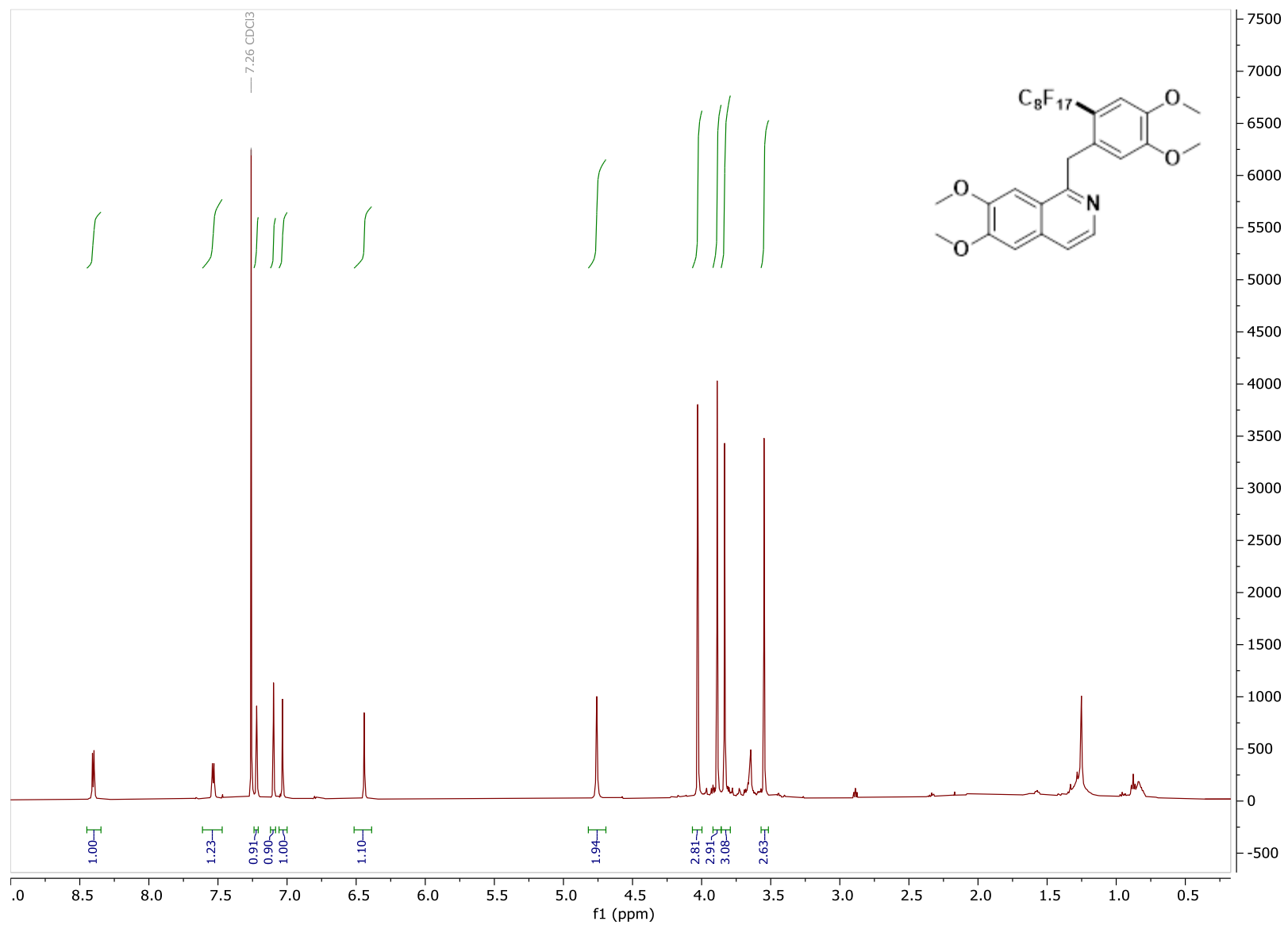
^{13}C NMR of **PF13**, CDCl_3 , 126 MHz



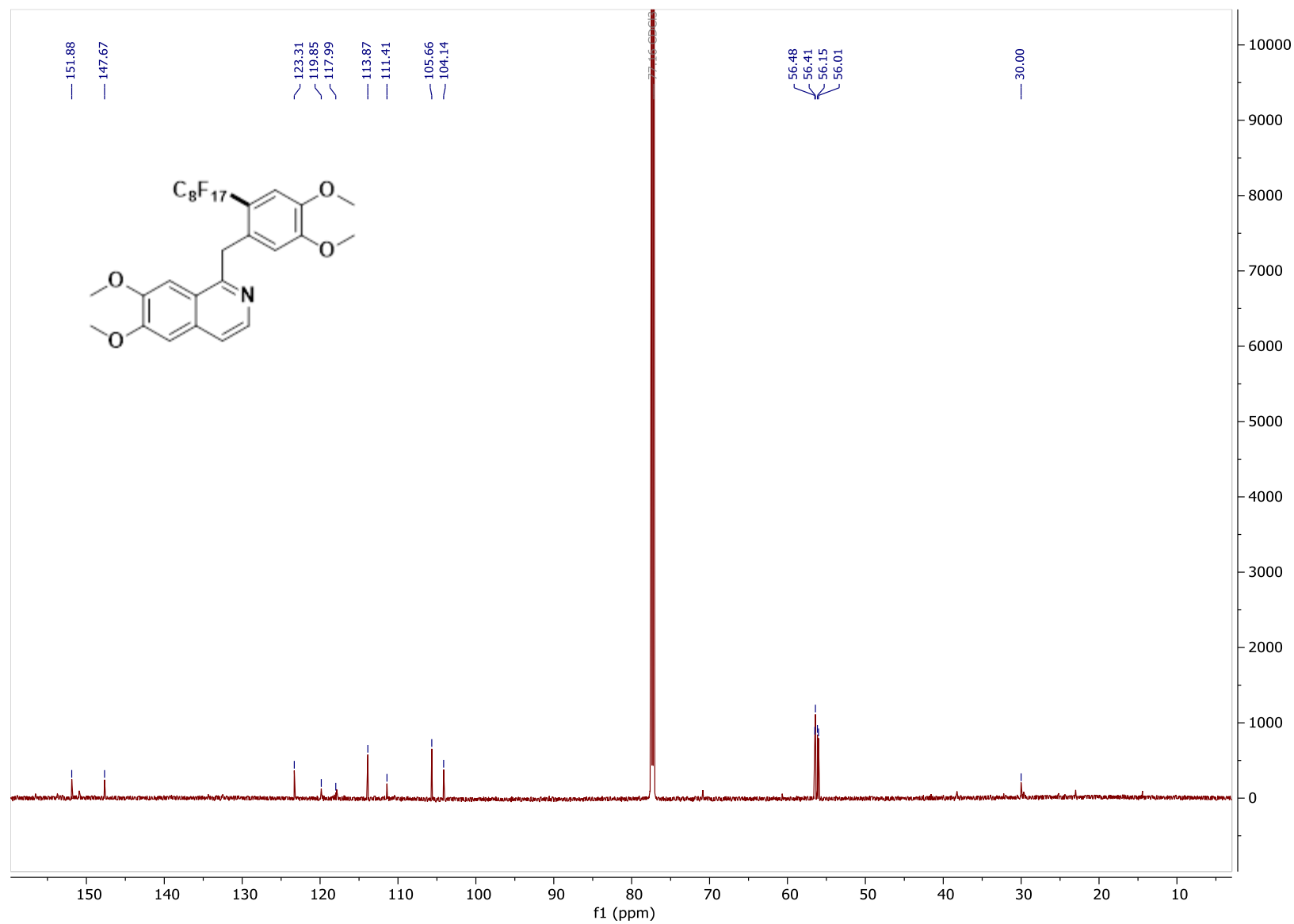
^{19}F NMR of **PF13**, CDCl_3 , 471 MHz



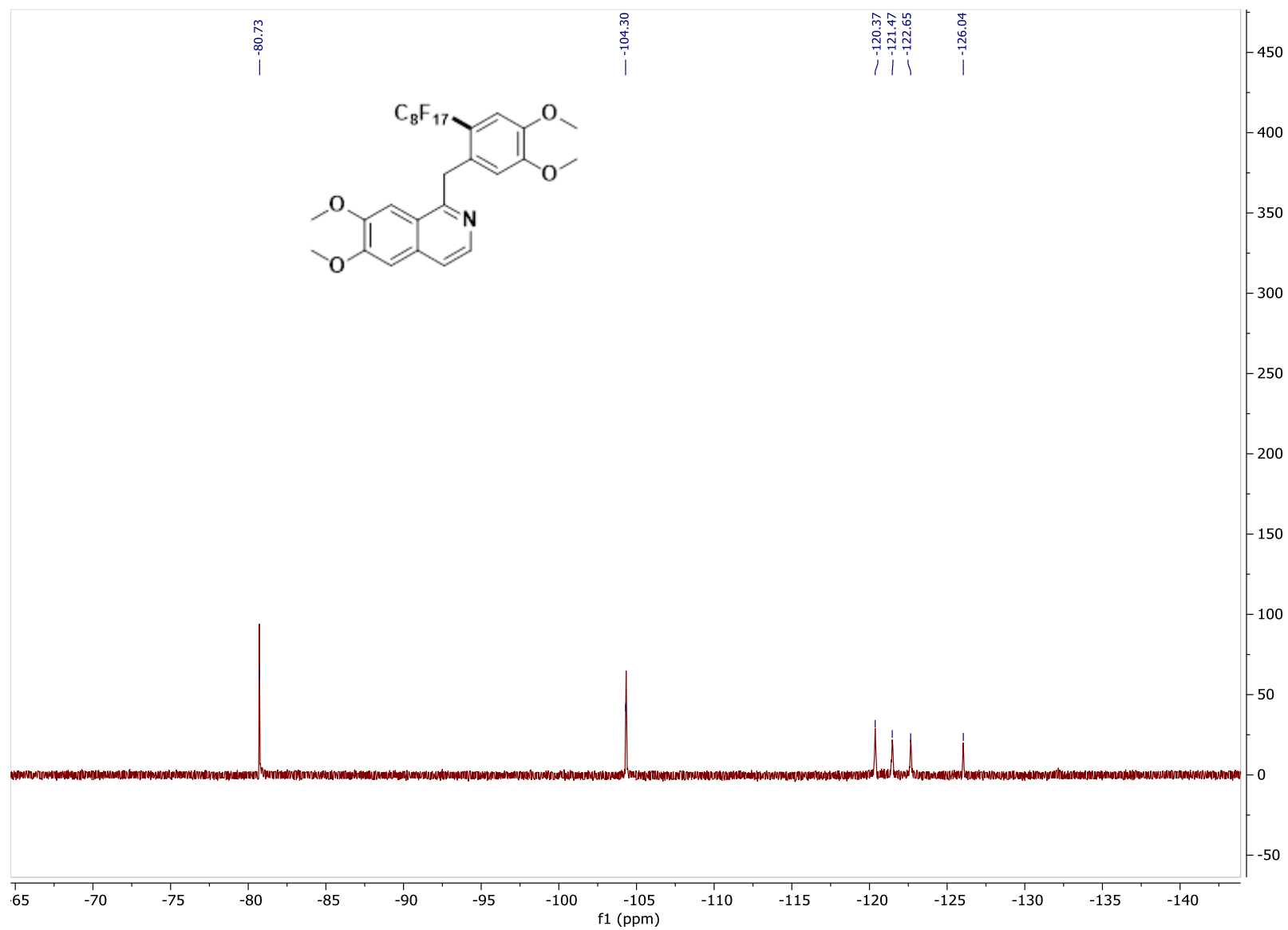
^1H - ^{19}F HMBC of PF13

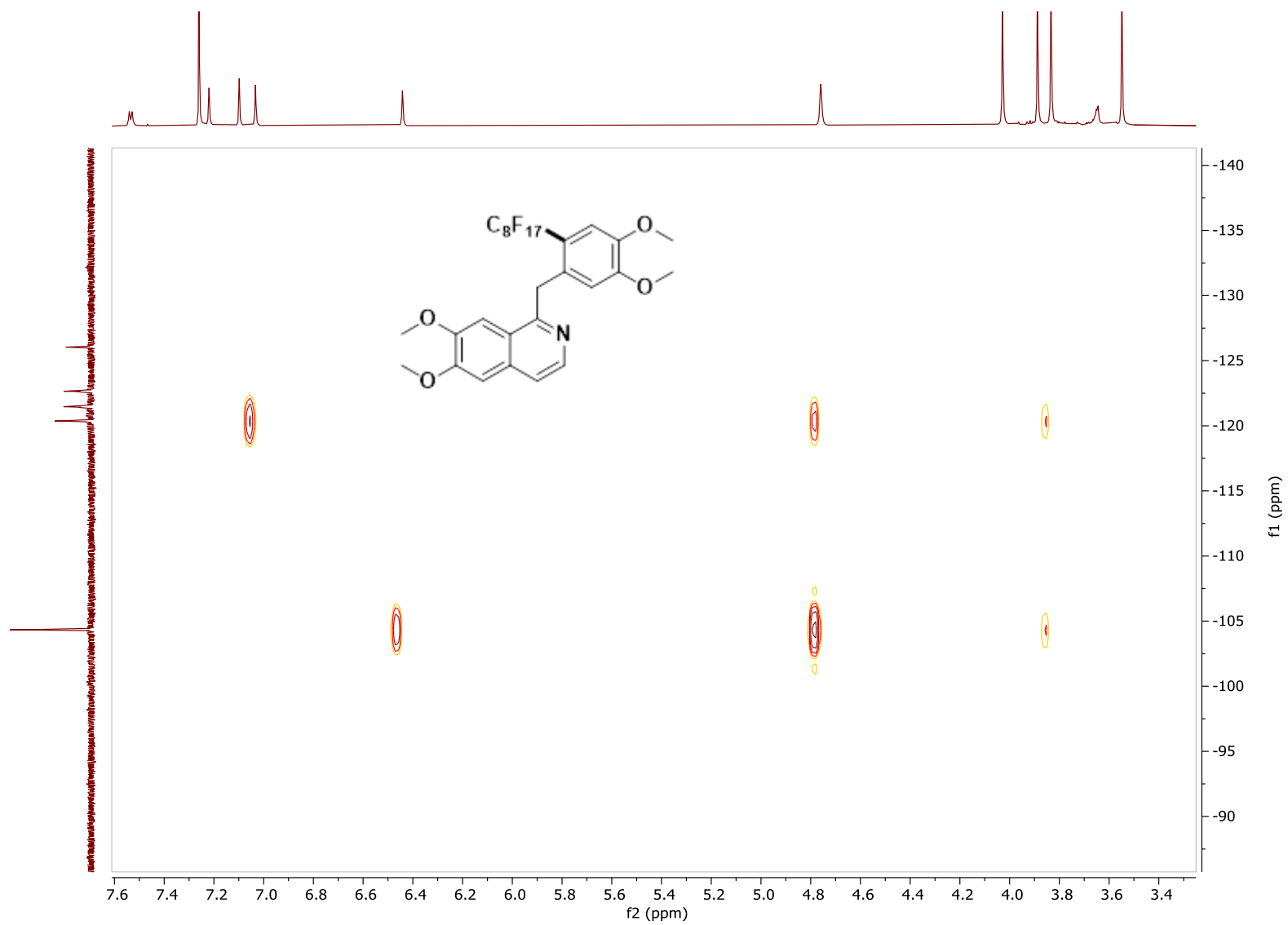
^1H NMR of PF14, CDCl_3 , 500 MHz

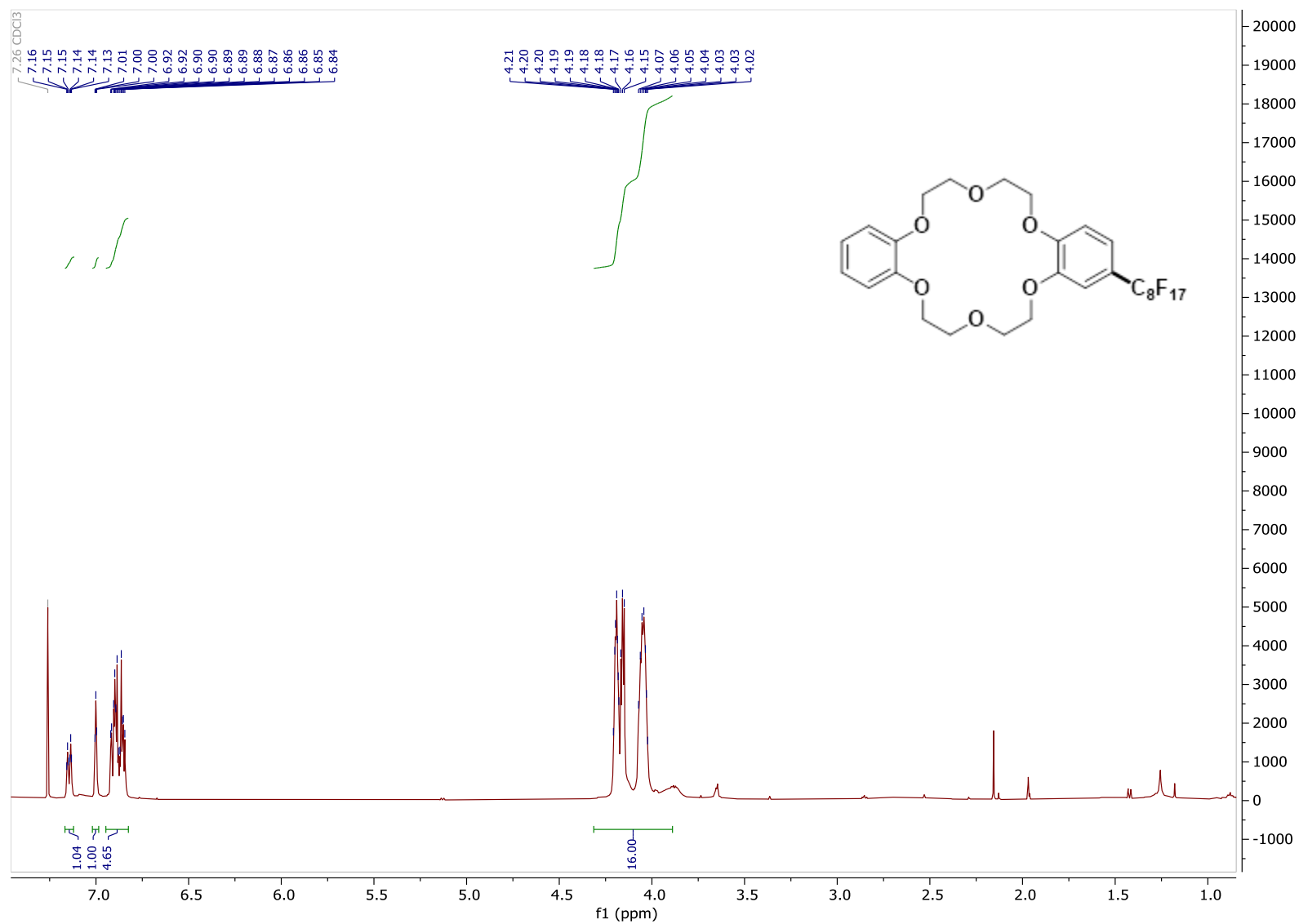
^{13}C NMR of **PF14**, CDCl_3 , 126 MHz



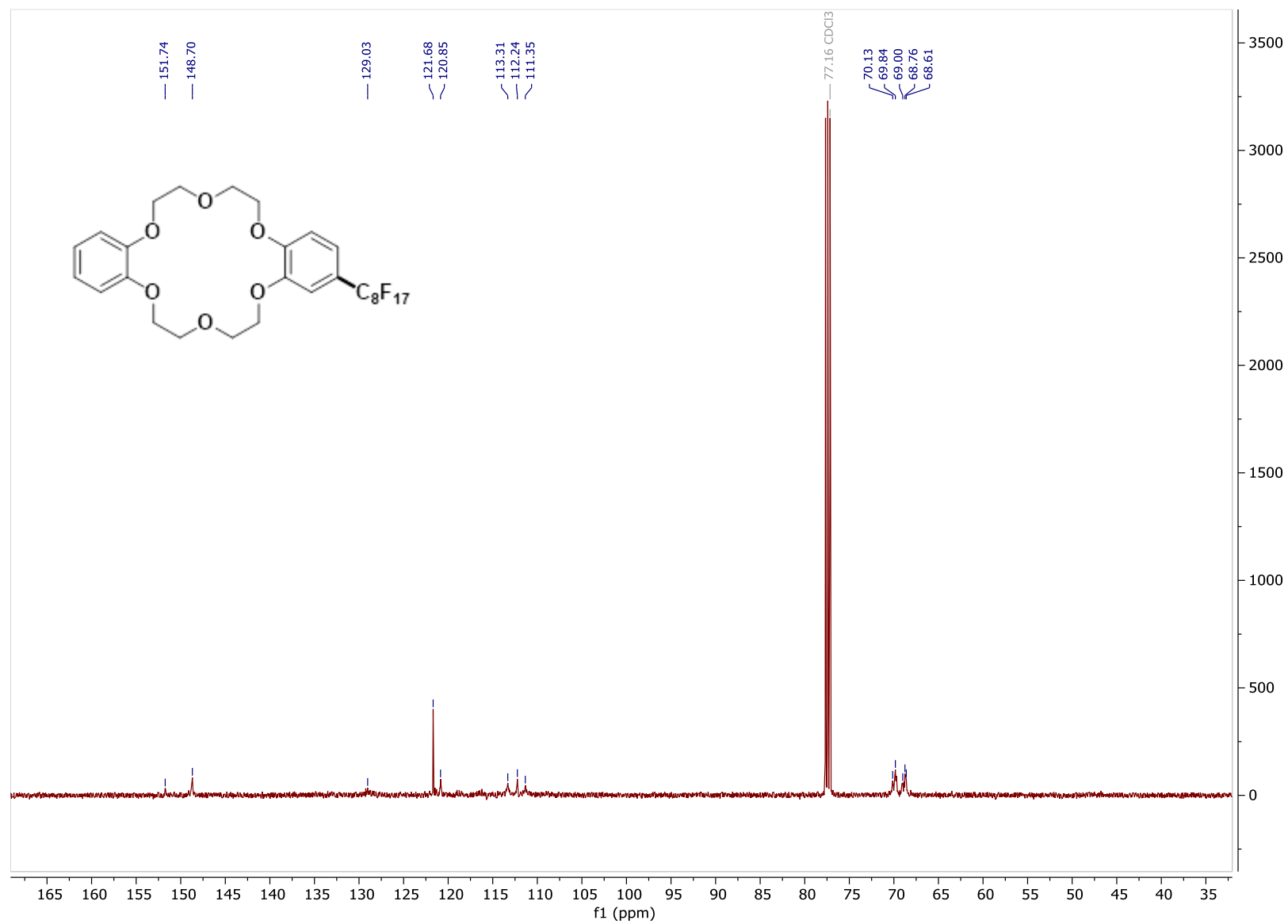
^{19}F NMR of **PF14**, CDCl_3 , 471 MHz



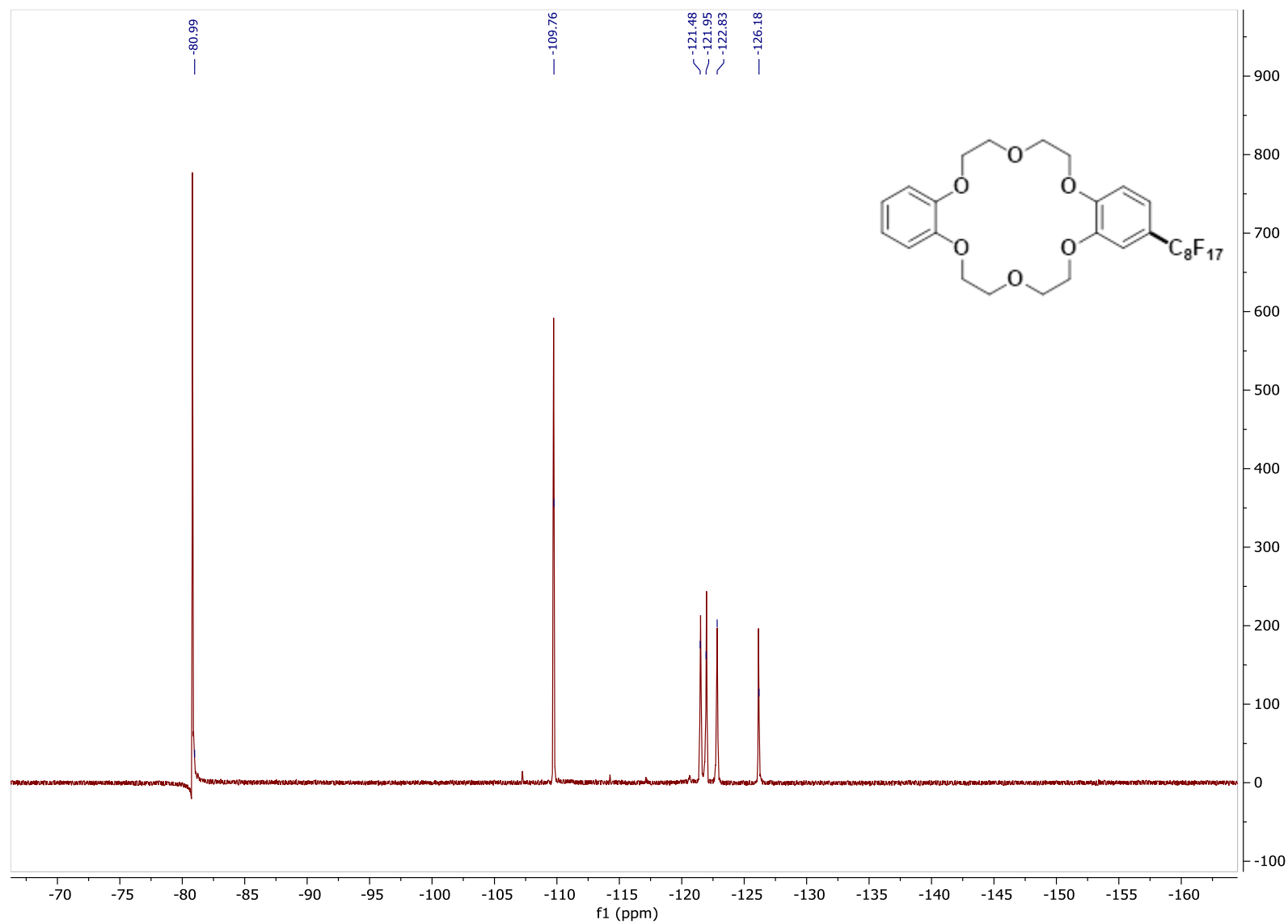
^1H - ^{19}F HMBC of PF14

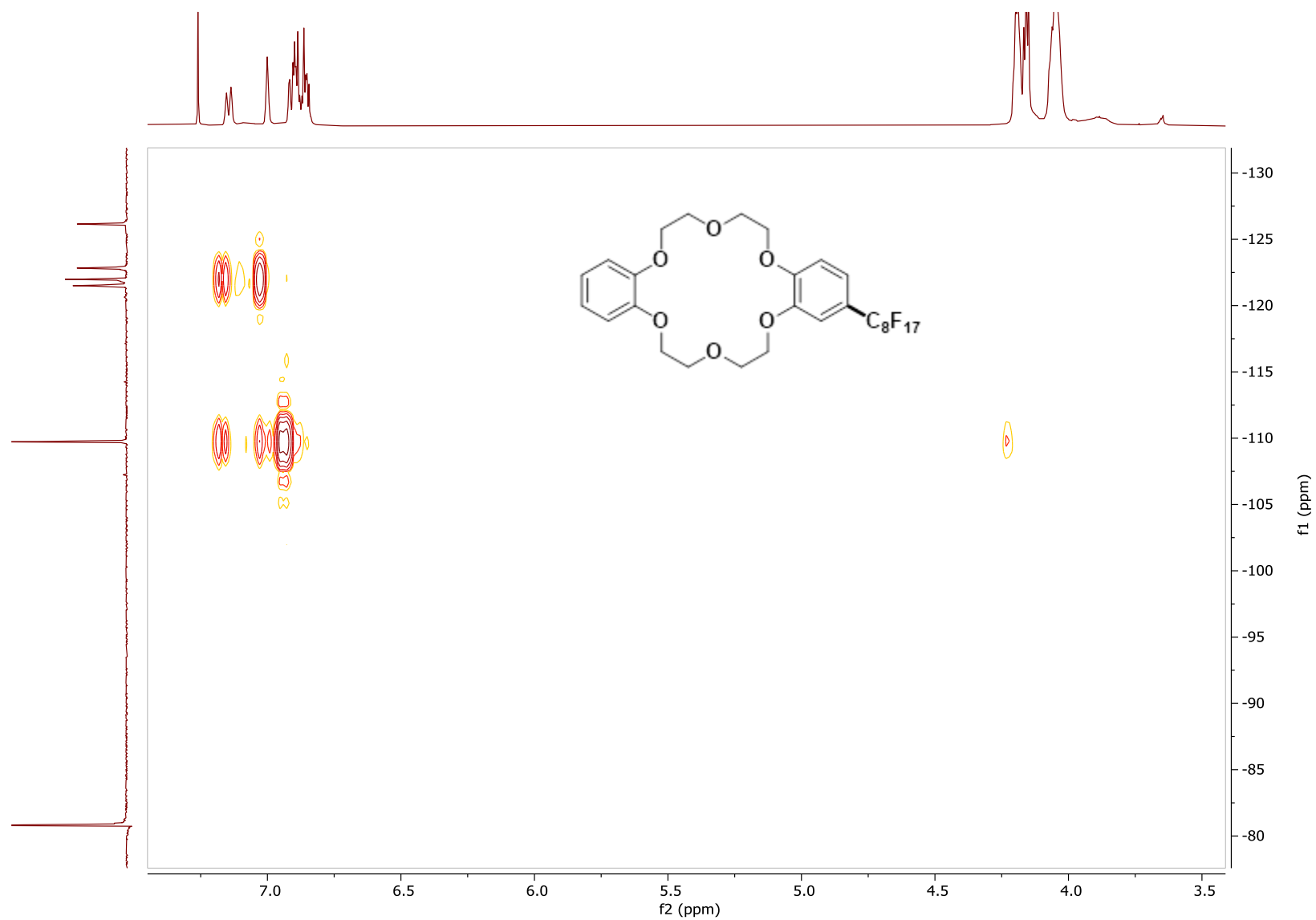
^1H NMR of PF15, CDCl_3 , 500 MHz

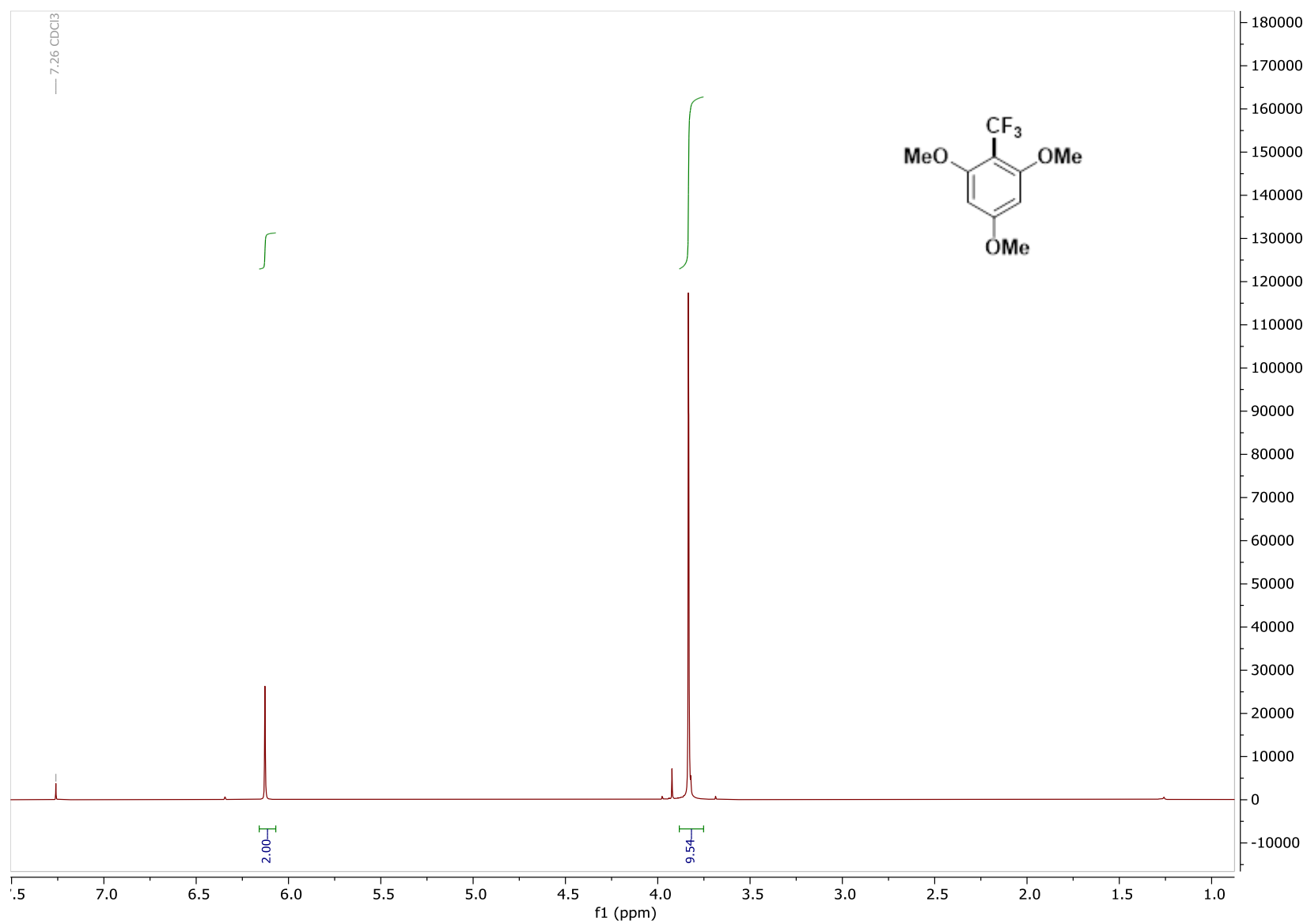
^{13}C NMR of **PF15**, CDCl_3 , 126 MHz



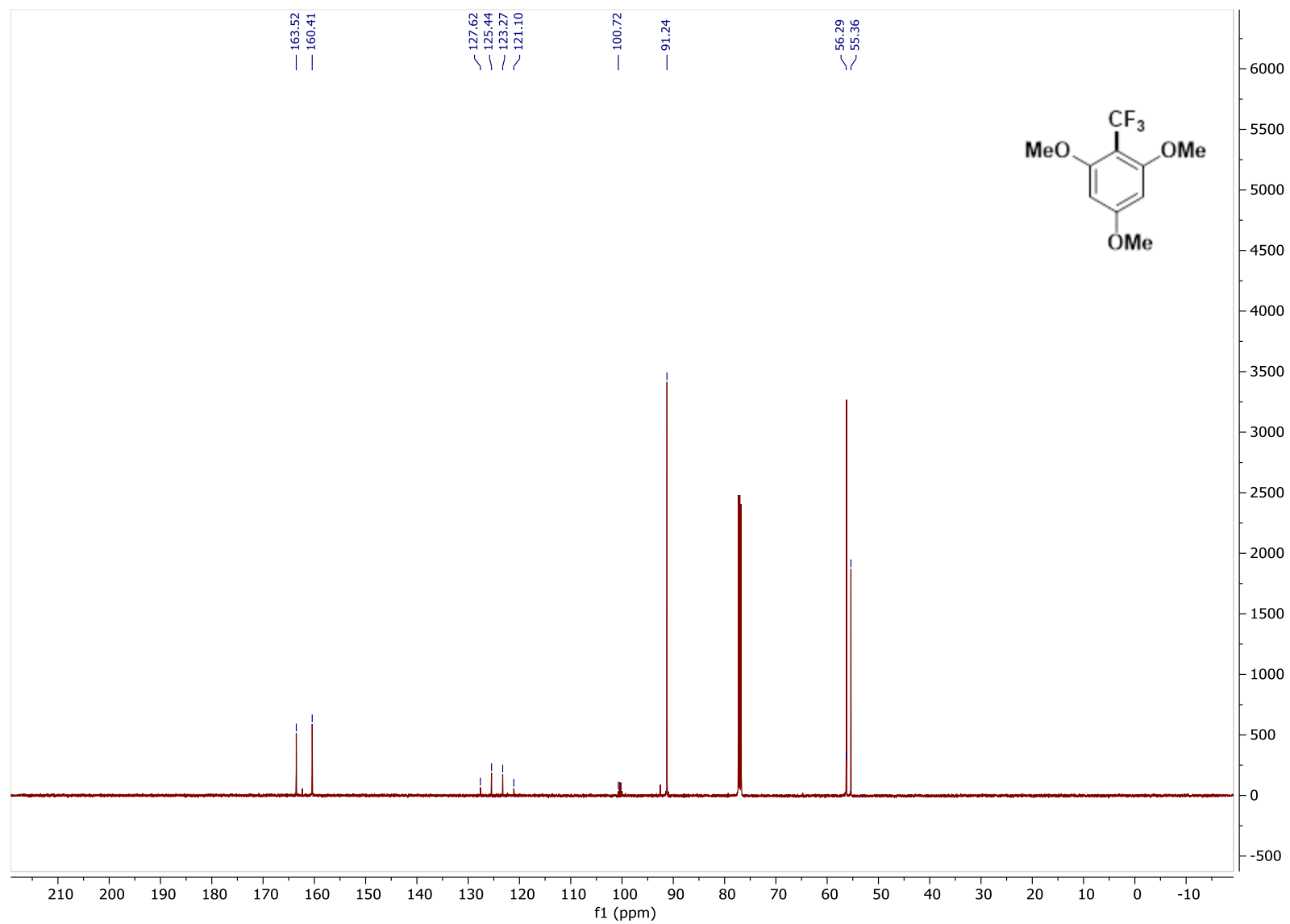
^{19}F NMR of **PF15**, CDCl_3 , 471 MHz



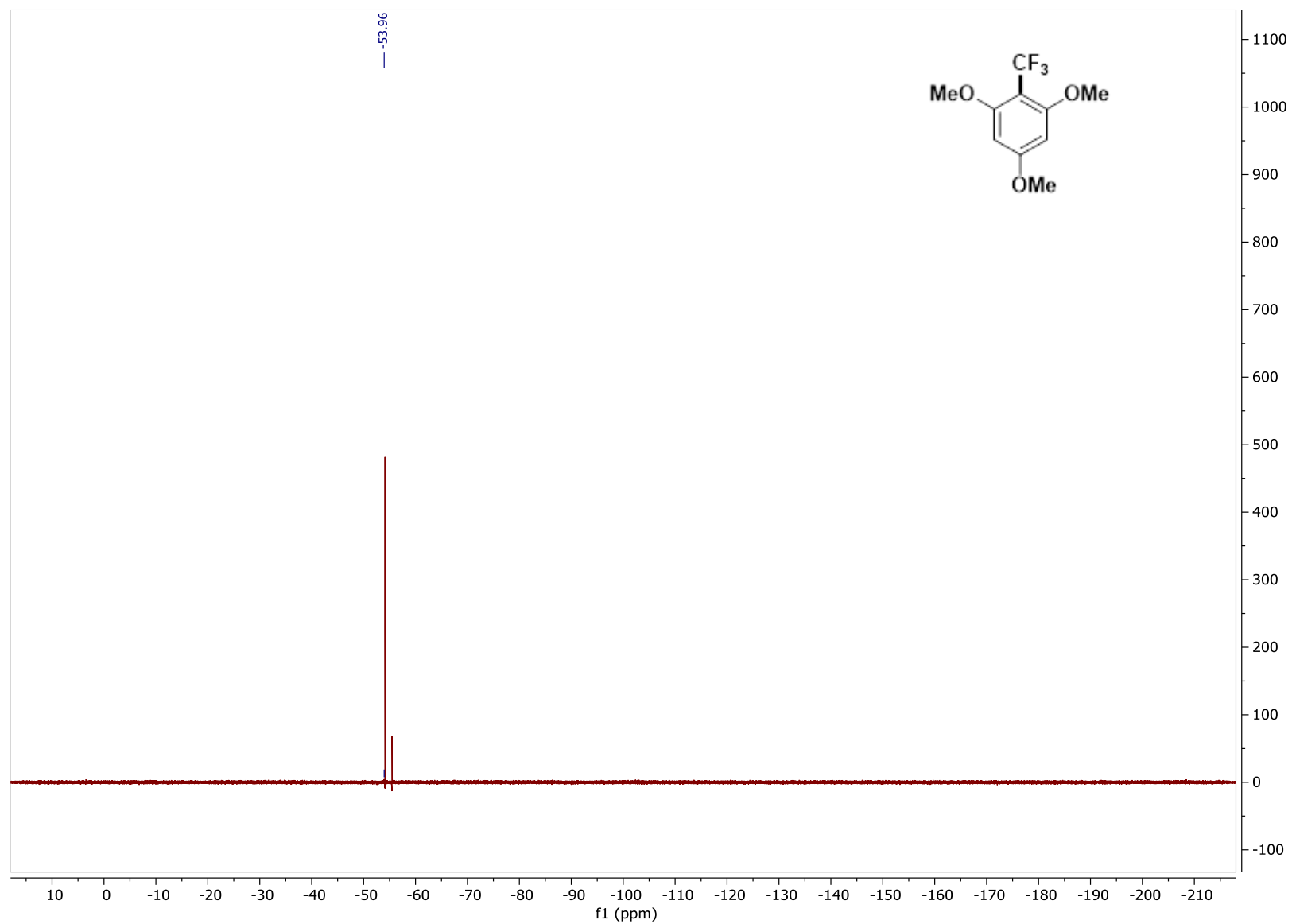
^1H - ^{19}F HMBC of PF15

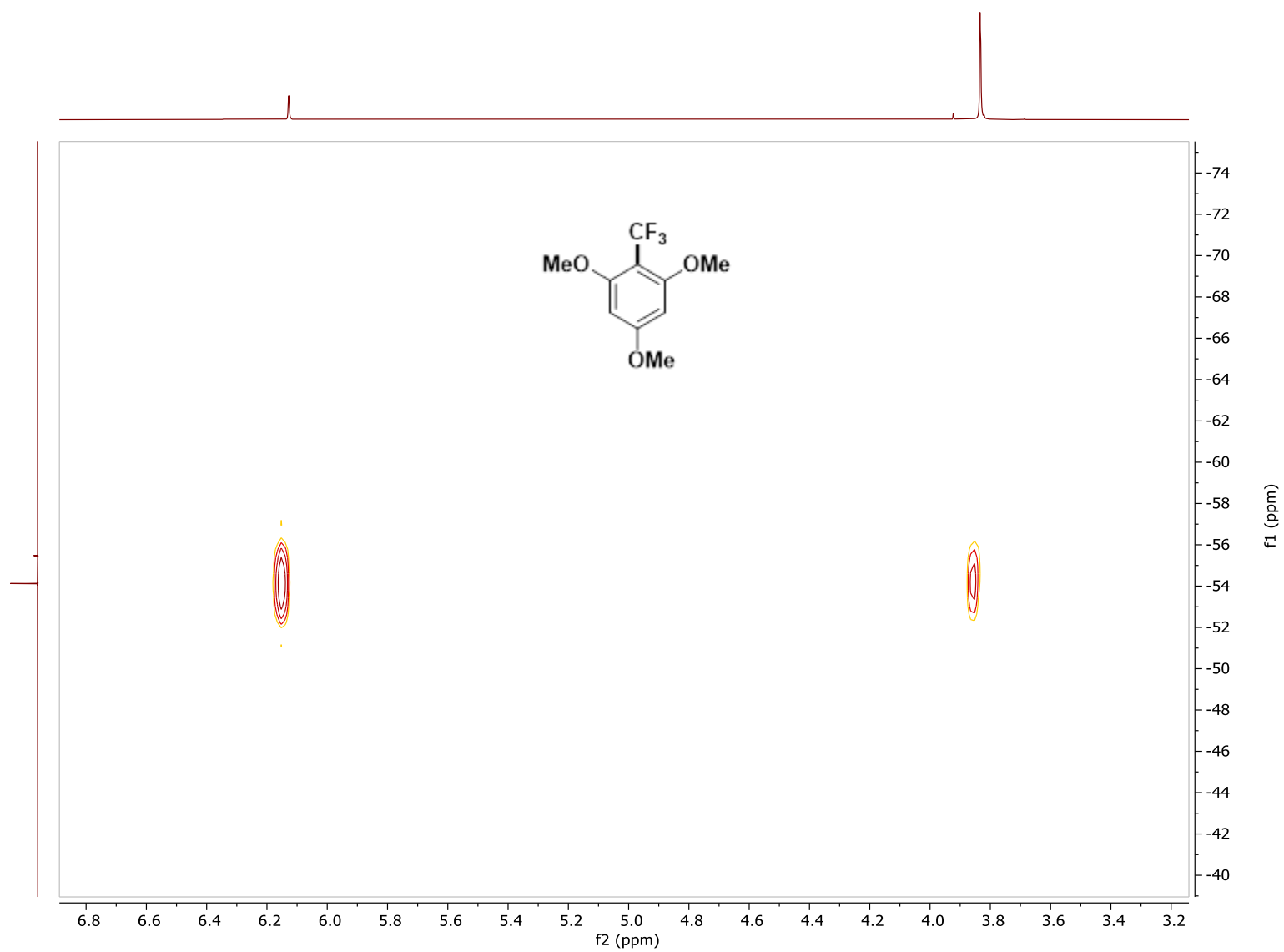
^1H NMR of TF1, CDCl_3 , 500 MHz

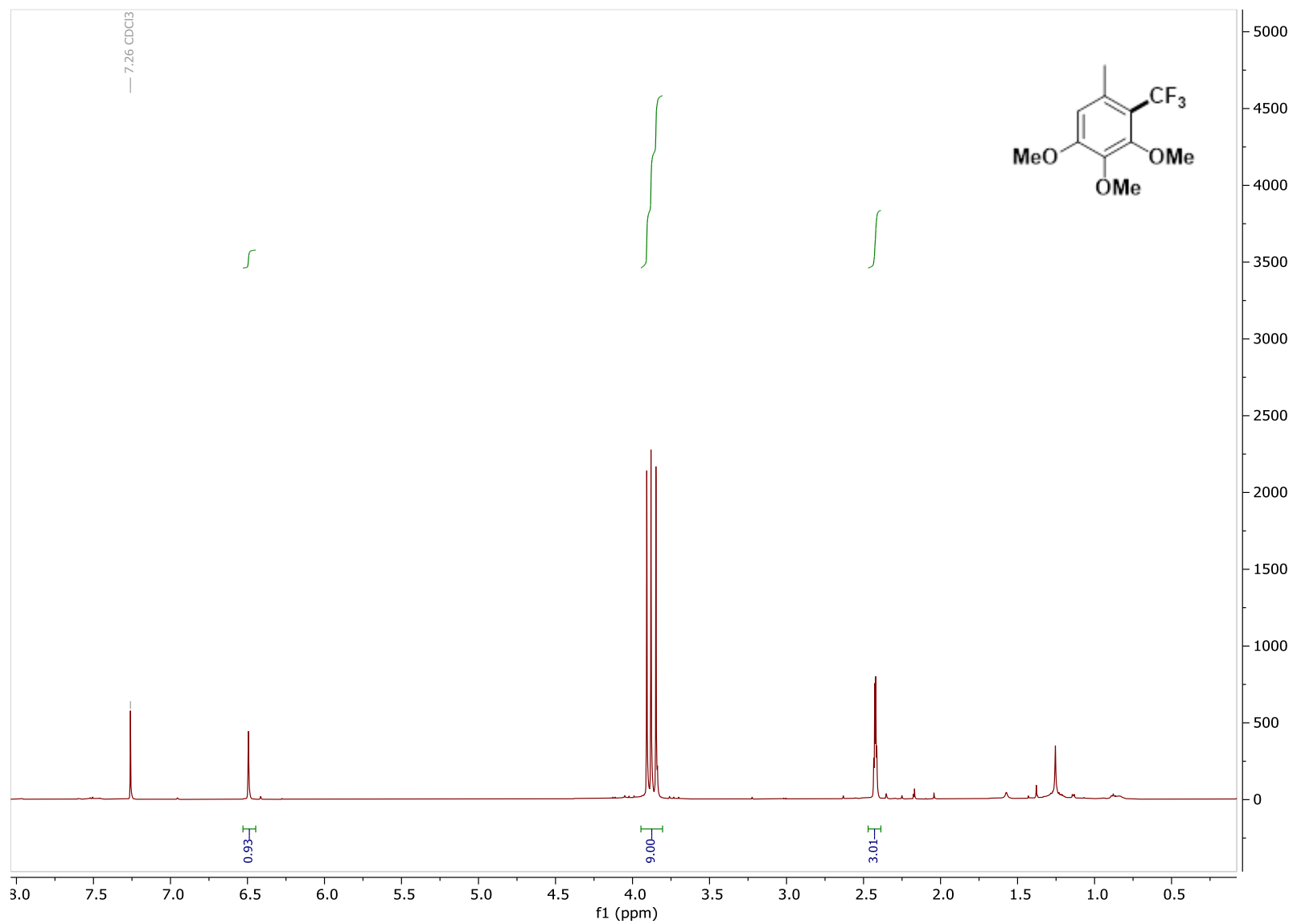
^{13}C NMR of TF1, CDCl_3 , 126 MHz



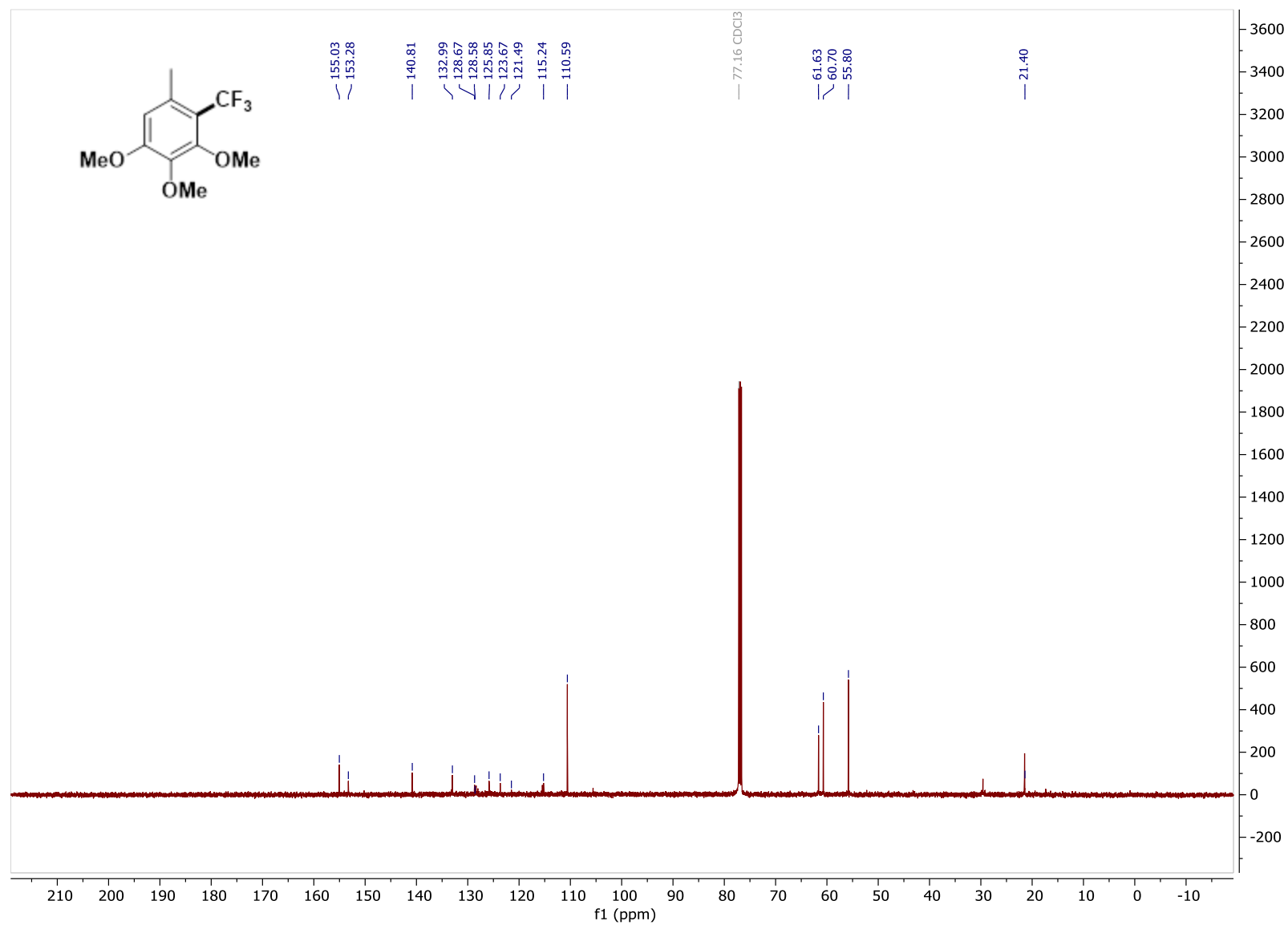
^{19}F NMR of **TF1**, CDCl_3 , 471 MHz



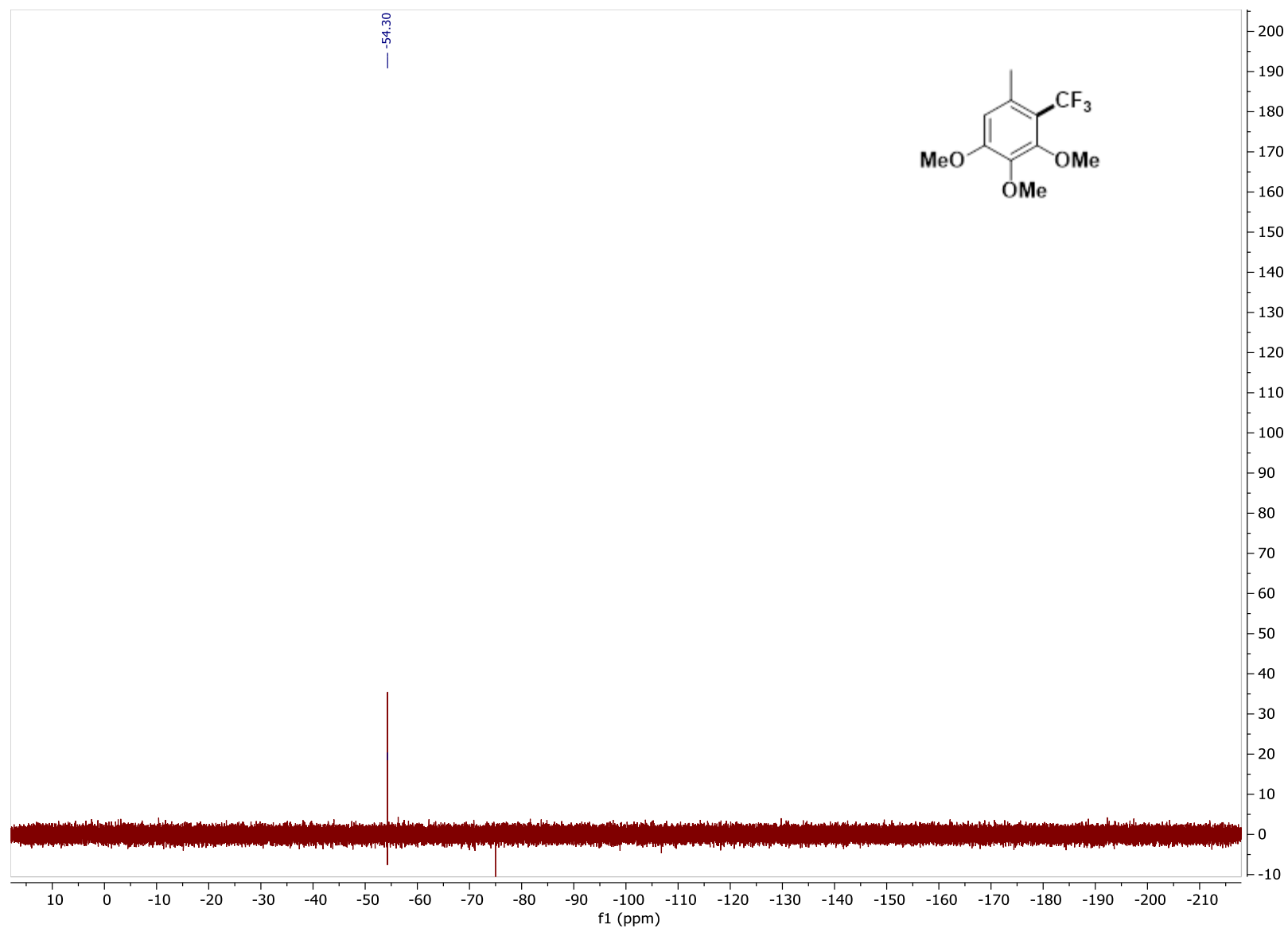
^1H - ^{19}F HMBC of TF1

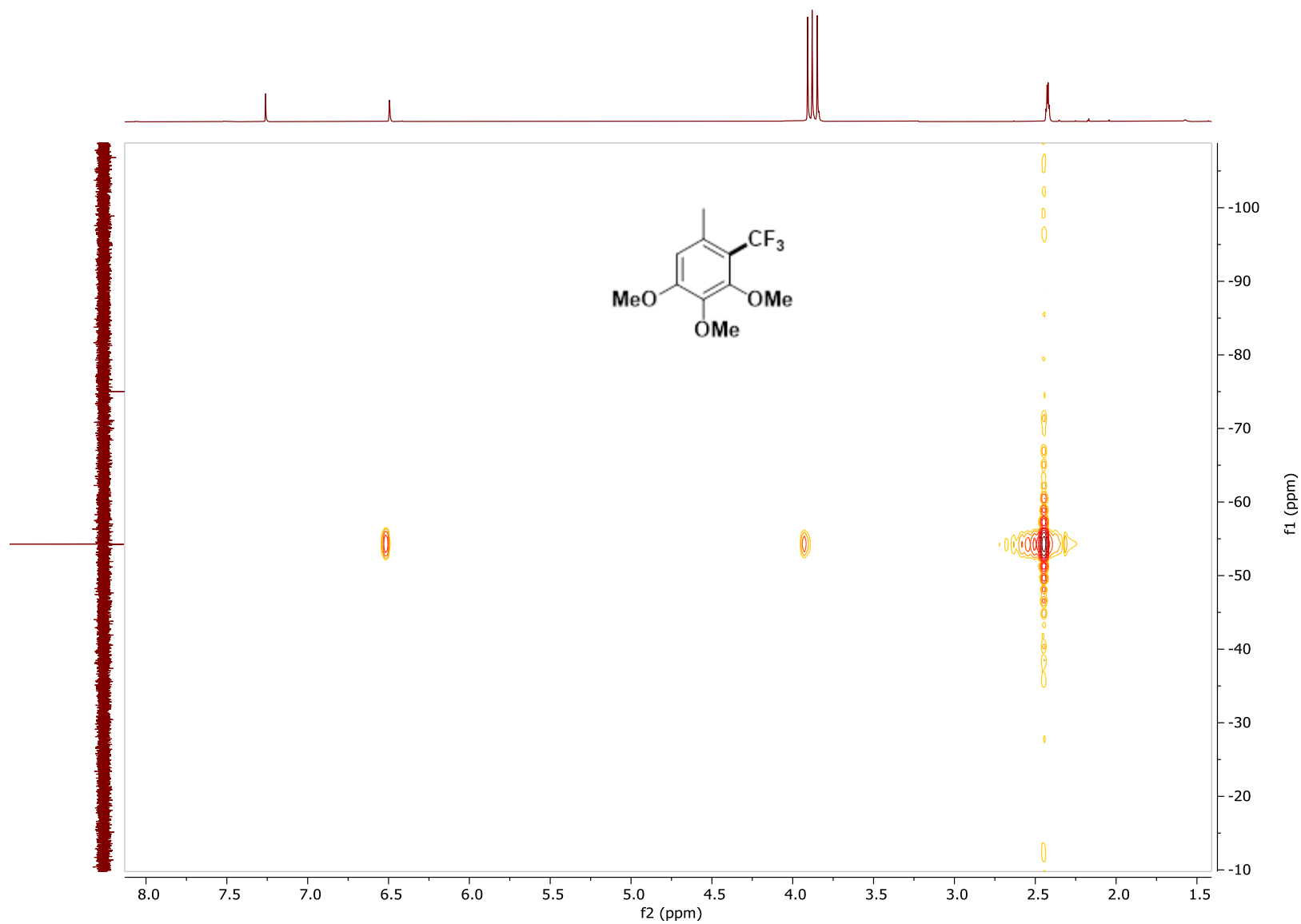
^1H NMR of **TF2**, CDCl_3 , 500 MHz

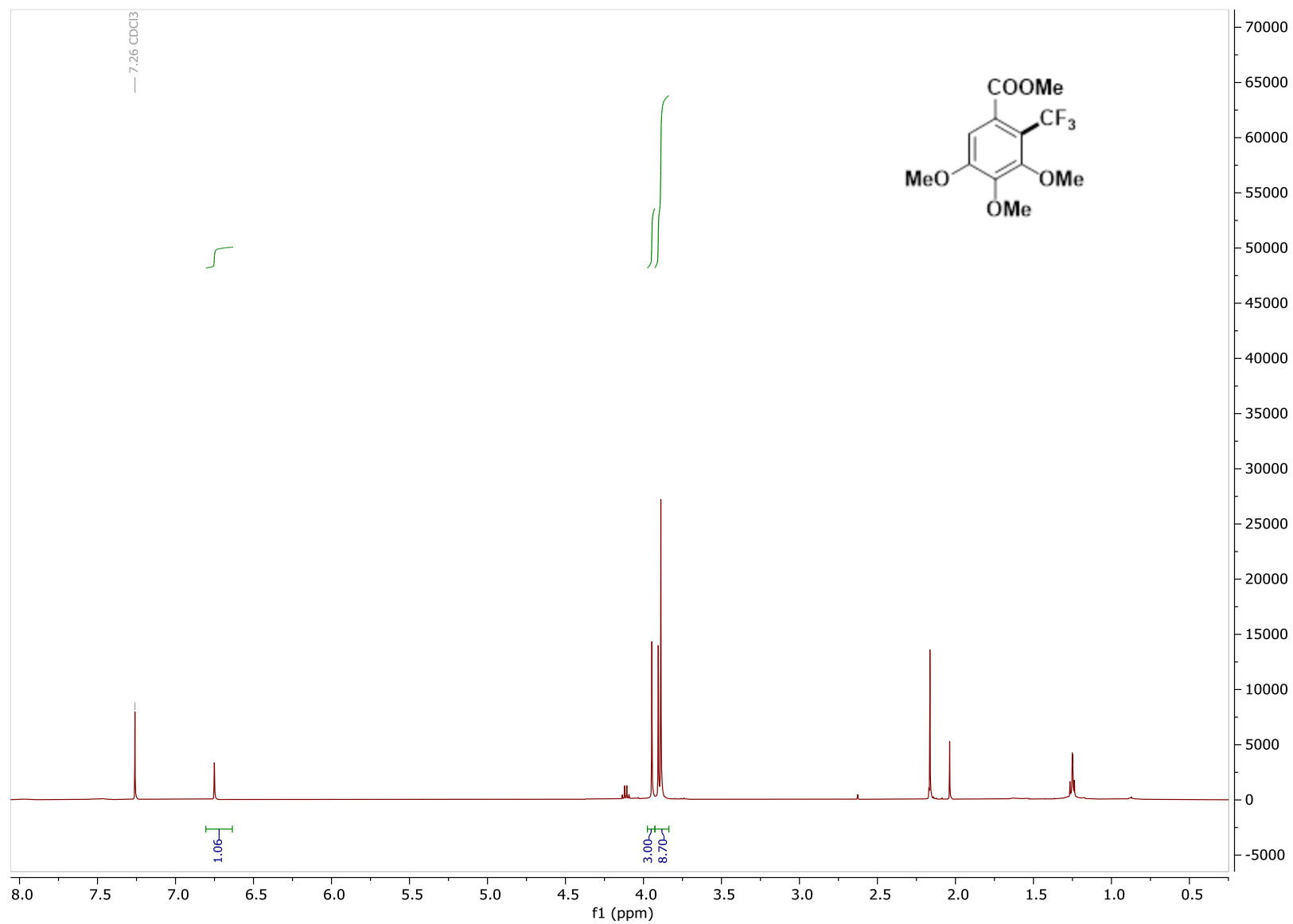
^{13}C NMR of TF2, CDCl_3 , 126 MHz

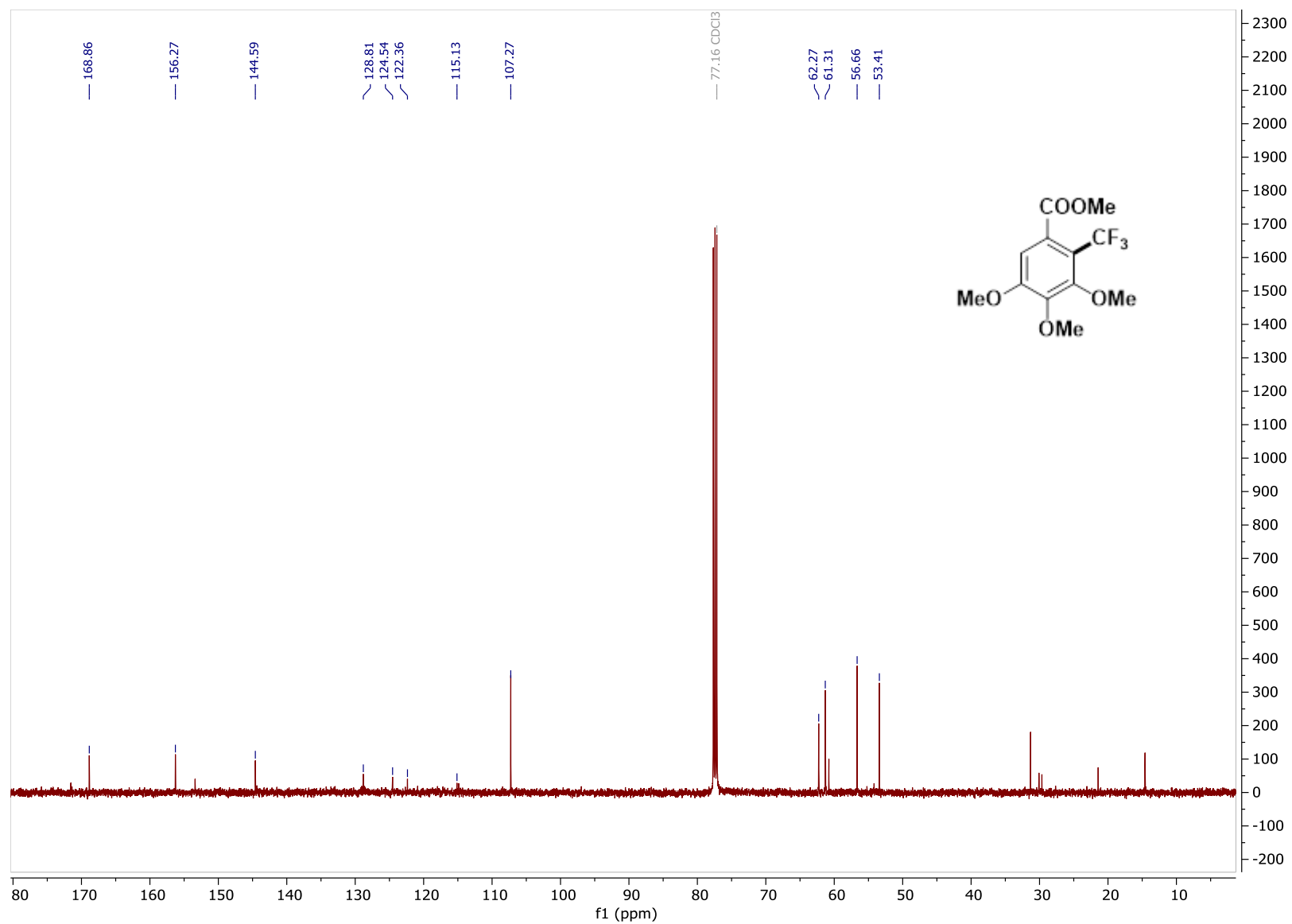


^{19}F NMR of **TF2**, CDCl_3 , 471 MHz

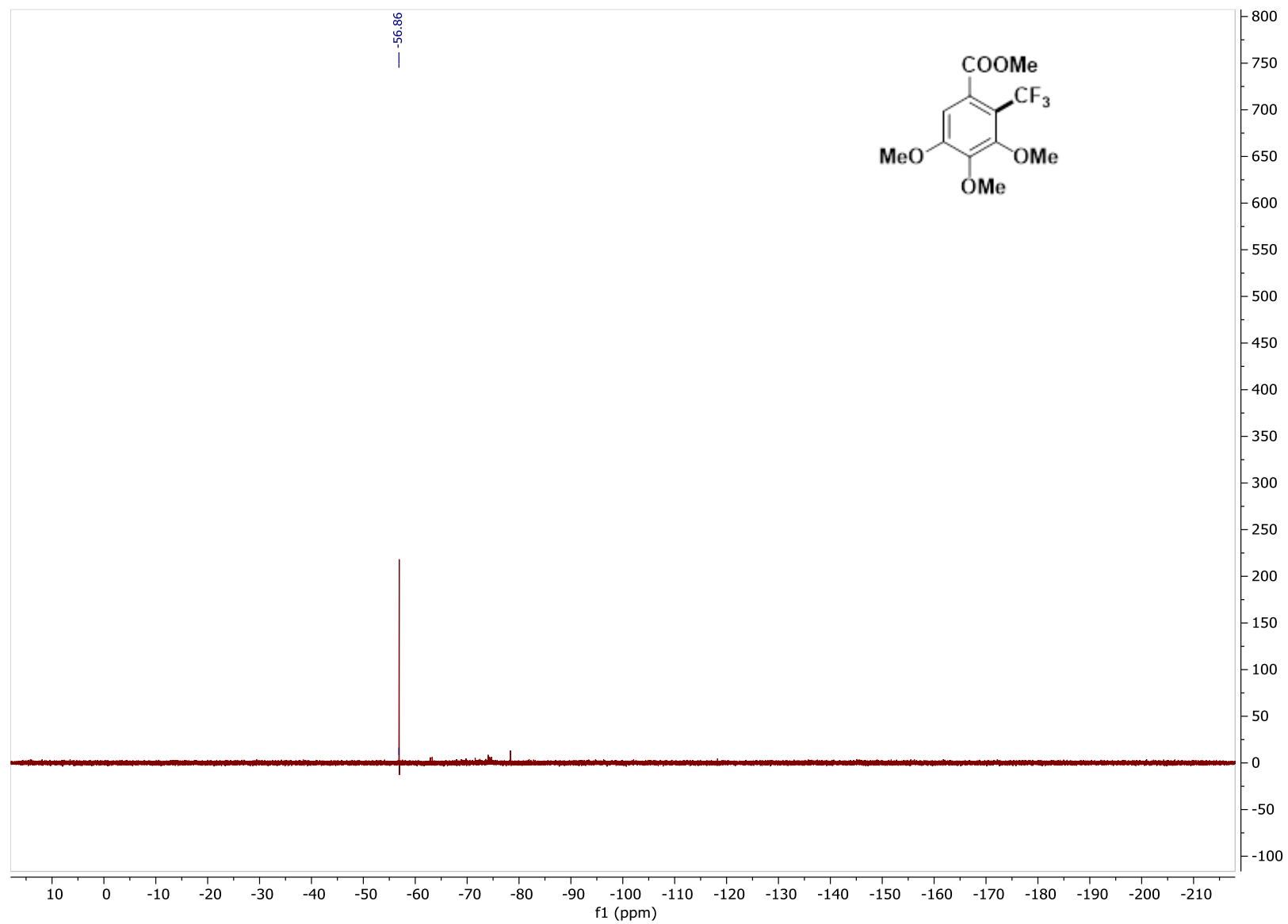


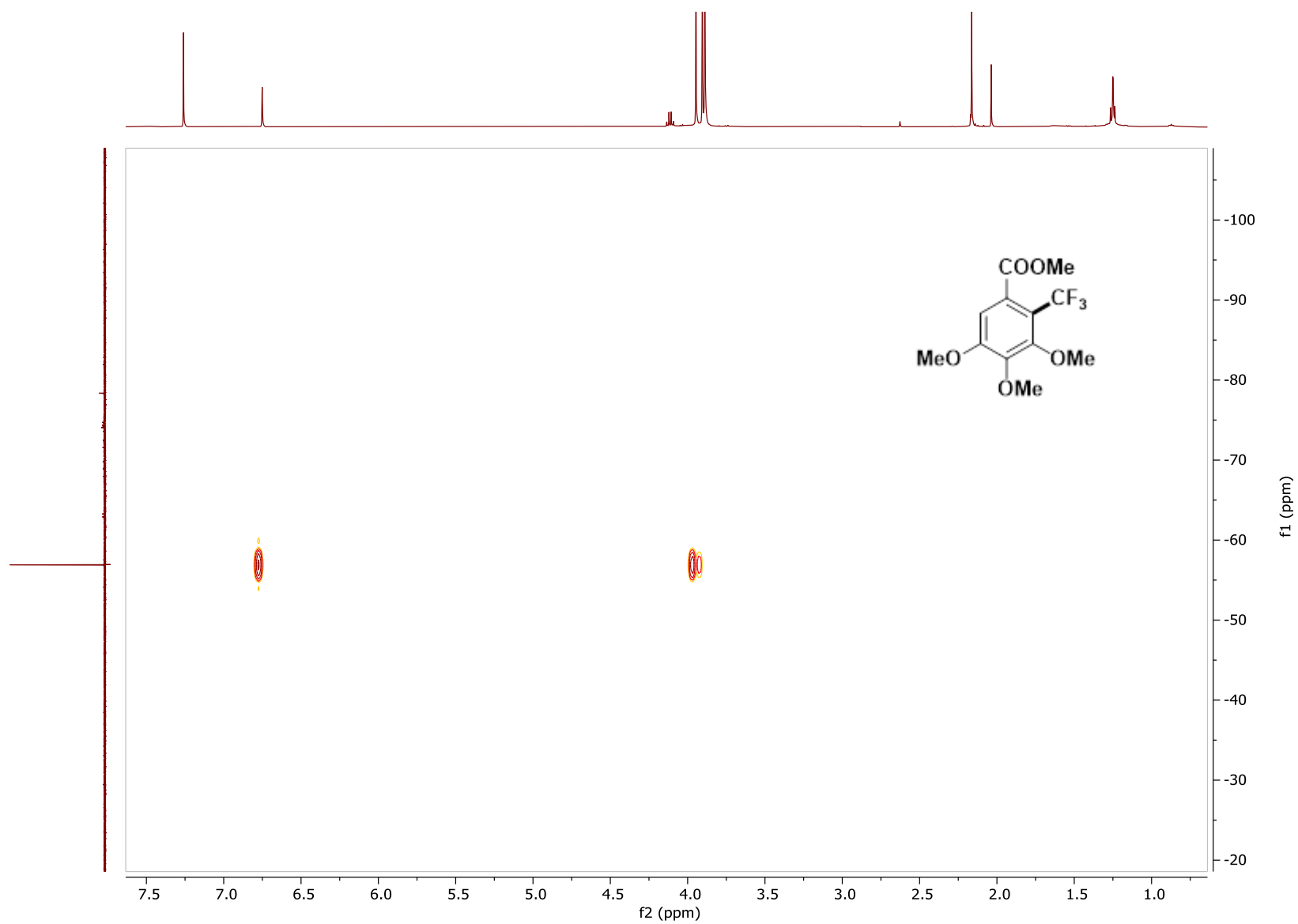
^1H - ^{19}F HMBC of TF2

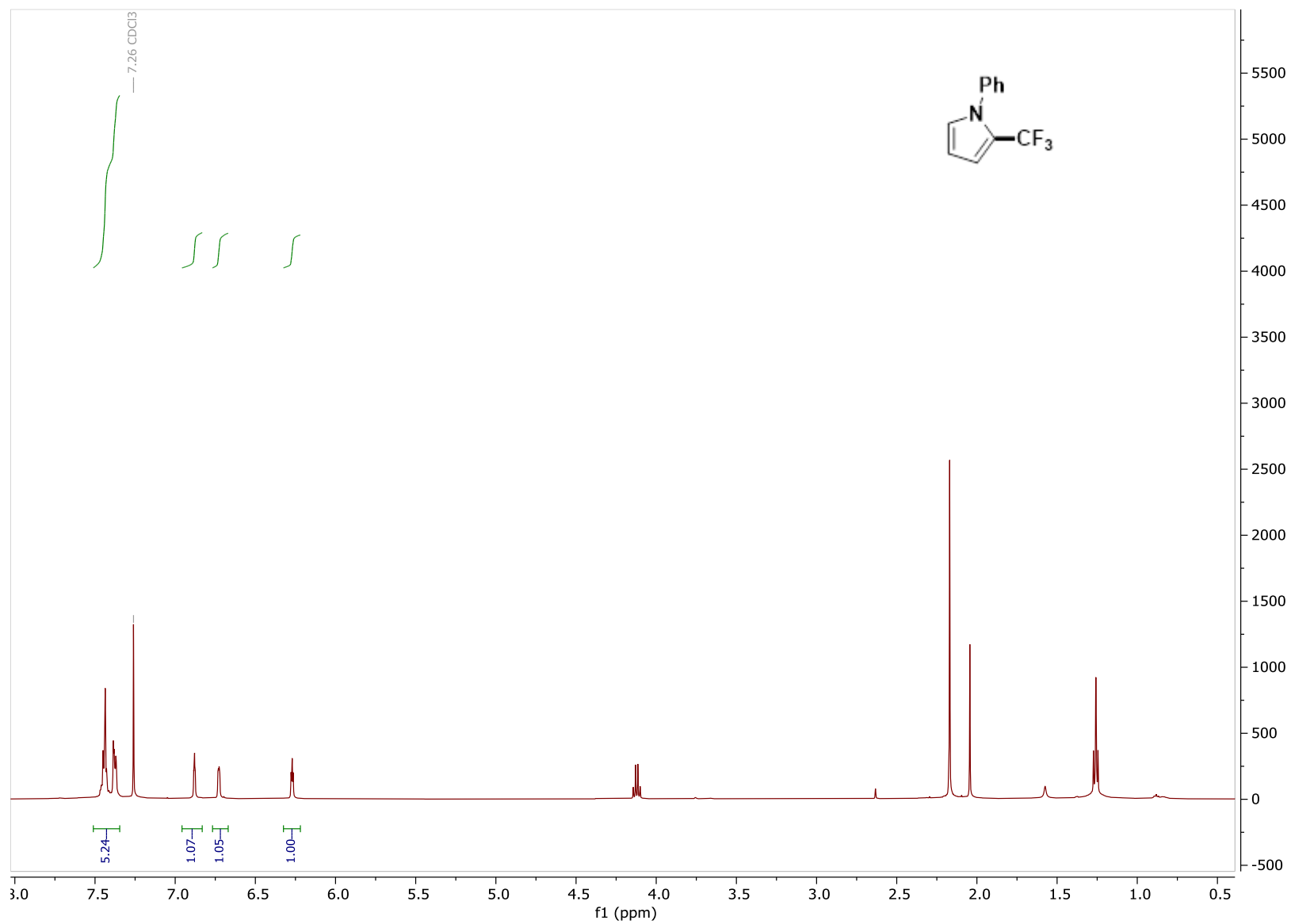
^1H NMR of **TF3**, CDCl_3 , 500 MHz

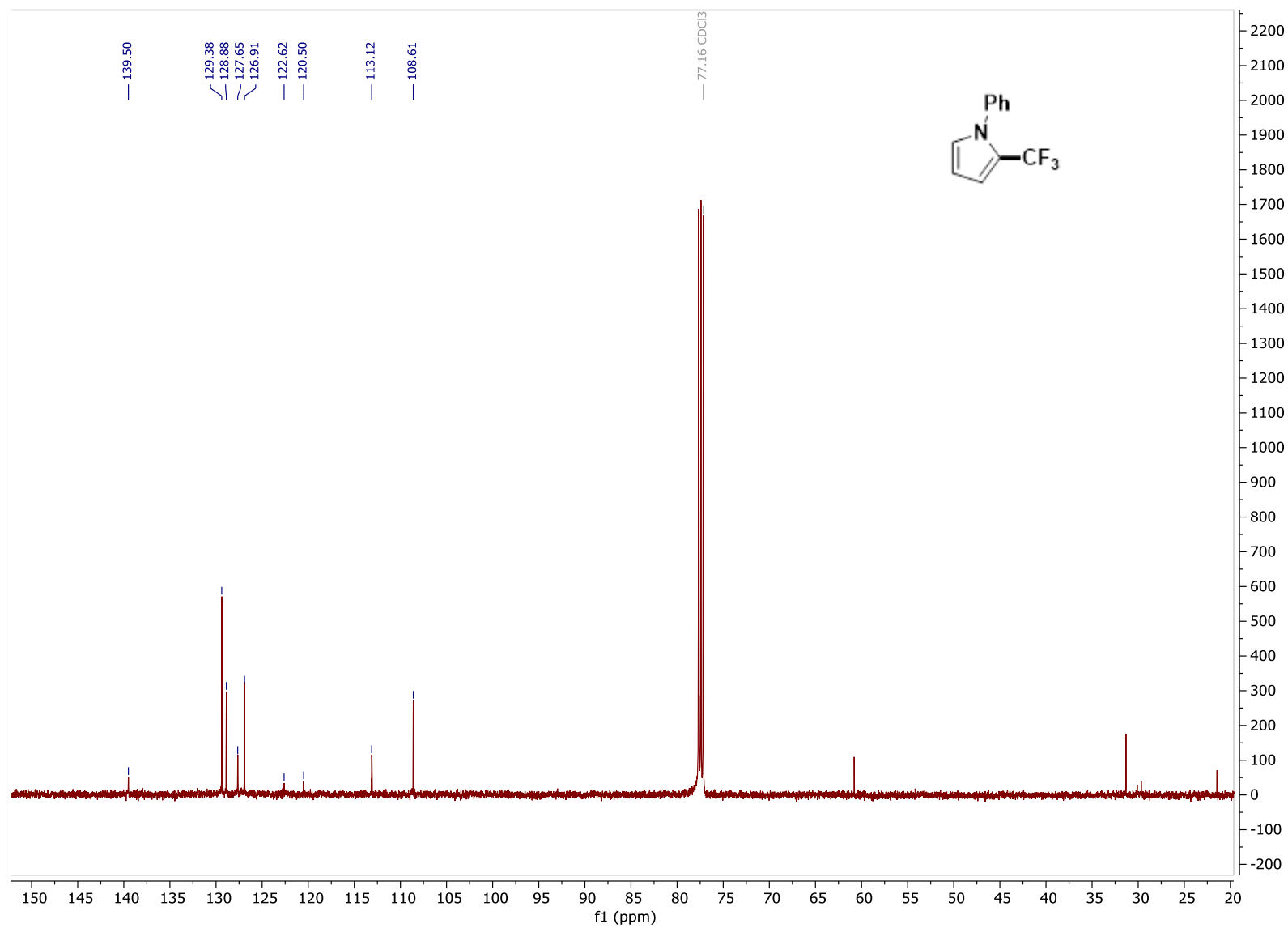
^{13}C NMR of TF3, CDCl_3 , 126 MHz

^{19}F NMR of **TF3**, CDCl_3 , 471 MHz

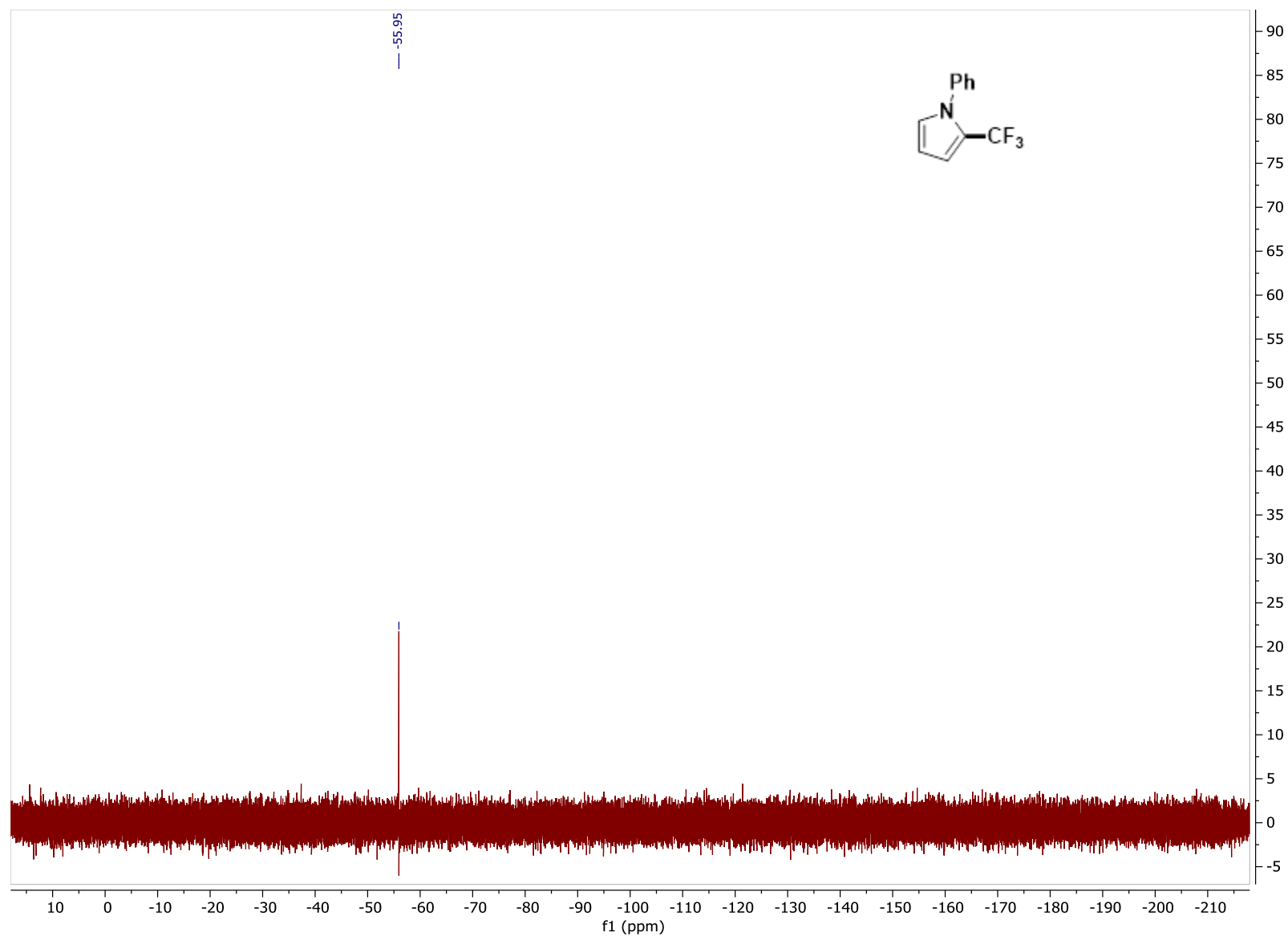


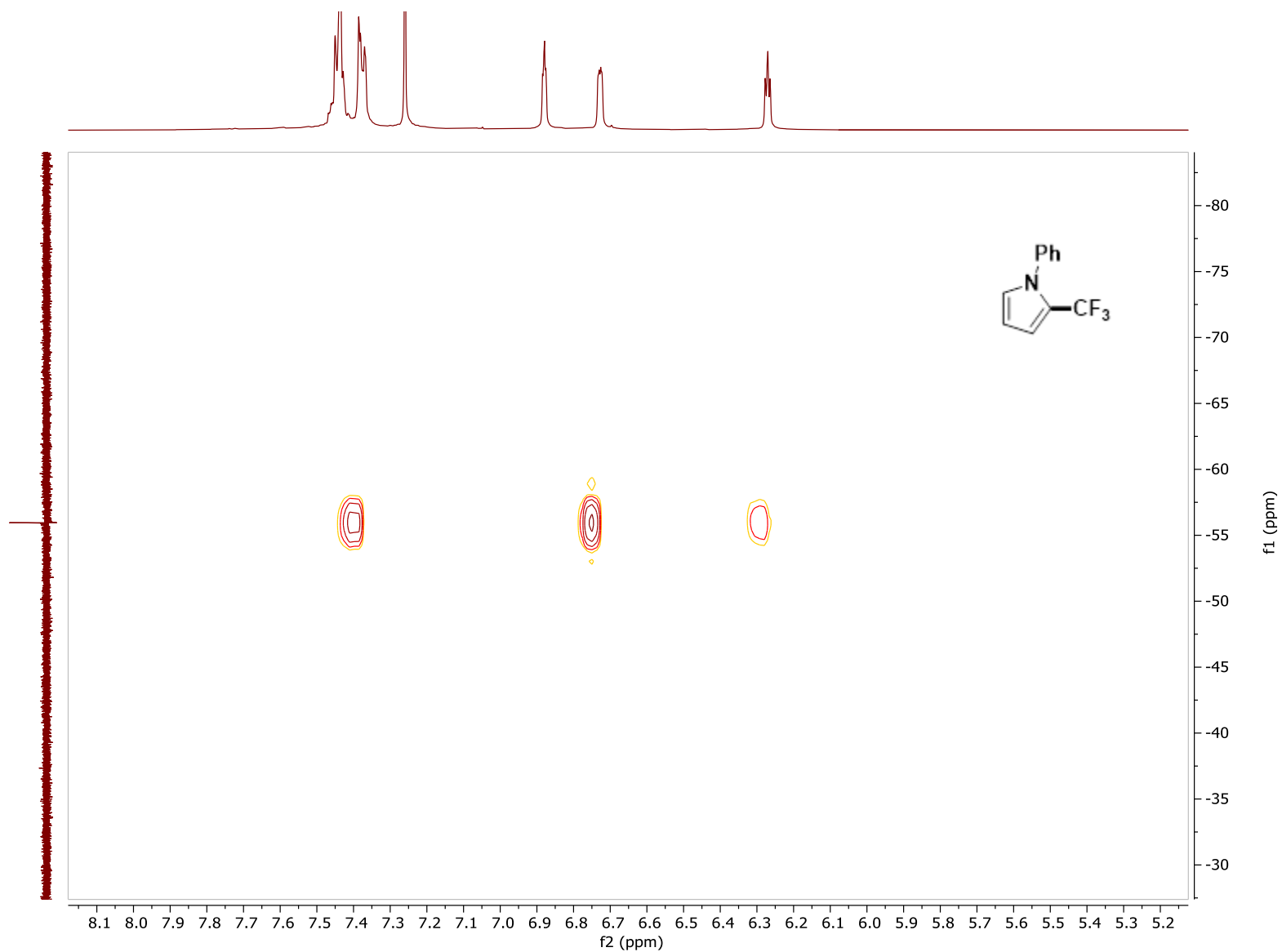
^1H - ^{19}F HMBC of TF3

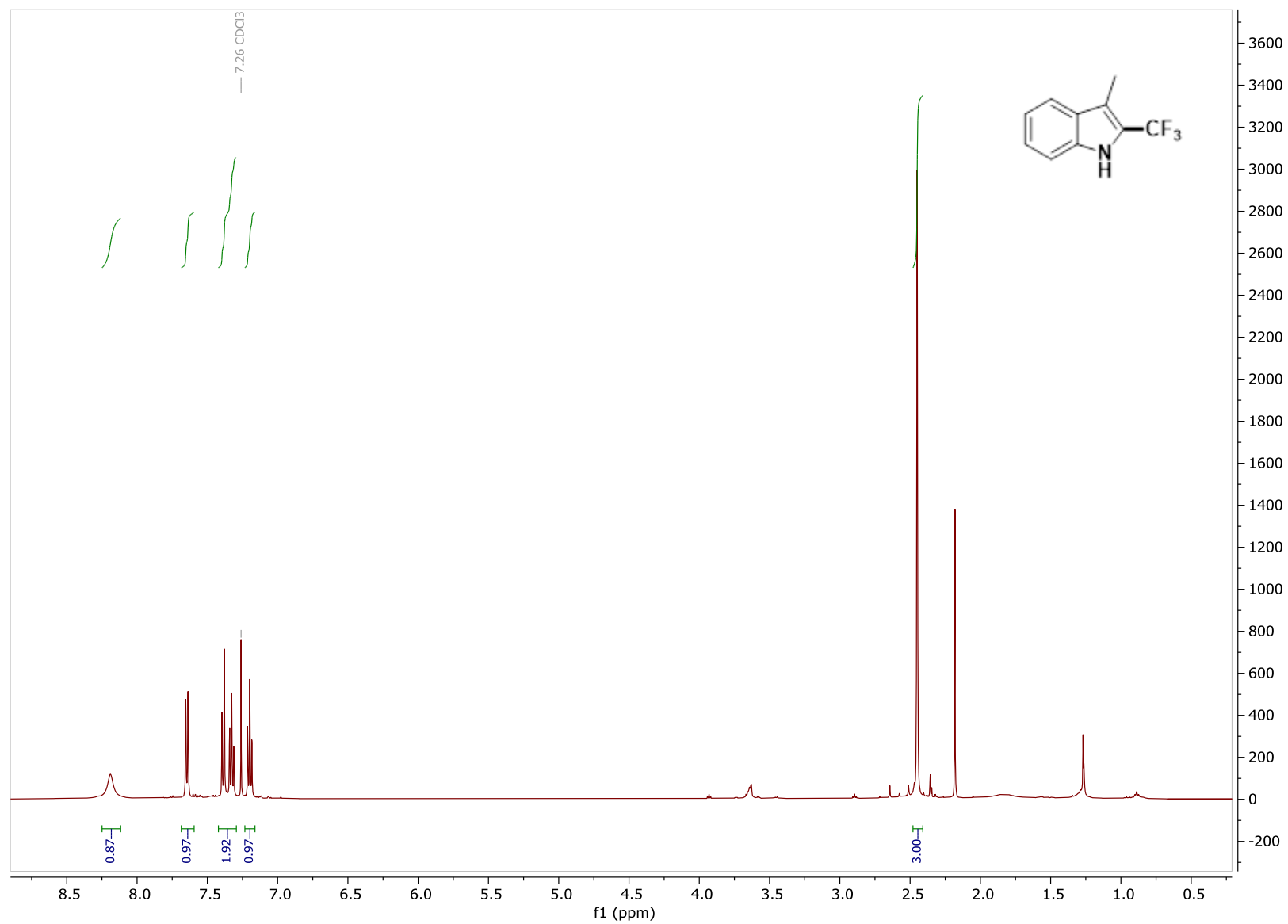
^1H NMR of TF4, CDCl_3 , 500 MHz

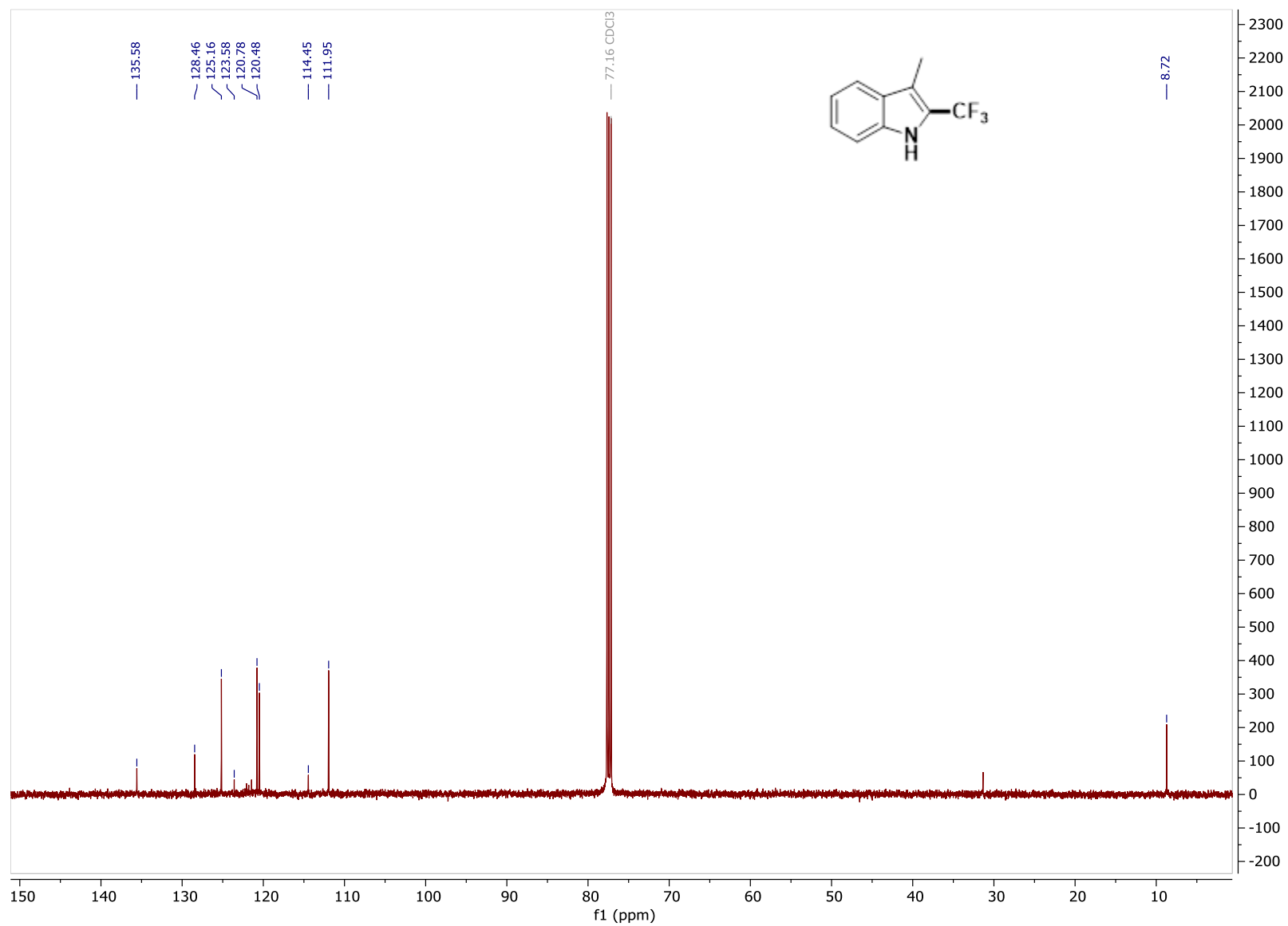
^{13}C NMR of TF4, CDCl_3 , 126 MHz

^{19}F NMR of **TF4**, CDCl_3 , 471 MHz

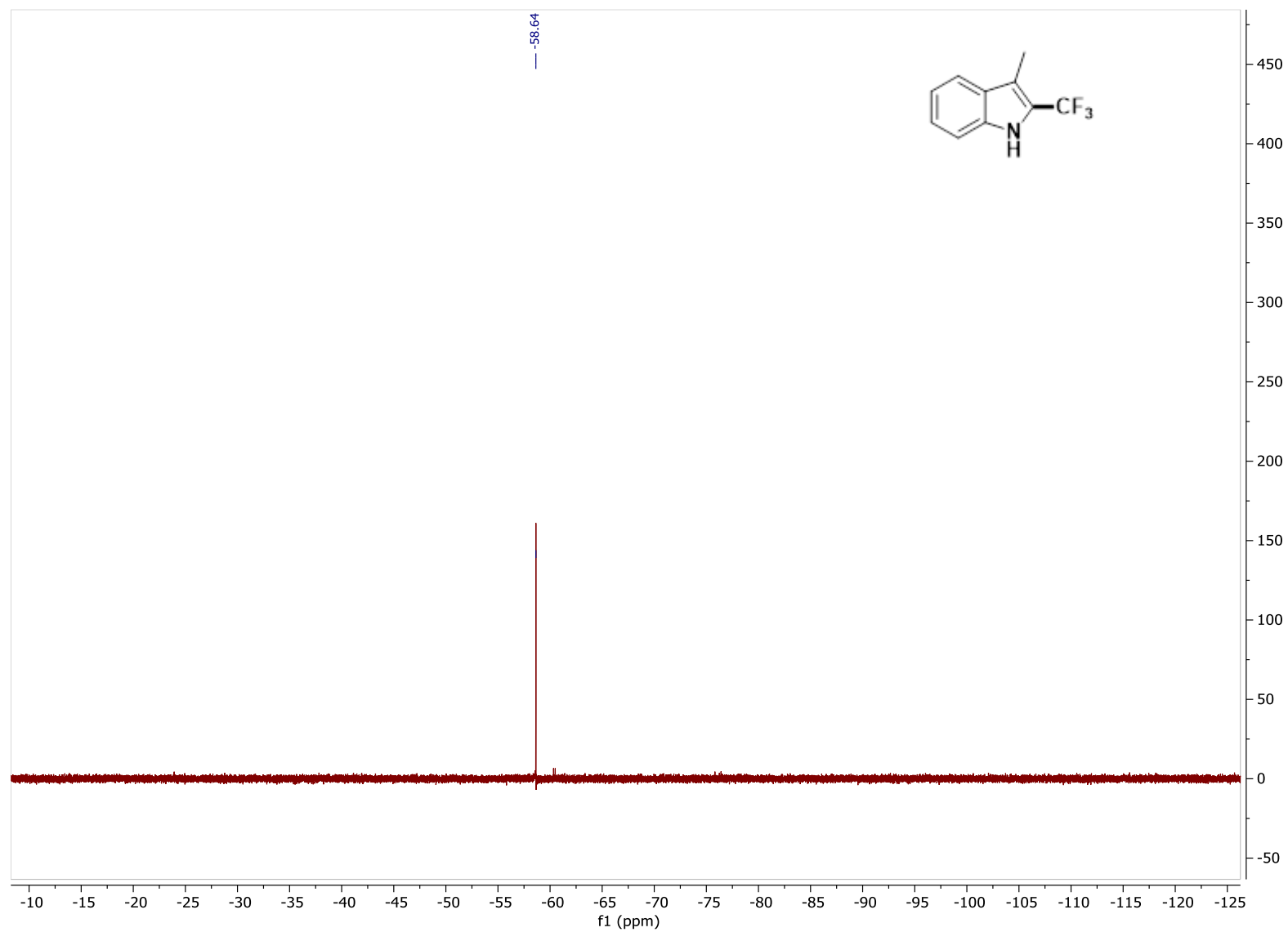


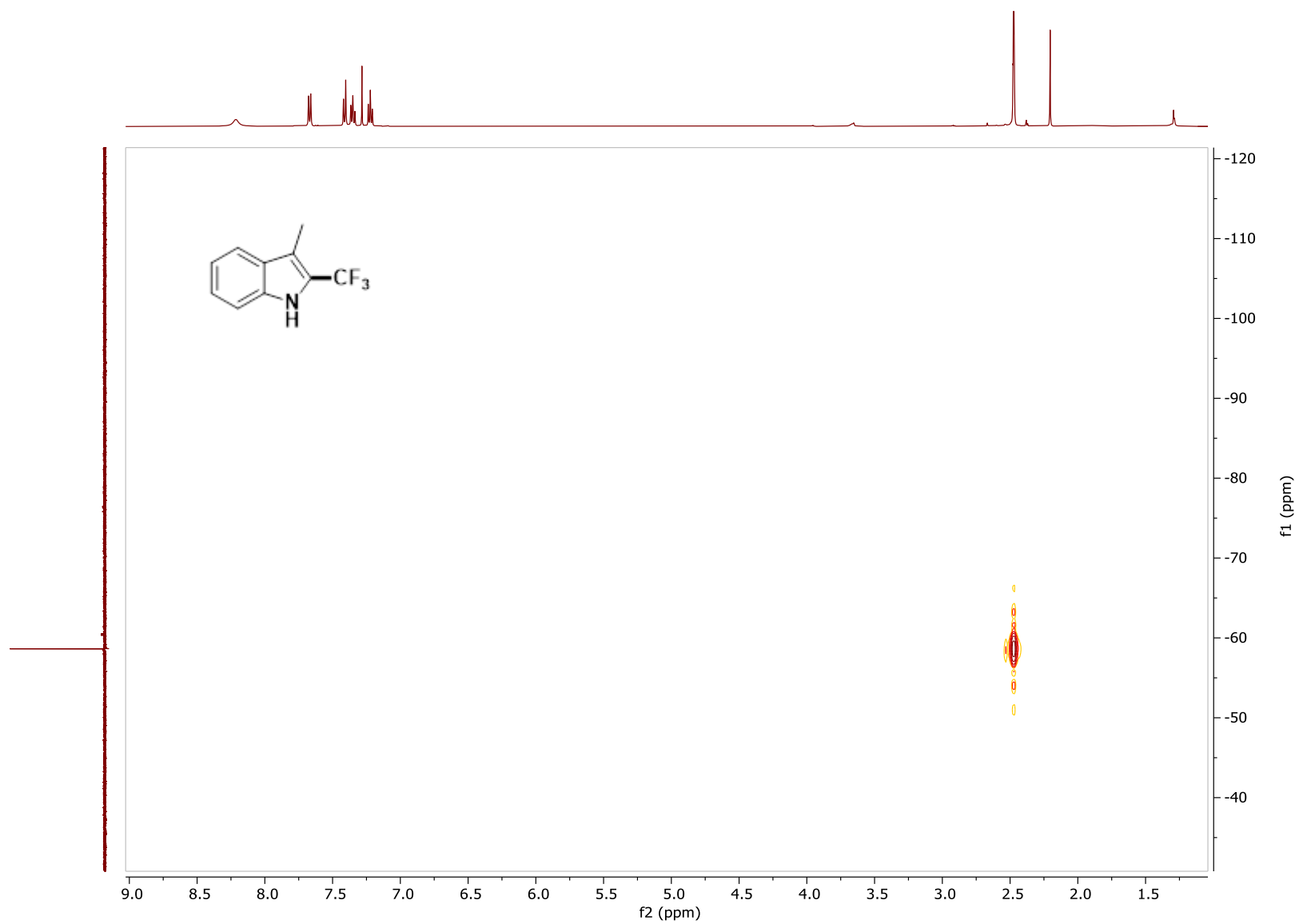
^1H - ^{19}F HMBC of TF4

^1H NMR of TF5, CDCl_3 , 500 MHz

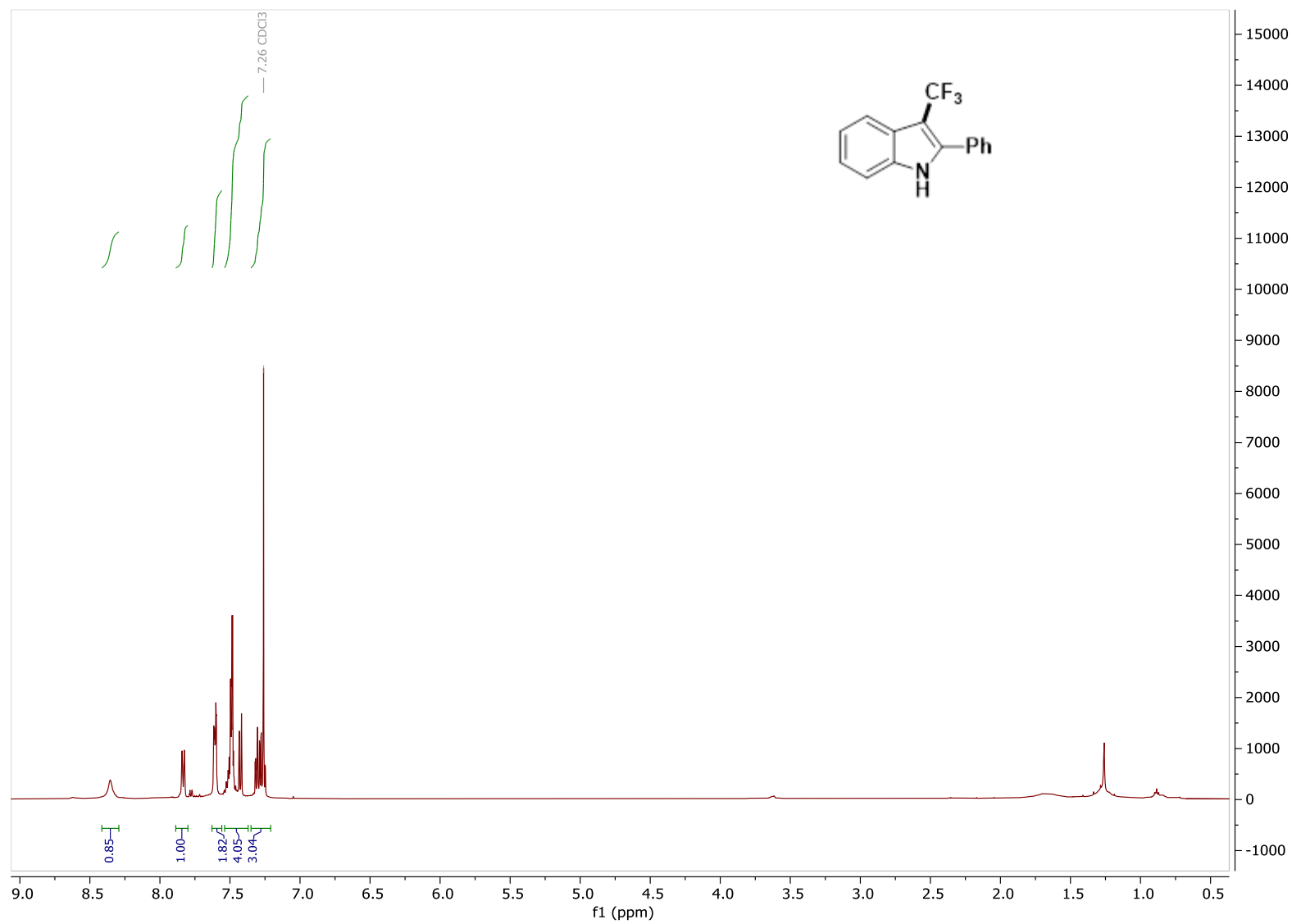
^{13}C NMR of **TF5**, CDCl_3 , 126 MHz

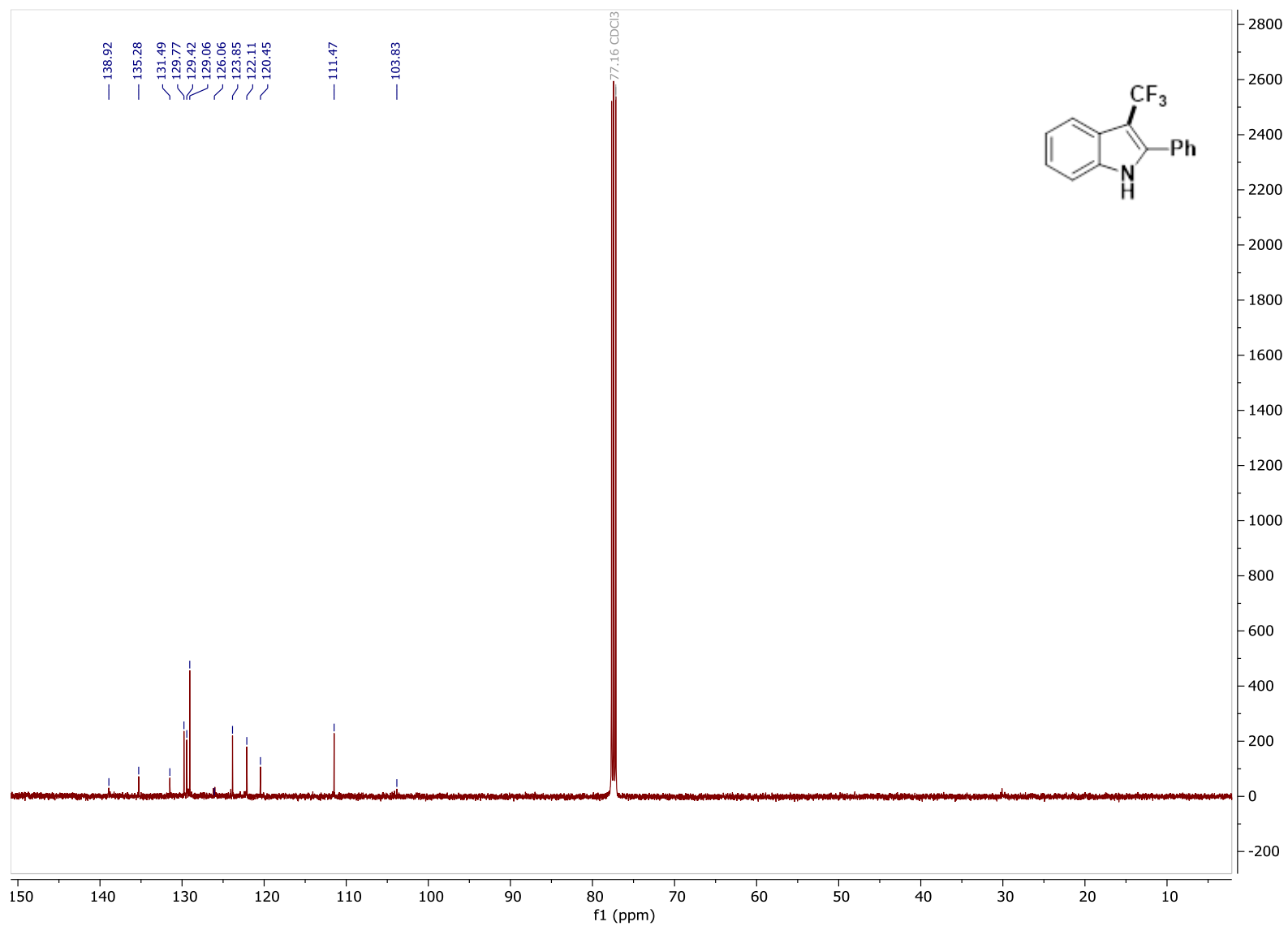
^{19}F NMR of **TF5**, CDCl_3 , 471 MHz



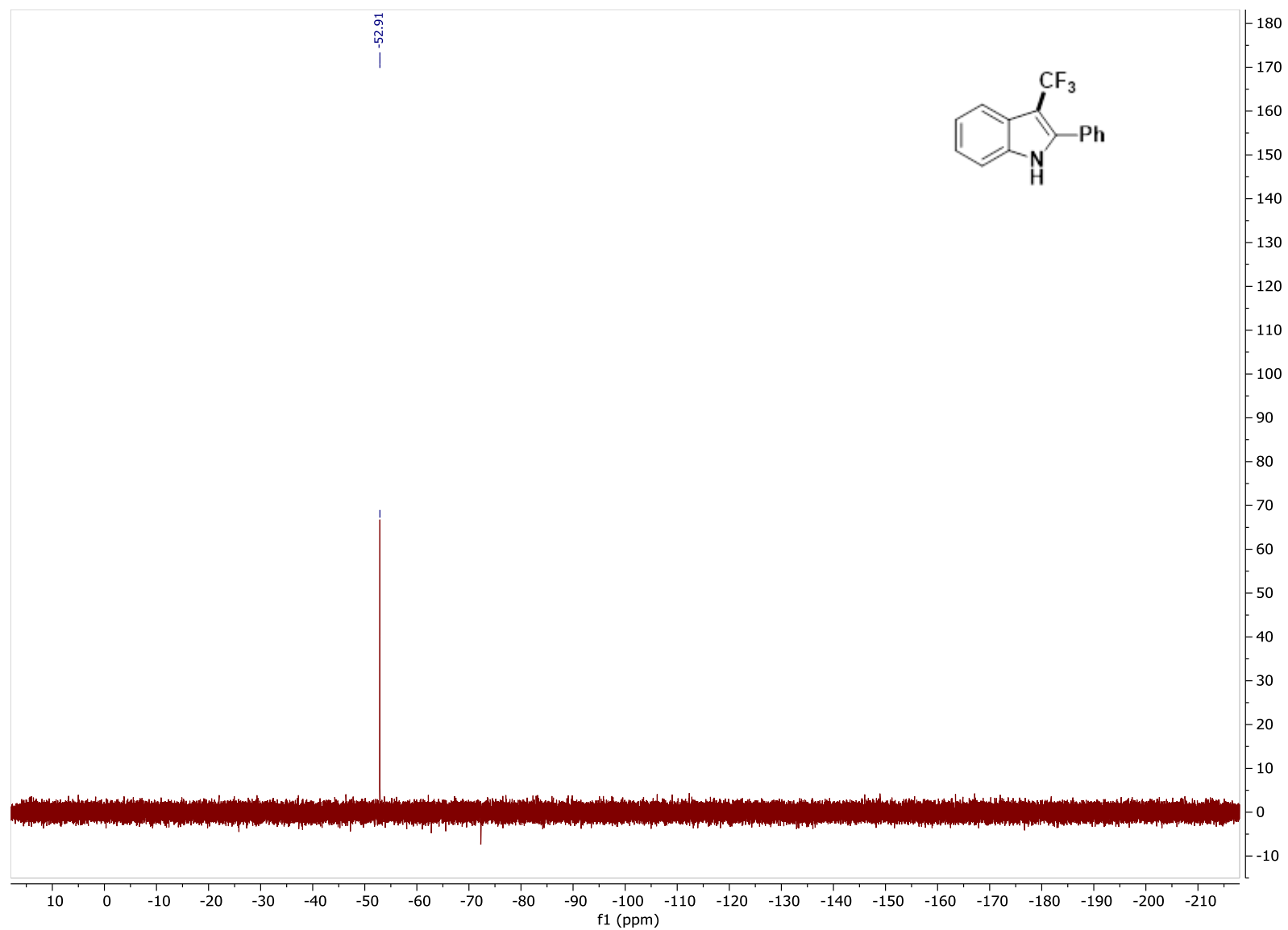
^1H - ^{19}F HMBC of TF5

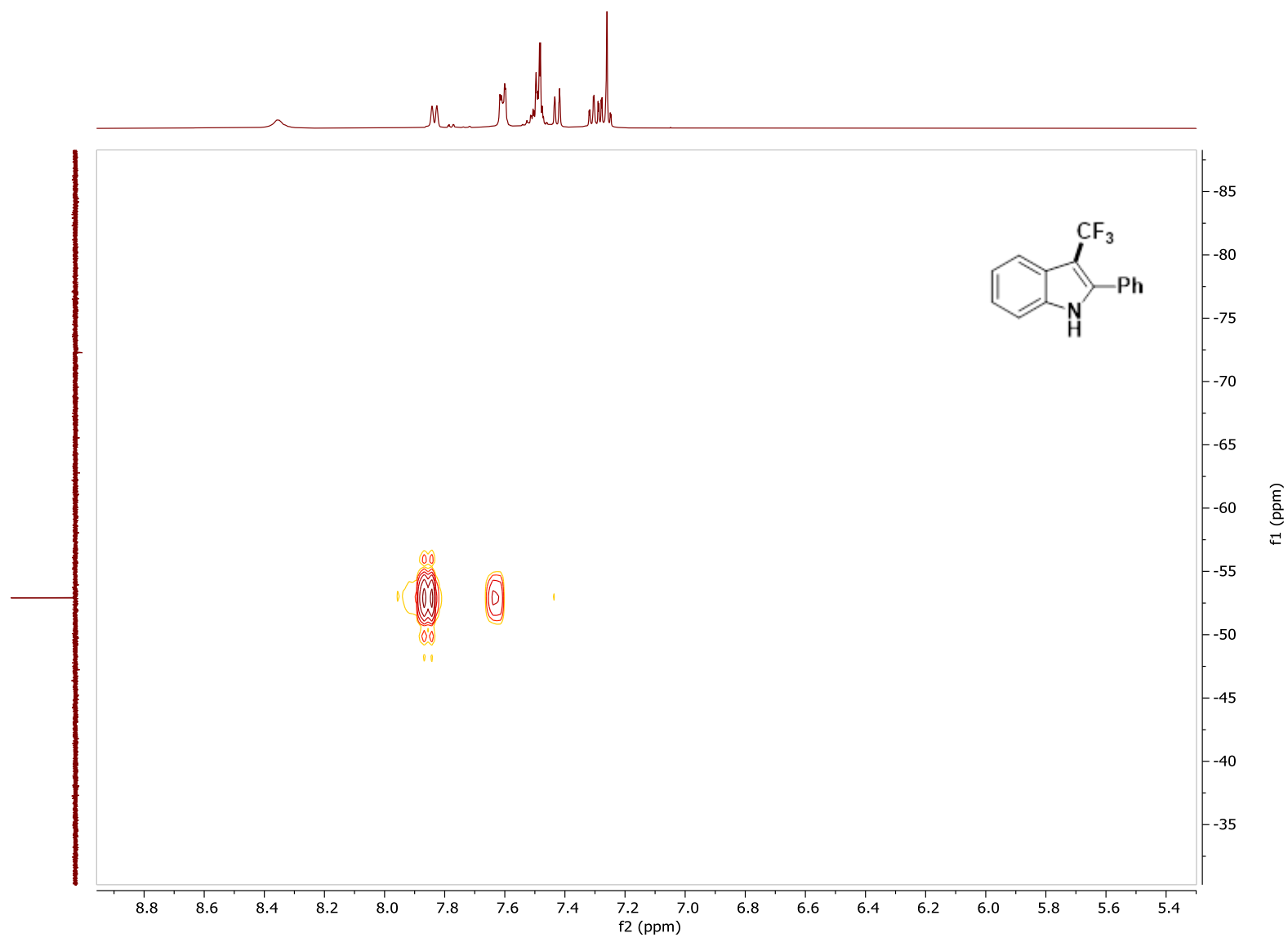
^1H NMR of **TF6**, CDCl_3 , 500 MHz

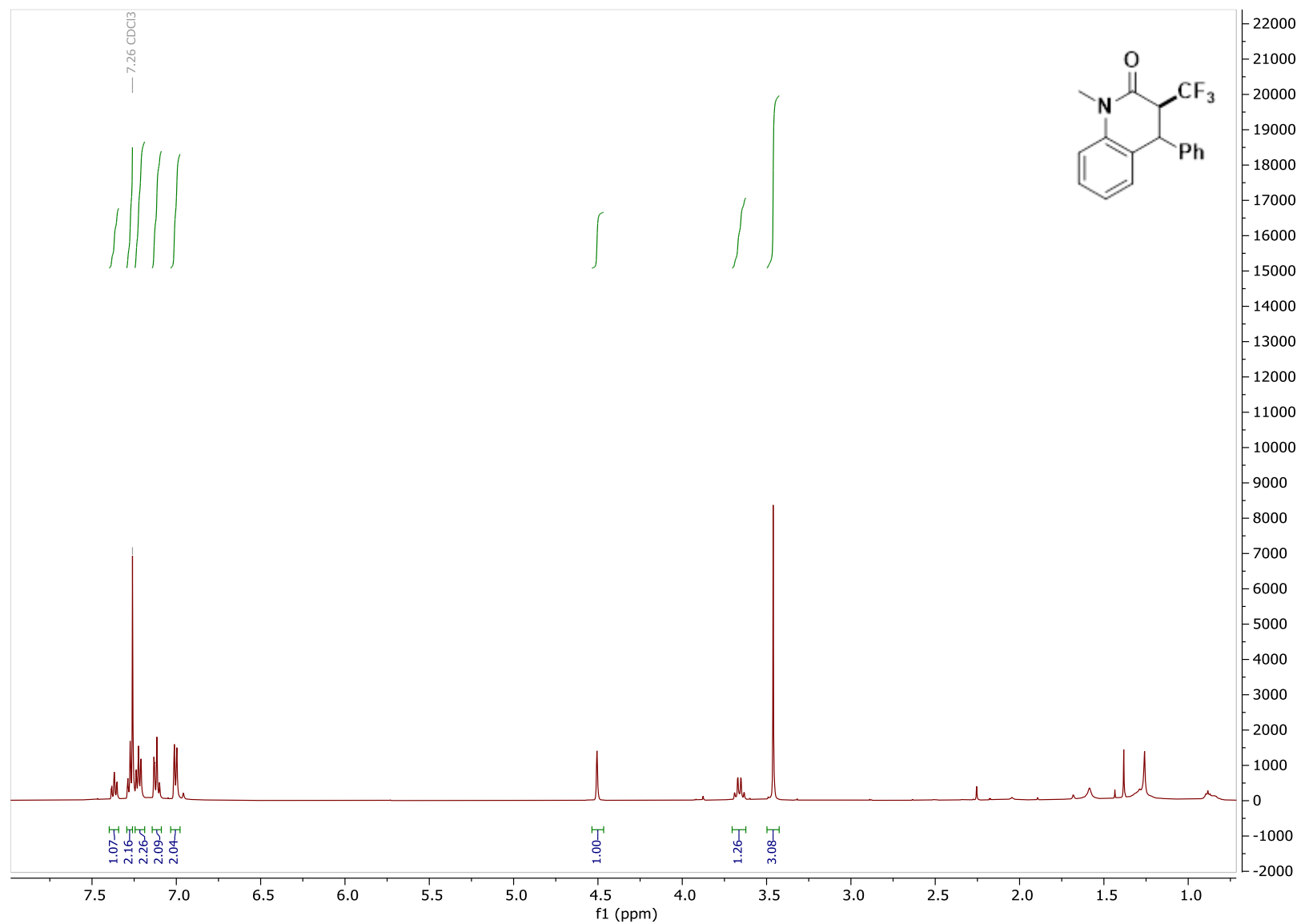


^{13}C NMR of TF6, CDCl_3 , 126 MHz

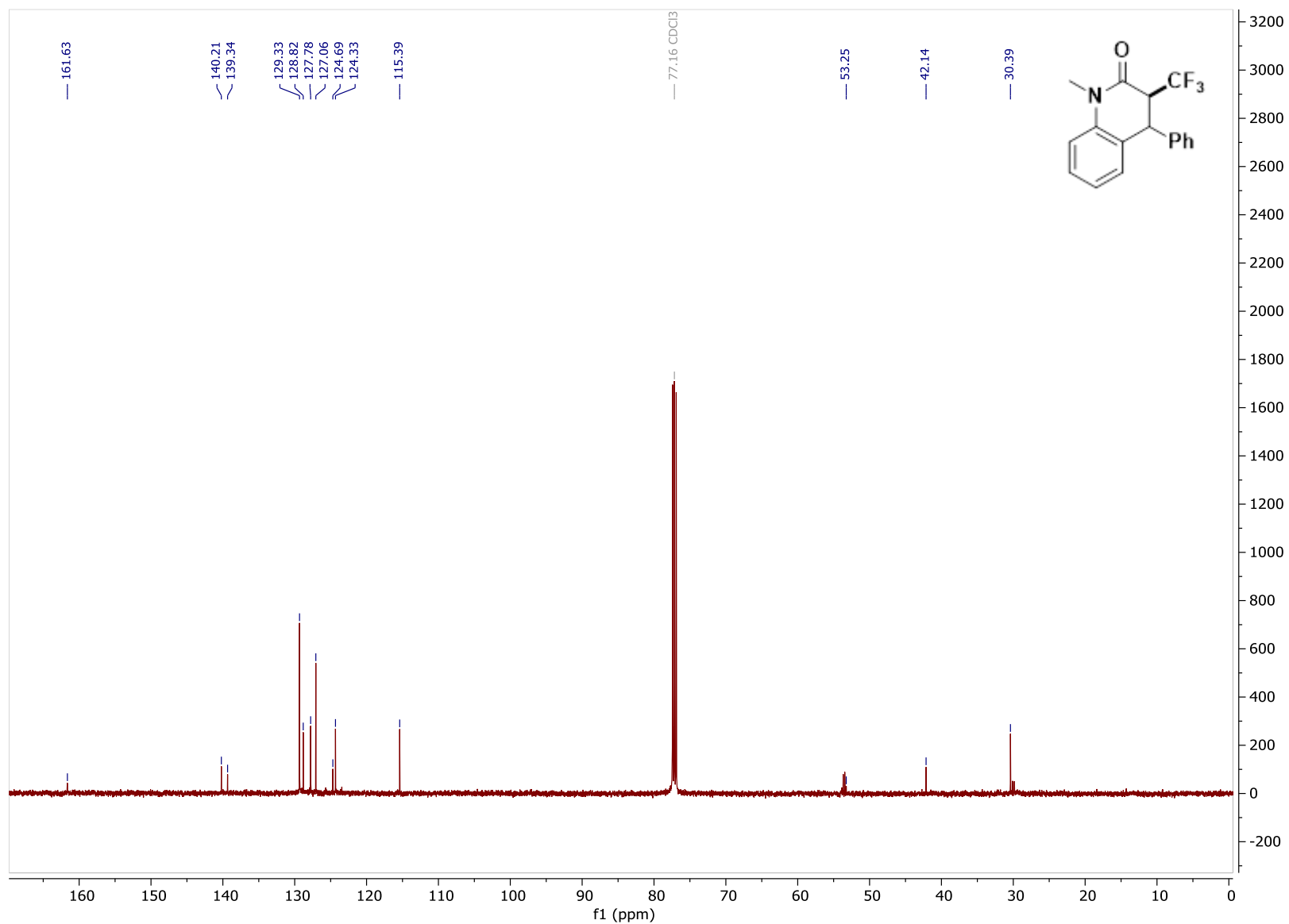
^{19}F NMR of **TF6**, CDCl_3 , 471 MHz



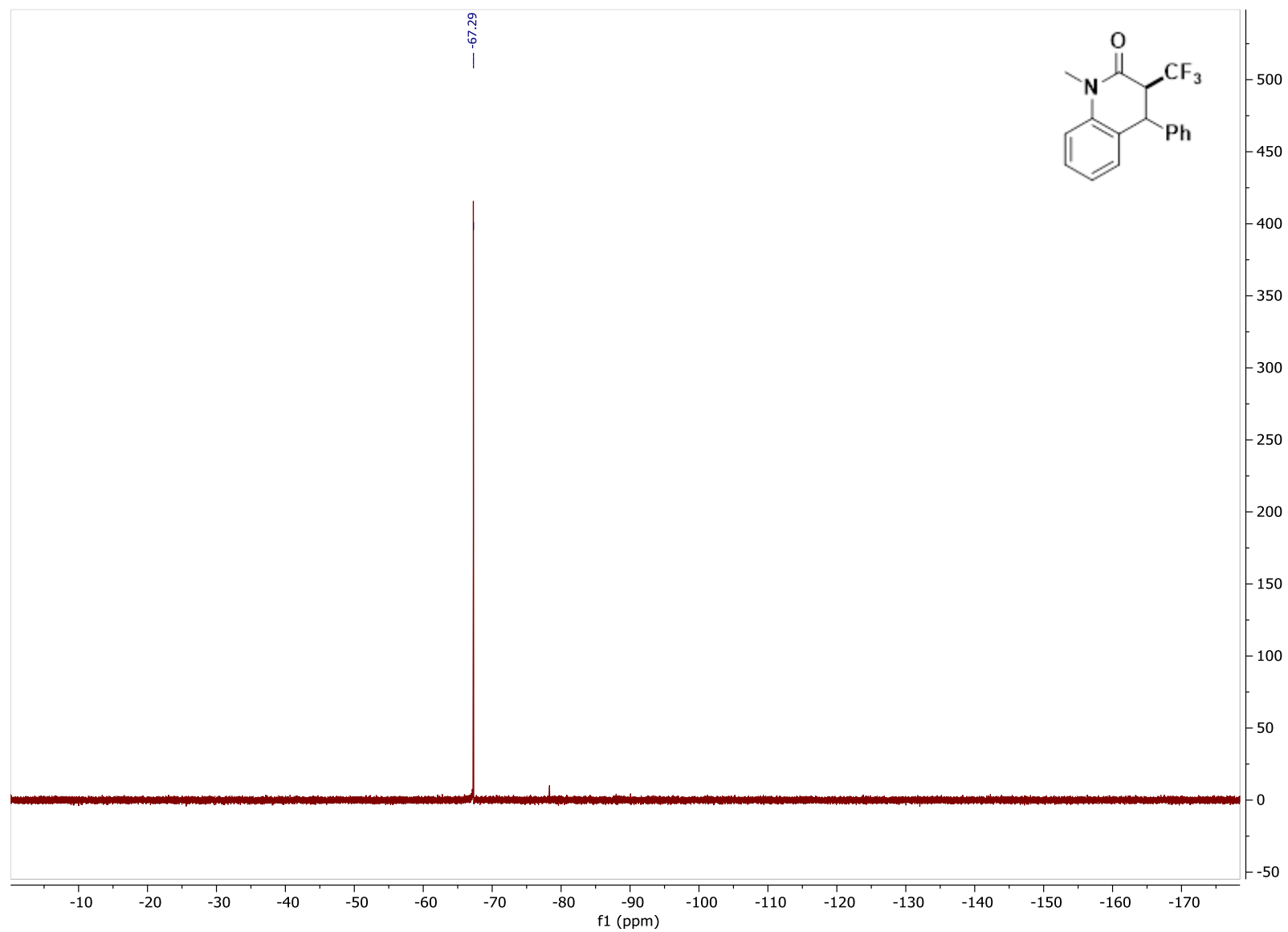
^1H - ^{19}F HMBC of TF6

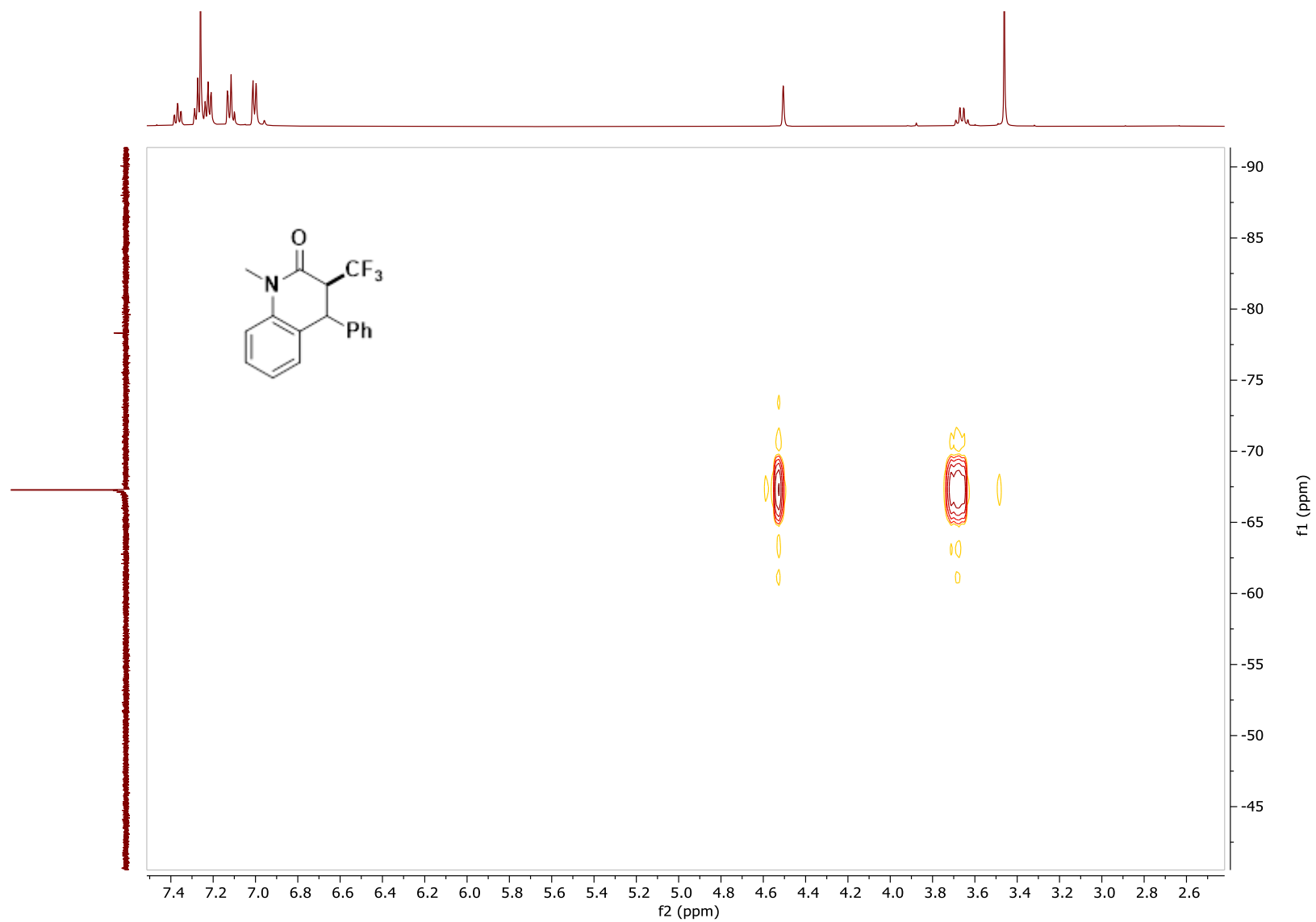
^1H NMR of **TF7**, CDCl_3 , 500 MHz

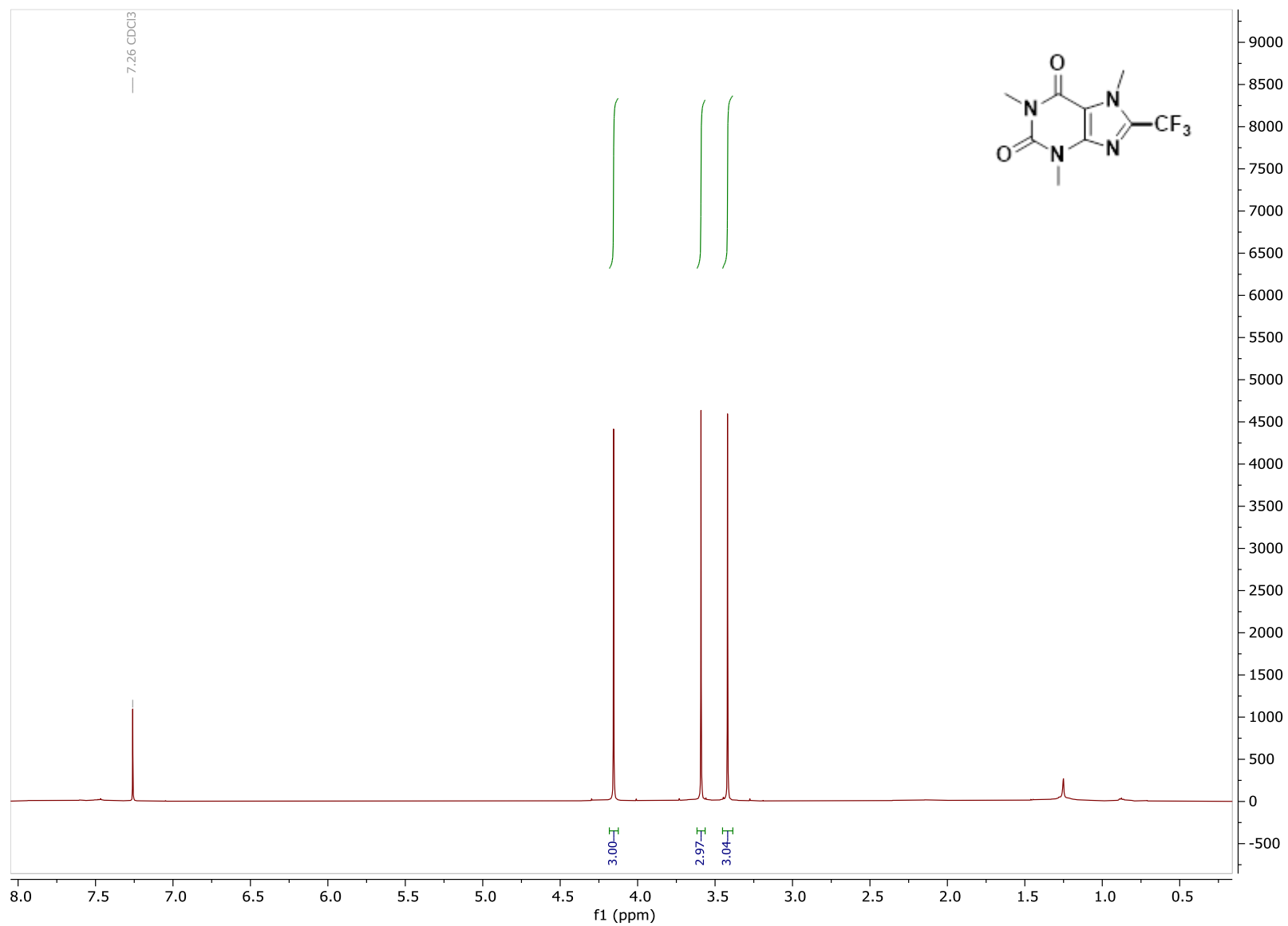
^{13}C NMR of TF7, CDCl_3 , 126 MHz



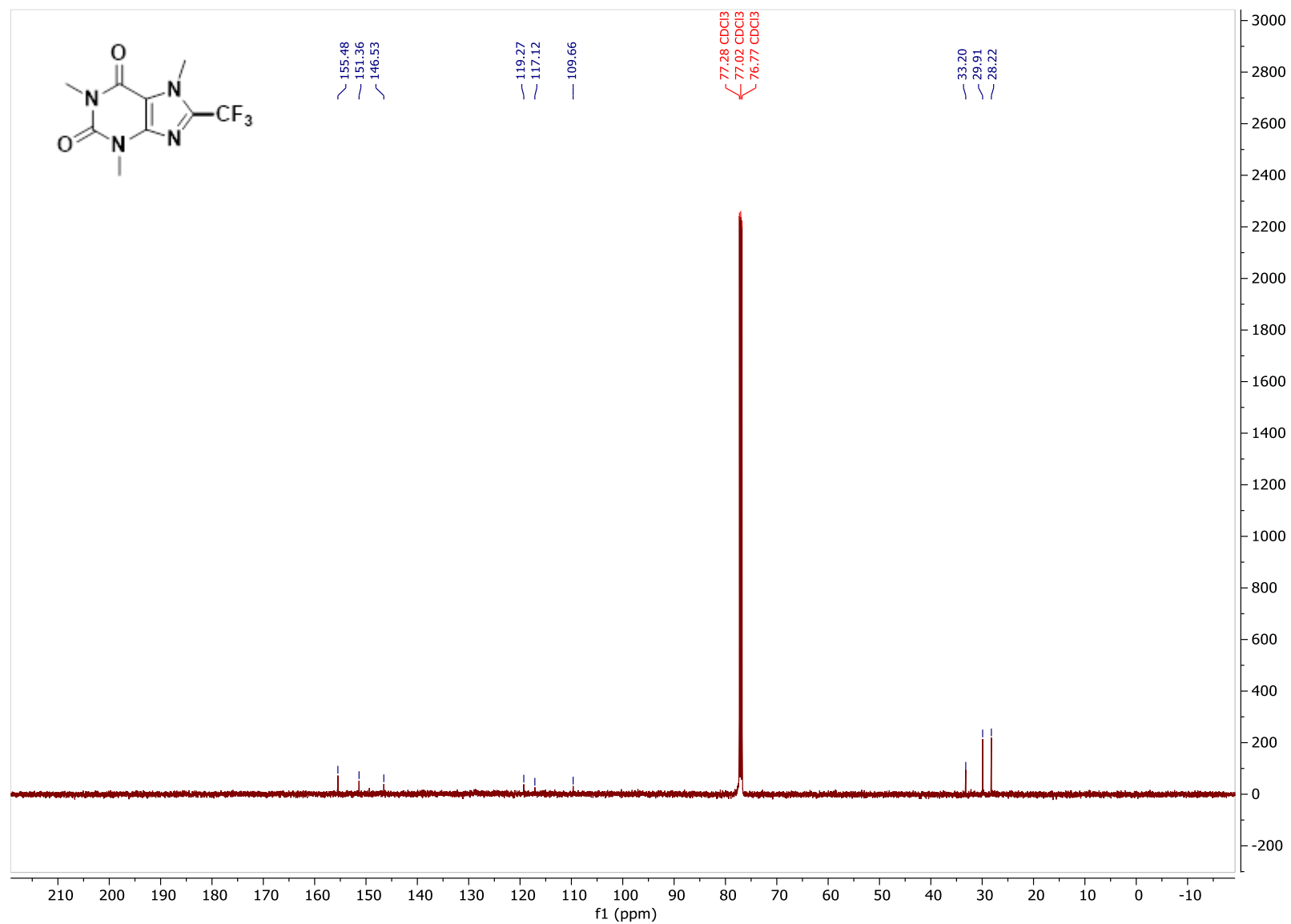
^{19}F NMR of **TF7**, CDCl_3 , 471 MHz



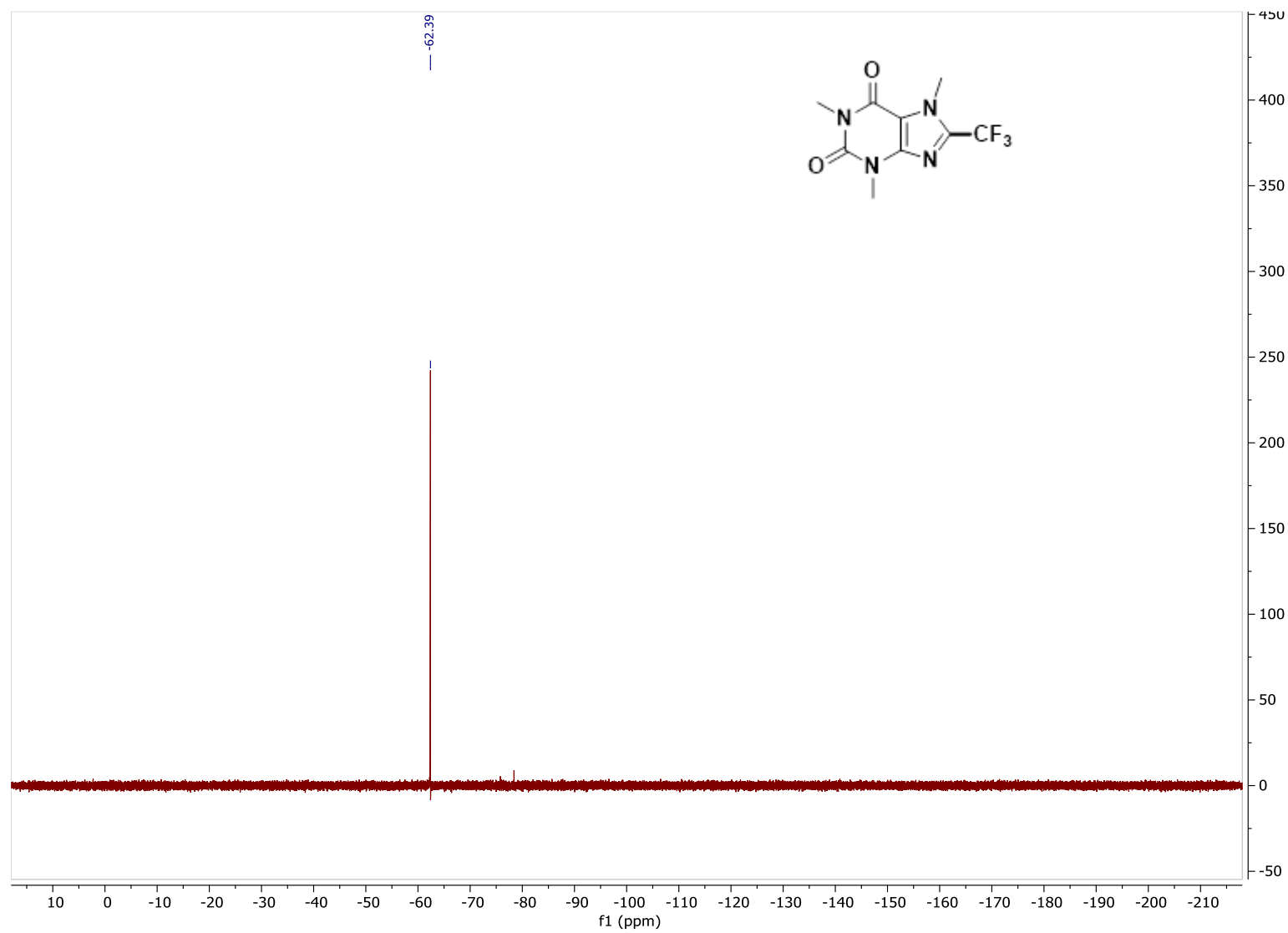
^1H - ^{19}F HMBC of TF7

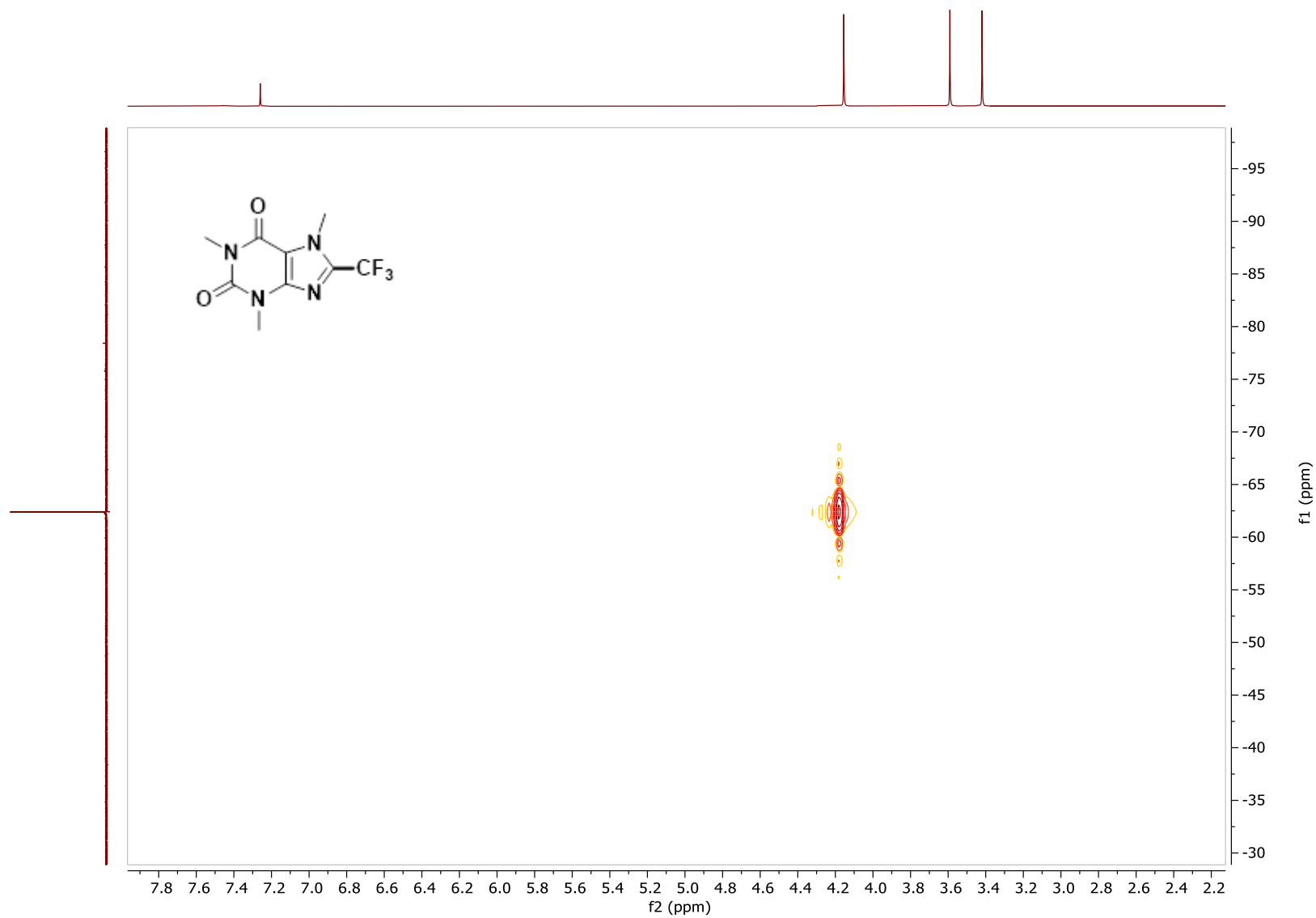
^1H NMR of **TF8**, CDCl_3 , 500 MHz

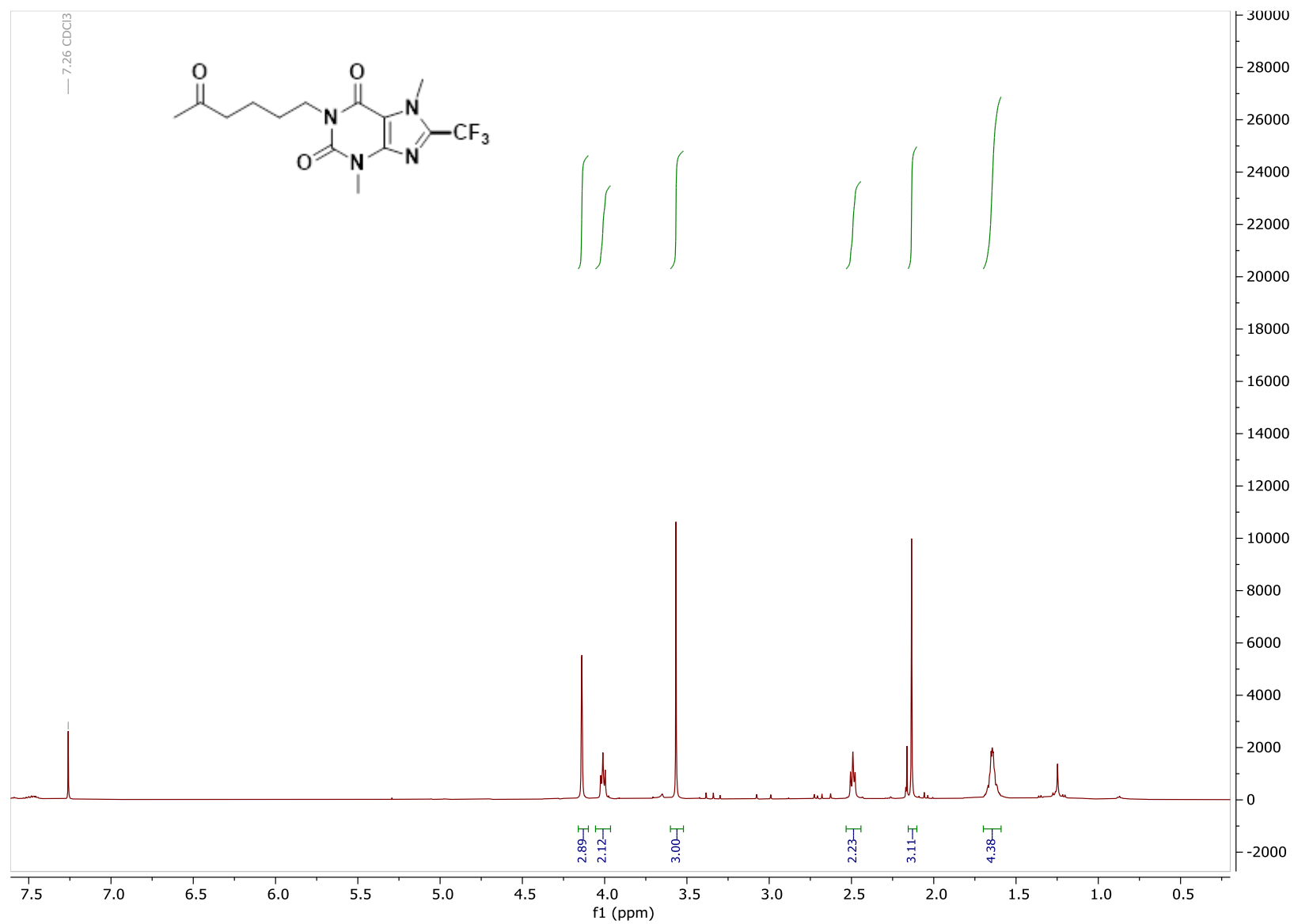
^{13}C NMR of **TF8**, CDCl_3 , 126 MHz

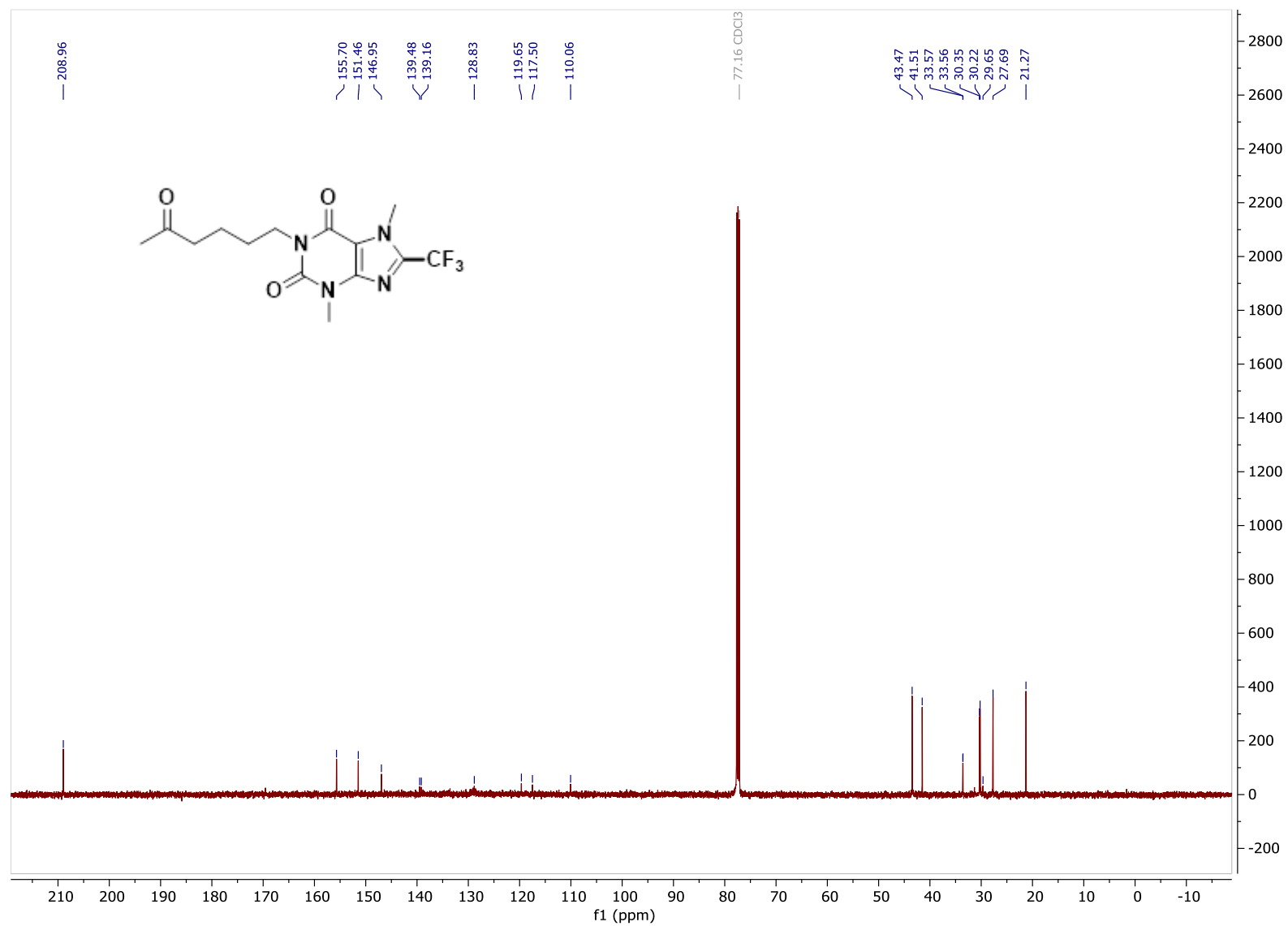


^{19}F NMR of **TF8**, CDCl_3 , 471 MHz

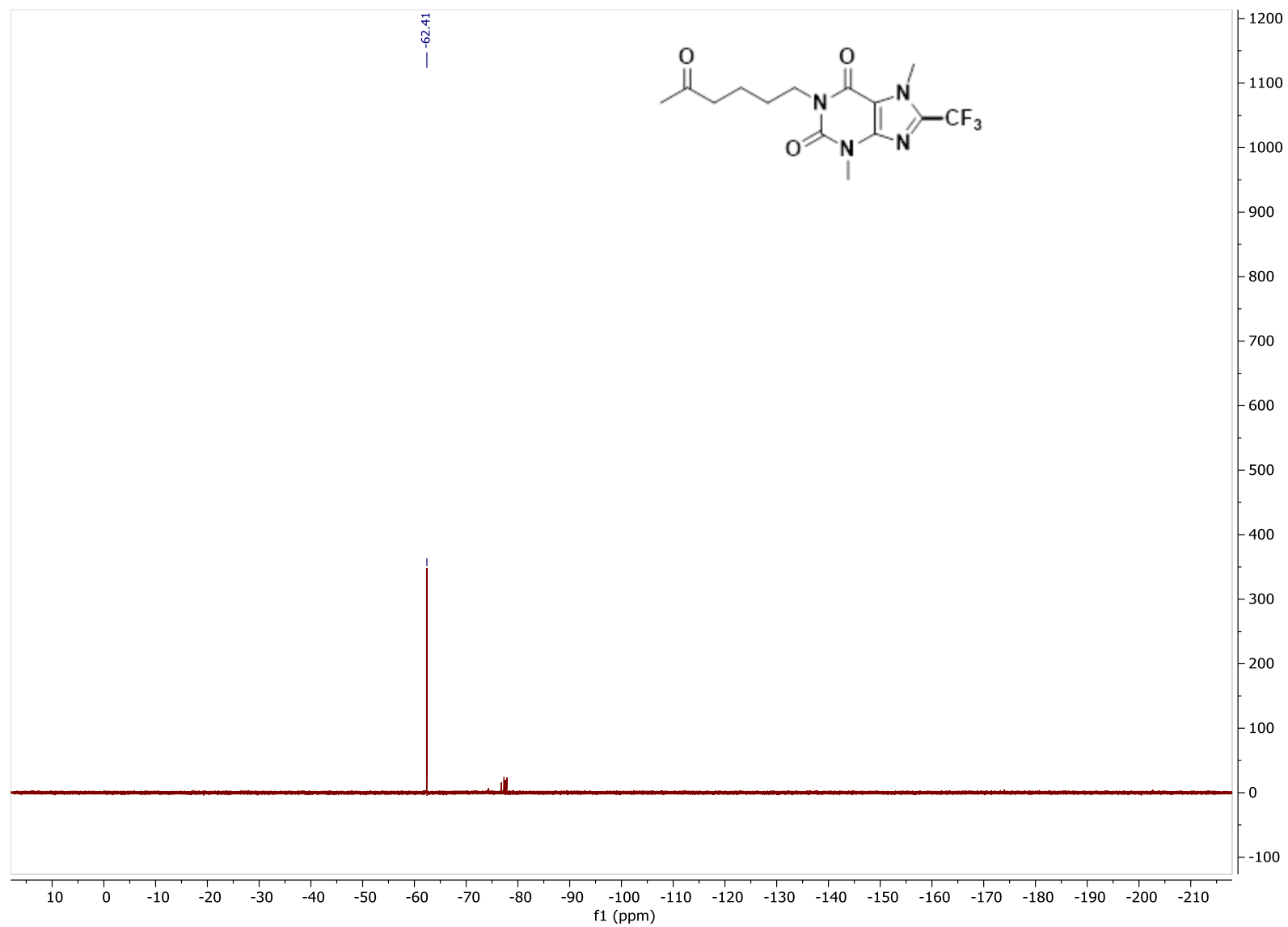


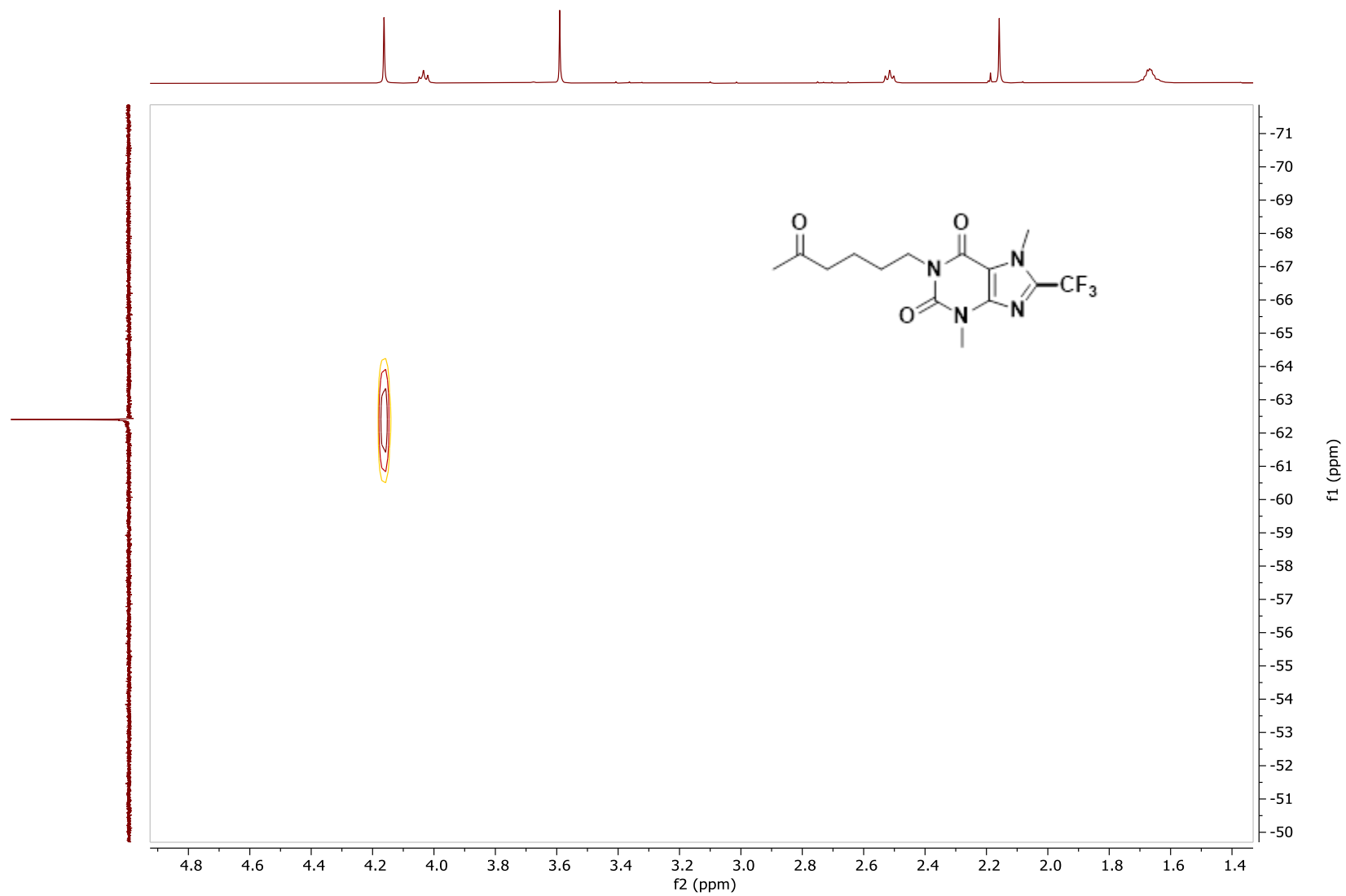
^1H - ^{19}F HMBC of TF8

^1H NMR of **TF9**, CDCl_3 , 500 MHz

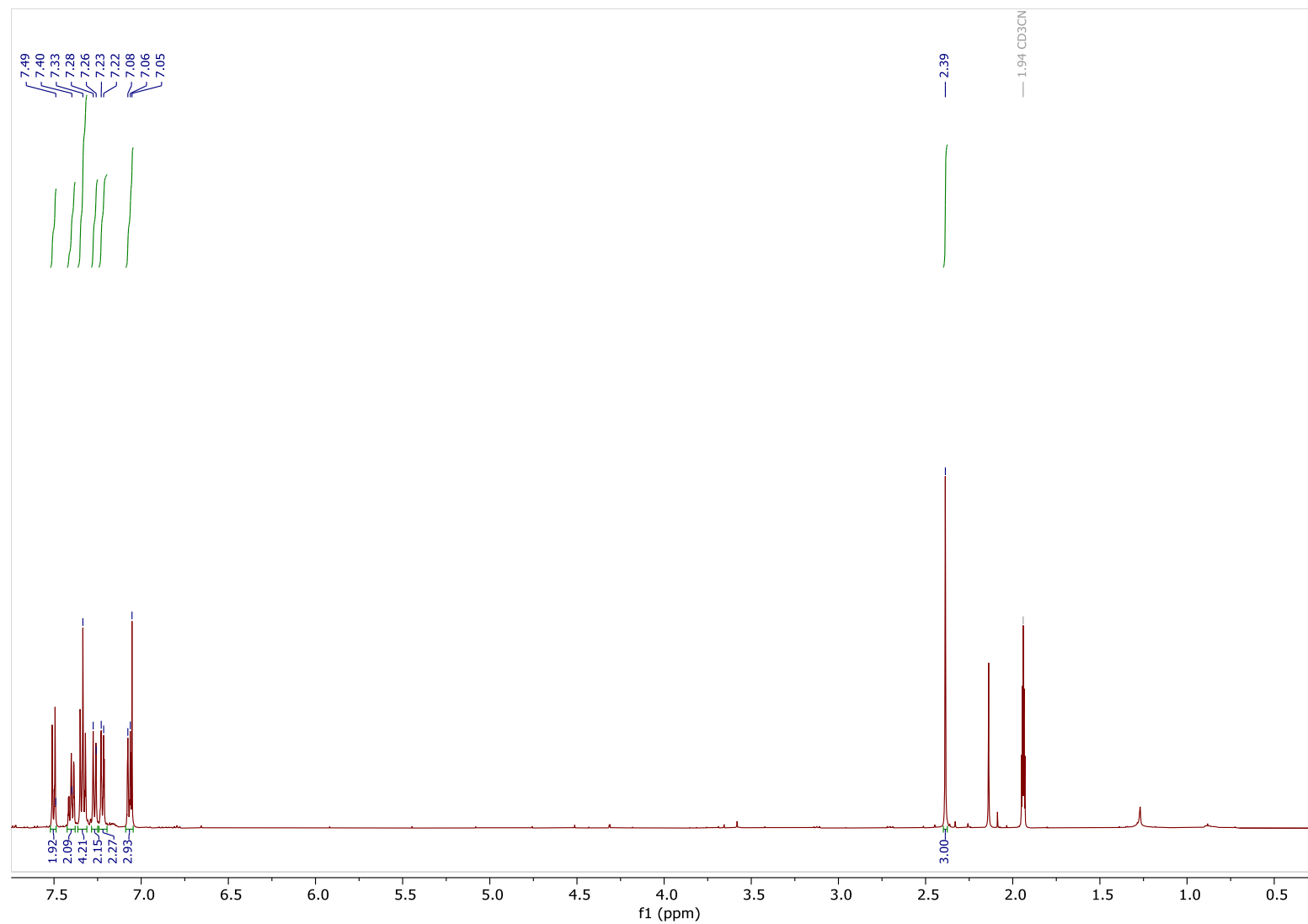
^{13}C NMR of TF9, CDCl_3 , 126 MHz

^{19}F NMR of **TF9**, CDCl_3 , 471 MHz



^1H - ^{19}F HMBC of TF9

Characterization data for Chapter 4

 ^1H NMR of **3**, CD_3CN , 500 MHz

^{13}C NMR of **3**, CD_3CN , 126 MHz

